



# **The ROSE Report: CAMD, Past, Present and Future**

**By**

**The Rose Committee:**

**Henry D Bellamy; Leslie G Butler; Doris Carver; Jin-Woo Choi; Lorraine Marceau-Day; Peter A Dowben; David Ederer; Jost S Goettert; Brooks Keel; Challa Kumar; Richard L Kurtz; Wen J Meng; Eizi Morilawa; Kevin Morris; Marcia E Newcomer; Erwin D Poliakoff; Amitava Roy; John D Scott; Phillip Sprunger; Craig P Stevens; Victor P Suller.**

**Additional Contributions from: Tabbetha Dobbins; Ken Hogstrum; Josef Hormes; Paul Russo; Ed Walker.**



## **Acknowledgements and CAMD Contact Information:**

This document was requested by the CAMD SAC has been the effort of a rather large committee listed as follows:

### Committee Members:

Dr. Amitava Roy, Assoc. Prof. Res., CAMD;  
Dr. Brooks Keel, Vice Chancellor, Research & Economic Development, LSU;  
Dr. Challa Kumar, Director of Nanofabrication and Nanomaterials, CAMD;  
Mr. Craig P Stevens, Assistant Director for Administration, CAMD;  
Dr. David Ederer, Interim Director, CAMD;  
Dr. Doris Carver, Assoc. Vice Chancellor, Research & Economic Development, LSU;  
Dr. Eizi Morikawa, Staff, CAMD;  
Dr. Erwin D Poliakoff, Professor of Chemistry, LSU;  
Dr. Henry D Bellamy, Assoc. Prof. Res., CAMD;  
Dr. Jin-Woo Choi, Desig. Professor, Electrical Engineering, LSU;  
Dr. John D Scott, Scientific Director, CAMD;  
Dr. Jost S Goettert, Director, Microfabrication, CAMD;  
Mr. Kevin J Morris, Deputy Director, Vacuum Group, CAMD;  
Dr. Leslie G Butler, Professor of Chemistry, LSU;  
Dr. Lorraine Marceau-Day, Radiation Safety Officer, CAMD;  
Dr. Marcia E Newcomer, Chair, Biological Sciences, LSU;  
Dr. Peter A Dowben, Professor of Physics, University of Nebraska;  
Dr. Phillip Sprunger, Assoc. Professor of Physics, LSU;  
Dr. Richard L Kurtz, Professor of Physics, LSU;  
Mr. Victor P Suller, Deputy Director, Accelerator Operations, CAMD;  
Dr. Wen J Meng, Desig Professor, Mechanical Engineering, LSU;

The co-chairs, Professor Brooks Keel, Vice Chancellor of Research and Economic Development and Professor David Ederer, Interim Director of CAMD are especially grateful to their colleagues who have contributed to this labor.

Contact: For information about CAMD visit our website: <http://www.camd.lsu.edu/>, or call  
Mr. Craig Stevens – 225-578-4603 or  
Dr. John Scott – 225-578-4605



## Table of Contents: Rose Report

			Page No.
		<b>Acknowledgements and CAMD Contact Information</b>	
<b>I</b>		<b>Executive Summary and Introduction</b>	1
	<b>A.</b>	<b>Description of CAMD</b>	3
	<b>B.</b>	<b>Layout of the CAMD Electron Storage Ring , its Operating Parameters, and Associated Beam Lines</b>	5
	<b>C.</b>	<b>Table of Beamlines</b>	7
	<b>D.</b>	<b>Microfabrication Facilities</b>	8
<b>II</b>		<b>CAMD Science: Current and Near Future</b>	9
		Introduction	10
	<b>A.</b>	<b>Material Sciences</b>	11
		1 Nanomaterials	11
		2 Polymers and Soft Materials	16
		3 Correlated and Magnetic Materials	20
	<b>B.</b>	<b>Chemical Sciences</b>	22
		1 Atomic, Molecular, Optical (AMO) Physics and Chemical Physics at CAMD: VUV Photoionization Research	22
		2 Opportunities at the intersection of nanoscience and combustion chemistry: X-ray characterization	28
		3 Catalysis Research at CAMD	31
	<b>C.</b>	<b>Environmental Sciences</b>	36
	<b>D.</b>	<b>Life Sciences</b>	40
		1 Macromolecular Crystallography at CAMD	40
		2 Biomedical Applications	43
	<b>E.</b>	<b>Clinical Science</b>	47
	<b>F.</b>	<b>Microfabrication</b>	52
		1 MEMS/LIGA Services at CAMD in 2006	52
		2 Applications	58
<b>III</b>		<b>CAMD Today</b>	81
		Introduction	82
	<b>A.</b>	<b>A Brief History of CAMD</b>	83
	<b>B.</b>	<b>Current Situation</b>	88
		1 The Ring	88
		a. Performance	88
		b. Reliability	90
		c. Opportunities and their limits	91
	<b>B.</b>	2 Beamlines (description, types of research, needs and justification, publications)	93
		2 a. VUV and IR	93
		b. X-ray (2-10 KeV)	110

<b>III</b>	<b>B.</b>		c.	Wavelength Shifter (7- 70 keV)	123
		3		CAMD Microfabrication: An Introduction	127
			a.	CAMD Microfabrication: A Unique LSU Resource	129
			b.	CAMD Microfabrication and LSU faculty: two examples of partnerships	130
	<b>B.</b>	4		Other Activities	137
			a.	CAMD Outreach	137
			b.	CAMD Safety	139
		5	a.	CAMD Organizational Structure	141
			b.	CAMD's Funding	151
			c.	CAMD Cleanroom	154
			d.	History and Overview of IT at CAMD	159
	<b>C.</b>			<b>CAMD User Statistics</b>	160
		1		CAMD Users from Louisiana	162
			a.	LSU	162
			b.	State of Louisiana [Excluding LSU]	164
		2		CAMD Users Outside Louisiana	165
		3		Degrees Based on CAMD Work	169
<b>IV</b>				<b>A Plan for a Transition between the Current Configuration of CAMD and a Future Microfabrication Laboratory and Light Source for the 21st Century</b>	171
				Introduction	172
	<b>A.</b>			<b>Planning for CAMD's Future in Microfabrication</b>	173
	<b>B.</b>			<b>Optimizing CAMD: Accelerator, Insertion Devices, and Beamlines</b>	174
	<b>B.</b>	1		Hard X-ray Wiggler	178
		2		Scientific Opportunities with Hard X-ray Wiggler	180
		2	a.	Macromolecular Crystallography	181
			b.	Tomography	184
			c.	Medical Radiology	185
			d.	Geosciences and Environmental Science	187
			e.	Catalysis and Energy Research	189
	<b>C.</b>			<b>Second Insertion Device (A Soft X-ray Wiggler)</b>	190
		1		Description of 3.5 Tesla Multi Pole Wiggler	190
		2		Scientific Case for the Soft X-ray Wiggler	198
			a.	Small-angle Scattering (SAXS)	198
			b.	Intermediate Energy EXAFS	199
			c.	Correlation of the microstructure of Perovskites and Related Oxides with their Physical Properties	200
	<b>D.</b>			<b>New VUV Wiggler</b>	202
		1		Description of the VUV wiggler	202
		2		Scientific Opportunities with the VUV Wiggler	204
			1.a.	Spin-polarization and Exchange in Room Temperature Metal-organic Ferromagnets	204

IV	D.	2	1.b.	Photoemission and Gas Phase Cluster Experiments (Dowbin)	205
	E.			<b>Upgrades to Existing Beamlines</b>	206
IV	E.	1		Upgrades to Existing X-Ray Bending Magnet Beamlines to Characterize Advanced Materials	206
	E.	1	b.	Scientific Benefits of Upgrading the VUV Beamlines	210
V				<b>The Future : A New Light Source for the Southeast Flagship Agenda: through new ring</b>	211
	A.			<b>Introduction</b>	212
	B.			<b>A Compact Third Generation Source: ROSE:</b>	215
	C.			<b>Defining the Road toward the Development of the “Light Source of the Future”: A report by the Source Breakout Group attending the workshop, Enabling Grand Challenge Science: The Light Source of the Future.</b>	218
	C.	1		Overview	218
		2		Electron Guns and Timing	220
		3		Bunch Compression and Pulse Length	220
		4		Undulators and Free Electron Lasers	221
		5		Superconducting LINACs	223
		6		Seed and Pump Lasers	224
		7		Inverse Compton Scatter Source	224
		8		Experimental Facilities	224
	D.			<b>Work Force Development Implicit with the Development of an Advanced Light Source</b>	227
		1		General Remarks	227
		2		Staffing Challenges to Develop and Accelerator..	228
		3		Workforce Development through an Existing LSU Program.	229
		4		Workforce Development through a University-Federal and State Partnership	229
	E.			<b>Conclusions</b>	230
				<b>Appendices</b>	231
	A.			<b>Appendix A: Publications 2005 - 2001</b>	232
	B.			<b>Appendix B: User Report 2006</b>	259
				Scientific Thrusts	260
				Life Sciences	260
				Environmental and Agricultural Sciences	284
				Nanoscience	335
				Material and Chemical Sciences	363
				Microfabrication	452
				Radiology	482
				BioMems	486
	C.			<b>Workshop Reports</b>	496
	C.	1		First Workshop to Evaluate a New Advanced Light Source November 2006	500
	C.	2		Second Workshop Enabling Grand Challenge Science: The Light Source of the Future,	519

		January 28-30, 2008	
		<b>List of Attendees</b>	524
		<b>Report: Enabling Grand Challenge Science: The Light Source of the Future, January 28-30, 2008</b>	526
	<b>D.</b>	<b>Second Insertion Device</b>	549
	<b>E.</b>	<b>Possible configuration for the source of the 21st Century</b>	553



# Section I

## Executive Summary and Introduction



## **CAMD: A Flower Whose Time To Bloom Is Coming!**

### **Executive Summary**

About twenty years ago, the faculty and administration at Louisiana State University (LSU) had a vision. It was to create a facility to stimulate economic growth in Louisiana. This facility would use synchrotron radiation as a cutting edge technique to work toward the development of microchip manufacture by x-ray lithography as had been pioneered by IBM Yorktown. Envisioned benefits would include x-radiation for scientific research and spin-off companies located in Baton Rouge near the source of the x-rays. The facility was named, "The J. Bennett Johnston Sr. Center for Advanced Microstructures and Devices,"(CAMD), and it became operational in 1992. The state made a commitment to support the facility at a level of about \$4,800,000 per year, and LSU made a commitment to hire four new faculty members who would focus their research at CAMD. Several beam lines for the soft x-ray region were constructed along with an x-ray beam line and clean rooms for lithography activities. By 2006 CAMD, under strong leadership, has grown to the present day facility of fifteen beamlines, 2100 square feet of class 100 clean room, 50 staff, and about 300 users who publish approximately 110 papers per year supported by over \$24,000,000/year in outside funding. Approximately, 30 members of the LSU faculty use CAMD for their research along with 70 undergraduate and graduate students.

Scientific research and technological development has broadened at CAMD to include research areas such as protein crystallography (first paper published in 2003), biophysics, cancer research, surface science, the study of electronic properties of materials, and environmental investigations. These advances have been achieved partially through grants obtained from the Louisiana Board of Regents and support from the DOE, NIH, and the NSF. Technological development in x-ray lithography has been fostered by contracts with DARPA as well, to the extent that micro and nanotechnologies engaged in at CAMD are among the most advanced in the world and have spun off two start-up companies, Mezzo Systems Inc., and Esperance Pharmaceuticals Inc. in the Baton Rouge area with memoranda of understanding established at several other institutions.

Yet, to fulfill its mission to enhance the quality of research and education at the undergraduate, graduate and postdoctoral levels through collaborations in synchrotron radiation-based research and micro- and nanofabrication capabilities, CAMD cannot remain quiescent but must continue to exploit the newest techniques available to develop and provide cutting edge research and development infrastructure for LSU, the state of Louisiana and national and international users. As part of this paradigm, in the near term, CAMD will strive to add two insertion devices as well as become a core part of a Frontier Materials Research and Development Center, to fully exploit its unique expertise in the areas of biosciences, materials development, and micro- and nano-science technologies. In addition to conducting research and development, these capabilities will be used to showcase the latest technology and research through educational outreach to the general public and to students K-12. Ultimately, during the coming decade, we propose to extend our vision toward the implementation of a southeast regional research and technical center that is centered on a new advanced light source providing the power, resolution and advanced technology to further extend materials science, bioscience, micro-and nano-science through microscopy, the analysis of dilute materials, and the utilization of sophisticated

materials. To achieve this vision, this report proposes a plan to augment CAMD’s staff to properly support the advanced research activities. Such a facility will enable progress toward advanced microfabrication technology that includes hand held labs on chips and other devices that may be commercialized. In addition to perfecting advanced microfabrication techniques, CAMD will advance nanoimprint lithography (NIL) techniques to develop “top-down” TMO/strongly correlated systems which will become test beds to probe material property effects as a function of size and dimension. These new facilities will provide cutting edge R&D capabilities for LSU, the state of Louisiana, and the southwest region of the United States, well into the 21<sup>st</sup> century.

**A set of bullets that give the key milestones of the past few years.**

	2003	2004	2005	2006	2007
<b>State Budget</b>	\$4.4M	\$4.6M	\$4.7M	\$4.8M	\$4.8 M
✓ Staff	54	55	49	50	51
✓ Users					
LSU‡	24	119	68	165	190
Louisiana				63	31
Total	215	292	289	298	301
✓ Papers U/S*	47/58	22/86	51/58	TBD	TBD
✓ Staff Funding	\$2.7M	\$1.4M	\$1.1M	\$1.5M	\$1.2 M
✓ User Funding†	\$11M	\$21M	\$21M	\$24M	\$28M
✓ Graduates between 2004-2006:	27 Ph.D , 15 M.S., 12 U. G., 4 Post Doc’s, 2 H.S.				

\* U/S: U and S are user and CAMD staff publications respectively

† Estimated based on an average grant size and the number of faculty users.

‡ LSU users include those from CAMD staff and LSU.

**The table shows that state funding has been heavily leveraged by funding from the User Community as well as CAMD staff, and that CAMD has made a significant contribution to the economic viability of the state through the training and research facilities it provides for faculty and students alike. CAMD provides another intrinsic value by serving as the medium where faculty and staff from various centers and departments at LSU and elsewhere can collaborate creatively.**

## I. Introduction

### I.A. Description of CAMD

The Louisiana State University J. Bennett Johnston, Sr., Center for Advanced Microstructures and Devices (LSU-CAMD) is a synchrotron-radiation research center of the Office of Research and Economic Development, directed by Vice-Chancellor for Research and Economic Development, Brooks Keel. The electron-storage ring, which is the heart of CAMD, has been in operation to produce intense and bright synchrotron radiation since September, 1992. The facility is located at 6980 Jefferson Highway, Baton Rouge, approximately five miles from the LSU campus. A brief history of the facility is included in Section III.A of this report and is also available online at the beginning of the **CAMD 2003 Annual Report** <http://www.camd.lsu.edu/newsletters/CAMD2003AR.pdf>

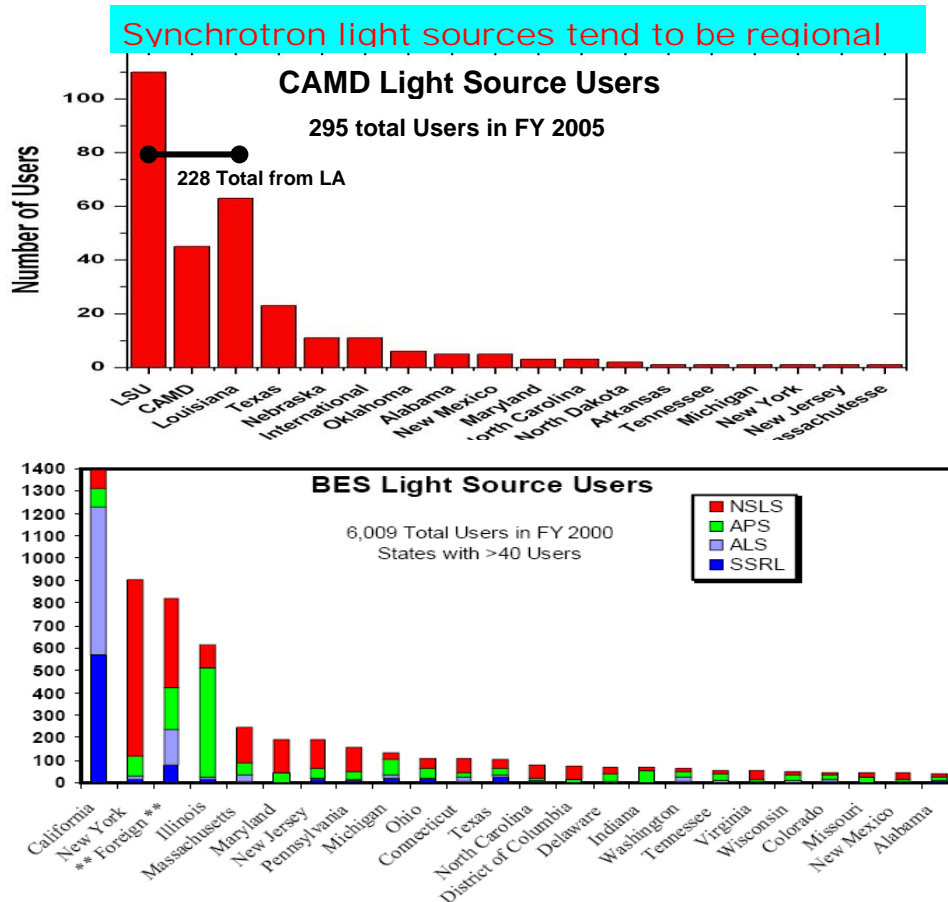
The synchrotron-radiation source, an electron storage ring operating at 1.3 GeV, with a 200-MeV-linear-accelerator injector, along with the CAMD Experiment Hall and Mechanical-Support Facility, were built with funding provided by a special Congressional appropriation of \$25M made in 1988. The principal operating budget of \$4.8M is provided by the State of Louisiana, as a part of the LSU budget.

The purpose of this report is to provide information to the LSU Administration documenting the achievements of CAMD and showing how CAMD supports scientists at LSU, the state of Louisiana and the United States, and especially how it will be able to play a role in the LSU Flagship Agenda.

CAMD has developed as a world class center for microfabrication and has scientific capabilities that include interdisciplinary collaborative work in LSU's Center for Biomolecular Multiscale Systems (CBMM), the Pennington Center, the AG Center, and the School of the Coast and Environment, as well as projects that include Louisiana Tech University. In addition, the research efforts of the 295 users of the facility, of whom 228 come from Louisiana and 165 from LSU and CAMD, add to the importance of CAMD's relevance to LSU's continued scientific development. In 2006, there were about 40 users who are faculty from LSU. These LSU faculty members send about 80 students to CAMD for research. About 35 faculty from other institutions in Louisiana and elsewhere send about 70 more students to CAMD. This visiting researchers attract approximately \$20,000,000/year in grant money to support their research. About 15 graduate students, who have been trained at CAMD, graduate each year with the Ph.D. or a master's degree.

Additionally, CAMD is the only synchrotron radiation source in the southern region of the United States. The regional nature of these sources is shown in figure 1. The upper panel illustrates how the number of users of CAMD clusters locally. This trend is also replicated elsewhere; a look at the lower panel in the same figure indicates that users of the Department of Energy Office of Basic Energy Science (BES) synchrotron sources are also clustered nearby the source. For example, the ALS and the SSRL sources are in California and most of their users come from California.

The importance of the CAMD synchrotron source as a regional source is borne out by the fact that CAMD supports a beam line for protein crystallography through the Gulf Coast Protein Crystallography Consortium (GCPCC). There are 25 user groups making use of this beamline and they have research support of approximately \$11,000,000 per year.



These users find the propinquity of CAMD particularly attractive because it is not expensive nor does it take a long time to travel to CAMD from their nearby locations. Delicate samples can be carried to and fro without fear of damage or loss by baggage handlers at an airport. In addition, beam time can often be scheduled on short notice, rather than waiting months to test an idea or a new procedure. Perhaps most important, students can work here and not worry about fitting their samples into the short time slots that are available at the light sources located at the National Labs. In fact, these features, propinquity and availability of beam time at short notice, were utilized by the 2006 Nobel Laureate in Chemistry, Professor Kornberg at Stanford, to carry out his research<sup>1</sup>.

CAMD has provided an important venue to carry out research even though it is several miles from the LSU Campus. One of our users, Professor Spivey, who studies catalysts, had this to say about his research experience at CAMD, "Among the LSU capabilities that have been essential to my ability to attract research funds in the area of catalysis/alternative fuels is the synchrotron line at CAMD. I wanted to make sure that I express to you that I believe it has been an essential, critical component of the grants we have rec'd in this area."

1] Roger Kornberg wins the Nobel Prize,

[http://www-ssrl.slac.stanford.edu/newsletters/headlines/headlines\\_10-06.html#Nobel](http://www-ssrl.slac.stanford.edu/newsletters/headlines/headlines_10-06.html#Nobel)

## I.B. Layout of the CAMD Electron Storage Ring , its Operating Parameters, and Associated Beam Lines:

Figure I.B.1 is a plan view of the CAMD electron storage ring and the associated x-ray, VUV, and lithographic beam lines. **Table I.B.1** contains the major operational parameters. The ring is injected by a 200 MeV (operated at 180 MeV) linear accelerator. Stored beam current accumulates over a period of a few minutes until a limit of up to about 200 mA is attained, at which point the beam energy is ramped to 1.3 GeV. Although the storage ring can be operated at energies up to 1.5 GeV, it is operated at this lower energy to achieve optimum reliability. Of the four straight sections, there are two straight sections available for insertion devices. One contains the x-ray wavelength shifter, and plans are being formulated for a second insertion device for the soft x-ray range. In addition to a flux increase of about 50, the energy range of this device will be especially suited for the study of magnetic materials because its energy range lies in the region of transition-metal L edges.

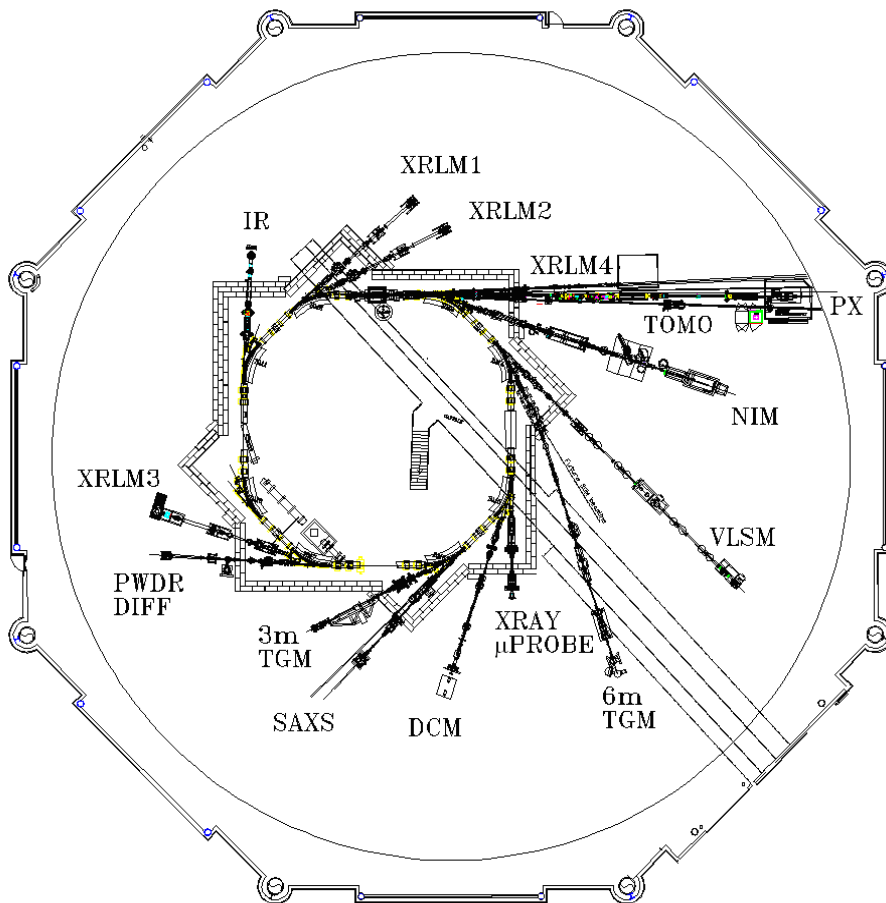
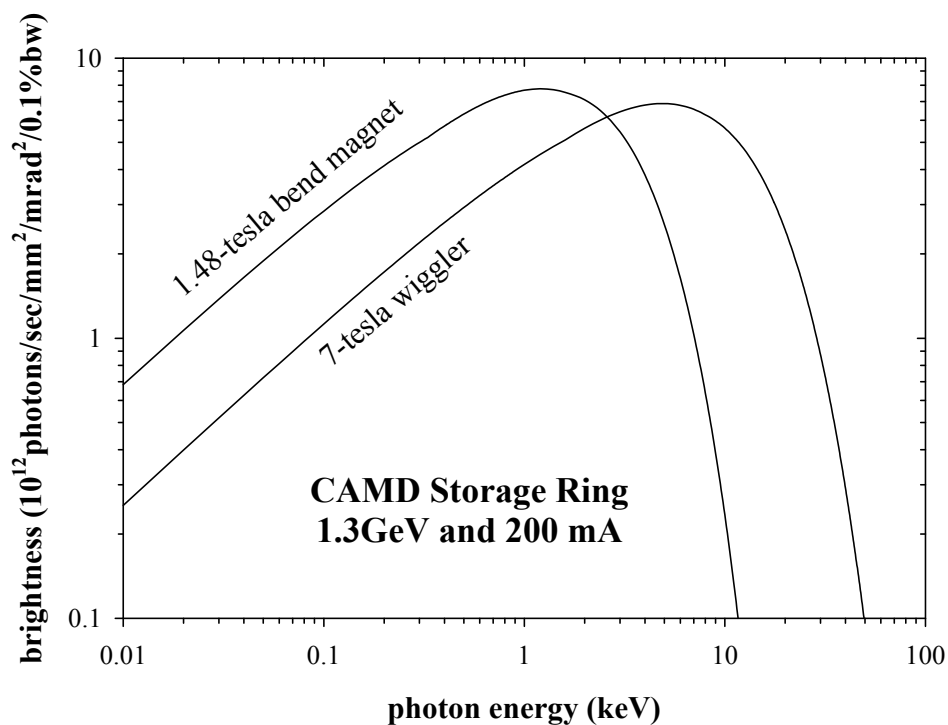


Figure I.B.1 (above) Plan view of the CAMD electron storage ring.



**Figure I.B.2 Brightness** of CAMD radiation produced in bending magnets and the wavelength shifter. Calculations based on machine parameters given in Table I.B.1 .

**Table I.B.1 CAMD Electron Storage-Ring Parameters**

Beam Energy (GeV)	1.3
Beam current (mA)	200
Bending radius (meters)	2.928
Critical wavelength, bend magnet (Å)	7.45
Critical energy, bend magnet (keV)	1.66
Critical energy, 7 Tesla wiggler (keV)	7.87
Beam lifetime at 200 mA (hours)	10
Harmonic number	92
Radiative (power) watts/mrad/mA	0.014
Injection energy (MeV)	180
Natural emittance (m-rad)	$3.5 \times 10^{-7}$

The accelerator serves 15 beamlines for scientific research and microfabrication purposes. Table I.C lists the beam lines, their function and operational parameters. The spectral range served by the accelerator extends from the i.r. to x-ray energies greater than 35 keV.



## I.C Table of CAMD Beamlines Available to Users; December, 2008

<b>FTIR Spectrometer &amp; Microscope</b> Port 1A, 50x50 mrad <sup>2</sup> acceptance	Installation completed; commissioning phase began 1/2004. <b>Biology, surface chemistry, environmental science, forensics</b>
<b>Micromachining I</b> Port 2A, 15 mrad	Variable-wavelength, variable high-pass (transmittance) and low-pass (reflectance) filters, Jenoptic DEX02 scanner. <b>Microfabrication</b>
<b>Micromachining II</b> Port 2B, 5 mrad	“White-light” beamline, $\epsilon_{\max} \approx 4$ keV, Jenoptic scanner. <b>Microfabrication</b>
<b>Micromachining IV</b> Port 3A, 10 mrad	Micromachining beamline mounted at the 7- tesla superconducting wavelength shifter. Ideal for deep resists. Jenoptik DEX03 scanner. <b>Microfabrication</b>
<b>High-Energy X-ray Spectroscopy</b> Port 3A, 2 mrad	The energy range 7 to 35 keV can be accessed at this beamline with a Bonn-designed, water-cooled double crystal monochromator. In the lower energy range Ge 422 crystals are used. The resolution is ca. 2 eV in this range. <b>Material-structure and environmental studies</b>
<b>Protein Crystallography</b> Port 3A, 2 mrad	Installed at 7-tesla wavelength shifter. Constructed with funding from NIH and NSF acquired by the Gulf Coast Protein Crystallography Consortium , <b>Protein Crystallography</b>
<b>X-ray-Microtomography</b> Port 3A, 3 mrad,	Covers spectral range from ca. 5 keV to 35 keV using double multilayer-mirror monochromator. Spatial resolution better than $5 \times 5 \mu^2$ . This beamline is also used by LSU Health Physicists for radiography test experiments.
<b>3-meter NIM</b> Port 3B, 70 mrad	High-resolution, high-flux beamline, , range 2 – 40 eV. Scienta electron analyzer with 10 meV resolution. <b>valence-electron excitation</b>
<b>VLSPGM</b> Port 4A, 7 mrad	Beamline recently modified from original PGM to current VLSPGM. Beamline is operational for simple absorption and photo-ionization spectroscopic investigations. Work is ongoing to enable circular-polarization-radiation experiments. Range, 200 – 1200 eV.
<b>6-meter TGM</b> Port 4B, 28 mrad	Range 15-300 eV with resolving power greater than 2000. High flux, moderate resolution. <b>Material and surface sciences</b>
<b>X-ray Microprobe</b> Port 5A, 2 mrad	Double-crystal monochromator and micro-focus/sample-alignment stage. Achieves spatial resolution of $50 \times 50 \mu\text{m}^2$ over range 2 - 15 keV. <b>Material-structure and environmental studies</b>
<b>EXAFS, DCM</b> Port 5B, 2 mrad	Range 1-15 keV with resolution from 0.5 eV (low energy) to 2 eV (high energy), currently configured for EXAFS. <b>Material-structure and environmental studies</b>
<b>SAXS/Graz.-Angle EXAFS</b> Port 6A, 2 mrad	Range 1-15 keV, DCM equipped, <b>Surface-structure studies:.</b>
<b>3-meter TGM</b> Port 6 B, 24 mrad	Range 15 - 350 eV with resolving power greater than 1000. <b>material and surface sciences</b>
<b>X-ray Powder Diffraction</b> Port 7A, 3 mrad	Double-crystal monochromator and 5-circle goniometer (currently, only 2 circles active).
<b>Micromachining III</b> Port 7B, 5 mrad	“White-light” beamline, scanner & mask/wafer chuck. <b>Microfabrication</b>

## I.D. Microfabrication Capabilities and Overview

When CAMD began operations in 1995, the establishment of x-ray based microfabrication technology was one of CAMD's key missions. The electronics industry was the initial market for this technology as x-ray based lithography was capable of achieving levels of miniaturization that were not believed possible using conventional UV-lithography. But, owing to various technological and business factors, and despite significant efforts by key players like IBM the semiconductor industry followed a path away from x-ray lithography in the 1990's. However, this period also saw the rapid rise of a nascent field called MEMS (Micro-Electro Mechanical Systems), a field that was bringing about a paradigm shift in the way we interacted with the microscopic world. Micron scale sensing and actuation methods and devices were being created that embodied concepts put forward by Dr. Richard Feynman in his famous 1959 lecture – "There's Plenty of Room at the Bottom". To fabricate these devices x-ray lithography is an extremely viable technology that is being used to produce results that are, even to date, impossible with any other competing method.

CAMD is one of the few research centers in the world uniquely positioned to implement x-ray lithography based microfabrication as part of the LIGA process – a MEMS process combining x-ray lithography, electroplating, and molding capable of fabricating precision microstructures in non-silicon materials like polymers, metals, and ceramics. Given the fact that CAMD is a synchrotron radiation facility process steps associated closely with x-ray lithography are the primary focus of our microfabrication technologies. Over the last years CAMD with substantial support from three DARPA's Hi-MEMS Alliance grants and the much appreciated state operating budget has invested in equipment, personnel, and process research and development and is today *one of the leading* x-ray based microfabrication centers in the world with active, joint research programs conducted primarily with partners in Germany (BESSY/AZM and ANKA/IMT) and recently Canada (CLS/TRLabs).

Over the years, by improving and expanding its microtechnology capabilities and establishing reliable baseline processes, the CAMD microfabrication group became also a key supporter for a diverse range of research projects at LSU and across the country. Besides effectively providing support to faculty and students, the microfabrication group at CAMD has also been prolific in its own rights as a research entity, producing numerous peer reviewed publications (about 40 in the past 5 years), conference presentations and patents. The microfabrication group has also collaborated on a number of proposals funded by state and federal agencies.

Besides in-house research efforts dedicated to continuously improve and expand its LIGA microfabrication expertise the group also provides user support ranging including access to its state-of-the-art equipment for expert LSU and external users, offering training and support in research projects for new users, partnering with collaborators in joint research and development projects, and providing paid services primarily for industrial customers for its unique LIGA capabilities.

## Section II:

# CAMD Science: Current and Future



## II. CAMD Science: Current and Near Future

### Introduction

In this section, vignettes of research conducted at CAMD by users and CAMD staff are presented. It will become clear to the reader that the facilities at CAMD are used for a very broad array of scientific endeavors ranging from uncovering the electronic properties of nanowires to understanding how carefully chosen proteins can inhibit the metabolism of bacteria and act as a magic bullet to possibly reduce the impact of infections such as the common cold.

Chemical processes that account for the function of catalysts, for example, are readily studied by LSU scientists. Other research efforts by CAMD users address the production of hydrogen for fuel cells. These studies make use of the broad spectral range of the radiation produced by CAMD to probe the electronic structure of the outermost (valence) electrons and the inner (core) electrons of atoms, to identify a specific signature of the core electron bonded to the atom.

LSU and CAMD scientists are using x-ray tomography to investigate a diverse range of subjects including the migration of oil and other compounds in oil-bearing formations and the structure of cat claws.

A project that showcases how CAMD's wide variety of research tools has been uniquely combined is the microfluidic study of the formation of cobalt nanoparticles. In this work, the capabilities at CAMD for the fabrication of nanoparticles, along with tools to manufacture microfluidic arrays, enabled researchers to use CAMD's x-ray microfocus beamline to realize that the nanoparticles form on millisecond time scales.

Research at CAMD resulted in over 100 papers in 2005 (See the CAMD Annual Report of 2005 at: <http://www.camd.lsu.edu/newsletters/Annual%20Report%202005rev.pdf>). Highlights of CAMD research can also be found in Appendix B of this report and at: <http://www.camd.lsu.edu/highlights.htm>.

The scientific justification for this modestly sized second-generation storage ring, supported in large part by the State of Louisiana, has evolved from being a catalyst for the industrial development of microstructures to a facility to catalyze synergistic collaborations between scientific and engineering disciplines within and outside of the LSU community. One of the purposes of this critical review document is to propose a course of growth that includes enhancing CAMD's infrastructure to make it more competitive (outlined in Section IV) by providing CAMD with cutting-edge equipment and an adequate number of support personnel (outlined in Section III.B.4.a.). Such enhancements will allow CAMD to sustain its scientific impact in the coming years and serve the nascent Materials Science Center of Excellence at LSU.

## II.A. Materials Science

Among the synchrotron light sources in the US, CAMD occupies an important niche with its capabilities in the vacuum ultra-violet (VUV) and the soft x-ray region. The VUV, especially, is a key photon energy region for materials science since it encompasses the photo-excitation energy range for the valence and core-electrons, spanning roughly 5-2000 eV. In this energy range, the fundamental physics and chemistry of photoexcitations can be studied, the properties of magnetic and correlated materials can be uncovered, and the electronic band structures of semi-infinite and reduced-dimensional materials can be mapped.

With the recent trends focusing on high-energy and high-brilliance synchrotron sources, as well as specialized beamlines designed for very specific measurements, the flexibility of most light sources for a range of materials science studies is becoming channeled. The next generation of synchrotron sources that are being proposed focus on deep core excitations which naturally lead toward an emphasis on the structural aspects of materials. Although there is plenty of good science to be done with this focus, the lower energy vacuum ultraviolet is particularly suited to electronic structure measurements which are the goal of many materials science efforts. At CAMD, we currently have four VUV beamlines (See Section III.B.2.a for a description) for basic materials science studies and they are all scheduled to the maximum of their availability, and there is significant unmet demand for more time. The flexibility and complementary energy ranges of these beamlines provide LSU with a unique advantage scientifically in the characterization of materials. With the mode of beam allocation currently applied, users have the ability and beam-time allocation to conduct time-consuming experiments involving thin-films and reduced-dimensional materials that is not available at other regional light sources. The x-ray spectral region is serviced by an additional suite of five beamlines. These facilities are further described in Section III.B.2.b.

The following vignettes are descriptions of scientific programs currently underway utilizing the VUV, IR and x-ray capabilities at CAMD, and provide arguments for additional resources to enhance these facilities. Specifically, the enhanced intensities (not necessarily brightness) available through a multipole wiggler insertion device described in Section IV.B. and IV.C. will provide for more rapid measurements and permit the characterization of new, reduced dimensional materials that will be important in the fields of correlated materials, combustion research, and advanced nanomaterials for solar hydrogen generation and energy production.

Although Materials Science could be interpreted to span nearly all of the research conducted at CAMD, this section will focus on 3 areas: **Nanomaterials**, Soft materials or **Polymers**, and **Correlated / Magnetic** materials.

### **Nanomaterials**

Nanomaterials research conducted at CAMD can be divided into two categories associated with the environment that they are synthesized in, either vacuum based using typically physical growth techniques or wet-chemical synthesized materials.

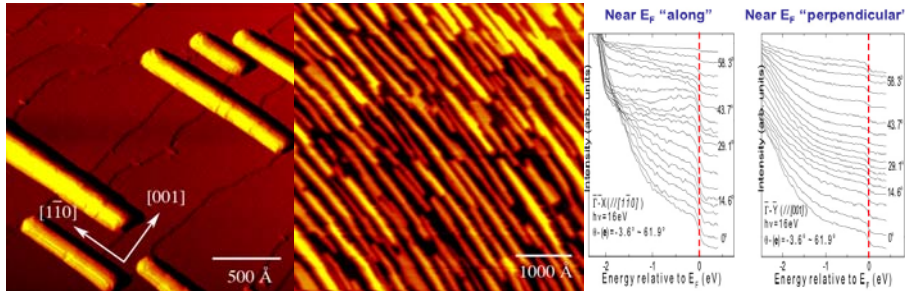


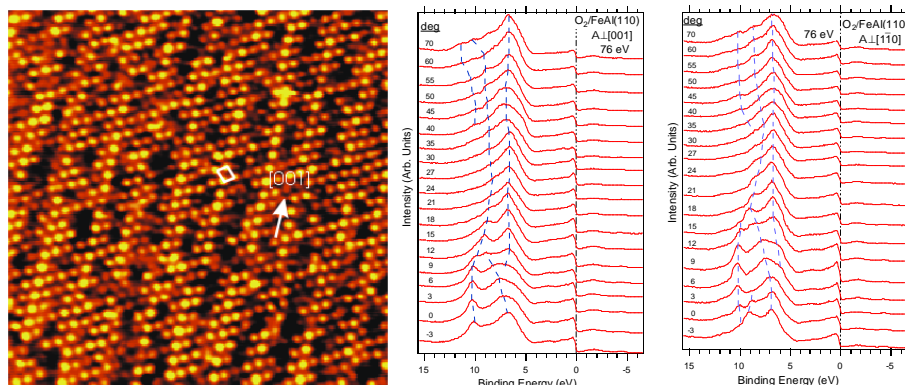
**Figure IIA.1.** Nanowires formed from 3 ML Ag/Cu(110), left panel, and ~20 ML Ag/Cu(110), middle. The wires grow perpendicular to the [001] axis. The right panel shows photoemission spectra near the Fermi level that show a band dispersing through at about 40° for directions along the wire but no such bands perpendicular.

The surface science group at LSU, led by Professors Kurtz and Sprunger, are interested in the fundamentally new properties exhibited by materials when their dimensions are reduced to the nanoscale. For example the Ag nanowires shown in Fig. IIA.1 exhibit unusual quasi-1D behavior.

Silver nanowires have been found to spontaneously grow on Cu(110) or on Ni(110), due to the  $C_{2v}$  symmetry and strain-mediated self-assembly. Figure IIA.1 shows STM images of the nanowires that grow on Cu(110) at 3 and 20 ML. Using angle-resolved photoemission at the NIM and at the 6-m beamlines they have found the nanowires to be insulating across the nanowire, since none of the electronic states disperse with angle and this is an atomic-like property. Along the nanowire, however bands are seen to cross the Fermi level indicating that they exhibit a 1-dimensional Fermi surface in the long direction. Because of this unusual conductivity, these nanowires should also exhibit new plasmon excitations and optical properties that are highly dependent on orientation. Additional work, including high-resolution electron energy loss spectroscopy (HREELS) is being done to further map out this unusual behavior. This research program is currently funded by NSF through the Division of Materials Research.

Another activity related to this NSF award is to successfully grow these reduced dimensional metals on ultra-thin oxides, where a large bandgap can minimize the hybridization/overlap with the underlying substrate band structure. Ultra-thin oxides serve as excellent templates because they provide a unique “insulating” substrate. Due to the nano-thickness of the oxide, electron spectroscopies (ARPES, STM, EELS) can be used without the problems associated with charging

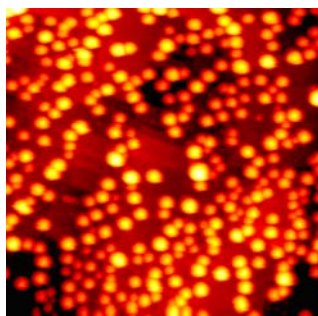
The electronic structure of ultra-thin aluminum oxide, grown on FeAl(110) has been investigated with angle-resolved photoemission spectroscopy. As shown, our scanning tunneling microscopy studies have revealed that exposing the clean FeAl(110) surface to 1000 L of oxygen at 850° C,



STM image (70x70 nm<sup>2</sup>) of oxidized FeAl(110) surface. The surface exposed to 1000 L of O<sub>2</sub> at 850 °C. The EDCs of Al<sub>2</sub>O<sub>3</sub> /FeAl(110) collected along high-symmetry directions of the substrate surface Brillouin zone. Dispersion of the oxide-induced states in both directions indicate a two dimensional electronic structure.

forms a homogeneous hexagonal oxide film with a thickness of approximately 10 Å. Core levels photoemission spectra of FeAl constituents indicate that Al is the only metal species present in the oxide film. As shown below, the measured band dispersion of oxide thin film indicates a 2-D electronic structure parallel to a plane of thin film due to the limited thickness of the oxide thin films.

The appearance of a peak in the anticipated band gap of bulk oxide film suggests the unique electronic structure of the 2-D oxide film. This latter observation is correlated with previous scanning tunneling microscopy results to elucidate the structure of the ultra-thin alumina film grown on FeAl(110). The results of this research will appear in the forthcoming issue of Applied Physics Journal (2007).



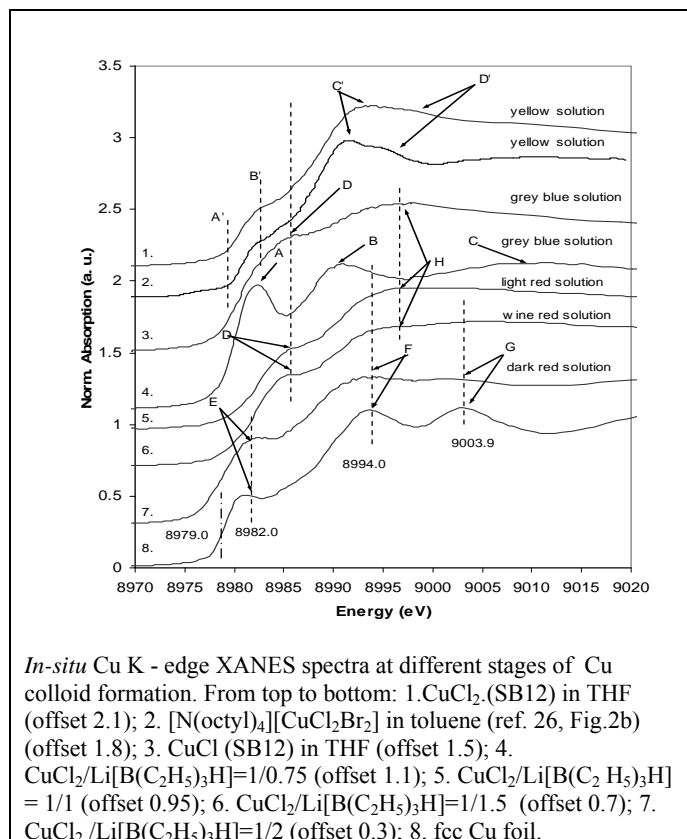
Ag nanoclusters on TiO<sub>2</sub>(110) imaged by STM (100nm<sup>2</sup>). Ag nanoclusters are ~5nm in diameter. F. Wang, P. Sprunger and R. Kurtz.

Another project in the LSU Surface Science Group involves nanoclusters supported on titania for solar hydrogen generation. TiO<sub>2</sub> (rutile) is a valuable catalyst for numerous reactions including environmentally-friendly acts of decomposing unwanted organics as well as being a promising source for photolysis – the generation of hydrogen from water using sunlight. This project seeks to enable these applications by enhancing the absorption of radiation in the near surface region through the judicious incorporation of nanometallic “antennas.” The figure shows 5 nm Ag clusters grown on TiO<sub>2</sub>(110).

Metallic nanoclusters on TiO<sub>2</sub> are well known to have unusual catalytic activities but they are also optically active and their inherent plasmon modes provide a potent means of absorbing radiation. Although the size distribution of the clusters *on* rutile can control the absorption energy somewhat, placing them *in* a dielectric matrix causes a broadening and a red-shift allowing their photoresponse to be tailored to the solar spectrum. A natural dielectric to consider is to encapsulate these metal clusters supported *on* TiO<sub>2</sub> with an overlayer *of* TiO<sub>2</sub>. Our ongoing measurements on the 6-m beamline at CAMD seek to characterize the electronic structure and specifically the nature of the electronic defects introduced into the TiO<sub>2</sub> due to the presence of the nanocluster. It is at these defects that the photolysis is thought to occur. This research is supported by NSF through the Division of Chemistry.

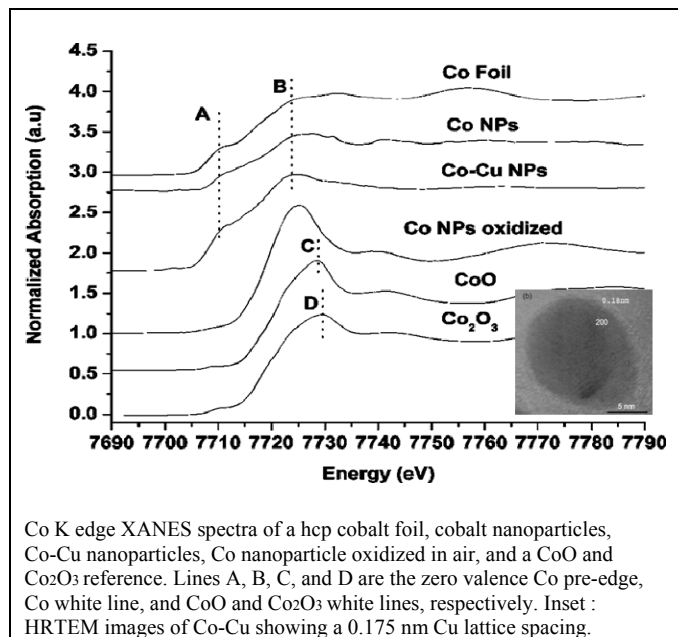
CAMD has initiated an in-house nanoresearch program in 2001, taking advantage of the well established infrastructure for X-ray absorption spectroscopy. The core competency of the ‘nano’ research group is to develop ‘bottom-up’ approaches using wet-chemical methods. The ability to design and conduct experiments to probe the mechanisms of nanomaterial formation in situ using synchrotron radiation based X-ray absorption spectroscopy provides a unique platform for CAMD and its users to control properties of nanomaterials. The wet chemical laboratory has necessary facilities and equipment to synthesize metallic mono, bi and core-shell metallic/polymer nanoparticles using techniques such as reverse micelle, sonochemical and surfactant mediated classical reduction. In addition to traditional ‘flask’ techniques, a unique polymeric micro reactor based nanomaterial synthetic technique is also developed. EXAFS (X-ray Absorption Fine Structure) and XANES (X-ray Absorption Near Edge Structure) are unique





more information J.Phys.Chem.B 109(19); 9330-9338, 2005.

In collaboration with E.J. Podlaha of LSU Chemical Engineering, Kumar and co-workers



involved in development of techniques to bind a variety of biomolecules such as proteins and peptides. A 23 amino acid synthetic lytic peptide (Hecate) was covalently linked to magnetite

tools and are being used to determine structures of metallic nanosystems, where the absence of long range order makes standard techniques such as X-Ray Diffraction less reliable.

The Nanofabrication group has recently investigated the mechanistic aspects of the formation of sulfobetaine-stabilized copper nanoparticles using *in situ* XANES supported by UV-vis spectroscopy and reaction calorimetry. The stability of the Cu(I) complex was found to be sensitive to the concentration of the sulfobetaine stabilizer and the addition rate of the reducing agent. A tetra-coordinated Cu(I) complex as an intermediate has also been postulated. Based on the understanding from these investigations, a micro fluidic process for copper nanoparticle synthesis was designed using sulfobetaine-Cu(I) complex as the starting material. See for

developed a novel route for core-shell structured nanoparticles. For example, copper shells around cobalt nanoparticles were fabricated by a displacement method around Co nanoparticles at room temperature in a copper-citrate aqueous electrolyte. Synchrotron radiation-based X-ray absorption near-edge structure analysis confirmed that cobalt oxide was not present in the nanoparticles upon exposure to air, consistent with a shell formation. See *Journal of The Electrochemical Society*, 152 (1) D1-D5, 2005 for more information.

Biofunctionalization of Nanomaterials is key to their application in life sciences. CAMD's nanofabrication group has been

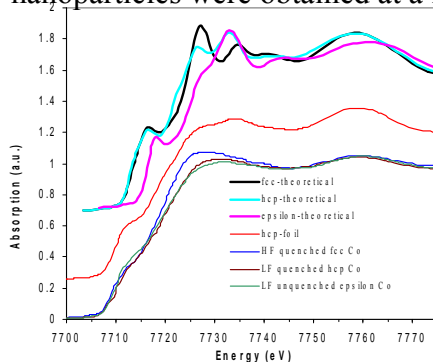


nanoparticles and the lytic peptide bound nanoparticles were characterized using X-Ray Absorption Near Edge Structure Spectroscopy (XANES), Transmission Electron Microscopy, and Electron Diffraction. Investigation of the magnetic properties using SQUID magnetometer has shown reduction in saturation magnetization ( $M_s$ ) of magnetite nanoparticles after binding with lytic peptide. *In vitro* cell culture assay using breast cancer cell lines MDA-MB-435S revealed that the lytic peptide bound magnetite nanoparticles were therapeutically active.

Similarly luteinizing hormone and releasing hormone (LHRH) bound iron oxide nanoparticles are routinely prepared as they are being investigated as novel MRI contrast agents.

In collaboration with Microfabrication group, CAMD's nanofabrication group has developed a unique polymeric micro reactor system for synthesis of nanomaterials. The main advantage of such a polymeric micro reactor system is that it is an inexpensive tool for not only nanomaterial production but also in general for production and process development of chemicals and pharmaceuticals. Possibilities for commercialization these new technologies are currently being explored.

Kumar and co-workers have recently synthesized Co nanoparticles with three different crystal structures sized using the polymeric microfluidic reactor through manipulation of reaction times, flow rates and quenching procedures. Cobalt nanoparticles of fcc ( $\beta$ ) phase were obtained from a high flow rate of the reactants followed by *in-situ* quenching of the reaction. Hcp and  $\epsilon$ -cobalt nanoparticles were obtained at a low flow rate of the reactants followed by *in-situ* quenching and



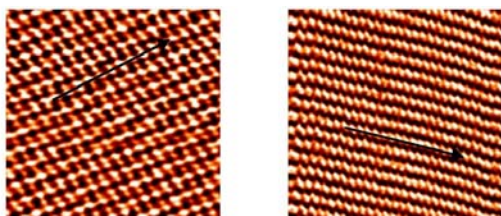
Co K-XANES spectra: a. (—) fcc Co nanoparticles synthesized at high flow rate and quenched immediately; b. (—) hcp Co nanoparticles synthesized at low flow rate and quenched immediately; c. (—) Co nanoparticles synthesized at low flow rate with delayed quenching; d. (—) hcp Co foil; e. (—) Theoretical hcp Co; f. (—) Theoretical fcc Co and g. (—) Theoretical  $\epsilon$  Co.

delayed quenching, respectively. The crystal structures were characterized using Co K-edge X-ray Absorption Near Edge Structure (XANES) spectroscopy, X-ray Diffraction (XRD) and Selected Area Electron Diffraction (SAED). For more information see the recent publication *Chemistry of Materials*, 18 (12), 2817 -2827, 2006.

In addition to the development of wet-chemical methods for synthesis of Nanomaterials and as well as their biofunctionalization, the Nanofabrication group is continuing its efforts to investigate the influence of organometallic precursors and surface active agents on the formation of cobalt nanoparticles. Investigations from CAMD's nanogroup reveal a new role for surfactants; influencing the reaction pathways, prior to nucleation, leading to formation of nanoparticles.

## Polymers and Soft Materials

The Nebraska MRSEC has been an active participant in research at CAMD through the leadership of Professor Peter Dowben. Recently their research has involved organic molecules and organometallic complexes. As an example of their research, they have been working to unravel the electronic structure of two related polymers with strong dipole ordering. Two different polymers, with large local electric dipoles, have been compared: copolymers of polyvinylidene fluoride with trifluoroethylene P(VDF-TrFE, 70%:30%) and polymethylvinylidenecyanide (PMVC).

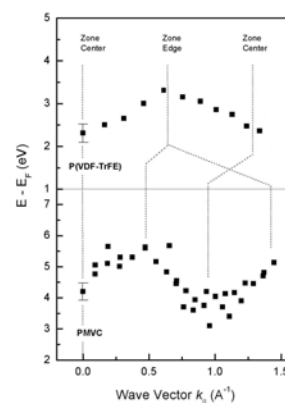


The surface structure of crystalline (left) P(VDF-TrFE) and (right) PMVC Langmuir-Blodgett films as ascertained from scanning tunneling microscopy. Arrows indicate chain direction.

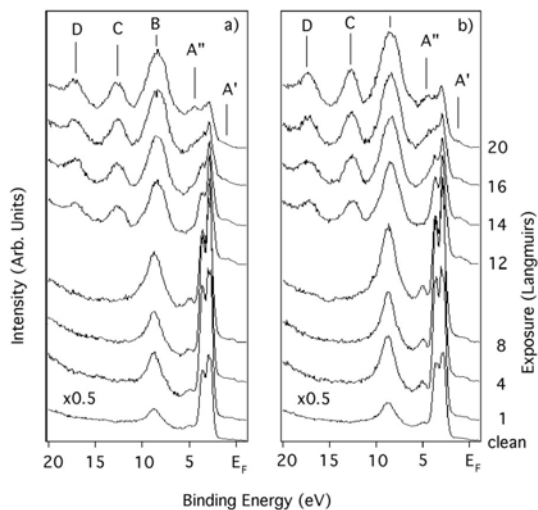
Poly(vinylidene fluoride) [PVDF,  $-(\text{CH}_2\text{-CF}_2)_n$ ] copolymers with trifluoroethylene [TrFE,  $-(\text{CHF-CF}_2)-$ ] can form highly ordered crystalline ferroelectric polymer ultrathin films as has been demonstrated by x-ray and neutron scattering, scanning tunneling microscopy, low energy electron diffraction and band mapping. Although not always evident in scanning tunneling microscopy, the band structure shows a characteristic super-periodicity dominated by  $-(\text{CH}_2\text{-CF}_2)_2$ - or  $-(\text{CH}_2\text{-CF}_2)-(\text{CHF-CF}_2)-$  “dimer” pairs in the ferroelectric phase. The copolymer P(VDF-TrFE, 70:30), in spite of the low overall symmetry does show all the characteristics of

high local symmetry and symmetry selection rules. The effects are quite significant in photoemission and electron energy loss spectroscopy. By comparing the copolymer P(VDF-TrFE, 70:30) to the highly dipole-ordered polymer polymethylvinylidenecyanide (PMVC), we can see the influence of local point group symmetry on the intra-molecular band structure. The results summarized here show that PMVC ( $-(\text{CH}(\text{CH}_3)\text{-C}(\text{CN})_2)_n$ ) has a much lower local point group symmetry than poly(vinylidene fluoride), although not a copolymer system. While the different local point group symmetries play a key role, both crystalline polymers exhibit intra-molecular band structure, though the Brillouin zone critical points differ.

Other work from the Nebraska group includes studies of the stability and structure of organometallic and metal organic complexes. The stability and structure of adsorbed molecular spin 1/2 organometallic and metal organic complexes are seen to be either less stable, or adopt a lower point group symmetry. When comparing initial cobaltocene adsorption on Cu(111) with other adsorbed metallocenes, it seems fairly clear that cobaltocene is far less stable as a molecule on surfaces than ferrocene (Z-1) or nickelocene (Z+1). Unlike the other metallocenes, initial adsorption is dissociative (see the Figure). Overall the big difference among these three metallocenes appears to be that the “nineteen electron” cobaltocene has a single unpaired electron



The band dispersion, from angle-resolved inverse photoemission, of the unoccupied feature closest to the Fermi level, along the polymer chains. The dashed lines indicate the different positions of the Brillouin zone

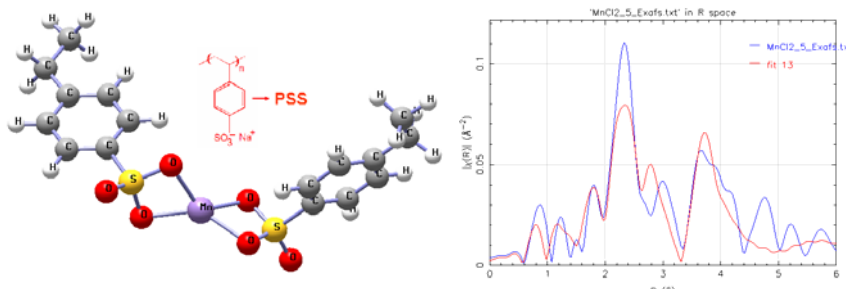


Coverage dependent angle-resolved photoemission spectra of cobaltocene on Cu(111) at 150 K. The photon energy of 36 eV and the photoelectrons are collected along the surface normal. The photoemission spectra were taken with s+p-polarized light (a) and more p-polarized light (b). The cobaltocene exposures are provided in units of Langmuirs ( $1\text{L} = 1.0 \times 10^{-6}\text{Torr}\cdot\text{sec}$ ).

in this case, EXAFS was applied to examine the salient features of conventional polyion assemblies.

The DFT calculations show the final geometry of a system consisting of 2 PSS monomer attached to a  $\text{Mn}^{2+}$  atom (figure below). Using the coordinates of the atoms from the DFT calculations the feff input file has been created. From the feff input file the scattering paths are calculated.

Using the first 10 scattering paths the data was fitted to the  $\text{MnCl}_2$  EXAFS data. Further analysis is required for a good fit of the data to find the coordination number and nearest neighbour distance of the central atom. One of the methods that can be adapted in our further studies is to get the normalized  $\chi\mu(E)$  Vs  $E(\text{eV})$  data from the DFT feff input files and compare it with the XANES(X-ray Absorption Near Edge Structure) data of  $\text{MnCl}_2$  Layer-by-layer nanofilms. Once a good fit is achieved that model could be used for the various cation species ( $\text{Fe}^{3+}$ ,  $\text{Mn}^{2+}$  and  $\text{Ti}^{3+}$ ) that will be added in our further studies on the Layer-by-layer nanofilms. This work is supported by NSF and the DOE.



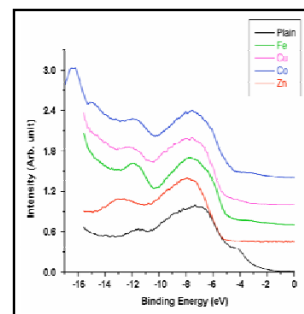
Geometry of the polyion studied as deduced from DFT calculations (left) and the R-space data fit to  $\text{MnCl}_2$  data.

resulting in a low ionization potential and facile decomposition. With absorption other than end-on, nickelocene MUST adopt a singlet state as the off normal adsorption orientation has reduced the molecular symmetry to such an extent that a triplet state is simply not possible.

Similarly, while both Co(II) ( $s=1/2$ ) and Ni(II) ( $s=0$ ) tetramethyldibenzo-tetraazaannulene molecular electronic structures are very similar, when the molecules are adsorbed on Au(111), the Ni(II) adopts a high symmetry molecular configuration upon adsorption, with a strong preferential orientation.

A group from Louisiana Tech in Ruston, LA led by Professor Tabbetha Dobbins is involved in studying the role of cation additions to polyelectrolyte solutions. These polyelectrolyte solutions are important in microelectronics and microfluidic systems for sensor applications. In

An additional study involving the Surface Science Group at LSU involves a collaboration with several faculty in the Chemistry Department including Professors Jayne Garno and Graca Vincente, and relates to the electronic structure of porphyrin films involving several different metal complexes. Porphyrins have practical applications in molecular electronic devices as light harvesting complexes, sensors, and photonic devices. The structural motif of the macrocycle, its peripheral groups and the addition of chelated metal ions result in the differences in their electrical, photophysical, magnetic and photo-electrical properties. The porphyrin backbone can be synthesized to contain a wide range of substituents, for example to enable directing the orientation in a side-on assembly or co-planar configuration. The organization of porphyrin molecule on surfaces as well as the attached substituents and/or coordinated metals dictate the resulting function, properties and efficiency in molecular devices.



The PES data of metallated (Fe(III), Co, Zn, Cu) and free-base porphyrin systems, acquired with a photon energy of 24 eV,

This study involved vuv measurements of the valence band electronic structures of several porphyrins complexed with Fe, Co, Zn, and Cu. The information regarding valence/band structure differences, particularly about the LDOS near  $E_F$ , provides insight for maximizing transport and photonic properties. The photoemission data of the prepared porphyrins on Si substrates is shown in the figure. From the present data, there appears to be subtle differences in the HOMO-LUMO gap as well as the nature of the density of states near  $E_F$ . To understand these differences, calculations are on-going. Moreover, AFM results indicate that there may be inhomogeneities in the porphyrin films.

The Associate Provost of Tulane, Brian S. Mitchell, is leading an investigation into the effect of near net shape manufacturing (NNSM) on polymer blending. Global Fourier-transform infrared spectroscopy (FT-IR) is often used to probe chemical changes in samples. The chemical structure (bonding arrangement, elements, etc) of the polymer determines which transitions can occur at specific wavenumbers for that polymer. Synchrotron IR, however, offers a unique set of advantages over global (thermal) IR. The brightness (photon flux emitted from unit source area and unit solid angle) is 100-1000 times greater than that of global sources – a phenomenon that allows for microspectroscopic (i.e., vibration-mode-selected mapping) investigations of both small and large size samples with heterogeneous regions. The focused beam produced by synchrotron radiation is thus much smaller in size and more intense than the global source and also provides a better signal-to-noise ratio.

The figure shows spectra taken at arbitrary points within area grids constructed over optical microscope images of PET/PS and PET/PMMA blends. In a row-by-row fashion, a spectrum is taken at each point in the grid. A characteristic peak is chosen for one of the polymers (typically the dispersed or minor phase), and the intensity of this peak is correlated to a color code such that maximum peak intensity is blue and nil is white.

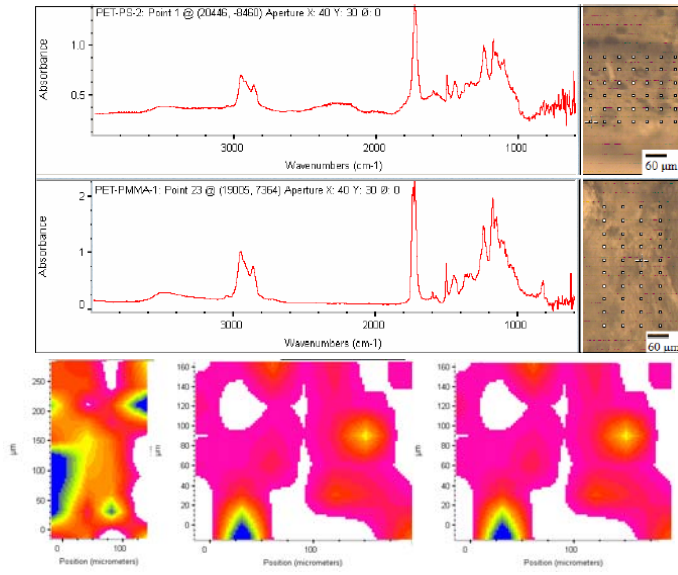


**Figure:** Optical micrographs of blends of PET/PS (top) and PET/PMMA (bottom) with arbitrary area grids superimposed on the images. The FT-IR spectra for the blends' respective crosshaired points are shown at left. The color coded lower panel shows PET/PMMA (left) and PET/PS (middle and right) compositional area maps.

elemental (Ti/Ta, Fe/Ta, Cr/Ta) distribution information obtained via XRF. Stimulated by these results, we have prepared an experimental strategy that employs grazing incidence XRF measurements to further correlate the structure of these systems with their optical loss characteristics.

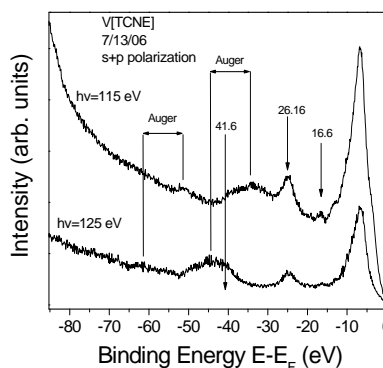
In the XRF experiments conducted thus far, clear signals are observable for the primary elements of interest, Ti and Ta. We have obtained data with excellent energy resolution and counting statistics at both of these edges. Relatively minor amounts Fe and Cr appear in a constant ratio for all samples which suggests that these elements are in the bulk, not in the coating. Our preliminary experiments indicate that grazing incidence beam measurements are required for XANES and EXAFS studies so as to minimize signals from the substrate. Complementary microbeam experiments are planned to determine spatial (x-y) uniformity of the element distributions. This work is supported by an NSF Physics grant.

E. Doomes and S. McGuire from Southern University use X-ray absorption spectroscopy to obtain detailed chemical composition and structure of titania ( $\text{TiO}_2$ )-doped tantala ( $\text{Ta}_2\text{O}_5$ ) multilayers fabricated via ion beam sputtering on  $\text{SiO}_2$  substrates. These dielectric multilayers play a major role as mirror coatings in high power laser applications such as laser interferometric gravity-wave detectors (LIGO) where noise in the mirrors must be kept to a minimum.

In the current study several samples having varying multilayer composition have been investigated. The measurements were performed at the CAMD Double Crystal Monochromator (DCM) beamline. Fluorescent X-rays were detected with a 13-element liquid nitrogen cooled Ge detector array. We obtained chemical and structural data obtained at the titanium K-edge and tantalum  $L_{III}$ -edge as well as relative

## Correlated and Magnetic Materials

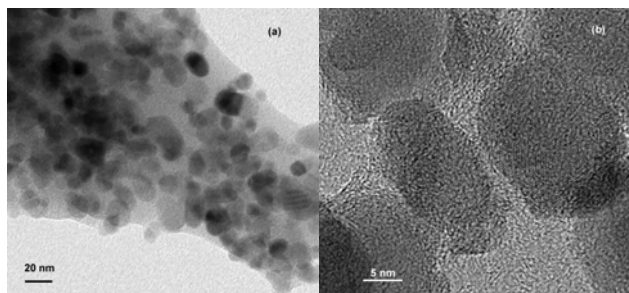
Tony Caruso, from North Dakota State University in Fargo is also interested in metal-organic materials that may exhibit magnetic and spintronic properties. Recent reports of room temperature remnant moments in thin film metal-organic materials (albeit few) are now reproducible. In order to progress in the development and utilization of organic and metal-organic materials in magnetic and spintronic devices, basic studies (i.e. spin polarized photoemission) must be completed to help reveal: (1) the mechanism(s) responsible for exchange; (2) where in binding energy the exchange occurs; and, (3) the raw polarization at the Fermi level.



Shallow core photoemission of V[TCNE] on evaporated Au completed with normally collected photoelectrons and incident s+p polarization.

It is for these reasons, they have completed an initial spin-integrated valence structure study of vanadium tetracyanoethylene or V[TCNE]. Due to the antiferromagnetic exchange between the carbon polarons and V(II), a distinct splitting should exist that is resolvable by photoemission. The figure shows shallow core photoemission demonstrating the oxygen free transfer of the thin films (no peak at -41.6 eV and no oxide shoulder on the V 3p) along with other photoemission lines which we have yet to account for. The V 3p binding energy position is roughly 2 eV higher in binding energy than expected for atomic V 3p indicating a very strong bond (increased binding energy) with the coordinating TCNE which helps further corroborate the superexchange mechanism. This work is supported by the Defense Microelectronics Activity, DMEA, and the NSF.

In continuing the theme of magnetic materials, Professor Jinke Tang (UNO) has been looking at the origin of enhanced spin polarization in magnetic oxides. Polystyrene coated Fe<sub>3</sub>O<sub>4</sub> nanoparticles exhibit intergranular tunneling magnetoresistance (MR) ratio of 22.8% at room temperature and a maximum MR of 40.9% at 110 K. The drastic enhancement of the MR ratio clearly suggests that there is high degree of spin polarization even at room temperature for half metallic Fe<sub>3</sub>O<sub>4</sub>. The derived spin polarization  $P$  is about 54% and 83% at room temperature and 110 K, respectively. Their work suggests further



TEM image for the Polystyrene coated Fe<sub>3</sub>O<sub>4</sub> sample indicating that Fe<sub>3</sub>O<sub>4</sub> nanoparticles are embedded in polymer matrix(left). High resolution TEM image showing that the Fe<sub>3</sub>O<sub>4</sub> particles are separated by a thin polymer layer of a few nanometers, forming tunnel barrier for electron transport (right).

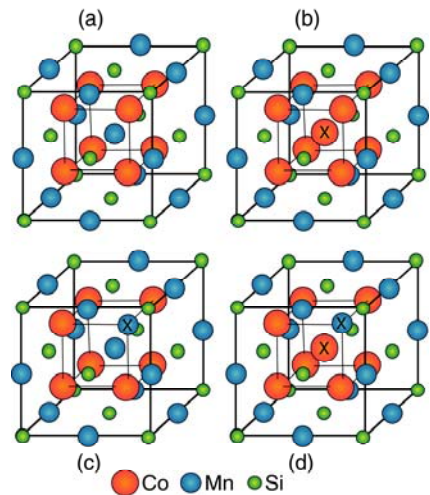
increase in the spin polarization can be achieved by preventing the oxidation of the surface of  $\text{Fe}_3\text{O}_4$  by a protective coating.

Tang's group have also investigated the magnetic properties of  $\text{HfO}_2$  films. Pure  $\text{HfO}_2$  and Gd-doped  $\text{HfO}_2$  thin films have been grown on different single crystal substrates (silicon,  $\text{R-Al}_2\text{O}_3$  and  $\text{LaAlO}_3$ ) by pulsed laser deposition. Very weak ferromagnetism is observed in pure and Gd-doped  $\text{HfO}_2$  films on different substrates at 300 K and 5 K, which is attributed to either impure target materials or signals from the substrates. The magnetic property does not change significantly with post deposition annealing for the  $\text{HfO}_2$  films. Their investigation casts doubt on the previously reported ferromagnetism in this material.

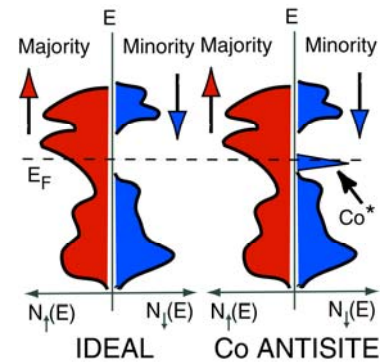
A final example of the materials science work conducted at CAMD is that of Professor Shane Stadler, University of Southern Illinois and potentially an LSU faculty member. His work involves magnetic materials that exhibit either half-metallic or magnetocaloric effects.

In the half-metallic Heusler alloys, as well as in other ordered magnetic materials, even slight deviations from the ideal structure, composition, and/or order can result in sub-optimal magnetic properties. A form of disorder occurs in  $\text{Co}_2\text{MnSi}$  and  $\text{Co}_2\text{MnGe}$  in which atoms in X sites occupy Mn sites and vice versa. This is called antisite disorder, and results in a reduced magnetic moment per formula unit since the spin on the antisite atom is usually antialigned with the other local spins. Antisite occupation alters the band structures of these materials, causing states to appear in the band gap of the minority carriers, and destroys the half-metallic character of the system.

Stadler's group have recently observed a reversible, giant magnetocaloric effect (MCE) in the Heusler alloy  $\text{Ni}_2\text{Mn}_{1-x}\text{Cu}_x\text{Ga}$  (Stadler *et al.*, *Applied Physics Letters* **88**, 192511 (2006)). The measured entropy change for this system is about  $-64 \text{ J K}^{-1}\text{kg}^{-1}$  (in an applied field of 5 T) at room temperature, i.e., more than double the largest value reported to date. This material also has a significant MCE effect ( $\sim 30 \text{ J K}^{-1}\text{kg}^{-1}$ ) in fields at or below 2 T, making it a strong candidate for employment in magnetocaloric refrigeration devices based on *permanent* magnets rather than on high-maintenance superconducting magnets. The parent alloy  $\text{Ni}_2\text{MnGa}$  undergoes two transitions: A second order paramagnetic/ferromagnetic transition at 376 K ( $T_c$ ), and a first order martensitic (structural) transition at 202 K ( $T_m$ ). Varying the stoichiometry by substitution has the effect of changing the transition temperatures  $T_m$  and  $T_c$ , and, in the case where Mn is substituted with Cu ( $x = 0.25$ ), the two transitions coincide. It is at this "compound transition" that



Various defects in the  $\text{Co}_2\text{MnSi}$  lattice: (a) no defects; (b) Co antisite; (c) Mn antisite; and (d) Co-Mn swap. Atoms marked with X are not in their ideal locations.



The effect of Co antisites ( $\text{Co}^*$ ) on the spin-projected densities of states of  $\text{Co}_2\text{MnSi}$ .



## **II.B. Chemical Science**

There are two dominant areas of research at CAMD that involve chemical sciences. First, there are studies that use the lower energy radiation, the vacuum ultraviolet (VUV) range, as a means of ejecting valence electrons from species of chemical interest. Secondly, there are many ongoing investigations that employ the x-rays from CAMD for the purpose of generating structural information as well as data on chemical speciation, both of which are relevant to a variety of research topics in the chemical sciences. In the simplest terms, the VUV studies provide information on the valence electrons that comprise the “glue” that binds atoms to form molecules, ions, clusters, radicals, and related species of interest to chemists, biochemists, and chemical engineers. In a similarly broad sense, x-rays provide data on structure, which is equally important for chemists and chemical engineers. Finally, it is important to note that CAMD can be fully competitive in the international arena in performing state-of-the-art research in chemistry and related disciplines, e.g., biochemistry, chemical engineering, nanochemistry, and chemical engineering, for example. The experiments described here do not require a small spot or high resolution, i.e., features that are available at third generation sources. The experiments require high flux and dependable operation, so CAMD can be and is competitive. The VUV research at CAMD has focused on molecular photoionization dynamics. VUV studies can have additional impact, and will given the activities planned for the near future. In particular, it has been demonstrated that important chemical information can be determined via generating ionization potential data for exotic species, e.g., reactive intermediates, cluster species, etc. Such studies are planned for CAMD, and there is the faculty and staff expertise at LSU and other nearby institutions that make such advances possible. Similarly, x-ray experiments provide structural and chemical speciation data in a routine fashion. Researchers who employ CAMD for such studies have done much in this area, particularly with regard to heterogeneous processes, and most particularly, with respect to research on catalyst structure and function.

There are two points requiring additional emphasis. Only a few examples are given in this section in the interest of brevity. They are meant solely to provide a case for representative accomplishments already achieved at CAMD, and also to provide a possible roadmap for near-term future directions. Secondly, chemistry is indeed the central science, so not all of the relevant chemistry examples are given in this section. There are important examples of chemistry research that is performed under the rubric of materials science, environmental science, nanoscience, and microfabrication. So there are many other examples of state-of-the-art chemistry research that appear in other parts of this document.

### **II.B.1.a Opportunities in Atomic, Molecular, Optical (AMO) Physics and Chemical Physics at CAMD: VUV Photoionization Research**

Many research programs in AMO and chemical physics focus on molecular photoionization, so it is not surprising that VUV spectroscopies have a major impact in modern research in these areas. Research focuses on two dominant themes: (1) fundamental molecular scattering dynamics – as photoionization is a theoretically tractable instance of a well-prepared half-scattering event of electron plus ion, and (2) applications that use photoionization as a detection scheme. CAMD is well-suited for several types of photoionization studies, because several research areas do not require high brightness. Thus, CAMD can play a major role in such research. In some cases, it

already has, while there are other identifiable areas where the source can be exploited more effectively.

One example of a fundamental topic in molecular photoionization is the study of correlated motion between electronic and nuclear degrees of freedom, such as vibrational and electronic motion, or rotational and electronic degrees of freedom. My research in molecular photoionization has used three techniques over the years: dispersed fluorescence spectroscopy, fluorescence polarization analysis, and photoelectron spectroscopy. The first two methods have been applied with considerable success at CAMD, while the third has been performed more recently at the ALS. As an example of what was performed previously at CAMD, rotationally resolved dispersed fluorescence spectra from  $N_2^+(B^2\Sigma_u^+)$  state photoions are shown below.

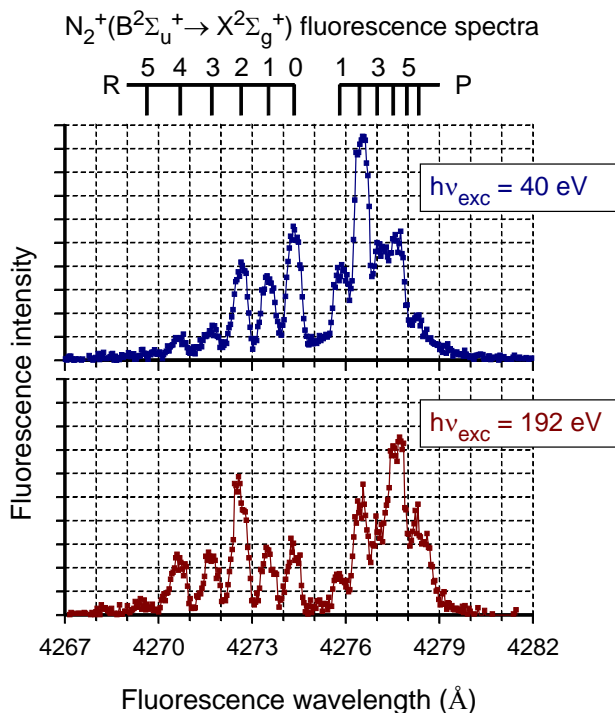


**Figure 1.** Dispersed fluorescence spectra from  $N_2^+(B^2\Sigma_u^+)$  photoions are shown at two selected photon energies [PRL **72**, 44 (1994)]. The radically different relative intensities result from changes in angular momentum partitioning between the photoelectron and the photoion. (The photoelectron kinetic energy is what has changed between these two data sets.) These data are representative of many results generated at the plane grating monochromator beamline that has been transformed into the new variable line spaced grating monochromator beamline.

Detailed information on the molecular scattering dynamics were generated from these data and several related studies because they illuminate microscopic insights into the molecular scattering dynamics by resolving molecular aspects of the phenomena. Indeed, the example shown in Fig. 1 was quite important because of the dramatic differences displayed between the  $N_2$  and CO data. This type of research utilizing fluorescence from photoions has been extremely productive at CAMD, generating Physical Review Letters [PRL **72**, 44 (1994); PRL **76**, 2666 (1996).], high-profile communications in the Journal of Chemical Physics [JCP **101**, 5402 (1994); JCP **113**, 899 (2000)], several journal articles and book chapters, as well as three National Science Foundation grants. Such studies are important for fundamental reasons in molecular physics because they provide new qualitative insights, and equally important, they serve to develop new spectroscopic tools of general importance. The outgrowths of this work are currently being funded by the Department of Energy for research performed at the ALS, namely the high resolution photoelectron spectroscopy experiments [PRL **92**, 1430021 (2004); JCP **125**, 164316 (2006)].

Other research directions that employ the strengths of CAMD are easily envisioned, and two cutting-edge experimental programs are currently being considered. First, it is possible to adapt

our gas-phase vibrationally-resolved photoelectron spectroscopy studies to a high resolution low energy beamline at CAMD. While it cannot be competitive with a beamline that generates high resolution data over a wide energy range (such as an ALS beamline), there are no limitations preventing high resolution data over a relatively narrow spectral range. Thus, Scienta-based photoelectron spectroscopy achieving 10 meV resolution would be useful, albeit for narrow ranges for the incident photon energy [e.g., A. Das *et al.*, J. Chem. Phys. **125**, 164316 (2006)]. Secondly, it would be very beneficial to use photoionization as a tool for other areas of research. One area that has generated tremendous interest is using synchrotron radiation as a source of tunable ionizing radiation to analyze the composition of flames using photoionization mass spectroscopy (PIMS) [Science **308**, 1887 (2005)]. There are several researchers doing first-rate combustion research at LSU, and it would be very beneficial to involve them in synchrotron-based research by performing relatively straightforward PIMS measurements. Again, such experiments do not require high brightness, simply high flux.

Note that work which has generated international interest and the proposed activities which can produce similarly favorable attention share some simple characteristics.

- Our previous successes emphasize important scientific niches where LSU academic departments have world-class research capabilities that dovetail naturally with the technical capabilities of CAMD.
- Previous successful research has exploited shared faculty and staff interests, goals, and capabilities.

There are additional issues which dictate the directions of future work (e.g., start-up costs and beamline development). Most of the new directions identified are not labor or equipment intensive, however. In order to achieve future success, it is important to have a machine that functions optimally and reliably. The machine physics expertise of several leaders (beginning with Ben Craft and currently being spearheaded by Vic Suller) have assured that this will not be a problem. The accelerator is operating very well, and a number of improvements continue to be made. Secondly, it is important to have optimally designed and maintained beamlines and endstations. The beamlines required for the work that is mentioned above do not have a natural home, and there are not appropriate staff to form a natural bridge for such work. Again, these obstacles are addressable, but they should be mentioned for completeness as well.

### **II.B.1.b. Time resolved x-ray absorption spectroscopy**

The ability to control the wet chemical synthesis of metallic nanoparticles and thus the properties of the final products requires a detailed understanding of the various processes taking place during the synthesis. To elucidate the process scientists at CAMD in collaboration with scientists at Bonn University undertook a study of the wet-chemical synthesis of Co nanoparticles in a microreactor system using a time resolved investigation by X-ray absorption spectroscopy. The experiment combined the x-ray, micro and nanofabrication facilities at CAMD to explore the development of Co nanoparticles on millisecond time scales.

The general mechanism for the formation of (metal) nanoclusters, which was proposed by Turkevich and Kim [1] in 1970, essentially consists of three steps: nucleation, growth and

agglomeration and is considered to be valid to-date. However, the exact mechanism for the different steps is still a matter of scientific discussion. There are two recent publications that used X-ray absorption spectroscopy for the time resolved in situ characterization of copper [2] and platinum nanoparticles, respectively [3]. In both cases no “free atoms” have been observed but rather complex intermediate compounds. Both studies demonstrate clearly that nanoparticle synthesis is a complex topic in which a lot of open questions remain to be solved. At the same time, they show the need to achieve improved time resolution, in order to close the “gap” between the precursor, metastable intermediate state and complete nanoparticle and to learn more about the nature of the fast nucleation process, which could not be resolved in a single one of these time-dependent experiments in spite of the fact that the entire reactions were rather slow.

Using in situ X-ray absorption spectroscopy in combination with a conventional wet-chemistry system imposes challenges as both possible XAS techniques: using an energy dispersive monochromator (EDM) or a conventional double crystal monochromator in “Quick-EXAFS mode” require significant integrations time per spectrum and per energy step, respectively, because of the normally relatively low concentration of the “active” components in the beaker. Thus, it is not possible to use the full potential of these techniques regarding their time resolution.

Also “inhomogeneties” in the chemical environment, temperature, concentration along the reactor chamber are draw backs of traditional batch reactor for in situ investigations. Just recently it was demonstrated that wet chemical synthesis of nanoparticles can also be carried out using micro fluidic reactors [4]. Using a microreactor system one can solve several of these problems, due to possibility rapidly mix reagents and better control over the temperature in the channel as well as exchange time with space resolved measurements. Here, the time resolution that is achieved is determined by the length of the channels of the microreactor, the retention time, and the size (here height) of the X-ray beam.

### *Experimental set-up*

Experiments were carried out at the 1.3 GeV electron storage ring at the Louisiana State University Center for Advanced Microstructure and Devices (CAMD) at the XMP beamline. Synchrotron radiation was monochromatized using a double crystal Lemonnier monochromator equipped with Ge 220 crystals. The monochromatic radiation was focused onto the channels of the microreactor system by a conventional Kirkpatrick Baez system resulting in a spot size of about  $40 \times 70 \mu\text{m}^2$ . Spectra were recorded in fluorescence mode using a single element Germanium detector. The XANES spectra were scanned within -20; +40; +80 eV intervals relative to the K-edge of a Co-metal foil with a step width 0.4 or 1 eV per respective interval with integration time of 3 s per step. Standard XANES data analysis (subtraction of a linear background, normalization at 7784 eV) was performed using the WINXAS97 software package.

The design of the microreactor used for the here reported experiments is shown in Figure 1. The size of channel is  $500 \times 500 \mu\text{m}^2$ . Components for the reactor were molded in polymethyl methacrylate (PMMA) by a hot embossing process. The reactor possesses three microfluidic ports: two inlets and one outlet. Flexible PTFE tubes (inner diameter: 0.8 mm) were used to deliver reagents and the product to/from the channel. Micro- dispensing, solenoid actuated pumps (Bio-chem valve inc., 120SP 24 Vdc) were used for filling the reactor with reagent solutions. Continuous flow rates in the order of  $1.3 \mu\text{l}/\text{min}$  were achieved. Spectra were collected

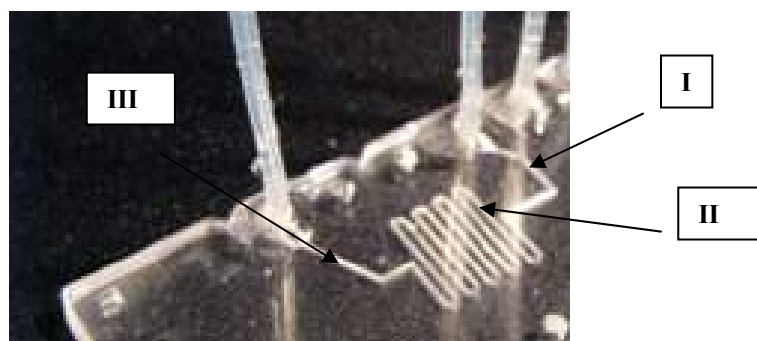
at three different points (cf. Fig1.): I) immediately after the mixing point, II) after the first curl of the snake mixer, and III) at the end of the channel system. With a channel length of 10 cm, a retention time of  $\sim 50$  seconds and a beam height of about  $40 \mu\text{m}$ , the time resolution of this system is better than 2 msec and thus at least a factor of 100 better compared to previous studies.

The synthesis of Co-nanoparticles in water was used for this experiment [5] with cobalt acetate tetrahydrate  $(\text{CH}_3\text{COO})_2\text{Co} \cdot 4\text{H}_2\text{O}$  as a precursor, N-dodecyl-N, -dimethyl-3-ammomio-1 propanosulfonate ( $\text{C}_{17}\text{H}_{37}\text{NO}_3\text{S}$ ) as a surfactant, and sodium borohydrate ( $\text{NaBH}_4$ ) as a reducing agent.

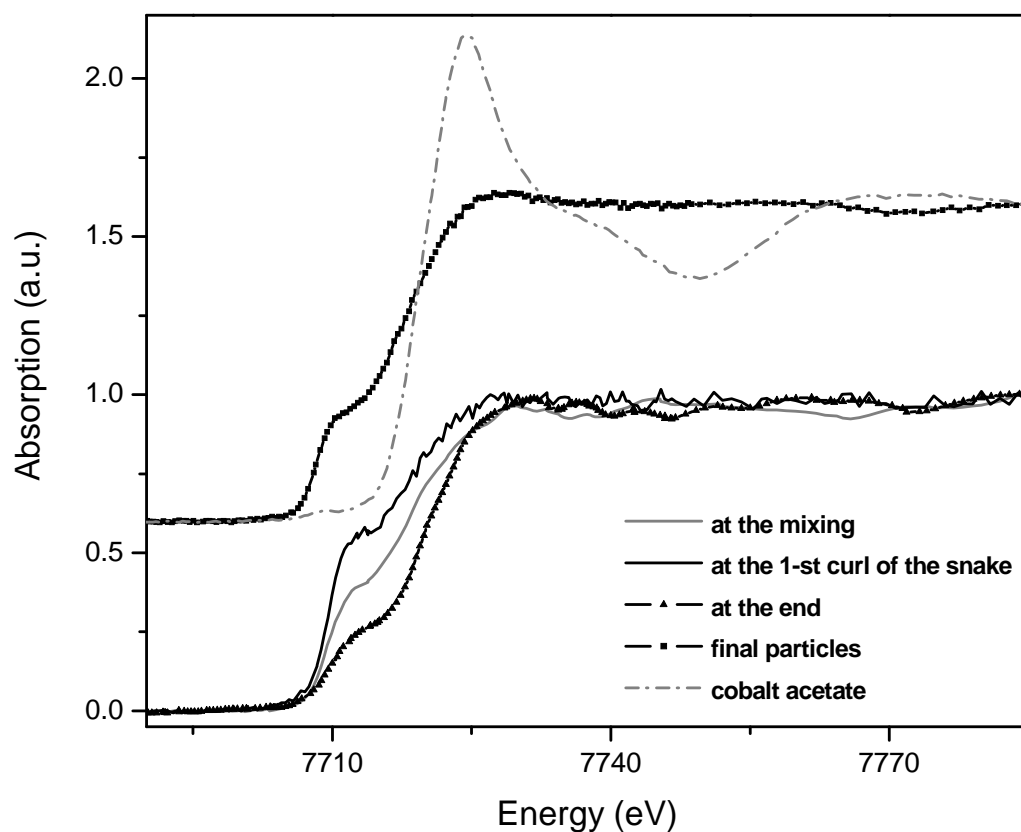
### *Results and Discussion*

Figure 2 shows the Co-K-XANES spectra that were recorded at the three positions described above together with the spectra of the precursor and the final product. It is obvious that all three spectra taken within the microreactor are different, demonstrating that actually different stages of the synthesis are observed. As the spectrum taken near the mixing point is different from the precursor it is also obvious that the first step of the reaction is extremely fast as the reaction time to this point is less than 0.5 s. Also the spectrum at point II does not show the typical resonance of an atomic transition metal K-shell spectrum that is dominated by the  $1s \rightarrow 4p$  resonance [6]. However as there is hardly any fine structure on the continuum it can be suspected that we have here very small Co-clusters. Eventhough the fine structure in the final spectrum is somewhat “washed out” the position and the intensity of the various peaks indicate strongly the presence of a Co-nanoparticles with an fcc structure.

Based on the preliminary results obtained so far, the quality of the spectra needs further improvement and it is also necessary to evaluate to what extent the laminar flow in the microchannels affect the spectra. However, we clearly demonstrated the potential of this new technique for fast time resolved in situ investigations not only for the synthesis of nanoparticles but also for the investigation of other chemical reactions.



**Figure. 1:** Picture of the microreactor system with points marked where spectra were taken



**Figure. 2:** Co K-edge XANES spectra recorded at three different positions of the microchannel together with reference spectra of the precursor and the final product collected at the end of microfluidic system.

### References:

1. Turkevich, J.; Kim, G.; Science 1970 169 872
2. Rothe, J.; Hormes, J.; Bönnemann, H.; Brijoux, W.; Siepen, K.; J. Am. Chem. Soc. 1998 120 6019-6023
3. Angermund, K.; Bühl, M.; Dinjus, E.; Endruschat, U.; Gassner, F.; Haubold, H.G.; Hormes, J.; Köhl, G.; Mauschick, F.T.; Modrow, H.; Mörtel, R.; Mynott, R.; Tesche, B.; Vad, T.; Waldöfner, N.; Bönnemann, H.; Angew. Chem. Int. Ed. 2002 41 4041-4044
4. Chan M. E., Mathies A. Richard and Alivisatos A. P. 2003 , *Nano Letters*, 3(2), 199-201.
5. Son S.U., Lee S.I., Chung Y.K., Kim S.-W., Hyeon T., *Organic letters*, 2002, Vol.4, No.2, 278.
6. Arp, U.; Lagutin, B.M.; Materlik, G.; Petrov, I.D.; Sonntag, B.; Sukhorukov, V.L.; J. Phys. B: At. Mol. Opt. Phys. 1993, 26 4381-4398

## II.B.2 Opportunities at the intersection of nanoscience and combustion chemistry: X-ray characterization studies

### *Introduction*

One of the most significant environmental issues of the decade is the effect of combustion-generated nanoparticles on human health and the environment. Numerous health effects studies have demonstrated that airborne fine particulate matter with a mean aerodynamic diameter of less than 2.5 microns (PM<sub>2.5</sub>) initiate cardiopulmonary disease and cancer in exposed human populations.<sup>1,2</sup> However, it has only been recently realized that the particles with the most demonstrable health impacts are in the nanometer regime (PM<sub>0.1</sub>) and are composed almost entirely of combustion-generated by-products.<sup>2-4</sup> The Nanoscience Group is currently engaged in fundamental, systematic studies of the origin, nature and reactivity of combustion-generated metal-containing nanoparticles. Because the nanoparticles and interfaces are typically rather complex, CAMD-based x-ray characterization methods (XANES and EXAFS) are invaluable tools, and can become even more central to this project.

Combustion processes generate nanoparticles with metal oxide nuclei, and these seed nuclei can undergo a variety of transformations. In the hot zones of combustion devices, the metal seed nuclei can promote reactions with gas-phase organic species to form a carbonaceous layer resulting in nanoparticle growth. In the cool zone ( $\leq 600$  °C), the metal nuclei can initiate formation of new pollutants. Accordingly, we will assess the role of the metal oxide nuclei in the growth and nature of nanoparticles, as well as determine how surface-condensed metal oxides and chlorides mediate formation of gas-phase as well as surface-associated pollutants. X-ray spectroscopy is important for characterizing both the nanoparticle composition and interfaces, as well as the chemical processes that take place at the interfaces.

### *Strategy: ongoing and proposed studies*

The group has recently developed a synthetic route that can control the cluster size for metal oxide nanoparticles tethered to silica “scaffolds”. These laboratory-based nanoparticles will be used as surrogates for the less well-defined particles that are generated in real combustion systems. The current method uses organic dendrimers in solution to form complexes with metal ions, and the resulting metal-containing complexes<sup>5</sup> are “calcined” on silica or alumina surfaces to generate immobilized metal oxide nanoparticles. The initial results demonstrate that viable strategies are viable for preparing well-defined metal oxide nanoparticles that will serve as surrogates for combustion-generated ultrafine particulate matter. Figure 1 presents a micrograph of a sample prepared in this way. The dark spots are CuO nanoclusters, and the translucent background is the silica.

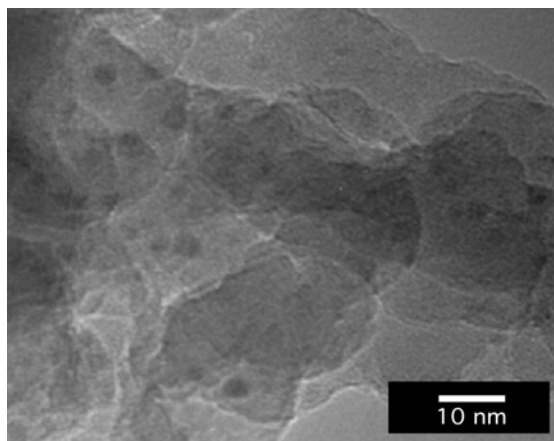


Figure 1: The translucent layers are the silica and the dark spots are the copper oxide nanoparticles. The mean size of the nanoparticles is 3.2 nm.

Moreover, the size of nanoclusters can be controlled by varying the amount of  $\text{Cu}^{2+}$  complexed by the dendrimer. The clusters detected on the surface of silica are extremely small. The average size was 3.2 nm for the particles shown in Figure 1. While our initial focus will be on copper oxide nanoclusters, other metal oxides will be important. We have performed Initial experiments that show that this method can be adapted to other metals. In addition to the Cu results shown, we have initial results on Ag and Fe, and we are currently developing methods appropriate for Ni and Cd. The results showing the capability of size selectivity in the preparative methods are shown in Figure 2.

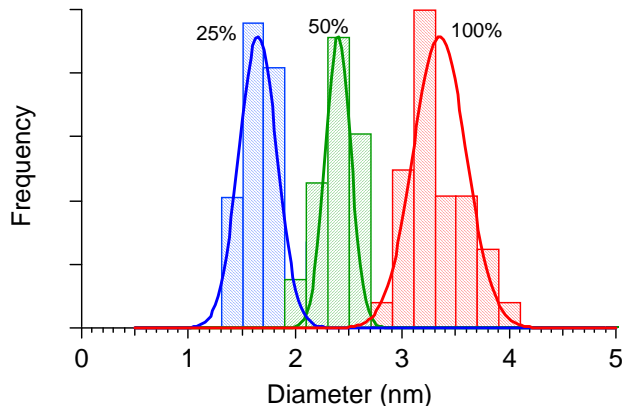


Figure 2: Histograms of nanoparticle size for different substitution ratios of  $\text{Cu}^{2+}$ /dendrimer in precursor. (The notation denotes the percentage relative to the stoichiometric maximum.)

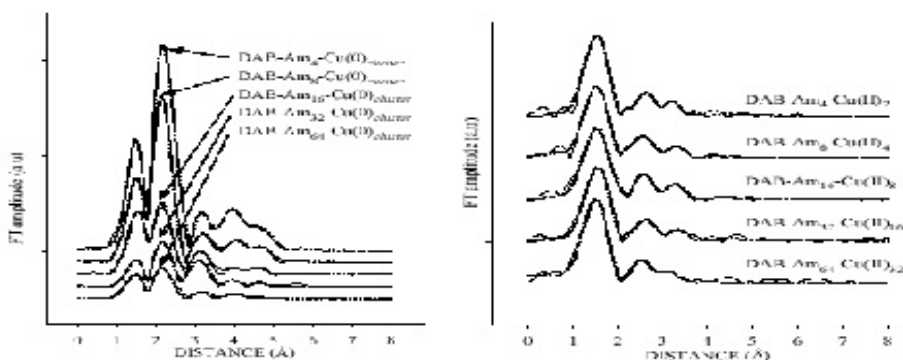


Figure 3: Fourier transforms of EXAFS spectra of Cu before (left) and after (right) reduction.

These studies are outgrowths of previous investigations into nanoparticle characterization and combustion chemistry. X-ray spectroscopy at CAMD has already played a central role in understanding the role of the dendrimer complexation, as is shown in “before and after” EXAFS results on the dendrimeric complexes processed in a reduction procedure used to generate zero-valent metallic Cu nanoparticles.<sup>5</sup>

Similarly, x-ray spectroscopy has been used to characterize combustion processes at metal oxide interfaces, such as uptake of dioxin precursors on metal oxide surfaces. A typical example is shown in Figure 4 below.<sup>6,7</sup> In this case, we were studying the effects of the metal oxide particle history on the chemical kinetics of 2-chlorophenol uptake (responsible for the production of dioxins and furans, examples of carcinogenic persistent organic pollutants).

X-ray based synchrotron studies are ideally suited for characterizing the oxidation state of the metal fraction in combustion systems, and several studies such as this have already been



performed at CAMD on micron-sized particles.<sup>6,7</sup> Preliminary measurements have also been performed on nanoparticles, and they are equally straightforward. Moreover, the CAMD component of this collaborative research is currently funded by an NSF NIRT grant (Nanoscience Interdisciplinary Research Team), as well as an NIH grant. The nanocluster group is planning to pursue this work vigorously in the near future.

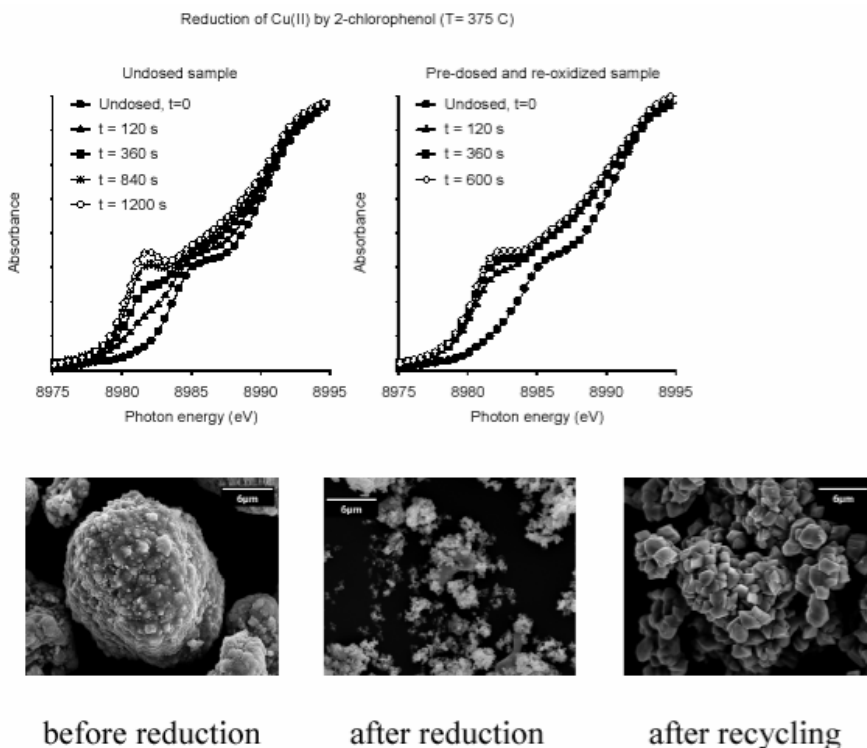


Figure 4a: XANES spectra of the Cu K-edge as a function of reaction time after exposure to 2-chlorophenol. The data in the left hand frame were taken for an undosed sample, while the data on the right were obtained for a sample that had been cycled (dosed and reoxidized).

Figure 4b: Scanning electron microscope images of CuO grains for samples before reaction, after reaction with 2-chlorophenol, and after re-oxidative cycling of the same grains. Grain size had strong effects on kinetics, and possibly on mechanism. Each from is 15  $\mu\text{m}$  wide.

### *Opportunities and Obstacles*

The opportunities are clearly defined in the preceding text. This is a project that lies at the nexus of fundamental and applied research, and we have the faculties and funding necessary to make the required progress. However, there needs to be additional work at the CAMD end by providing the beamline with a beam that is stable and stationary, and using sensitive detectors which are readily available and reliable, particularly multielement fluorescence detectors. Finally, additional staff with extensive expertise in x-ray instrumentation and methods need to be hired, in part to fill the void left by the tragic death of CAMD staff scientist Roland Tittsworth.

1. D.W. Dockery, C.A. Pope III, X. Xu, J.D. Spengler, J.H. Ware, M.E. Fay, New England Journal of Medicine; **329**, 1753 (1993).
2. C.A. Pope III, R.T. Burnett, M.J. Thun, E.E. Calle, D. Krewski, K. Ito, JAMA **287**,1132 (2002).
3. R.J. Delfino, H. Gong, W.S. Linn, E.D. Pellizzari, Y. Hu. Environmental Health Perspectives **111**, 647 (2003).
4. Air Quality Criteria for Particulate Matter; EPA/600/P-95-001 aF thru cF: U.S. Environmental Protection Agency; 1996.
5. P.N. Floriano, C.O. Noble, IV, J.M. Schoonmaker, E.D. Poliakoff, and R.L. McCarley, J. Am. Chem. Soc. **123**, 10545 (2001)
6. S.L. Alderman, George R. Farquar, E.D. Poliakoff, B. Dellinger, Proc. Combustion Institute, **30**, 1255 (2005).
7. S.L. Alderman, G.R. Farquar, E.D. Poliakoff, and B. Dellinger, Environ. Sci. Technol. **39**, 7396 (2005).

### II.B.3.a. X-ray absorption spectroscopy in studies of catalysis and combustion

X-ray absorption spectroscopy (XAS) is a critically important tool for researchers studying catalysts and other heterogeneous chemical processes. Such studies are some of the earliest applications of both EXAFS (extended x-ray absorption fine structure) and XANES (x-ray absorption near edge spectroscopy). X-ray spectroscopy remains one of the primary and most useful tools for chemists and chemical engineers who study processes involving disordered and complex media, generally, and catalysts in particular. Moreover, many researchers have been using CAMD for such studies since its inception, and continue to do so today. This is not surprising, as CAMD is competitive with other sources around the world for such research, as CAMD capabilities are well-suited for most catalytic processes are often carried out at higher temperatures and pressures with reactive gases, and x-ray spectroscopy is well-suited for such in-situ measurements for studying these reactions.

Many LSU researchers have used CAMD for x-ray catalysis research. Here, a few examples are highlighted to illustrate the potential that such studies have. In particular, we mention some ongoing activities of Profs. Kerry Dooley and J. Jerry Spivey of the LSU Chemical Engineering Department, as well as those of Profs. Dellinger, Poliakoff, and McCarley of the LSU Chemistry Department. These faculty members have also brought researchers from the nation as their collaborators to CAMD.

One example of catalysis research is the work of Prof. Dooley's and coworkers, who are trying to determine the electronic structure and coordination environment of Ce and other dopants in mixed metal oxide catalysts used for the manufacture of methylketones. XANES and EXAFS spectra were collected at room temperature and at 420°C (a typical reaction temperature). X-ray absorption spectroscopy is a very useful technique for determining both the electronic structure and the structural environment of the absorbing atom while EXAFS spectroscopy provides more detailed structural data. The coordination environment of Ce was explored using XANES and EXAFS under different doping conditions. Normalized Ce L<sub>III</sub> XANES spectra of the CeO<sub>2</sub>/Al<sub>2</sub>O<sub>3</sub> catalysts are shown in Figure 1. The catalyst containing 0.8% Pd has a higher intensity peak corresponding to Ce(III) than does the undoped sample, while the catalyst containing 2.4% Co has a lower intensity peak; for 0.8% Co the change in peak height is small. For the K-containing samples (not shown here), the peak heights corresponding to Ce(III) were lower. From such data, we are able to ascertain the electronic structure, and in particular, can estimate the number of oxygen vacancies that can be related to the catalytic properties.

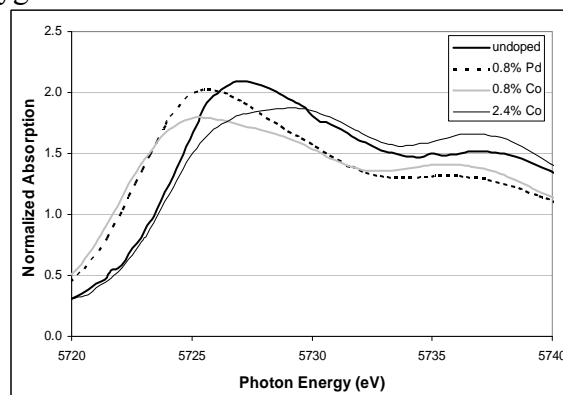


**Figure 1.** Ce L<sub>III</sub> XANES spectra of CeO<sub>2</sub>/Al<sub>2</sub>O<sub>3</sub> catalysts reduced in 10% H<sub>2</sub>/N<sub>2</sub> at 420°C.

The average number of oxygen vacancies in the coordination shell of the dopant Ce atoms was determined from such data, and the effects of different treatments (e.g., H<sub>2</sub> reduction) were also ascertained. Important information results from these data on the Co structure. Specifically, these data indicate that Co is in a different electronic state from CoO in the catalyst, due to substitution of Co into CeO<sub>2</sub>. Since some of the cobalt atoms in Co<sub>3</sub>O<sub>4</sub> have tetrahedral oxygen coordination, while in CoO all Co atoms are octahedrally coordinated, these results suggest that more Co in the catalysts is tetrahedrally coordinated by oxygen as a solid solution with CeO<sub>2</sub>. EXAFS data were also acquired, and those results ruled out the possibility that most of the cobalt is in a separate oxidic or metallic phase. Such a detailed microscopic picture of the catalysts is important for understanding the microscopic details of the catalysts, thereby aiding in the design and preparation of improved and lower cost catalysts for real processes.

Chemists perform a wide array of x-ray based research that is closely related to the catalysis studies performed by chemical engineers. For example, Profs. Dellinger, Poliakoff, and McCarley (LSU Chemistry) are investigating the electronic and geometric structure changes that are related to the unwanted production of pollutants that occurs on metal oxide surfaces in combustion processes. Analogous to the chemical engineering catalysis research, such measurements provide an unambiguous picture of the processes that produce the persistent organic pollutants that occur on metal oxide surfaces. Such investigations are moving into new directions, including the nanochemistry that is related to soot formation and reactivity in combustion. All of this work is well-funded. In the case of the chemistry research, the major sponsor has been (and continues to be) the National Science Foundation, while industrial and other federal agencies have been reliable in supporting the high quality research performed in the Chemical Engineering Department at LSU.

### **II.B. 3.b. Catalysis Research at CAMD in Professor Spivey's Group**

X-ray absorption spectroscopy (XAS) was embraced by catalyst researchers as a very attractive technique immediately after some of the first spectra were taken at Stanford University (Lytle et al., 1977). The classic review article on application of XAS in catalysis research by Prins and Koningsberger (Prins and Koningsberger, 1988) is still very relevant after almost 20 years. Along with XAS, X-ray diffractometry has also been extensively used in this type of research. Beamlines using combined XAS and XRD are very useful in this field (Ref? Thomas?). Catalytic processes are often carried out at higher temperatures and pressures with reactive gases, and synchrotron-light based techniques are inherently suitable for studying these reactions.

Some in-situ experiments were performed at CAMD in the mid 1990s with a modified Lytle cell but the effort was not sustained. Over the past few years there has been renewed interest at CAMD in catalysis research. This effort has been spearheaded by Drs. Kerry Dooley and J. Jerry Spivey of the Chemical Engineering Department at LSU. A variety of catalysts, for wide ranging applications, are being investigated or will be studied. These faculty members have brought researchers from the nation as their collaborators to CAMD.

Among current and past projects related to catalysis research are alumina supported ceria catalysts for ketone production; Fischer-Tropsch catalysts for ethanol production from biomass and ethanol from coal; barium hexa-aluminate for hydrogen production from diesel fuel; and

zinc ortho-titanate as a sorbent for integrated gas combined cycle gasification process. Several of these projects are funded by the Department of Energy.

Dr. Kerry Dooley from Chemical Engineering at LSU recently investigated new catalysts for methylketone manufacture. Asymmetric (non-symmetric) ketones can be produced by the catalytic decarboxylative condensation of carboxylic acids. Dr. Dooley has formulated improved catalysts to manufacture two typical ketones of industrial interest, methylnonylketone (MNK) and diisopropyl ketone (DIPK). MNK is formed from acetic and decanoic acids, while DIPK is the coupling product of isobutyric acid (IBA). These ketones are useful as solvents for elastomers, polyvinyl acetate and other plastics. They are also used as reaction/extraction solvents, animal repellants, in nutrients, fragrances and flavors, and as intermediates in making pesticides, herbicides, and pharmaceuticals. Metal-doped, supported  $\text{CeO}_2/\text{Al}_2\text{O}_3$  catalysts are effective for the high temperature catalytic decarboxylative condensation of carboxylic acids to produce ketones. Controlled addition of cobalt, palladium, manganese, potassium and praeisodmium improved the activity, stability and selectivity of the catalyst. The objective of the project was to obtain the best performing catalyst.

The K edge of cobalt and L edge of cerium and palladium were probed. Experiments were conducted at room temperature and in-situ conditions at temperature of  $420^\circ\text{C}$ . In this case there is little relationship between the number of oxygen vacancies as determined by XANES and the reaction rate for ketonization, because of the relative ease at which a dehydrogenated ketene-like intermediate can be produced from acetic acid. Cobalt seems to be a useful additive for either type of reaction, fulfilling either role. In concentrations of  $<15$  at.% in  $\text{CeO}_2$ , it inserts easily into the rare earth oxide, in tetrahedral coordination, boosting the number of oxygen vacancies formed under reducing conditions. In much higher concentrations the cobalt can also form separate reduced oxide domains, but with less power to dehydrogenate than, e.g., palladium.

There is a high demand in the United States to develop alternative fuels and it is increasingly apparent that using domestic resources is the most attractive way to become energy independent. The United States has over four times the energy in coal reserves than the entire Middle East in petroleum reserves. Although there are engineering issues with coal-to-liquid Fischer Tropsch, rising prices in petroleum as well as innovative research is creating a favorable environment for large-scale implementation of coal-to-liquid processes in the US. Bulk iron catalysts are advantageous for coal and biomass Fischer-Tropsch due to their relatively low cost, high water gas shift activity (for the low  $\text{H}_2/\text{CO}$  synthesis gas ratio of coal and biomass), and low methane selectivity.

Dr. Spivey is working with researchers from Clemson University to investigate iron-based Fischer Tropsch catalysts containing minor metals. The premise of adding a minor metal is that it forms a mixed metal carbide which improves activity, stability, and selectivity due to iron-secondary metal interactions. Formation of these mixed metal carbides is difficult to establish by X-ray diffractometry as they form mostly on the surface where the catalytic activity usually occurs. X-ray absorption spectroscopy with the electron yield detection mode, which probes only the top few hundred nanometers, has been very helpful in this research. In one experiment the role of molybdenum as a minor metal in these catalysts was probed. Both K and L edges of molybdenum were measured and the L edge is more sensitive to the electronic structure,

symmetry and the oxidation state. The K edge measurements were performed at the National Synchrotron Light Source. There was no evidence of mixed carbide formation. The  $L_{III}$  edge XANES spectrum of molybdenum showed that it is in tetrahedral coordination. X-ray diffractometry showed that the calcined catalysts mostly had nanometer-sized hematite ( $Fe_2O_3$ ) domains. Passivation of the catalysts reduced the proportion of hematite and produced cohenite ( $\theta-Fe_3C$ ; analogous to cementite) with about 100Å domain size.

Dr. Spivey recently also received funding from the Department of Energy for the project “Catalytic Process for the Conversion of Coal-derived Syngas to Ethanol.” His co-investigators include researchers from Clemson (Jim G. Goodwin, Jr), Conoco-Phillips (Ed Sughrue) and Oak Ridge National Lab (Steve Overbury). The objective of the project is to develop a coal-based process for the conversion of low  $H_2/CO$  synthesis gas to ethanol. The development of an economically viable, coal-based process producing ethanol provides a way in which hydrogen can be easily transported, with ethanol being reformed at the point of use to provide hydrogen. This process also takes advantage of the large domestic coal resources in the US to help move toward energy independence.

Clean coal-derived synthesis gas is produced using Conoco-Phillips’ proven E-Gas technology. Because the synthesis gas has a  $H_2/CO$  ratio of  $\sim 0.7/1$ , the composition must be adjusted for optimal ethanol synthesis. This is done using a gas-solid reaction step in which the water gas shift reaction is used to adjust the synthesis gas  $H_2/CO$  ratio from  $\sim 0.7/1$  to the 2/1 ratio required for ethanol synthesis (while also generating high purity  $CO_2$ ). The final step is the selective catalytic conversion to ethanol. This project focuses on the last two steps. Rhodium-based Fischer-Tropsch catalysts will be used in this project. The K edge of rhodium (23.220 keV) will require the new wavelength shifter XAS beamline for measurements.

Dr. Spivey is participating in another project initiated at the University of West Virginia, related to the production of hydrogen from fuel cell. The catalytic partial oxidation of diesel fuel is an attractive source of  $H_2$  and CO for fuel cell applications. However, the deposition of carbon onto the surface of the catalyst and the migration and loss of active metals remain the principal issues in the development of a suitable catalyst. The formation of elemental carbon onto the surface of a catalyst has been shown to be related to both the size of the active metal cluster and its coordination. The substitution of a catalytic metal into the lattice of hexa-aluminate compounds may serve to reduce the size of active metal clusters and to increase their dispersion thereby reducing their susceptibility toward carbon deposition. Interactions between neighboring substituted metals and the hexaaluminate lattice may serve to suppress active metal mobility. In this project, a series of barium hexaaluminate catalysts with Ni substituted into the lattice were prepared with the general formula,  $BaNi_yAl_{12-y}O_{19-\delta}$  ( $y = 0.2, 0.6$  and  $1.0$ ). The average Ni coordination was characterized by Extended X-ray Absorption Fine Structure Spectroscopy (EXAFS) for the as synthesized catalysts. Catalyst activity and selectivity was assessed by  $H_2$  and CO yields obtained from n-tetradecane ( $C_{14}H_{30}$ ) catalytic partial oxidation. Post-run characterization of the catalysts was undertaken by temperature programmed oxidation to locate and quantify the amount of carbon deposited onto the catalysts.

EXAFS analysis of the  $BaNi_yAl_{12-y}O_{19-\delta}$  catalyst showed that the average Ni-O bond distance to be relatively insensitive to increasing Ni substitution, however increasing Ni substitution

decreased Ni-O coordination. Catalyst activity and selectivity was shown to be strongly dependant on the Ni substitution. Temperature programmed oxidation of the reacted catalysts indicates that carbon deposited onto the surface of the catalysts was directly related to their activity and selectivity.

In another project, Dr. Spivey's group in collaboration with researchers from the University of Pittsburgh, is studying novel sorbent materials for integrated gas combined cycle coal gasification process. The high efficiency of this process offers potentially clean energy production via gasification of coal into synthesis gas, followed by use of steam from the gasification process in steam turbines and combustion of the synthesis gas to power gas turbines. As coal typically contains atomic impurities such as S, As, Se, Cl, Hg, etc, possible gasification byproducts contaminating the synthesis gas can include species like H<sub>2</sub>S, AsH<sub>3</sub>, H<sub>2</sub>Se, HCl, HgCl. The release of these compounds into the environment is widely known to have negative consequences; similarly, the relatively high concentration of H<sub>2</sub>S as a contaminant gasifier byproduct can foul later stages of the integrated gas combined cycle coal gasification process. Current technologies in the integrated gas combined cycle coal gasification typically use a multi-stage/material process for contaminant removal. For process intensification, a low cost high uptake sorbent is needed to capture these species simultaneously.

Zinc Orthotitanate, Zn<sub>2</sub>TiO<sub>4</sub> has been proposed as such a sorbent. It combines high thermal stability with reactive surface chemistry required for the removal of species like H<sub>2</sub>S, AsX, XSe and other contaminants from hot coal gas. It has been shown that this material is regenerable with minimal performance loss between cycles. To aid in the development of these materials, an atomic scale understanding of the zinc orthotitanate surface and bulk chemistry is needed as there is little known experimentally about this material, or the atomic-scale processes that make it potentially viable as a multi-contaminant sorbent for the IGCC. While it is known that bulk zinc orthotitanate is an inverse spinel structure with Zn atoms occupying T-sites and both Zn and Ti atoms occupying O-sites, the distribution of Zn and Ti in the O-sites has remained confusing and uncertain. X-ray absorption fine structure spectroscopy (EXAFS), and along with density functional theory, was used to improve our understanding of the atomic scale properties of this material. EXAFS was performed with both calcined and uncalcined crystals to investigate the changes during the sorption process.

The future of catalysis research at CAMD appears very promising. The addition of the wavelength shifter beamline will allow more user time and access to higher energies. Drs. Kerry Dooley and K.T. Valsaraj in the Chemical Engineering Department at LSU are synthesizing mesoporous materials as catalysts. Characterization of this material requires high quality powder diffraction pattern at very low angles. The new powder diffraction beamline has already been useful for characterization of Fischer-Tropsch catalysts and can be used for the mesoporous catalysts.

#### **References:**

- Lytle, F.W., Via, G.H., and Sinfelt, J.H. (1977) New Application Of Extended X-Ray Absorption Fine-Structure (EXAFS) as a Surface Probe-Nature of Oxygen Interaction With a Ruthenium Catalyst. *Journal Of Chemical Physics*, 67(8), 3831-3832.
- Prins, R., and Koningsberger, D.C. (1988) Catalysis. In D.C. Koningsberger, and R. Prins, Eds. *X-Ray Absorption Principles, Applications, Techniques of EXAFS, SEXAFS and XANES*, 92, p. 321-372. John Wiley & Sons, New York.

## II.C. Environmental Sciences

Many problems in environmental and agricultural sciences have been investigated at CAMD. These include studying the role of bacteria in global sulfur cycle, sediments from New Orleans after hurricane Katrina, and the mobility of phosphorus and zinc in bio-solids amended agricultural land. Along with X-ray absorption spectroscopy and X-ray microprobe, Fourier transform infrared spectro-microscopy has also been utilized in environmental research. Both XAS beamlines used in environmental research are “windowless,” i.e., only a thin Kapton™ window separates the beamlines from the ring, and thus providing high flux at low energies. Additional highlights can also be found in Appendix B of this report.

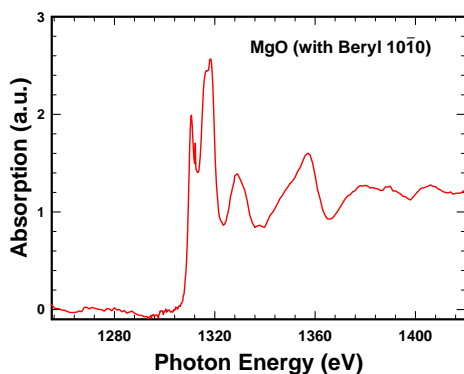


Figure II.C.1

Periclase (MgO) absorption spectrum obtained at the DCM beamline

Dr. Annette Summer Engel from the Department of Geology and Geophysics and Biological sciences at LSU recently studied the role of bacteria in sulfur speciation in ancient deposits which are often used in the interpretation of the geologic record in the broader context of the sulfur geobiocycle<sup>1</sup>. This work was performed in collaboration with Dr. Alexander Prange from Hochschule Niederrhein, Germany. XAS was used in conjunction with an evaluation of habitat geochemistry, microbial community compositions, and sulfur isotope systematic. The XAS measurements by Drs. Engel and Prange showed that there is some preferential accumulation of cyclo-octasulfur ( $S_8$ ) compared with polymeric sulfur ( $S_n$ ). Sulfur isotope composition confirmed that sulfur content and sulfur speciation may not correlate to microbial metabolic processes in natural samples, thereby complicating the interpretation of modern and ancient sulfur records.

In another project Dr. Prange, along with his collaborators (including Dr. Josef Hormes, University of Bonn and CAMD), is studying the role of anoxygenic phototrophic sulfur bacteria in the global sulfur cycle. The particular bacterium they studied is *Allochroamatium vinosum* (f. *Chromatium vinosum*). The elemental sulfur is taken up, transformed into intracellular sulfur globules and oxidized to sulfate by this bacterium. Sulfur speciation was analyzed using X-ray absorption spectroscopy and sulfate contents were determined by high pressure liquid chromatography (HPLC) to quantify the amount

of elemental sulfur being taken up and oxidized by *Alc. vinosum*. The results show that *Alc. vinosum* uses only the polymeric sulfur ( $(S_n)_m$ , sulfur chain) fraction of elemental sulfur and is probably unable to take up and form sulfur globules from *cyclo*-octasulfur ( $S_8$ ).

Understanding the speciation of an element in soil or waste is very important as it is the chemical form which determines its bioavailability or toxicity. XANES spectroscopy has made significant contribution to such determination since it became accessible to agronomists and environmental scientists. Traditionally, speciation of an element is defined operationally, based on its sequential dissolution in acids of certain strengths. XANES spectroscopy has showed that such definition has little scientific validity for elements like chromium and manganese. Dr. Wang, who is a soil chemist in the Department of Agronomy and Environmental Management at LSU, extended this observation to phosphorus. He found that since chemical fractionation contained a large residual-P fraction which could not be partitioned into chemically defined phosphorus forms, XANES estimates of soil total Ca-phosphates and the total Fe-/Al-P species was more effective than the chemical phosphorus fractionation procedure even though XANES could not differentiate phosphorus sorbed onto Fe or Al oxides.

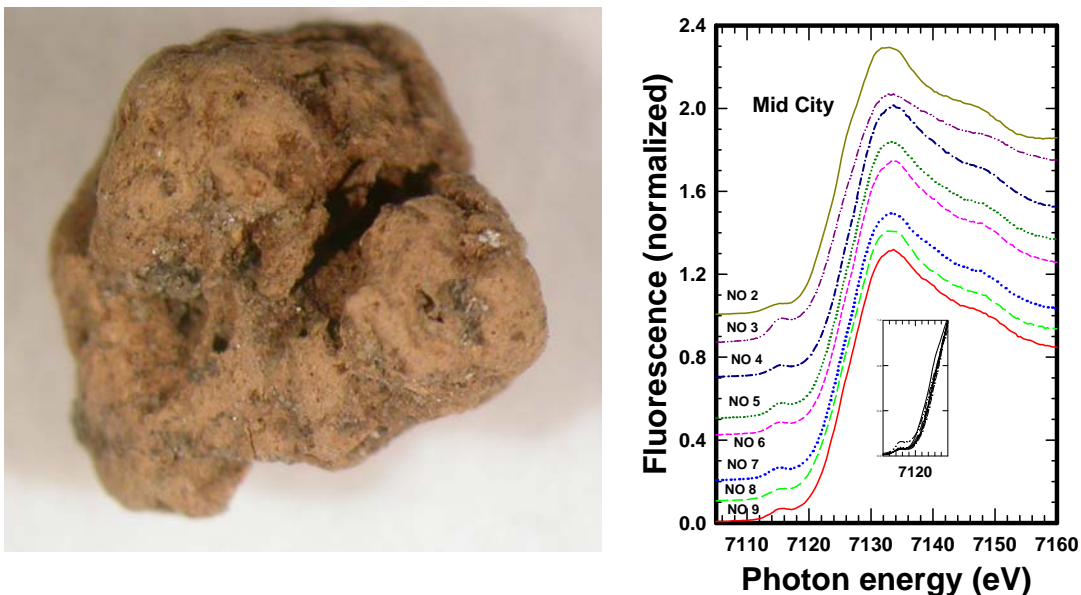


Figure II.C.2

An iron-rich sediment particle (left) from Mid City New Orleans and XANES spectroscopy of sediments from New Orleans (right)

A USGS funded project investigating the sediments in New Orleans after Katrina flooding was recently completed. Similar to the flood water<sup>2</sup>, the sediments were also high in iron and zinc, and locally in copper, arsenic, and lead. Hundreds of measurements of these elements in the soil have been performed but practically no speciation studies have been conducted<sup>3</sup>.

Dr. Engel from LSU also studies the role of arsenic and antimony in the life cycle of



bacteria in some extreme environments. Her geomicrobiological studies can provide insight into early Precambrian terrestrial habitats, and may offer insights to the origin of adaptations to extreme environmental conditions. Some of the material that Dr. Engel will be studying comes from El Tatio, a hot spring at 12,000 foot elevation, in Chile. The water in the hot spring has very high arsenic concentration and contaminates the drinking water in the surrounding region. She is working in this project with researchers from the Universidad Catolica in Santiago, Chile.

It is widely recognized now that surface-mediated reactions generate many of the pollutants in the atmosphere during combustion. The dioxins in the atmosphere are most likely produced by this process in reactions involving transition metals, hydrocarbons and a chlorine source. Dr. Irwin Poliakoff and Dr. Barry Dellinger in the Chemistry Department at LSU are investigating the pathways of dioxin production during incineration. They have studied a surrogate system silica-copper oxide-2-chlorophenol by XAS at high temperatures. During the experiment, monitored by XAS, copper oxide was easily reduced to metallic copper. Preliminary results from this study have been published but more work is needed<sup>4</sup>.

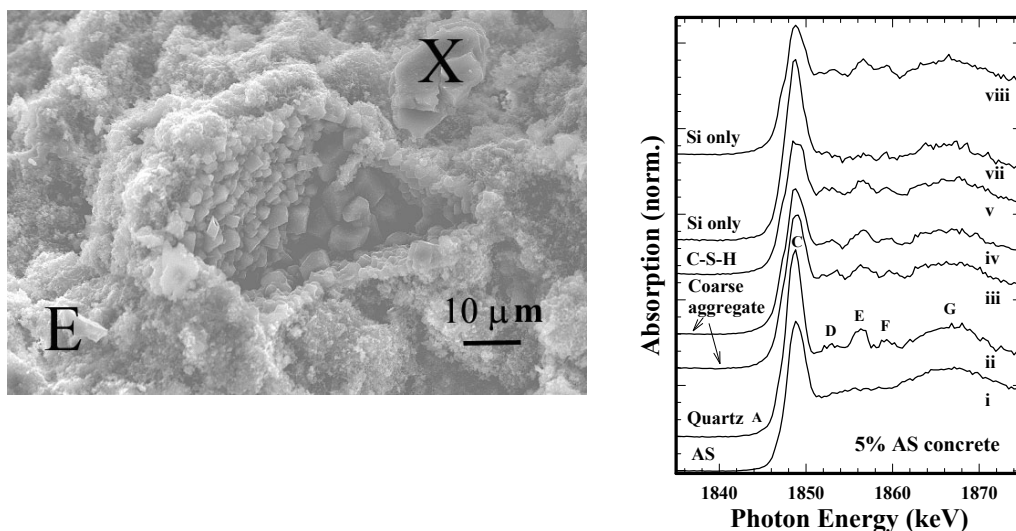


Figure II.C.3

The nanometer-size amorphous silica crystallized into quartz in concrete

A manufacturing plant in Louisiana produces nanometer-scale amorphous silica ( $\text{SiO}_2$ ) as a by-product which is presently sent to the landfill. Preliminary studies showed that incorporation of this silica into portland cement concrete produced significant strength gain. It was difficult, however, to ascertain the exact role of this silica in the concrete as concrete contains many silicate phases, including quartz, a form of silica. It is also important to know the role of this silica as formation of unstable phases may lead to deterioration of the properties of this concrete over the long term. An analytical technique was needed which would identify different silica forms and spatially resolve them. The X-ray microprobe at CAMD proved to be the right tool for this problem. Spatially resolved XANES analysis showed that by-product silica was crystallizing into

the most stable form of silica, quartz. It increased the bonding between the large aggregate in concrete and the cement matrix and thereby increased the strength<sup>5</sup>.

- <sup>1</sup> A. S. Engel, H. Lichtenberg, A. Prange et al., *Fems Microbiology Letters* **269** (1), 54 (2007).
- <sup>2</sup> J.H. Pardue, W.M. Moe, D. McInnis et al., *ES&T Web Edition* (October 11th) (2005).
- <sup>3</sup> A. Roy, C. Bianchetti, R. Tittsworth et al., presented at the Thirteenth International X-Ray Absorption Fine Structure Conference Stanford University, Palo Alto, California, 2006a (unpublished).
- <sup>4</sup> G. R. Farquar, S. L. Alderman, E. D. Poliakoff et al., *Environmental Science & Technology* **37** (5), 931 (2003).
- <sup>5</sup> A. Roy, N. Moelders, P. J. Schilling et al., *Journal of Materials in Civil Engineering* **18** (6), 747 (2006).

## II.D. Life Sciences

Synchrotrons play a large and increasingly vital role in life-science research. The unique characteristics of synchrotron radiation provide better data and, in many cases, allow experiments to be done which would otherwise be impossible. Here at CAMD life-science research falls into four major categories, macromolecular crystallography, X-ray absorption spectroscopy, X-ray tomography, and infrared spectroscopy.

### II.D.1 Macromolecular Crystallography at CAMD

Macromolecular Crystallography (also known as Protein Crystallography) seeks to explain the functioning of biological macromolecules, such as proteins and DNA. The technique is used to determine the structures of biological molecules, that is the location of the atoms that make up the molecule and how the atoms are connected to each other. Long an area of basic research, macromolecular crystallography has over the last decade become an important tool in drug discovery and development. Drugs function by binding to macromolecules and changing their behavior. By determining the structure of a complex between a target macromolecule (generally an enzyme) and a candidate drug, crystallographers can advise the pharmaceutical chemists on how to modify the drug to enhance its activity or increase the drug's specificity thereby reducing side effects.

Synchrotrons have become the dominant data source for macromolecular crystallography. In 2006 79% of the publicly released structures were obtained from synchrotron data. CAMD has had a macromolecular crystallography beamline since 2002 which is operated and funded by the Gulf Coast Protein Crystallography Consortium (GCPCC), a group of 8 institutions in LA TX and OK. The beamline has been a steady and increasingly productive source of macromolecular structures. Below we give a few examples of protein structures solved with data from CAMD and explain their significance.

The Waldrop lab (LSU) has solved the structure of the bacterial enzyme biotin carboxylase with a drug candidate bound to it. The drug inhibits the activity of the enzyme; since active enzyme is required by the bacteria an inhibitor has great promise as an antibiotic. The biotin carboxylase used in this work comes from the medically important bacterium *staphylococcus aureas* and is thus an excellent target for development of novel inhibitors to combat the rise in antibiotic-resistant staphylococca infections. This work is sponsored by a pharmaceutical company and the Waldrop lab is now using the knowledge gained from the structure to produce modifications to the drug candidate to design compounds with improved properties.

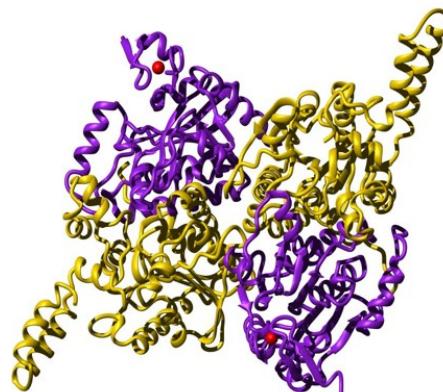


Figure 1, Biotin carboxylase dimer

The Watowich lab at the University of Texas Medical Branch in Galveston has determined the structure of the active part of the protein NSP2 from the Venezuelan equine encephalitis virus (VEEV). VEEV is a significant cause of human illness in Central and South America with mortality rates of ~1%. There is currently no specific treatment for VEEV infection and the vaccine provides incomplete protection. NSP2 is essential for viral replication, making it an attractive target for development of antiviral drugs to treat VEEV infection. The availability of a structure for the protease domain of VEEV NSP2 will be of great use in the drug discovery process. A vast database of known compounds can be screened by computers to find drug candidates and the structure can be used to guide the design of new compounds. The data from CAMD enabled the structure to be determined in much greater detail than could be done with non-synchrotron data. The greater detail is essential for the design of new inhibitors of NSP2.

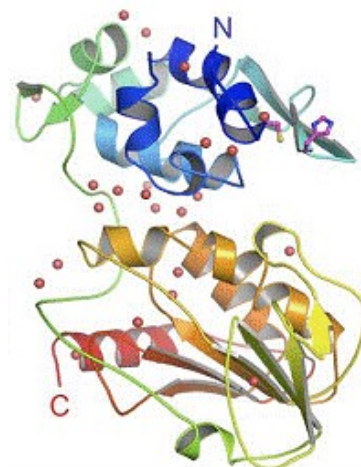


Figure 5, Ribbon diagram of NSP2 colored from blue (N-terminus) to red (C-terminus). Spheres are bound water molecules

The laboratory of Yong-Hwan Lee (LSU) is focused on the development of novel therapeutics for the treatment of cancer. Recent developments have shown that the increased metabolic rates observed in cancer cells are driven by an unusually high concentrations of the regulatory molecule fructose-2,6-bis-phosphate, the concentration of which is controlled by the enzyme 6-phosphofructo-2-kinase/fructose-2,6-bisphosphatase (PFKFB3). As part of their efforts to understand its structural architecture and provide a molecular scaffold for the design of novel cancer therapeutics, the Lee laboratory has used data from CAMD to determine the structure of this enzyme in complex with inhibitors. Given the large unit cell of the PFKFB crystals, data collection at a synchrotron source is essential.

The Worthylake lab from the LSU Health Sciences Center in New Orleans has solved the structure of a fragment of the protein IQGAP1 using multi wavelength data from CAMD. Only a synchrotron can provide the tunable x-ray beam needed for multi-wavelength data collection. IQGAP1 is a "molecular scaffold" protein which is important for cell adhesion and cell motility. It behaves anomalously compared to homologous proteins and the fragment of IQGAP1 that has been solved is believed to be responsible for the anomalous behavior. A manuscript describing the structure is in preparation.

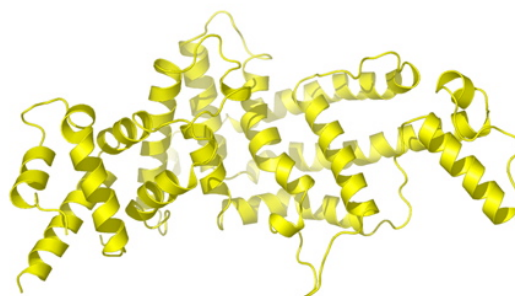
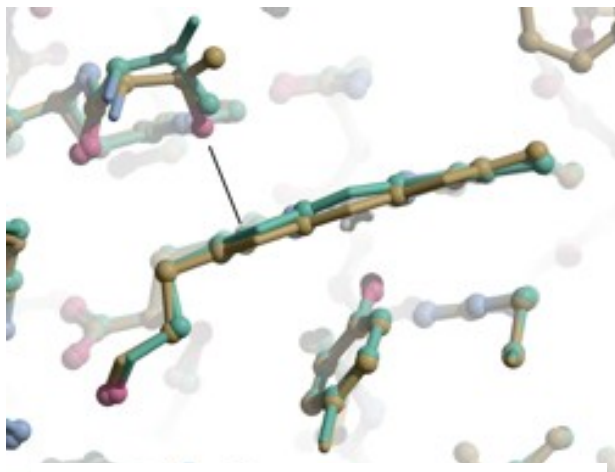


Figure 6, Ribbon diagram of IQGAP1

The Newcomer lab at LSU has solved the structure of Allene Oxide Synthase (AOS) from a soft coral *Plexaura Homomalla*. They see a clear structural relationship between AOS and Catalase, an enzyme that protects cells by breaking down hydrogen peroxide. Both are heme enzymes with a near identical conformation for most of their structures. Nevertheless they have distinct

enzymatic activities which appears to be due to modest differences in the environment around their hemes. To investigate this puzzle the Newcomer lab has prepared and solved the structures of AOS with single amino-acid substitutions. A mutation, T66V, that exhibits some catalase activity was solved at 1.8 Å and has a non-planar heme like catalase whereas native AOS has a planar heme. They have proposed a mechanism which prevents the AOS heme from reacting with hydrogen peroxide which, on the basis of its size, should be able to reach the heme.



**Figure 7**, The effect of the T66V substitution on heme planarity. AOS (gold), AOS:T66V (green)

The First lab at LSU Health Sciences Center in Shreveport grew crystals of the enzyme Tyrosyl-tRNA synthetase (TyrRS) which plays an essential role in protein synthesis. Specifically it catalyzes the attachment of tyrosine to the 3' end of tRNA<sup>Tyr</sup>. Understanding how TyrRS catalyzes this reaction is important because of both the central role that this process plays in protein synthesis and the potential for using this enzyme to introduce unnatural amino acids into proteins.

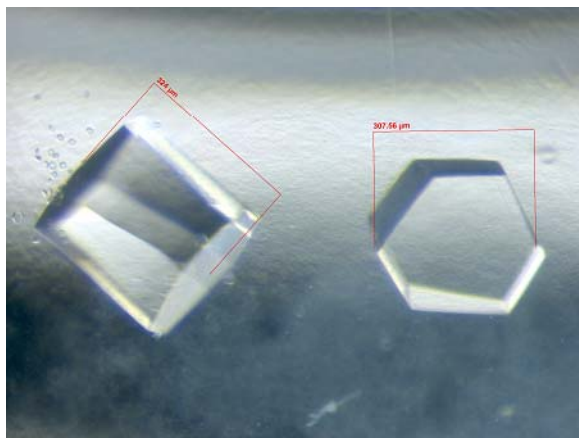


**Figure 8**, Wild-type TyrRS-D Tyrosine complex crystals.

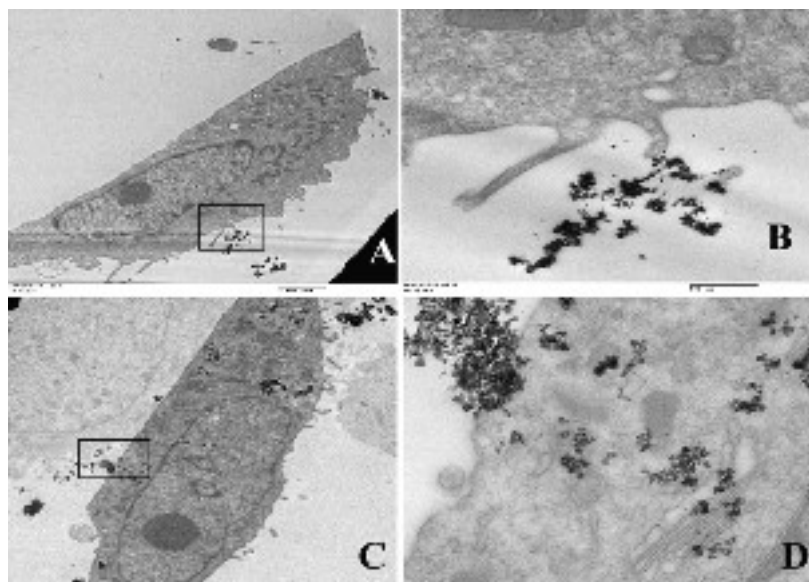
In contrast to other aminoacyl-tRNA synthetases, TyrRS is able to catalyze the attachment of both the L- and D-stereoisomers of its cognate amino acid to tRNA. (Only the L stereoisomers of amino acids are used to make proteins.) The First lab prepared and crystallized complexes of TyrRS with both D and L tyrosine for both native and mutated enzyme. During the fourth quarter of 2006 they collected data at CAMD from native and a mutant each with L and D tyrosine bound. They are currently determining the structures of these complexes using molecular replacement methods.

## II.D.2 Biomedical Applications

### Biomedical Application of Nanomaterials Designed, Synthesized and Characterized Using XAS in CAMD

One of the major areas of interest for CAMD's Nanofabrication group is to explore the opportunities that exist for magnetic Nanomaterials in biomedicine. Through appropriate collaboration with external users, Nanofabrication group has been able to develop few unique patentable technologies in the area of medical diagnosis, drug delivery and tissue engineering.

In collaboration with Prof. Leuschner at Pennington Biomedical Research Center, superparamagnetic iron oxide nanoparticles coupled with LHRH hormones are being developed as novel contrast agents for enhancing the contrast in MRI of primary tumors as well as of micrometastases. LHRH acts as a targeting agent. Targeted delivery of superparamagnetic iron oxide nanoparticles (SPIONs) could facilitate their accumulation in metastatic cancer cells in peripheral tissues, lymph nodes and bones and enhance the sensitivity of magnetic resonance imaging (MRI). The specificities of luteinizing hormone releasing hormone (LHRH) and luteinizing hormone/chorionic gonadotropin (LH/CG)- bound SPIONs were tested in human breast cancer cells *in vitro* and were found to be dependent on the receptor expression of the target cells, the time of incubation and showed saturation kinetics. In incubations with MDA-MB-435S.luc cells, the highest iron accumulation was 452.6 pg Fe/ cell with

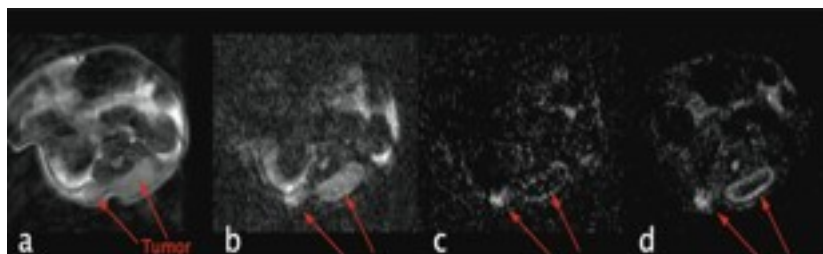


Sub-cellular location of LHRH-SPION in MDA-MB-435S.luc cells after incubation at 4 °C for 3 h (A, B) and 37 °C (C, D) for 0.5 h. LHRH-SPIONs were taken up by the cells and accumulate in the cytosolic compartment (bars in A, C) 2 micron, (B) 500 nm, (D) 100 nm

LHRH-SPIONs, 203.6 pg Fe/cell with b-CG-SPIONs and 51.3 pg Fe/cell with SPIONs. Incubations at 4 °C resulted in 1.1 pg Fe/cell. Co-incubation with the same ligands (bCG or LHRH) decreased the iron accumulation in each case. LHRH-SPIONs were poorly incorporated by macrophages. Tumors and metastatic cells from breast cancer xenografts were targeted *in vivo* in a nude mouse model. LHRH-SPION specifically accumulated in cells of human breast cancer xenografts. In collaboration with Prof. Soboyejo of Princeton University, sub-cellular accumulation of LHRH-SPIONs was investigated using high resolution TEM analysis. The amount of LHRH-SPION in the lungs was directly dependent on the number of metastatic cells and amounted to 77.8 pg Fe/metastatic cell. In contrast, unconjugated SPIONs accumulated in the liver, showed poor affinity to the tumor, and were not detectable in metastatic lesions in the lungs. LHRH-SPION accumulated in the cytosolic compartment of the target cells and formed clusters. LHRH-SPIONs did not accumulate in livers of normal mice. In conclusion, LHRH conjugated SPIONs

may serve as a contrast agent for MR imaging *in vivo* and increase the sensitivity for the detection of metastases and disseminated cells in lymph nodes, bones and peripheral organs. For more information read the publication: *Breast Cancer Research and Treatment*, 99(2), 163-176, 2006. Using a first-of-its-kind x-ray microscope recently built for the Advanced Light Source (ALS) of the Lawrence Berkeley National Laboratory (Berkeley Lab), the morphology and chemical integrity of LHRH bound magnetite nanomaterials within the cancer cells is currently being investigated in collaboration with Dr. Carolyn Larabell. Dr. Larabell is the Head, National Center for X-ray Microscopy and also PBD Faculty Scientist, Department of Advanced Microscopies at UC San Francisco. She is carrying out the experiments which will help us to understand how the LHRH-SPIONs are interacting within the cancer cell through utilization of nanotomography experiments.

In collaboration with Prof. Warren Warren of Duke University, where Intermolecular multiple quantum coherence (iMQC) imaging which is a new advanced technique that provides information not available from conventional MR imaging has been developed, LHRH-SPIONs were

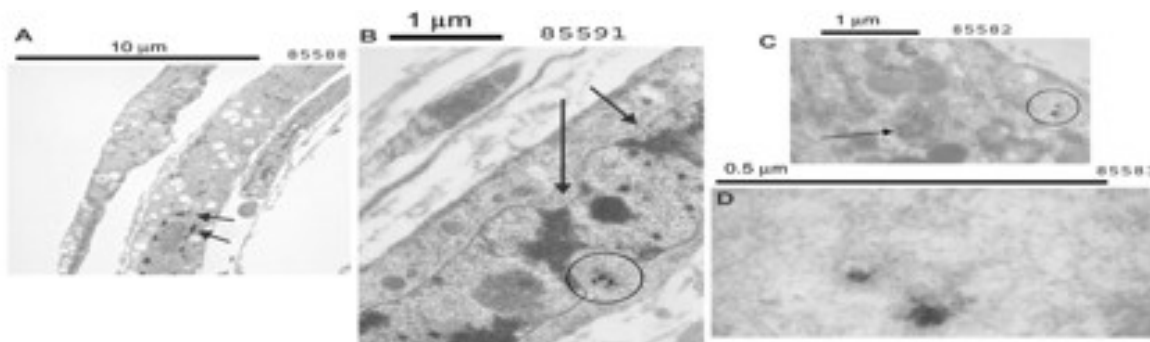


a) *in vivo* axial spin echo image of the mice breast tumor; b) *in vivo* iDQC image; c) *in vivo* iDQC anisotropy map image; d) post mortem iDQC anisotropy map image

tested for their ability to enhance contrast in MRI. Mice were first inoculated with human breast cancer cells. After the tumor vascularization the mice received an injection of LHRH-SPION (luteinising hormone-releasing hormone-

conjugated superparamagnetic nanoparticles). Standard spin echo and a series of three in-

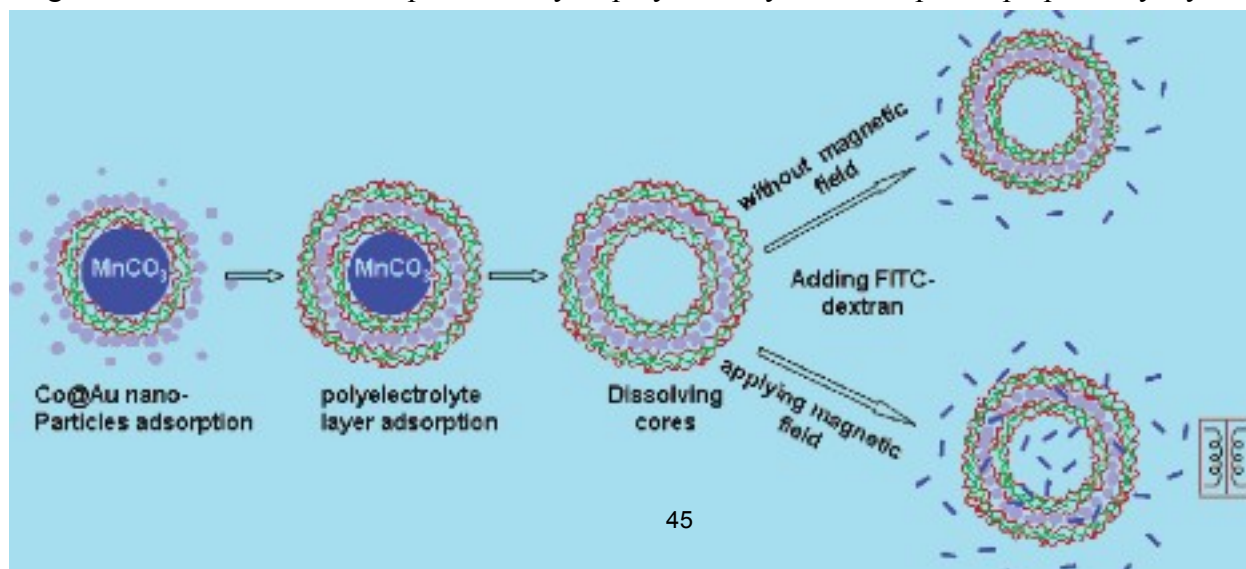
termolecular double quantum images (iDQC) were acquired *in vivo* and *post mortem*. The combination of three different iDQC images (with the correlation gradient pointing in three orthogonal directions) gave us the anisotropy map. The figure shows *in vivo* standard spin echo and the iDQC anisotropy map images. The iDQC anisotropy image shows an interesting new feature: tumor region highlighting. From theoretical derivations regions of high intensity signal correspond to regions of high anisotropy. An example of high anisotropy region is tumor masses which will be emphasized using this methodology, therefore improving MRI soft tissue characterization.



Transmission electron microscopy of BMVECs in culture after treatment with copper-cobalt nanoparticles. Panel A shows cell injury indicated by numerous vacuoles within cells and condensed, nuclear chromatin as indicated by arrows. Panel B shows detail of condensed, nuclear chromatin (arrows), and possible nanoparticle aggregates within another cell as indicated by the circled area. Panel C shows another cell with cobalt nanoparticle aggregates (circled) and nearby mitochondria shown for size perspective (indicated by arrow); circled area of nanoparticle aggregates is shown magnified in Panel D. Magnification of each micrograph is indicated by scale bar

As a part of a just-concluded DARPA funded project, the nanofabrication group collaborated with Prof. Mark DeCoster of LSU Neurosciences, New Orleans to evaluate potential toxic effects of magnetic nanoparticles on brain tissues and cells. It is expected that brain microvascular endothelial cells (BMVECs), and also brain astrocytes, could be exposed to nanoparticles introduced to the periphery of the animal or person as they are the cells which line the brain's blood vessels. These cells might therefore be the first brain cells to suffer toxic exposure to nanoparticles. Consequently, determining the potential toxicity of magnetic and metals-based nanoparticles will be important for further guiding development of these materials for effective biomedical applications. This collaborative effort led to investigation of the effect of cobalt core metal shell and other types of magnetic nanoparticles on BMVECs and brain astrocytes in vitro. The cytotoxicity of cobalt and metal protected cobalt particles using gold or copper shells were compared. While cobalt (oxidized) and gold shell cobalt nanoparticles were found to be non-toxic at 25  $\mu\text{g/ml}$ , non-oxidized cobalt, copper shell cobalt, and copper nanoparticles were significantly toxic to BMVECs and astrocytes. The biocompatibility of cobalt core gold shell magnetic nanoparticles may therefore lead to development of future biomedical tools.

In collaboration with Prof. Yuri Lvov of Institute for Micro manufacturing, Louisiana Tech University, Ruston and Prof. Leuschner of PBRC a novel magnetic nanoparticle-based drug delivery system for controlled release is being developed. As a proof of concept, We explored using a magnetic field to modulate the permeability of polyelectrolyte microcapsules prepared by layer-





by-layer self-assembly. Ferromagnetic gold-coated cobalt (Co@Au) nanoparticles (3 nm diameter) were embedded inside the capsule walls. The final 5  $\mu\text{m}$  diameter microcapsules had wall structures consisting of 4 bilayers of poly(sodium styrene sulfonate)/poly(allylamine hydrochloride) (PSS/PAH), 1 layer of Co@Au, and 5 bilayers of PSS/PAH. External alternating magnetic fields of 100-300 Hz and 1200 Oe were applied to rotate the embedded Co@Au nanoparticles, which subsequently disturbed and distorted the capsule wall and drastically increased its permeability to macromolecules like FITC-labeled dextran. The capsule permeability change was estimated by taking the capsule interior and exterior fluorescent intensity ratio using confocal laser scanning microscopy. Capsules with 1 layer of Co@Au nanoparticles and 10 polyelectrolyte bilayers are optimal for magnetically controlling permeability. A theoretical explanation was proposed for the permeability control mechanisms. "Switching on" of these microcapsules using a magnetic field makes this method a good candidate for controlled drug delivery in biomedical applications. For more information see *Langmuir*, 21(5), 2042-2050, 2005.

Infection is a dangerous complication that can develop after placement of a prosthesis. If the infection goes untreated, it may require additional surgery to replace or even remove the prosthesis completely. Current treatment for serious infections is usually administered systematically through intravenous means or by injection which can then be followed by further surgery. However, systematic dosages are limited by drug toxicity at high concentrations. Higher concentrations of an antibiotic would be beneficial if administered locally where it is needed. In collaboration with Prof. Cato Laurencin of Department of Orthopaedic Surgery, University of Virginia, Charlottesville, VA, Dr. Challa Kumar has obtained a seed funding from National Academy of Sciences, Keck Foundation to investigate, by means of an alternating magnetic field, the controlled release of the antibiotic gentamicin; which will be regulated to turn on and off as needed. The antibiotic will be loaded into microspheres containing magnetic nanoparticles that alter sphere permeability in response to the magnetic field. The magnetic switching of the particles will allow for complete conservation of the drug when no infection is present as well as immediate delivery when required. These microspheres will be immobilized in a poly(ether-etherketone) (PEEK) film and deposited in a thin layer on the surface of a prosthesis. Release from this compound layer will be compared to release of drug loaded directly into the PEEK film. The PEEK film itself also contributes to improvement of the structural-tissue interface as it has been shown to be biocompatible, is nondegradable, and is also wear resistant for joint replacement applications. Modeling of the system will begin with the mathematical description of how the drug reaches its target. This is accomplished by modeling the interaction and diffusion of gentamicin from the device into surrounding tissue. A second step in the modeling process will be to describe the relationship between the magnetic field parameters and how the drug is released.

## II.E Clinical Science

### II.E.1 Auger Electron Radiotherapy and Dosimetry

A collaboration of LSU Medical Physics, MXISystems (Fairview, TN), and CAMD personnel under the leadership of Kenneth Hogstrom (LSU) begun in 2005 continues to study monochromatic Auger electron radiotherapy, dosimetry, and treatment planning as well as monochromatic x-ray imaging in medicine. This work has been done on the tomography beamline at CAMD. The tomography beamline receives light from the 7 T superconducting wavelength shifter and can provide either monochromatic light or "white light" (all wavelengths).

The researchers first sought to characterize the monochromatic beam to provide physical data for theoretical calculations and designing future experiments. Beam data include beam intensity, mean energy, spatial distribution, and beam divergence. Two independent methods were used to measure the mean energy of the beam: Compton spectroscopy and powder diffraction (crystallography). At several monochromator settings between 15-40 keV, results from both methods and the expected output from the monochromator were in adequate agreement verifying both the accuracy of the monochromator control and our ability to measure the beam's mean energy.

They then measured the spatial distribution and angular divergence of the beam using GAFCHROMIC<sup>®</sup> film. Spatial distribution of beam intensity (pixel values) was shown to decrease by an average of  $7.2 \pm 1.1\%$  from left to right across the full 3 cm beam width and remain relatively constant across the approximately 1 mm height of the well-collimated beam. Beam divergence, measured from films spaced a known distance apart, was shown to be less than 2.5 mrad horizontally and less than 0.5 mrad vertically.

Beam intensity and fluence rate were calculated from Compton scattering data, ion chamber measurements, and film measurements for narrow and broad x-ray beams. Table 1 shows the Compton scattering results for the average of multiple measurements made at scattering angles from 15-60°. The incident fluence was calculated from the number of photons scattered into our detector and the Klein-Nishina collisional cross section for polarized incident radiation. Ion chamber results were calculated using the ideal narrow beam relationship between fluence and dose from extrapolated phantom surface doses on measured depth versus dose curves. Measurements showed the photon fluence rate in the beam ranged from  $1 \times 10^{11}$  photons·cm<sup>-2</sup>·s<sup>-1</sup> to  $2 \times 10^{11}$  photons·cm<sup>-2</sup>·s<sup>-1</sup> per 100 mA of ring current at beam energies near 35 keV (suitable for reaching the iodine K-edge in DNA-incorporated IUdR to initiate Auger electron cascades).

FLUENCE (PHOTONS·CM <sup>-2</sup> ·S <sup>-1</sup> ) PER 100 MILLIAMPS BEAM CURRENT			
<i>Experiment Date</i>	<i>Energy [keV]</i>	<i>Compton Spectroscopy</i>	<i>Ion Chamber</i>
August 21, 2006	40.7 ± 0.5	$1.37 \pm 0.2 \times 10^{11}$	$1.82 \times 10^{11}$
September 18, 2006	25.4 ± 0.5	$1.56 \pm 0.2 \times 10^{11}$	$1.30 \times 10^{11}$
September 19, 2006	35.8 ± 0.5	$1.73 \pm 0.2 \times 10^{11}$	$1.97 \times 10^{11}$
November 11, 2006	35.0 ± 0.5	N/A	$1.96 \times 10^{11}$
December 2, 2006	35.0 ± 0.5	$1.19 \pm 0.1 \times 10^{11}$	N/A

**Table 1:** Results for narrow beam fluence measurements.

The X-ray dosimetry involved (a) Measurement of the central-axis dose versus depth for a broad beam ( $3 \times 3 \text{ cm}^2$ ) in a homogeneous plastic phantom (PMMA) and in inhomogeneous phantoms (PMMA, bone-equivalent plastic, and lung-equivalent plastic) for dose intercomparisons between measurements (ion chamber, radiochromic film) and Monte Carlo calculations. (b) Verification of dose distributions in phantom simulations of small animals as preparation for future animal trials.

To do this a broad beam was created by vertically oscillating the irradiation target through a well-collimated, 0.9-mm height beam using a motorized screw-drive stage under computer control. Beamline collimation limits the useable beam width to 2.75 cm. Radiochromic film measurements showed that spatial and dose distributions are uniform within the broad beam generated in this fashion with the expected horizontal falloff noted above. Broad-beam, central-axis depth-dose measurements were made in a homogeneous plastic phantom (PMMA) and inhomogeneous phantoms (PMMA and bone plastic, PMMA and lung plastic) using radiochromic film and ion chamber dosimetry. Results comparing ion chamber and film depth-dose curves are shown in Figure 1

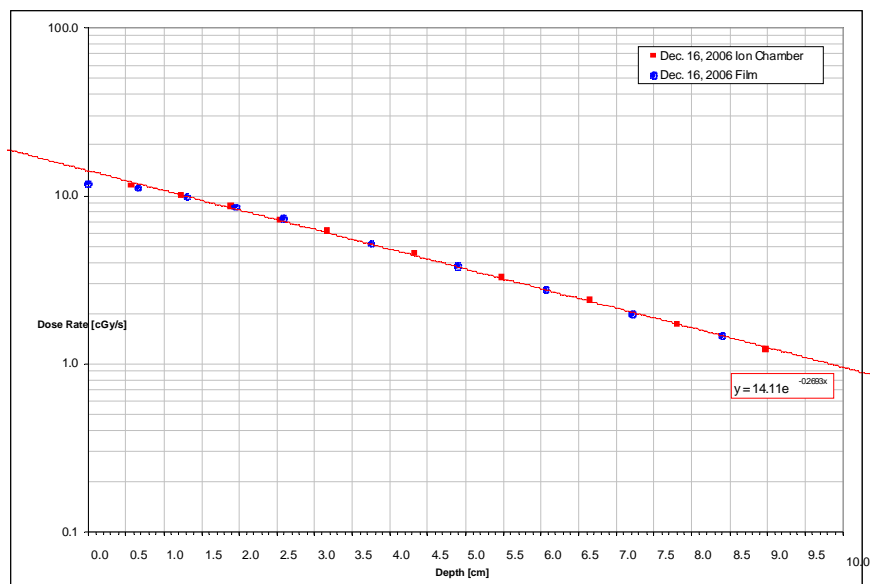


**Figure 1:** Depth dose measurements with film and ion chamber for broad beam geometries. Dose rates are given for within the narrow beam used to create the irradiated area.

Using the beam measured beam properties, the beam specifications and phantom geometry have been modeled using the MCNP5 Monte Carlo. Comparisons between Monte Carlo generated and measured dose distributions are currently being performed.

The idea behind Auger electron radiotherapy is to use radiation at an absorption edge of an element, such as iodine, which can be specifically added to the target organ. The added element will produce Auger electrons when it absorbs x-ray photons. These electrons are low energy (*i.e.* short range) so they only damage and kill the cells in the target organ. Measurement of the dose-response of Chinese hamster ovary (CHO) cells

with and without DNA-incorporated IUdR (iodo-deoxyuridine) serves as a validation of the potential dose enhancement resulting from Auger electron radiotherapy.

The dose-response of CHO cells was measured by irradiating monolayers of log-phase cells at doses

from 1 to 8 Gy using 35 keV x-rays. Clonogenic assays were performed at the Pennington Biomedical Research Center by MarieVarnes in collaboration with Carola Leuschner's laboratory. Irradiated cells were plated, incubated, and allowed to grow for 1 week. Cells were then fixed and stained with crystal violet (Figure 2); colonies of 50 or more cells were scored as survivors. Survival curves, (cf. Figure 3) are consistent with previously published data. This result indicates that we should soon be ready to commence experiments incorporating IUdR into the growth medium of the cells prior to irradiation in order to evaluate the amount of iodine uptake into the DNA and the attainable dose enhancement resulting from Auger electron radiotherapy.

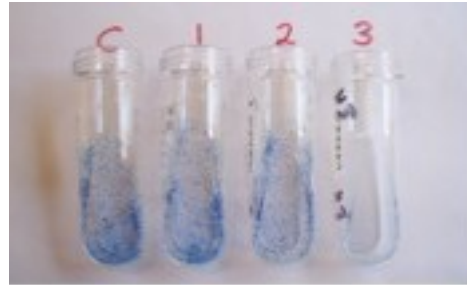


**Figure 2:** Growth of cell colonies after 1 week of incubation from cells irradiated with 0 Gy (C), 1 Gy (1), 2 Gy (2) and 4 Gy (3).

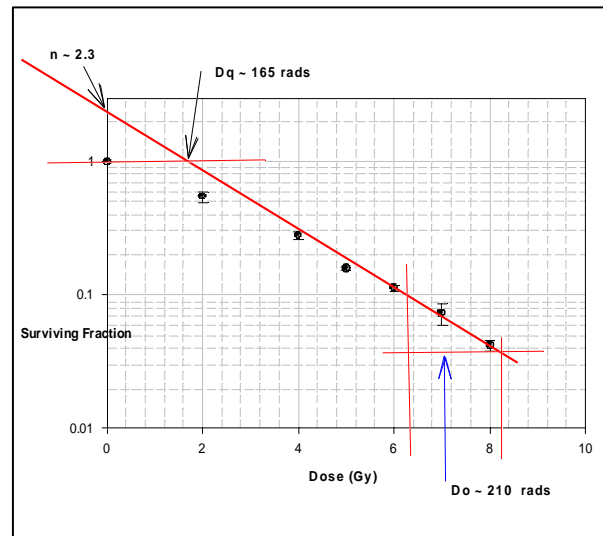


**Figure 3:** CHO dose-response from Dec. 16, 2006.

## II.E.2 Development of LHRH-SPIONs as Novel Contrast Agents for MRI of Tumors and Metastases

CAMD's Nanofabrication Group has been collaborating with Pennington Biomedical Research Center in developing LHRH-SPIONs as novel contrast agents for MRI for sensitive detection of primary as well as metastatic tumor cells. See for more information the following publications: Carola Leuschner et al., *Breast Cancer Research and Treatment* (2006), 99(2), 163-176 and Jikou Zhou et al., *Biomaterials* (2006), 27(9), 2001-2008. As a part of these investigations, LHRH-SPIONs of different sizes and shapes are being synthesized and characterized using CAMD's synchrotron radiation based X-ray absorption spectroscopy. One of the key questions that remain unanswered is how these particles behave within the cancer cells in comparison with normal cells. This is where the utility of X-ray microscopy comes into play.

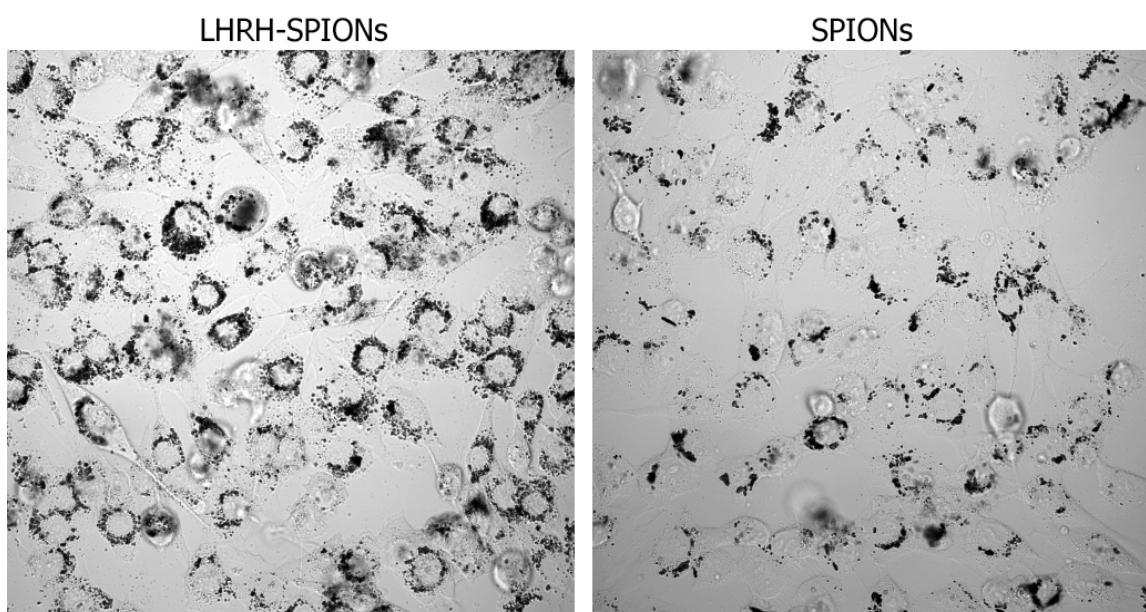


**Figure 1:** Scanning Transmission X-ray Microscope (STXM) images of cells treated with SPIONs with and without LHRH attached

X-ray microscopy, which can bridge the gap between light and electron microscopy, is an emerging new technology that will expand the existing imaging toolbox for cell and molecular biologists and biomedical nanotechnologists. A first-of-its-kind x-ray microscope recently built for the Advanced Light Source (ALS) of the Lawrence Berkeley National Laboratory (Berkeley Lab) offers the promise of studying the impact of nanomaterials within biological cells. Using these state of the art techniques, the morphology and chemical integrity of LHRH bound magnetite nanomaterials within the cancer cells are currently being investigated in collaboration with Dr. Carolyn Larabell. Dr. Larabell is head of the National Center for X-ray Microscopy and also a PBD Faculty Scientist, Department of Advanced Microscopies at UC San Francisco. Her lab is carrying out experiments which will help us to understand how the LHRH-SPIONs interact within the cancer cell. This understanding is crucial not only to gain fundamental knowledge of the behavior of nanoscale magnetic materials within cancer cells but also to complete product development for commercialization of this new class of contrast agents.

Results from initial experiments using STXM are shown in the figure given above. The images show the comparative perinuclear accumulation of the LHRH-SPION particles and SPIONs in MDA-MB-435S human breast cancer cells detected using STXM. It is clear from the images that a larger number of LHRH-SPIONs enter the cancer cells than SPIONs alone. The STXM can't do tomography and nanotomography investigations will be carried out once the new x-ray microscope at the ALS is commissioned.

## II.F.1 MEMS/LIGA Services at CAMD

### Summary

The MEMS/LIGA Service Group at CAMD has continued to provide a multitude of MEMS related services to the MEMS community, primarily at LSU, but also the wider LIGA community in the world. Besides well-established routine services including thin film deposition, X-ray masks, optical and X-ray lithography (print-shop), electroplating of Ni, Ni-Fe, Cu, and Au, mold insert fabrication, and hot embossing the group also offers novel capabilities including thick SU-8 patterning and UDXRL patterning at the CAMD wiggler. Nano-composite materials and nano-size lithographic patterning have been explored and further improved. These R&D efforts were inspired by interacting with customers and understanding their process and application requirements as well as the desire to establish internal R&D projects with focus on meeting requirements of future applications, and generating new funding opportunities.

In addition the service group focused on writing proposals to enhance the existing process equipment process infrastructure expanding capabilities and better meet future R&D demands.

The following contributions briefly summarize service and beamline statistics, the enhancement activities, and some of the ongoing R&D efforts.

### Overview of currently provided microfabrication services

Tables 1 and 2 summarize the base processes and process modules offered by the MEMS/LiGA Services Group at CAMD. All services are offered to customers on a pay basis. These services are mostly comparable to the ones offered in 2004 and 2005<sup>1</sup> with some minor adjustments marked at the bottom of each table.

**Table 1:** Services provided by the CAMD Service Group in 2006

Service Type	Materials	Specifications	
<b>E-beam deposition</b>	Cr, Au, Cu, Ni, Ti	0-2000 Å	
<b>Surface modification</b>	Ti oxidation	2 µm	
<b>Printshop (X-ray exposure)</b>	PMMA	1-2000 µm	
	SU-8 <sup>(1)</sup>	1-3000 µm	
<b>Electroplating</b>	Ni	1-5000 µm	
	Cu	1-500 µm	
	Au	1-100 µm	
	Ni-Fe	1-500 µm	
<b>Hot-embossing</b>	PMMA, PC	CD > 10 µm Aspect-ratio 10:1	
<b>Flycutting</b>	PMMA, SU-8	50 µm – any	
<b>Metrology:</b>			
	<b>SEM</b>	Any	< 4" DIA
	<b>EDAX</b>		
<b>WYKO</b>	Any	Any	

<sup>(1)</sup>SU-8 substrates are to be provided by customer, CAMD is not offering application of thick (>500µm) SU-8 resists at this time.

<sup>1</sup> Y. Desta et al: 'MEMS/LIGA Services at CAMD in 2004', CAMD Annual Report 2004. J. Goettert et al: 'MEMS/LIGA Services at CAMD in 2005', CAMD Annual Report 2005.

**Table 2:** Process modules offered by the CAMD Service Group in 2006

Module Type	Materials	Specifications
UDXRL Substrates	PMMA	100-2000 $\mu\text{m}$
X-ray masks	Au on Be, C, SiNx, or Kapton	5-40 $\mu\text{m}$ Au thickness, 5 $\mu\text{m}$ CD
Mold inserts	Nickel	5 $\mu\text{m}$ CD, 4"-6" DIA
	Brass (machined) <sup>(1)</sup>	20 $\mu\text{m}$ CD

<sup>(1)</sup>Machined mold inserts made from Brass is a rapid prototyping service provided through CBM2/Jason Guy; while evaluating the customer's design and specification CAMD staff is recommending the most suitable fabrication approach to make a mold insert. Precision machined mold inserts are especially attractive for microfluidic applications and design iteration but are typically limited to Aspect Ratios (AR) <4.

**Table 3:** Summary of service jobs completed in 2006 and compared with service jobs in 2006

Service type	Customers	Number of Jobs 2006	Number of Jobs 2005
Thin film deposition	LSU, Industrial	389 (993 substrates)	519 (1591 substrates)
Surface modification	LSU, Industrial	258	NA
UDXRL Substrates	Industrial	5 (116)	5(27 substrates)
X-ray masks	LSU, Industrial	12	21
Mold inserts	LSU, Industrial	75 (2 LiGA)	4
Electroplating	LSU, Industrial	12 (211)	46 (112 substrates)
X-ray Exposure	LSU, Industrial	592 substrates	598 (661 substrates)
Hot embossing	LSU, Industrial	75 (950)	57(930)
Metrology	LSU, Industrial	10 (71 samples)	30 (105 samples)
Fly cutting	Industrial	20 (162 substrates)	22 (191 substrates)
Polishing	Industrial	4 (20 substrates)	4 (16 substrates)

Overall the number of service jobs remained constant indicating a stable demand for MEMS services provided by CAMD. It should be noted that new customers for microfluidic applications could be attracted through collaboration with CBM<sup>2</sup>. Most of their current needs can be satisfied by micromachining and molding and do not need (at least initially) lithography based services. This account partly for the dramatic increase in mold inserts fabrication.

### User statistics – X-ray lithography exposures

The two charts in Fig. 1 represent the distribution of exposed substrates (left) and exposure dose (right) from different user groups (CAMD, External, LSU) at all four lithography beamlines for 2006. The user groups include CAMD with currently one major project (accounting for approx. 60% of the CAMD substrates and funded through DARPA-MTO, MGA project; for details see



contribution from A. Bhushan and D. Yemane in Sect II.F.2) and 4 smaller projects, while external print-shop users include HT Micro, Mezzo, and Creatv Inc and LSU users are from Mechanical (2 professors) and Chemical (1 professor) Engineering at LSU.

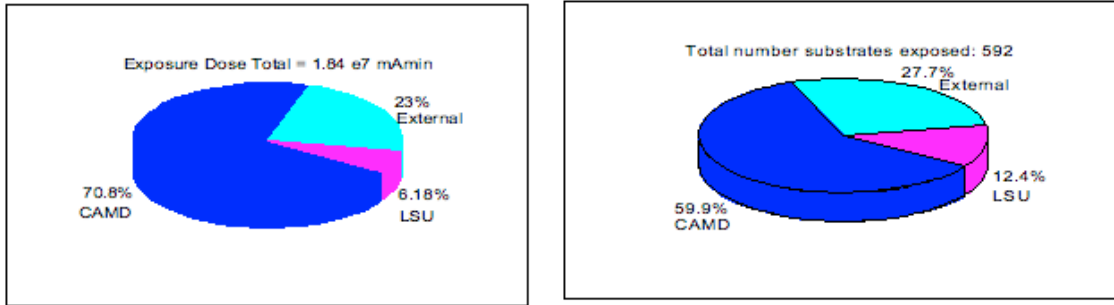


Figure 1: Distribution of the total number of substrates (left) and exposure dose (right) for all beamlines among the three main user groups – CAMD, LSU professors and students, and external, industrial customers. The total number of substrates was 592.

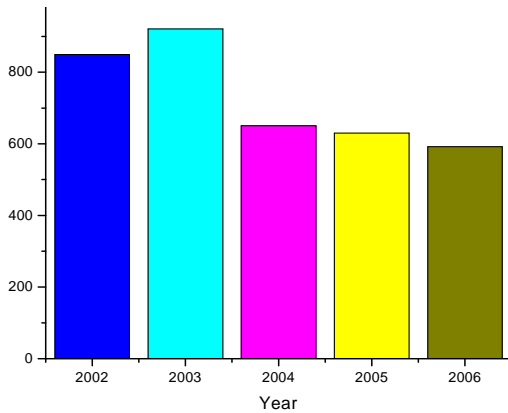


Figure 2: Total numbers of substrates exposed in the last 5 years at all beamlines.

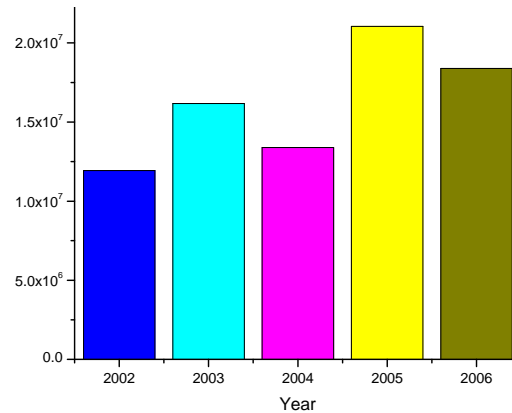


Figure 3: Total exposure dose in the last 5 years accumulated at all beamlines.

When comparing these numbers with previous years (Figs. 2 and 3) the following observations can be made:

- The higher numbers of exposed substrates in 2002 and 2003 was stimulated through CAMD research projects funded through DARPA. After 2004 the number stabilized around 600 substrates per year.
- The trend for total exposure dose is slightly increasing over time. This indicates a desire for longer exposures per substrate caused by thicker resists/taller structures and larger mask areas/larger scanning distance. This also reflects an improvement in technology as we are now able to fabricate X-ray masks with large open areas (80mm) as well as patterning thick resist layers beyond 500 $\mu$ m thickness.

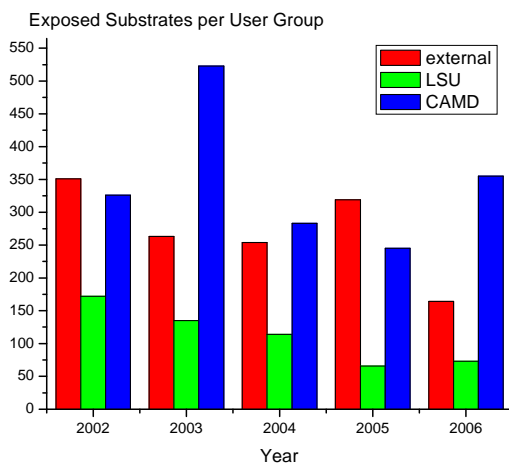


Figure 4: Number of substrates exposed by the main user groups over the past 5 years.

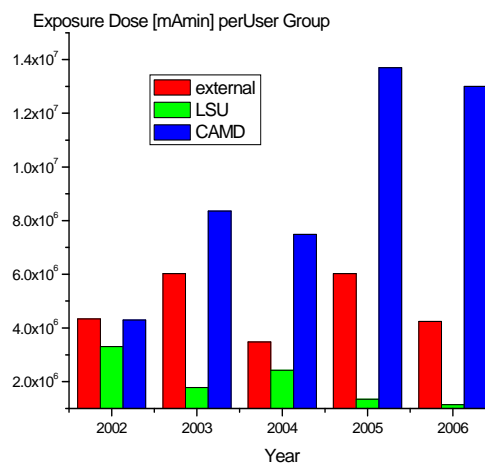


Figure 5: Exposure dose accumulated by the main user groups over the past 5 years.

While these overall trends demonstrate a certain stability of operation and a reasonable interest in using LIGA technology a closer look at the three main user groups shown in Figures 4 and 5 leads to the following observations:

- The number of substrates from LSU users is decreasing somewhat continuously over the past 5 years; there is mainly one active user (E. Podlaha, Chem. Eng.) who uses X-ray lithography to pattern templates for plating tests; all other users choose alternative approaches (micromachining, optical lithography) and only turn to x-ray lithography when in need of highest quality.
- The external users experienced a dramatic dip (~50%) in 2006 mainly because HT Micro – the leading customer in 2005 – had significantly fewer substrates to expose. However, the exposure dose didn't decrease at the same rate indicating the need to expose thicker substrates.
- The CAMD portion increased primarily because of the demand for GC samples needed for column coating and chromatography tests; however, due to process optimization the exposure dose for these samples could be reduced.

In conclusion, x-ray lithography capabilities are under-utilized and find fewer and fewer users. The LSU community in particular seems to shy away from this technology and favors alternative options, namely micromachining and molding. This approach is certainly appropriate for many microfluidic applications, a focus of researchers at LSU's CBMM center. CAMD researchers have become the main user group and strong efforts and good progress are present when funding is available. Smaller research efforts (see contribution by Jost Goettert *et al.* in this report) are ongoing and are stimulated by customer interest but cannot be pursued with high priority due to a lack of funding.

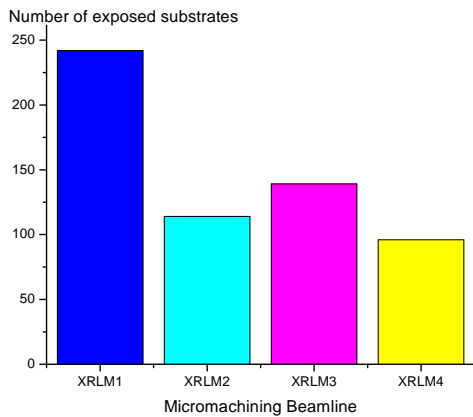


Figure 6: Number of substrates exposed at the CAMD micromachining beamlines.

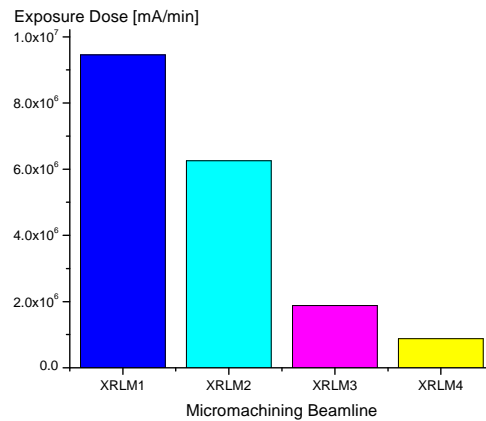


Figure 7: Accumulated exposure dose at the CAMD micromachining beamlines.

Data from Figures 6 and 7 provides closer look at the amount and nature of the use of the four beamlines:

- XRLM1 exposes the majority of substrates and provides the highest accumulated dose; this is mainly due to the versatility of this beamline allowing a switch between a soft x-ray spectrum and the regular bending magnet spectrum by inserting two mirrors into the beam; demand for the soft x-ray photons arose from projects associated with micrometer down to sub-micrometer structures.
- XRLM 2 and 3 expose approx. the same number of substrates; however the exposure dose at XRLM 2 is ~3x higher as this beamline is used for thicker substrates (longer exposure times) and larger scan range (larger mask areas); it should be noted that XRLM 2 could easily accommodate all exposure requests for both beamlines.
- There is an increasing interest in hard x-ray radiation for UDXRL samples which are now available at the DEX 3 scanner (modifications of the substrate fixture and cooling circuit resulted in stable, reliable exposure conditions); however, despite the increased resist thickness (typ. 1-1.5mm) exposure dose is low as the wiggler spectrum is harder and overall power output is significantly higher. There is certainly opportunity to provide more print-shop services at this beamline in the future.

In conclusion, the CAMD microfabrication group should consider reducing the number of operating micromachining beamlines from 4 to 3 (XRLM 1 and 4 and either XRLM 2 or 3). There is a need for a versatile exposure spectrum using the mirror option or the wiggler source. There is a growing interest for smaller (sub-micrometer) structures requiring soft x-ray lithography (applications include for example photonic crystals, RF MEMS devices, and filter structures for microfluidic applications) and an interest in very tall structures patterned by hard x-rays from the wiggler beamline. It should also be noted that process improvements (meaning R&D) are needed to establish a standard service in these areas. For example, patterning of ultra-thick resist structures needs systematic studies on dose and development parameters to ensure the desired structure quality for PMMA and there is always interest in reducing exposure dose by replacing PMMA with the more sensitive SU-8 resist (see contribution J. Goettert *et al.* in this report).

## Enhancement proposals

The Louisiana Board of Regents (BoR) provides annual funding opportunities for enhancement of infrastructure. The CAMD microfabrication group regularly submits proposals for equipment that is of interest to a larger user community and allows the microfabrication community to stay on the cutting edge of R&D infrastructure and capabilities.

The following proposals have been submitted in 2006. The abstract for each proposal is included and further details can be requested from the PI directly.

Biocompatible Coating (Parylene) Deposition System.  
(P.I. V. Singh, funds requested \$98,690)

Analytical equipment for *in-situ* detection in MEMS and NEMS systems.  
(P.I. C. Kumar, funds requested \$134,686)

## II.F.2 Applications

The following examples describe some of the ongoing research projects in the CAMD microfabrication group. They are summarized in no particular order in the form of brief abstracts or reports. It should be mentioned that the efforts can be grouped into two major categories that supplement each other and greatly benefit from the expertise and knowhow of the microfabrication staff/researchers – efforts towards MEMS and NEMS system development, and improvement and expansion of existing microfabrication capabilities to better serve our users and enable novel applications. Because funding in MEMS and NEMS is increasingly provided for system solutions rather than process improvement future microfabrication efforts will need to shift in this direction. A first step is CAMD's participation in LSU's Center for BioModular Multi-Scale System (CBM<sup>2</sup>) in which CAMD's role is two-fold – as a provider of infrastructure and a supporter of process expertise, and as an enabler of business opportunities by transferring research results into marketable products/prototypes through its well-established service capabilities. These aspects are further discussed in chapter IV.E.

### Fabrication of High Aspect Ratio Nanostructures Using Soft X-Ray Lithography

Fabrication and development of submicron/nanostructures with high aspect ratios using soft x-ray LIGA has been revived in order to fabricate mold insert templates for Nano-Imprint-Lithography (NIL) efforts associated with CBM<sup>2</sup> (Prof. Sunggook Park). Novel methods and advances in nanotechnology have generated an ever increasing desire and need for such fabrication ability, highly relevant to nearly all fields of current research. Examples include biomimetry, or the artificial mimicking of natural biological submicron and nanostructures such as gecko foot hairs<sup>1</sup> or the Lotus effect<sup>2</sup>; environmental engineering, such as using fabricated photonic nanocrystals in thin polymeric films for the construction of photovoltaic cells to harness solar energy<sup>3</sup>; nanoelectromechanical systems or NEMS, an exciting new field innately derived from the popular microelectromechanical systems (MEMS) field.

One approach to make nanosize structures is using soft X-ray lithography initially developed to fabricate the next generation microelectronic chips<sup>4</sup>. While structure height for microelectronics is typically a few 100 nanometers the aforementioned applications require high aspect ratio submicron and/or nanosize structures. There are a number of ways of making these structures. For example nano-embossing of the fine probe tip of an AFM or STM is used to produce nano-scaled indentations into soft, impressionable substrates<sup>1</sup>. As with any embossing or molding method, difficulty in fabrication arises in releasing substrate from the molds without structural loss and without compromising structural precision, particularly when dealing with high aspect-ratio features. Electron or E-beam lithography is another method shown to produce very precise nanostructures in the lateral dimension. This approach has limitations regarding high aspect ratio structures requiring high electron energies (100keV) and exhibits feature broadening because of scattering. X-ray LIGA either used in a conventional shadow printing setup<sup>5</sup> or as interference lithography<sup>6</sup> method is another technique capable of achieving high precision submicron/nanostructures, and also may provide a cost effective solution for nanoscale patterning by copying many structures in parallel.

High aspect ratio submicron/nanoscale patterning of PMMA is accomplished with synchrotron x-rays at CAMD. The XRLM1 microfabrication beamline is equipped with a double-mirror sys-

tem which provides soft x-rays<sup>7</sup>. The patterning process utilized a silicon nitride membrane mask with gold absorber structures (posts) of 750 nm diameter fabricated by E-beam lithography<sup>5</sup>. The substrate for exposure was PMMA spin coated to approximately 4  $\mu\text{m}$  on a gold coated silicon wafer. The resulting PMMA structures are cylindrical posts with a diameter of 750 nm and a height of  $\sim 4 \mu\text{m}$  giving a high aspect ratio of 5. Wet development of the structures from unexposed PMMA may be problematic due to the tendency to stick together. In order to avoid this, a method was devised for developing without the use of liquids which will be further discussed. Subsequently, nickel electroplating around the post structures was done and as a final step the PMMA posts were dissolved. Figure 1 shows the top view of the LIGA structures. The diameter of each hole is 750 nm with a depth of 4  $\mu\text{m}$ .

Issues associated with high-aspect ratio nanostructure fabrication include 1) exposure doses using the XRLM1 double-mirror system, 2) the development of the structures and preventing sticking, and 3) nickel electroplating to achieve high uniformity and ease of handling of the fragile structures.

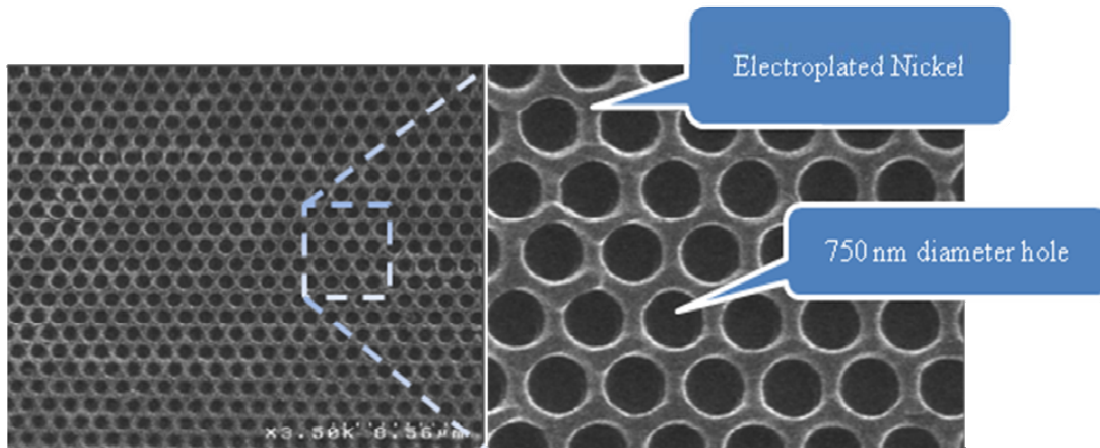


Fig. 1: SEM images of a wide view (left), and magnified view (right) of x-ray LIGA fabricated high aspect ratio nanostructures. Surrounded with electroplated Ni, the holes have a diameter of 750 nm at a depth of 4  $\mu\text{m}$ .

## References

1. Sitti, M. "High Aspect Ratio Polymer Mico/Nano-structure Manufacturing using Nanoembossing, Nanomolding and Directed Self-Assembly", Proceedings of the 2003 IEEE/ASME International Conference on Advanced Intelligent Mechatronics (AIM), 2003.
2. Blossey, R. (2003): *Self-cleaning surfaces - virtual realities* ; Nature materials 2: 301-306
3. Sinkkonen, J, Novikov, S, Ovchinnikov, V, Toivola, T. "Light Emission From Si/Sio<sub>2</sub> Nanostructures", 3<sup>rd</sup> World Conference on Photovoltaic Energy Conversion, May 11-18, 2003.
4. Cerrina, F. ; *X-ray Lithography* ; in : Rai-Choudhury, P. (Ed.) SPIE Handbook of Microlithography. Micromachining, and Microfabrication, Vol. 1 (1997), 251-320.
5. L. Wang, T. Christenson, Y.M. Desta, R.K. Fettig and J. Goettert; "High Resolution X-ray Masks for High Aspect Ratio MEMS Applications" Journal of Micromechanics and Microengineering, 14 (2004) S.722-26.
6. For more details on x-ray interference lithography check the PSI-Laboratory for Micro- and Nanotechnology webpage at <http://lmn.web.psi.ch/xil/intro.htm>.
7. For details see <http://www.camd.lsu.edu/beamlines.htm>

## Preliminary Studies of Thick SU-8 Laminate for Ultra-Deep X-ray Lithography

In the past various efforts have been reported to apply millimeter thick SU-8 as resist for ultra-deep X-ray lithography (UDXRL) applications<sup>1,3</sup>. Methods include multiple spin-coating, casting, and dry-chip casting<sup>3</sup>. A major challenge with these methods besides the time-consuming fabrication of the films is a non-uniform solvent content across the thick resist layer which affects patterning accuracy and structure quality. In comparison to these tedious efforts thick PMMA resists are built by bonding thick sheet material onto a substrate ensuring uniform material properties throughout the height.

F. Dawan, Z. Ling, and J. Goettert are collaborating with D. Johnson and W. Dai, of MicroChem Corp<sup>4</sup> which is developing a novel SU-8 formulation. This formulation is designed specifically for thick X-ray applications and is designed to be available in sheets in thicknesses up to several millimeters. The formulation contains added flexibilizing agents plus a reduced PAG concentration and is totally solvent-free. This novel material, XP MicroForm 4000NX, can be laminated at low temperatures and pressures directly onto most substrate materials and then rapidly processed. Because of the manufacturing process<sup>5</sup> the sheets potentially provide highest sheet-to-sheet consistency, excellent thickness uniformity without degradation from the baking process, and no requirement to bake or dry the films prior to use. Since the sheets are solvent-free there is no solvent gradient within the film which further improves the imaging process.

Initial X-ray lithography experiments on developmental laminated films were conducted at the XRLM 1 beamline using the CAMD bending magnet spectrum. Exposure and process parameters were screened in a range comparable with previous studies<sup>1</sup> (see Table 1). The results demonstrate the potential and also the remaining challenges of this new resist as illustrated in Figures 1-4. From the initial experiments it is evident that the low PAG concentration requires a slightly higher exposure dose (30-40J/cm<sup>3</sup>) and that a smaller top to bottom dose ratio (3:1) is advantageous for this resist formulation. Also adhesion needs to be further improved and the development for open (post arrays) and closed (hole arrays) structures patterned simultaneously must be optimized. Previously reported top-scum or skin was eliminated using a Kapton sheet placed between the resist and the mask preventing any unwanted exposure during the sample loading and also reduced secondary radiation caused by the mask.

### References

1. Y. Desta, H. Miller, J. Goettert, C. Stockhofe, V. Singh, O. Kizilkaya, Y. Jin, D. Johnson, W. Weber; *Deep X-ray Lithography of SU-8 Photoresist: Influence of Process Parameters and Conditions on Microstructure Quality*, Book of Abstracts, HARMST05, June 10-13, 2005, Gyeongju, Korea, pp. 70-71, 2005; June 2005.
2. Becnel, C; Desta, Y; and Kelly, K, *Ultra-deep x-ray lithography of densely packed SU-8 features: I&II*. Journal of Micromechanics and Microengineering, 2005(6): p. 1242.
3. Daniel Bernhardt; *Fabrication and structure-analysis of ultra-tall HARM made in SU-8 and PMMA*, Master Thesis Fachhochschule Gelsenkirchen (2003).
4. MicroChem Corp., Newton, Massachusetts. For more information about MCC resist products visit <http://www.microchem.com/index.htm> .
5. Johnson, D U.S. Patent Application.

Table 1: Summary of Experimental Parameters

Constant Parameters	Value	Variables	Value
Laminate SU-8	PAG 1%	Dose	Bottom dose from 15 – 60 J/cm <sup>3</sup>
Substrate	Si-wafer, Cr/Au	Dose ratio	3:1; 7:1
Exposure source	CAMD bending magnet; E <sub>c</sub> = 1.6 keV	PEB temperature	60°C, 95°C and 60 plus 95°C
Mask	250µm graphite, 80µm Au	PEB time	Range 5 – 40min
Developer	PGMEA at RT, beaker; time 60-150min	Relaxation after bake	Range 15hrs – 30hrs
Rinse	PGMEA/IPA		

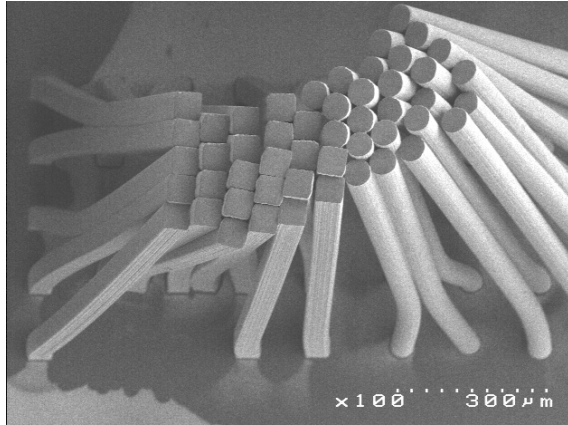


Fig. 1: Post array with ~20µm wide dimensions.

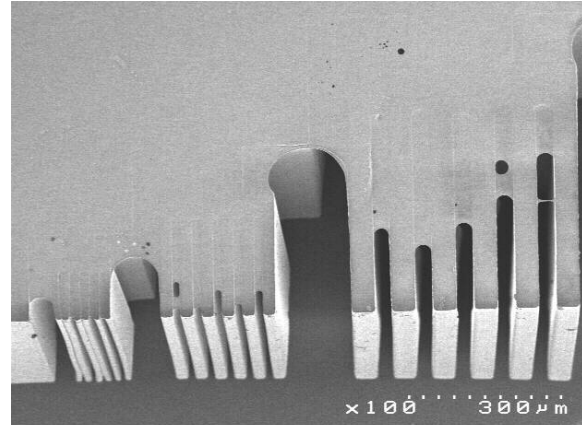


Fig. 2: Fork test pattern with smallest features of ~20µm

Figures 1 and 2: Samples have been prebaked after delivery to release any stress caused by transportation; the resulting structures appear ‘soft’ (Fig. 1, low dose 20J/cm<sup>3</sup>; Fig. 2, high dose 40J/cm<sup>3</sup>). The effect of pre-baking prior to exposure is not yet understood. The skin formation was caused by not placing a Kapton absorber between the mask and resist.

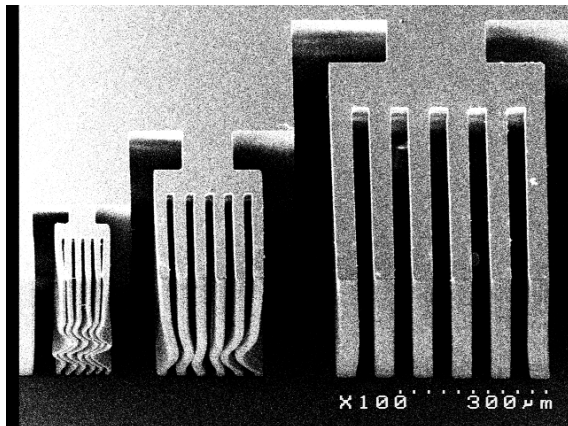


Fig. 3: Fork test pattern exposed with low dose (15J/cm<sup>3</sup>).

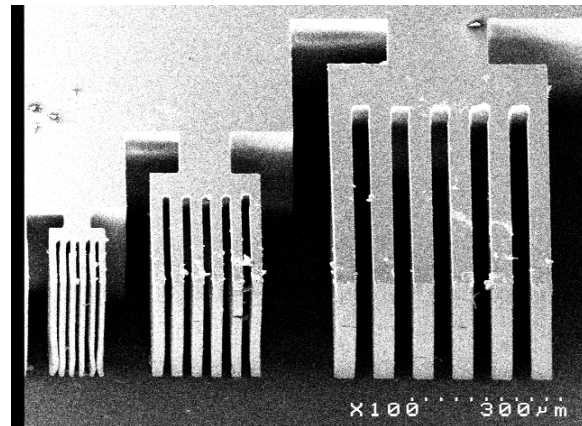


Fig. 4: Fork test pattern exposed with high dose (30J/cm<sup>3</sup>).

Figures 3 and 4: This sample has been exposed as received, exposure with 15 J/cm<sup>3</sup> (Fig. 3) and 30 J/cm<sup>3</sup> (Fig. 4) demonstrate improved structure stability; samples with even higher exposure doses were delaminated from the substrate and couldn’t be analyzed; skin was prevented by using a 50µm Kapton filter placed between the mask and resist.



## Mechanical and Optical Applications of Ultra-precise LIGA Microstructures

Direct LIGA fabrication combining precision patterning of PMMA and SU-8 microstructures using X-ray lithography with high-quality electroplating and advanced assembly and integration techniques offers a wide range of advantages for a number of applications in microfluidics, microoptics and precision microengineering.

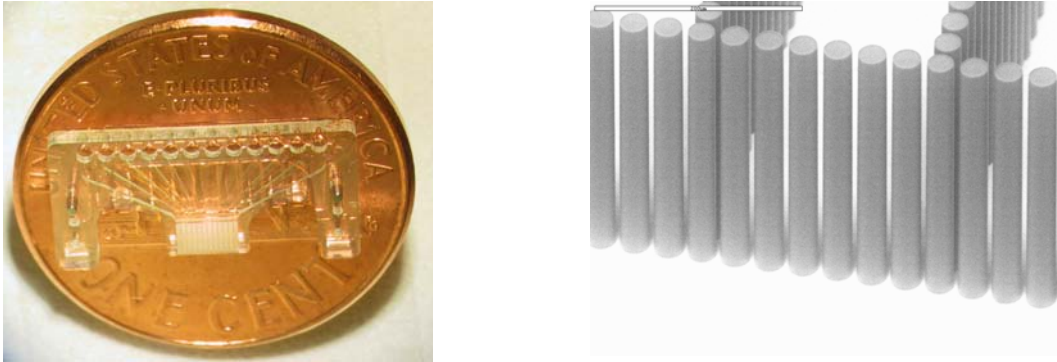
In the past years CAMD has supported HT Micro in its exploration of commercial opportunities which has fabricated prototype devices for a number of customers. Main efforts have been focused on the fabrication of LIGA structures with the ultimate pattern quality as well as high quality electroplated materials meeting the application requirements. These key issues require continued development on optimizing procedures and processes to ensure high repeatability and full control of structure properties<sup>1</sup>. In order to fully utilize this potential and also provide easy and convenient access to X-ray lithography capabilities CAMD provides a paid printshop and LIGA support service to customers like HT Micro. CAMD operates 4 beamlines with different exposure spectra and scanner capabilities to enable patterning of a variety of structures ranging from nanometer scale lateral features to millimeter in height<sup>2</sup>. It also provides professional user support via a so-called printshop service which allows customers to send masks and wafers and have CAMD experts perform the exposure process. Partnership and collaboration with CAMD is highly flexible and can include joint research projects, for example exploring new resist materials or improve process capabilities, or simply consists of services like exposing customer substrates with X-ray photons.

Z. Ling, and J. Goettert are working in collaboration with T. Christenson, and D. Elerath of HT Micro<sup>3</sup>, which is currently building prototype devices for a number of applications. As one example, a biofluidic interface structures is shown in Figure 1 comprised entirely of PMMA and fabricated by X-ray lithography. Within this component are 12 channels that feed 12 reservoirs “caged” in by PMMA pillars as shown in the detail photographs in Figure 1. The PMMA cage structures consist of rows of 30  $\mu\text{m}$  diameter cylindrical pillars with 300  $\mu\text{m}$  height that reside on 33  $\mu\text{m}$  centers resulting in rows of 3 x 300  $\mu\text{m}$  gaps. Another set of components, springs, combines precision patterning using deep X-ray lithography and electroplating of high yield-strength materials such as NiFe alloys<sup>4</sup>. By controlling precisely the structure features a simple spring-mass acceleration switch may be realized as shown in Figures 2. The spiral spring supports a ring which when accelerated will contact the outer rim or top (not shown) and bottom shoulder at a predefined acceleration threshold. Another example area includes micro-actuators where small, micrometer-wide working gaps can be maintained through relatively much larger thickness with overlap stroke dimensions of several hundred microns. When coupled with compliant springs resonant actuators can be built and applied to generate structured light sources for use in miniature confocal microscopes. Figures 3, left shows a microscope developed at the University of Arizona using an “optical bench” for alignment and support of miniature optics as well as resonant amplitude grating (right) that provides structured light into the microscope when illuminated from a dc source<sup>5</sup>.

### References:

1. T. Christenson, “X-ray-based fabrication” Micro-Nano Newsletter, Vol 10, No10, Oct 2005.
2. For details about the LIGA microfabrication beamlines see CAMD homepage at [www.camd.lsu.edu](http://www.camd.lsu.edu).
3. HT MicroAnalytical Inc, Albuquerque, NM. Further information about their products can be obtained from the HT MicroAnalytical webpage, <http://www.htmicro.com/>

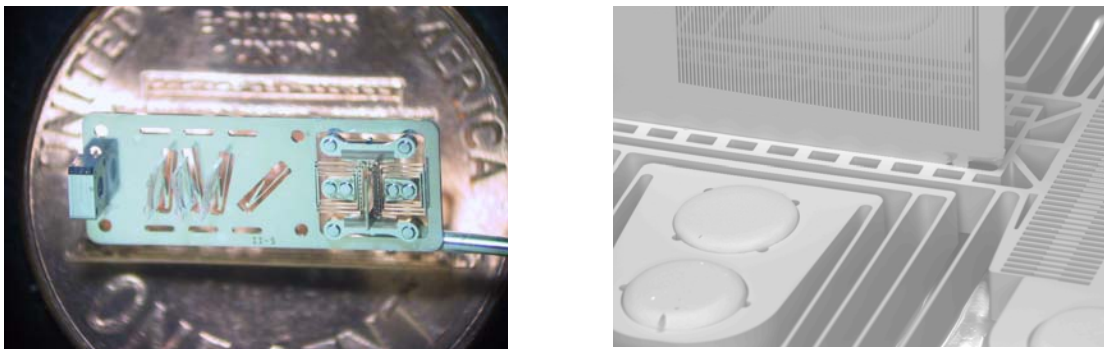
4. Schlossmacher, P., Yamasaki, T., Ehrlich, K., Bade, K., Bacher, W.; "Production and Characterization of Ni-based Alloys for Applications in Microsystems Technology", FZKA Nachrichten, 30 (1998), pp. 207-214.
5. T.S. Tkaczyk, J.D. Rogers, M. Rahman, T.C. Christenson, S. Gaalema, E.L. Dereniak, R. Richards-Kortum, M.R. Descour; "Multi-modal miniature microscope : 4M Device for bio-imaging applications – an overview of the system"; Proc. SPIE Vol. 5959, 2005, pp. 138-146.



Figs. 1: Examples of PMMA microfluidic devices made by X-ray lithography; interface chip bridging macro-fluidic connectors with microchannels (left), reservoir with flow filter structures (right).



Figs. 2: Precision mechanical switching devices made from NiFe alloy; acceleration switch (left) and acceleration sensitive latching surety components (right).



Figs. 3: Example of a micro-optical bench with integrated electrostatic actuator (left). A close-up view of the resonant actuator is shown in Fig. 3, right. The electrostatic comb drive is capable of resonating the grating at  $\pm 100 \mu\text{m}$  amplitude with 10 Volts with quality factors at atmosphere of over 50.

## Ultra-tall, High Aspect Ratio Metal Microstructures and Imaging Applications

Z. Ling, D. Yemane, V. Singh, and J. Goettert are working in collaboration with O.V. Makarova, C.M. Tang, and G. Yang, of Creatv MicroTech Inc.<sup>1</sup> to utilize x-ray lithography and electroplating to make exceptionally high quality, high-aspect ratio metal and composite microstructures used as x-ray anti-scatter grids and nuclear collimators for various optical, x-ray and  $\gamma$ -ray applications, or high-definition integrated circuit interconnects<sup>2-5</sup>. Depending upon the application microstructures with small lateral dimensions of a few tens of micrometers and heights up to 15 mm made from high Z material are required on areas as large as 70x70 mm<sup>2</sup>. Typically the devices are assembled from several layers of identical microstructures with individual thickness up to 1mm. CAMD provides X-ray lithography ‘print-shop’ services from various sources (white light and mirror light from a bending magnet, hard X-rays from a wiggler insertion device) and supports customers in their effort to improve and optimize the lithography and development fabrication steps<sup>5</sup>.

Recent progress in fabricating tall microstructures, up to 2 mm, with lateral dimensions as small as 25 $\mu$ m using the CAMD 7T wiggler light source<sup>6</sup> will be reported here. X-ray masks made from graphite substrates with up to 60  $\mu$ m thick Au absorber (see Fig. 1) define the initial structure and are made by thick SU-8 optical lithography and gold electroplating<sup>4,7</sup>. Substrates made from silicon and graphite are used and thick PMMA sheets (up to 3 mm) are glued to them using a PMMA/MMA glue. For x-ray lithography the CAMD wiggler beamline is used providing a hard x-ray spectrum with photon energies up to 40 keV. A DEX 3 scanner (Fig. 2) with efficient cooling for mask and substrate is used for pattern transfer. Process optimization of bottom dose and top/bottom dose ratio resulted in minimum bottom dose of  $\sim 3.8$  KJ/cm<sup>3</sup> for a 1.3mm tall structure and a dose ratio of less than 2.5:1. Development time could be significantly reduced by employing megasonic development without compromising the structure quality (see Fig. 3). Copper electroforming was performed using a copper sulfate plating bath. After electroforming, the copper microstructures along with the PMMA mold were released from the plating base by abrasive removal of graphite. Both sides of the copper microstructure were polished using aluminum oxide pads. Finally, the PMMA mold was dissolved in acetone, resulting in the finished freestanding metal part shown in Figure 4.

Collimators capable of higher resolution and optimized for greater sensitivity can significantly improve the imaging from  $\gamma$ -cameras used in planar scintigraphy of small animals for single-photon-emission computed tomography. The collimator under development is designed for <sup>125</sup>I high-resolution  $\gamma$ -camera. The desirable height of collimator of 5.5 mm will be achieved by stacking the appropriate number of copper layers using high precision alignment pins.

### References:

1. Creatv MicroTech Inc, Potomac, MD. For more details about their products visit Creatv’s webpage, <http://www.creatvmicrotech.com/>
2. O.V. Makarova, D.C. Mancini, N. Moldovan, R. Divan, C.-M. Tang, D.G. Ryding, R.H. Lee, *Sensors and Actuators A* **2003**,103, 182-186.
3. O.V. Makarova, D.C. Mancini, N. Moldovan, R. Divan, V.N. Zyryanov, C.-M. Tang, *Microsystem Technologies* **2004**, 10, 540-543.
4. O.V. Makarova, G. Yang, C.-M. Tang, D.C. Mancini, R. Divan, J. Yaeger, *Proc.SPIE* **2004**, 5539, 126-132.
5. O.V. Makarova, G. Yang, C.-M. Tang, *HARMST 2007*.
6. J. Goettert, P. Datta, Y. Desta, Y. Jin, Z. Ling, V. Singh, *IOP Journal of Physics: Conference Series* **34**

(2006) 912-918.

7. J. Goettert; "The LIGA Process ", in: W. Wang, S. Soper (Eds.) *Bio-MEMS: Technologies and Applications*, CRC Press (2006), 45-94.
8. R. Divan, D.C. Mancini, S.M. Gallagher, J. Booske and D. Van der Weide, *Microsystem Technologies* **2004**, *10*, 728-734.

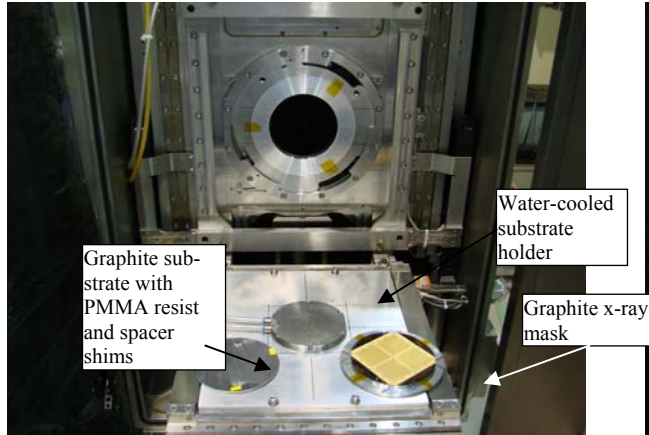


Fig. 1: Graphite substrate and mask inside the DEX3 scanner prior to assembling on a special, water-cooled substrate mount.

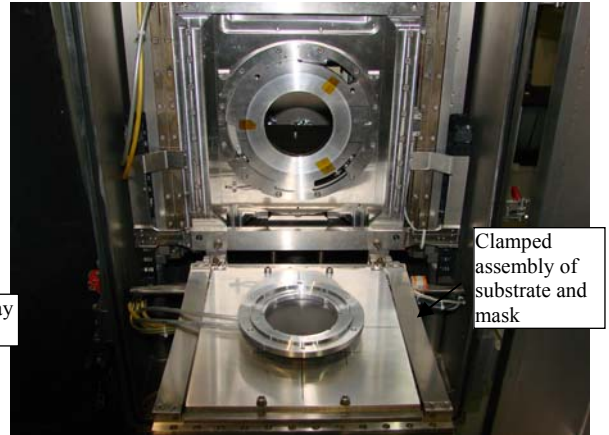


Fig. 2: Stack of substrate and mask clamped on scanner back plate before loading.

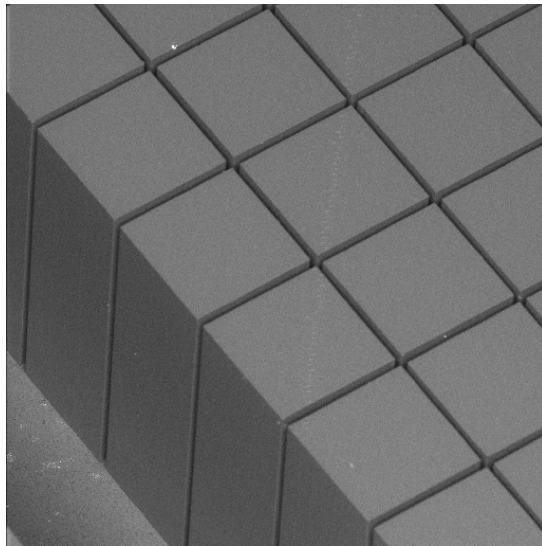


Fig. 3: SEM image of 1.5 mm deep and 25 μm wide microchannels in PMMA resist exposed at the CAMD wiggler beamline.

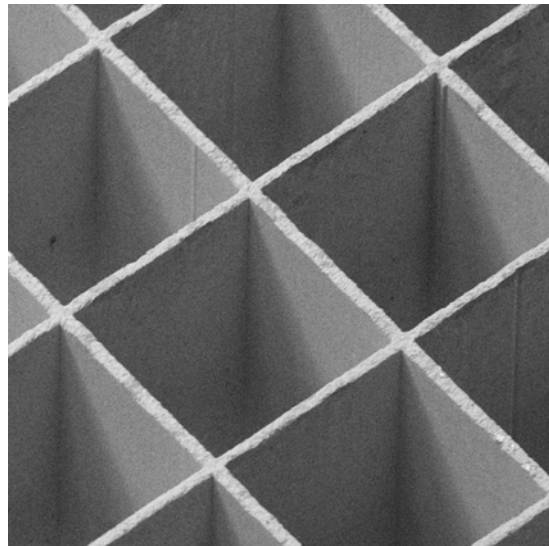


Fig. 4: SEM image of copper collimator with 25 μm wide septa electroplated into the PMMA template shown in Figure 3.

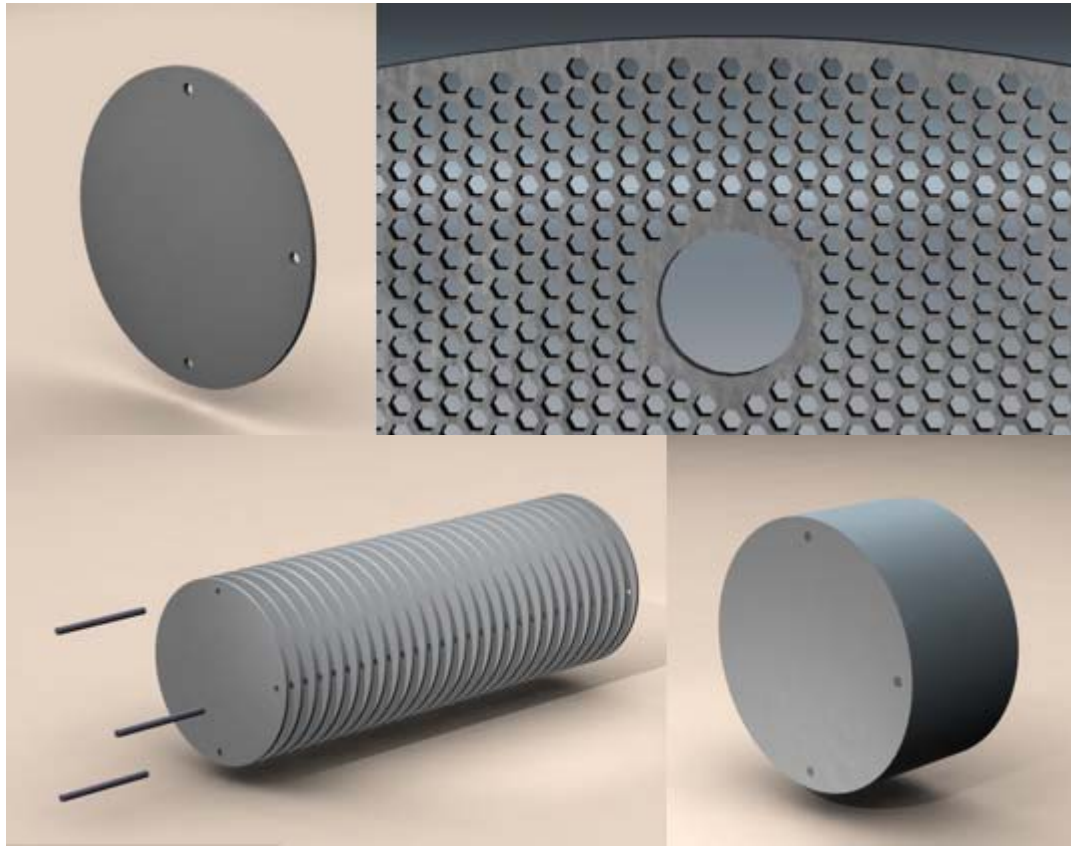
## Regenerators - A Commercial Application for LIGA Microstructures

LIGA offers the possibility of producing small, well-defined features in tall, large area structures, an important advantage for heat exchanger and cooling device applications. Kevin Kelly, the president of Mezzo Technologies and his colleagues have been pursuing the development of these heat exchangers<sup>1</sup>. One example is a cryo-cooler, a device that removes heat from an environment that needs to be maintained at cryogenic temperature<sup>2</sup>. Regenerative heat engines and cryo-coolers use a regenerator to absorb and release energy at appropriate times within a process cycle. Regenerators are heat exchangers that are crucial components of Stirling heat engines and cryocoolers. In either case, a regenerator is a device where heat is transferred between a gas and a solid matrix. The gas oscillates back and forth through the solid matrix, picking up energy from the matrix in one direction, releasing the energy back to the matrix in the other. The regenerator should offer high heat transfer/volume, low pressure drop, sufficient heat capacity, and low cost. The regenerator performance has a dramatic effect on the overall performance of the product (heat engine or cryocooler). A regenerator functions best when the temperature difference between the solid and the gas at any position within the regenerator is minimal, the pressure drop of the gas across the regenerator is minimal, the axial conduction within the solid matrix in the flow direction is minimal, and the dead space (total volume associated with the pores in the regenerator) is small. In addition to these thermodynamic parameters, the regenerator should be made from a material that is strong and tough and resistant to damage from shock loads, compression, and other factors.

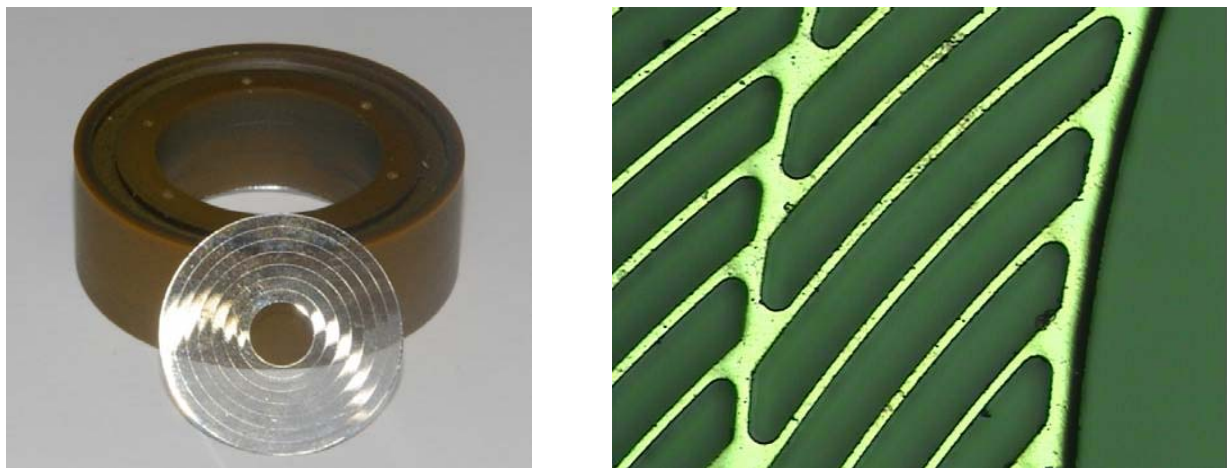
Based on theoretical modeling a high performance regenerator can be built from a well-aligned stack of thin, perforated metal disks with large open areas and small connecting grid pattern (see Figs. 1 and 2). Each disk is fabricated using X-ray lithography and nickel electroplating fabrication steps<sup>3</sup>. Besides high yield and stable processing important for any commercial application is an inexpensive production. This last aspect is achieved by utilizing the printshop services offered by CAMD<sup>4</sup>. Simple access and technical support for established processes as well as joint, collaborative R&D partnerships to improve existing processes and develop new capabilities are key points for successfully use LIGA for commercial applications.

### References:

1. Mezzo Technologies, Bon Carre Business Center, Baton Rouge, La; for more details on their MEMS products visit [http://www.mezzotech.net/4\\_products.htm](http://www.mezzotech.net/4_products.htm).
2. R. Ackerman; "Cryogenic Regenerative Heat Exchangers", Plenum Press, New York (1997).
3. D. Guidry, J. Parker, A. McCandless, S. Motakef, K. Kelly, "X-ray Lithography Fabricated Microchannel Regenerators for Cryocoolers", Cryocoolers 13, 2004 International Cryocooler Conference, pp. 405-409.
4. For more details of CAMD capabilities supporting LIGA see <http://www.camd.lsu.edu/beamlines.htm> and <http://www.camd.lsu.edu/microfabrication/>



Figs. 1: The building block of Mezzo regenerators is a stack of high porosity thin disks. Each disk is identical and the stack forms a continuous passage through the regenerator for easy flow. Assembly of the stack is simple and made possible through holes and pins.



Figs. 2: Single nickel disk of ~25mm  $\varnothing$  and mounting jig (left) and close up view of channel walls 14 $\mu$ m wide and 250 $\mu$ m tall (right).

## Sweat/Saliva Stick Volume Meter

This R&D work started in the second half of 2002<sup>1</sup> as part of a DARPA grant and was continued by the CAMD group in 2004 to modify and build the sweatstick demonstrator devices for preliminary testing to be conducted at University of Houston<sup>2</sup>. The design of the device was further modified in 2005 to make it more versatile and this modified device was designed to collect both sweat and saliva from humans<sup>3</sup>. The work was further continued by the CAMD group in 2006. The results from previous work<sup>4</sup> showed that the design needed to be modified to improve its saliva (a more viscous fluid than sweat) collection efficiency without the help of trained personnel. Therefore, 5 saliva sticks with a modified design were fabricated and assembled to perform the preliminary testing to compare the results with other saliva collecting techniques. Further, the work on fabricating a portable device was also continued<sup>5</sup> and a presentation at the COMS2006 conference sparked some interest in commercialization of the sweat stick device for health monitoring<sup>6</sup>. Despite the promising results and also market opportunities with the end of the DARPA project in 2006 the systematic and continuous research on this project had to be stopped and only a small effort (senior design project) partly funded through an undergraduate research grant for an amount of \$1300 was continued.

Figure 1 shows the schematic of the modified saliva collection device. The device has 1 mm wide channels all around it at an angle of 20°. Saliva is collected in these channels and flows into the tube connected to the device when the device is spun at high speed in a centrifuge. Two vent channels, on the right side in figure 1, ensure free flow of saliva by preventing any vacuum. Preliminary results show that the volume of saliva collected is much smaller than expected requiring a modified design of the collecting device in future efforts.

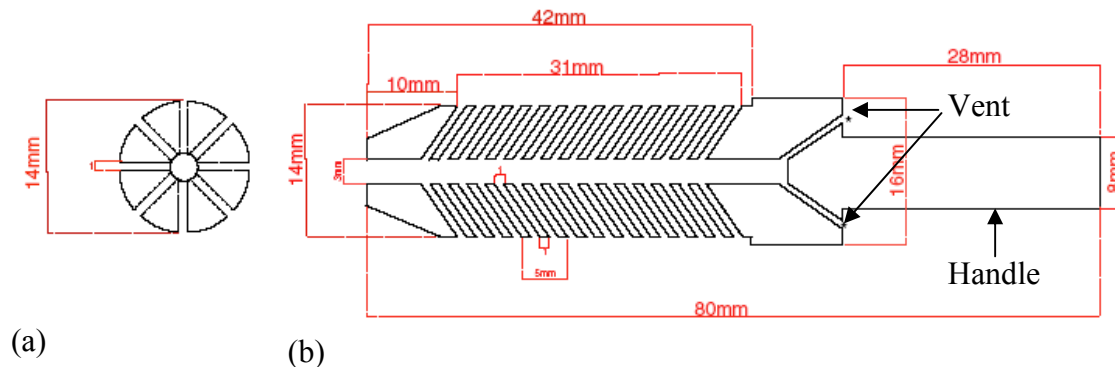


Fig. 1: Schematic view of the device (a) Top (X-section), (b) Longitudinal (X-section).

The main focus of this project was to design and build an optical detection system to detect a specific target (for example Calcium) in the sample using a fluorescent marker. Fig.2 shows the schematic of the point-of-care, non-invasive, diagnostic device.

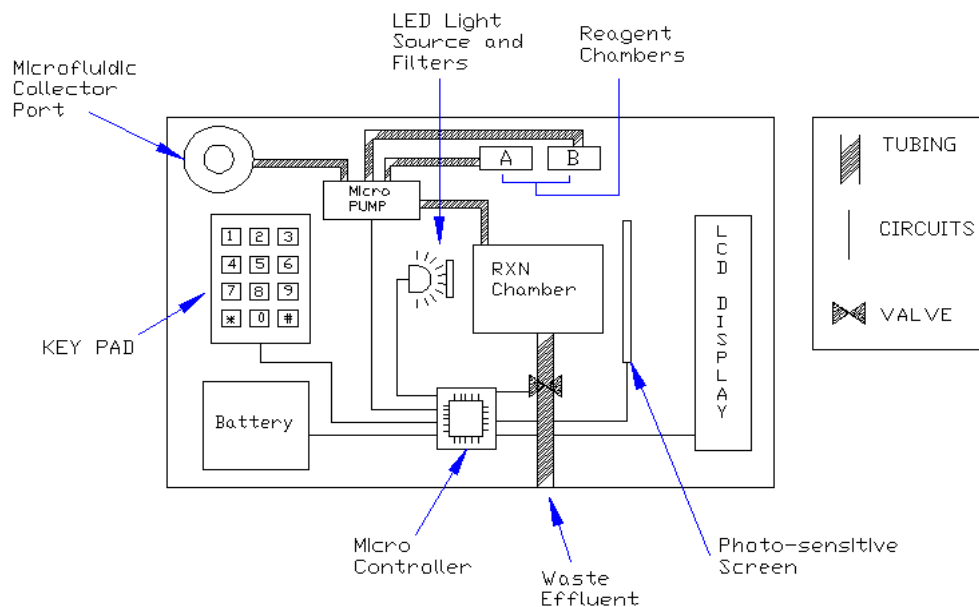


Fig. 2: A Schematic of the design.

### Conclusions and future work

The project has progressed further but has not reached the point where tests can be performed routinely that will allow evaluation of sweat/saliva stick prototype devices and comparison of their performance with existing solutions. It should be mentioned that osteoporosis is a serious health issue and simple diagnostic tools that allow monitoring indicators such as calcium and success of treatment are in growing demand. However, the experience from our research efforts indicate that, besides a number of technical issues that need to be solved and which delay development of a competitive prototype, collaboration with medical partners (doctors, hospitals,...) is critical to guide the development resulting in a useful device. Here, the integration in a bigger, focused center effort like CBM<sup>2</sup> is crucial because it not only provides the complementary (to the CAMD engineering and materials expertise) research expertise in biology and medicine but also gives credibility and visibility crucial for acceptance in the medical community.

### References:

1. J. Weimert, 'Development and Fabrication of Volumetric Sensor for Analysis of Sweat Samples', Master thesis, University of Applied Science in Gelsenkirchen (Germany), Dec. 2003.
2. V. Singh, J. Goettert, 'Sweat Stick Project', CAMD Annual Report 2004.
3. V. Singh, J. Goettert, 'Sweat Stick Project', CAMD Annual Report 2005.
4. D. Englert, R. Nelson, Q. Nguyen, T. Qureshi, 'A portable, non-invasive, diagnostic device for osteoporosis', LSU research project (advisors V. Singh, T. Monroe), 2006.
5. Varshni Singh, Yohannes Desta, Proyag Datta, Jason Guy, Mark Clarke, Daniel L. Feedback, J. Weimert, Jost Goettert; "A hybrid approach for fabrication of polymeric BIOMEMS devices", *Microsyst Technol* (2007) 13: 369–377.
6. J. Goettert, P. Datta, Y. Jin, K. Kelly, Z. Ling, V. Singh, 'Microfluidic Applications of LIGA Microstructures', *Proc. COMS 2006*, St. Petersburg, Florida, Aug. 27-31, 2006.
7. More information about osteoporosis can be found at <http://www.nof.org/>.



## Microfluidic Stack – A microfluidic development platform for life science application

Biological-Microelectromechanical Systems (Bio-MEMS) devices and Lab-on-chip or  $\mu$ -Total Analysis Systems ( $\mu$ TAS) have the potential to provide attractive solutions for a variety of sensing and diagnostic needs in life-science, medical and environmental monitoring applications. Since its initial steps in the early 1990 significant research has been carried out to develop simple microfluidic components such as mixers, splitters and valves and to integrate them into complex systems such as blood analysis devices and capillary electrophoresis systems which are entering the market as first-generation products. While stand-alone, very sophisticated solutions for specific tasks exist the general use of microfluidic solutions in many science and engineering areas is not fully established due to a lack of easy access to the technology and inconveniences of operation. In order to fully explore the potential of Bio-MEMS and  $\mu$ -TAS solutions for a broader user community the equivalent to what the printed circuit board is for microelectronics application is needed in microfluidics - a user-friendly, standardized microfluidic development platform.

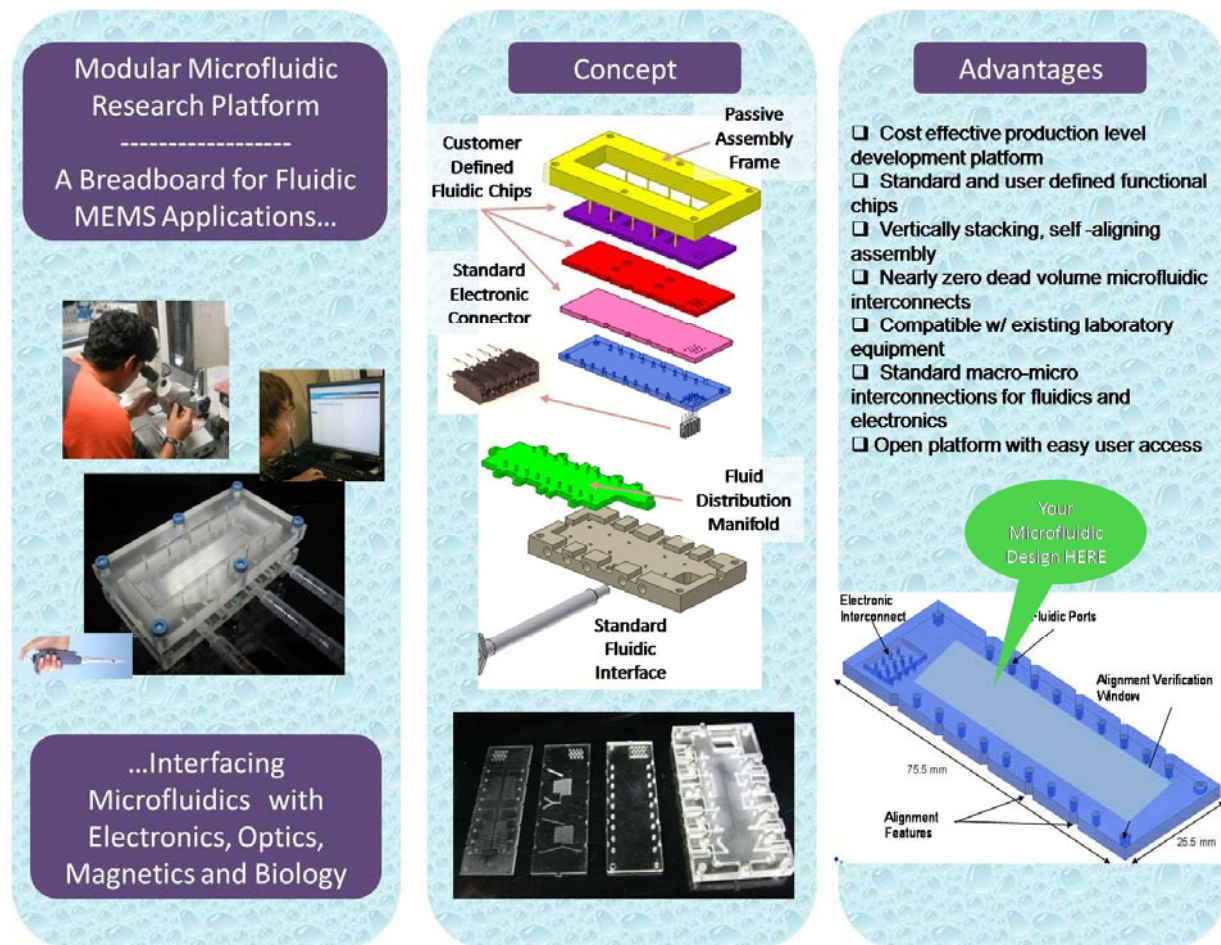


Fig. 1: Concept and features of the microfluidic development platform

The research for the design, fabrication and test of the microfluidic development platform was conducted as part of a PhD thesis<sup>1,2</sup>. Figure 1 illustrates the basic ideas of the development platform and is a description of its benefits.

The designed platform is modular in nature with individual polymer modules integrated through vertical stacking of individual chips to form a complete system. Each module may contain multi-domain components such as microfluidic elements, optical waveguides, electronic wiring, magnetic parts, and biological surfaces. The system addresses macro-micro and micro-micro inter-connection issues and provides the user with a flexible, modular and easy-to-use experimental setup which provides a framework of basic functions and also a high degree of flexibility to meet specific user demands.

The potential of the microfluidic development platform was verified in a number of customer-driven experiments including cell culture for Hansen’s disease studies, development of giant magnetoresistive (GMR) based bio sensor, optical interrogation of DNA, magnetic separation of paramagnetic microbeads, microreactor for wet-chemical synthesis of magnetic nanoparticles including in-situ EXAFS analysis, and a crystal growth test chip for protein crystallography experiments as shown in Figure 2.

**Who are we?**

Louisiana State University (LSU) operates, with financial support from the State of Louisiana, the J. Bennett Johnston Sr., Center for Advanced Microstructures and Devices (CAMD), a 2<sup>nd</sup> generation, 1.3 GeV electron storage ring. CAMD provides user access to its state-of-the-art equipment and offers training, research and development as well as paid services in synchrotron radiation based science, analysis, and technology. In the area of analytical services CAMD supports techniques including IR, VUV, and X-ray spectroscopy, X-ray diffraction, X-ray tomography, and protein crystallography to characterize materials and correlate their macroscopic properties to the atomic structure. In the area of microfabrication CAMD support is focused on offering easy access to LIGA fabrication processes and support for academic and industry customers in prototype development, proof-of-concept studies, and small-scale fabrication.


**The CAMD Microfabrication Capabilities**  
We provide professional microfabrication services to academia and industry since 2003. Our patterning capabilities include microstructures with dimensions from sub-micrometer to millimeters made from a variety of metals and polymers. You can contact us for further details or price information.

**Contact Information**  
Proyag Datta ([pdatta1@lsu.edu](mailto:pdatta1@lsu.edu))  
Jost Goettert ([jost@lsu.edu](mailto:jost@lsu.edu))


**Application**




Chip with integrated waveguide for generating a fluorescence signal from spotted areas inside the fluidic channel



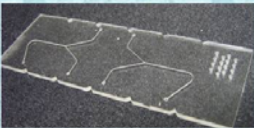
Chip for rare population cell growth experiments



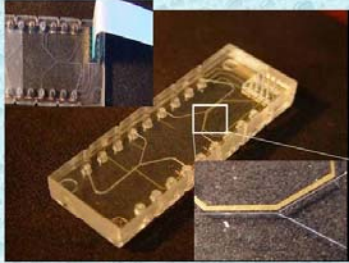
Chip with silicon dies for surface chemistry experiments



Chips with basic mixing and splitting structures required for many microfluidic applications



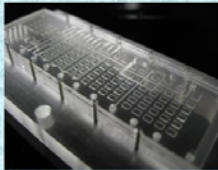
**Application**



Thin film wiring deposited on polymer microfluidic chips and connected via ribbon cable for sensing and control applications



Standard macro interface to syringes (or other customer-specified fluidic connectors) coupled with the stack distribution manifold



Crystal growth experiment using a multi-chip stack for parallel screening of different growth conditions

Fig. 2: Examples and possible applications of the microfluidic development platform.

### References:

1. P. Datta, ‘Modular, Polymeric Development Platform for Microfluidic Applications - Design, Fabrication, Testing and Examples’, PhD Thesis University Karlsruhe, 2007.
2. P. Datta, J. Hammacher, M. Pease, S. Gurung, J. Goettert; “Development of an Integrated Polymer Microfluidic Stack”, IOP, Journal of Physics: Conference Series 34 (2006) 853-858.

## Development of Magnetic Nanomaterials and Devices for Biological Applications

In support<sup>1</sup> of DARPA's overall goal to develop a handheld Bio-Sensor using GMR detection of bio-functionalized magnetic nanoparticles, CAMD researchers contributed to two major tasks related to (1) the fabrication, assembly, integration and testing of GMR sensors integrated into microfluidic systems and (2) the synthesis and characterization of bio-functionalized magnetic nanoparticles. This contribution briefly summarizes the main research accomplishments related to microfluidics and system integration.

Figure 1 below illustrates the two main efforts in relation to the overall project goal. Two critical aspects essential to achieve the overall goal are the integration of silicon based GMR magnetic sensor chips into microfluidic platforms including bio-functionalized surface modification, and the synthesis of dedicated magnetic nanoparticles with surface properties enabling the detection of selective bio-species (this part is covered elsewhere in the ROSE report in Nano-science by Challa Kumar). It should be emphasized that research efforts include a number of CAMD micro-fabrication staff and greatly benefit from support through the service group members. It also was an excellent example how complicated MEMS system development is and how challenging multi-disciplinary projects are combining contributions from MEMS engineers, electrical and mechanical engineers, and material and life scientists.

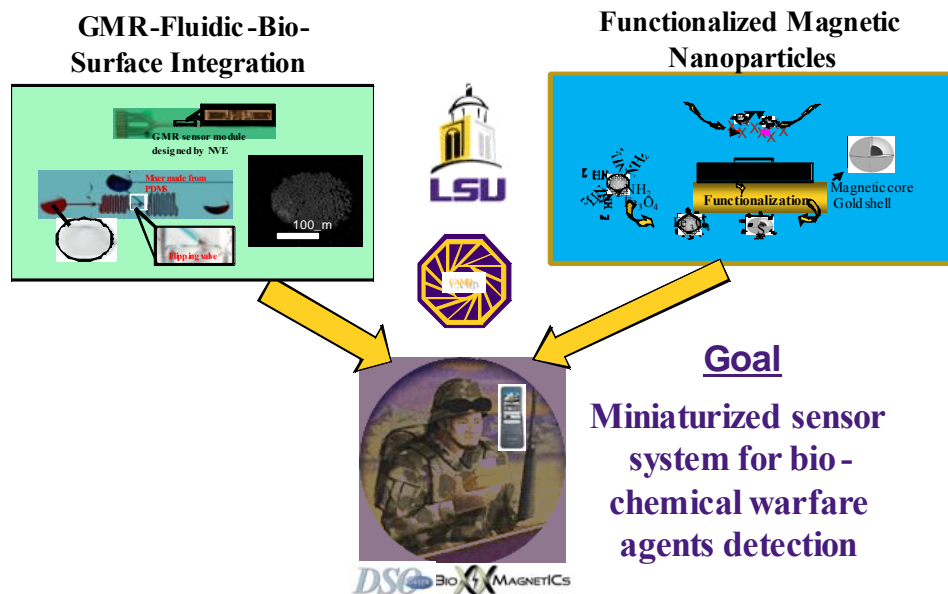


Fig. 1: Overview of CAMD research focus in the DARPA Bio-Magnetics project.

### Sensor System Fabrication and Integration

Figure 2 shows the main tasks associated with the integration of GMR sensor chips into polymer microfluidic handling system including surface bio-functionalization to selectively bind functionalized magnetic nanoparticles.

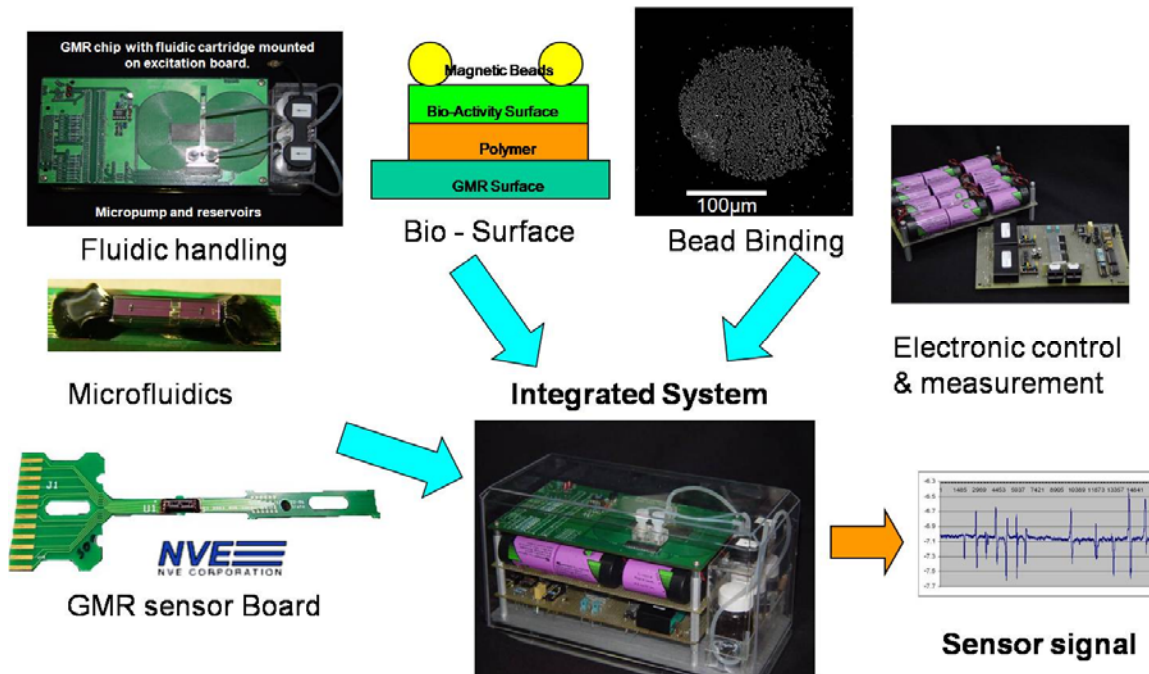


Fig. 2: Major CAMD tasks associated with fabrication and integration of the Magnetic Biosensor.

The GMR sensor chips were provided by NVE Corporation (also partner and sub-contractor in this DARPA program) in a pre-assembled form mounted on a special PCB board (so-called diving board). The sensor surface is protected by a thin  $\text{Si}_3\text{N}_4$  film ensuring that the sensors were not shorted when fluid was passed across the surface. This surface film is also the interface for the bio-functionalization chemistry.

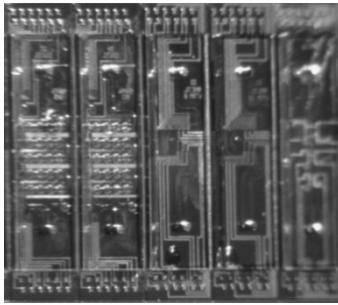
### Fluidic Cartridge for GMR sensors

Microfluidic channels were patterned on top of the GMR sensors using an aligned optical lithography process in SU-8 resist. Channels with lateral dimensions down to  $10\mu\text{m}$  and up to  $50\mu\text{m}$  tall have been patterned and successfully sealed with an SU-8 film using a novel process called semi-solid transfer. An additional SU-8 layer is providing relatively large ( $0.5\text{mm}$  diameter) inlet and outlet structures interfacing the chip with a fluidic cartridge. The SU-8 lithography process was done on a wafer-scale producing nearly 1000 GMR sensor dies in a parallel fabrication process. After wafer dicing the individual sensor chips were mounted onto the electronic diving board and electrically connected via wire-bonding. The diving-board mounted sensors were interfaced with a fluidic cartridge that provided a robust and user-friendly macroscopic fluidic interface using standard fluid connectors. This setting enables researcher to easily mount the diving board onto the excitation board and run fluids across the GMR surface in a well-defined manner. Figures 3 show some of the accomplishments and results.

This integration approach combines GMR silicon sensor chips with micro-macrofluidic handling systems delivering a ‘hard’ plastic structure with superior fluid flow control. Additional attributes are

- Lithographically defined microfluidic structures with smallest features down to  $10\mu\text{m}$  and heights up to  $50\mu\text{m}$  will allow guiding fluidic samples even to very small sensor chips;

- Lithographically defined micro-macrofluidic interface enabling relatively simple connection to fluidic reservoirs and fluid operation using a custom-made, reusable cartridge;
- Microfluidic structures are batch processed using aligned optical lithography on a pre-structured GMR sensor silicon wafer enabling a cost-effective, large-scale fabrication of GMR sensor chips with added microchannels;
- Microfluidic channels are sealed with the same hard-plastic material (SU-8) providing a uniform environment for the fluid.



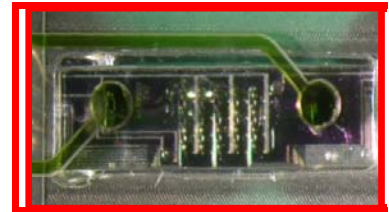
5 sensor dices with added fluidic microchannels on a full 4" wafer.



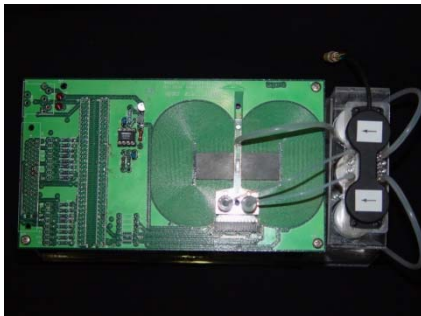
GMR chip with microfluidic structure mounted onto diving board and wire-bond connected. The wires are protected with epoxy glue.



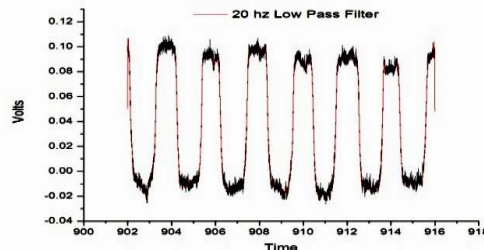
Fluidic cartridge providing an interface between microfluidic channels and macroscopic fluidic connectors.



Microfluidic inlet/outlet with channel system patterned on GMR chip (wafer-scale) using optical lithography. Colored water proves no leak.



GMR sensor with fluidic cartridge mounted onto magnetic excitation board and connected to fluidic reservoirs with ferrofluid and oil samples.

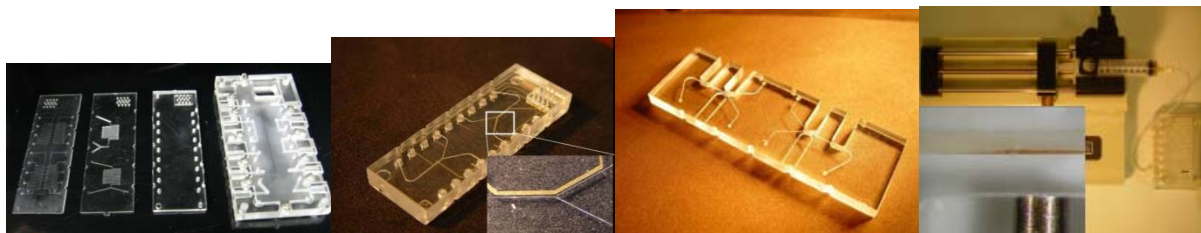


Ferrofluid/oil plugs pumped into the cartridge and the microfluidic channels generating a GMR signal when the ferrofluid is passing across the sensor surface.

Figs. 3: Steps in the fabrication and testing procedure of GMR-microfluidic chips.

### Vertical Microfluidic Development Platform

In order to allow simple access to the GMR surface (surface functionalization, visual inspection of surface chemistry after an experiment, taking surface samples) an alternative concept has been developed utilizing the microfluidic stack described in a previous highlight. CAMD has started building a library of dedicated chips designed for specific functions including fluidic mixing, magnetic separation, GMR sensing, and optical inspection.



Figs 4: Examples of stack compatible fluidic chips. Left to right, Distribution plate and different fluidic chips after fabrication and prior to assembly. Fluidic chip with conductive wire pattern for bead manipulation and electrical detection. Magnetic pre-concentrator chip with fluidic y-junction. Bead concentration measurement.

Each chip function can be tested individually or in an arbitrary combination due to the use of standardized microfluidic interconnects. Chip stacking uses the concept of elastic averaging to passively align polymer chips (typically made from PMMA and PC) in an easy, user-friendly fashion. Chips are molded using hot embossing and are either sealed permanently with a thermowelding process or temporarily using a soft gasket. The gasket provides the opportunity to disassemble the stack after completing the experiments and closely investigate the surface.

The stack allows the convenient use of microfluidic designs and solutions in a fast, cost-effective way. The modular approach using a simple assembly process is highly flexible and can easily accommodate user needs. A drawback is the limited minimum size of fluidic channels (typically about  $100\mu\text{m}$ ) determined by the fabrication process which uses a combination of precision micromachining and molding. Using a LIGA fabrication approach, however, it will be possible to fabricate a mold insert with smaller dimensions.

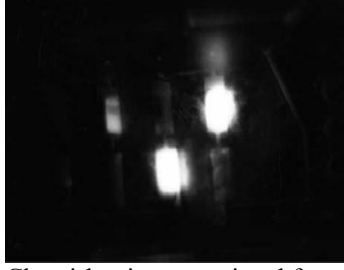
### GMR Surface Functionalization

Surface functionalization of GMR chips with a thin layer of biomolecules which allows selective binding or target molecules is typically an add-on process, for example using spotting. However, complex procedures had to be developed to optimize bonding selectivity and optimize signal-to-noise ratios. The fluidic stack was successfully utilized for systematic studies of bio-functionalized surfaces and their preparation. In addition, executing the bio-protocol - a specific fluidic procedure with different chemicals required to activating the surface, reacting the sample molecules, removing any unwanted, non-specifically bound molecules through washing, and finally detecting the sample - in a microfluidic environment resembling the actual sensor dimension is accelerating the development dramatically and will allow quick transition from basic research to sensor prototype devices. Figures 5 below show as an example a test chip containing up to 10 GMR chips treated with different surface chemistry and undergoing the identical bio-protocol. It should be noted that these tests used fluorescent-labeled nanoparticles instead of magnetic labels due to problems with the electronic signal stability.

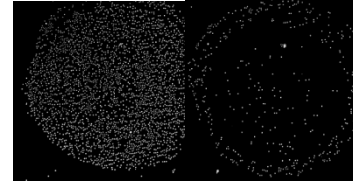
In conclusion the flexibility and simplicity of the fluidic stack development platform makes it an ideal research tool not only for this sensor project but for a number of other projects and life science applications currently being investigated. Continuously using this platform will increase the number of fluidic chips available for a particular experiment and will accelerate using microfluidic solutions in a wide range of life science applications including cell analysis, protein crystal growth, sensor chips for optical detection of bound bio-molecules, and microreactor based synthesis of specialty chemicals, in particular nanoparticles.



Fluidic test chip with 10 GMR chips prepared with different surface coatings for screening tests.



Chemi-luminescent signal from captured molecules from different chips on a light sensitive film



Photographs of bound beads (3µm Dynabeads) on a 200µm diameter spotted surface. Passivation of the outside area reduces the non-selective binding of the beads and thus increases signal-to-noise ratio.

Figs. 5: Fluidic chips and stack assembly for systematic studies of bio-functionalized surfaces on GMR sensor chips.

### Project Summary:

The GMR-microfluidic integration efforts are still work in progress and haven't resulted in a stable solution and a handheld Bio-Sensor device suitable for serious testing. The following list provides some key lessons learned that should guide future research efforts:

- The pre-defined GMR electronic package (diving board, excitation) is a very strict boundary condition for integrating a microfluidic system; alternative, more rigid solutions might be possible starting with the naked silicon chip directly embedded into the polymer chips or using more reliable platforms such as DIP IC chip carrier.
- The vertical fluidic development platform is an enabling research tool giving users a microfluidic handling system with convenient interface features to standard laboratory equipment such as syringe pumps, pipettes, fluorescent microscopes, and similar; there is already a set of designs for basic fluidic functions available that can be easily extended to new, customer-defined chip designs further supporting its use in life science applications.
- Bio-functionalization of the GMR sensor surface is an important issue and significantly compromises MEMS fabrication and ultimately sensor fabrication costs; while flow sensing applications (for example detecting beads passing across the surface) are feasible bio-sensing may require alternative approaches decoupling the actual bio-reaction from the GMR signal generation.
- Use of magnetic forces to 'manipulate' bead loaded liquid flow is an interesting concept and should be further explored within the stack confinement for basic fluid processing operations such as mixing, pre-concentrating, and re-directing.

The general sensor system research is continuing within the Post-Katrina project funded through Louisiana's Board of Regents and led by AMRI, University of New Orleans. In this project the fluidic stack platform will be utilized as research and development tool to explore Biosensors using bio-functionalized nano-wires embedded into microfluidic channels and interconnected to microsize conductive layers.

### Reference:

1. Prime Contract to AMRI/University of New Orleans from Defense Advanced Research Projects Agency (DARPA).

## Design Aspects and Performance Tests of Miniaturized Gas Chromatography Sensors<sup>1</sup>

Rapid and comprehensive on-site analysis of chemicals in applications ranging from industrial process control to homeland security is of significant importance to improve the environment and ensure a better life. A gas chromatograph (GC), often-termed “a needle in a haystack” instrument<sup>2</sup>, is one of the most widely used analytical devices, with applications in the chemical process industry, oil exploration, environmental monitoring, purification of substances, and general organic compound analysis. Apart from these traditional uses, GCs are playing an important role in the detection of chemical warfare agents, the detection of diseases<sup>3</sup>, and even in quality control of coffee beans<sup>4</sup>. Industrial process control is one of the major applications of GCs, with instruments in chemical plants continuously monitoring chemical processes and contributing to quality control. The need for sensors that are fast, reliable, and portable has never been greater. For the challenging task of on-site instrumentation, where power sources can be limited, shrinking the size of the device is the most effective way to conserve power. Although gas chromatography is a mature technique well suited for these applications, current instrumentation has deficiencies that limit its usage. Speed of analysis and non-portability are severe hindrances to using the bench top and portable instruments for on-site applications. The focus of this DARPA project is develop MEMS technologies that enable the fabrication of handheld size GC-based sensors that are fast, reliable, and portable and meet the demand for on-site analysis.

From the many components of a GC sensor, the separation column primarily defines the resolution and selectivity<sup>5</sup>. However, sample handling and especially dead volumes introduced along the path compromise the analytical performance of the separation column and make it advantageous to include functional components such as sample loop, pre-concentration, split injector, and makeup gas manifold into the design. The design shown in Figure 1 integrates the sample loop and possible pre-concentrator with the column thermally isolated from the column by air gaps. This way, when performing temperature cycling independent of the column, the sample loop, filled with an adsorbent, will act as a second stage, integrated concentrator. Another important feature is temperature programming and the optimized system package. As the overall system is built from different discrete components major emphasis of the research has been put on system integration and interconnection technologies shown in Figures 2. The system design and column layout was supported by modeling theoretical performance taking into account real systems especially considering dead volume. For both isothermal and temperature programming operation, the column performance is reduced drastically by dead volumes. Also, in a real system, a narrow width, high aspect ratio column will perform better than similar dimension circular or square columns. Through process control, a device yield of over 90% was achieved. Tests on these columns yielded more than 20,000 plates for unretained species. Four hydrocarbons were separated in less than 2 s at 100 °C on a 50 µm wide by 600 µm tall by 0.5 m long coated LiGA column. For the first time reported, 2-D GC was implemented using MEMS columns as shown in the chromatogram of Figure 3<sup>6</sup>.

While system integration aspects are crucial for the GC sensor chromatographic performance the single most challenging fabrication aspect is related to high aspect ratio LiGA nickel columns with typical lateral dimensions of a few ten micrometer and heights up to 1mm. Based on a model developed by Giddings et al.<sup>7</sup>, rectangular columns offer significant advantages over circular columns because separation or column resolution can be optimized by changing the lateral width, while tall heights provide sufficient volumetric flow to detect a measurable signal. By us-



ing X-ray LiGA technology, fabrication of columns with serpentine like arrangement ranging 0.5m to 2m long, 50 $\mu$ m wide, and up to 650 $\mu$ m tall nickel GC columns with aspect ratios of more than 10 have been fabricated<sup>8</sup> as shown in Figures 4 and 5. Research was performed at CAMD and BESSY synchrotron source to further improve these dimensions towards smaller lateral dimensions (down to 20 $\mu$ m) and higher aspect ratios (up to 20). Some of the means used to optimize process steps are exposing samples with adjusted dose and the use of acoustic agitation (megasonic) to enhance the development rate. By adjusting the bottom dose from 4.0 to 3.25kJ/cm<sup>3</sup> at 1.3 GeV energy and dose ratio of 4.1, exposure time was reduced from 5hrs to 3hrs. Also, by means of megasonic agitation at 10W/cm<sup>2</sup> power in GG developer followed by DI-water rinse we were able to reduce development time from 5.5hrs to 2.5hrs. Adjusted bath temperature and sample cycling duration had significant factor in minimizing development time. Due to the optimized exposure time and development means, we have achieved a high yield (80-90%) in our column production.

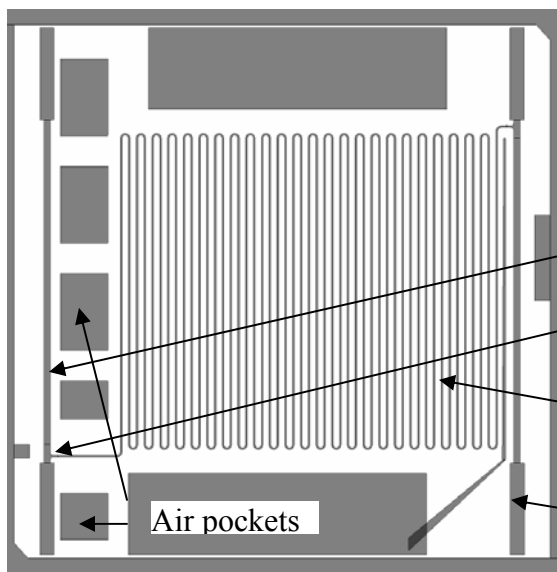


Fig. 1: Schematic of an advanced micro-GC column with integrated sample injector, pre-concentrator, and gas manifold.

Thermally isolated sample inlet loop

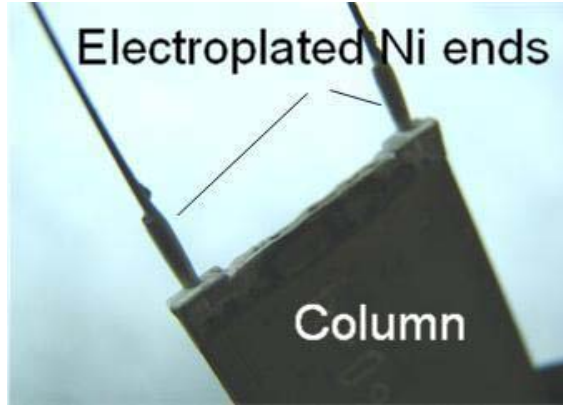
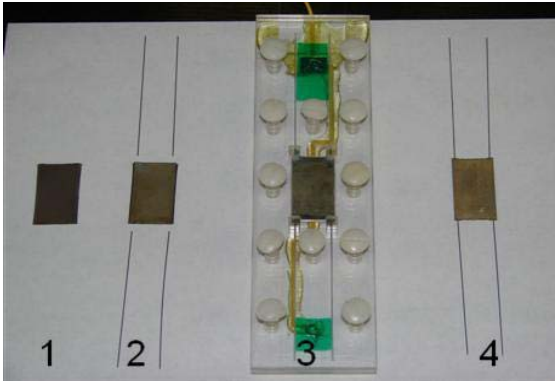
Split injector

Separation column

Detector outlet

Air pockets

The GC sensor project is another example of a multi-disciplinary project in which the initial CAMD microfabrication capability to produce LiGA Ni columns was complemented by system integration knowhow, surface chemistry (column coating) and, very important, GC expertise (Prof. Ed Overton, LSU-Environmental Studies). This DARPA funded project is currently transitioning into Phase III with LSU remaining a sub-contractor involved with the chromatography performance tests of the prototype systems mainly built from Si MEMS components fabricated at Sandia National Laboratory because reliably coating of the inside of the Ni columns is still an unsolved material challenge.



Figs. 2: Parts and plating jig for tube interconnects with the micro-metal column (left); close up of the electroplated tubes mounted to the metal column (right).

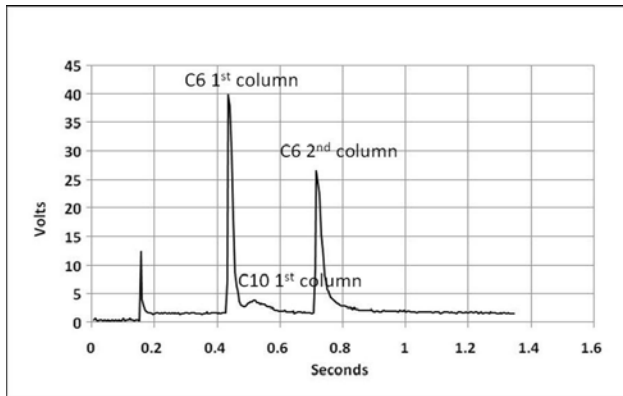
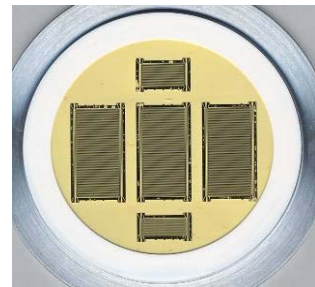
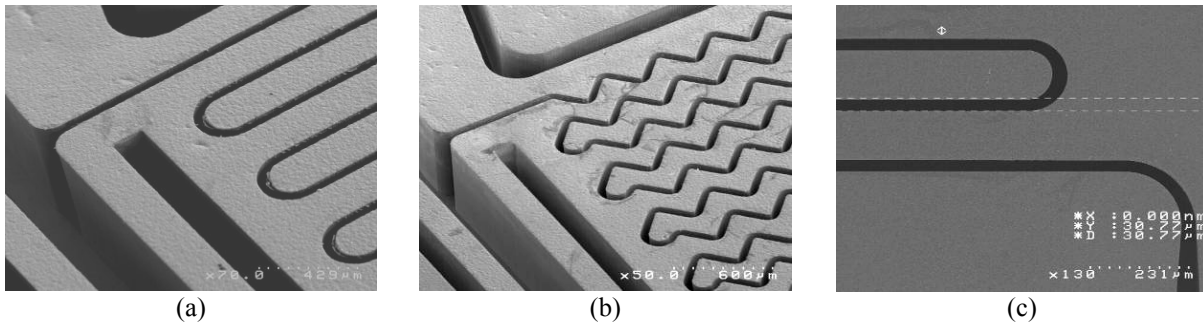


Fig. 3: Separation of hexane and decane using 2D GC on a 50  $\mu\text{m}$  by 600  $\mu\text{m}$  by 0.5 m first column, coated with 0.1  $\mu\text{m}$  OV-1 and an uncoated 50  $\mu\text{m}$  by 600  $\mu\text{m}$  by 1 m second column. The column head pressure was 40 psi, the split for the second column was set to 100% open, and the makeup gas pressure for both the columns was set at 15 psi.



Figs. 4: Silicon wafer with TiOx seed layer and PMMA resist of 650 $\mu\text{m}$  and 1mm, resp., (left); 4" silicon nitride membrane mask with different column designs routinely used for exposures at CAMD and BESSY (1 $\mu\text{m}$  thick membrane with  $\sim$ 10 $\mu\text{m}$  thick Au).



Figs 5: SEM pictures of plated Ni columns; (a) split injector in a  $50\mu\text{m} \times 650\mu\text{m}$  straight column design; (b) split injector in a  $50\mu\text{m} \times 650\mu\text{m}$  corrugated column design, (c)  $30\mu\text{m} \times 650\mu\text{m}$  wide straight channel.

### References:

1. Prime Contract to Sandia National Laboratory, Albuquerque, NW from Defense Advanced Research Projects Agency (DARPA).
2. J. V. Hinshaw, "Finding a needle in a haystack," *LCGC North America*, v 22, no 10, 2004.
3. M. J. Felton, "GC and systems biology," *Today's Chemist at Work*, pp 26-29, June 2004.
4. M. S. Lesney, "GC and the coffee bean crisis," *Today's Chemist at Work*, pp 30-34, June 2004.
5. A. Bhushan, "System Optimization for Realizing a miniaturized Gas Chromatograph Sensor for rapid chemical Analysis", PhD thesis, LSU (2006).
6. Abhinav Bhushan, Dawit Yemane, Edward B. Overton, Jost Goettert, Michael C. Murphy" Fabrication and Preliminary Results for LiGA Fabricated Nickel Micro Gas Chromatograph Columns", *JMEMS* Vol. 16, NO. 2 (2007): 383-393.
7. J.C. Giddings, J.P. Chang, M.N. Myers, J.M. Davis, and K.D. Caldwell, *J. Chromatogr.*, v 255 (1983), 359-379.
8. A. Bhushan, D. Yemane, D. Trudell, E. B. Overton, and J. Goettert, "Fabrication of micro-gas chromatograph columns for fast chromatography," *Microsyst. Technol.*, published online DOI 10.1007/s00542-006-0210-3, 2006.



## Section III

### CAMD Today



### **III. CAMD Today**

#### **Introduction**

In this section, the reader will find a description of CAMD today (2008). The section begins with a short history of the facility that includes some of the policies that influenced its formation and continue to have impact to this day. In addition to documenting CAMD's history, the performance and current upgrades of the accelerator, the beamlines, microfabrication facilities, and other infrastructure are presented, along with a profile of the user community, our outreach program, and the administrative structure (III.B.5.a). This section also contains current organization charts that include proposed basic increases to enhance the overall performance of the facility. The budget and funding for the facility is documented for the past three years in part III.B.5.b.

It should be clear to the reader, after reading Section II, that the 15 beam lines and microfabrication facilities at CAMD are used for a very broad array of scientific and technological endeavors. The detailed descriptions of the facility, including personnel, beamlines and other hardware, given in this section include performance, current staffing and productivity levels.

Staffing levels at CAMD are substantially less than that at other synchrotron radiation facilities and thus CAMD provides excellent value for the dollar invested, while maintaining quality service to our approximately 300 users. It is an administrative goal to fill key vacant positions and provide even better service in this new federal funding environment (2009).

In this section and in Section IV, arguments will be made to recommend and support a strategic increase in facility upgrades and technical staff to assist the user community.

### III.A. A Brief History of CAMD

CAMD is a designated research center of the Louisiana State University and Agricultural and Mechanical College and, administratively, is in the Office of Research and Economic Development. The Head of this Office is Vice Chancellor Brooks Keel. The electron-storage ring, which is the heart of CAMD, has been in operation to produce intense and bright synchrotron radiation since September, 1992. CAMD's electron storage ring is considered a second-generation synchrotron-light source. At the time of its design and construction, five second-generation light sources were in existence in the US; the SSRL at the DoE-funded SLAC Laboratory at Stanford University. The NSF-funded the SRC at the University of Wisconsin, CHESS using the NSF-funded CESR ring at Cornell University, the DoE-funded NSLS (actually consisting of a low-energy VUV ring and a higher-energy X-ray ring) at Brookhaven National Lab on Long Island and the Department-of-Commerce-funded ring, SURF, at NIST in Gaithersburg, Maryland. At this time, two third-generation rings were funded through the DoE; the Advanced Light Source, a soft-X-ray ring, at Lawrence Berkeley Laboratory and the Advanced Photon Source, a very-high energy X-ray ring at the Argonne National Laboratory. It should be noted that these synchrotron-radiation sources, other than CAMD, were located in three geographic regions; the Bay Area of California (two rings), the Chicago area (2 rings) and the Washington DC to southern New York area (3 facilities, 4 rings). This remains the situation, even today.

This accelerator and the building that houses it, the *CAMD Experiment Hall and Mechanical-Support Facility*, were built with funding provided by a special US-Congressional appropriation of \$25M made in 1987-1988 through the DoE. At the forefront of the effort to obtain this funding were Dr. Gary Findley (currently, Chemistry Professor, University of Louisiana at Monroe), Sean McGlynn (then LSU Vice Chancellor for Research, currently, Professor Emeritus, Chemistry, LSU), Professor Pratul Ajmira (currently, Professor, Electrical and Computer Engineering, LSU) and Professor Harvill Eaton (then Associate Dean of Engineering LSU and soon to become Vice Chancellor of Research LSU, currently, President of Cumberland University, Lebanon, Tennessee) working with Senator J. Bennett Johnston, Jr. The reasons underlying the funding of the CAMD electron storage ring and conventional facility were toward providing a viable technology to enable commercial utilization of X-ray lithography-production of sub-micrometer-feature integrated circuits. Research programs, in the US, with which CAMD was cooperating in this effort, were the Center for X-ray Lithography (CXrL), University of Wisconsin and SRC, IBM and Sematech, the government-industry organization for SEMiconductor MANufacturing TECHnology. During 1987 and 88, several workshops were held at LSU in which leaders from these other organizations were active participants.

Also, in 1987, Dr. Findley, Director of the CAMD Project Office, formed the first CAMD external advisory committee, consisting of well-known scientists in the fields of micro-circuit design and fabrication and synchrotron-radiation-based science; Martha Krebs, Herman Winick, Russ Huebner, Mike Knotek and Franco Cerrina. In 1988, Dr. Findley worked with a small team of advisors to write the procurement-bid specifications for the electron-storage ring and successfully selected the Brobeck Division of Maxwell Laboratory, San Diego, to design, build and commission the accelerators and associated systems. He also worked with the LSU System Office and the Louisiana Architect Board to select the excellent team of architects, Baton-Rouge-based *Tech IV* (Bobby Crump, Tom Holden, Trey Trahan and Mike Wilson), to design and



oversee the building of the conventional facility. Tech IV, under the advisement of Dr. Findley, chose the firm of Lester B. Knight to be the project engineers; Knight and Company was involved in the engineering of the conventional facility for the Advanced Photon Source. Jules Godel, of the National Synchrotron Light Source, was chosen by Dr. Findley as a consulting engineer to advise CAMD regarding the engineering of the conventional facility. Dr. Findley also worked with the LSU System Office to help convince the System's Board of Supervisors to locate CAMD on LSU property across the street from the College of Engineering and Business Administration (CEBA) building. This was done before the awarding of the \$25M from the DoE; January, 1988. Dr. Findley resigned his position at LSU in the spring of 1989.

Soon after Dr. Findley's resignation, the LSU administration decided to not use the on-campus site that had been carefully chosen by the LSU Office of Facility Planning in conjunction with the LSU System Vice President of Institutional Services. The reason for the decision was that an estimated cost of ca. \$250K for engineering to counteract the hydrostatic pressure caused by the Mississippi River in flood stage would be required if CAMD were to be built at the on-campus site. No consideration was given to proximity convenience of the facility for its LSU users or to the difference in the utility charges on campus versus the "stand-alone-facility" charges off campus. It was over one year before a 15-acre site, generously donated at 6980 Jefferson Highway, approximately five miles north-east of the LSU campus, was finally accepted by the State of Louisiana. About 20% of the Louisiana-state-provided CAMD budget is used each year to pay utilities and, up to 2007, no effort has been made on the part of the LSU administration to support a public transportation for students and faculty to travel between campus and the laboratory.

There were some exciting (to say the least) times during the search for a suitable site, the shrinking time to build on that site and the contract date for a place for Maxwell-Brobeck to assemble the storage ring and commission it so that they might receive full payment. Professor Volker Saile, from DESY in Hamburg Germany, began as Director of the CAMD Project in November, 1989. His first task was to help the CAMD staff overcome the problems caused by not having a site to house the storage ring that had been under design and construction in Berkeley, California for almost one year. During the first part of 1990, the site was secured and a Tech-IV design for an excellent but rapid-construction building was created. The conventional facility was constructed in about eleven months, completed almost one month ahead of contract schedule. The 45,000-square-foot facility included a 25,000-square-foot experiment hall where the storage ring and beamlines would be housed. The components of the ring were delivered during late spring, 1991 and by early October of the same year, injection from the 200 MeV LinAc was accomplished with, initially, four orbits. By August, 1992, full-energy ramp of the ring to 1.4 GeV and 250 mA, with stable radiation beams from the dipole ports, was accomplished and LSU took ownership of the synchrotron-radiation source. Professor Saile was now Director of CAMD, the light source!

The State of Louisiana, Legislature and Governor, provided \$3M for research infrastructure almost immediately after the ring was shown to be successful. One-half of the money was designated for basic science and the other half for X-ray lithography and research in the area of using X rays to fabricate sub-micrometer-feature integrated circuits. The basic science part of the funding went to the acquisition of vacuum-ultraviolet, high-resolution-spectroscopy beamline designed by CAMD staff scientists and LSU faculty recently hired (1988-1991) specifically

because of outstanding research records in synchrotron-radiation-based spectroscopic research. The X-ray-lithography part of the funding went to acquisition of an X-ray-lithography beamline (designed by CAMD staff scientists and built by Maxwell Laboratories), a 1000 square-foot, class 100 clean room, and an mask stepper developed as a joint effort by LSU Electrical Engineering faculty and CAMD staff scientists. The stepper was supplied radiation by the beamline and was housed in the class-100 clean room.

Within a few years after CAMD became an operational synchrotron-radiation source, an advance in using ultraviolet radiation and a technology developed at IBM, the phase-shift mask, made the need for X-ray lithography unnecessary for sub-micrometer features in integrated circuits. The other matter that led to the demise of X-ray lithography for circuit manufacture was gravity. Traditional stepper-scanners used for optical (lithographic) fabrication of microcircuits move in the horizontal plane, perpendicular to the force of gravity. As synchrotrons were the only viable source of X rays for lithography, the scanner-stepper was required to move vertically and the positions of the assemblies of masks and wafers, particularly during the process of stepping the mask and wafer relative to one another, could not be controlled to the nanometer precision required when over twenty levels of an integrated circuit had to be layered on each other. CAMD (the name involves micro structures and devices, not just microcircuits) has been from its beginning involved in the field of MEMS (Micro-Electronic-Mechanical-Systems). In fact, even early in its life, CAMD was partnered with the Institute for Micromanufacturing (IfM) at Louisiana Tech University. At the same time that the special-language appropriation was made by Congress to fund CAMD, IfM was also funded by a similar appropriation. Two of the earliest beamlines to be installed at CAMD were property of IfM and were designed for X-ray-lithographic manufacture of micrometer-sized-feature mechanical devices. During this time, CAMD installed a “home-made” beamline and scanner on which to fabricate micro-mechanical devices. It should be mentioned that, during the push to develop the X-ray circuit-fabrication technology, IBM purchased a compact super-conducting storage ring from Oxford in England and the NSLS received a total of \$35M to design and build a compact super-conducting ring for similar industrial applications. IBM’s ring was installed in its new Advanced Lithography Facility (ALF) and the ring was decommissioned in the late ‘90’s and now resides at the Jefferson Lab in Newport News, Virginia. The NSLS succeeded in building a warm-magnet mock-up of the super-conducting ring but never built the cold ring. CAMD has been very successful in developing the technology of X-ray LiGA; German acronym for X-ray lithography (*X-ray Lithographie*), Electroplating (*Galvanoformung*), and Molding (*Abformung*). This process in microtechnology was developed in the early 1980s by a team under the leadership of Erwin Willy Becker and Wolfgang Ehrfeld at the Institute for Nuclear Process Engineering at the Karlsruhe Nuclear Research Center.

Under the leadership of Professor Saile, the research infrastructure quickly grew, by the mid 1990’s, to include three more synchrotron-radiation beamlines in addition to the five described above. These beamlines were equipped with a variety of end stations. Volker Saile resigned at the end of 1997 and became Director of the Institute for Microstructure Technology (IHT) at the Forschzentrum Karlsruhe as well as a tenured professor at the Karlsruhe University. The ANKA synchrotron facility on the FZK campus supports X-ray lithography programs at the IHT. Before his departure, Professor Saile saw an additional 1500-square feet of class-100 clean room installed as well as directed the procurements of three additional basic-science beamlines and the 7-tesla super-conducting wiggler.

In October, 1999, Professor Josef Hormes joined CAMD as Director and remained in that position through June, 2006, when he made the difficult decision to return to Bonn University, where he was a Professor of Physics and had been informed by them that he must return actively to the faculty at Bonn or lose a substantial portion of his retirement income. Under his direction for over seven years, the three afore-mentioned beamlines were installed and/or commissioned by the CAMD staff, the new grazing-angle-absorption/small-angle-scattering X-ray beamline was built to replace one of the existing beamlines and funding/procuring of three additional beamlines was obtained resulting in a total of fifteen beamlines either operational or in some stage of construction at the close of 2003. The precise status and utilization of each of these fifteen beamlines, as of February 1, 2006, are presented in tabular format and narrative description in the following paragraphs.

Professor Hormes, in addition to directing the CAMD staff and cooperating with LSU faculty to design and acquire the afore-mentioned infrastructure has guided CAMD to establish several important programs. These programs have definitely increased the impact CAMD is having on science and engineering research at LSU, throughout the state of Louisiana and in other parts of the nation and world as well as on education of undergraduate and graduate students and faculty from colleges and universities throughout the nation. Some of Professor Horm's accomplishments include:

- He re-established the external advisory committee, in fact he established three committees; a Science Advisory Committee (SAC), a Machine Advisory Committee (MAC) and an Industrial Advisory Committee (IAC). The first two committees are composed of internationally-known scientists and engineers from US and European synchrotron-radiation facilities and faculty from US universities and laboratories who are well-established and well-respected users of synchrotron radiation and/or experts in microfabrication. The latter committee is composed of Baton Rouge area representatives of industry, technology and community involvement (e.g., Chamber of Commerce and news media).
- Dr. Hormes also established outreach and educational activities. CAMD staff have, from the beginning, been very active in giving presentations and tours to school classes, community organizations and university audiences (LSU, Louisiana and neighboring states); however, Professor Hormes led CAMD to expand this type of activity by:
  - Having the staff seek and obtain funding for an NSF-and-CAMD-sponsored REU (Research Experiences for Undergraduate Students) Program. Since the summer of 2000, there have been more than 50 undergraduate students from across the nation involved in the 10-week program each summer.
  - Also, beginning in 2000, each summer one of the CAMD scientists has organized a one-week workshop or summer-institute to educate students and faculty of Louisiana and regional universities. The subjects covered have included synchrotron radiation in material-science research, in environmental-science research, in biological research and also subjects in biomedical research, microfabrication and nanomaterial science.
- Professor Hormes made a strong effort to improve the dependability and quality of the synchrotron radiation produced at CAMD; his aims were to improve beam stability, up-

time and ring current. To achieve these things, he invited two respected and experienced accelerator physicists to come to CAMD for extended periods of time. The result of the intense effort has been to achieve great increase in the qualities mentioned and, in addition, the brightness of the user light has also been increased significantly. Dr Vic Suller, from Darsbury Laboratory and one of the designers/builders of the new UK ring Diamond, has been at CAMD fairly regularly for four years and currently is a full-time staff member, the Accelerator Director. He currently is leading the Accelerator group to establish “mini-beta” injection for the purpose of accommodating new insertion devices that CAMD is currently considering and for which funding is being actively sought.

- He, along with Dr. Suller and other accelerator physicists with international reputation, proposed a new third-generation synchrotron-radiation source for the Southeast, SEALS (South East Advanced Light Source). This is a serious proposal and remains a top priority of the CAMD staff.

When Professor Hormes announced his planned resignation to a joint meeting of the SAC and MAC on March 2, 2006, the members of these committees nominated Professor David Ederer, a member of the SAC, to serve as Interim Director of CAMD. Professor Ederer is Emeritus Professor of Physics at Tulane University and, at the time of his nomination, a Senior Scientist at Argonne National Laboratory. LSU Vice Chancellor of Research Dr. Harold Silverman chose Professor Ederer from a field of several candidates and he joined CAMD as Director in July, 2006. David has guided CAMD through a number of critical issues including;

- The search for a Director
- The writing of an NSF MRI proposal to obtain a new multi-pole high-field superconducting wiggler (\$1.5M). He coordinated an interdisciplinary effort with participants (as PI's) from LSU Biological Sciences, Chemistry and CAMD (accelerator and X-ray science).
- Establishing close ties with the LSU Office of Research and Economic Development and the new Vice Chancellor of Research, Dr. Brooks Keel. Already, together they are seeking ways of increasing funding for CAMD operations and have visited NSF and DoE with presentation of CAMD's capabilities and user base.
- The writing of a comprehensive CAMD report (this ROSE report), based in part on the past Annual Reports and intended for use as a report to the Vice Chancellor as well as the basis for reports and proposals to appropriate agencies for future CAMD funding and, ultimately, to agencies which are possible funding sources for a new third-generation synchrotron-radiation source for the South and/or Southeast.

### III.B. Current Situation

#### III.B.1. The Ring

##### III.B.1. a. Performance

The CAMD Light Source is conventionally described as a 2<sup>nd</sup> generation synchrotron radiation facility. This means the storage ring accelerator, which is the basic source of the radiation, is designed to generate that radiation primarily in its bending magnets and not in specialized insertion devices. This fitted well with the role of CAMD as it was envisioned in 1992, namely to provide cutting edge x-ray lithographic facilities for micro structure development and research.

The structure of the storage ring itself consists of 4 identical sub-units or cells. Each cell contains 2 bending magnets, a number of focusing magnets and a 2.5 m long straight section. Two straight sections contain the injection system and the radio frequency accelerating cavity, while the other two were initially left empty. A diagram of the storage ring layout is shown in Figure 1.

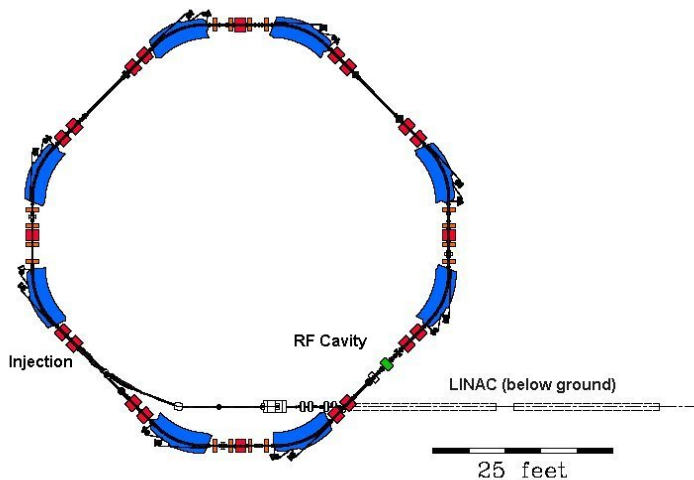


**Figure 1.** A diagrammatic layout of the CAMD storage ring.

A subsidiary accelerator, the LINAC shown in fig 1, is used to inject a beam of electrons into the storage ring at an energy of 200 MeV. After a few minutes of injection, once a substantial beam of electrons (up to 250 mA) has accumulated, injection is stopped and the stored beam of electrons in the ring is accelerated to an energy of 1.3 GeV. This is the operating energy of CAMD at which the beam is held for a period of about 8 hours. Owing to several inherent processes the beam, after 8 hours, will decrease in intensity by about 50% so the injection cycle is repeated. This is done 3 times a day as the facility is in use on a 24 hours basis. In a repeating 2 week cycle the accelerator operates 10 days for research and 4 days for maintenance or development.

During this time radiation is produced continuously in the bending magnets and is transported to the experimental stations by 15 beamlines, each of which operates simultaneously and independently. The distribution of beamlines around the accelerator is shown in Figure 2.

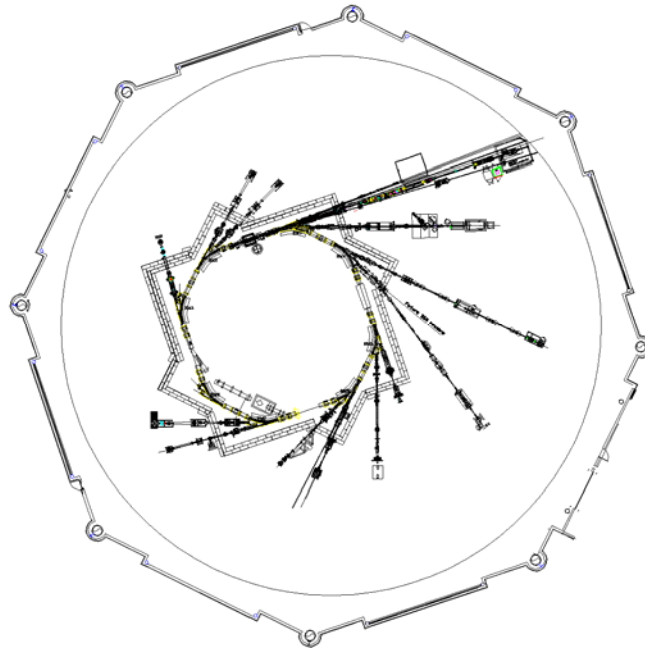


**Figure 2.** The distribution of beamlines around the CAMD accelerator.

After operating CAMD for several years it was decided to extend the range of photon energies available at the facility into the hard X-ray region by installing a Wavelength Shifter. This Insertion Device (ID) is located in one of the free straight sections of the storage ring where, by applying a localized region of very high magnetic field (almost 5 times stronger than in the CAMD bending magnets), it generates a beam of hard X-rays. The wavelength shifter was commissioned in 1998 and is presently used for protein crystallography, micro-tomography and deep lithography.

The wavelength shifter applies a magnetic field of 7 Tesla to the beam and such high fields can only be generated by using superconducting technology. The ID itself is kept at a temperature of 4 degrees above absolute zero by immersing it in liquid Helium which is contained within a cryostat. Heat leakage into the liquid Helium, which causes it to evaporate and be lost into the atmosphere, is minimized by using super insulation and a heat shield cooled with liquid Nitrogen. The wavelength shifter in its cryostat is shown in Figure 3.

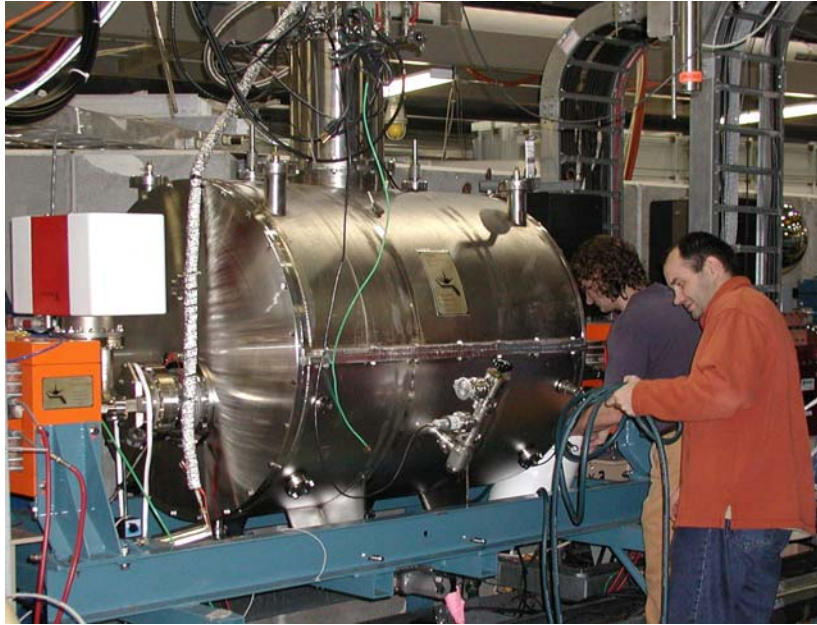


**Figure 3.** A view of the 7 Tesla superconducting Wavelength Shifter in its cryostat.

The CAMD wavelength shifter is amongst the few IDs worldwide which can operate at 7 Tesla or above. It performs well and is highly reliable but a minor drawback is that it needs to be refilled with liquid helium 3 times a week. A possible upgrade would be to replace the cryostat with a modern low loss design which includes a closed cycle helium cryo-cooler. This would remove the need to refill the ID with liquid helium on a regular basis, thereby reducing downtime and costs and helping to conserve the Earth's limited inventory of helium.

Since coming into operation in 1992 the CAMD Light Source has steadily broadened the scope of its research program. At the present time (2007) the 15 beam lines are in use not only for micro-fabrication but also for spectroscopy, spectro-microscopy, micro-tomography, and molecular and crystalline structure determination. The addition of a high field wavelength shifter into one of the straight sections has increased the range of photon energies available at CAMD from the previous limit of 10 keV to 65 keV.

### **III.B.1.b. Reliability**

The accelerator is scheduled to run approximately 450 hours per month for research, although in 2006 it was necessary to limit operating hours January thru April because of budget restrictions in the aftermath of Hurricane Katrina. The reliability with which this schedule is met is highly important for a productive research program. The data for both scheduled beam time and delivered beam time is shown in fig 3 for the year 2006. The reasons why the schedule may not be fully met include disturbances to the incoming electrical supply (thunderstorms and hurricanes) as well as accelerator equipment faults. The overall efficiency achieved by CAMD in 2006 was 97.9% and the integrated beam intensity

was 640 Ampere-hours with an average beam current of 147 mA. This performance is competitive with the best international standards achieved by synchrotron light sources.

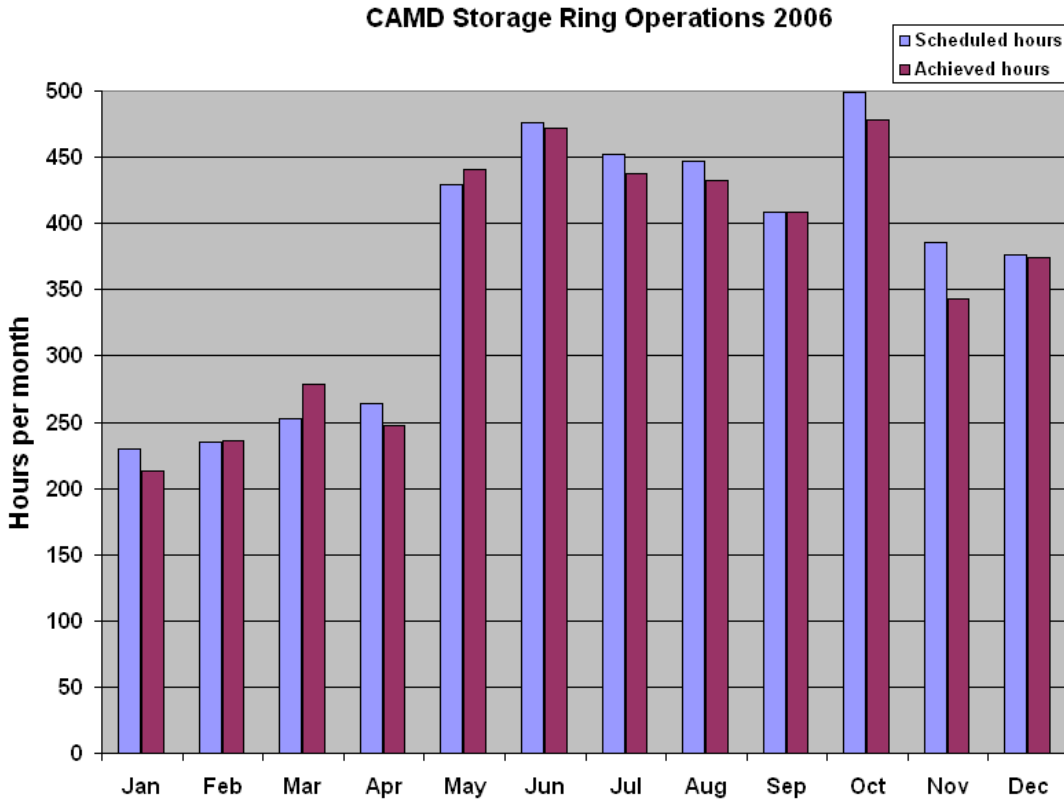


Figure 4. Scheduled and achieved beam hours per month for CAMD in 2006.

### III.B.1.c. Opportunities and their limits

These paragraphs describe in a general sense the opportunities to improve the performance of CAMD as it now exists. Detailed descriptions and costs will be given in IV A, B, C.

#### *Higher beam current*

The beam current is limited by instabilities and by the finite RF power available to replenish the loss due to radiation. The first priority would be to overcome the instabilities, for which there are several countermeasures available such as a third harmonic RF cavity and a set of well distributed octupole magnets. Once higher currents, greater than say 300 mA, are routine it will be necessary to increase the available RF power by either up-rating the klystron and or by installing new cavities. At some level of beam current, which might be many hundreds of milli-Amperes the cooling of the radiation absorbers would need to be improved.

#### *Increased beam brightness*

The brightness of the CAMD light source, which is a measure of how its beams can be focused to a small spot with low divergence, has been increased by about a factor 10 by



Careful optimization of the focusing magnets in the storage ring. This has probably fully exploited the improvement potential by this route; however some small additional gains (20%/30%) could be obtained by using more complex settings for the focusing magnets...However, a further increase in brightness of a factor 3 could be obtained by installing additional corrector magnets, skew quadrupoles, to improve the vertical beam size. These steps would bring the CAMD storage ring to its ultimate brightness potential, other than entirely rebuilding its structure.

### ***Increased flux density***

Some experiments benefit from increased flux density even without an increase in beam brightness. This technique has been applied since 2002 to the protein crystallography beam line which uses the wavelength shifter. It increases the flux density at the wiggler source point by a factor 5 by shrinking the vertical beam size through use of a special operating mode of the storage ring. This is called the Minibeta and it increases the flux density at the wiggler source point by a factor 5 by shrinking the vertical beam size there. It will be possible to make an additional Minibeta at another straight section should a second ID be installed. These improvements could be obtained without significant additional costs.

### ***Beam position stabilization***

The electron beam source position is stabilized continuously and achieves typically +/- 50 micron variation over the life of a user beam fill. Using modern digital electronics would allow the beam stabilization to be improved by reducing the variation and increasing the rate at which correction is applied. A further improvement would be to install photon position monitors on all beamlines, to allow beam angle to be stabilized in addition to source position. In view of the relatively large beam source size in CAMD +/- 10 micron variation could represent the most cost effective improved performance.

### ***Beam lifetime***

By reducing the pressure inside the storage ring vacuum chamber the beam lifetime could be increased from its well conditioned value of 15 hours. It is not easy to accomplish a reduced pressure because the CAMD system is already operating in the Ultra High Vacuum regime with pressure approximately  $10^{-9}$  torr. However, by redesigning the vacuum chamber and vacuum pumps it should be possible to more than double the beam lifetime. This would be an expensive development for the CAMD storage ring with a long period of down-time, but it would increase the integrated flux for research by at least 25% and would benefit the more demanding research requiring excellent source stability.

### ***Accelerator infrastructure improvements***

Although the accelerator itself is very reliable, the infrastructure which underpins its operation is inevitably showing signs of degradation after nearly 15 years of use. Furthermore, there have been advances in technology since the CAMD infrastructure was designed about 20 years ago and the facility reliability would benefit from this new technology. A program of replacing and upgrading the numerous items would significantly assist the operation of the storage ring and could be carried out on a rolling basis over several years.

### III. B. 2 Beamlines

#### a. VUV and IR

##### a-1. Variable-Line-Spacing Plane Grating Monochromator (VLSPGM) Beamline

###### Beamline Description

A varied-line-space plane-grating monochromator for the energy range of 200 – 1,200 eV is an upgrade of the aged CAMD plane grating monochromator beamline. Ray-tracing simulations predict performance improvements in both resolving power and throughput. An increase in resolving power from ~3,000 to the range 28,000 – 8,000 (from low to high energy) throughput increase of 50 – 400% are expected. In contrast to the large enhancement of performance, the upgrade is relatively inexpensive because of extensive utilization of the current beamline components. Some of the beamline parameters are summarized below.

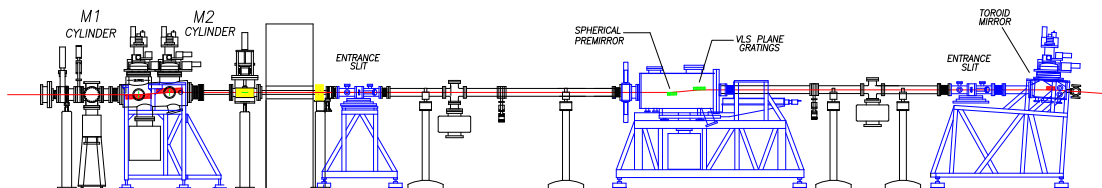
Grating: two variable-line-spacing plane gratings (500 and 1000 gr/mm)

Bending magnet: ~7 mrad horizontal acceptance

Range: 200 – 1,200 eV

Resolution: >1,000 @ 100 micron slits (theoretical)

Throughput: ~1 x 10<sup>10</sup> photons/sec·100mA with 100 micron slits (measured)



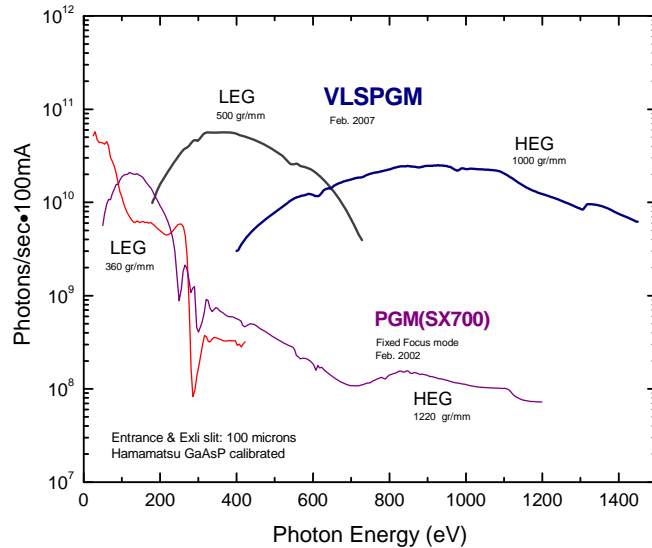
Drawing of the VLSPGM Beamline



Photograph of the VLSPGM Beamline

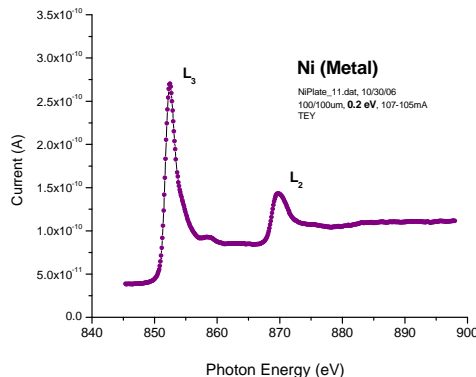
## Current Status

The beamline is operational but still the final commissioning phase. Preliminary performance results confirm the performance upgrade. The beamline throughputs (measured at 100 micron entrance and exit slit) were measured by a calibrated photodiode. The result (figure below) indicates nearly two order of magnitude better flux than the old PGM in the soft x-ray (200 – 1200 eV) energy region. This improvement in flux is results of the clean (non-carbon contaminated) optical surfaces and the VLSPGM



The measured photon flux from the VLSPGM beamline and the old PGM beamline

design which is utilizing one less reflection surfaces (mirrors) than those of the old PGM design. It must be noted that very slight carbon contamination in the carbon-edge ( $\sim 285$  eV) in the measured flux which promises possibility of NEXAFS (near-edge x-ray absorption fine structure) spectroscopy in organic samples which were not possible with the old PGM in the past. Experiments such as MCD (magnetic circular dichroism) and PEEM (photoemission electron microscope) are also planned with this new VLSPGM beamline. As an example of the beamline performance, the absorption spectrum of Ni metal is given in the figure below, which was measured by total electron yield method. The spectrum indicates reasonable signal strength and resolution.



New variable line spacing gratings (~\$80,000) has been purchased from: “Enhancement of Synchrotron Beamline for Magnetics Research”, R. Kurtz, P. Dowben, G. Mankey, P. Sprunger, S. Stadler, NSF, 2002.

### Publications

The publication record of the PGM beamline is listed below. The old PGM beamline was one of the working-horse beamline at CAMD during 1992 – 2001. The beamline was used by the three major user groups (LSU/Physics, LSU/Chemistry, and CAMD) with their own end stations. Mostly ARUPS (angle-resolved photoemission) spectroscopy and gas phase fluorescence measurements were performed. In these measurements, the beamline was used at the fixed energy with the photon energy under 200 eV. Serious NEXAFS measurements were rarely performed. Due to lack of the working end stations and the limited performance of the beamline, the usage of the beamline decreased gradually since 2002. These facts motivated upgrading the old PGM beamline with the VLSPGM design.

Year	2000	2001	2002	2003	2004	2005	2006
Publications	5	3	4	1	2	4	0

Selected publications are listed below.

“The electronic structure of  $\text{CaMnO}_x$  with  $2.66 \leq x \leq 3.00$  studied with photoemission and X-ray absorption spectroscopy”, G. Zampieri, F. Prado, A. Caneiro, J. Briatico, M. T. Causa, M. Tovar, B. Alascio, M. Abbate, and E. Morikawa, *Phys. Rev. B*, **58**, 3755 (1998).

“Photoemission study of pristine and photo-degraded poly-(methylmethacrylate)”, K. K. Okudaira, S. Hasegawa, E. Morikawa, P. T. Sprunger, V. Saile, K. Seki, Y. Harada, and N. Ueno, *J. Apply. Phys.*, **83**, 4292 (1998).

“Sulfur on  $\text{TiO}_2(110)$  studied with resonant photoemission”, E. L. D. Hebenstreit, W. Hebenstreit, H. Geisler, S. N. Thornburg, C. A. Ventrice, Jr., D. A. Hite, P. T. Sprunger, and U. Diebold, *Phys. Rev. B* **64**, 115418 (2001).

“Surface resonances and reduced symmetry in the heteroepitaxial Ag/Cu(110) system”, D.A. Hite, O. Kizilkaya, P.T. Sprunger, E. Laegsgaard, F. Besenbacher, *Phys. Rev. B* **65**, 113411 (2002).

As stated the above, the preliminary performance of the VLSPGM beamline confirmed major upgrade from the old PGM beamline. This new soft x-ray beamline provides new research opportunities in the fields such as NEXAFS, MCD, and PEEM, and expects to attract more new users to the CAMD facility.

## a-2. Fourier Transfer Infrared (FT-IR) Microscopy Beamline

### Beamline Description

The infrared microscopy beamline utilizes a pair of mirrors (plane and toroid) to provide focus of the infrared radiation from the bending magnet to the outside of the radiation shielding wall through a diamond window. This focus serves as a new source point for the FT-IR spectrometer and the IR microscope. The beam is then reflected by an off-axis parabolical mirror, which collimates the beam to the spectrometer and the microscope. The beamline parameters are summarized below.

Bending magnet: 50 mrad in vertical and 50 mrad in horizontal acceptances with newly commissioned dipole chamber

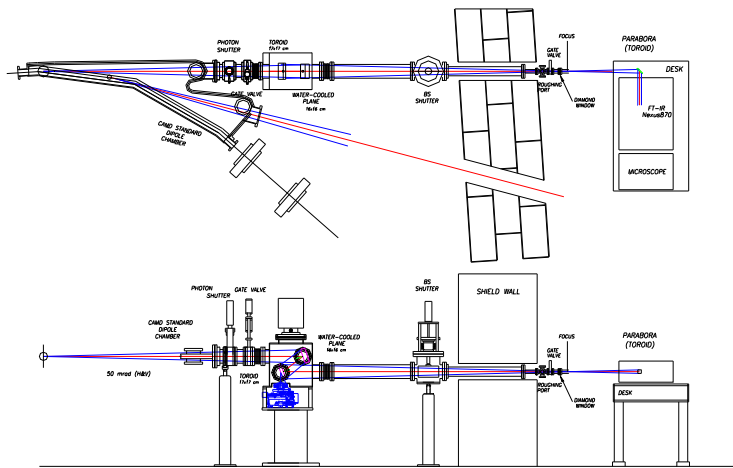
Nicolet FT-IR spectrometer

Nicolet IR microscope (MTC-A and MTC-B detectors)

Spectral Range: MCT-B for  $11,700 - 400 \text{ cm}^{-1}$ , MCT-A for  $11,700 - 600 \text{ cm}^{-1}$

Spectral Resolution: max.  $0.125 \text{ cm}^{-1}$

Spatial resolution: max.  $\sim 15 \times 15 \mu\text{m}^2$



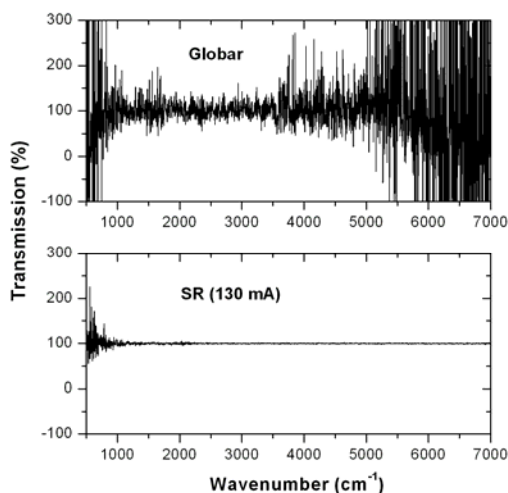
Drawing of the FT-IR Microscopy Beamline



Photographs of the FT-IR Beamline. The mirror chamber located inside of the radiation shielding is shown in the photo on the left, and the FT-IR spectrometer and microscope are shown on the right.

### Current Status

The beamline is in operational since it was commissioned in 2004. The most important component of the IR system is the microscope which utilizes Schwarzschild optics, two objectives and one condenser, allowing both reflection-and-transmission-mode data acquisitions. The maximum spatial resolution is approximately 15  $\mu\text{m}$  with the synchrotron radiation source. The mercury cadmium telluride (MCT) microscope detector covers the mid-IR spectral range of 11,700 - 400  $\text{cm}^{-1}$ . Chemical imaging, namely 2-dimensional IR mapping, can be performed by computer controlled XY-stage of the microscope. High brightness provided by synchrotron source is especially advantageous for microspectroscopic investigations of small size samples from a wide variety of fields including physics, chemistry, biology, and material science. This high brightness yields a superior S/N ration when compared to conventional source. The figure below shows the comparison of 100% transmission line measured using at 10x10  $\mu\text{m}^2$  microscope aperture for the synchrotron and a conventional globar source.



The S/N ratio in the 100% transmission line of the synchrotron and conventional globar sources.

The IR beamline recently received major performance upgrades. A new aluminum dipole chamber (picture shown below) has been installed successfully during the shutdown in January 2007. The new dipole chamber allows acceptance of 50 mrad (horizontal) and 50 mrad (vertical) radiations as compared to 15 mrad and 50 mrad with the previous dipole chamber. In addition, a new detector (MTC-A) was also installed at the microscope. These modifications provide more infrared flux in the mid-IR as well as far-IR ranges.



Photograph of new dipole chamber for the IR beamline

The new dipole chamber was funded by Louisiana Board of Regents, “Modification of infrared (IR) beamline to enhance far-IR and Thz microscopy capability”, E. Morikawa (CAMD/LSU) and J. D. Scott (CAMD/LSU), 2005-2006.

#### Publications

The IR beamline produced six papers since 2004 as shown in the table below. The number of publications is low compared to the similar IR beamline at other synchrotron facilities such as NSLS, ALS, and SRC. The reason is small size of the users. Currently we have seven users, from University of Louisiana at Lafayette (Pitting corrosion), University of Bonn (Plants), University of Nebraska (Organic materials), Tulane University (Polymers), LSU (Geological samples) and CAMD (Minerals). Total usage of the IR beamline with all users is in average less than 10 weeks in a year. Since the CAMD IR beamline performance is competitive as compared to beamlines at other synchrotron facilities, more new users have to be developed.

Year	2004	2005	2006
Publications	1	2	3

Selected articles are given below.

“Performance of the Infrared Microspectroscopy Beamline at CAMD”, O. Kizilkaya, J. D. Scott, E. Morikawa, J. D. Garber, and R. S. Perkins, *Rev. Sci. Instrum.* **76**, 013703 (2005).

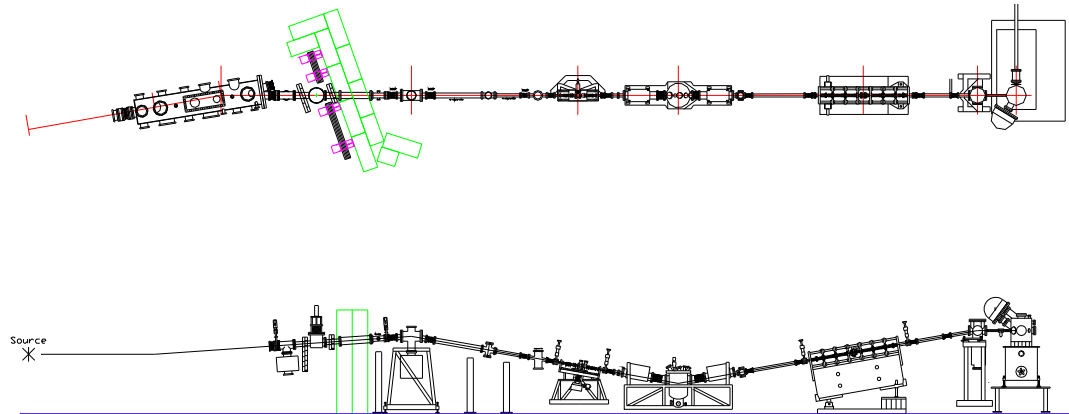
“Functionalization of Gold and Glass Surfaces with Magnetic Nanoparticles Using Biomolecular Interactions”, B. G. Nidumolu, M. C. Urbina, J. Hormes, C. Kumar, and W. T. Monroe, *Biotechnology Progress*, 22(1), 91-95, (2006).

“The electronic structure of 1,2-PCB10H11 molecular films: a precursor to a novel semiconductor”, S. Balaz, Di Dimov, NM Boag, K. Nelson, B. Montag, JI. Brand, PA Dowben, *Applied Physics A- Materials Science & Processing* 84(1-2):149-159, 2006.

### a-3. 6-meter Toroidal Grating Monochromator (6m-TGM) Beamline

#### Beamline Description

The monochromator featuring interchangeable three toroidal gratings for providing monochromatic photons in the VUV range. The beamline was initially operated at the National Synchrotron Light Source (Brookhaven) and moved to CAMD in 1996. Some of the beamline parameters are summarized below.



The 6m-Toroidal Grating Monochromator Beamline (top and side views)

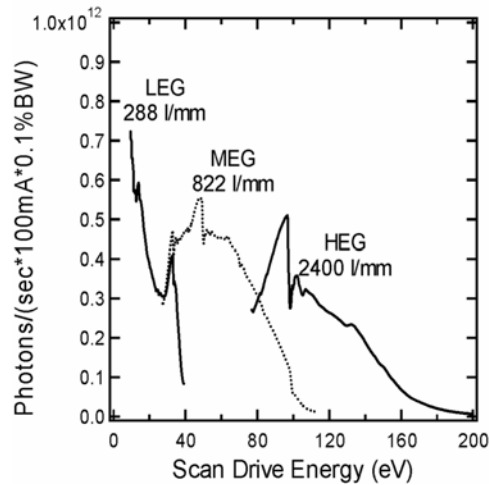


Photograph of the 6m-Toroidal Grating Monochromator Beamline

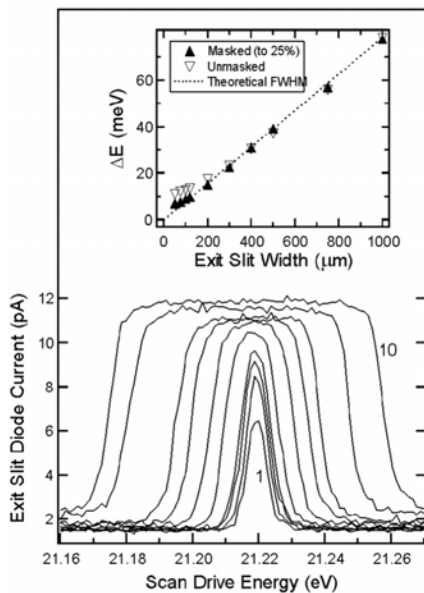


Gratings: toroid (288, 822, and 2400 gr/mm)  
 Operational Range: 15 – 200 eV  
 Bending magnet: 28 mrad horizontal acceptance  
 Spectral Resolution: ~2,000 @ 100 micron slits  
 Throughput:  $\sim 3 \times 10^{11}$  photons/sec·100mA

The measured beamline flux measured with a silicon photodiode and normalized to ring current is plotted in the figure below for the three toroidal gratings.



The measured beamline flux of the 6m-TGM beamline



Resolution tests were performed with He I radiation (discharge lamp) and a silicon diode behind the exit slit. The results are given in the left figure. The ultimate resolution (7 meV) increases to 11 meV for the unmasked grating. Removing the grating masks enhanced the flux by a factor of four. The ultimate resolving power is about 2000.

### Current Status

The beamline has been operational since 1998. A photoemission station developed and owned by J. Erskine (Texas A&M) was mounted at the beamline as a permanent end station until 2003. After the end station was removed, the beamline was used as a source for a medium resolution angle-resolved ultraviolet photoemission spectroscopy (ARUPS) station developed by the physics department at LSU. Currently the beamline is providing monochromatic photons to a newly commissioned high-resolution ARUPS station which was funded by Louisiana Board of Regent, “Louisiana High-Resolution Photoemission End station”, P. Sprunger (LSU), R. Kurtz (LSU), C. Ventrice (UNO), H. Geisler (Xavier), E. Morikawa (CAMD), in 2002.

The 6m-TGM beamline provides adequate intensity and resolution for the medium resolution photoemission spectroscopy measurements. The beamline control program was modified recently for more user friendly beamline operation.

### Publications

The publication record of the 6m-TGM beamline is listed below. The Texas UPS end station, mounted permanently at the beamline until 2003, was extensively used for Ph.D. thesis work from a graduated student of Texas A&M. The UPS endstation employed between 2004 and 2005 was found to be having technical problems later. These facts reflect the lack of publication for this beamline history.

Year	2000	2001	2002	2003	2004	2005	2006
Publications	0	0	1	0	1	0	0

A new high-resolution ARUPS end station (LSU/Physics) was commissioned successfully at the 6m-TGM beamline in spring 2007. As soon as the endstation became operational, the beamtime of the 6m-TGM beamline was fully booked, indicating strong demands for active endstation in VUV photoemission spectroscopy. More publications are expected from the beamline in near future.

The selected publications are listed below.

“CAMD 6-m toroidal grating monochromator beamline”, K.D. Koch, C.V. Mohan, J.L. Erskine, P.T. Sprunger, and J.D. Scott, Nuclear Instruments & Methods in Physics Research Section A, 483 (2002) 821-829.

“Surface reconstruction of FeAl(110) studied by scanning tunnelling microscopy and angle-resolved photoemission spectroscopy”, O. Kizilkaya, D. A. Hite, D. M. Zehner, P.T. Sprunger, Journal of Physics-Condensed Matter, 16(30), 5395-5406 (2004).

#### a-4, 3-meter Toroidal Grating Monochromator (3m-TGM) Beamline

##### Beamline Description

The 3-m TGM beamline is a high-flux medium resolution instrument which delivers monochromatic radiation the energy range between 10 eV and 150 eV with the two toroid gratings (380 gr/mm and 1800 gr/mm). The first toroid mirror accepts 24 mrad of synchrotron radiation in horizontal direction, and reflects the radiation to the toroid grating through the entrance slit. Monochromatized radiation from the grating then passes through the exit slit, and is focused at the sample position by the ellipsoidal refocusing mirror. The photon energy is scanned by simple rotation of the grating. The beamline was operated at the National Synchrotron Light Source (Brookhaven) and moved to CAMD in 1997. Owing to the height difference between the NSLS VUV ring and the CAMD ring, the 3m-TGM beamline layout was modified by adding a plane mirror located after the exit slit to make the output beam parallel to the experimental floor.

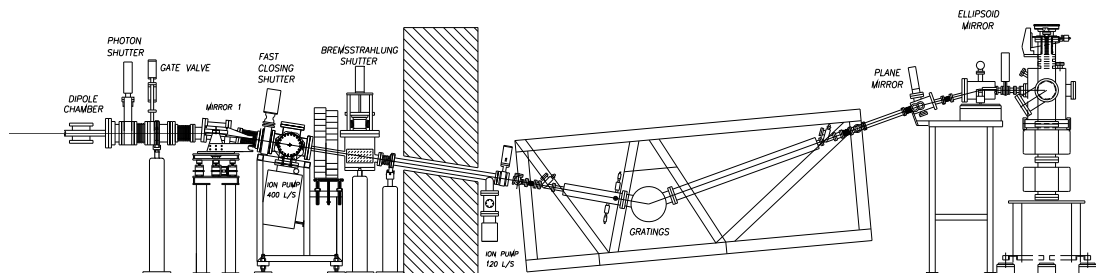
Gratings: toroidal gratings (380 and 1800 gr/mm)

Operational Range: 10 – 150 eV

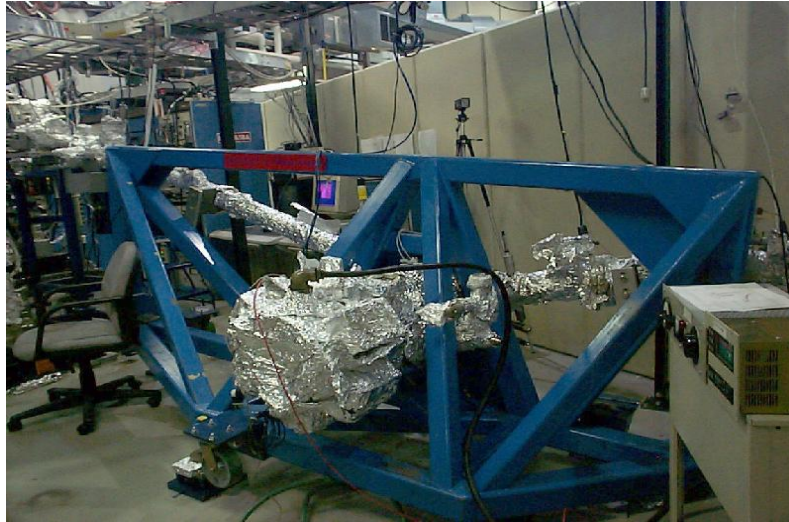
Bending magnet: 24 mrad horizontal acceptance

Resolution: 200-700

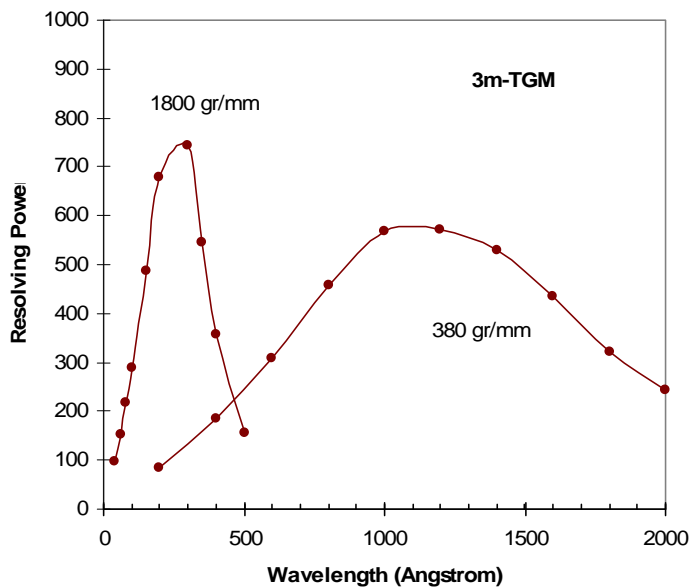
Throughput:  $\sim 10^{11}$  photons/sec·100mA



Drawing (side view) of the 3m-TGM Beamline



Photograph (grating chamber) of the 3m-TGM Beamline



Simulated resolution of the 3mTGM beamline with 380 gr/mm and 1800 gr/mm gratings.

### Current Status

The beamline was commissioned in 2000. Since then the beamline is fully operational and it produces adequate flux and resolution to the designated end station designed for angle-resolved ultraviolet photoemission spectroscopy (ARUPS) measurements where photoelectrons are monitored by a 50 mm semispherical electron analyzer. The ARUPS station possesses standard surface science sample preparation capabilities (sample

heating, cooling, and sample loading). The beamline control program allows performing resonant photoemission (i.e. constant initial state spectroscopy) measurements. The combined beamline and analyzer resolution is ~70 meV.

After the 3mTGM beamline was moved from Brookhaven to CAMD, new first mirror (toroid) with a chamber and two toroidal gratings were purchased from the fund awarded by the National Science Foundation – DCI, "Upgrade of a synchrotron Beamline for Surface Chemistry", P. Dowben (Univ. of Nebraska), E. Morikawa (CAMD/LSU), P. T. Sprunger (CAMD/LSU), A. Moewes (CAMD/LSU), and M. Langell (Univ. of Nebraska), in 1998-1999.

### Publications

This beamline is the most heavily used of the VUV beamlines at CAMD. The beamtime was heavily overbooked especially in recent years. The number of users increased steadily from 2000, and it counts 29 users until present. As a result many publications are produced from data obtained on this beamline. The publication history of the beamline (and ARUPS end station) is listed in table below. There were 5 publications until 2001. However, there were total 78 publications between 2002 and 2006. This extremely high productivity indicates that existence of the strong VUV photoemission users in the CAMD user community. Photon energy tune ability allowable from the synchrotron radiation is essential in the VUV photoemission spectroscopy.

Year	2000	2001	2002	2003	2004	2005	2006
Publications	1	4	11	11	15	25	19

Selected publications are listed below.

"The Electronic Structure of ErAs(100)", Takashi Komesu, Hae-Kyung Jeong, Jaewu Choi, C.N. Borca, P.A. Dowben, A.G. Petukhov, B.D. Schultz, and C.J. Palmstrøm, , Phys. Rev. B 67 (2003) 035104.

"The surface structure of TiO<sub>2</sub>(011)-2x1", T. J. Beck, A. Klust, M. Batzill, C. DiValentin, A. Selloni, U. Diebold, Phys. Rev. Lett. 93, (2004) 036104.

"Orientation and bonding of 4,4'-biphenyldiisocyanide", A.N. Caruso, R. Rajesh, G. Gallup, J. Redepenning and P. A. Dowben, Journal of Physical Chemistry, B108 (2004) 6910-6914.

"Gas phase-dependent properties of SnO<sub>2</sub> (110), (100), and (101) single crystal surfaces: structure, composition, and electronic properties", M. Batzill, K. Katsiev, J.M. Burst, U. Diebold, A.M. Chaka, B. Delley, Phys. Rev. B 72, 165414 (2005).

"Strain Induced half metal to semiconductor transition in GdN", Chun-gang Duan, R.F. Sabiryanov, Jianjun Liu, W.N. Mei, P.A. Dowben and J.R. Hardy, Phys. Rev. Letters, **94** (2005) 237201.

"Gas phase-dependent properties of low index SnO<sub>2</sub> single crystal surfaces II: electronic structure", M. Batzill, K. Katsiev, J.M. Burst, U. Diebold, A.M. Chaka, B. Delley, Phys. Rev. B 72 (2005) 165414.

### a-5. 3-meter Normal Incidence Monochromator (3m-NIM) Beamline

#### Beamline Description

The beamline was designed primary for high-resolution photoelectron spectroscopy utilizing a Scienta electron analyzer, which is permanently placed as an endstation at the beamline. In order to expand utilization of the beamline, an additional beamline-tail (2<sup>nd</sup> tail) will be built.

Gratings: 2 spherical gratings (1200 gr/mm Au coated and 1200 gr/mm Al coated)

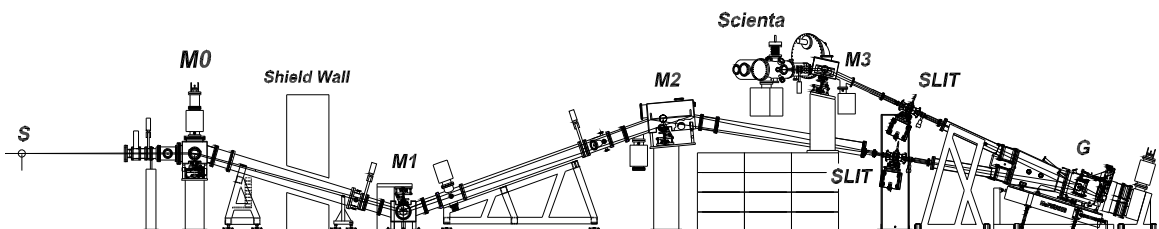
Operational Range: 5 – 30 eV

Bending magnet: 70 mrad horizontal acceptance

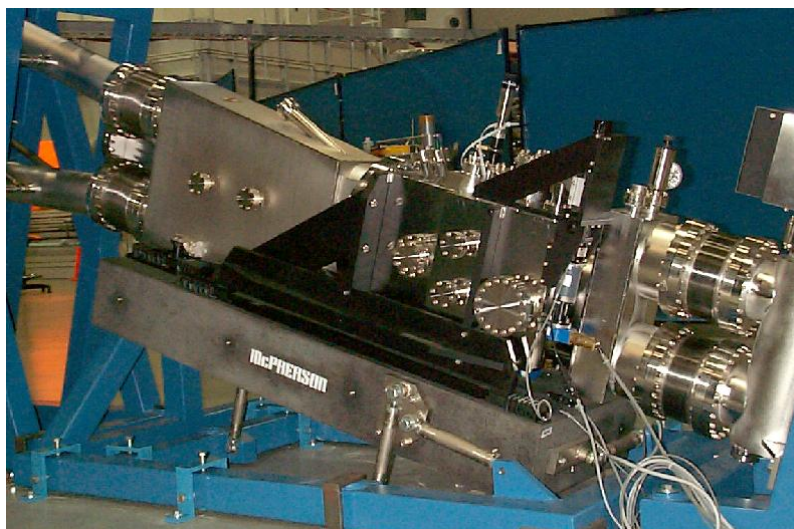
Resolution: 10,000 – 50,000

Throughput:  $\sim 2 \times 10^{10}$  photons/sec·100mA

Layout of the 3-m NIM beamline is shown the figure below. The water-cooled ellipsoidal mirror ( $M_0$ ) accepts a full 70 mrad of horizontal radiation from a dipole magnet. By using two cylindrical mirrors ( $M_1$  and  $M_2$ ), each producing the same coma but oppositely signed, a coma-free image at the entrance slit can be produced in the vertical (meridian) direction. The best monochromators, with regard to resolution, over the desired spectral region, use spherical gratings with incidence angles near normal and equal length of source and objective arms. By considering geometric constraints of the experiment hall along with resolving power, it was decided to utilize the McPherson mount with an optimal focal length of 3.00 meters. This mount requires the rotation and the translation of the grating during the wavelength scan. The monochromator is equipped with two inter-changeable spherical gratings. The ellipsoidal mirror ( $M_3$ ) focuses the exited beam from the grating onto a sample with a demagnification factor of  $\sim 1/2$ .

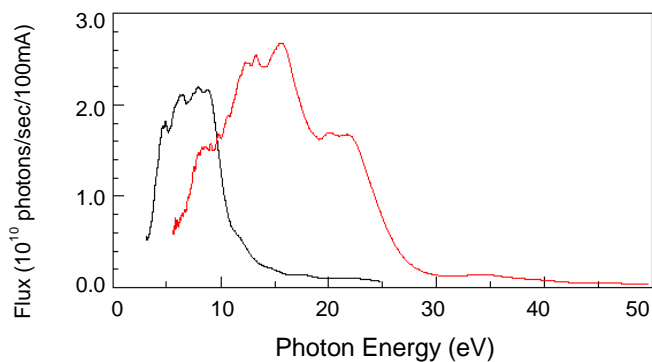


Layout of the 3m-NIM beamline



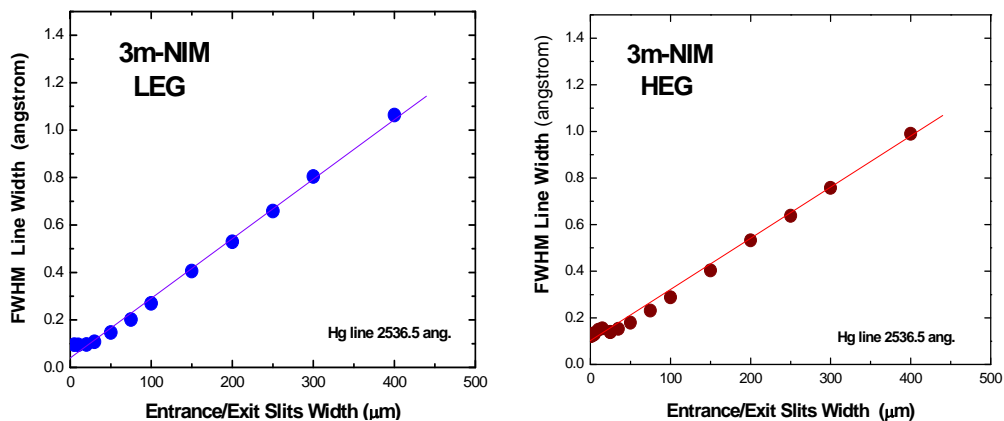
Photograph of the 3m-NIM beamline (grating section)

Photon intensity at the sample position (entrance and exit slits, 100  $\mu\text{m}$ ) was measured by a photodiode. The measured flux was normalized to ring current of 100 mA and corrected by absolute quantum efficiency of the diode.



Measured beamline flux at the sample position

The width (FWHM) of a major intense line 2536.5  $\text{\AA}$  from the Hg-lamp was measured as a function of the monochromator slit widths (shown below). By using the zero slit width value and assuming a natural width of the Hg-line as 0.09  $\text{\AA}$  FWHM, the instrumental resolutions for the both high and low energy gratings are evaluated to be  $\lambda/\Delta\lambda = 57,600$ .



Measured resolution of the 3m-NIM beamline

### Current Status

The beamline is fully operational since 2002. The beamline software program (LabView) controls not only the wavelength scan but also performs data acquisition with multi-channel AD converter. Currently the 3m-NIM beamline is dedicated for high-resolution photoemission spectroscopy. A high-resolution electron analyzer Scienta 200 for ARUPS was re-commissioned in 2004. The ultimate resolution of Scienta analyzer was measured to be  $\sim 5\text{meV}$  by employing argon gas, which is slightly better than the company specification value. It was also confirmed that the detector performs well in the angular mode which provides information regarding angular distribution of the photo-emitted electrons from the sample.

The 3m-NIM beamline was funded by National Science Foundation, "The Development of a Low Energy, High Resolution Synchrotron Radiation Beamline", E.W. Plummer, J.W. Allen, P.A. Dowben, J.L. Erskine, R. Gooden, and V. Saile, NSF, DMR-9512275, in 1995.

### Publications

Publication history of the beamline is listed in the table below. Because of insufficient manpower and technical complications, the Scienta analyzer required unexpectedly much longer time for full commissioning. This is evident from the publication record. Most of the early publications are related to the beamline instrumentations. It was found in 2006 that the micro-channel-plate detector of the Scienta analyzer needed replacement, which contributed to an additional down time. Although it is not reflected in the publication history, there were reasonable numbers of users after the re-commission of the analyzer in 2004. Scienta analyzer especially in its early model as ours is known to be a difficult instrument to operate. At least, one full time personal, is needed for maintain the maximum performance of the Scienta analyzer. Currently the Scienta is managed by a CAMD staff in addition to the duties at the 3m-TGM beamline.



Year	2000	2001	2002	2003	2004	2005	2006
Publications	1	1	2	0	0	2	1

The selected publications are listed below.

“The New Normal-Incidence-Monochromator Facility at CAMD”, E. Morikawa, C. M. Evans, and J. D. Scott, Proceedings of Application of Accelerators in Research and Industry:- Sixteenth International Conference, AIP Conference Proceedings, **576**, 730 (2001).

“The Double-Tailed Normal-Incidence-Monochromator Beamline at CAMD”, E. Morikawa, C. M. Evans, and J. D. Scott, Rev. Sci. Instrum., **73** (2002) 1557.

“Electron phonon coupling and the temperature dependent initial energy shifts of the surface states on Be (1010)”, S. -J. Tang, Ismail, P. T. Sprunger, E. W. Plummer, Phys Rev B **65**, 235428 (2002).

“Vibronic Coupling in the Valence Band Photoemission of the Ferroelectric Copolymer: poly(vinylidene fluoride) (70%) and trifluoroethylene (30%)”, Luis G. Rosa, Ya.B. Losovyj, Jaewu Choi, and P.A. Dowben, Journal of Physical Chemistry B **109** (2005) 7817-7820.

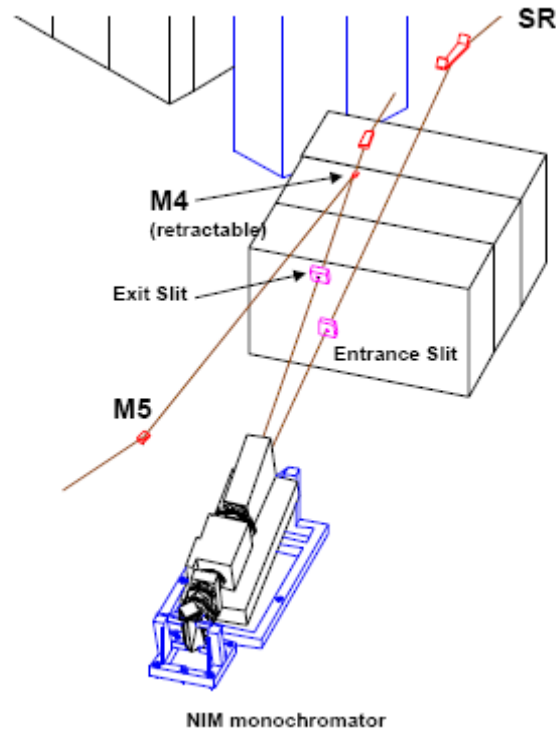
“Photohole Screening Effects in Polythiophenes with Pendant Groups”, D.-Q. Feng, A.N. Caruso, D.L. Schulz, Ya.B. Losovyj and P.A. Dowben, , *J. Phys. Chem. B* **109** (2005) 16382-16389

“The Semiconductor to Insulator Transition in Poly(3-hexylthiophene)”, A.N. Caruso, D.-Q. Feng, Ya.B. Losovyj, D. Schulz, Snjezana Balaz, Luis G. Rosa, A. Sokolov, B. Doudin and P.A. Dowben, , *Physica Status Solidi B* (2006) in press.

Since the Scienta analyzer is permanently placed as an endstation for high-resolution photoemission spectroscopy studies, 2<sup>nd</sup> tail of the beamline was considered in order to allow for a broader range of scientific activity, such as photo-ionizations and photo-absorptions of atoms and molecules. This 2<sup>nd</sup> tail project was recently funded by Louisiana Board of Regents Support Fund “Modification of the Normal-Incidence-Monochromator Beamline at CAMD to Provide a Double-Tailed Beamline for Spectroscopy in the Far Ultraviolet”, J. D. Scott (CAMD) and E. Morikawa (CAMD) in 2005.

In design of the 2<sup>nd</sup> tail (shown in the figure below), beam after passing through the exit slit is reflected horizontally and backward by a retractable cylindrical mirror, then reflected up vertically by a toroidal mirror. The output beam from the toroid mirror is parallel to the floor with a reasonable beam height for most end stations. A total demagnification factor of 3.48 is achieved in horizontal direction. In vertical direction, an intermediate focus is made between the cylinder and the toroid mirrors, which allows the use of a relatively small mirror for the toroidal mirror. The total magnification factor in vertical direction is 1.85. Throughput from the 2<sup>nd</sup> tail is ~2-3 times less intensity compared to one from the 1<sup>st</sup> tail at the photon energy of < 30 eV, and is about one order of magnitude less at >30 eV, due to additional reflecting surface and the large incidence angle. However, spot size at the sample position at the 2<sup>nd</sup> tail is relatively small due to

the larger horizontal demagnification factor, therefore, the effective intensity is expected to be comparable between the 1<sup>st</sup> and 2<sup>nd</sup> tails.



Layout of the 2<sup>nd</sup> tail of the 3m-NIM beamline

The type of research that could be performed at the 2<sup>nd</sup> tail of the NIM beamline include (1) angle resolved photoemission and photoionization spectroscopies, (2) high-resolution atomic and molecular spectroscopies (photoionization, absorption, and magnetic circular dichroism) involving valence-shell bonding and chemically active electrons, (3) high-resolution solid-state spectroscopies (reflectance, transmission, spin-resolved-electron ionization and magnetic circular dichroism) of conduction band electrons and electrons involved in metal-substrate bonding in important inorganic, organic and biological materials and (4) materials research in the area of UV hardening of electronic devices used in space and selective study of UV-sensitive photo resists for deep-UV lithography applications. Currently three researchers from University of Nebraska, University of Texas Galveston, and University of Louisiana Monroe, two LSU faculties from Physics and Chemistry departments, and four staff from CAMD are expressed their strong interests in using the 2<sup>nd</sup> Tail when it becomes available. Most of the key components (mirrors, mirror chamber, ion pumps, and gate valves) are already in house. Thus it is expected that construction and commissioning of the 2<sup>nd</sup> tail will begin in near future.

## Section III.B.2

### b.1 - Double Crystal Monochromator (DCM)

#### Beamline Description

The CAMD XAS beamline has been in operation since the fall of 1994, first using a double-crystal monochromator (DCM) from the Laboratório Nacional de Luz Síncrotron (LNLS), followed by using one from Bonn University. The lowest energy at which data has been successfully measured is the Cu L<sub>III</sub> edge at 932.5 eV, the highest is the Mo K edge at 20,000 eV. Data have been collected from a wide variety of samples associated with research in materials science, catalysis, geology, and environmental science. It is the workhorse of the X-ray group, sees maximum usage, and usually overbooked.

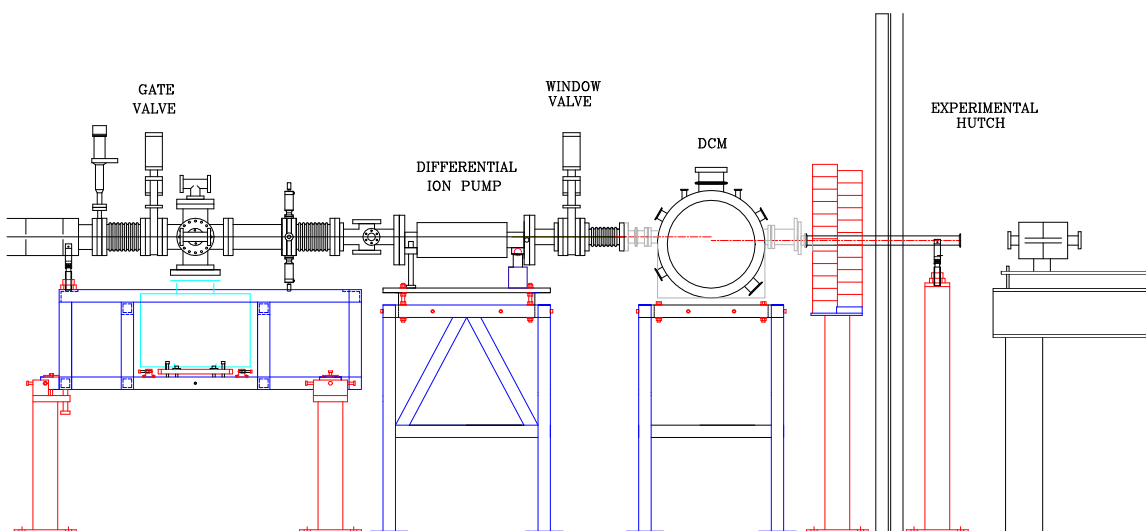


Figure III.B.b.1  
Schematic Drawing of DCM beamline

The DCM beamline is located on port 5b (bending magnet 5 dipole chamber, port b). It accepts 2mrad of radiation from the bending magnet. The monochromator is equipped with two crystals and Lemmonier-Bonn type. It has a fixed exit and it is vacuum compatible. The angular range of the monochromator is roughly 15° - 65°. The available crystals and the corresponding energy range for operation are summarized in Table III.B.b.1. The current beamline has been optimized for operation in the soft x-ray region to take advantage of the source intensity distribution. A differential ion pump immediately upstream of monochromator allows operation with only a thin (seven to 13

μm) Kapton™ window. The crystals in the monochromator can be changed very rapidly, in less than two hours. A photon beam position monitor allows monitoring of the beam position all the time. The beamline operates well over a 1 keV - 12 keV range with the upper limit defined by the drop in source intensity above 10 keV. The resolution is 0.5 eV at low energies and 2 eV at high energies.

**Table III.B.b.1**  
Monochromator Crystals

Crystal	$2d$ (Å)	E (eV)
KAP (001)	26.632	510 - 1800
Beryl (10 $\bar{1}$ 0)	15.954	860 - 3000
YB <sub>66</sub> (400)	11.72	1170 - 4090
InSb (111)	7.481	1830 - 6400
Si (111)	6.271	2180 - 7640
Ge (220)	4.00	3420 - 11980
Si (220)	3.840	3560 - 12470
Ge (422)	2.306	5930 - 20770

XAS can be measured in transmission, fluorescence, and electron yield modes. Detectors available include ionization chambers, a Peltier-cooled Si(Li) detector, and Lytle fluorescence and electron yield detectors. A Lytle furnace is available for *in situ* measurements from liquid nitrogen temperature up to 750° C in controlled atmosphere up to 1 atm pressure. In addition, the monochromator has the potential for performing time-resolved (QEXAFS) studies and implementation of this feature is planned for the near future.

A Canberra 13-element high purity germanium diode array detector was added to the arsenal in 2002. Since then it has become a very important component of the beamline. It is a workhorse on the DCM, and has really enhanced the ability of CAMD to examine low absorber concentration samples, which are often of most relevance to meaningful scientific investigations in many disciplines; such as; biochemistry, catalysis, environmental science, geology, materials science, etc.

In 2003, a second bremsstrahlung shutter was added downstream of the monochromator, with the appropriate RIS and Allen Bradley control system hardware and programming, which allowed one to work at the experimental station in the second hutch and keep light on the DCM crystals, allowing them to stay thermally stable.

Partial List of Funding associated with DCM

Collaborative Research: Biogeochemical Controls on Antimony and Arsenic Mobility in a Siliceous Hydrothermal Systems, P.I.: Annette Summer Engel, \$109,452, 9/15/2006-8/31/08, NSF

Iron-Based Mixed Metal Carbide Fischer-Tropsch Catalysts, J.J. Spivey, Chemical Engineering at LSU, in collaboration with Clemson University, \$ 224,948.00, 8/31/2005 – 8/31/2008, DOE

Staffing

Staff opening (0.75)  
 Gregory Merchan (1.0)  
 Rusty Louis (0.1)

Current Status

The DCM beamline is operational for XAS. It is a general user beamline and is scheduled for constant operation. It has historically been overbooked

Selected Publications

Dooley, K.M., Bhat, A.K., Plaisance, C.P., and Roy, A. (2007) Ketones from acid condensation using supported CeO<sub>2</sub> catalysts: Effect of additives. *Applied Catalysis A: General*, 320, 122-133.

Engel, A.S., Lichtenberg, H., Prange, A., and Hormes, J. (2007) Speciation of sulfur from filamentous microbial mats from sulfidic cave springs using X-ray absorption near-edge spectroscopy. *Fems Microbiology Letters*, 269(1), 54-62.

Farquar, G.R., Alderman, S.L., Poliakoff, E.D., and Dellinger, B. (2003) X-ray spectroscopic studies of the high temperature reduction of Cu(II)O by 2-chlorophenol on a simulated fly ash surface. *Environmental Science & Technology*, 37(5), 931-935.

Meng, W.J., Zhang, X.D., Shi, B., Jiang, J.C., Rehn, L.E., Baldo, P.M., and Tittsworth, R.C. (2003) Structure and mechanical properties of Ti-Si-N ceramic nanocomposite coatings. *Surface & Coatings Technology*, 163, 251-259.

Prange, A., Oerke, E.C., Steiner, U., Bianchetti, C.M., Hormes, J., and Modrow, H. (2005) Spatially resolved sulphur K-edge XANES spectroscopy for in situ characterization of the fungus-plant interaction *Puccinia triticina* and wheat leaves. *Journal of Phytopathology*, 153(10), 627-632.

**Table III.B.b.2: Summary of Beamline Staff and Publications**

Year	2000	2001	2002	2003	2004	2005	2006
Manager	R. Tittsworth	R. Tittsworth	R. Tittsworth	R. Tittsworth	R. Tittsworth	R. Tittsworth	A. Roy
B-L Scientist	R. Tittsworth	R. Tittsworth	R. Tittsworth	R. Tittsworth	R. Tittsworth	R. Tittsworth	A. Roy
Publications	6	7	9	11	7	11	10

## b.2 - X-ray Microprobe (XMP)

### Beamline Description

The XMP beamline is currently used both as an X-ray absorption spectroscopy beamline and an X-ray microprobe beamline. The beamline was reconfigured in 2002 to be very similar to the DCM beamline on port 5b (accepting 2 mrad), except for the added microprobe capability. It is hoped that once the new wiggler beamline is available for XAS, this beamline can be rededicated for X-ray microprobe work only.

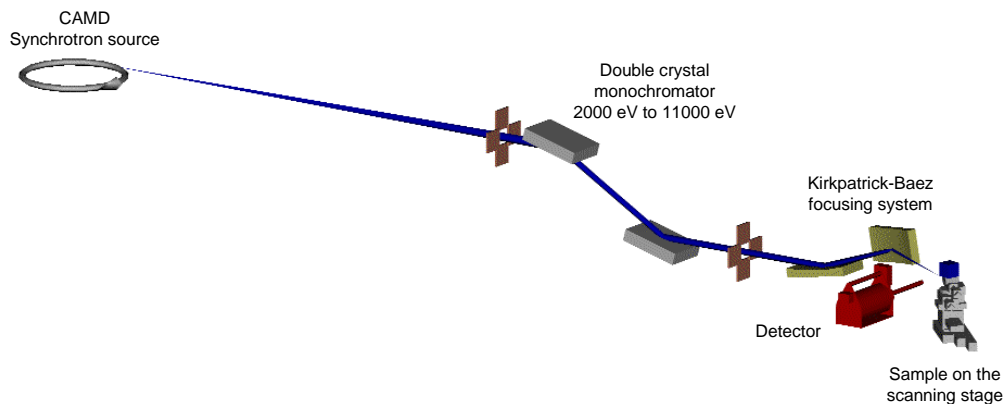


Figure III.B.b.2  
Schematic Drawing of the XMP beamline

Historically, the beamline was built as a collaborative effort between the Argonne National Laboratory and CAMD. The micro-focusing optics was built with the help from Mark Rivers and Peter Eng from the GSE-CARS group at the University of Chicago. A schematic drawing of the beamline and detailed one of the microprobe are shown in Figures III.B.b.2 and Figure III.B.b.3

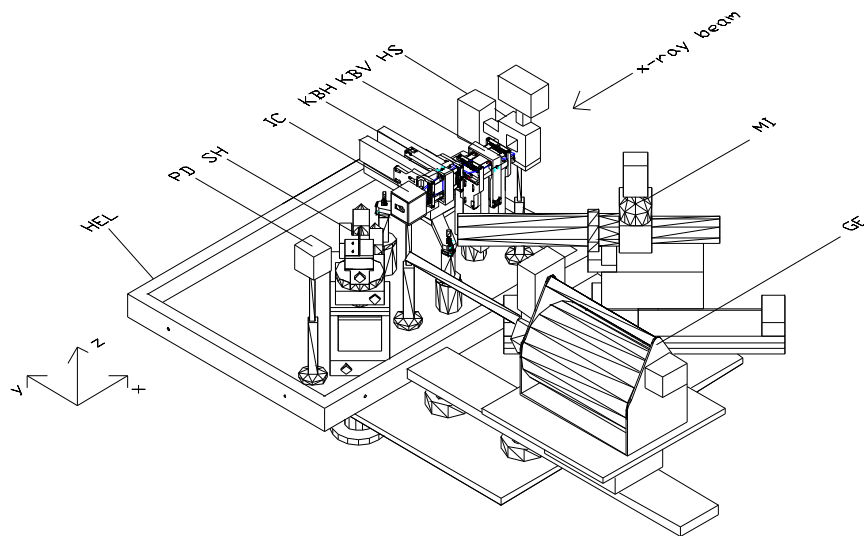


Figure III.B.b.3  
XMP Microfocusing Optics

The incident white or monochromatic x-ray beam (indicated by an arrow) passes through a motorized 4-jaw entrance slit, defining the beam size, which illuminates the vertical and horizontal focusing mirror of the Kirkpatrick-Baez system (KBV, KBH) . After being reflected off the KB system, the beam travels through a 1" long ion chamber (IC) and impinges as a small spot on the sample. The sample, with a typical size of 45 mm x 15 mm, is mounted to the sample holder (SH), which is located on the motorized goniometric sample stage assembly. The sample stage assembly, consisting of 2 translation stages (x, z) and 2 rotation stages (phi, chi), is positioned under 45° to the incident beam. To collect data in transmission a photo-diode is positioned behind the sample in the direct beam. Fluorescence data, on the other hand, is acquired with an energy-dispersive germanium detector, which is also coupled in to the helium atmosphere. To obtain an optical microscope image of the sample, a long-working distance microscope (MI) is pointed through a view port under 90° to the sample.

The initial design consisted of a plexiglass chamber around the micro-focusing system which allowed low-Z measurements when it was filled with helium. In 2005 a large metal chamber replaced the original plexiglass chamber which allowed operation at moderately low vacuum in addition to helium atmosphere. Measurements have been made at phosphorus and sulfur K edges in 2006.

As mentioned earlier, the design of the beamline is very similar to that of the DCM except the absence of the second bremsstrahlung shutter. The crystal sets used at the DCM are also interchangeably used at this beamline. The same detectors from DCM can also be used at the XMP.

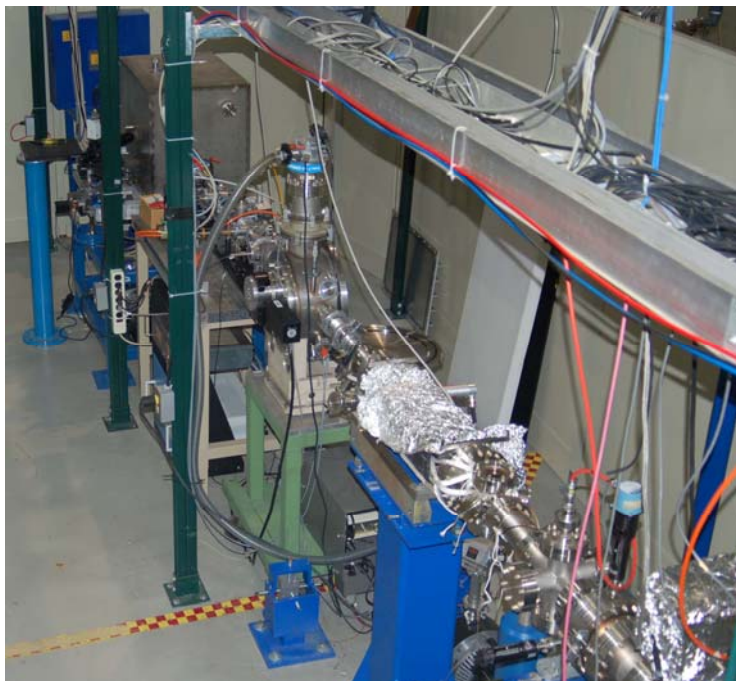


Figure III.B.b.4  
XMP Experimental Hutch

Figure 3 shows a photograph of the X-ray microprobe beamline. The double crystal monochromator is in the middle. At the top middle is the experimental chamber.



Figure III.B.b.5  
XMP Experimental Chamber

A new PC based beamline control and data acquisition system has been installed to replace the original VMS/VAX Alpha system. However, there are still old very old motion controllers that need to be replaced.



Service to the CAMD Nanofabrication group constituted a large part of the experimental time allotted at the XMP during 2002. The relationship between the XMP beamline and the CAMD Nanofabrication group allowed for quick characterization of cobalt-based nanoparticles as well as Fe K-edge analysis of magnetite nanoparticles.

### Current Status

The beamline is operational for standard XAS experiments and as an X-ray microprobe. There has been a surge of interest in using the X-ray microprobe in 2007. In early 2000, a spot size of 20  $\mu\text{m}$  (vertical) x 40  $\mu\text{m}$  (horizontal) could be routinely achieved. At present (June 2007) that size is ca. 80 $\mu\text{m}$  x 50  $\mu\text{m}$ . The mirrors are now almost ten years old and need replacement. This should allow attainment of previous spot size. In addition, the brightness of the ring has improved over the past ten years. This should result in better flux at the XMP beam line.

### Staffing

Vadim Palshin (0.5)

Rusty Louis (0.2)

### Selected Publications

- de Silva, R.M., Palshin, V., Hormes, J., Fronczek, F.R., and Kumar, C.S.S.R. (2007) Investigation of the Influence of Organometallic Precursors on the Formation of Cobalt Nanoparticles. *Journal of Physical Chemistry C*.
- Modrow, H., Palina, N., Kumar, C.S.S.R., Doomes, E.E., Aghasyan, M., Palshin, V., Tittsworth, R., Jiang, J.C., and Hormes, J. (2005) Characterization of Size Dependent Structural and Electronic Properties of CTAB-Stabilized Cobalt Nanoparticles by X-ray Absorption Spectroscopy. *Physica Scripta*, T115, p. 790-793.
- Molders, N., Schilling, P.J., Wong, J., Roos, J.W., and Smith, I.L. (2001) X-ray Fluorescence Mapping and micro-XANES Spectroscopic Characterization of Exhaust particulates Emitted From auto engines Burning MMT-Added Gasoline. *Environmental Science and Technology*, 35(15), 3122-3129.
- Palshin, V., de Silva, R.M., Hormes, J., and Kumar, C.S.S.R. (2007) Effect of Precursor on the Electronic and Geometric Properties of Cobalt Nanoparticles Investigated by Co-K XANES and EXAFS. In B. Hedman, and P. Pianetta, Eds. *X-Ray Absorption Fine Structure - XAFS13*, 882, p. 758-760. American Institute of Physics, Palo Alto, California.
- Roy, A., Moelders, N., Schilling, P.J., and Seals, R.K. (2006) Role of an amorphous silica in portland cement concrete. *Journal of Materials in Civil Engineering*, 18(6), 747-753.
- Song, Y.J., Modrow, H., Henry, L.L., Saw, C.K., Doomes, E.E., Palshin, V., Hormes, J., and Kumar, C.S.S.R. (2006) Microfluidic synthesis of cobalt nanoparticles. *Chemistry of Materials*, 18(12), 2817-2827.

Zinoveva, S., Datta, P., deSilva, R.M., Louis, R., Kumar, C.S.S.R., and Hormes, J. (2007)  
 Time resolved observation of the wet-chemical synthesis of nanoparticles by  
 spatially-resolved X-ray spectroscopy. In E. Morikawa, J. Scott, and A. Roy, Eds.  
 Synchrotron Radiation Instrumentation 2007. Elsevier, Baton Rouge, Louisiana.

**Table III.B.b.3: Summary of Beamline Staff and Publications**

Year	2000	2001	2002	2003	2004	2005	2006
Manager			V. Palshin	V. Palshin	V. Palshin	V. Palshin	V. Palshin
B-L Scientist			V. Palshin	V. Palshin	V. Palshin	V. Palshin	V. Palshin
Publications	1	1	1	1	1	1	2

### **b.3 - Small Angle X-Ray Scattering (SAXS)**

#### Beamline Description

The equipment for the small angle X-ray scattering (SAXS) end station was bought with funding from a National Science Foundation's Integrative Graduate Education and Research Traineeship (IGERT) to Dr. Paul Russo of the Chemistry Department at LSU. The beamline has been installed at port 6a<sub>1</sub> (bending magnet 6, dipole chamber port a<sub>1</sub>...port a is split to accommodate 2 beamlines). A second bremsstrahlung shutter is present in the first hutch to allow for white light on monochromator crystals at all times during operation. CAMD provided the double crystal monochromator. The Brazilian (LNLS) designed double crystal monochromator has Golvchenko geometry, usable for both SAXS and XAS with up to three crystal sets mountable, Si(111), Si(220) and InSb(111), covering the energy range 1.8 keV -14 keV. A differential ion pump immediately upstream of monochromator allows operation with only a Kapton™ window between the ring and the experimental station.

A multiwire gas proportional 2d detector. (Gabriel type, manufactured by Molecular Metrology) is used for signal detection. Optical benches with pinhole apertures, sample chamber, etc, are present.

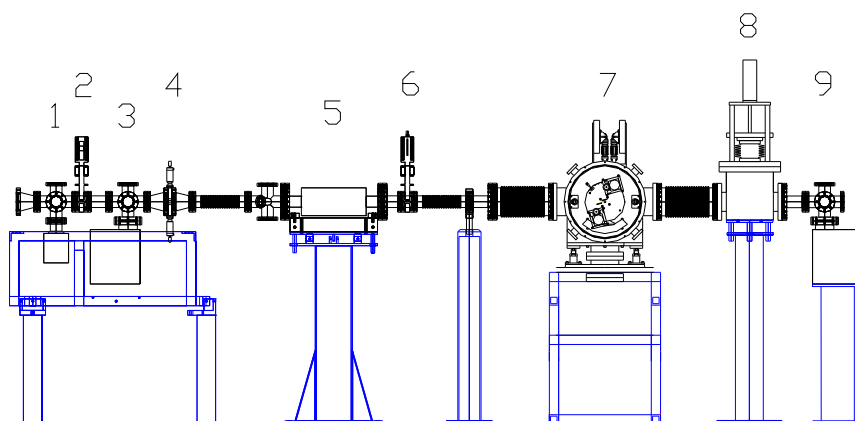


Figure III.B.b.6  
Hutch 1 of the SAX/GIXAFS beamline

- 1 Ion Pump (55 l/s)
- 2 Pneumatic Gate Valve
- 3 Ion Pump (150 l/s)
- 4 Motorized Adjustable Slits
- 5 Differential Ion Pump
- 6 Manual Gate Valve
- 7 Double Crystal Monochromator
- 8 Bremsstrahlung Shutter
- 9 Ion Pump (200 l/s)



Figure III.B.b.7  
SAXS beamline in small angle (left) and wide angle (right) configuration.

### Staffing

Paul Russo, (a Professor in Chemistry and his student )  
Staff scientist (0.3)  
Staff electronic specialist (0.1)

#### Current Status

Though funding for this beamline was obtained in 2000 it became fully operational only in January 2007.

#### Publications

Graduate thesis in preparation 2007.

### **b.4 - Grazing Angle Incidence Extended X-Ray Absorption Fine Structure**

#### Beamline Description

The grazing incidence X-ray absorption fine structure (GIXAFS) beamline was built with funding from the Louisiana Board of Regents in 2000 to Paul Schilling (UNO Mechanical Engineering) and Philip Sprunger (LSU Physics). This end station shares the beamline with the SAXS end station. The GIXAFS endstation consists of a vacuum chamber (built by Advanced Design Consulting) with optical rail built in, for mounting ion chambers, sample manipulation stages, goniometers, slit systems, all remotely controlled (Figure III.B.b.8). The main beamline description is otherwise identical to the SAXS beamline.



Figure III.B.b.8  
GIXAFS vacuum enclosure.

## Current Status

User interest in using the GIXAFS beamline has not been high. Several recent users at the DCM beamline are investigating thin films. These materials can be more easily studied at the GIXAFS beamline.

## Publications

none.

## **b.5 - X-Ray Diffractometry (XRD) Beamline**

### Beamline Description

The XRD beamline was built with a \$78,000 grant from the Louisiana Board of Regents and commissioned in 2006. It consists of a Brazilian-designed (LNLS) double crystal monochromator, a Huber four-circle diffractometer ( $0.001^\circ$  minimum step size), and a Canberra germanium solid state detector. The monochromator is equipped with Si 111 and Ge 220 crystals. The Canberra high purity germanium solid state detector has a resolution of 130 eV at Mn  $K_\alpha$ . For typical use, the diffractometer circle is set to 17 cm, and the source and receiving slits have been set to 300 micrometers and 200 micrometers, respectively. A sample spinner is used for improved particle size averaging. Wavelength can be shifted in a matter of minutes. There is adequate flux to operate the powder diffraction beamline between five and 10 keV (Cr  $K_\alpha$  (2.2896 Å) and Zn  $K_\alpha$  (1.4354 Å) lines, approximately). The diffractometer is placed on a motorized optical bench. The source slit is motorized to allow dynamic slit scanning and slit width variation. All the motors are controlled by two XPS motion controllers, with up to eight cards in each.

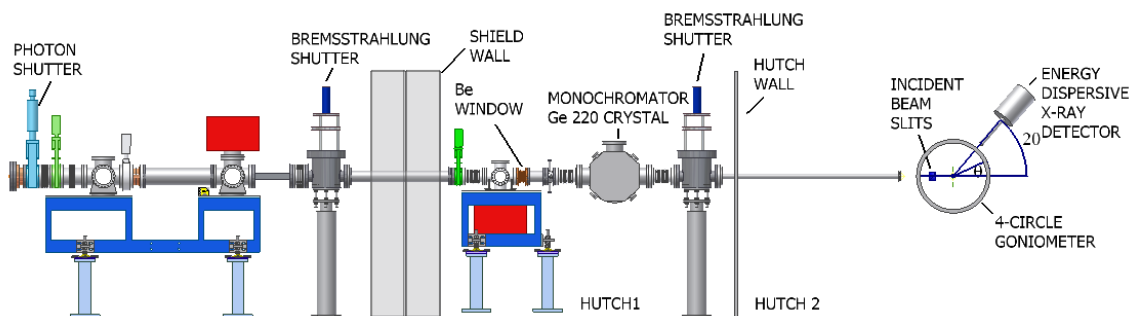


Figure III.B.b.9  
XRD beamline

The XRD beamline is located on port 7a and accepts 3 mrad radiation from the ring. Figure III.B.b.9 shows a schematic drawing of the beamline. The beamline is separated from the main ring by a 250 micrometer thick beryllium window in the first hutch. A double crystal monochromator is placed in one hutch and the diffractometer in a separate

hutch, with a bremsstrahlung shutter in between. The second bremsstrahlung shutter, just before the experimental hutch, allows light to stay incident on the monochromator crystals while samples are being changed. Very little time is thus lost between samples.

At the beamline, the user can use MDI's Jade version 7.5 software which automates many powder diffraction analysis. The user also has access to International Center for Diffraction Data's Powder Diffraction File-2 database consisting of more than 163,000 inorganic entries and International Center for Structure Data's crystal structure database with more than 93,000 entries.

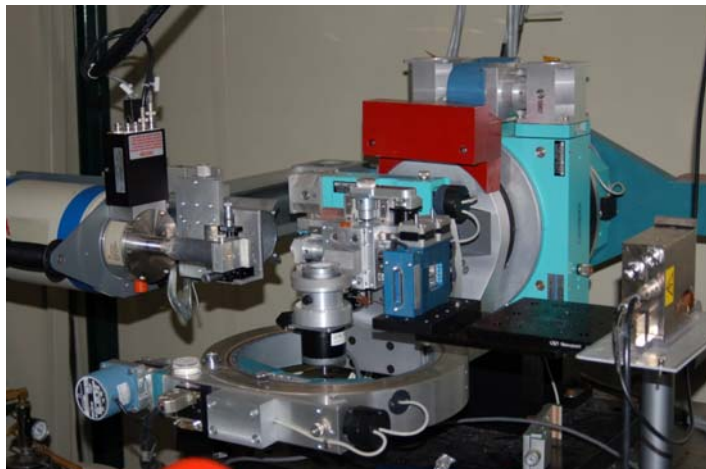


Figure III.B.b.10  
Four-circle Huber powder diffractometer at XRD beamline

The present configuration of this beamline allows only powder samples to be run, but other sample geometries are possible. For example, thin films have been measured.

#### Partial List of Funding associated with DCM

Iron-Based Mixed Metal Carbide Fischer-Tropsch Catalysts, J.J. Spivey, Chemical Engineering at LSU, in collaboration with Clemson University, \$ 224,948.00, 8/31/2005 – 8/31/2008, DOE

#### Staffing

Amitava Roy (0.2)  
Rusty Louis (0.2),

#### Current Status

The beamline is close to routine operation. Typically, a 3° to 70° diffraction run, with 0.02° step size and 2 seconds integration time, requires six hours. The monochromator requires further upgrade in software for routine scanning.

## Publications

Louis, R., Bianchetti, C., Roy, A., Merchan, G., Morris, K., and Jiles, R. (2007) Synchrotron Powder X-Ray Diffractometer Beamline at J. Bennett Johnston Sr., Center for Advanced Microstructures and Devices. In E. Morikawa, J. Scott, and A. Roy, Eds. Synchrotron Radiation Instrumentation 2007 Elsevier, Baton Rouge, Louisiana.

**Table III.B.b.4: Summary of Beamline Staff and Publications**

Year	2000	2001	2002	2003	2004	2005	2006	2007
Manager	Funding obtained through Louisiana Board of Regents						A. Roy	
B-L Scientist	in 2004 to build the beamline; completed in late 2006.						A. Roy	
Publications							0	1

### III. B.2.c. Wavelength Shifter (7-70 keV)

***The Gulf Coast Protein Crystallography Consortium (GCPCC) beamline at CAMD.*** The protein crystallography beam line at CAMD is operated by the GCPCC which comprises 8 institutions; Rice University, Texas A & M, Baylor College of Medicine, University of Houston, University of Texas Medical Branch, University of Texas, Oklahoma Medical Research Foundation and LSU. The consortium secured the funding to construct the beamline through a joint NSF-NIH grant and continues to partially fund its operation. The beamline, along with 2 (soon to be 3) other beamlines, receives x-rays from a 7.0 T superconducting wavelength shifter. The wavelength shifter provides "hard" (high energy) x-rays otherwise not produced by the CAMD ring due to its relatively low electron-beam energy. The cost of running the wiggler, about \$90K/year for liquid He, is entirely paid for by CAMD. The Louisiana Governor's Biotechnology Initiative (GBI) also contributes to the cost of operating the beamline. Use of the beamline ("beamtime") is allocated to labs from GCPCC member institutions and also to general (non-GCPCC) users. It is a requirement of the NIH that at least 25% of the beamtime be available to general users.

Unlike "home" X-ray sources, which generate only CuK $\alpha$  radiation (1.5418 Å), a synchrotron beamline is "tunable". The experimenter can collect data with x-rays of whatever wavelength is most suited for the experiment. Tunability allows structures to be solved by the Multiwavelength Anomalous Dispersion (MAD) technique which exploits changes in the x-ray properties of elements as the wavelength is varied. Many crystallographic projects, such as those involving drug development where numerous structures of the target protein complexed with lead compounds are determined, do not require such tunability, but are still facilitated by the increased intensity available at synchrotron beamlines.

The GCPCC beamline at CAMD is equipped with 2 focusing mirrors to concentrate the beam on the sample and 2 monochromators to select the desired x-ray wavelength. The monochromators have different band passes and the experimenter can select which one to use depending on whether the experiment would most benefit from higher x-ray flux or greater spectral purity. The beamline is controlled by a locally modified version of MX which is a program package written for use at the Advanced Photon Source.

Data are collected with Mar 165mm CCD detector mounted on a Mar dtb base which provides a single-axis goniostat with a 2-theta motion for collecting higher resolution data. Data collection is controlled by vendor-supplied software and the data can be processed at the beamline on PCs running Linux and a selection of popular protein crystallography data processing packages. An Oxford Instruments Cryojet maintains samples at ~100 K for data collection. (Macromolecular crystals are about 1000 times more resistant to radiation damage at 100 K than at room temperature.) A small wet lab equipped with a fume hood, incubators, walk-in cold room etc. is being constructed near the beamline and will be finished by this summer. We have purchased most of the equipment for the lab with funds from the Louisiana Governor's Biotechnology Initiative (GBI). The lab will serve users testing heavy atom derivatives for MIR



phasing as they will be able to modify soaking conditions rapidly in response to the results of beamline crystal screening. It will also house an anaerobic chamber, purchased with GBI funds, for work with oxygen-sensitive proteins. It can be difficult to maintain anaerobic conditions while transporting crystals to the beamline so we believe that the ability to anaerobically prepare and store crystals at the beamline will prove to be essential. The lab will have four adjustable-temperature incubators, also purchased with GBI funds, for storage and growth of crystals.

The beamline at CAMD has proven to be an invaluable asset over the past several years, and multiple MAD structures at the Se and Fe edges have been solved with CAMD data. Moreover, in the case of at least one FeMAD structure, the anomalous scatterer was present at below what is considered reasonable to produce a good signal (1 per 373 amino acids rather than 1 per 175 amino acids), yet the signal was of excellent quality. There are now six LSU crystallographic groups that share the LSU beamtime allotment, four in Baton Rouge, and one each in New Orleans and Shreveport. There are also other groups at LSU that will require occasional access (*e.g.* the Aboul-Ela lab which principally uses NMR).

Despite the considerable success which has attended its operation there are aspects of the beamline that could be significantly improved. The primary one is the intensity of the x-rays. Although stronger than a home source the x-ray beam is considerably less intense than the beam at most beamlines at other synchrotrons. We have recently submitted an application to the NSF Major Research Instrumentation (MRI) program for \$1.63M to purchase a multipole wiggler to replace the wavelength shifter which now produces the x-rays for the CAMD hard x-ray beamlines. If installed, the new wiggler will increase the x-ray flux by at least 10 fold for all the beamlines now served by the wavelength shifter. With the new wiggler the GCPCC beamline at CAMD will have a flux competitive with most macromolecular crystallography beamlines at other rings. (There are beamlines that are far stronger but they generally have to attenuate their beam for macromolecular applications.) We expect to hear whether our application was successful in July of this year. We will need to make some modifications to the beamline to handle the increased heating produced by the higher x-ray flux but they are relatively minor.

In recent years many macromolecular crystallography beamlines have installed robots to mount and retrieve samples while maintaining them at 100 K. The robots enable beamline users to bring large numbers of crystals pre-frozen in liquid nitrogen and to screen them to find the best crystals to collect data from. Robotic crystal screening can greatly increase the efficiency of beamline usage, crystals can be removed from the storage Dewar, tested and returned to the Dewar more quickly because the experimenter does not have to enter the hutch each time. Crystals can also be screened when there is no user at the beamline such as overnight. Software for evaluating the screening results and selecting the best crystal is available in the public domain. Many beamlines at other rings have also been installing software which allows them to be operated remotely over the internet. Remote operation combines synergistically with robotics to allow researchers to ship pre-frozen crystals to the beamline, screen them and to collect and process the data from the best of the screened crystals without having to be at the beamline. We are in the process

of implementing remote operation of the beamline. We have most of the beamline electronics under software control and we expect to include the remaining equipment in the next few months. We have installed a pan-tilt-zoom camera in the hutch so that remote users can monitor the data collection equipment. We will install software such as the Stanford Synchrotron Radiation Laboratory (SSRL) World-Wide Image Viewer to allow users to view the diffraction images remotely and evaluate crystal quality. The recent addition of a high speed (10baseT) connection between CAMD and LSU will greatly facilitate remote access to the beamline. What remains is to acquire a sample-mounting robot. MAR Research, the manufacturer of our dtb system, makes a robot designed to integrate with the dtb for about \$115K. We are currently pursuing funding to acquire this system.

The necessity of remote operation might be questioned on the basis that most of the LSU groups are in Baton Rouge and therefore not all that “remote” from the beamline. However, researchers at the LSU medical schools are a significant distance away in New Orleans and Shreveport and we hope that the increased ease of use will encourage use from the medical schools and the other campuses of the LSU system. An additional point is that the remote operation system will enable PIs to advise and guide their students in real time without having to come to CAMD. The remote operation system will therefore be useful even when data is being collected by students who are present at the beamline.

The GCPCC beamline at CAMD is the source of 17 macromolecular structures in the Protein Data Bank, a worldwide repository for protein structures. The deposited structures are reported in 15 papers, all published in refereed journals. Additional information is given in the table below.

<b>Protein</b>	<b>Purpose of study</b>	<b>PDB ID</b>	<b>Principal Investigator</b>	<b>Institution</b>
YedU	<i>E. coli heat shock protein</i>	1ONS	Robert O. Fox	UTMB Galveston
Rab5/Rababin5 complex	mediation of endocytosis	1TU4	X. Cai Zhang	Oklahoma Medical Research Foundation
Calmodulin/Calcium channel complex	Heart disease	2F3Y & 2F3Z	Florante Quiocho	Baylor College of Medicine
UDP-glycosyl transferase	glycosylation of plant natural products	2ACV	Xiaoqiang Wang	Samuel R. Noble Foundation
<i>B. stearothermophilus</i> HPr	understanding protein folding	1Y4Y	James C. Sacchettini	Texas A&M
Coral allene oxide synthase	prostaglandin synthesis in coral, modeling inflammatory response in humans	1U5U	Marcia E. Newcomer	LSU

<i>D. radiourans HucR</i>	DNA transcription regulation, cellular response to oxidative stress	2FBK	Marcia E. Newcomer	LSU
YciF	<i>E. coli stress protein</i>	2GS4	Robert O. Fox	UTMB Galveston
hypoxia-inducible 6-phosphofructo-2-kinase-2,6-bisphosphatase	attenuation of glycolysis and gluconeogenesis	2AXN	Yong-Hwan Lee	LSU
C2 domain of phosphatidylinositide 3-kinase	cell proliferation signaling	2B3R	Wayne Zhou	LSU
Venezuealan equine encephalitis alphavirus nsP2 protease	alphavirus replication	2HWK	Stanley J. Watowich	UTMB Galveston
PrP19 U-box	ubiquination (protein post-translational modification)	2BAY	Marcia E. Newcomer	LSU
<i>M. tuberculosis b-ketoacyl acyl carrier protein synthase</i>	investigation of tuberculosis	2GP6	James C. Sacchettini	Texas A&M

### III. B.3. CAMD Microfabrication: An Introduction

The CAMD microfabrication group is addressing several aspects unique to CAMD that go beyond the sole use of synchrotron radiation. Originally the microfabrication efforts were geared towards microelectronic applications that required the development of soft-x-ray lithography as a tool for Next Generation Lithography (NGL). With the decision of the IC industry to focus on alternative techniques such as EUV and the advent of the High-MEMS Alliance program, an US initiative to implement LIGA technology in the United States, CAMD’s microfabrication group focused its research activities on other applications including precision engineering, microfluidic, BioMEMS, and material science. At the same time the group provided user access to its unique infrastructure including class 100 clean room facilities with conventional MEMS microfabrication equipment, four microfabrication beamlines, electroplating, hot embossing and basic metrology and material analysis tools. Besides user access to its infrastructure, synchrotron and non-synchrotron, the microfabrication group also added in-depth user training and education support for user projects, and technical services to LSU as well as other educational and industrial users to its support portfolio. Figure III.B.2.i. illustrates the activities and impact of the CAMD microfabrication team in its effort to support current and future LSU research activities.

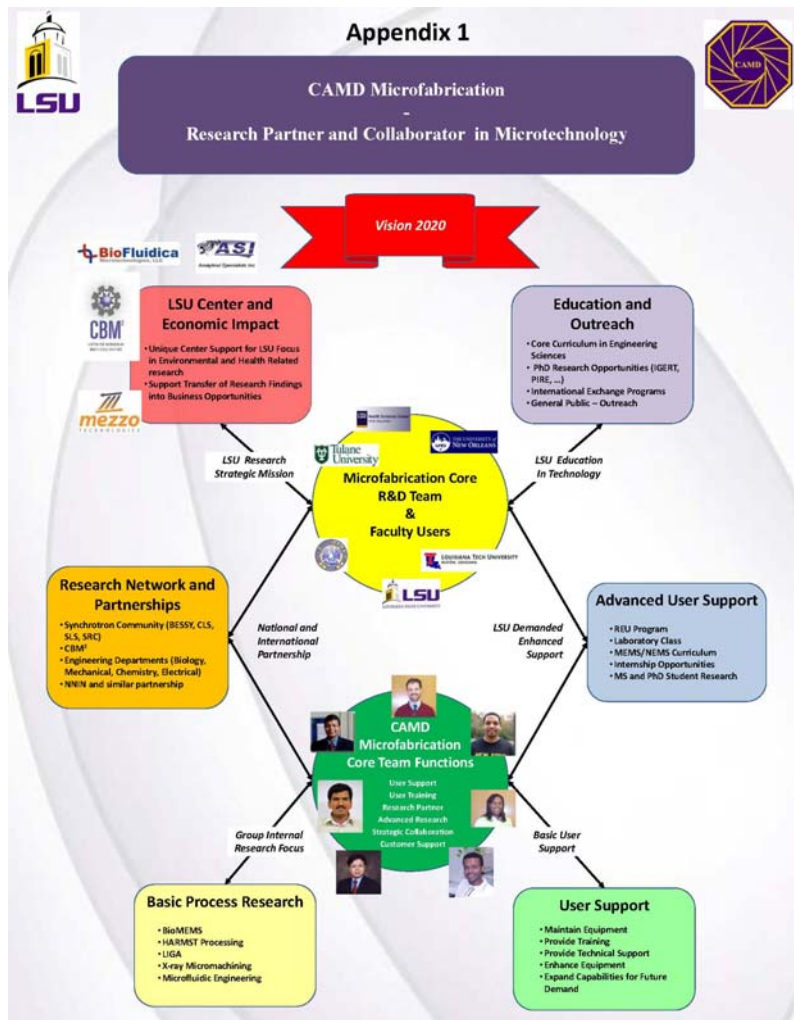


Fig. III.B.3.i:

Appendix 1 illustrates two key areas of our activities: **R&D focus** and **Education and Outreach**. It also provides an outline of the current, near-term, and long-term efforts designed to best support LSU’s Flagship Agenda and Louisiana’s Vision 2020 in research related to biomedical, micro-nanotechnology, energy, environment, and material science applications.

The core team, shown as the green insert at the bottom of the figure, consists of seven key members (4 PhDs) who provide dual functions of user support and independent research. They assist users with their research efforts, maintain equipment and processes in proper working order and also conduct basic process research related to the unique microfabrication capabilities offered by CAMD. Their presence also strongly supports LSU research efforts like CBM<sup>2</sup> and other material science research projects. The core team is supported by about 6 student workers who also conduct their thesis research under the immediate supervision of the team members. Ideally, these CAMD staff members would be jointly affiliated with different academic departments to best serve these students and ensure continuity in our educational and research support, and also open faculty career opportunities for long-term personal growth. The CAMD team is a respected partner in the world-wide HARMST (**H**igh **A**spect **R**atio **M**icrostructure **T**echnology) community, which is an interest group for all aspects of LIGA microstructure fabrication ranging from process R&D efforts to materials and commercial applications. In order to keep its leading position in this community the group also conducts internal research in areas focused on x-ray lithography, for example x-ray mask fabrication, ultra-deep x-ray lithography and testing and optimizing process parameters for novel resist materials.

As outlined in Fig. III.B.3.i research and education are the main areas and adapting to future needs remains an important effort. In the near future improved student training and research experiences will be achieved by expanding educational activities through dedicated teaching and training programs at CAMD and on campus. Ultimately, a focused MEMS/NEMS educational curriculum including lectures and hands-on laboratory classes with a strong materials science component will be jointly developed with LSU faculty and addressing the nation's need for a well-educated, technology-savvy workforce. This will also strengthen research at LSU and other universities boosting our competitiveness in attracting R&D funding in critical areas like environment, energy, health and medicine. Part of these future efforts will be devoted to the discussion of a centralized facility for micro and nanotechnology established either on the LSU campus or at South Campus. Concentrating wide-spread activities in a central laboratory will be the most-effective way to enable cutting-edge research in many of the traditional departments. The Vice Chancellor for Research's Committee to evaluate South Campus argued that South Campus would be acceptable with certain caveats such as more efficient transportation, but came to the conclusion that a facility on campus would be the most effective. Furthermore, a central laboratory will position LSU's research community to compete with the best in micro- and nanotechnology in the nation. A diverse, shared research facility supported by university, state, federal resources and private funding will become the home of an interdisciplinary team of scientists and engineers performing cutting-edge research with outstanding results. This unique research capability will enable faculty and students alike to develop novel micro and nanofabricated devices and materials helping to solve some of our societal needs, and will also set the stage for spin-off companies that will help promote the economic development of technology in the state.

It is important in preparation for the future to carefully evaluate the current situation, identify immediate and future needs, and combine this with the state's future economic goals that will enable CAMD/LSU to participate and contribute according to LSU's flagship university agenda. The following paragraphs provide more detail to this discussion.

### III. B.3.a. CAMD Microfabrication: A Unique LSU Resource

CAMD provides unique x-ray research capabilities in LIGA, and MEMS, that is outlined in Figure III.B.3.ii (Appendix 2).

CAMD offers a complete program in x-ray lithography with four beamlines providing different x-ray exposure spectra that allow us to pattern microstructures with dimensions ranging from nanometers to millimeters, extremely high aspect ratios, and in different engineering materials that are *extremely* difficult to achieve with any other MEMS technology.

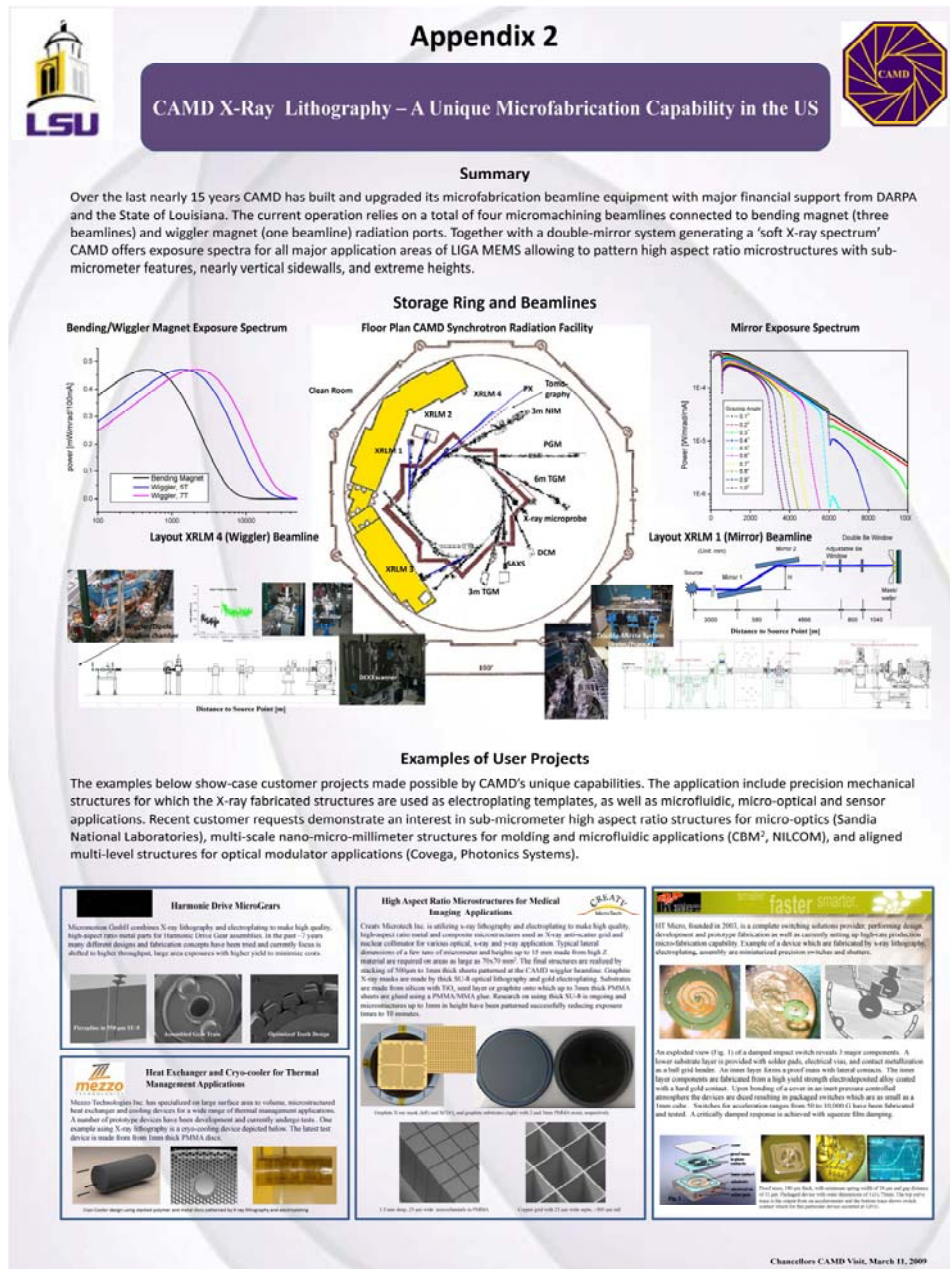


Fig. III.B.3.ii: Appendix 2 illustrates CAMD’s unique x-ray microfabrication capabilities and shows examples of industrial projects that are supported by the CAMD microfabrication group.

The x-ray lithography capabilities also include a number of clean room based equipment and process technologies necessary to make x-ray masks, perform resist application and development, as well as electroplating for metal structures and metrology for structure and material analysis. Funds to build this infrastructure came from the DARPA Hi-MEMS Alliance, and totaled about \$ 7.5M. Funds were also used from CAMD's state budget, and were supplemented by Board of Regents Enhancement grants. The combination of the right equipment, an open, user-oriented and inter-disciplinary working environment, and expert staff make this entire operation a success producing outstanding results from the CAMD group and its user community. It should also be emphasized that with our current strength of 7 active staff members, the CAMD group competes and collaborates successfully with similar centers, for example BESSY/AZM with about 12 permanent staff, and ANKA/IMT with about 25 staff.

CAMD's microfabrication program attracts a number of commercial customers and partners who utilize the x-ray lithography and molding services. Some examples of customer projects, focusing on micromechanical precision metal parts as well as microfluidic and microoptic polymer parts are shown in the three lower panels of Fig. III.B.3.ii. As a member of the original Hi-MEMS Alliance, CAMD had established a 'print-shop' service dedicated to industrial users enabling them to easily/conveniently access this service in a turnkey manner. While this service is excellent, unique, and highly appreciated by our customers it is not commercially profitable because all our customers require low production volumes and typically need only a few exposures of one design to make hundreds or even thousands of parts and meet their market demands. On the other hand new business for emerging applications such as RF-MEMS (Radio Frequency) or multi-level mold inserts require significant investment in research and technology development before commercially viable products and processes can be produced. This research effort does not require a dedicated exposure service but expertise in the broader field of microfabrication exploring and testing the best solution for a specific product development. The CAMD group, a team with complementary expertise and skills, has a track record in this type of partnership especially with their MEMS Exchange (<http://www.mems-exchange.org/>) activities and will continue to explore these opportunities through joint research projects.

The output of the current operation is described in Sec. II.F.1. and II.F.2, while the program structure is reflected in Figure 4 in Sec. III.B.5.a. and shows the main activities of the group. Access and training to beamlines and clean room equipment is provided as major service and involves senior and junior staff. This Education and Outreach activity reflects CAMD's unique role for the LSU community. Approximately 60-70 students each year benefit from our training program.

### **III. B.3.b. CAMD Microfabrication and LSU faculty: two examples of partnerships**

While infrastructure and support for industrial customers is critical aligning our research efforts with programs from LSU faculty is another important aspect of the group's operation as the combined expertise is resulting in cutting-edge research results competitive for federal funding. This section is a brief summary of the information presented in Appendix 3 (Figures III.B.b.iii-iv) that highlights two examples of long-term, very successful partnerships between CAMD staff and LSU faculty. Some details of the ongoing research are documented in the four figures with further information available from an extensive list of publications.

**Cross-disciplinary, inter-departmental research education and collaboration** is a major ingredient for favorable research in the field of BioMEMS focusing on developing technology solutions (BioChips, Point-of-Care, Lab-on-a-chip) for health and medical applications. Figure Fig. III.B.2.iii by Matt Hupert/CBM<sup>2</sup> is a summary of a recent conference paper that demonstrates the bandwidth of research necessary to successfully build an analytical chip for tuberculosis diagnosis.

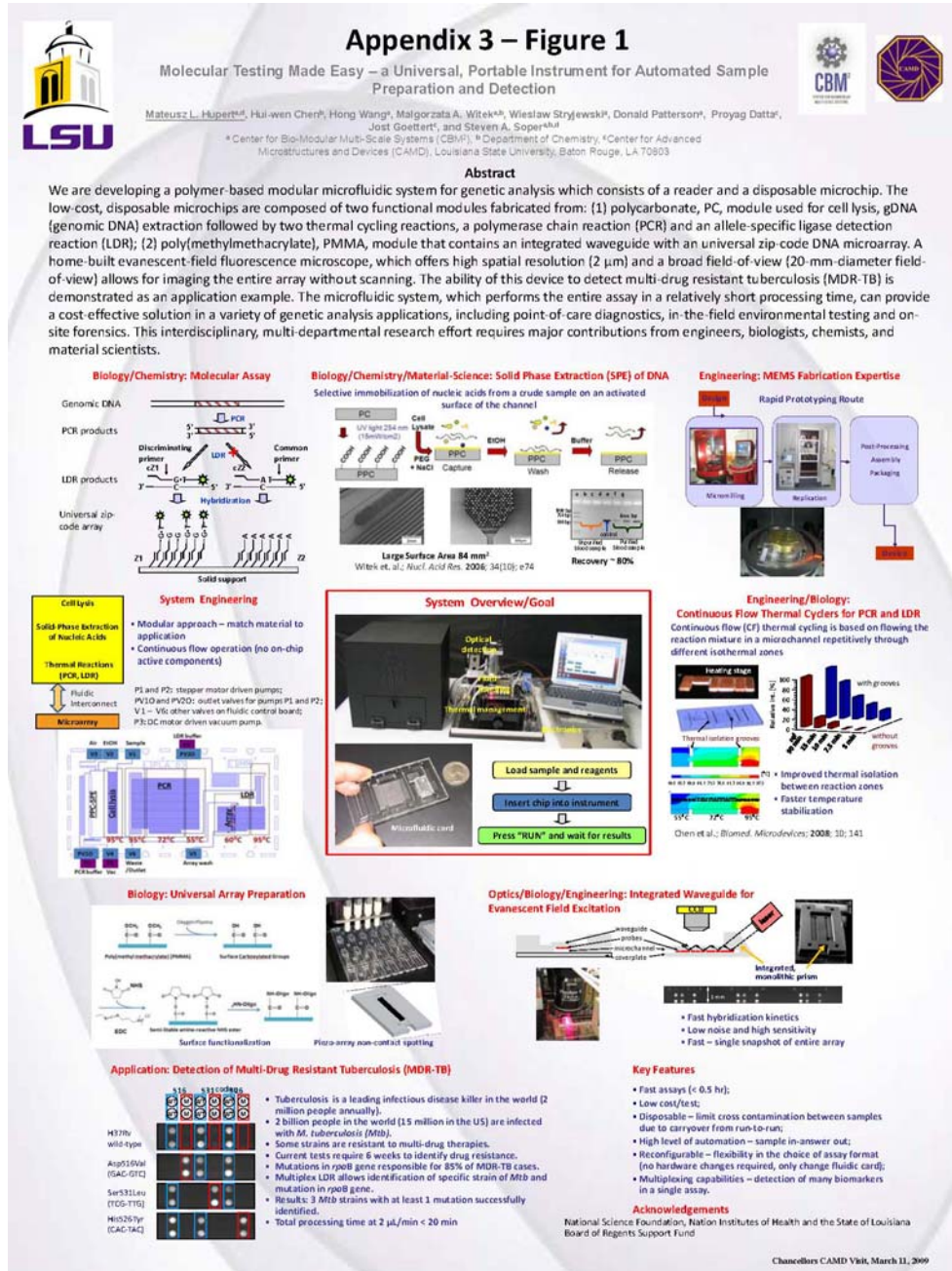


Fig. III.B.3.iii: Example of a BioSensor system project and the complexity of the task requiring inter-disciplinary research with contributions from several groups.



Contributions from different disciplines including biology, engineering, material science, micro- and nanofabrication as well as surface science and engineering, each of which is valuable research in its own right, are required to design and build a complete device. This type of synergistic cooperative research blossoms readily in the open, highly interactive environment of CBM<sup>2</sup>. CAMD's expert staff permits timely results to be obtained, allowing market exploration or new funding opportunities, and also provides researchers associated with CBM<sup>2</sup> research projects a centralized facility with state-of-the-art equipment. CAMD's facilities not only boosts the quality of LSU scientist's research but attracts new users from academia as well as spawns business opportunities through spin-off companies, who will benefit from strong research collaborations and first-class infrastructure support.

***Advanced engineering solutions*** in microfluidics, displayed in Figure III.B.3.iv from Proyag Datta, were initially started by the demand from CBM<sup>2</sup> scientists to obtain useable chips which can easily interface with CBM<sup>2</sup> existing laboratory equipment and also provide access to advanced MEMS solutions in the form of unique fluidic chips. This concept – a modular, easily reconfigurable stack with standardized fluidic, electrical, and optical interfaces – is now at a level where it attracts not only new research funding opportunities (i.e. with University of New Orleans' Advanced Materials Research Institute, AMRI, to develop Biosensors) but also attracts the attention as an educational tool for non-MEMS experts in especially the life sciences and chemical engineering disciplines. CAMD is currently exploring funding opportunities in this direction and also explores strategic partnerships with companies to further improve the stack concept into a marketable educational and research tool. Another important research project has been formulated from this effort, namely the combination of different micro- and nanofabrication technologies to build complex, multi-level, multi-scale templates for mold inserts. This project takes full advantage of CAMD's x-ray lithography process capabilities and expertise and is at the heart of a proposal to the NSF that seeks support for the funding of an Engineering Research Center, that will partner CAMD staff with faculty from LSU and other universities.

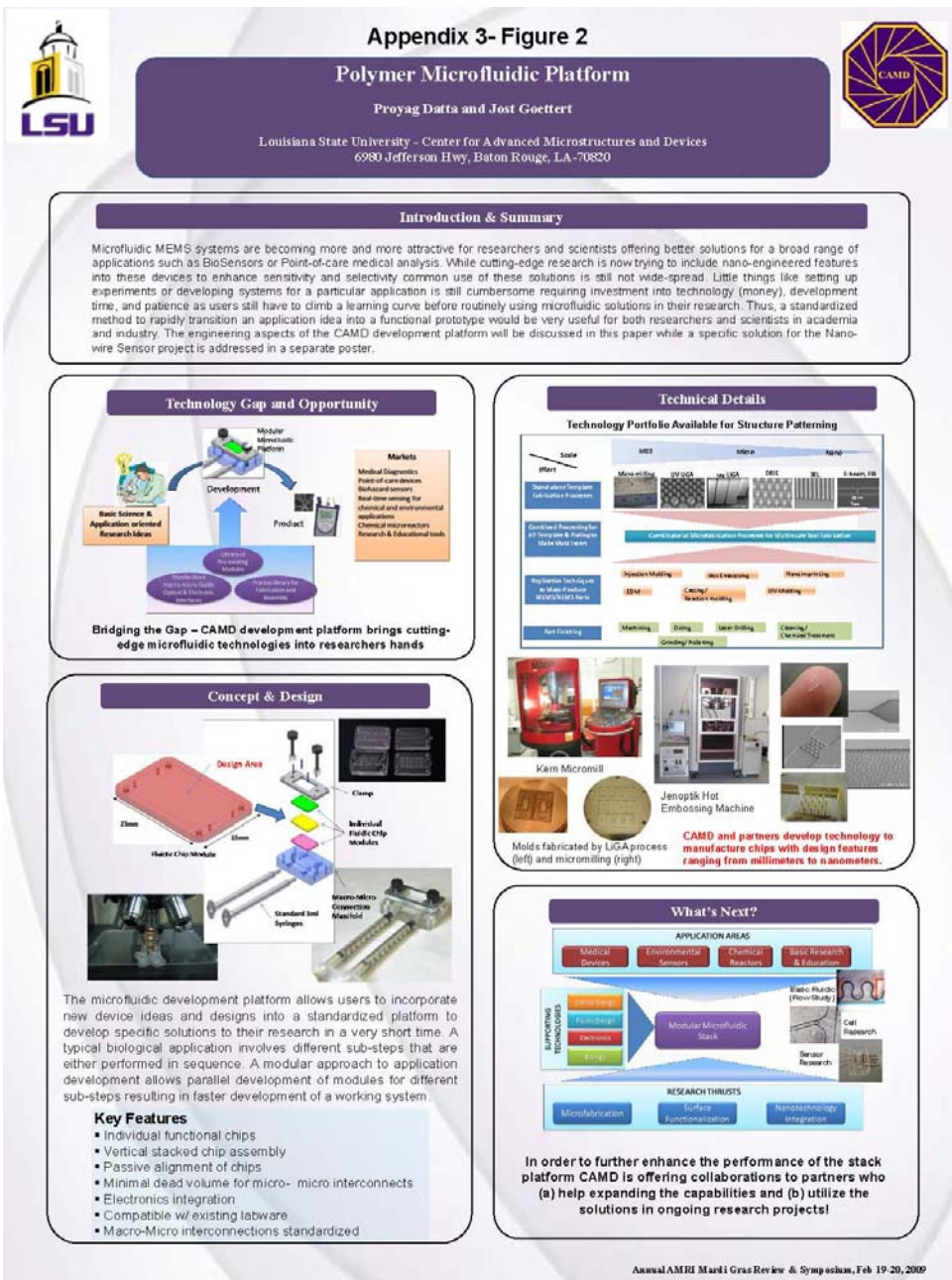


Figure III.B.3.iv: Concept and engineering details of microfluidic development platform crucial for BioMEMS and microreactor research projects.

Figure III.B.3.v illustrates the efforts of *commercializing the CBM<sup>2</sup> research results* through a spin-off company, BioFluidica. It highlights the market needs for Biochips solutions for a wide range of medical and sensor applications. The commercial approach is based on developing and manufacturing complete, chip-based diagnostic designs, that include advanced fluidic devices using cost-effective mass-production, bio-specific surface functionalization, and user-friendly handling. These devices will be easily loaded with sample liquid, and inserted into a ‘reader’ automatically executing a protocol and producing results with minimum user interference.

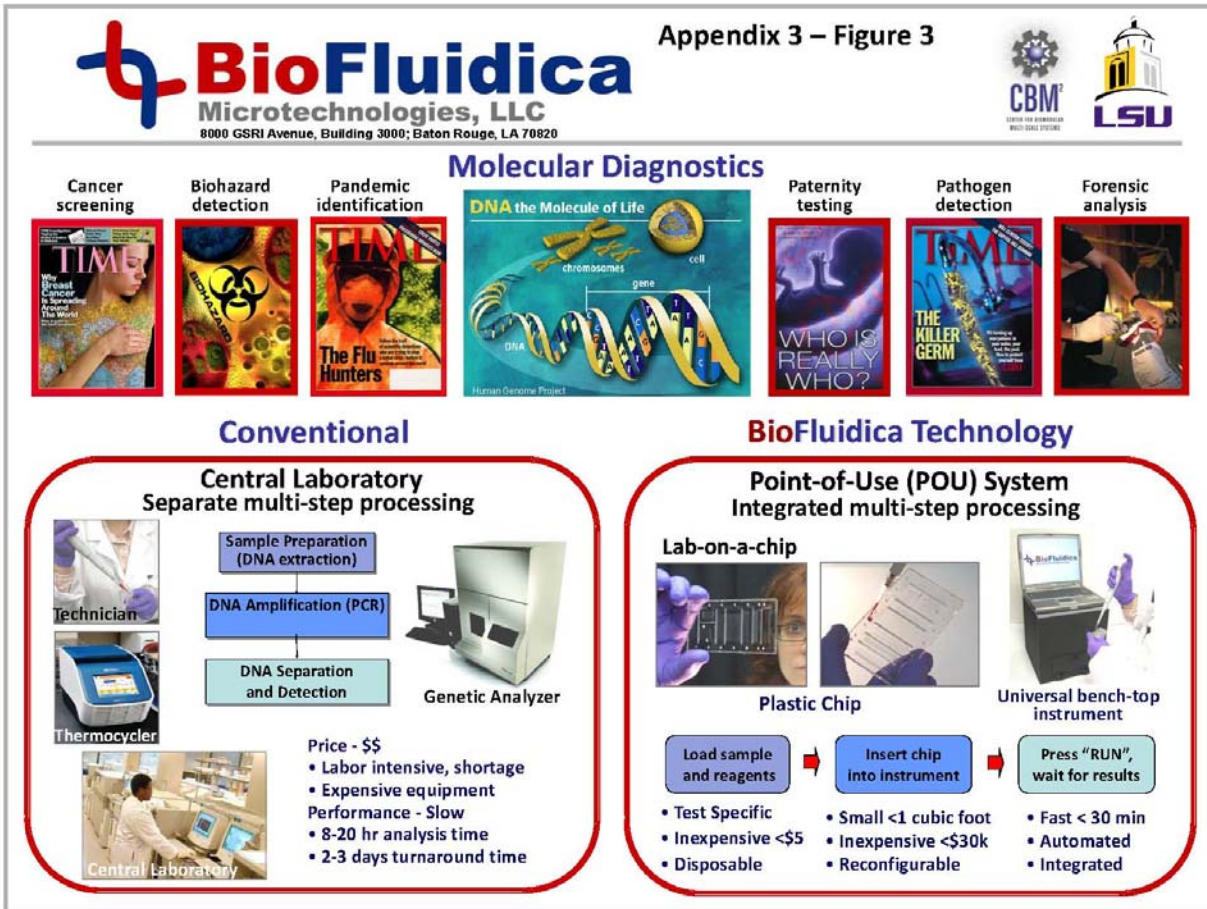


Figure III.B.3.v: BioFluidica, a CBM<sup>2</sup> spin-off company explores commercialization opportunities of point-of-use BioMEMS solutions utilizing LSU research results.

Figures III.B.3.iii-v demonstrate on one hand the complexity of chip based research and on the other show that LSU is in an excellent position to successfully compete in the area of BioMEMS owing to the strong inter-disciplinary collaboration on campus and with external partners. Further strengthening these partnership bonds is crucial for successfully meeting the Louisiana Vision 2020 goals and ensuring LSU's leadership position among the outstanding research universities who conduct research in BioMEMS.

Another example of a long-term collaboration of about 15 years is the development of a **miniaturized environmental sensor** based on gas chromatography (GC). Under the leadership of Prof. Ed Overton (Environmental Sciences) the team has applied microtechnology solutions, in particular x-ray lithography and nickel electroplating, to design and build compact, small GC systems, which find broad use in the chemical industry, environmental monitoring, food industry, and more recently homeland security and health and medicine for the analysis of gas and liquid mixtures. These new instruments surpass the existing bench-top instruments and enable today field measurements in minutes, bringing the analytical laboratory into the field rather than samples into a central laboratory.

The idea of a miniaturized GC sensor has first been suggested in the late 70's and was proposed as one of the key application for MEMS technologies. Yet, the complexity of an analytical MEMS sensor and the research effort required to transfer an idea into reality has been underestimated and only recently some first instruments with promising performance have been introduced in the market. Similarly, LSU's efforts went through a learning experience starting from learning and perfecting MEMS fabrication to system design, integration of control functions, and optimizing system performance rather than individual components as outlined in Fig. III.B.3.vi.



Fig. III.B.3.vi: Development efforts at LSU towards a miniaturized, ultra-fast GC sensor.

The technical part of Fig. III.B.3.vi illustrates ongoing research efforts, for example coating the inside of a LIGA fabricated metal column with a special, few 100nm thick polymer (so-called stationary phase) that helps separate the components of a complex mixture. Another major accomplishment has been made with regard to integrated column design that allows narrow sample plug formation. This feature is essential for fast chromatography, and the assembly of the entire system with minimum dead volume and cold spots. Many lessons have been learned and small but crucial improvements have resulted in a working prototype that outperforms bench top systems in terms of speed and is rugged for in-the-field-operation. These efforts have been partly funded through the DARPA-MGA program (<http://www.darpa.mil/MTO/programs/mga/index.html>) in which the LSU team was working with partners from Sandia and other universities to develop a micro-GC system for homeland security applications. As with the previous example the complexity of the task requires close inter-disciplinary research from engineers, material scientists, and end-users and the slow progress is an example of how much time it takes to have a team understand all the nuances of an application and advice a system design that can be transferred into a working prototype.

In summary CAMD's LIGA efforts initially were aimed towards industrial users and print-shop activities as part of the Hi-MEMS alliance enabling access to CAMD's unique x-ray lithography capabilities. However, as has also been proven by efforts from other LIGA groups, the transition from prototype to mass production is not straight forward but requires substantial research to fine-tune existing processes where commercial quality is achieved with outstanding reliability and cost-effective fabrication. This approach towards commercialization is not a stronghold of a university based research entity and thus cannot be the only goal of the CAMD group. However, with the equipment and expertise accumulated it is possible to carry out cutting-edge research at the interface of micro- and nanotechnology. These efforts can be combined with the unique research expertise available in various departments at LSU and is an excellent basis for building the outstanding research program evolving through CBM<sup>2</sup>. This complimentary research combined with training, education, and outreach to align these efforts with programs within LSU will allow LSU to enhance its position as a leading research university in the US. Further discussion of these ideas will be continued in Chapter IV.

### III.B.4. CAMD Other Activities

#### III.B.4.a. CAMD Outreach

Outreach to the LSU, scientific and local communities is one of the top priorities of CAMD's mission. Part of this mission is to "spread the good news," through the use of the media available at LSU, in the local newspapers, and TV stations. Towards this end, we have engaged the part-time services of Dr. Sumita Roy, who is helping CAMD with publicity at the site and those of Ms. Ashley Berthalot of the LSU Office of Public Affairs. In the works are a revised CAMD website with research highlights, and a new video showcasing CAMD's outstanding facilities. Other efforts at outreach include:

- **Tours of CAMD:**  
We welcome high and grammar school classes, university classes, other student groups, professional organizations and societies, as well as civic organizations, teachers, government people, and private individuals to visit our facilities. Such "official tours" for groups of visitors are arranged in advance. For approximate numbers of visitors for 1999-2006, please see Table 2.
- **Presentations:**  
Our staff perform science demonstrations and deliver talks in schools, provide public lectures for college and tech school classes and for public interest groups as well.
- **CAMD Open House:**  
One Saturday each year, the CAMD staff host a "hands-on" open house at the CAMD Laboratory. It includes guided tours of the accelerator, beamlines, and clean rooms. Around 12-15 demonstration booths set up by CAMD staff and synchrotron users encourage visitors, especially children in the K-12 range, to participate in the wonders of science. However, in 2000, the Open House was more structured in that visitors were enrolled in three distinct seminar workshops with a general visit to the Experimental Hall. For additional details on these events from 2000-2006, please see Table 3.
- **NSF-Sponsored Research Experience for Undergraduates Program (REU):**  
Undergraduates from LSU and other colleges and universities participate in research projects with CAMD staff scientists.
- **CAMD Science Teacher Program:**  
CAMD scientists work with science teachers to enhance primary and secondary science education in the state. In addition to the CAMD tours described above, this work includes helping teachers by providing equipment for their classroom use, traveling to schools to lecture and give demonstrations that pertain to CAMD and/or general science, judging science fairs and helping students with science fair projects.

- **CAMD “Summer School”:**  
Each year, CAMD conducts a two week summer school/workshop that is directed towards the application of synchrotron radiation to a specific research area. These “Summer Schools” are intended for graduate students and young scientists in academia and industry. For more details, please see Table 4.  
**“Emerging Faculty Program”**  
CAMD also sponsors a program that enables non-tenured faculty to be employed at CAMD during the summer months
- **Miscellaneous:**  
During the course of the year, CAMD conducts courses to train students to use the clean rooms. CAMD also hosts a Seminar Series with other departments, where research topics that include lectures on surface science, environmental research, nano-and micro-technologies are offered by outstanding experts.  
**Science Fair Participation:** There are approximately 12 science and technical staff at CAMD who participate in Science Fair judging at the local school level and up to the state and national levels. At least two of our staff will work with students to plan and help with individual projects.

### **CAMD Summer Research Program:**

#### **Undergraduates, High School Teachers, and Students:**

For 10 weeks during the summer, CAMD scientists work individually with undergraduate students from LSU, Louisiana universities and universities from across the nation to involve the participants in “real-life” laboratory research efforts. During the summers of 2000 and 2005, the program was funded by the CAMD state budget to support 14 and 5 undergraduate students, respectively, and, in addition, one high school student was supported in 2005. During the remaining summers from 2001 – 2007, undergraduate and high-school students and teachers were supported by funds obtained from the NSF REU Program, the Louisiana Board of Regents, individual faculty research grants and the state budget. Specifically, during these six years, there were a total of 54 undergraduate students, two high-school students and two teachers sponsored by the NSF (DMR-0097784 and -0553484). Also, two undergraduates were sponsored by the CAMD state budget (they were foreign students not eligible for NSF REU Program support) and one teacher plus acquisition of teacher-aid material was sponsored by a \$10K grant from the Louisiana Board of Regents. NSF support for the 2006 and 2007 programs was provided by the AFOSR through the NSF DMR. In summary, a total of 78 undergraduates have participated in NSF and CAMD-sponsored summer programs. Of these, 25 students were from LSU, 22 (28%) from minority-serving institutions (Southern University, Xavier University, Grambling State University and Texas Southern University) and 17 were women (23%). In addition, two high school science teachers received financial support (combination of NSF and Louisiana funds) to participate in summer research programs and three high-school students received support. Please see Tables 1(a) and (b) in Appendix A.

### III.B.4.b. CAMD Safety

CAMD gives safety the highest priority. The radiation safety of all users is addressed via a 3 step process. First, all users receive radiation safety training [test-certifiable] prior to gaining access to the facility. The elements covered in radiation safety pertain uniquely to the CAMD facility. Annual recertification of all users in radiation safety is also mandated. This recertification process is different from year to year – and is predicated on the most up to date information on the hazards of ionizing radiation. Second, all users are monitored using a passive integrating device developed by an accredited laboratory [P1 Type]. These personnel badges are read quarterly. In the past, they were read monthly with always zero readings. Third, users are protected from the hazards of radiation through the judicious use of interlock systems.

Interlocks are re-certified quarterly, during the commissioning of a new beamline [beamline portion only], or if there is an apparent failure. All interlocks are redundant and are fabricated so as to fail only in a fail-safe manner. For example, Bremsstrahlung shutters are mechanically operated using compressed air. Should the air fail, these shutters would sit in the beamline, blocking any radiation from coming upstream towards the end-stations. All shutters are forced closed during the injection process.

In addition to radiation surveys, several facility and environmental monitoring stations are also in place using TLD's. Within the experimental hall, there are 25 sites dedicated to photon measurement and 6 additional sites dedicated to neutron monitoring. The Neutron TLDs' also have the capability to discern between X-rays and electrons, as well as neutrons. As with all passive monitoring devices used at CAMD, all TLD's are posted in duplicate [and sometimes in triplicate, as for special research projects]. Special efforts are put into place to extensively monitor and alleviate any concerns that might be brought up by our neighbors. Should the need arise, we have long-term data supporting the observation that radiation levels at CAMD are below the dose set for the public. Active real-time monitoring is also available in the form of radiation detection instruments.

Radiation Instrumentation is selected based on the machine characteristics [pulse or continuous fields], as well as whether we are dealing with Bremsstrahlung or Synchrotron radiation. All instruments are calibrated at the Louisiana State University Radiation Safety Office, which is under contract with CAMD to provide said service. Instruments are calibrated either annually or semi-annually, depending on their use. Such instruments provide real-time monitoring ability which is not achieved by TLD's.

In the past 15 years of operation, no single user has been exposed to a level of radiation exceeding the public dose limit [100 mrem /year]. Nevertheless, all users are badged as per the licensing agreement with the Department of Environmental Quality, State of Louisiana.

CAMD is also conscious of the need for active programs in General Safety, Industrial Hygiene, and Industrial Safety. To this end, CAMD has implemented several different programs, training regimens, and on-line access to hazards mitigation.

Approximately ¼ of the CAMD staff is trained in First Aid, CPR and the use of an automatic external defibrillator [hands-on and written testing protocols are required]. The training is Red



Cross certified and is administered by a certified trainer from the main campus of Louisiana State University.

Cleanroom training is provided for all users who need to use these specialized facilities. It includes material on emergency procedures, handling of chemical hazards, as well as gowning and cleanroom protocols and hands-on experience and select training on a variety of cleanroom instruments. Individualized training is also available for special access instrumentation.

The use of specific chemicals or mixtures of chemicals requires a safety review process. Similar procedures are in place for potential biological hazards. Each user is given a safety approval form that delineates the maximum volume or concentration and the use conditions for each experiment.

Suitable personnel protective equipment is provided to all CAMD users and, upon review of their specific protocol[s], recommendations are made. Personalized training for specific chemical hazards or specific circumstances is available on an as need basis.

Save driving courses are required of all CAMD users who wish to certify to use the CAMD Van. Similar training is available for using the Forklift or the Crane. Though written testing is required, Forklift and Crane training have an additional proficiency testing of how to handle these devices prior to obtaining certification. Generally, Forklift and Crane training is restricted to CAMD staff. Such courses are given intermittently, on an as need basis.

The National Electrical Code is used as the basis for all electrical connections in facility. The facility manager and the assistant facility manager at CAMD are both certified Commercial and Industrial Electricians. All signal cable [low-voltage], is segregated from high voltage cables in cable trays. The use of extension cords is allowed only during commissioning activities.

In the past 16 years, CAMD has suffered only minor injuries, including a broken finger, and two set of stitches for cuts to the hand in a population of 1233 trained users. We are proud of this record and think it is a reflection of the high priority CAMD sets for safety.

### III.B.5.a. CAMD Organizational Structure

CAMD is presently organized into five operating units as shown in Figure 1

#### CAMD Organizational Chart

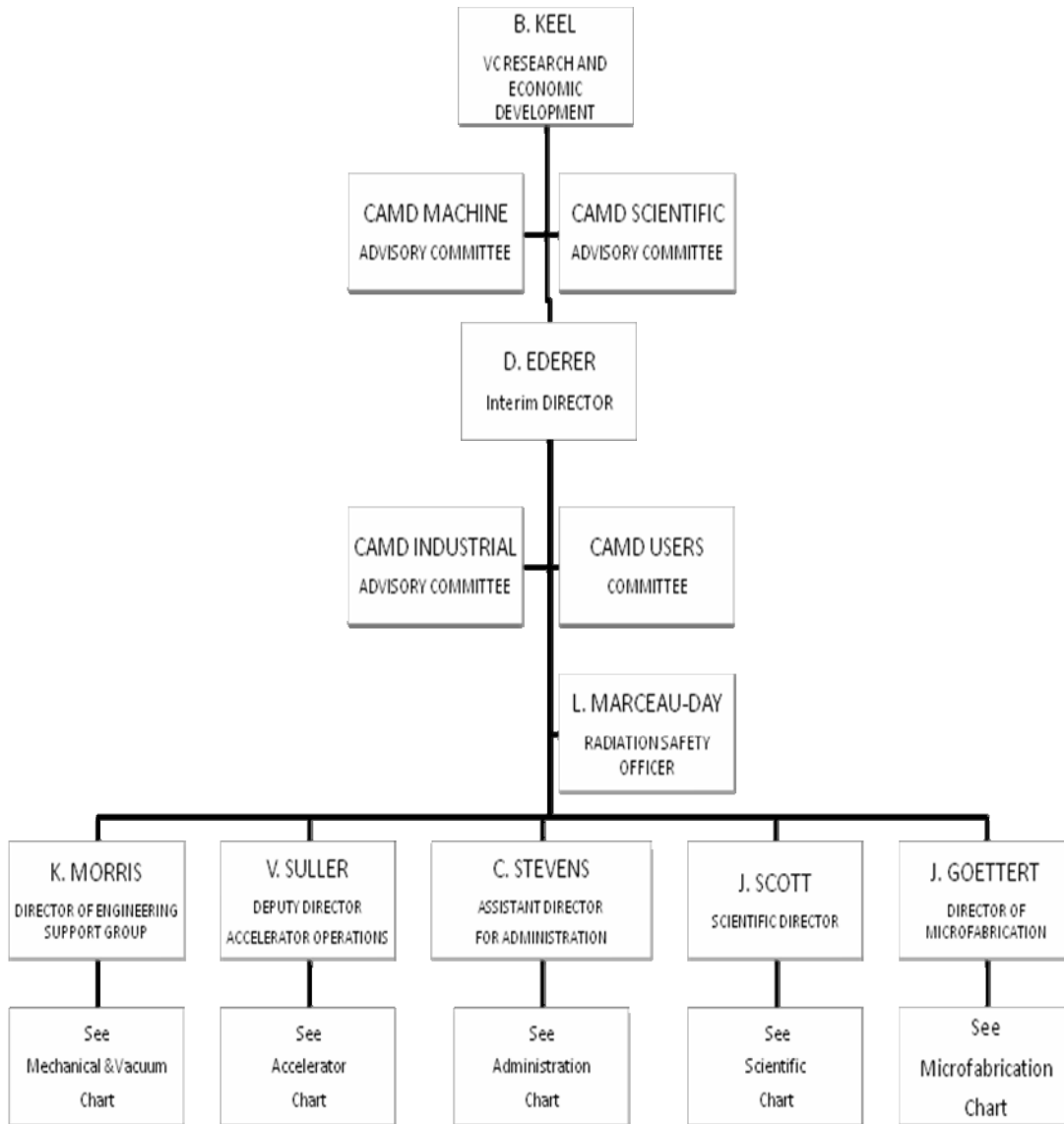
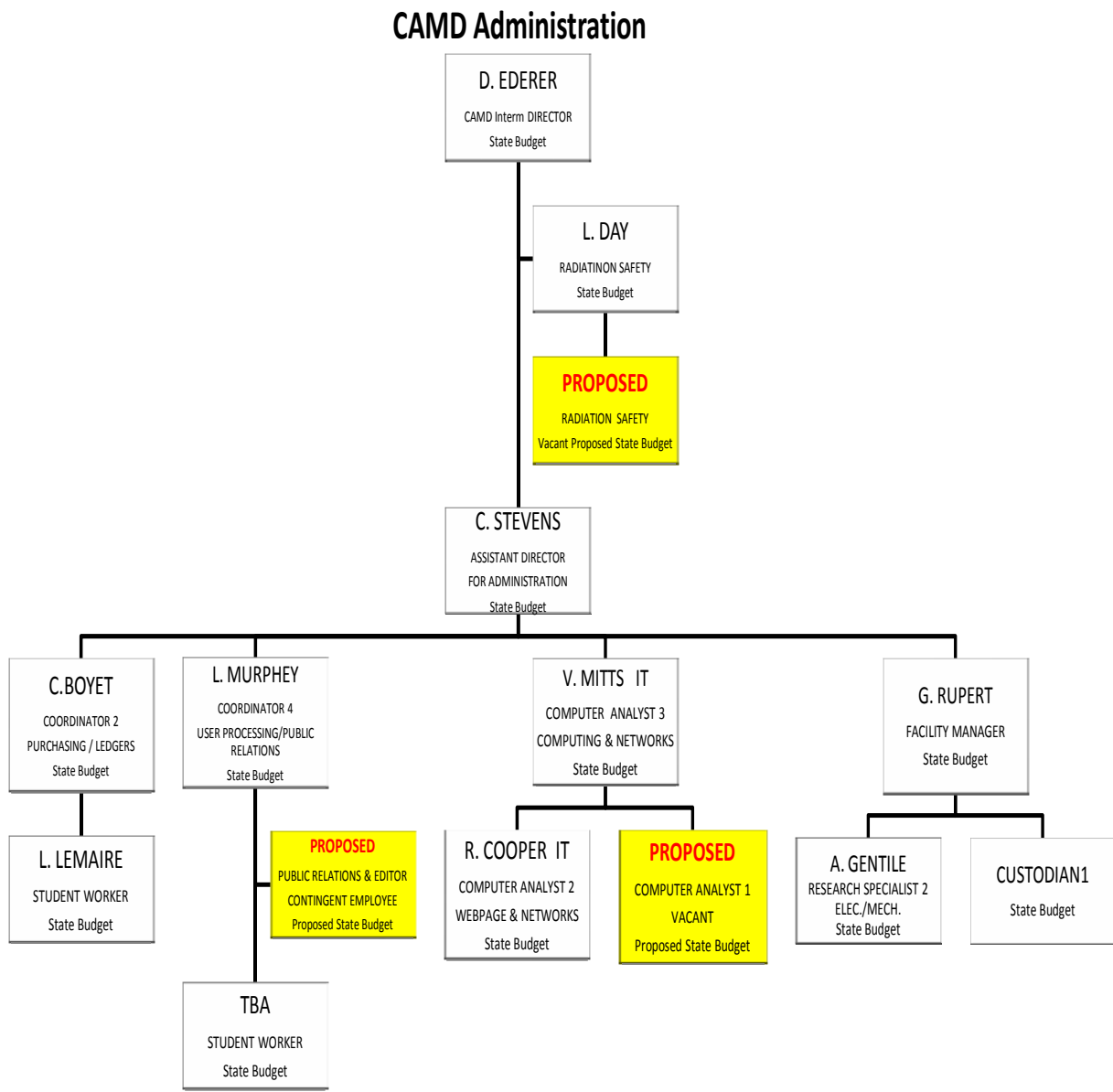


Figure 1: CAMD Organization Chart

## Overview

The Center is responsible to the Office of the Vice-Chancellor for Research and Economic Development (R&ED). CAMD's Director reports directly to the Vice-Chancellor as does CAMD's Scientific Advisory Committee (SAC). Several other committees serve to advise CAMD's Director and Vice-Director and they include the Machine Advisory Committee (MAC), the CAMD Users Committee (CUC), and the Industrial Advisory Committee (IAC). Typically, these committees meet once a year and compile an Annual Report for the Directors and the Vice-Chancellor.

CAMD's organizational structure is broken into the following five groups: Assistant Director for Administration, the Scientific Director, Director of Microfabrication, the Deputy Director for Accelerator Operations, and the Deputy Director for Engineering Support. The existing organizational structure of these groups is shown in black in Figures 2-5. The current document recommends changes within the organizational structure that will allow CAMD to restructure itself to meet the changing and new demands from the LSU community, e.g. the Materials Science Center (MSC) and the needs of its growing user community. These proposed adjustments to the staff are shown in red within a colored box.



**Figure 2:** CAMD’s Administrative breakdown.

**Administrative Group:** The Administrative Group is responsible for the facility, security, purchases, mail, mailings, accounting, job descriptions, and a myriad of other housekeeping (literally and figuratively), and financial activities. All costs to maintain the facility are borne through CAMD’s operating budget – including custodial services and general upkeep of the facility, services that are typically provided by the University for Campus Departments. Such maintenance costs will continue to grow in order to cope with an aging facility that requires

much-needed improvements. Radiation and other safety issues are also important responsibilities of the Administrative Group.

There are three areas that need strengthening. The first is safety. CAMD has maintained safety with a high priority. The details of our efforts to maintain a safe working environment is discussed in Section III.B.3.d. The result of our diligence is essentially an unblemished safety record. At present, the responsibilities fall almost entirely on the safety officer, Dr. Lorraine Day, who has part-time back up from Mr. Gentile, a research specialist and from Ms. Shaloma Malveaux, a research specialist, who provides chemical safety assistance in the microfabrication group. Hiring an assistant safety officer to help maintain records, such as user profiles, and documentation, such as Materials Safety Data Sheets (MSDS) would be an important addition.

The second area is communication. We would like to add a person whose responsibility is to provide information for the community. It is surprising to learn that many within the LSU campus are not aware of the role CAMD plays in scientific research. It is even more surprising to learn that many scientists at other synchrotron radiation facilities do not know about CAMD. This is the result of poor communications. We would like to further utilize the services of the Office of Research and Economic Development and the LSU Public Relations office to increase the awareness of the LSU community, state, nation and beyond about CAMD. During the spring of 2007, CAMD and LSU hosted the Synchrotron Radiation Instrumentation Conference in Baton Rouge. It was refreshing to learn that the many participants who visited CAMD's research facilities, expressed their delight in finding such a user-friendly facility. This year, with the help of a part-time writer, editor and information specialist, we implemented a News and Highlights link, <http://www.camd.lsu.edu/news.htm>, and <http://www.camd.lsu.edu/highlights.htm>, respectively, on our website, in an attempt to provide research highlights for the lay community. Sites such as these serve as important tools to showcase the latest discoveries and can be found at every other synchrotron facility website.

Finally, there is a need for an additional IT specialist. There is a need to grow a strong relationship with the community by networking through LONI/CCT to enable improved access to CAMD for its many users.. Thanks to the tireless efforts of our two specialists, CAMD has a nice website; however, they can barely keep up with computer updates and hardware management; much less devote time to continue developing the website. Some of these critical needs are discussed in Section III.B.4.e.

***Scientific and Nanotechnology Group:*** Scientific research activities are broken down into the VUV/IR and X-ray research groups. The organizational structure of these groups is depicted in Figure 3 shown below.

## CAMD Scientific Group

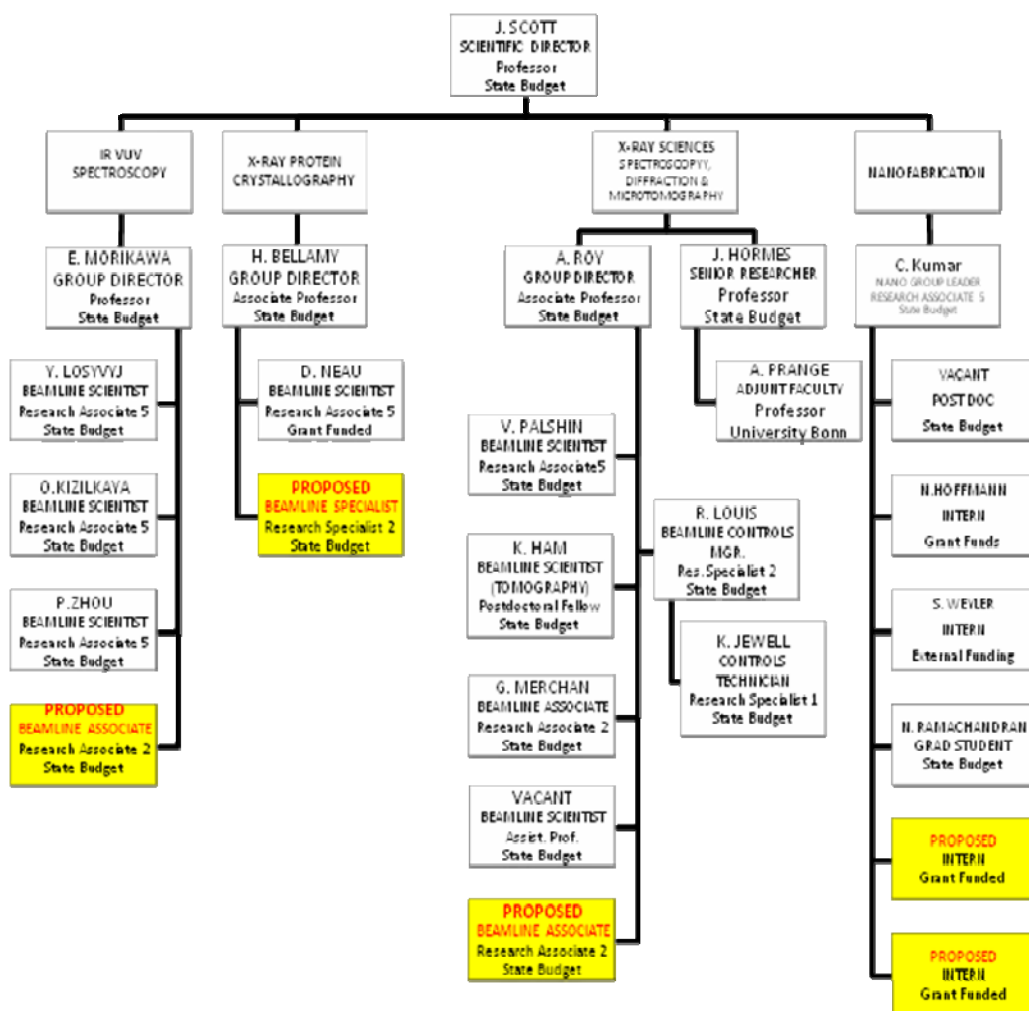


**Figure 3:** CAMD’s Scientific Research Groups.

Currently, the VUV/IR Group is composed of a group leader and three scientists to service four VUV and one IR beam lines. Technical and other service work is shared with the X-ray Group. By comparison with any other SR facility, this is a woefully small number of people to provide adequate support for these productive facilities; consequently, we have a great deal of “deferred maintenance.”

A glance at the VUV/IR subgroup, shown in the left hand portion of Figure 3, suggests that the scientific support for this subsection is reasonable, with about one scientist per beamline. However, technical support for these beamlines is lacking. Technical support is shared with the X-ray group, and as a result, improvements and developments to the VUV/IR beamlines must be

scheduled to fit in with the schedules of the X-ray technicians, who are extremely busy with their duties managing the five X-ray beamlines. These are complex beamlines requiring a great deal of technical and programming support, far greater than we are currently able to provide. We are proposing adding one or two research specialists to strengthen technical support.

The X-ray Group is split into two subgroups, one utilizing the wavelength shifter for protein crystallography (PX) and the other managing four X-ray spectroscopy beamlines including Tomography, XMP, Diffraction, DCM, and X-ray Microprobe (with another under construction for the wavelength shifter beam line during the summer of 2007). The X-ray Group Leader is assisted part-time by CAMD's former director, Josef Hormes, and three research associates. These staff members, in addition to assisting users on the x-ray beam lines, are also on call to aid the VUV/IR group with problems associated with software and other issues relevant to beam line control and construction. We are presently engaged in a search for an x-ray beam line scientist and are in the process of hiring a research specialist. The addition of these members of staff will alleviate the staffing shortage to a degree. To bring up the staffing levels to something that is approximately competitive to meet the needs of our user community, it is proposed to increase the technical scientific staff by three more members that would include two beam line managers and a technician or an engineer.

The nanotechnology group, (shown as the column on the far right of Figure 3), reports to the scientific director and was established to allow CAMD and its users the opportunity to actively participate in the emerging field of nanotechnology.. It has been heavily supported with outside funding and currently is seeking to fill a vacancy, and as activities and funding progress, it will be augmented with two additional interns. The activities of the Nanotechnology group are described in Section II.A.1 and, III.B.3b.

### ***Microfabrication Group:***

CAMD microfabrication group is addressing several aspects unique to CAMD and going beyond the sole use of synchrotron radiation. The writing of this report coincides with the ongoing focus on the Microfabrication Group, and its current organizational structure is shown in Figure 4.

In the initial stages, microfabrication efforts at CAMD, were geared towards microelectronic applications developing softX-ray lithography as tool for the Next Generation Lithography (NGL). With the decision of the IC industry to focus on alternative techniques such as EUV and the advent of the High-MEMS Alliance program, an US initiative to implement LIGA technology in the United States, CAMD's microfabrication group focused its research activities on other applications including precision engineering, microfluidic, BioMEMS, and material science. At the same time, the group enabled access to its unique infrastructure including class 100 clean room facilities with conventional MEMS microfabrication infrastructure, four microfabrication beamlines, electroplating, hot embossing, and some basic material analytical tools; it also provides in-depth training and education as well as user service.

The current operation, as shown in Fig. 4, indicates the main activities of the group. Access and training to beamlines and clean room equipment is provided as a major service and involves the participation of senior and junior staff. This Education and Outreach activity reflects CAMD's unique role for the LSU community. Approximately, 60-70 students benefit each year from this service. CAMD's LIGA work has always been geared towards serving the needs of industrial users, enabling them to access benefits from this US-wide unique capability.

The microfabrication group provides a broad range of services to the academic and industrial users and closely collaborates with several companies in developing LIGA- based products. In order to maintain cutting-edge expertise and also continuously improve processing skills and material knowledge in LIGA, these services are complemented by conducting dedicated research projects spearheaded by the senior staff members. Such on-going research projects reflect customers' future needs that rely upon and use CAMD staff expertise; funding is provided partly through the operating budget, as well as from service income.

A third effort is called independent R&D projects that are typically externally funded and are collaborative efforts with external partners. While these projects benefit from the existing infrastructure and available expertise at CAMD, their goals are strongly future-oriented and embedded into larger, LSU- wide efforts, for example, the CBMM and Materials Science Center Initiative.



# CAMD Microfabrication Group

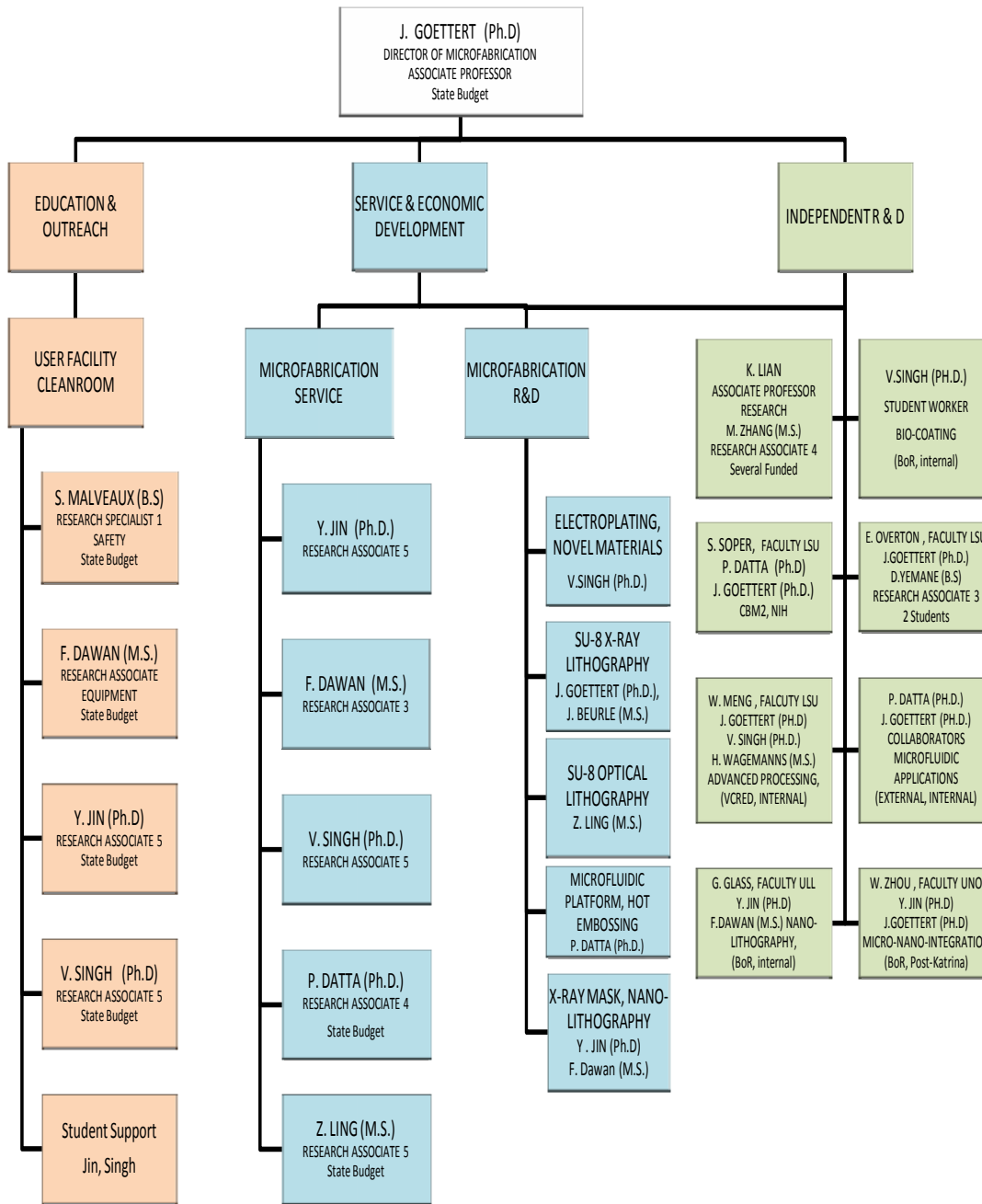
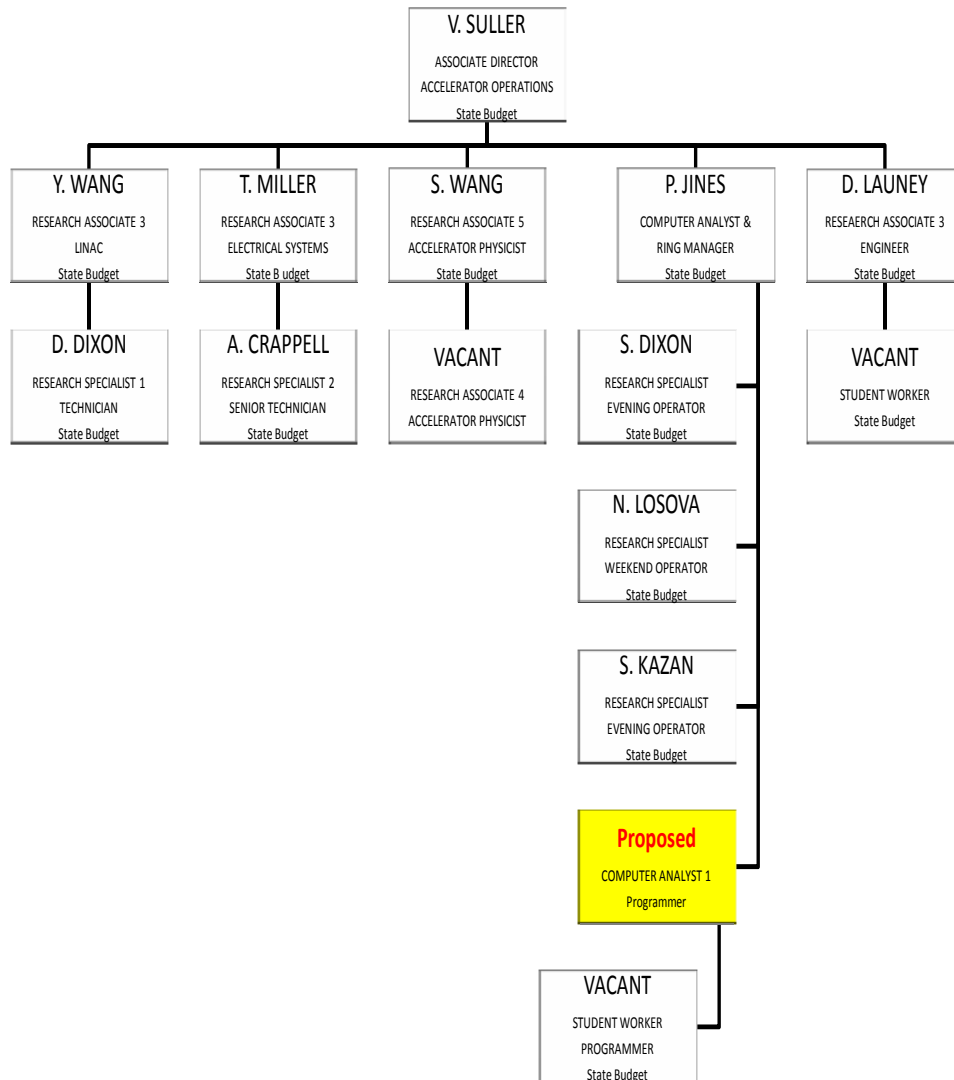


Figure 4: CAMD’s Micro- and Nano-fabrication Research Groups.

**The Accelerator Engineering and Support Group:** The Accelerator group has attained the exceptional efficiency of 97% (efficiency defined as the ratio of beam delivered to beam scheduled). The 11 people on the staff include three evening and weekend operators.

### CAMD Accelerator Group



**Figure 5:** CAMD’s Accelerator Group.

At present, CAMD is filling one accelerator physicist vacancy. (what is the purpose of this sentence?) However, if plans to upgrade the accelerator and ring components are to be fulfilled, two more staff should be hired in the near term. The multipole wiggler insertion device is under consideration as the first upgrade to the ring, and there are plans to decrease the emittance at injection to accommodate a second insertion device.

**Engineering Support Group:** The final group is the Mechanical and Vacuum Engineering Group. This tiny group supports *all* mechanical, vacuum maintenance, improvements, as well as engineering developments, for the ring and the hardware attached to it. A mammoth task carried out by four extremely capable engineers, one of whom is currently serving in Iraq for the year 2007-2008. As the plans to upgrade CAMD mature, this team will require staff additions for a timely implementation of the upgrades.

### CAMD Engineering Support Group

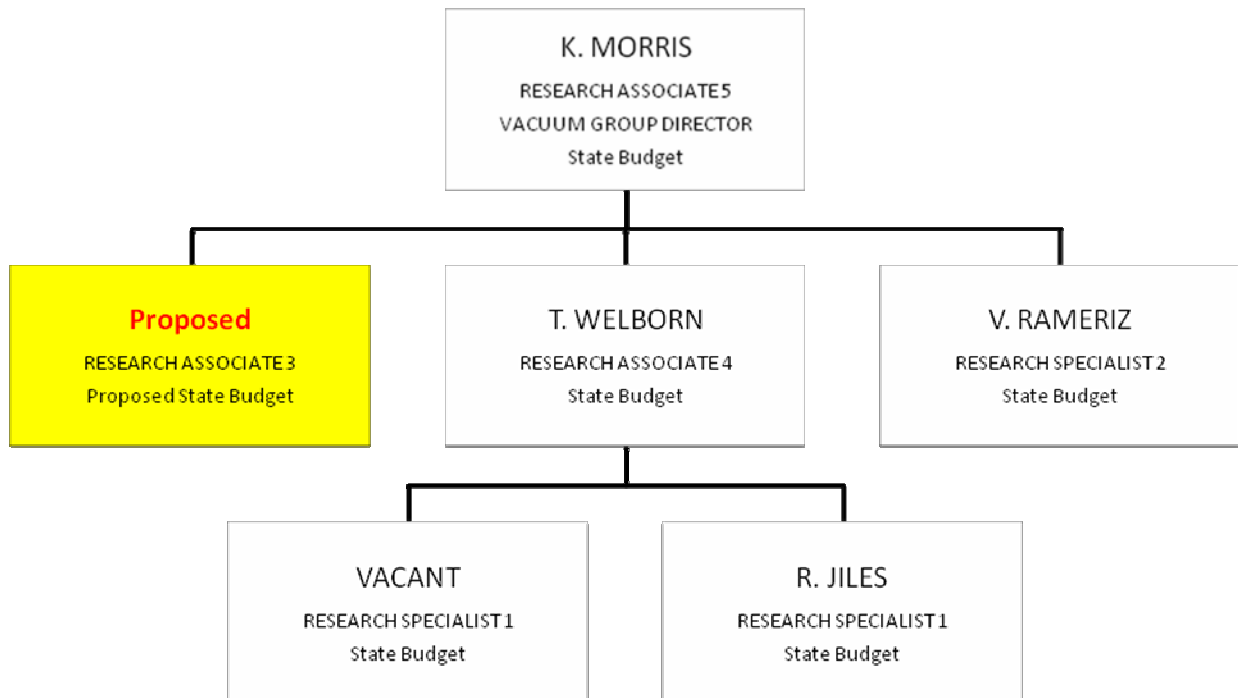


**Figure 6:** CAMD’s Mechanical and Vacuum Engineering Support Group.

### III.B.5.b. CAMD's Funding

The CAMD state funded operating budget has increased slowly during the past four years with increases in the budget coming only from legislative mandated staff pay raises and changes to the fringe benefit rates. There was no salary increases in the 2005/2006 fiscal year owing to hurricanes Katrina and Rita. The actual numbers are shown in Table I, along with the full time equivalent number of employees (FTE). Owing to budget cuts in the 2005/2006 fiscal year, six positions were eliminated, bringing the total employee positions to 49 positions.

During the 2006/2007 fiscal year, we split a position to create two part-time positions in order to have two weekend caretakers rather than just one, bringing us up to 50 funded positions. The 2007/2008 fiscal year operating budget includes 51 positions due to a further split of another position to support a faculty line at 50% effort. A complete breakdown of the current employment picture and the plans to prepare CAMD for its role in the LSU Materials Center has been presented in III.B.4.a.

**Table 1:** The Operational Budget at CAMD from 2003-2008, Full Time Equivalent (FTE)

FY	2003/2004	2004/2005	2005/2006	2006/2007	2007/2008
Dollars	\$4,412,288	\$ 4,651,280	\$ 4,667,380	\$4,838,146	\$5,124,134
CAMD Extramural	\$ 2,700,000	\$1,400,000	\$1,100,000	\$1,500,000	\$2,800,000
FTE	54	55	49	50	51

The following graph provides a breakdown of the yearly allocation of the state operational budget funds from 2003/2004-2006/2007 at CAMD:

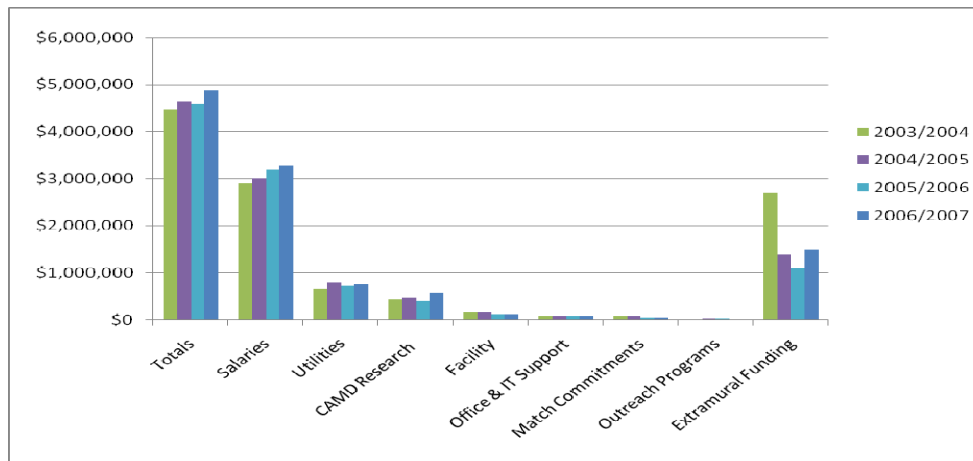


**Figure 1:** CAMD's operating budget breakdown for 2003-2006.

A glance at Figure 1 tells the tale of how the budget increases have been absorbed by increasing personnel and utility costs reducing, thereby, discretionary funds. These funds provide resources for spare parts, office supplies, custodial services, and staff travel. The cost of helium for the

wavelength shifter is also included in the facility costs. It amounted to \$83,000 in FY 2006-07 and will increase in 2008 by 30% to 50% because of decreasing supplies of helium, thus eroding CAMD's discretionary budget further. CAMD staff realized that helium costs would become untenable in the near future and applied for and received Louisiana Board of Regents funding to partially cover the cost of converting the liquid helium cooled cryostat to a closed-cycle helium cooler, eliminating the use of liquid helium completely. The components for the cryocooler will be ordered during fiscal year 2007-08.

Utility costs and custodial services (trash removal, lawn care, etc.) that are usually absorbed by the university through overhead, also constitute a part of the CAMD budget.

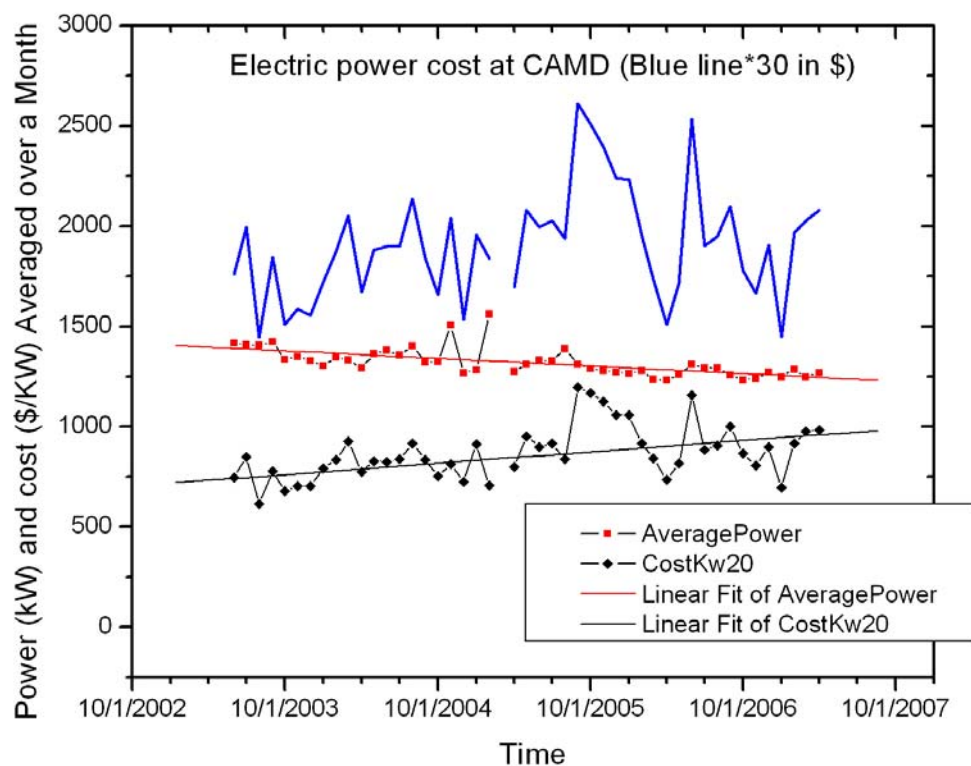


**Figure 2:** Average electric power consumption and cost at CAMD's between 2002 and 2007.

The CAMD power bill consumes about 17% of CAMD's budget (\$769 k in FY 2006-07). Utility costs have increased slowly during the past five years since the power cost has risen at about 5%/year; however, the power usage has decreased by about 3% per year, owing to a more efficient use of the ring. Assuming the ring will operate on the same schedule, we foresee a leveling in the average power consumption and thus a rise in the power costs. Of course, Katrina in late August 2005 generated rather significant fluctuations for several months into 2006.

The amount of external funding CAMD staff generated is shown in the third row in Table 1, and in the last set of bars in Figure 1. The spike in 2003 was produced by DARPA funding for the

development of a microstructure-based lab on a chip. However, this funding is winding down as DARPA has redirected its resources to other projects.

While CAMD's outreach program is partially supported by the NSF REU program, CAMD adds about \$25,000 to the approximately \$80,000 that the NSF provides for the REU program annually for a more extensive outreach to the general public and minorities through tours, open houses, and publications. Because of the importance of outreach, CAMD has used some of its resources to add a temporary public relations staff person to develop press releases describing CAMD's research for the CAMD website, LSU publicity releases, and other publications.

It is pretty clear, considering the budget trends, that CAMD must reposition itself for its role in the proposed LSU Materials Center, as an x-ray source for the state, and as a regional resource in the south. Initially this may be accomplished by creative financing. For example if the University absorbed the utility costs for CAMD as it does for other centers, it would effectively add \$770,000 to the budget that could be used to support additional staff and add needed upgrades to the facility, as well as playing a more proactive role in the activities of the new Material Center of Excellence.

### **III.B.5.c. CAMD Cleanroom**

#### **Summary**

The cleanroom is a major part of the User facility at CAMD and provides the main LSU infrastructure resource for standard MEMS (MicroElectroMechanicalSystems) processes supporting different LSU departments, professors and students in their research projects. It is complemented by additional ‘clean’ working space in various departments on LSU campus (ME, ECE, South Campus) and is a major contributor to hands-on microfabrication education and research at LSU. It is also open and available to industrial users. Infrastructure, training, and education allow US and international researchers and students to complete their microfabrication projects either independently or with various levels of support from CAMD staff. Additionally, CAMD staff offers paid services and provides clients with professional fabrication results especially dedicated to its unique LIGA microfabrication capabilities. The cleanroom infrastructure is more than 10 years in operation and CAMD staff used DARPA and State funds to upgrade and continuously maintain the equipment to offer state-of-the-art support.

It is important to mention that the cleanroom is not immediately connected to the synchrotron operation as initially anticipated and required for microelectronic applications. It is first and foremost a central piece of infrastructure serving the entire LSU research community in education and research in microtechnology. Though efforts are ongoing to ‘continuously’ upgrade and expand the equipment and process capabilities (mainly through BoR Enhancement programs), it is evident that a major LSU wide effort is needed to best prepare the LSU community for the future demands and challenges in micro- and nanotechnology.

#### **User Information**

User support for cleanroom activities is a vital part of the CAMD user facility operation. Support of students includes education and training for each entering individuals. Education of cleanroom function and equipment, along with general processing guidelines are included in the initial cleanroom training. Detailed training in cleanroom protocol and chemical, electrical, fire, and emergency safety are included. Training on machine use and safety completes initial training on twelve processing machines, which is typically required for user projects. Training is offered on an individual need basis for more specialized machines such as the optical profiler, scanning electron microscope, spectrophotometer, and upgraded mask aligner. Detailed training for acid use inside the cleanroom is necessary to ensure adequate understanding of properties of acids and first aid and emergency protocol required in case of mishap.

The cleanroom has supported many students in their pursuit of project completion for undergraduate, graduate, and post-doc work. Figure III.B.5.c.1 indicates the types of degrees earned by students who worked actively on projects in the CAMD cleanroom since 2001.

**Levels of Degrees Earned by CAMD Cleanroom Users 2001-2006**

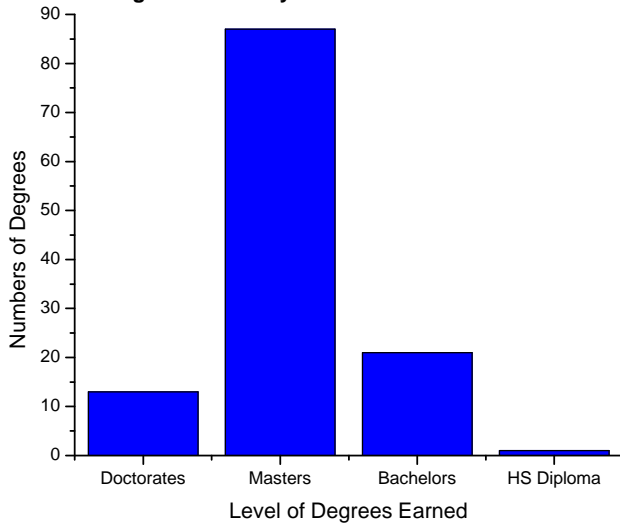


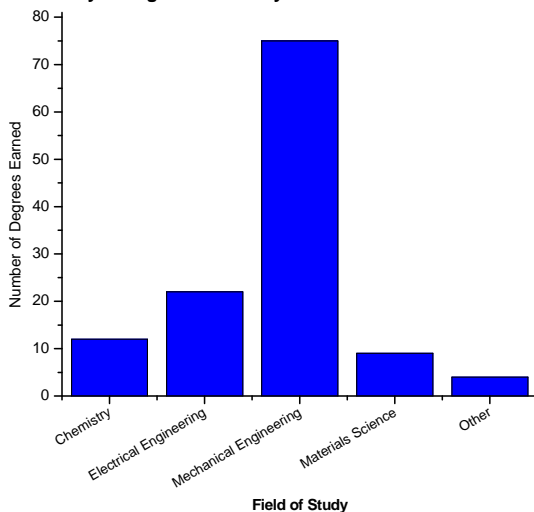
**Figure III.B.5.c.1**

Degree levels earned by students working in the CAMD cleanroom. The total number of degrees earned from 2001 until end of 2006 is 122.

As the chart indicates, master-level students are the most common. Post-doctorate work is not indicated in this graph or the following, which constitute another 15 Users over the past 6 years.

The most common field of study for cleanroom users is Mechanical Engineering, as indicated in Figure III.B.5.c.2. The strong interest of users from the ME department reflects that the major areas of interest in LSU’s MEMS research are driven by this user community focusing on mechanical, fluidic, thermal, optical applications and materials issues related to MEMS fabrication and research, and that the typical MEMS stronghold and driver (electrical engineering) is of less importance for LSU’s efforts. The ‘other’ category in Figure 2 includes students from Chemical and Biological Engineering.

**Field of Study of Degrees Earned by CAMD Cleanroom Users 2001 - 2006**



**Affiliation of Earned Degrees by CAMD Cleanroom Users 2001-2006**

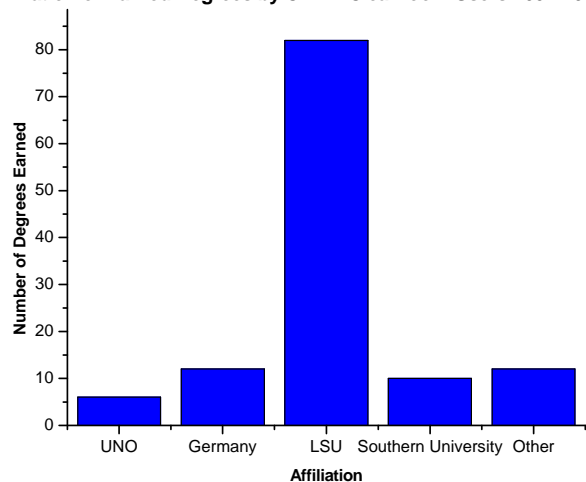


**Figure III.B.5.c.2**

Concentrated field of study for degrees earned by students using the CAMD cleanroom for their projects.

**Figure III.B.5.c.3**

Affiliation of degrees earned by CAMD cleanroom users.



Another substantial R&D training effort is CAMD's NSF funded REU (Research Experiences for Undergraduates) program with a total of 10 of the undergraduates having received their degrees. The status of their research and graduate education can be followed in the NSF-REU yearly report, available upon request.

Academic Users are typically working on funded projects from the NSF, DARPA, NIH, BoR EPSCoR and others. The academic students are primarily local, serving Louisiana State University and Southern University, as indicated in Figure 3. A significant number of internationally affiliated universities, especially Germany, commonly use the CAMD cleanroom in support of their master's thesis projects, too.

The cleanroom does assist in supporting industry from Mezzo International, an LSU spin-off company, to HT Micro (Albuquerque, NM), Creatv Inc. (Potomac, MD), and Micromotion GmbH (Mainz, Germany) as well as the CAMD Service group, which offers standard processing and metrology services through MEMS Exchange and other affiliations.

## **Operations**

Cleanroom activity is determined by monitoring machine use, which is accomplished by compiling data created from machine login through our uniquely developed Login system. Each time a machine is run it must be logged in through the Login computer. The user's name, affiliation, the date, machine name, and time logged in are recorded. Comparisons of cleanroom activity along with accurate accounts of machine use time are available through this system.

It is to be emphasized that CAMD's cleanroom is not designed to accommodate a large number of users at any given time without compromising the 'cleanroom quality'. Thus, a maximum number of 5 users is allowed inside the cleanroom processing or inspecting samples. It would be highly recommended to separate the cleanroom in two areas for different purposes – student training and advanced research. This will also allow students to 'practice' techniques and processes skills using 'old' equipment and will keep the 'advanced research tools' in better conditions performing at the highest level. In addition, an intensive hands-on laboratory class could/should be established that would be part of the curriculum and students would be required to take this class prior to become a CAMD cleanroom user. This program would elevate the level of education in MEMS/NEMS technologies and also result in enhanced research productivity.

## **Cost Center**

The cost center is a fee schedule in which rates for a single piece of equipment were derived using CAMD's expense and usage history according to guidelines provided by the university. Strict guidelines for rate derivation were provided by PS-103 through LSU's department of Budget and Planning. Jim Bates, Director of Sponsored Programs, guided and approved the rates of each cost center in October 2005. Rates are subject to yearly adjustment in order to ensure best estimates of generated revenue, which are to be kept at or below cost. The Cleanroom has a cost center for each piece of equipment of which time is to be charged.

The cost centers were derived in order to allow all Users (including CAMD staff) to contribute their portion of used resources to the operation and maintenance of the facility. It was apparent in 2001 from trends of other labs around the country and foresight of Microfabrication's funding

future that led to the long process of deriving and approving the cost centers. Over the past year it has been determined the immediate future of user access and affordability of the Cleanroom and its equipment is increasingly precarious. It costs approximately \$250,000 per year to supply and maintain the Cleanroom infrastructure and supplies, and 100% of these funds are pulled from CAMD's reduced budget (it should be noted that some DARPA project funds were also used to pay for CAMD's part of the research efforts). Thus, successful implementation of the cost centers in the future would contribute to the operation and maintenance of the Cleanroom, thereby allowing CAMD to continue to serve its user community.

The discussion about cost center or, more general, user contribution to cleanroom operational costs is reoccurring and needs to be addressed in the 'bigger picture' of LSU research. A cleanroom is to be considered a major research tool supporting many students from a variety of departments. It's a central piece of research infrastructure with relatively high costs for service and maintenance as well as a continuous need for investment to maintain 'state-of-the-art' capabilities. Thus, it is a major decision impacting many departments if (a) a cleanroom infrastructure is needed for LSU's research efforts, and (b) how to pay for the operational costs. While historically it made sense to keep the cleanroom at CAMD it has certainly a number of advantages to have this tool centralized on campus making it easily accessible to many student users and their projects.

Thus, a more detailed discussion is needed to determine affordability by both CAMD and the user community, and CAMD is committed to working with campus faculty and LSU administration to resolve this dilemma for successful operation and access of the facility for everyone.

## **Training**

The Annual Cleanroom Refresher is held each spring. Instruction on the new safety and cleanroom protocols are included, along with etiquette and operational reminders to Users on specific issues that were subsequently improved upon by the Users.

For training to be most effective, theoretical knowledge of processing and background of the project would be required, along with applied skills development. While CAMD cannot affect the background research of another user's project, increased instruction through an engineering class of theoretical and applied processing for micro and nano lithography as well as LIGA would properly prepare each student for effective and thorough project completion. Additional instruction on research tools and ethics would provide a bold complement to this research enhancement program. The student laboratory space described above would afford the infrastructure for the applied portion of instruction, which is vitally important to student skill development in micro and nano processing. Due to lack of funds and cooperation between CAMD and LSU, this educational opportunity has continued to elude the local academic community. Future efforts should be promoted and actively pursued by embedding this class in an LSU wide strategic plan to achieve excellence in materials science utilizing advanced micro- and nanotechnologies.

## **Future Cleanroom Infrastructure**

CAMD microfabrication group has regularly submitted proposals to the BoR to acquire new equipment/process capabilities and/or upgrade existing ones. These proposals were fairly successful but do not reflect a cohesive strategic plan to elevate the Cleanroom operation to the 'next level'. Equipment proposed and purchased is mainly identified to immediate internal and user needs.

The following pieces of equipment and/or upgrades are in the process of being installed:

- Nano-hood; a dedicated ultra-clean workspace for nanolithography research;
- Ebeam writing capability for Hitachi SEM (includes stages, current control, and software allowing to use the SEM electron beam for writing of submicrometer structures, ~100nm);
- RIE-ICP, dry etching capability with inductively coupled plasma to allow submicrometer etching of silicon substrates as tools for Nano-Imprint-Lithography (NIL);
- Parylene coater, a dedicated machine to apply conformal Parylene coating on fluidic chips and other MEMS devices.

In order to better prepare for future research and user needs it is necessary to (a) identify the long-term research goals for the LSU community, (b) prepare a list of equipment/infrastructure needed to reach these goals, (c) plan to acquire the equipment, (d) decide where to locate and how to operate the cleanroom (cost center, free-of-charge user facility, technical support staff,...) and how to finance maintenance and service. This effort requires leadership by LSU's Vice-Chancellor for Research and needs active contributions (not only ideas but also financial commitment) from all LSU departments' interested and utilizing micro-and nanotechnologies. CAMD certainly can provide 10 years of experience as a user facility and its experienced staff is ready to support this campus wide effort.

### **III.B.5.d. History and Overview of IT at CAMD**

In 1998, Computer Analyst , Vincent G. Mitts, was given permission to completely replace the existing CAMD network and telecommunications equipment, which allowed for the expansion of three additional office buildings and the integration of the CAMD telephone system with LSU's Telecommunications department. New fiber optic cables were installed for the network backbone, connecting all the internal network routing switches together with Gigabit Ethernet, and all additional network cables were replaced with new Category 5e Ethernet cable. A new Lucent G3 PBX system was also installed which allowed CAMD to be connected directly with LSU's telecommunications system, providing the CAMD department with new campus telephone extensions.

In addition, in 2006, CAMD's main internet connection with BellSouth was upgraded from a T1 line (1.5Mbps) to a standard Ethernet connection (10Mbps). This upgrade helped alleviate some of the network congestion problems CAMD was experiencing while accessing the internet during peak network traffic times of the day.

Analyst Mitts and his colleague Rebecca Cooper are responsible for a large array of equipment including, routers and switches, ninety desktop computers and 31 laptop computers, as well as six servers. In addition to this formidable array of computational equipment, these two staff members sustain the communication connections, website and software integrity for the entire facility.

### **Immediate and Future Needs of IT at CAMD**

- A. There is an immediate need for at least one additional staff member to care for Help Desk needs, computer maintenance, software and security updates, and other computer related issues.
- B. There is a future need to upgrade CAMD's internet connection with LSU from its current 10Mbps (standard Ethernet) at \$494.85 per month to 100Mbps (fast Ethernet) at \$875.00 per month. This will enable the future growth of CAMD's network, providing the necessary bandwidth for video conferencing and large data transfers with campus and other remote users. This has been one of the most frequent requests received from outside users. Many have agreed that this would also help bridge the physical gap between the LSU campus and CAMD.
- C. CAMD's existing network infrastructure is reaching the end of its life cycle (ten years or more). Therefore, planning and budgeting considerations should be discussed to anticipate the inevitable upgrade and/or replacement of existing infrastructure hardware.
- D. CAMD has the option of integrating its current network domain with LSU's Active Directory domain. However, careful planning is needed to ensure that proper control remains in place at CAMD, once it is integrated into LSU's Active Directory.

### III.C. CAMD User Statistics

#### 1. Introduction

It is important to define the terms of CAMD user, both active and inactive and CAMD collaborator at the outset of this information.

CAMD User	A person who has passed radiation safety training, and is assigned a badge
CAMD Active User	A person who has maintained annual radiation training re-certification and has a radiation badge
CAMD Inactive User	A person whose training has lapsed, a person who has graduated, has moved or a person who no longer wishes to use the CAMD facility
CAMD Collaborator	A person who has not maintained his/her training requirements, but who sends samples to CAMD staff, or mentors students to conduct research at CAMD.

#### 2. User Statistics

This section of the document will focus on a geographical distribution of the CAMD user community: LSU; Louisiana; United States and foreign users. For the LSU community, the numbers of individuals from each department will be highlighted. Groups are assigned as Faculty, Post-Doctoral Fellows, Staff, Graduate Students, Under-Graduate Students, Visiting Researchers, Teachers [High School] and High School Students. It is important to note that the

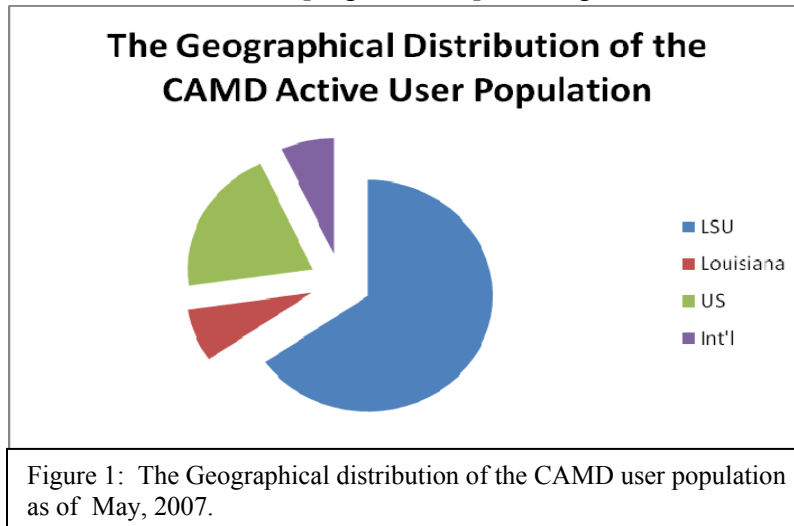


Figure 1: The Geographical distribution of the CAMD user population as of May, 2007.

active user participation list is a fluid, dynamic document, subject to daily fluctuations. Therefore, data from May of 2007 will be used for comparative purposes. The use of this data is further explained under section III.C.2.

Only those CAMD faculty and staff who are actively using the facility for research, including process development are included in the statistics for Figure 1. CAMD administrative

staff, the accelerator group and facility support personnel are specifically excluded from these statistics. Four additional persons are included: The CAMD Director, the CAMD Scientific Director, the Accelerator Group Head and the Microfabrication Director.

Figure 1 illustrates the distribution of the active user community utilizing the CAMD facility effective May, 2007. As anticipated, LSU has the lion's share of total users accounting for 61% of the total active user community. This is in line with other Synchrotron Radiation Facilities, that tend to serve a regional populace. As of 05/2007, there were 241 total active users working

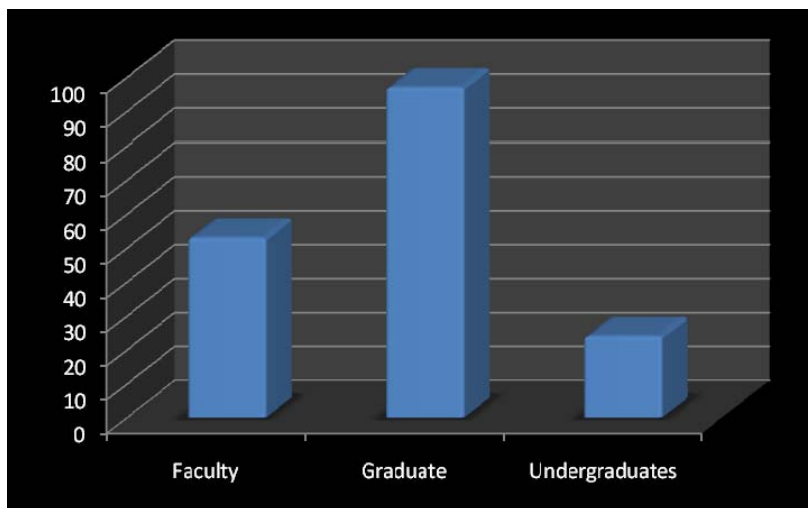


Figure 2: Numbers of active participants at CAMD as of May 2007

at CAMD including 59 total CAMD staff members (Figure 2). This includes 53 active faculty members, 97 graduate students and 24 undergraduates. The number fluctuates annually due, in part, to an influx of summer students in the REU program, or to incoming graduate students. These figures were also taken in the month of May, a time when many students graduate and so are no longer counted as active participants. Another reason for the lower numbers at this time

of year is associated with the fact that rolls are purged annually in May, of those individuals who have not maintained their training requirements. CAMD's certificate to operate the synchrotron is predicated on the basis of annual radiation safety re-training. In practice, many allow their training to lapse and re-train only when they have allotted time at a beamline or if a research proposal has been funded.

Participant numbers for the past 5 years are tabulated in Table 1. Values are valid through May of 2007, and are also shown graphically in Figure 3. Not included in the 2007 data are 13 PhD, 8 Master's Level and 6 Bachelor's level graduates as well as one Law Doctorate who graduated this past year. All of these individuals either worked at CAMD or conducted a significant portion of their research at CAMD. Further information on the number of degrees granted to active CAMD users is available in Section III.C.3.

**Table 1**

Numbers of active users for the CAMD facility by year including total, faculty, graduate and undergraduate populations for years 2003-2007 [effective through 05/2007]

Year	Total	Faculty	Graduate	Undergrads	Visiting	Staff	Teachers	High School
2007	241	53	97	24	2	59	0	0
2006	298	94	120	32	0	48	0	4
2005	289	80	111	25	7	63	2	1
2004	292	85	106	34	5	59	2	2
2003	215	46	69	35	1	63	1	0

### III.C.1. CAMD Users from Louisiana

#### a.LSU

As of May, 2007, there were 241 active users of the CAMD facility. This includes 31 members of CAMD who actively participate in research activities out of a total of 55 staff and faculty members [not included in Figure 1]. From the LSU community, there are 147 active participants representing 16 distinct departments. Figure 1 shows the distribution of active participants from various LSU departments. As expected, LSU faculty, staff and students represent the lion's share of users at the facility [61%] [Figure 1, Section IIIC]. The largest number of graduate students comes from the LSU department of Mechanical Engineering [Figures 1 and 3]. Figure 2 is a composite of the distribution of LSU faculty from Agronomy through Civil and Environmental Engineering and from Computer Science through Physics. The sheer physical

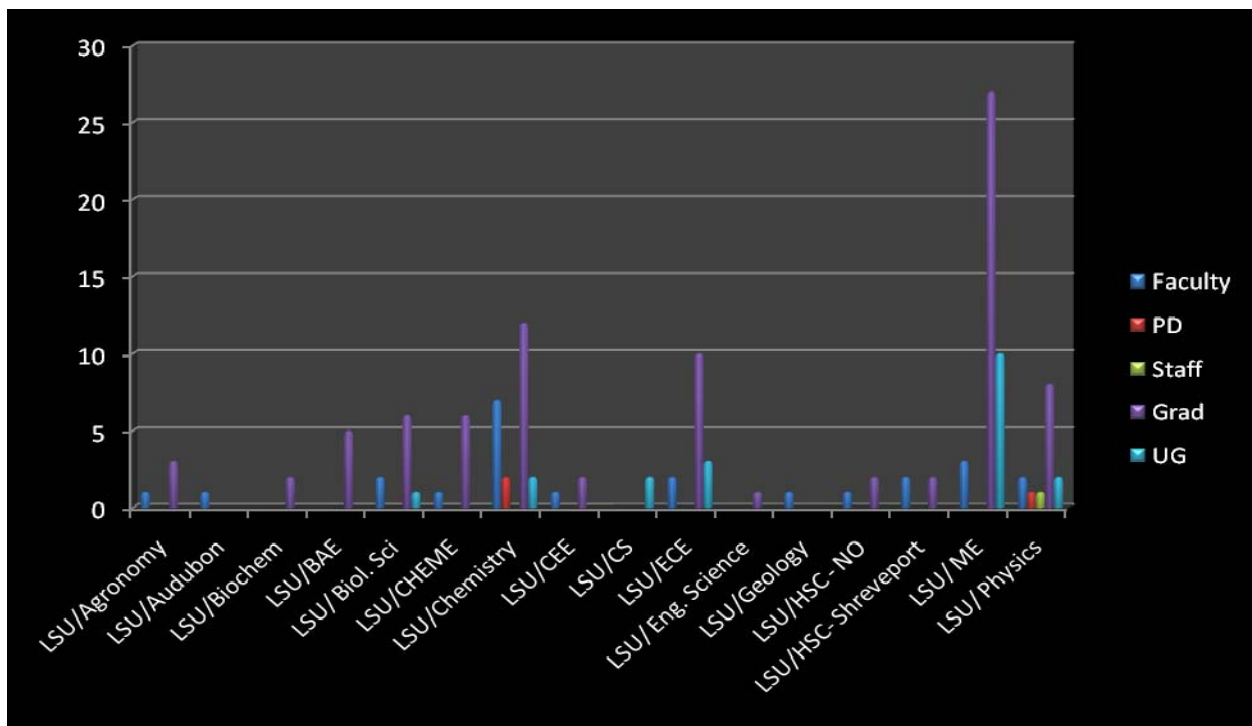


Figure 1: The current distribution of CAMD active users from Louisiana State University [including both Health Science Centers in New Orleans and in Shreveport] as of May, 2007

number of departments involved precluded the use of a single pie chart. There is no common denominator between the numbers of active LSU faculty members and the numbers of graduate students from the same department [Figures 2 and 3]

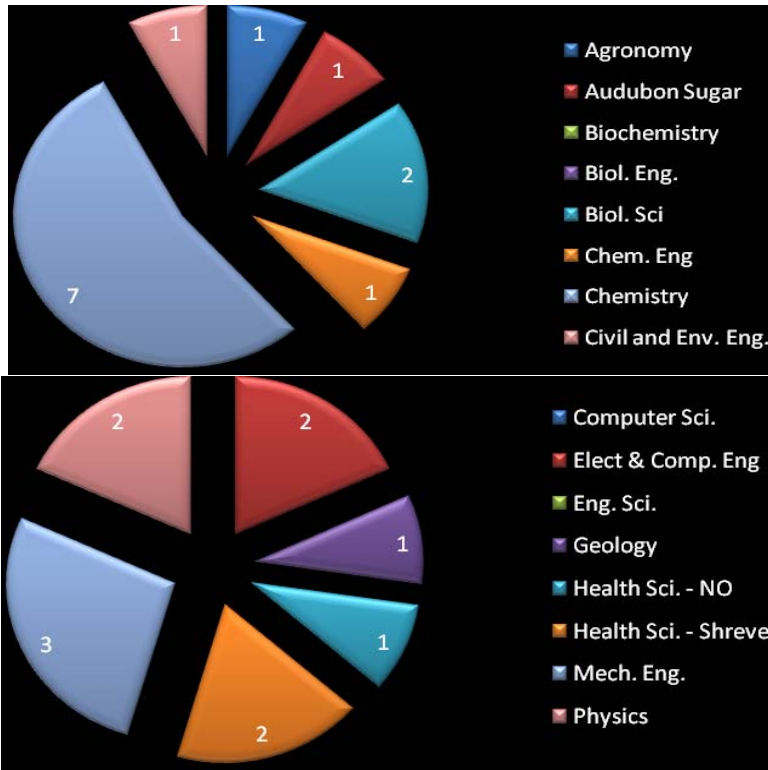


Figure 2: The distribution of LSU Faculty from various departments. Individual departments, are alphabetically grouped

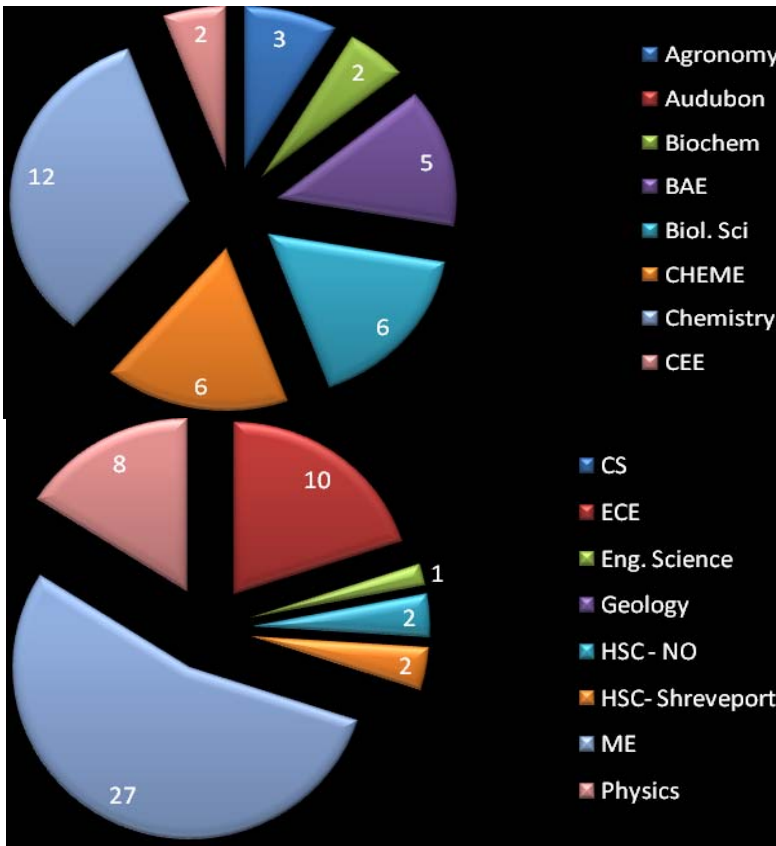


Figure 3: Graduate students per department 2006-2007

There are also a significant number of graduate students from the Department of Electrical and Computer Engineering. Several undergraduate students are employed as part-time technicians at CAMD. The majority of these individuals come either from LSU's department of mechanical engineering or from LSU's department of Electrical and Computer Engineering. Additionally, there is a strong faculty presence from the LSU Chemistry Department. Both LSU health science centers [*i.e.* Shreveport and New Orleans] are represented as well as the Audubon Sugar Institute, a part of the LSU Agricultural Center, considered a separate campus of the university. It is clear, that CAMD interacts well with members of the LSU university community, as can be seen in Figure 1 [above]. Figure 2 is the distribution of LSU faculty from various departments, Agronomy through Civil and Environmental Engineering, and Computer Science through Physics. It shows that the highest concentration of active LSU faculty members is in the Department of Chemistry [7] followed by the Mechanical Engineering department. Although, there are fewer actively participating faculty from the Department of Mechanical Engineering, they support the most graduate student projects at CAMD [currently 27 graduate students from 2006 to the present] as shown in Figure 3.



**b. State of Louisiana [Excluding LSU]**

There is also representation from several other Louisiana Universities and businesses. Among these are Southern University Baton Rouge, Louisiana Tech University, University of Louisiana

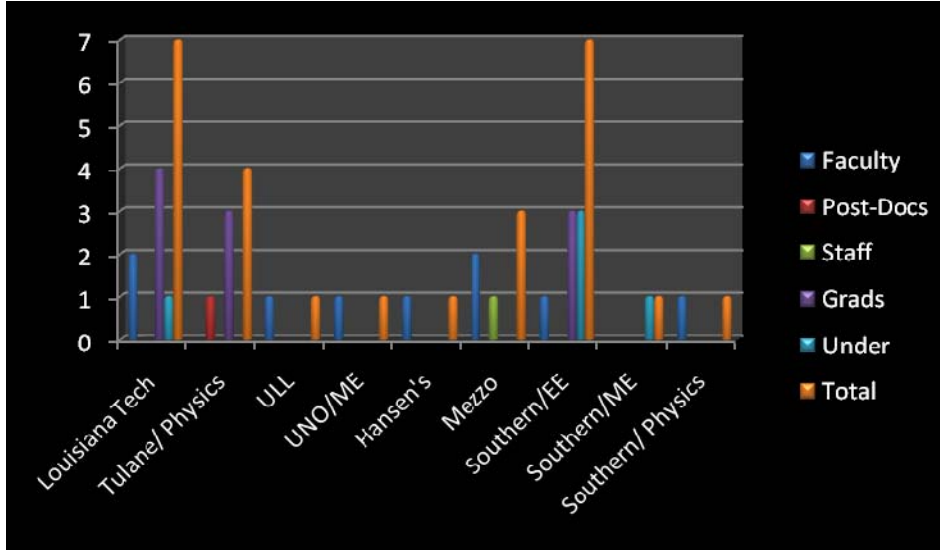


Figure 2: Representation of users from the Louisiana community, excluding members of Louisiana State University, May, 2007

at Lafayette, Tulane University and the University of New Orleans, Mezzo Systems and The National Hansen's Disease Center located in Baton Rouge. Mezzo Systems represents the first spin-off company from CAMD. Figure 2 gives the distribution of Louisiana Universities and research centers, excluding LSU's contribution.

Together, residents of Louisiana account for 75% of the CAMD user community[Figure 3].

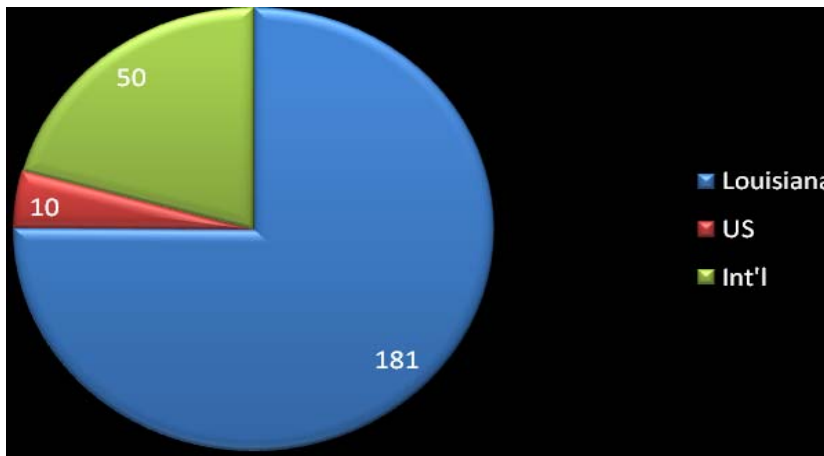


Figure 3: Distribution of Louisiana Residents using the CAMD facility. 75% of the users are from the state of Louisiana

Southern University has 3 active departments, including the Department of Electrical Engineering, the Department of Mechanical Engineering and the Department of Physics. Not included in these figures are interactions between one CAMD faculty member and the Southern University Agricultural Center. Several undergraduate students at Southern University have also participated in REU

[research experience for undergraduates] programs hosted at CAMD since its inception in 2000 [not shown]. Within the state of Louisiana, the largest numbers of users come from Louisiana Tech University and Southern University's department of Electrical Engineering.

### III.C.2. CAMD Users Outside Louisiana

#### US Participation:

Within the US, several states are represented. Most of the user population comes from Texas,

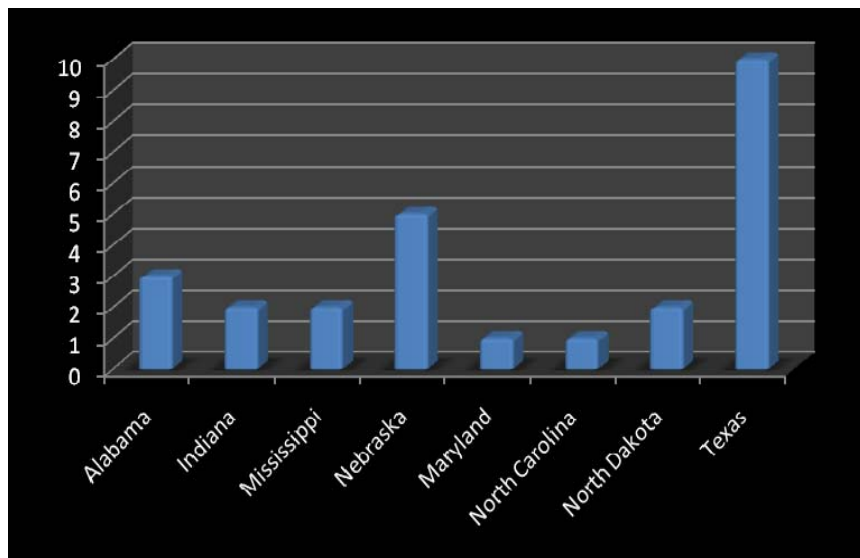


Figure 1: The contribution of various U.S. states to the active CAMD user community.

Alabama and the States of Nebraska and Oklahoma. Texas, Oklahoma and Louisiana are members of the Gulf Coast Protein Crystallography Consortium [GCPCC]. Representatives from other Louisiana institutions are also major contributors of graduate students, and to a lesser extent, of undergraduate students. As of 06/27/2007, CAMD had about 25 active users from 8 different US states.

A common occurrence is that students using the facility and graduating then

go on to other academic institutions but continue to utilize the CAMD facility [*i.e.* a generational effect].

Some examples include Dr. Tony Caruso who graduated from the University of Nebraska but is now at North Dakota State University. Dr. Ruihua Cheng, another graduate of the University of Nebraska, is now at Indiana University /Purdue University and has begun training a new generation of graduate students at CAMD. Similarly, a former LSU / Physics post-doctoral fellow is now sending his students from the University of Alabama to use the facility. It is gratifying that the experience of these users has been so positive that they want to create a similar experience for their own students.

#### CAMD Collaborators:

As defined in section IIIC, there exists a subset of CAMD users who send students and/or samples for analysis. These individuals do not maintain active user status but are clearly users of the CAMD facility. Their publications require input from CAMD staff, or through their own students collecting data at CAMD. Examples of such individuals include Prof. Steve Soper, Director of CBM2; Prof. Michael Murphey; Mechanical Engineering [this individual currently supports 15 graduate students working at CAMD], Prof. Kevin Kelly; Mechanical Engineering and Mezzo International and Prof. Fritz Goetz; Gelsenkirchen University; as well as Prof. Ed Overton of Environmental Sciences. Many of these individuals have sent dozens of personnel [undergraduates, graduate students or post-doctoral fellows] to work at CAMD since records

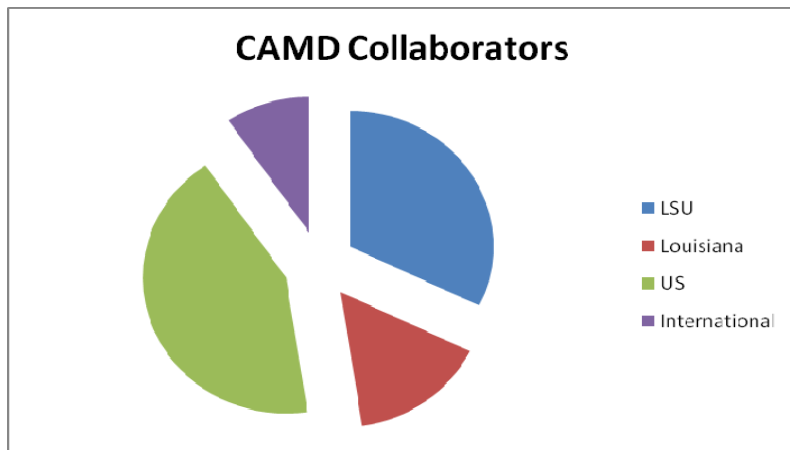


Figure 2: CAMD Collaborating Faculty members from LSU, Louisiana, the United States and the International Community.

were comprehensively initiated [1997]. For year 2006, these research colleagues represent 44 separate departments or institutions. 27 of these faculty members are from LSU with an additional 13 from other universities in the state of Louisiana. Also within this population, 36 collaborators from 17 US states are represented as well as individuals from 8 foreign countries.

Since 1997, there have been 135 CAMD users from various US institutions, excluding the user community from the state of Louisiana. Some of the participants from the northeast include Harvard University, Johns Hopkins University, The University of Maryland and the University of New Hampshire. The states of North Carolina, Tennessee and Alabama are also represented. Participating universities from Texas include, The Baylor College of Medicine, Rice University, and The University of Texas Medical Branch at Galveston, UT-Austin, TAMU, and The University of Houston through the GCCPC [Gulf Coast Consortium on Protein Crystallography] and UTEP {Chemistry}. The state of Texas accounts for 52 trained participants, with an additional 9 researchers from the state of Oklahoma. Oklahoma institutions include Oklahoma Medical Research Foundation and the Samuel Roberts Nobel Foundation and the Oklahoma University Medical Center.

The University of Nebraska Lincoln has sent 17 participants, primarily from Dr. Peter Dowben's Physics Lab as well as several from the Department of Chemical Engineering [Dr. Jennifer Brand] who shares a joint appointment at Nebraska Wesleyan University. One REU student came from the University of Arkansas, Fayetteville. Recently, CAMD has conducted individual tours for Mississippi professors {Mississippi State and University of Mississippi} visiting LSU. To date, these introductions have not yet blossomed into active research projects but CAMD continues to conduct such tours as an outreach tool.

## Europe

Many universities from Germany have sent dozens of students from various campuses including Bonn University; Zwickau University; the Technical University of Karlsruhe; Neidderhein University; The University of Hannover; Feiburg University, and Bielefeld, to name but a few. Other European nations represented include France, Denmark and Finland.

## **Asia**

Korea has sent individuals from Chonbuk, Pohang and Chonnam Universities while Japan has sent no fewer than 8 individuals from such universities as Kobe and Toyama. One individual who conducted the major share of his dissertation research at CAMD came from Singapore. A visiting professor has recently returned to her Faculty position at the University of Colombo, Sri Lanka.

## **South America**

Five different universities from Brazil have sent researchers to the CAMD Facility. Historically, CAMD formed an early association with the Brazilian Light Source located in Campinas [LNLS-Laboratorio Nazionale de Luz Sincrotron]. CAMD's first beamline [the 3MTGM] was partially built with the help of our Brazilian colleagues, as was CAMD's first monochromator. The Brazilians used CAMD to gain experience in building their own Light Source, which is now both larger and brighter than the current CAMD facility. A total of 22 Brazilians trained, participated or were visiting professors, graduate or undergraduates students at CAMD. At least 3 professors came to CAMD to work during their sabbatical leave from their respective universities.

## **Historical Perspectives**

Since 1997, some 700 LSU affiliated individuals have been active users. In addition to this LSU participation, 154 individuals from other Louisiana Universities have also been trained since 1996. Participants include members of Faculty or Student populations from Tulane University, McNeese University, University of New Orleans, Xavier University, and Southeast Louisiana University, The University of Louisiana at Lafayette [SWLU] as well as the La Tech University [including the Institute for Micromanufacturing [IfM], Grambling University, Southern University of Baton Rouge, Nicholls State University, Louisiana College, Louisiana State University Health Sciences Center, Shreveport; Louisiana State University Health Sciences Center, New Orleans; The LSU Agricultural Center [The Audubon Sugar Institute]; The Pennington Biomedical Research Center and the University of Monroe. In all some 17 Louisiana Universities or select research institutes are engaged.

In the past 13 years, LSU/CAMD has interacted with over 700 LSU faculty, staff and students (Table 2). Several departments of Louisiana State University have also conducted research at CAMD. From the college of Engineering: Chemical Engineering; Electrical Engineering; Mechanical Engineering; from the College of Agriculture: Biological and Agricultural Engineering; Agronomy and Forestry; from the College of Basic Sciences: Biological Sciences [including Zoology and Biochemistry], Chemistry [including Physical Chemistry, Organic Chemistry, Metallo-Organic Chemistry, Environmental, Inorganic Chemistry, Polymers, Analytical]; Experimental Statistics, Geology, and Physics.

In addition to the LSU participation, 154 individuals from other Louisiana Universities have also been trained since 1996. Participants include members of Faculty or Student populations from Tulane University, McNeese University, University of New Orleans, Xavier University, and Southeast Louisiana University, The University of Louisiana at Lafayette [SWLU] as well as the

La Tech University [including the Institute for Micromanufacturing [IfM], Grambling University, Southern University of Baton Rouge, Nicholls State University, Louisiana College, Louisiana State University Health Sciences Center, Shreveport; Louisiana State University Health Sciences Center, New Orleans; The LSU Agricultural Center [The Audubon Sugar Institute]; The Pennington Biomedical Research Center and the University of Monroe. In all some 17 Louisiana Universities or select research institutes are engaged.

Institution	Participants
Africa	3
Brazil	22
France	2
Germany	40
Japan	8
Korea	4
Louisiana /not LSU	154
LSU	728
Mid-West	12
Nebraska	17
Northeast	4
Oklahoma	9
South-East	14
Texas	52
US, Other	27
<b>TOTAL</b>	<b>1096</b>

Some other undergraduate students specializing in French, English, Accounting or Advertising have also had the opportunity for exposure to CAMD’s unique environment, helping to broaden their horizons. Excluding facility services personnel, 1241 individuals have been trained by CAMD to use or enter the facility. Table 1 depicts the major geographical distributions for approximately 1100 of these participants.

**Table 1**  
The geographical distributions for approximately 1100 participants working at CAMD from 1994-2007

### **III.C.3. Degrees Based on CAMD Work**

#### **REU**

REU is the NSF funded research experience for undergraduates program hosted at CAMD since 2000 [for more information on this program see section VB8]. Excluding the 2007 students, CAMD has hosted 45 students in its NSF-funded REU programs, primarily from historically minority institutions. These programs give the students hands-on experience at conducting meaningful research and the opportunity to prepare and present their research in a formal setting.

#### **Undergraduates:**

At the Bachelor's level, CAMD has supported 9 BA students, 1 Education major; 313 Bachelor of Science students – from LSU, Southern, LaTech, and Bonn University since 1994 for a total of 323 Bachelor level students. This number excludes the REU student population, although a few students have continued to work at CAMD after completing their REU program. In the Bachelor of Science option, 5 students have participated from Biological Sciences; 3 from Biochemistry; 4 from Civil and Environmental Engineering; 15 from Chemical Engineering; 16 from Chemistry [including Southern and Xavier Universities]; 13 from Computer Science; 35 from Electrical and Computer Engineering and 28 from Electrical Engineering at Southern University; 5 from Industrial Engineering; 47 from Mechanical Engineering [including 1 student from Southern University]; 48 from Physics [including Southern, LaTech University and Bonn University] and 3 from Zoology.

#### **Masters Level**

In addition, 254 MS students have undertaken research at CAMD. Though the majority of these students were from LSU, others came from Bonn University and from Brazil, as well as from Southern University [Baton Rouge] and Tulane University. Some 25 students were trained in Chemistry including UC Santa Barbara, 100 in Physics [including Southern, University of Pennsylvania, McNeese, Nicholls State, Grambling, Stuttgart, Bonn, Karlsruhe, UFMG de Sol, Brazil, University of Rio and Gelsenkirchen University]. 51 were trained in Electrical Engineering, 50 students in Mechanical Engineering and 20 in other engineering disciplines.

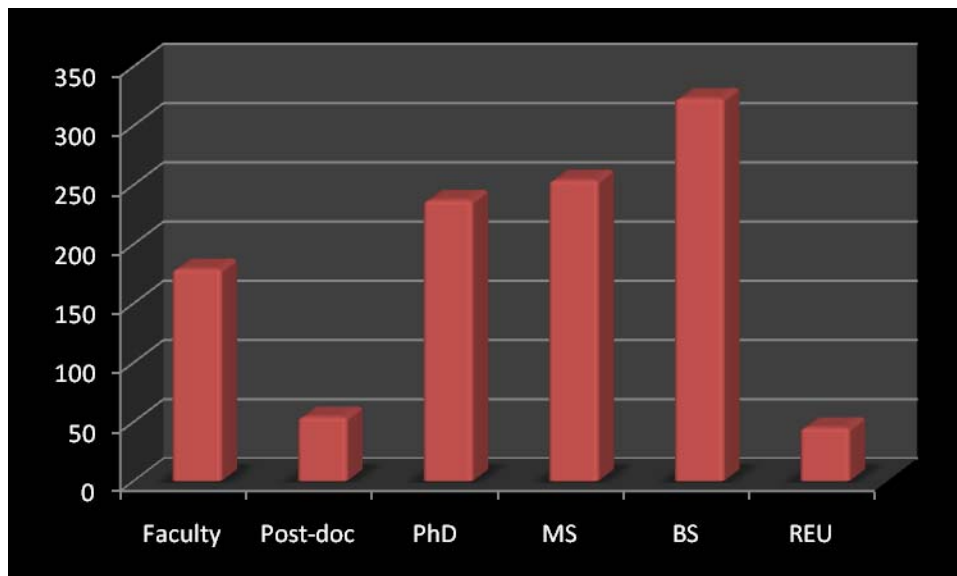
#### **PhD Level**

The number of PhD students who have relied on CAMD, for at least part of their research is also substantial [237]. This includes 3 Agronomy students [LSU]; 8 Biochemistry students [Rice, UT-Austin, TAMU]; 11 Biol. Sci. [LSU, UT-Austin, Vanderbilt]; 5 Civil and Environmental engineering, 9 Chemical Engineering; 52 Chemistry [including Brasilia Univ. and Case Western Reserve]; 14 Electrical and Computer Engineering; 46 Mechanical Engineering and 14 Molecular Biology students [Houston, Vanderbilt, UTMB, Baylor College of Medicine, LSU Medical Center, Shreveport and UT-Austin]

### **Post-Doctoral Level**

CAMD has given support to 54 post-doctoral fellows from the US, from Germany, from Japan

The numbers of graduates from these programs is not available, but nevertheless, all of



these individuals received substantial training in the applications and use of Synchrotron Radiation. In all 859 students have been trained at CAMD to use her facilities, to learn about synchrotron radiation and to conduct research, and publish their results.

### **Faculty**

Some 179 faculty have actively conducted research at CAMD. This is in addition to 88 participants identified in section IIIC, who are not in the active list of CAMD users as of May, 2007; though some of these 88 had previously been active users of the facility [including Steve Soper, Pratul Ajmera, Michael Murphy and Kevin Kelly]

### **Staff**

Since its inception, CAMD has had 100 staff members. Many of these were former students at LSU, who either after graduating, joined the CAMD family, or continued to work on their degrees while CAMD staff members including Drs. Varshni Singh, Yoonyoung Jin; Yohannes Desta and Abhinav Bhushan.





## Section IV

A Plan for a Transition between the Current Configuration of CAMD and a Future Microfabrication Laboratory and Light Source for the 21<sup>st</sup> Century



## Section IV

## Introduction

Section I provided a brief introduction to CAMD. Section II contained a summary of the scientific highlights from users who carried out research at CAMD, as well as their ideas for future research projects. Section III gave a more detailed description of the presently available facilities and their current condition. Section III also presented the current organization and made suggestions for resolving the staffing deficiency. Summaries of the funding history and user community were also included in this section.

We now shift emphasis to the future. In this section we propose near future upgrades to keep CAMD competitive while the scientific case is being developed for a major new advanced light source to serve the scientific community of the southeast (ROSE). Some of the options for ROSE will be discussed in Section V.

In particular CAMD's role in the newly organized Materials Science component of the Multidisciplinary Hiring Initiative at LSU will be addressed. CAMD's expertise and mission to support materials and microstructure research at LSU and the state of Louisiana make it an important and essential component to essential of this momentous initiative.

Thus, in this section, up-grades to the accelerator will be described (Section IVA). Three insertion devices, a 7.5 T multipole wiggler to produce x-ray energies to 70 keV, to enhance tomography and structural biology, a 2.5 T multipole wiggler for small-angle scattering and EXAFS will be discussed in Sections IV.B and IV.C. The third insertion device will be aimed at the very soft portion of the x-ray spectrum (100 eV- 1000 eV) and will be discussed in Section IV.D. Micro-fabrication is discussed in section IV.E. Finally upgrades to the existing beam lines will be described in Section IV.F.

**It should be understood that the recommendations are not fully self consistent because they depend on multiple funding proposals that will be submitted in 2009-2010. Exactly how these improvements are implemented will depend on the funding order of the proposals.**

#### **IV.A. Planning for CAMD's Future in Microfabrication**

The importance of micro- and nanotechnology for many faculty projects has come into sharp focus recently as discussions arose about moving the CAMD clean room (including equipment) and other micro- and nanotechnology infrastructure into renovated South Campus facilities. It is argued that a central micro/nanotechnology facility will allow for the sharing of expensive and complex cutting-edge research instrumentation while providing for maintenance and continuous development by dedicated experts. However, a center at South Campus is hampered at the present time by a lack of funds and efficient transportation between the LSU main campus and South Campus. Nevertheless, the presence of such a central facility will enhance interaction among users and the microfabrication group, improving efficiency as well as the quality of scientific results. Consolidating equipment and employing expert staff will make the use of technology more affordable and cost-effective. Students at LSU stand to benefit greatly from this as senior members of the microfabrication group will take a more active role in technical education of students at all levels by a combination of formalized classroom teaching and laboratory courses to be offered as part of LSU curriculum. Last but not least, a central micro- nano-fabrication hub will boost the university's research visibility and will attract grants for major upgrades (NSF-MRI funding), enable faculty and staff to successfully compete for major center funding (NSF-CBM<sup>2</sup>), support the community and state in developing new commercial ventures based on technology research, and help Louisiana to move forward to achieve its Vision 2020 goals. A centralized facility will enable us to be more competitive with other leading research universities like Georgia Tech, Cornell, or UCLA, and become a partner in nation-wide research networks like the *National Nanotechnology Infrastructure Network* (NNIN) and help Louisiana move forward to achieve its Vision 2020 goals. A central facility at South Campus or, preferably, on the main campus could have an enormous impact on LSU achieving the goals of Vision 2020.

CAMD's microfabrication group has been a strong supporter of LSU faculty and students during the past 10 years and is committed to continue its efforts helping LSU to reach its 'LSU Forever' goals in the areas of research and technology. Information summarized in this brief report provides a general idea of our activities and how it supports the LSU community.

## IV.B. Optimizing CAMD: Accelerator, Insertion Devices, and Beamlines

Since 1992 there has been a continued evolution of the CAMD facility through a steady development of the performance of the storage ring as well as through the addition of beam lines. This has been achieved by a process of investment in equipment and resources and the potential has by no means been exhausted. There is still considerable scope for further development of the CAMD accelerator which will enhance the research capabilities of the facility. These possible developments will be described in the following sections.

### *Improved beam current*

The intensity of the radiation generated by a synchrotron light source is proportional to the intensity of the stored electron beam current. The CAMD beam current has steadily been increased since the facility came into operation, mainly as a better understanding has been achieved of the current-limiting effects which occur. The principal limitations arise when the beam energy is low, such as during injection and the early part of the ramp which increases the beam energy to 1.3 GeV. It is here that instabilities can be encountered which cause losses in the stored electron beam current. Studies devoted to these effects have largely resulted in their being circumvented so that at 1.3 GeV over 200 mA can be stored in CAMD. However the instabilities are somewhat variable and it would be beneficial to apply a combination of techniques to improve the reliability with high beam current, such as lengthening the electron bunches and applying high-order magnetic fields such as octupole. A set of high order field magnets could be installed as well as a low-power third harmonic cavity for bunch lengthening.

A different technique to alleviate low energy instabilities would be to raise the energy of injection into the storage ring. The present linac has two accelerating sections which deliver beam at a nominal 200 MeV energy. There is sufficient room in the linac vault to allow a third accelerating section to be installed and that would raise the energy to 300 MeV. This would significantly remove the influence of low energy instabilities and improve the beam current. A surplus section of linac from the decommissioned HELIOS accelerator has been made available to CAMD and it is intended to install it when funds become available to complete the project.

Above 200 mA another type of instability arises, due to Higher Order Mode resonances in the RF accelerating cavity and these are certainly experienced in CAMD. To overcome these instabilities and raise the current limit above 200 mA will require refinement of the CAMD RF cavity to reduce the modes. This can be done at relatively modest cost by designing damping systems which can be fitted to the cavity. A more expensive but technically superior solution would be to replace the cavity with one of the modern designs which are available and which have significantly reduced modes. An example of such a cavity is shown in Figure 1.

Once the current at injection energy is increased beyond 300 mA it will be necessary to increase the power which can be delivered by the RF power source when the beam energy is 1.3 GeV. This is because the RF power is used to replace the energy which the electrons emit as synchrotron radiation and for a beam current of 300 mA all the available power would be used.

Several options exist which would result in greater RF power being available to support increased beam current. One would be to replace the existing power source which is rated at 60 kW with an 80 kW source. This would allow 450 mA of beam current with a consequent increase in radiation intensity by 50%. A second would be to install the existing spare RF power

source and cavity which would permit at least double the beam current. This, however, would have the disadvantage of adding more modes which could drive beam instabilities and thus limit the current.

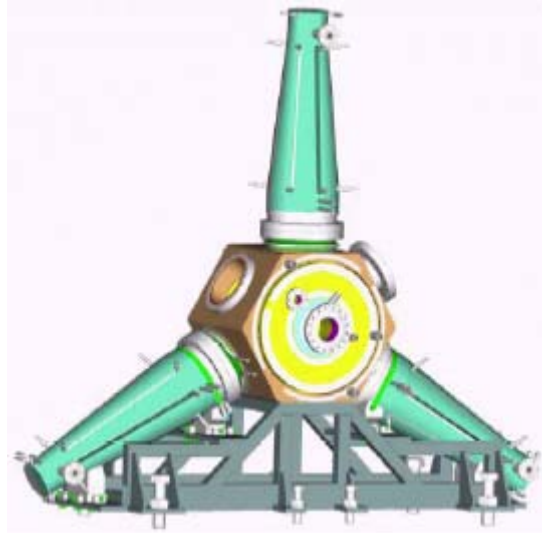


**Figure 1.** An RF cavity with reduced Higher Order Modes designed for Synchrotron Light Sources.

Very approximate costs associated with these schemes are:-

Low power third harmonic RF cavity	\$75k
Set of higher order field magnets and power supplies	\$100k
Increase linac energy to 300 MeV	\$250k
Reduced HOM RF cavity	\$500k

### ***Increased beam brightness***

The brightness parameter of a beam of photons emanating from a synchrotron light source is a measure of the radiation intensity and of both the area and divergence of the emitting electron beam. High brightness is desirable for most experiments because it allows the beam to be focused to a small spot with low divergence. The brightness of the CAMD light source has been increased by about a factor 10 by careful optimization of the focusing magnets in the storage ring. We have probably fully exploited the improvement potential by this route; however some small additional gains (20%/30%) could be obtained by using more complex settings for the focusing magnets. This would be accomplished by using separate power supplies for many of the focusing magnets and independently controlling them.

A much bigger improvement to brightness would be obtained by minimizing the vertical size of the beam. The vertical beam size is determined by a number of factors; coupling, spurious vertical dispersion, etc, which are currently being studied at CAMD. The vertical size is now very

small, typically 200 microns and can only be measured satisfactorily by using an X-ray pinhole camera. An image of the electron beam at the source point as measured with the CAMD X-ray pinhole camera is shown in Figure 2. Additional corrector magnets, skew quadrupoles, will be needed to improve the vertical beam size and perhaps a further increase in brightness of a factor 3 could be obtained.

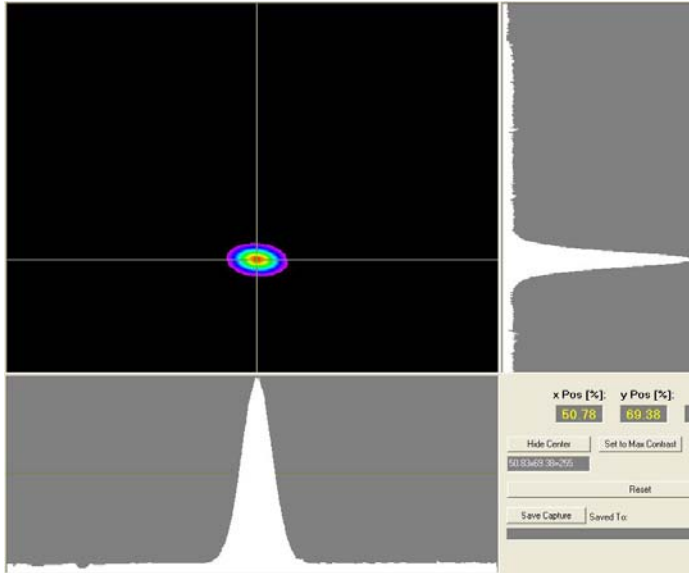


**Figure 2.** An image of the electron beam at the source point measured with the CAMD X-ray pinhole camera. The beam size is approximately 450 microns by 250 microns.

Approximate costs associated with increasing the brightness are:-

Additional skew quadrupoles	\$50k
Independent quadrupole power supplies	\$150k

### ***Increased flux density***

Some experiments benefit from increased flux density even without an increase in beam brightness. The protein crystallography beam line which uses the wavelength shifter falls into this category so a special operating mode has been developed for the storage ring. This is called the Minibeta which has been in use since 2002. It increases the flux density at the wiggler source point by a factor 5 by shrinking the vertical beam size. It will be possible to make Minibetas at every straight section should a second ID be installed. These improvements could be obtained without significant additional costs.

### ***Beam Position Stabilization***

All experiments using synchrotron light transport the photon beam to the experiment using some kind of optical system. Thus it is important to keep the source position stable and repeatable and this is done by monitoring and controlling the electron-beam position at about 20 pick-up sta-

tions distributed around the storage ring. Several years ago the original beam monitoring system in CAMD was upgraded with new pick-ups and high performance electronics. Using sophisticated software the electron beam position is stabilized continuously and achieves typically  $\pm 50$  micron variation in the photon beam position at the end of a beamline.

A useful upgrade of the position control system would be to replace the present high performance analogue electronics with a digital system. This would allow the beam stabilization to be improved by reducing the variation and increasing the rate at which correction is applied. A further improvement would be to install photon position monitors on all beamlines, which would allow their information to be included in the stabilization algorithm.

Approximate costs associated with improved beam position stability are:-

Digital electron position monitor electronics	\$175k
Beamline photon monitors	\$100k

### ***Beam Lifetime***

There are several mechanisms which cause the loss of individual electrons from the stored electron beam and for CAMD the most significant is collisions between electrons and molecules of residual gas inside the vacuum chamber. Over about 8 hours approximately half of the stored electrons in CAMD will suffer such a collision so that over this period the beam current will reduce by a half. The time constant over which the beam decreases is termed the beam lifetime. Figure 3 is a plot of the beam current in CAMD over 24 hours and between the peaks, which indicate the regular re-injections of beam, the reduction due to the beam lifetime effect can clearly be seen.

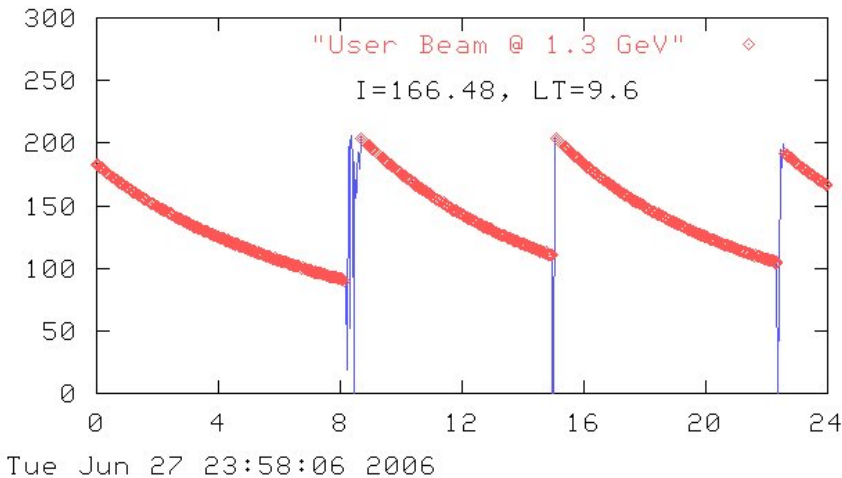


**Figure 3.** Plot of the beam current in CAMD over 24 hours showing the beam lifetime effect.



By reducing the pressure inside the storage ring vacuum chamber the beam lifetime can be increased. It is not easy to accomplish a reduced pressure because the CAMD system is already operating in the Ultra High Vacuum regime with pressure approximately  $10^{-9}$  torr. However, by redesigning the vacuum chamber and including special Non Evaporable Getter pumps near where the synchrotron radiation impinges on the chamber wall it should be possible to more than double the beam lifetime. This would be an expensive but profitable development for the CAMD storage ring because it would increase the integrated flux for research by at least 25%. The estimated cost for replacing the entire vacuum chamber and new pumps would be about \$2.0 million.

***Accelerator infrastructure improvements***

Although the accelerator itself is very reliable, the infrastructure which underpins its operation is inevitably showing signs of wear and tear after nearly 15 years of use. Furthermore, there have been advances in technology since the CAMD infrastructure was designed about 20 years ago and the accelerator performance would benefit from this new technology. A program of replacing and upgrading the following items would significantly assist the operation of the storage ring:-

New computer control systems:	\$100k
Improved diagnostic equipment for the control room:	\$75k
New technology RF power source.	\$100k

**IV.B.1. Hard X-ray Wiggler**

We want to replace the present 7 T wavelength shifter with a multipole wiggler (MPW) which will deliver beams with higher brightness. A straightforward replacement of the wavelength shifter with the new MPW should cause minimum disruption to CAMD schedule of operations and permit the existing beamlines to utilize the increased brightness, albeit after being suitably upgraded.

In contrast to the wavelength shifter, the new MPW will have multiple poles of alternating direction high field. The radiation from each of the poles will overlap and combine to greatly increase the total flux of photons into the beamlines served by the wiggler. Multi Pole Wigglers are being successfully operated at almost all x-ray synchrotron sources, including two examples with fields greater than 7 T.

The number of poles which can be included in the MPW depends on the length of the device and the vertical aperture within it. The vertical aperture, for a desired field level, dictates the length of the individual poles.

In CAMD the vertical aperture must accommodate the beam at the injection energy. Because this energy is quite low, 175 MeV, the radiation damping time is long and the beam is sensitive to instabilities which increase the beam size and hence the required aperture. The present limiting vertical aperture is in the wavelength shifter, where the vacuum chamber vertical size is 31.5 mm. By changing the quadrupole settings in CAMD, a condition can be produced which squeezes the vertical beam size at the wavelength shifter, thereby reducing the required vertical aperture. This mode has been successfully tested at injection energy in CAMD and from the re-

sults it is calculated that the vertical aperture in the new MPW could be reduced to 20 mm over a 2.5 m length without significantly impacting on the injected beam current.

With a vacuum chamber vertical aperture of 20 mm, the gap between the magnetic poles in the new MPW will be 40 mm. This allows for the finite thickness of the vacuum chamber walls and for thermal insulation between the chamber and the superconducting elements. By scaling the parameters from other superconducting MPW designs it can be calculated that a peak field of 7.5 T can be realized with a 40 mm pole gap if the pole length is 135 mm.

In addition to the main high field poles there need to be end poles which each bend the beam half of the bend angle in a main pole, in order to return the beam to its proper trajectory in the straight. The field in such an end pole is conventionally at a lower level than the main poles, to simplify the photon source point parameters. For the proposed MPW the end poles would be at 1.5 T.

With these parameters established it is possible to outline a MPW with the required 7.5 T field and pole length 135 mm. It would contain 11 main poles, two 1.5 T end poles, and the necessary spaces and clearances in a total length of 2.565 m between flanges. This is shown diagrammatically in figure 4.

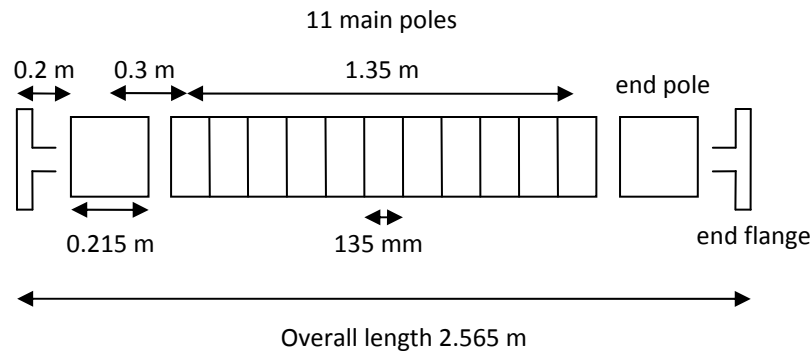


**Figure 4.** Schematic of the 11 pole MPW.

The bend angle produced by each of the main poles will be 149 mr, so that the radiation from each pole will overlap and increase the flux delivered into the beamline. The spectral flux, in comparison with the flux from the 7Tesla wavelength shifter and a dipole magnet, is shown in Figure 5.

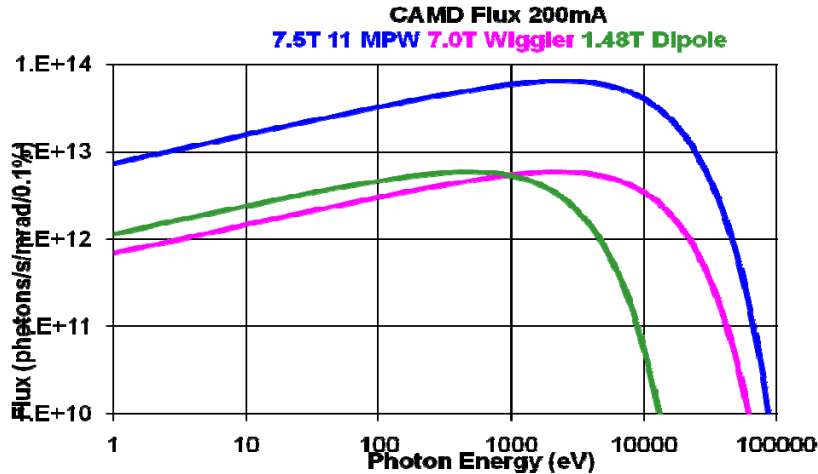


Figure 5. Logarithmic plot of Dipole, Wavelength Shifter and MPW flux.

From Figure 5 it can be seen that the MPW in the spectral region from 10 to 50 keV will provide about an order of magnitude greater flux than the wavelength shifter. For a beam current of 200 mA in the storage ring, the total power generated by the MPW will be 18 kW.

***Budget Estimate for 7.5 Tesla Multipole Wiggler.***

Wiggler and cryostat	0.85	M\$
Cryocooler	0.19	M\$
New vacuum chamber and pumps	0.33	M\$
New electron beam position monitors	0.09	M\$
New power supplies	0.07	M\$
Changes to RF system	0.15	M\$
Skew multipole magnets	0.27	M\$
TOTAL	1.95	M\$

**IV.B.2. Scientific Opportunities with the Multipole X-ray Wiggler**

The increased photon flux will greatly assist the current programs and allow new R&D opportunities. We expect the number of users for the protein crystallographic beamline to double and that 10-15 new research groups will be served at a fourth beamline that CAMD is now commissioning for X-ray absorption spectroscopy (EXAFS). The more intense X-ray flux will enable users to perform experiments on smaller crystals and more dilute samples. This is a crucial advantage as researchers are increasingly investigating proteins that do not readily crystallize such as membrane proteins. Although EXAFS is an important technique for investigating the function of metal atoms in enzymes, the concentration is so low that a very intense X-ray beam is required to get good data. Samples used for environmental research frequently have a very low concentration of the material of interest.

The higher X-ray energy will make the X-ray absorption edges of heavier elements such as arsenic and lead accessible for research projects that are environmentally important. The greatly increased flux in the 30 keV range from the new wiggler will enable studies of bone structure which allow scientists to learn how diseases such as laminitis in horses can be understood and treated.[3] The higher energy X-rays also have a greater penetrating power and will enable X-ray dosimetry and cell irradiation at the iodine K edge, which is medically significant. In addition, the higher flux will enable new-generation experiments such as phase-contrast tomography, an imaging method based on changing sample density at interfaces. Phase-contrast tomography has proven advantages for imaging biological structures. An ongoing project at CAMD employs both phase contrast imaging at the Advanced Light Source and contrast agents (Cs salts, iodinated organics) to explore complex structures in feline claws.

This multipole wiggler is the beginning of a several-year plan toward developing a third/fourth generation synchrotron radiation source at LSU which will provide scientists at Louisiana State University, the state of Louisiana, and regional scientists from adjoining states with a new regional synchrotron radiation center. As lagniappe, the new wiggler will use an electromechanical cryocooler to greatly reduce liquid helium consumption, yielding a cost savings for liquid helium of about \$120k/yr.

We believe that the advantages to LSU of having this source of intense high-energy X-rays at CAMD are considerable. An example of the benefits of propinquity is the 2006 Nobel Prize for Chemistry, which was awarded to Roger Kornberg of the Stanford Medical School for solving the structure of RNA polymerase II.<sup>1</sup> His capacity to overcome the many roadblocks to completing his research in protein crystallography depended critically on the fact that the Stanford Synchrotron was close by, enabling him to use bits and snatches of beam time for testing. Accordingly, the new wiggler will enable LSU researchers and their regional colleagues to conduct cutting-edge research with high energy X-rays. A straightforward replacement of the 7 T wavelength shifter with a new MPW will cause minimum disruption to the CAMD operations schedule and permit the existing beamlines to utilize the increased brightness, with only minor modifications.

<sup>1</sup> <http://mednews.stanford.edu/kornberg/slac.html>

Highlights of the science that will be enabled by this new capability experiments will be described in the following paragraphs.

#### **IV.B.2.a. Macromolecular Crystallography**

**Towards a Model for Understanding the Regio-specificity of Lipoxygenases.** (Marcia Newcomer, LSU-BR)

Recent studies firmly establish a role for 5-Lipoxygenase (5-LOX) in the development of heart disease. Mice deficient in the enzyme are afforded protection from atherosclerosis[5]. Promoter variants for 5-LOX and 5-LOX activating protein (FLAP) are associated with changes in the risk of stroke [6-8]. Furthermore, 5-LOX is found in human atherosclerotic lesions[9, 10]. Thus it has been proposed that 5-LOX inhibitors have application in the treatment of cardiovascular disease [11] and some are currently in clinical trials for the treatment of acute coronary syndromes [12]. In addition, 12/15-LOX activity has also been linked to atherosclerosis[13-15]. Furthermore, the

problems linked to Cyclooxygenase(COX)-selective inhibitors such as Vioxx have led to the suggestion that balanced inhibition of both LOX and COX pathways is preferable to inhibition of a single pathway—which would result in an inadvertent increased flux through the non-inhibited inflammatory pathway [16, 17]. Consequently, dual COX/LOX inhibitors are in development [18, 19] one of which is currently in phase III trials for the treatment of osteoarthritis. Efforts to develop drugs to target LOX, and the quest for dual COX/LOX inhibitors, clearly establish a need for structural data for 5-LOX.

While lipoxygenases are iron enzymes inhibited by iron chelators or redox active compounds, these modes of inhibition are inherently non-specific. However, the strict product specificity of the various animal lipoxygenase isozymes indicates that selective inhibition of the 5-LOX isozyme is feasible, a requisite feature of an effective therapeutic strategy. In order to engineer specificity into any inhibitor, more structural information for this enzyme family is required. There are no animal LOX structures that provide a model for how substrate binds in the active site, a model central to the development of isozyme-specific inhibitors. A mechanistic understanding of substrate recognition, when all lipoxygenases recognize the same substrate, yet generate different products, can be used to help guide the design of novel inhibitors. The primary goal of our work is to describe the structural basis for lipoxygenase product specificity to provide a framework for the design of 5-LOX specific inhibitors.

There is no crystal structure of a lipoxygenase in complex with its substrate arachidonic acid (AA) to reveal the structural basis for product specificity in this family of enzymes. We have established a robust experimental system that is amenable to crystallization of an animal LOX-AA complex under anaerobic conditions. Experiments to determine the structure of the ternary complex, with nitric oxide as a dioxygen mimic, are also underway. Our recent 1.85 Å resolution structure of 8*R*-LOX, obtained with data collected at CAMD, provides a solid foundation for this work.

The high-resolution animal LOX structure has led us to propose an alternative to the boot-shaped cavity model for substrate binding which is based on the position of an inhibitor in the 15-LOX binding site (Fig. 6 gray stick). The “new” cavity overlaps with the previous model but there are key differences. Furthermore, it provides a firm structural basis to explain some puzzling issues relating to product specificity, such as the relationship defined by Coffa and Brash [33] between product stereochemistry and the presence of a conserved Gly in *R*- lipoxygenases and Ala in *S*- lipoxygenases. Fig 6 is a slab through the molecule with mesh outlining the surface. The mesh reveals a U-shaped channel that is open on both ends in the 8*R*-LOX. This channel also exists in the 15-LOX structure (gray mesh, pdb code 1LOX)—except that the end where the methyl terminus of the AA

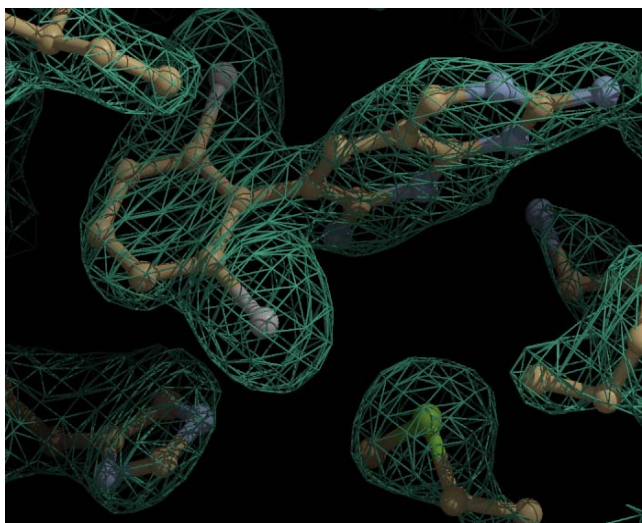


**Figure 6**, AA is positioned in a U-shaped cavity outlined with a surface mesh. 8*R*-LOX is blue, 15-LOX (1LOX) is gray. The Gly that determines which C reacts with the O<sub>2</sub> is indicated in red. RS7 is in gray stick.

(orange stick) is positioned is closed. The fit of AA is not precise—it is simply placed to provide the reader with a scale to gauge cavity volume and shape. In any case, one can see that the AA could enter the channel from either side. This suggests a mechanism for “inverse substrate orientation” that has been proposed to explain product specificity in 5-LOX. Isozymes might favor entry in one or the other direction. In addition, the position of the Gly/Ala residues that determines product stereochemistry is colored in red in Fig 6. One can easily imagine how the presence of an Ala or Gly at this site could determine which carbon in the substrate is the site of peroxidation.

Access to a synchrotron beamline with high brilliance is essential for this project, as the crystals grow only as thin plates. In addition, *a source in close proximity will allow the Newcomer laboratory to develop anaerobic crystallization protocols that minimize sample handling*, as crystals can be prepared *on site* just prior to when beamtime becomes available.

### ***Development of novel antibiotics that inhibit the synthesis of fatty acids by bacteria (Grover Waldrop, LSU-BR)***

The overuse of antibiotics in medicine and agriculture has created a significant increase in the number of antibiotic-resistant strains of *Staphylococcus aureus*. Bacteria need to synthesize fatty acids to form their cell membranes and, therefore, to grow. Thus, inhibition of the enzymes involved in fatty acid biosynthesis is an attractive strategy for the design of novel antibiotics. The Waldrop laboratory, in collaboration with scientists at Pfizer, is currently developing inhibitors of fatty acid synthesis that may ultimately serve as antibiotics. Figure 7 shows an inhibitor they have identified for the enzyme biotin carboxylase from *H. influenzae* a bacteria closely related to *S. aureus*.

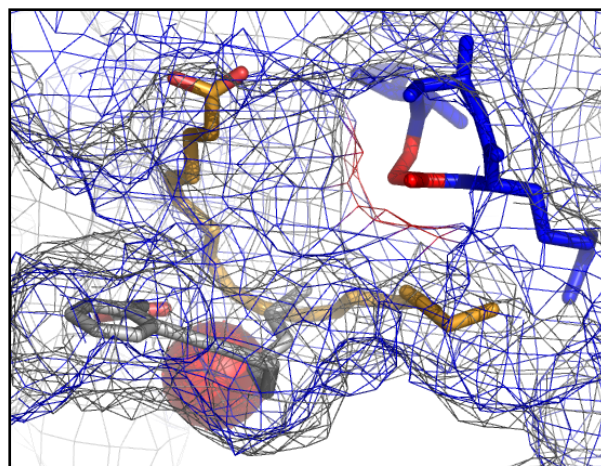


**Figure 7**, Inhibitor/Drug Candidate (blue) bound to an essential enzyme from the pathogen *Hemophilus influenzae*. A portion of the enzyme is shown in yellow.

### ***Control of metabolism of cancer cells. (Yong-Hwan Lee, LSU-BR)***

Recent developments have shown that the increased metabolic rates in cancer cells are driven by an unusually high concentration of a regulatory molecule produced by a tumor-specific form of the metabolic enzyme phosphofructokinase. The Lee laboratory has recently determined the structure of this tumor-specific enzyme as well as complexes of the enzyme and substrate analogs. They now have a molecular model for the design of inhibitors that could be used in chemotherapy.

For both the Waldrop and the Lee project the higher intensity provided by the multiple wiggler will allow complexes containing candidate drugs to be screened more rapidly and for the structures to be determined to higher resolution. The higher resolution will greatly assist interpretation of the details of the binding of the candidate drugs to the enzymes.

### IV.B.2.b. Tomography

Synchrotron X-ray tomography performance is dependent upon flux, energy range, beam size, divergence, evenness, stability, and coherence. With the proposed installation of the 7.5 T, multipole wiggler, we expect a near order-of-magnitude improvement in data acquisition rate based on greater flux (Figure 5) and somewhat improved phase contrast capabilities. Both of these improvements are extremely useful for ongoing research projects. Comparisons of the photon flux from proposed 11-pole, 7.5 T wiggler versus the current wavelength shifter show that tomography will enjoy 12- and 15-fold increases at 13.47 and 33.17 keV (Br and I K edges).

The CAMD tomography beamline started operation in 2000 at a bending magnet with white beam sample illumination. It was principally used for sample assessments for projects completed at the Advanced Photon Source tomography beamlines. In 2004 CAMD tomography research was transferred to a new beamline on the wavelength shifter, where the much "harder" x-ray output of the wavelength shifter enabled data collection at energies generally used for tomography, e.g. 30 keV. The CAMD tomography beamline is one of about 10 in the USA. A 3D data set at 4.5  $\mu\text{m}$  resolution over a field of view of about 1500 x 1500 x 200 voxels can be acquired in several hours with monochromatic X-rays from 6 to 40 keV. Based on the optimal projection ordering work of Köhler and Kazantsev *et al.*, we converted from standard fixed angle increment to an angle order based upon the Greek golden ratio; this angle order yields faster convergence to the final 3D image.

Competitor beamlines worldwide have several advantages, principally faster data collection. The APS GEOCARs 13BM can collect a near  $1\text{k}^3$  voxel data set in less than 30 minutes, and because of a 5 mm beam height, can more easily study larger samples; at CAMD, we are limited to acquiring successive volumes over a range of sample positions in order to study the larger samples. As detailed below essentially all the tomography projects will benefit from the increased flux provided by the new wiggler which will enable energy-selective near-micron resolution imaging for materials science, engineering, and biological systems. The increased

flux will also enable us to use a pinhole near the wiggler source to produce a partially coherent beam, which can be used to test and evaluate phase contrast imaging.

Recent applications of the beamline include biology, engineering, and chemistry. Tomography is revealing previously unknown structures in a cat claw; the goal of this work is to better understand cornified tissues, as shown in Figure 6. Increased flux will enable such structures to be imaged at higher resolution.

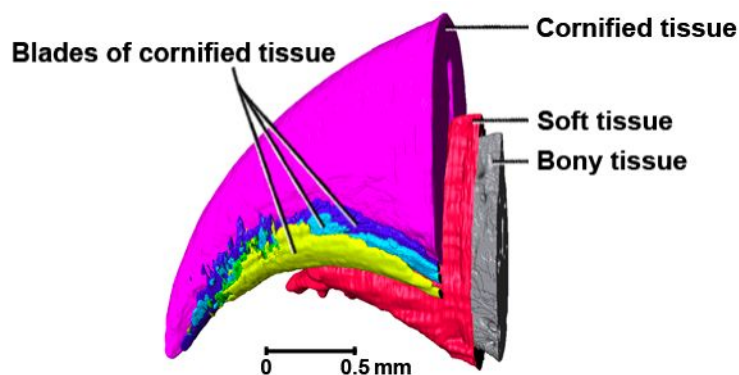


**Figure 8,** Composite image of a 3D-reconstruction of tomography data, showing the relative positions of the basic tissues in the tip of the claw of the fifth digit of an adult cat (specimen #12, left paw) through synchrotron X-ray phase contrast tomography.

In environmental engineering, fundamental aspects of hydrocarbon pollutant flow through aquifers are studied in 3D with tomography of synthetic and real aquifer materials and multiple fluids, as shown in Figure 9.

These experiments are often performed as a function of a variable, such as pressure and therefore greatly benefit from rapid image analysis. Has the sample stabilized at the new pressure setting? Mass transfer experiments, investigating the rate at which hydrocarbon dissolve into the water, are performed as a function of time. Rapid feedback regarding the temporally-varying hydrocarbon mass and distribution is crucial. Data collection time will decrease proportionally to the increase in flux.

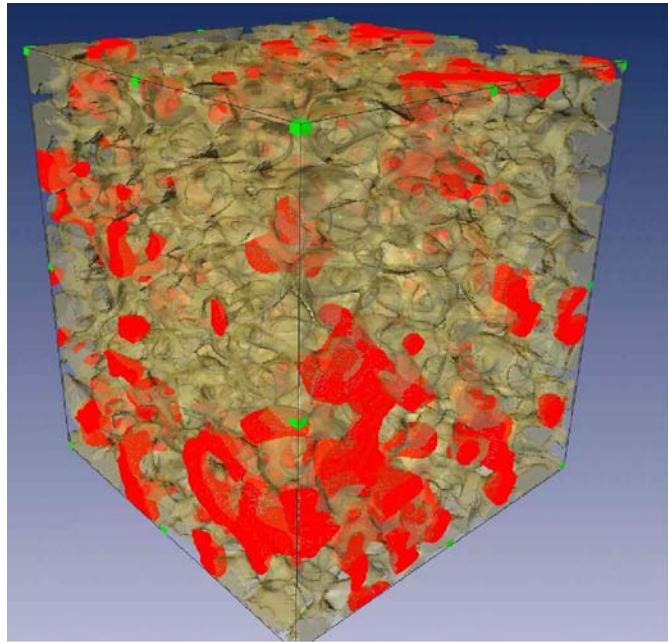


**Figure 9,** 3D rendering of sand (semi-transparent brown), entrapped oil (red), and water imaged at 12 micron voxel resolution with multi-energy synchrotron X-rays. tomogra-

#### **IV.B.2.c. Medical Radiology**

**Perspective:** Monochromatic X-rays offer relatively new opportunities in diagnostic radiology and radiation therapy. Monochromatic X-rays from conventional X-ray tubes have not provided adequate fluences for general medical use. Synchrotrons can produce suitable fluences; however, the beam area is usually limited to dimensions of a few cm, adequate for research, but not for human utilization. Tunable X-ray sources which collide high-intensity laser beams with MeV electron beams are being developed.[39, 40] While this technology develops over the next decade, the synchrotron will be an important platform for R&D on technology that can be translated to these future sources. The proposed MPW will be important to such a medical radiology research program.

**Current Research Program:** The LSU Medical Physics Program in collaboration (via a formal agreement) with the Mary Bird Perkins Cancer Center (MBPCC) is committed to research in the medical radiological use of monochromatic X-rays. Also, the LSU Medical Physics Program has a non-binding collaboration with MXISystems, Inc., developer of one of the laser X-ray accelerators for medical radiology, through which it hopes to have access to one of the early clinical devices, when manufactured.

**Radiation Therapy (K-edge Capture Therapy):** A major focus of our current research is a relatively new type of potential radiation therapy called K-edge capture therapy [41] in which the dose is localized by means of a drug that targets the DNA or other sensitive sites within cancer



cells (e.g. iododeoxyuridine or IUdR). Localization is caused by using monochromatic X-rays with energies just above that of the K-edge of a high-Z atom (e.g. iodine) attached to the drug. The proposed MPW is important to future research of K-edge capture therapy due to its ca. 13-fold higher flux at the iodine K edge (33.1 keV). Dr. Kenneth Hogstrom, who directs this program, has provided funding for a postdoctoral fellow, part-time radiation biologist, and graduate students. This group's research is aimed at (1) developing clinically useful methods for beam dosimetry, (2) validating methods of dose calculations to be used for patient treatment planning, and (3) improving our understanding of the radiation biology associated with K-edge capture therapy.[41, 42]

The tomography beamline provides a 1 mm×30 mm X-ray beam. By translating a base plate vertically a larger area can be irradiated. For a 30 mm×30 mm radiation field, a maximum dose rate of approximately 1 Gy/min can be achieved at 40 keV. A field of this size can be used for dose measurements and verifying dose calculations, but it is minimally acceptable for radiation biological studies of cells and small animals. The order of magnitude increase in beam intensity from the multipole wiggler will provide two benefits. It will shorten irradiation times at 40 keV, making IUdR studies easier, and it will allow us to conduct studies using higher-Z atoms, e.g. Gd, which has a K-edge of 50.2 keV.

**Diagnostic Radiology:** The proposed MPW directly affects the performance of tomographic imaging [43], including K-edge imaging or diffraction-enhanced imaging [44, 45], of high-Z labeled compounds, which is necessary for treatment planning of K-edge capture therapy. An important task in evaluating the targeting of a labeled compound is assessing its distribution in vivo; for pharmaceutical development, this usually involves many serial studies sacrificing a large number of animal subjects. By contrast, K-edge and diffraction-enhanced imaging allows one to characterize the 3-dimensional concentration of a compound, ideally in vivo with a single animal which can be used for serial dose-response studies. The high-resolution X-ray images can also be fused to functional images of the same compound labeled with a radioisotope of the high-Z element or of another compound such as FDG (18F-fluorodeoxyglucose) that images tumor metabolism. The MPW facilitates two improvements for measuring the temporal and spatial bio-distribution of high-Z drugs: (1) a higher flux provides a combination of shorter imaging times with higher resolution and (2) the higher X-ray energies allow the use of Gd imaging contrast agents.

Another focus in diagnostic imaging with monochromatic X-rays is dual-energy K-edge imaging, which has potential for improving disease diagnosis and showing the distribution of drugs required for dose calculations in K-edge capture therapy.[43] The proposed MPW will also facilitate projects relevant to breast cancer imaging and therapy. While CAMD is not a clinical imaging site, it provides a facility for researching improvements to breast cancer diagnostic and therapeutic techniques which could be implemented in the future on clinical monochromatic X-ray devices. For breast radiology, several cancer types have been reported to alter the radiation contrast of breast tissue [46, 47], providing a diagnostic means to identify breast cancer. CAMD can provide the monochromatic X-ray beams to measure these subtle changes.[48] The higher flux and improved energy range from the MPW also facilitate phase-contrast imaging wherein X-ray refraction at tissue boundaries provides information on tissue morphology and composition that is unavailable with conventional X-rays.

#### IV.B.2.d. Geoscience and Environmental Science

In the early days of environmental awareness the total concentration of a pollutant was more or less equated with its toxicity. The realization occurred in the 1960s that the toxicity of a metal depends on its speciation rather than its total concentration. Efforts are now being made to include speciation information explicitly in environmental regulations. There are very few techniques, however, which can yield direct information about speciation of metals, X-ray absorption spectroscopy being one. One of the best advantages of XAS may be that, unlike many other methods, it requires practically no sample preparation and thus the matrix remains unaltered.

One constraint of CAMD as a storage ring is the limit of detection and if realistic environmental samples can be analyzed with our present flux/brightness. A new multipole wiggler or a third generation source would greatly increase the brightness and thus allow us to investigate more realistic environmental problems. For example, the concentration at which mercury can be problematic is low parts per million or even lower. Similarly, the safe drinking water limit for arsenic is 10 ppb.

#### Mercury in Global Geobiocycle

Mercury is a neurotoxin. Mercury pollution is becoming quite widespread in the nation. Two of the main sources of mercury are burning of fossil fuels and landfills containing mercury-laden waste. There are also natural sources of mercury such as volcanoes. The relative contributions of these different sources are not precisely known. The landfills are the source of the more toxic methyl mercury form produced by methylating bacteria. Under the 1990 Clean Air Act Amendments (CAAA), the U.S. Environmental Protection Agency conducted a comprehensive study of hazardous air pollutant emissions from coal-fired utility plants which found that the more volatile elements or compounds such as mercury pass through the emissions-control equipment and are emitted to the atmosphere. The volatile mercury gets deposited close to a power plant and accumulates in the food chain through prey-predator relationships, particularly fish.

Several competing technologies are being investigated for mercury removal during coal burning. At present, the most promising technology for mercury removal appears to be activated carbon of mercury. However, the same technology for mercury removal cannot be applied to all coals as each coal is different. The exact technology that will be used for mercury removal in the future is unknown and so is the by-product of coal burning. Coal can contain several hundred ppm of mercury. The fate of mercury and other metals such as arsenic in the coal burning process can be investigated (even *in situ*) by XAS. XAS can also be used to investigate and improve mercury removal processes. The mercury level in the environment is a lot lower. The typical concentration in a predatory fish is several ppb. The increased flux from the MPW will significantly lower the metal concentrations required for XAS at CAMD.

#### Metal Transport in Riverine systems

The Mississippi River is the source of drinking water for many communities along its banks. The aquatic life in the River water depends on its water quality. The heavy metals in the

Mississippi are derived from principally from two sources: natural, due to erosion, and anthropogenic. The levels of many toxic heavy metals in the Mississippi have increased over the last several decades due to anthropogenic input. The anthropogenic inputs are sewage, agricultural waste and runoff, stormwater runoff, etc.

Filtration of drinking water may not be able to remove all of the adsorbed load. In the last two decades there has been an increasing realization that the so-called “dissolved” fraction includes metals adsorbed on finer colloidal matter which can easily pass through the fine filters (< 0.45 or 0.4  $\mu\text{m}$ ) normally used for separation. The concentrations of metals in these waters are in low ppm range and can be measured only with a strong X-ray source.

The behavior of a metal in river water depends on its chemical properties. The distribution of the metals between the dissolved and adsorbed fraction reach some sort of equilibrium and can be described by a distribution coefficient. For most metals the adsorbed fraction is usually many times greater than the dissolved fraction. In fact, binding of trace metals to natural organic matter is not very well understood. There may be several types of binding sites of differing strengths in natural organic matter in water. With increased metal loading different sites are utilized. Thus different techniques with different detection limits have yielded different values for distribution coefficients. With XAS the occurrence of an element of interest in different sites (within a mineral, adsorbed), can be easily identified. The adsorption sites can also be characterized to some extent by the atomic number of the site. Not much work has been found in the literature related to metal speciation in particulates in the Mississippi River. A better understanding of bio-availability of heavy metals in the Mississippi is necessary for improvement of its water quality. Any modeling of the metal transport process would require identification of quantity and nature of the adsorption sites. It may also allow us to identify inputs from different sources. As with mercury from coal, a strong X-ray source is required to investigate metal binding at the naturally occurring concentrations.

### Biological Sciences

Researchers from Biological Sciences at LSU and from the National Hansen’s Disease Program are interested in XANES and EXAFS of iron in protein, enzyme and bacteria. Measurements at the bending magnet beamline produced very noisy EXAFS spectra, with very limited k range. The close proximity of CAMD to the laboratory of these researchers provided great flexibility in their sample preparation. Some of these research projects are:

- As part of a larger effort to understand the biosynthetic reactions responsible for the synthesis of leukotrienes, Dr. Newcomer (NIH funding) is studying lipoxygenases and allene oxide synthases. The former are non-heme iron enzymes, and the latter heme enzymes that structurally resemble catalase. Determination of the state of Fe in both types of enzymes is an essential step in this process.
- Another user at CAMD (Dr. Huangen Ding from Biological Sciences and his undergraduate student) is interested in identifying the nature of the ligand between iron and iron sulfur protein cluster A (IscA). The protein is suspected to transport iron in many biological processes.
- Drs. Thomas Gillis and Ramanuj Lahiri from National Hansens’s Disease Program are interested in iron transport in leprosy bacteria *Mycobacterium leprae*. A scan of the leprosy bacteria genome shows no siderophore-like proteins. Thus the exact mechanism by

which it transports iron is not fully understood. The iron concentration in the bacteria is also low, ca. 700 ppm. Some preliminary data from the experiment will allow the researchers to seek further funding from the NIH.

The K pre-edge region of transition elements contains information about coordination, spin and valence. However, because of low absorption in this region and highly overlapping resonance peaks, high resolution data is needed to deconvolute these features. Much higher flux than presently available at the bending magnet beamlines is needed for these experiments. The new EXAFS beamline on the wavelength shifter will greatly help but the MPW would be a far better source.

#### **IV.B.2.e. Catalysis and Energy Research**

CAMD currently has a strong and vibrant research program in catalysis. Some of this research can be conducted at the bending magnet beamlines but higher flux and energy range will certainly aid in this area of investigation. Dr. J. Jerry Spivey from the Chemical Engineering Department at LSU presently has several projects for catalyst studies, funded by DOE, related to Fischer-Tropsch processes for production of ethanol from coal or some other types of biomass. The iron-based Fischer-Tropsch catalysts are cheaper than those made from other metals and have been effective in increasing the hydrogen to carbon monoxide ratio in the synthesis gas. Addition of other transition metals, such as copper, manganese, rhodium, tungsten, etc., to the iron has increased the productivity of these catalysts. These metals form alloys with iron and also mixed metal carbides. In recent laboratory studies, as a part of this project, zirconium has been found to be most effective additive to the iron-based catalyst. K edge of zirconium (17.998 keV) experiments at high energy along with L edge (2.22 to 2.53 keV) measurements at the bending magnet beamline can provide a more complete picture of the catalytic process. In another project, rhodium (K edge - 23.220 keV) has been found to be an effective additive to the iron-based Fischer-Tropsch catalyst. In yet another project nickel-substituted barium hexa-aluminate catalysts for generation of hydrogen from diesel fuel in solid oxide cells for production of electricity is being investigated. A high energy XAS beamline will allow easy access to the Ba K edge (37.441 keV) in these catalysts. There is very little atomic level information available about these catalysts in the literature. As with the environmental research the new beamline on the wavelength shifter will be a vast improvement over the bend magnet beamlines for the K edge transition measurements. The further increased flux provided by the MPW will allow more sensitive measurements and will provide enough flux to allow the use of a very small beam to spatially characterize the catalysts.

## IV.C Second Insertion Device (A Soft X-ray Wiggler)

### IV.C.1 Description of 3.5 Tesla Multi Pole Wiggler

It is proposed to install in the 3<sup>rd</sup> straight section of the CAMD ring, which is presently unoccupied, a multipole wiggler (MPW) which will deliver beams with higher brightness. This MPW will have a magnetic field of 3.5 T and will therefore produce softer (lower energy) x-rays than the 7 T wavelength shifter or the 7.5 T MPW which may replace the wavelength shifter. The 3.5 T MPW is a separate project from the 7.5 T MPW and will go in a different part of the ring. MPWs have multiple poles of alternating direction high field. The radiation from each of the poles overlaps and combines to greatly increase the total flux of photons into the beamline served by the wiggler. Multipole wigglers are being successfully operated at almost all x-ray synchrotron sources, including superconducting examples with fields between 2.2 and 7.5 T.

The number of poles which can be included in the MPW depends on the length of the device and the vertical aperture within it. The vertical aperture, for a desired field level, determines the length of the individual poles.

In CAMD the vertical aperture must accommodate the beam at the injection energy. Since this energy is quite low, 180 MeV, the radiation damping time is long and the beam is sensitive to instabilities which increase the beam size and hence the required aperture. The present limiting vertical aperture is in the wavelength shifter, where the vacuum chamber vertical size is 31.5 mm. By changing the quadrupole settings in CAMD, a condition can be produced which squeezes the vertical beam size in each of the straight sections, thereby reducing the required vertical aperture. This mode has been successfully tested in CAMD and from the results it is calculated that the vertical aperture in the new MPW could be reduced to 10 mm over a 1.0 m length without significantly affecting the injected beam current.

The science research programs to which this MPW would be applied are Small Angle Scattering and EXAFS, for which X-rays extending to 20 keV would be required. Thus the proposed MPW needs to operate at a moderately high magnetic field such as 3.5 Tesla and be superconducting. At the DIAMOND Light Source in UK there is a MPW currently in operation with the required field, aperture and pole length, and it is proposed to install in CAMD a 1.0 m long version of this MPW (the DIAMOND MPW is 1.5 m long). The major parameters of the DIAMOND MPW and the proposed CAMD MPW are given in Table 1.

	Magnetic Field (T)	Poles Main+end	Magnetic Gap (mm)	Pole length (mm)	MPW length (m)	Vertical Aperture (mm)	Bend angle per pole (mr)	Radiation power (kW)	
DIAMOND	3.5	45+4	16.4	30	1.54	10	6.7	50	
CAMD	3.5	25+4	16.4	30	1.0	10	15.4	2.0	

Table 1. Main parameters of the DIAMOND and proposed CAMD MPWs.

In an MPW there need to be end poles in addition to the main high-field poles, in order to return the beam to its proper trajectory in the straight. The end poles are either shorter than the main

poles or at a lower field. The proposed arrangement of 2 end poles at either end of the MPW, bending the beam through one quarter and three quarters of the main pole angle, results in a beam trajectory through the MPW which is centered about the axis. This is convenient for the beam line if it is required to operate the MPW at lower fields than 3.5 T.

A diagram of a superconducting MPW designed and built by the Budker Institute is shown in Figure 7. It can be seen that the MPW is contained within a cryostat which is cooled by a number of cryocoolers. Although the MPW contains approximately 200 liters of liquid helium, the efficient arrangement of insulation and cooled screens ensures that any boil-off of helium is recondensed without loss by the cryocoolers

The bend angle produced by each of the main poles will be 15.4 mr, so that the radiation from each pole will overlap and increase the flux delivered into the beamline. The electron beam will be deflected by 147  $\mu\text{m}$  peak to peak which is about 10% of the horizontal beam size so the source size will not be appreciably increased. The K value is 19.61 so the spectrum will have no undulator characteristics. The spectral flux, in comparison with the flux from the 7 Tesla wavelength shifter and a dipole magnet, is shown in Figure 1. Figure 1a shows the data plotted logarithmically, whilst figure 1b shows the same data with linear scales.

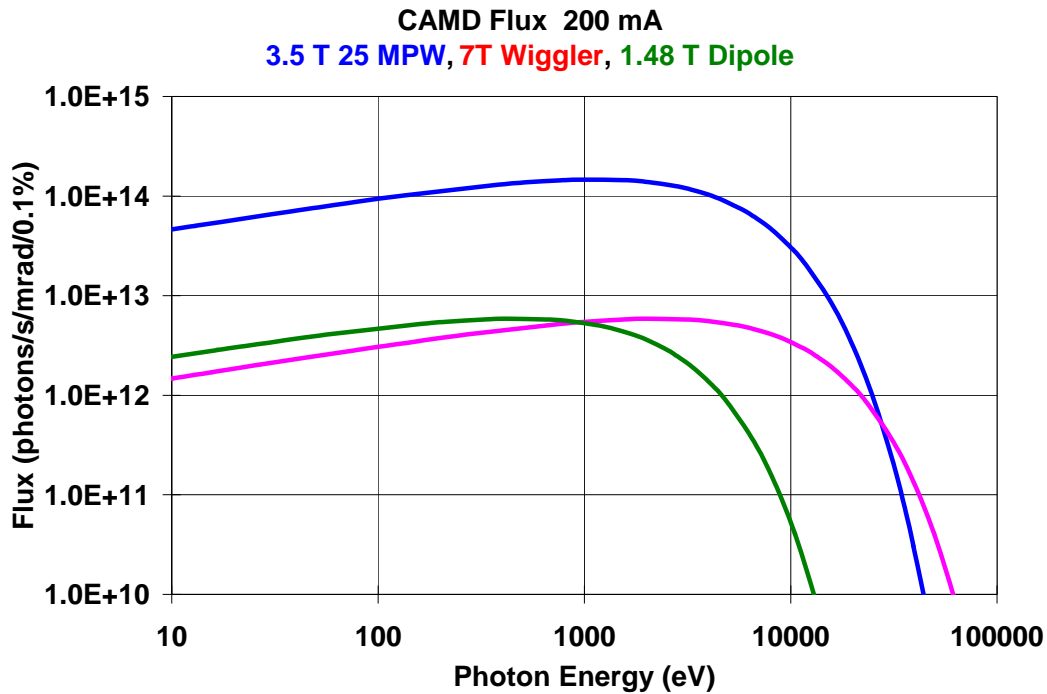


Figure 1a. Logarithmic plot of Dipole, Wavelength Shifter and MPW flux.

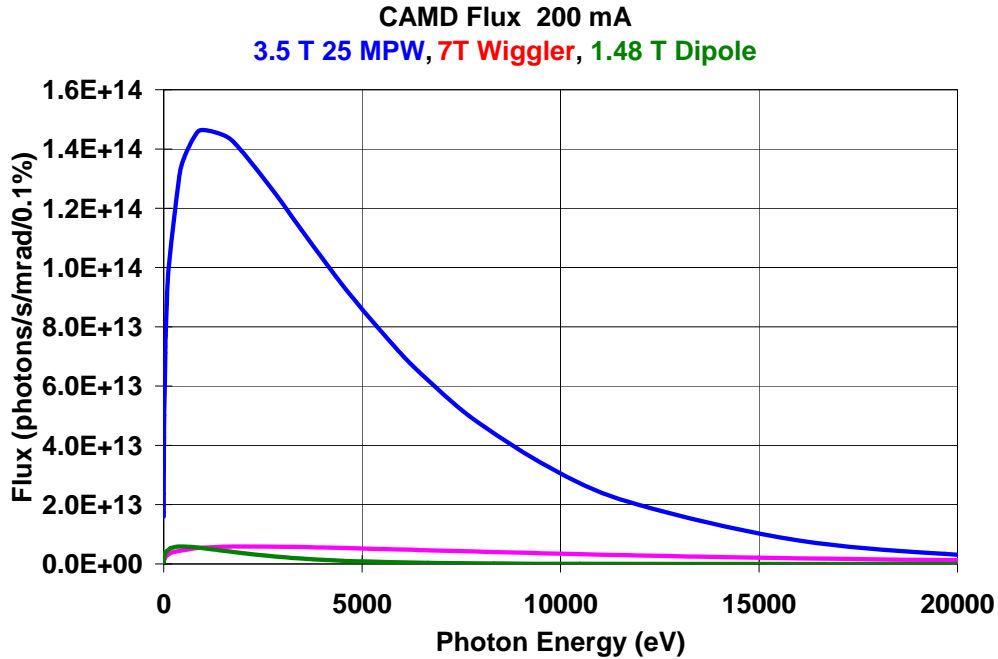


Figure 1b. Linear plot of Dipole, Wavelength Shifter and MPW flux.

From Figure 1 it can be seen that the MPW in the spectral region from 1 to 10 keV will provide over an order of magnitude greater flux than the wavelength shifter and will continue to give greater flux up to about 20 keV. For a beam current of 200 mA in the storage ring, the total power generated by the MPW will be 2 kW.

We have used the programs SHADOW-VUI (Franco Cerrina, Center for Nano Technology, University of Wisconsin and Manuel Sanchez del Rio, ESRF) and XOP2 (Manuel Sanchez del Rio) to model the output from the wiggler. The assumptions about the electron beam characteristics are given in Table 2

Parameter (units)	Value
Energy (GeV)	1.3
Beam Current used in calculations (mA)	100
$\sigma_x$ (mm)	1.4
$\sigma_z$ (mm)	0.2
$\sigma_x'$ (mrad)	0.0116
$\sigma_z'$ (mrad)	0.0053

Table 2. Synchrotron Beam Characteristics (waist at center of straight section)

The electron beam, wiggler and resulting photon beam have been modeled and the results are:

- Scatter-gram images of the modeled radiation impinging on a screen placed, perpendicular to the longitudinal axis of the wiggler and 10 m from the center of the wiggler; The scatter-grams are of the real-space (x horizontal, z vertical and y along the photon beam) distribution of the rays (photons) striking the plane and of the horizontal phase space (x and x'), which demonstrates the angular distribution of the photons' trajectories as a function of the horizontal distance from the where the optic axis penetrates the plane. To save space, the photon range, 1 to 20 keV, is divided into three subranges, 1-5 keV, 5-10 keV and 10-20 keV; therefore each distribution plot contains all of the photons in a given range.
- Plots of the photon fluxes of the total radiation emitted from the wiggler, the radiation from the wiggler transmitted through a 40 x 20 mm<sup>2</sup> aperture centered around the optic axis at the plane 10 meters from the wiggler, and, for comparison, the radiation modeled for a normal CAMD bend magnet (3-m radius) and transmitted through the same aperture (i.e., 4 mrad horizontal acceptance).
- The final plots are ratios of the fluxes and brightnesses from the modeled wiggler and bend-magnet sources that account for the radiation transmitted through the 40 mm aperture. "Brightness" of extended sources such as a multi-pole wiggler or a finite-aperture bend magnet is admittedly not straightforward because of the significant source-volume components y and y'. As several assumptions and approximations were made in the calculations, absolute values of brightness are not given, only the ratio of wiggler to bend-magnet, for the purpose of a comparison.

Energy Range (keV)	Total Photons in Range at 100 mA	$\sigma_x'$ (mrad)	$\sigma_z'$ (mrad)	$\sigma_x$ (mm)	$\sigma_z$ (mm)
1.0-5.0	$1.4520 \times 10^{18}$	16	0.8	5.3	0.54
5.0-10.0	$2.1996 \times 10^{17}$	9.8	0.5 / 0.5	3.7	0.52
10.0-20.0	$4.3528 \times 10^{16}$	8	0.5 / 0.32	3.9	0.51

Table 3. Radiation/Source Parameters of Wiggler as Measured for Modeled Source

The following 3 figures show the results of ray-tracing modeling of the wiggler over the three photon-energy ranges. The data are for rays impinging on a perpendicular screen placed 10 meters from center of wiggler. Plot A is a scatter-gram of the rays (photons) in real space and Plot B is of the same rays in phase space as indicated. The 40-mm aperture is indicated by the vertical lines in Plots A and B and a 4-mrad aperture is indicated by the horizontal lines in Plot B. Plot C is a bar graph of the total radiation intensity over the range.

### Discussion of scatter-gram images:

The distribution of the x-ray radiation is into fairly narrow region of space. This is the result of the relatively low K of the proposed wiggler. As the photon energy increases, the fan of radiation narrows significantly. This is, of course, a highly desirable characteristic. The width of the phase-space plot is characteristic of an extended-source, multi-pole wiggler. This and a similar situation for the z-z' relationship (not shown here) result in a significant lowering of the brightness of a wiggler source. There may be some adjustments that can be made in the wiggler de-



sign, but the current design parameters are very close to optimum considering what is needed with regard to radiation and what is exists with regard to machine and facility parameters and constraints.

An important matter regarding SAXS measurements with this wiggler can be found in the phase-space plots. The angular spread in the horizontal plane can be determined from the angular thickness of the plot (ca. 1.5 – 2 mrad). This width would basically remain even if the beam were optically collimated and then transmitted through a pin hole. In other words, SAXS would be performed with a beam having range of maximum angular divergence of  $\pm 0.75$  mrad. Likewise, the vertical-angular distribution (from  $z$   $z'$  plot, not shown) would be ca.  $\pm 0.1$  mrad.

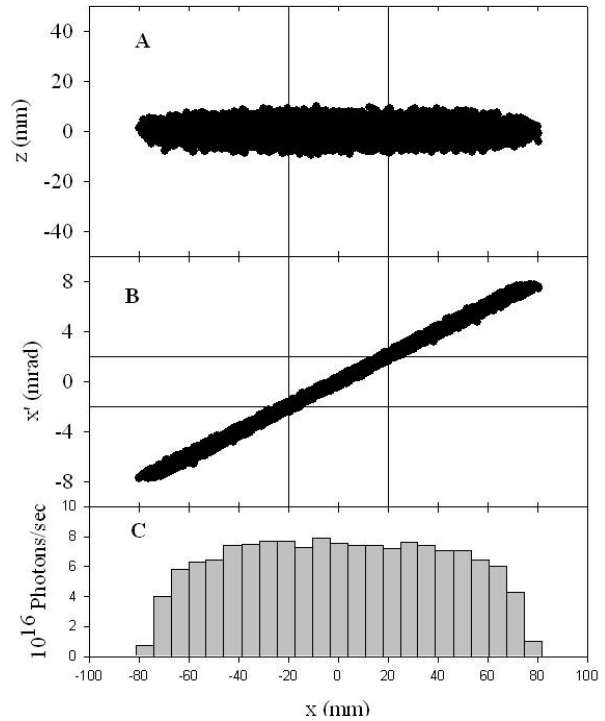


Figure 2. 1- 5 keV Scatter-gram

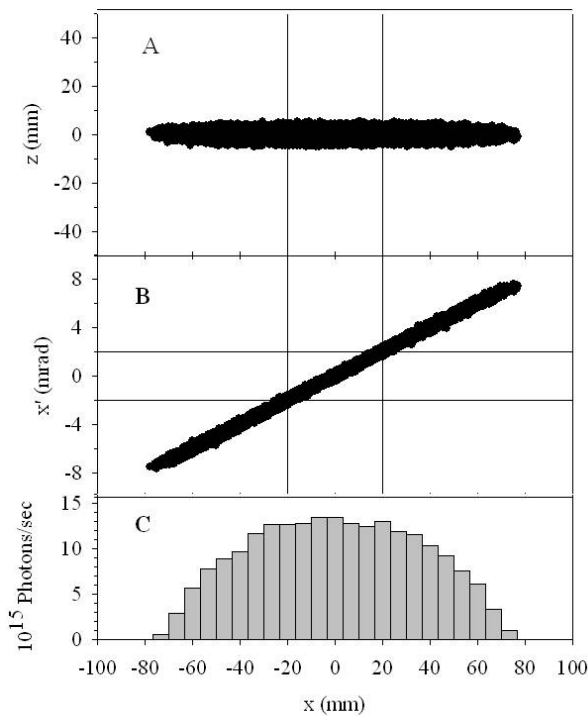


Figure 3. 5 -10 keV Scatter-gram

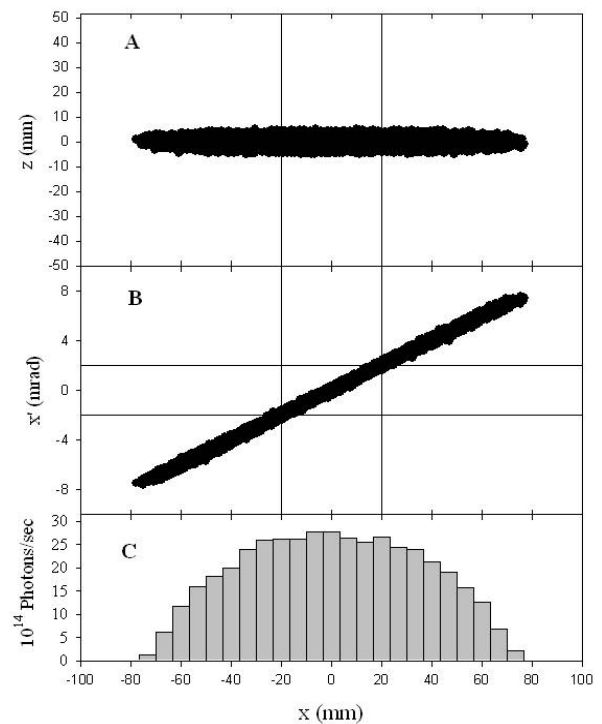


Figure 4. 10 -20 keV Scatter-gram

### Useable Flux Delivered to Beamline:

Comparing plots 1 and 2 in Figure 5 demonstrates the loss of radiation from an aperture which approximates the maximum acceptance of the proposed beamline. As the photon energy increases, it can be seen that an increasing portion of the radiation transmits through the 40 mm aperture. Figure 6 shows the ratios of wiggler to bend-magnet radiation, transmitted by the aperture. The flux ratio is from plots 2 and 3 in Figure 6. Flux production is, however, not the only relevant quality in determining if the proposed wiggler will provide a significantly improved x-ray beam. The brightness ratio curve demonstrates the flux ratio modified by the sizes of the respective sources. This ratio increases with photon energy because of the flux-ratio increase as well as because the size of the wiggler source decreases with increasing photon energy at a greater rate than does the bend magnet source size. It can be seen that the brightness-ratio increase is principally attributable to the flux ratios.

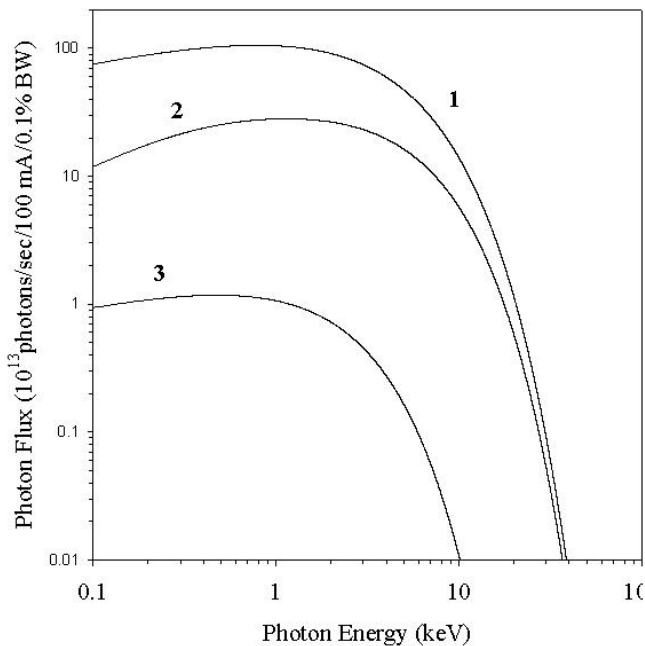


Figure 5. Plots of photon flux (0.1% bandwidth resolution) for total wiggler radiation (1), wiggler radiation transmitted through 40 mm aperture (2), 4 mrad (horizontal acceptance) radiation from CAMD bend magnet (3).

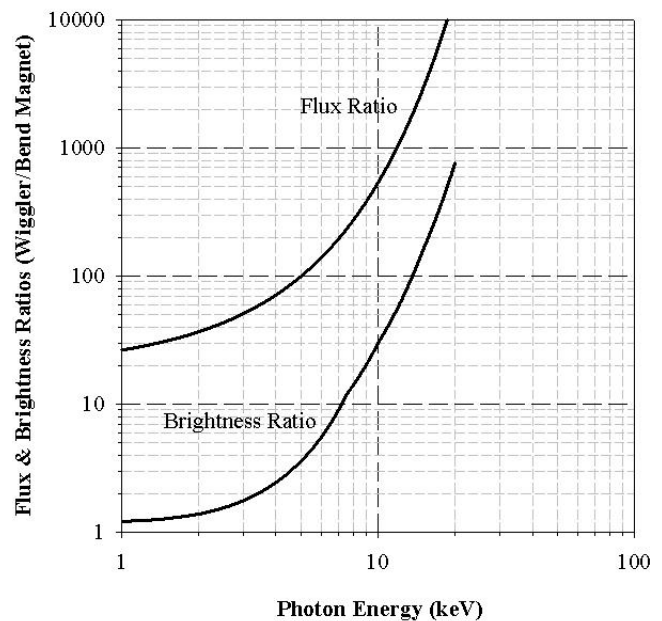


Figure 6. Plots of ratios (wiggler to 4-mrad-acceptance bend magnet) of radiation transmitted through 40-mm aperture, 10-meters from source.

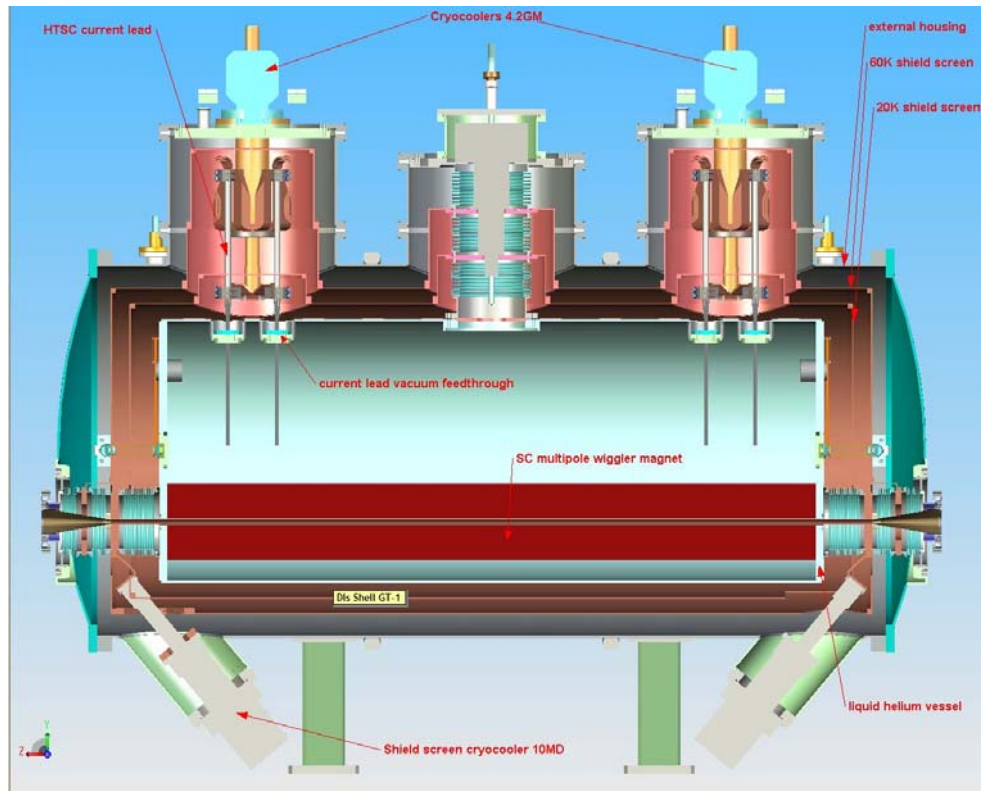


Figure 7. Diagram of a superconducting MPW with cryocoolers designed by Budker Institute.

**Budget Estimate for 3.5 Tesla Multipole Wiggler.**

Wiggler and cryostat	0.80	M\$
Cryocoolers	0.19	M\$
New vacuum chamber and pumps	0.35	M\$
New electron beam position monitors	0.10	M\$
New power supplies	0.06	M\$
Changes to RF system	0.15	M\$
Skew multipole magnets	0.27	M\$
<b>TOTAL</b>	<b>1.92</b>	<b>M\$</b>

## **Budget Justification**

The estimate above makes allowance for all components for the multipole wiggler itself and the associated and necessary changes to the CAMD storage ring. Beamline costs and those for instrumentation and research equipment are not included.

The wiggler and cryostat estimate has been made in consultation with the Budker Institute, Russia who are the leading constructors and suppliers of superconducting wigglers for synchrotron light sources worldwide. The existing 7 T wiggler at CAMD was supplied by Budker Institute. Nevertheless we would expect to be able to enter a competitive bidding situation because the companies ACCEL, GmbH in Germany and Advanced Design Consulting USA, Inc also have the capability to manufacture such a device.

A new vacuum chamber with electron beam position monitors will be required in order to safely handle the very high power density (2 kW) in the beam generated by the multipole wiggler. The estimate is based on CAMD's recent (within the last 5 years) experience of purchasing such items.

New power supplies will be required to power the MPW and the skew multipole magnets will counteract the tendency of the MPW to increase the vertical beam size. The main ring quadrupole power supplies need to be up-rated for the minibeta mode which squeezes the vertical beam size. The new skew multipole magnets will reduce the vertical size of the electron beam.

The multipole wiggler will greatly increase the power emitted by the electron beam in the CAMD storage ring and the lost power has to be resupplied by the RF system. It will be necessary to install a 2nd RF cavity into the storage ring, and this together with its power source is already available. The estimate given above will cover the additional waveguide and other miscellaneous hardware needed and replacement of spares which will be used for the 2<sup>nd</sup> system.

## **IV.C.2 Scientific Case for a Soft X-ray Wiggler**

### **IV.C.2.a Small-angle Scattering (SAXS)**

The SAXS technique comes in many flavors. The simplest relies on phase shifts of essentially monochromatic light, which occur at nonzero detection angles for particles (or other “inhomogeneities”) of finite size. The method is versatile, and can be used to obtain information regarding the dispersion and size of nanoparticles and short/medium range density fluctuations from solid/solid as well as solid/liquid systems. One example of solid/liquid systems is the so-called nanofluids, where nanoparticles are suspended in fluids such as water or ethylene glycol. Such nanofluids possess increased thermal conductivity and are potentially useful for advanced heat transfer applications. Russo (LSU Chemistry) has funding from the NSF to investigate new phases occurring in mixtures of nanoscale rods and colloidal spheres; the expected structures are in the range accessible to SAXS. He also enjoys funding from the American Chemical Society for the investigation of diffusion of polyelectrolytes through matrices composed of other polyelectrolytes. The average matrix dimension, or “correlation length”, is to be measured by SAXS. So far, these and other measurements have been made at SSRL beamline 1-3,

SAXS is potentially sensitive to very small changes in size or shape, especially for uniform particles. The Licata lab (LSU Chemistry) has been investigating polymerases using SAXS facilities around the globe (APS, SSRL (2 different instruments, LNLS and The Photon Factory).

The Russo group has been engaged in building, testing and optimizing the SAXS facility at CAMD. This three-pinhole device uses a 2D multiwire detector usually chosen for weaker lab sources; as a result, the detectable flux is better than one might expect from a standard CAMD bending magnet and double-crystal monochromator. Most of the studies performed by Russo’s group at SSRL could now be performed at CAMD. A significant concern is the continued health of the multiwire detector, which is sensitive to overexposure, expensive to repair, and not backed up by a spare detector as some facilities do. A secondary concern is the precision with which flux can be measured. It is not yet clear whether the SAXS at CAMD can succeed in measurements of polymerases or other dilute proteins. These experiments require careful sample positioning and/or sophisticated liquid cells. The accuracy of transmission and flux measurements is critical. Small details in any scattering experiment come at the highest angles; therefore, baseline corrections (camera stability) are also important. Improvements to the flux of the source itself and to camera sensitivity (minimizing the time over which the camera must remain stable) are desirable.

There is good reason to believe the existing SAXS facility will grow its user base. Tulane’s Vijay John (surfactant self-assemblies) and the University of Cincinnati’s Greg Beaucage (flame-produced nanoparticles) have expressed interest. Additional LSU users will include Negulescu and Sabliov (studies of biobased polymer structures, including drug delivery particles); McCauley (dendrimers and vesicle systems); and, Spivak (molecular recognition substrates). If one looks to an upgraded facility, there would be interest in XPCS (X-ray photon correlation spectroscopy) using coherent beam technology to build on a long tradition of visible light photon correlation scattering for complex fluid dynamics. Extra intensity would benefit anomalous SAXS

investigations of multicomponent systems to optimize contrast through wavelength adjustments that presently bump against CAMD's limited abilities to generate hard x-rays.

In addition to XAS, from which quantitative information regarding the short and medium range order can be extracted from nanocrystalline materials, small angle X-ray scattering (SAXS) can be used to obtain quantitative and statistically significant information regarding size distribution of nanoparticles. One example is shown in Fig. 4, where statistically significant information regarding TiC nanoparticles distribution (shown in Fig. 3) can be extracted.

#### References:

- 1) Matrix Fluorescence Photobleaching Recovery for Polymer Molecular Weight Distributions and Other Applications, G. J. Doucet, D. Dorman, R. Cueto, D. Neau, P. S. Russo, D. DeKee, J. Pople *Macromolecules*, 2006, 39(26), 9446 – 9455;
- 2) Diffusion of Dextran Probes in a Self-assembled Fibrous Gel Composed of Two-dimensional Arborols, Jirun Sun, Bethany F. Lyles, Keunok Han Yu, Jaime Weddell, John Pople, Max Hetzer, Daniel De Kee and Paul S. Russo, *J. Phys. Chem. B*, 2008, 112(1); 29-35.
- 3) **Temperature dependence and thermodynamics of Klenow polymerase binding to primed template DNA.** Datta, Kausiki; Wowor, Andy J.; Richard, Allison J.; LiCata, Vince J., *Biophysical Journal* (2006), 90(5), 1739-1751.

#### IV.C.2.b Intermediate Energy EXAFS

The 3.5 T MPW will be a stronger source of x-rays than the 7.5 T MPW at energies less than about 20 keV and as such will be well suited to K-edge measurements of the first row transition elements and most L edges. Examples of such research follow. It should be noted that if this project is not funded intermediate energy EXAFS will benefit from the new beamline on the wavelength shifter and even more from the 7.5 T MPW should that be funded. However, at the Ti K edge (4966 eV) the flux from the 3.5 T MPW will be 20 fold that of the 7.5 T MPW.

Drs. Stephen McGuire and Edward Doomes from Southern University (HBCU) are investigating multilayer mirror coatings by XAS. These multilayers of TiO<sub>2</sub>, doped with Ta<sub>2</sub>O<sub>5</sub>, are used as mirror coatings in high power laser applications. Currently, how the microscopic features of the coatings influence their optical properties is poorly understood. EXAFS and XANES measurements of the primary coating constituents (Ti and Ta) and trace elements (Fe, Cr, etc.) will be made. This work is supported by NSF (PHY-0101177).

Dr. Tabbetha Dobbins (Louisiana Tech University and Grambling State University (HBCU)) has a DOE-funded research program at CAMD to explore the behavior of transition metal catalysts added to complex metal hydrides. The goal is to find improved materials for hydrogen storage. They examined by XAS TiCl<sub>3</sub>-doped NaAlH<sub>4</sub> powders milled for various times and showed that the absorption energy may shift from Ti<sup>3+</sup> to Ti<sup>0</sup> during high energy milling to introduce the catalyst. [51]

#### **IV.C.2.c Correlation of the microstructure of Perovskites and Related Oxides with their Physical Properties, Edwin H. Walker, Jr., Chemistry, Southern University**

Our work in material science focuses on understanding the mechanisms that govern ion transport in perovskites and related oxides (PRO) with interesting and useful ionic transport properties. We are interested in correlating the microstructure of PROs with their physical properties. Experiments conducted in our group involve the synthesis of nanocrystalline PROs prepared with the novel gel method that we have developed.<sup>1,2</sup> In our studies, nanocrystalline PROs with varying compositions and crystallite size are prepared and characterized using X-ray diffraction and HRTEM in conjunction with impedance spectroscopy to investigate the relationship between structure, composition, and physical properties (ion transport in particular). Specifically, the structural and compositional factors that influence the ionic conductivity are the target of our investigations. We are interested in correlating structural and conductivity data to determine the effects of grain size, grain boundaries, defects and vacancies on bulk ion diffusion.

Recently, a low temperature precursor method has been recently developed by the P.I.<sup>1</sup> for the synthesis of nanocrystalline ternary oxide materials from a 3,3',3''-nitriлотripropionic acid (NTP) precursor solution. Due to the high degree of hydrogen bonding with water, NTP forms a viscous liquid that can absorb many times its own weight of water. The reaction occurs in the NTP system due to the condensation of ammonia with the vinyl group of acrylic acid *via* an internal rearrangement, which occurs by the classic Michael addition mechanism. Metal salts can be readily introduced into the NTP gel as either solids or aqueous solutions. While any water-soluble metal salt might suffice, the Walker group has found that metal acrylates are particularly compatible with the gelling agent. When ordinarily insoluble metal acrylate salts are introduced to the viscous liquid amino acid solution, the nucleophilic amine reacts with the metal acrylate, which results in an elaborate network of amine-connected metal propionates. Specifically, the condensation reactions with the vinyl groups on the metal acrylate-substituted amine will lead to metal immobilization in the hydrogen-bonded gel network. In addition, the increase in viscosity of the solution will tremendously slow the diffusion of metal ions and kinetically impair the separation of two or more metal acrylates. Finally, any free metal ions in aqueous solution will be locked in small aqueous domains that are integrated into the hydrogen-bonded organic network of the gel. Thus, the metals will be restricted to small domains limiting desegregation.

The very homogeneous viscous precursor metal-propionates liquid can easily be applied to a substrate. During thermal decomposition, the organic constituents of the gel precursor are removed by combustion. This results in the deposition of metal oxides that convert to crystalline polymetallic phases at low temperatures. The gel network prevents segregation of metal ions during deposition processes and provides control over the particle size with a narrow size distribution.

Small Angle X-ray Scattering (SAXS) coupled with differential scanning calorimetry will enhance our understanding of how the kinetics and thermodynamics of the elaborate highly hydrogen-bonded NTP interplay in the formation of these materials and will aid us in optimizing the preparation of the nanocrystalline ternary oxide materials. Although SAXS can be done in home labs there is no suitable equipment at Southern University. Furthermore the characteristics of synchrotron radiation provide much better SAXS data than a home lab system. due to higher intensity and lower beam divergence. In addition the synchrotron beam is tunable (that is the x-ray photon energy can be changed). This can be of great use for identifying the distribution of

metals in these materials by collecting data sets above and below the absorption edges of the metals of interest. The EXAFS facility which will be part of the proposed beamline will also be of great use in determining the environment around metal atoms at various stages in the preparation of the metal oxides. The development of the Louisiana and Gulf South Region X-ray Facility will therefore greatly enhance the research efforts in our group.



## IV.D New VUV Wiggler

### IV.D.1 Description of the VUV wiggler

CAMD is proposing to acquire and install a VUV wiggler in a short straight section. At the present time, a 1-Tesla, 100-mm-period-length, 21-pole device is being considered. The following tables give the wiggler parameters and the beam characteristics in the region of the ring proposed for wiggler installation.

**Proposed-CAMD-Wiggler Parameters**

Parameter (units)	Value
Peak Field (Tesla)	1.0
Period Length (mm)	100.0
K	9.34
n (number of poles)	20

**Synchrotron Beam Characteristics at wiggler center**

Parameter (units)	Value
Energy (GeV)	1.3
Beam Current used in calculations (mA)	100
$\sigma_x$ (mm)	1.4
$\sigma_z$ (mm)	0.2
$\epsilon_x$ (mm-rad)	$5.08 \times 10^{-5}$
$\epsilon_z$ (mm-rad)	$3.33 \times 10^{-6}$

The following figure contains plots of photon fluxes from the wiggler and a bend magnet in the CAMD electron storage ring. The total flux produced in the wiggler and that accepted into 1 mrad horizontal plane from a bend magnet are shown. For comparison, as indicated in the figure caption, wiggler radiation accepted in a nominal 1 mrad horizontal-plane angle is shown. The ratio of plot B to plot C is a measure of the wiggler to bend-magnet radiation.

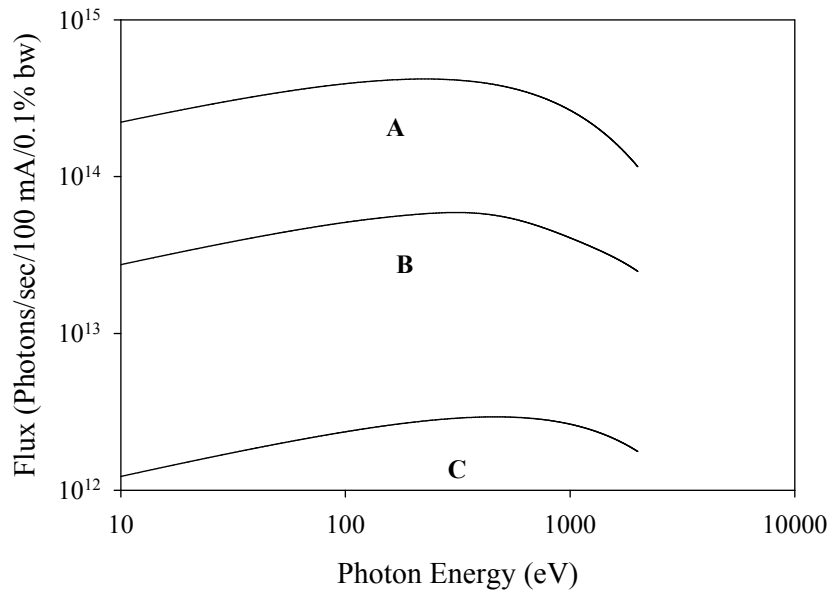


**Figure 1.** Plots of flux spectra of radiation produced by the CAMD electron storage ring operating at 1.3 GeV and 100 mA eam current. **Plot C** is radiation emitted into 1 mrad horizontal acceptance angle from a CAMD 3-meter bend magnet. **Plot A** is the full acceptance of all radiation (from 10-2000 eV) emitted by the proposed VUV wiggler. For comparison with the bend magnet flux, **Plot B** is nominally 1 mrad horizontal acceptance from the wiggler. This was modeled as the radiation transmitted through a 10-mm (horizontal) aperture (full vertical acceptance) placed 10 meters from the center of the wiggler.

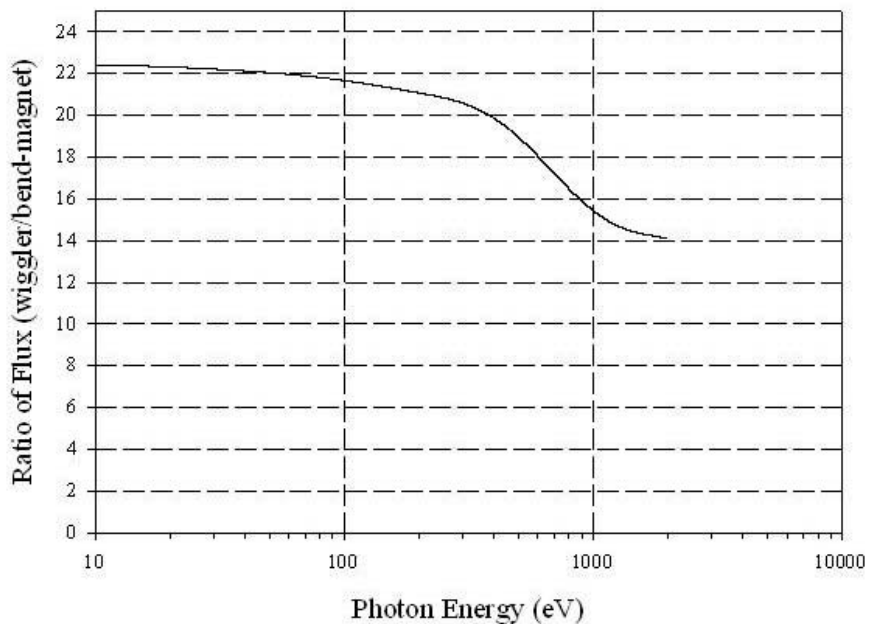


**Figure 2.** Ratio of Plots B and C in Figure 1.

## **IV.D.2 Scientific Opportunities with the VUV Wiggler.**

### **IV.D.2.1.a Spin-polarization and Exchange in Room Temperature Metal-organic Ferromagnets**

A.N. Caruso, North Dakota State University

Room temperature ferromagnetism in thin film metal-organic materials (albeit few) is now reproducible and of sufficient technological and basic interest. The use of such films in functional magnetic and spintronic devices have been limited due not only to the difficulty in fabricating the films and their atmospheric stability, but in the lack of understanding of their magnetic origin and determination of spin polarization. In order to progress in the development and utilization of organic and metal-organic materials in magnetic and spintronic devices, basic experiments such as spin polarized photoemission must be completed to help reveal: (1) the mechanism(s) responsible for exchange; (2) where in binding energy the exchange occurs; and, (3) the raw polarization at the Fermi energy. From a basic view there is a lack of understanding with regard to the exchange between metal centers through polaron or neutral organic ligands. Specifically there is a lack of understanding regarding the role of: (1) orbital orthogonality; (2) electron-phonon coupling; (3) conjugation; and, (4) degree of localization. Temperature dependent valence band spin polarized photoemission will indeed help understand, guide and corroborate theoretical predictions regarding the above questions, which ultimately hold the key to further development of this tremendously important and significant area in both the basic and applied communities.

In order to complete the above studies, a very high intensity source is required due to four main experimental limitations: (1) the measurement is angle resolved, such that very few of the photoejected electrons are collected in the  $\pm 0.5^\circ$  aperture; (2) the light must be polarized to provide for symmetry and selection rules; (3) the photoejected spin polarized electrons are collected after scattering off of a Mott polarimeter, whose efficiency is poor and greatly reduces the number of counts relative to spin integrated photoelectron spectroscopies; and (4), the pass energies need to be on the order of 2 eV or less and the slits need to be cut down so that features less than 50 meV wide may be resolved (especially in the case of spin polarized polaronic states). To put it simply, high resolution angle resolved spin polarized photoemission is an important experiment that cannot presently be completed because of the low number of counts; with a high intensity photon source, afforded by the insertion device in question, such studies may be completed.

An even more exotic experiment, that is deemed as “quantum mechanically complete” is to use incident circularly polarized light rather than linearly polarized light, to provide an additional angular momentum selection rule that can help to understand non-paramagnetic polarization and hybridization, such as transition metals mediated by carbon or oxygen for temperatures greater than 100K.

Presently, there is not a machine in the world that can fulfill the requirements stated above. With the existence of such an insertion device to provide the photons, combined with an existing end station at CAMD residing on the 3m-NIM beamline, CAMD would become a sole source for such important work in both the magnetic, spintronic and multiferroic fields whose necessity in applications is paramount over the next 15 years.

#### **IV.D.2.1.b Photoemission and Gas Phase Cluster Experiments (Dowbin)**

There are now five VUV beamlines at CAMD available for experiments. In section IV.F.2 we discuss improvements to the existing bending magnet beamlines. While improvements to the existing beamlines are very desirable an insertion device in the VUV is even more desirable because such a facility at CAMD would be unique to the southeast and makes possible resonant high resolution photoemission experiments and other photon “hungry” experiments that would be competitive or superior to other VUV facilities elsewhere in North America.

While interest in gas phase cluster experiments has waned in the US, this has not been the case elsewhere. COLd Target “Recoil” Ion Momentum Spectroscopy (COTRIMS) experiments on clusters have been one of the great successes of the FEL at the Hamburg synchrotron. A number of CAMD users have an interest in this area of research. The planned future work in chemical dynamics (See Section II.B.1) could also make use of this technique through an infrastructure expansion to include gas-phase cluster experiments.

Promising areas of research where CAMD could effectively compete include double and triple ion fragmentation experiments in core-to-bound excitation studies of clusters. Theory has certainly been motivated by those few experiments that have been undertaken, and with little effort, CAMD could be a major player on the international stage by supporting such experiments. The staff at CAMD understands that such experiments need large, but infrequent allotments of synchrotron time: a concept that scientists at many other synchrotrons have failed to grasp. The experiments are difficult and signal intensities are low, but CAMD could assume a leadership role with a little help from interested users at LSU and other institutions. A step toward this goal would be to build the soft x-ray undulator to produce both the necessary photon flux, as well as the necessary beam focus and polarization modulation.

## IV.E Upgrades to Existing Beamlines

### IV.E.1 Upgrades to Existing X-Ray Bending Magnet Beamlines to Characterize Advanced Materials

X-ray spectroscopic and diffractometric techniques are basic research tools at every major synchrotron facility, and will be an important resource for the current MS&E initiative at LSU. In what follows, potential applications of X-ray techniques to characterization of *advanced metallic and ceramic materials* are illustrated with past research examples.

#### X-ray absorption spectroscopy (XAS)

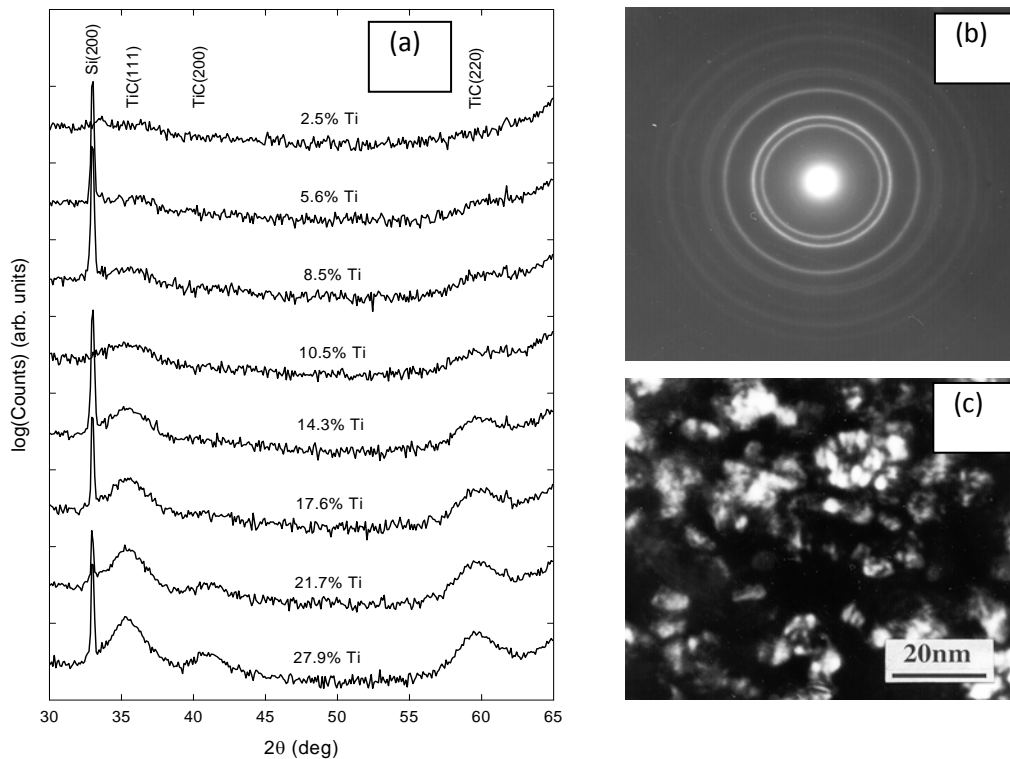


**Figure 1.** XRD and TEM examination of TiC nanocrystals embedded with an amorphous hydrogenated carbon matrix: (a) XRD patterns; (b) electron diffraction pattern; (c) TEM image.

Figure 1 shows the result of X-ray diffraction (XRD) and transmission electron microscopy (TEM) examination of a pseudo-binary composite of nanocrystalline TiC and amorphous hydrogenated carbon (a-C:H) in thin film form, which offers an example of nanocrystalline ceramic materials. Nanocrystals, ~5nm in size, are uniformly embedded within an a-C:H matrix. Although X-ray and electron diffraction patterns confirm the crystalline nature of the TiC phase, severe particle size broadening is present due to the small grain size of the TiC phase. Detailed

structural information regarding coordination, short and medium range order, etc, is difficult to obtain from conventional diffractometry and electron microscopy.

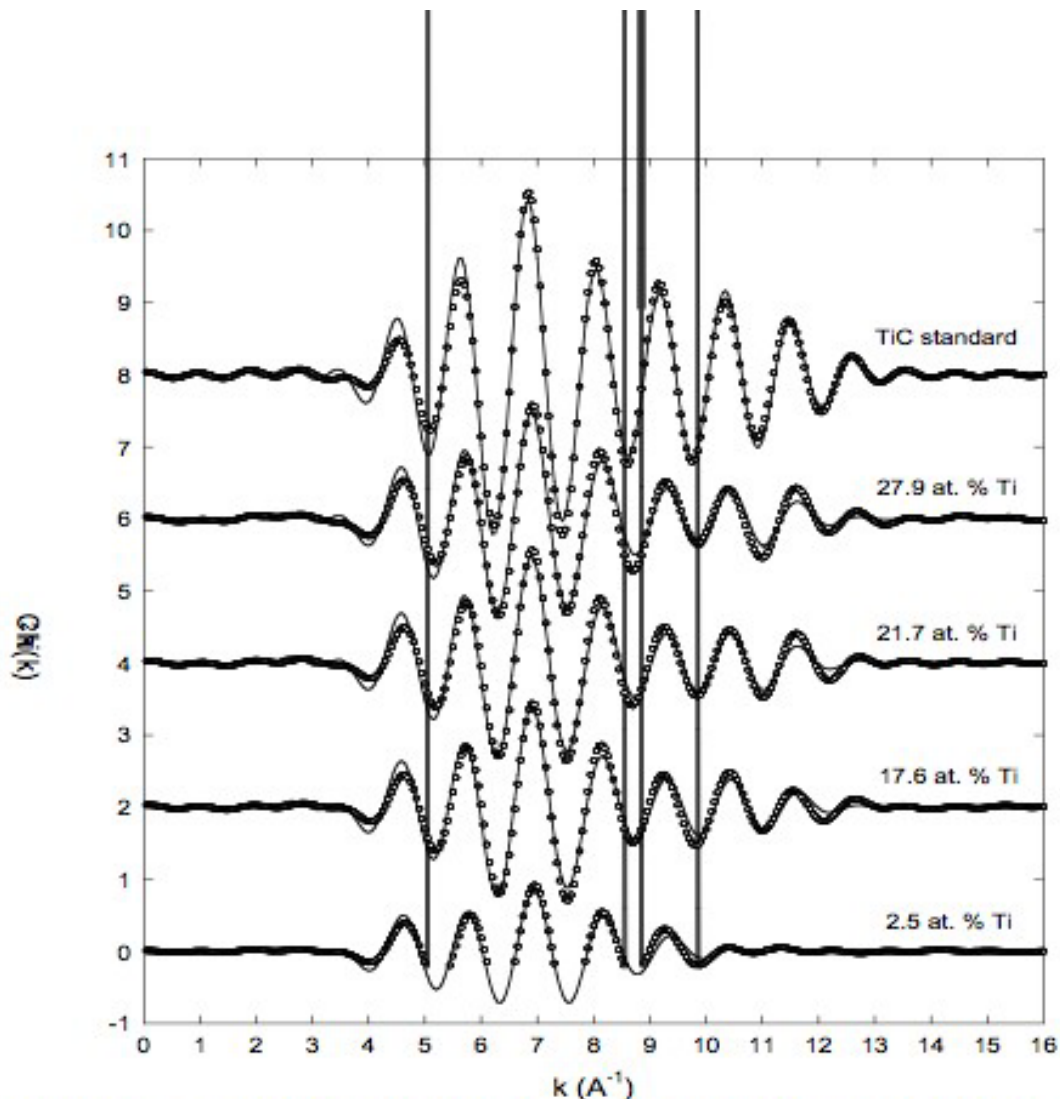


**Figure 2**, Filtered Fourier back transforms of Ti K-edge EXAFS spectra obtained from TiC/a-C:H nanocomposite thin films of different Ti composition.

XAS ideally complements XRD and TEM in the examination of nanocrystalline materials. Figure 2 shows a series of Ti K-edge Extended X-ray Absorption Fine Structure (EXAFS) spectra obtained from TiC/a-C:H nanocomposite thin films. Detailed fitting of such EXAFS spectra offers quantitative information regarding bond distance and average coordination number as a function of Ti composition, and indicates that Ti bonding environments largely conform to that in bulk crystalline TiC.<sup>i</sup> Such detailed characterization offers structural basis on which the mechanical and tribological properties of TiC/a-C:H thin films can be understood.<sup>ii, iii</sup>

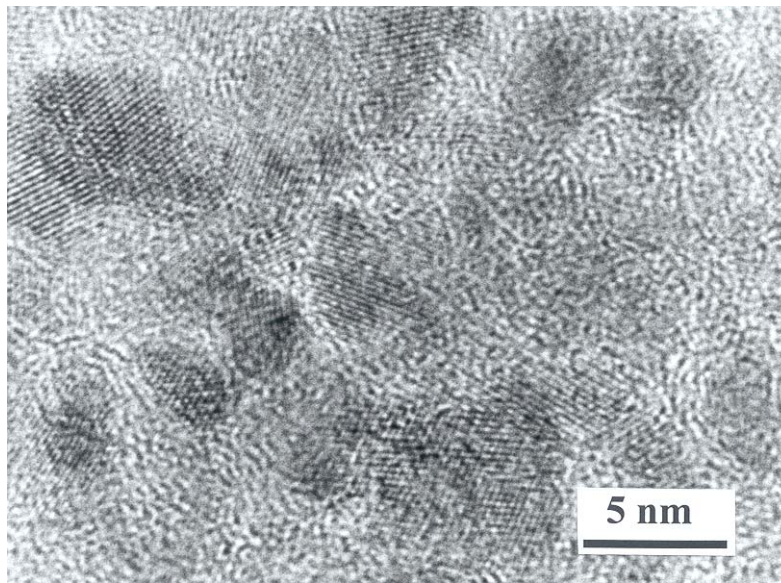


**Figure 3.** High resolution TEM micrograph of a TiC/a-C:H nanocomposite thin film, showing the presence of numerous TiC nanocrystals within the a-C:H matrix

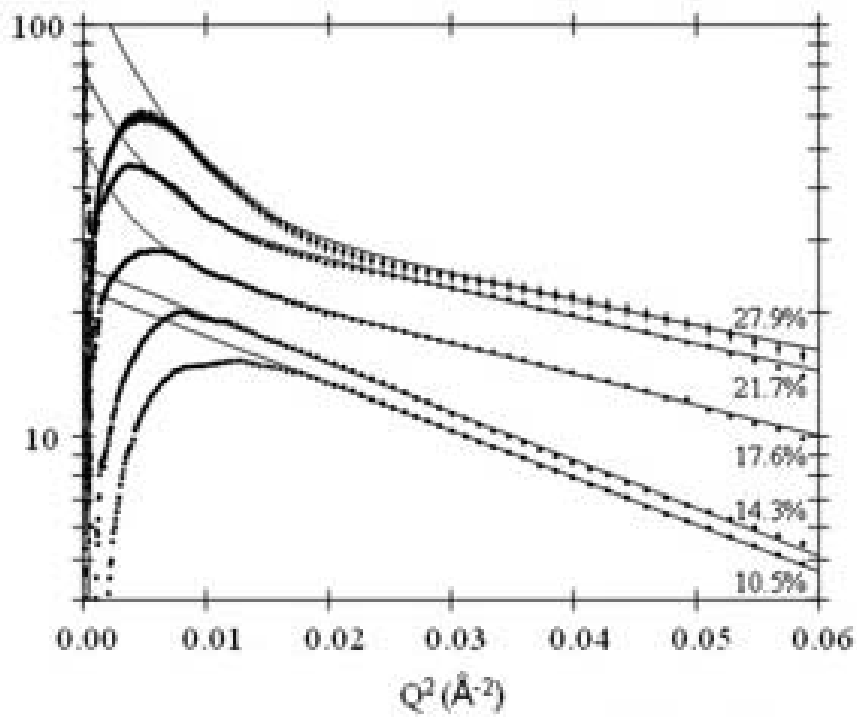


**Figure 4.** SAXS patterns of TiC/a-C:H nanocomposite thin films with different Ti compositions. Contrast arises from the difference in the electron density between the TiC and aC:H phases.

### Four-circle X-ray diffractometry (XRD)

This most basic materials characterization technique is applicable to wide ranging materials problems, including epitaxial thin film growth on substrates,<sup>iv</sup> determination of orientational order in polycrystals,<sup>v</sup> internal stresses, long-range ordering. Modern applications include glancing incidence X-ray scattering (GIXS), ultra-fast time-resolved studies, and others.

In summary, it is suggested that CAMD devotes a part of its resource to ensure that the techniques of XAS, SAXS, and XRD are up to date, fully supported, and remain competitive with other synchrotron facilities.

#### References:

- 
- <sup>i</sup> W. J. Meng, R. C. Tittsworth, J. C. Jiang, B. Feng, D. M. Cao, K. Winkler, V. Palshin, "Ti atomic bonding environment in Ti-containing hydrocarbon coatings", *J. Appl. Phys.*, 88, 2415 (2000).
  - <sup>ii</sup> D. M. Cao, B. Feng, W. J. Meng, L. E. Rehn, P. M. Baldo, M. M. Khonsari, "Friction and wear characteristics of ceramic nanocomposite coatings: titanium carbide/amorphous hydrocarbon", *Appl. Phys. Lett.* 79, 329 (2001).
  - <sup>iii</sup> B. Shi, W. J. Meng, L. E. Rehn, P. M. Baldo, "Intrinsic Stress Development in Ti-C:H Ceramic Nanocomposite Coatings", *Appl. Phys. Lett.* 81, 352 (2002).
  - <sup>iv</sup> W. J. Meng, J. Heremans, Y. T. Cheng, "Epitaxial growth of aluminum nitride on Si(111) by reactive sputtering", *Appl. Phys. Lett.* 59, 2097 (1991).
  - <sup>v</sup> W. J. Meng, G. L. Eesley, "Growth and mechanical anisotropy of TiN thin films", *Thin Solid Films* 271, 108 (1995).



---

#### IV.E.1.b Scientific Benefits of Upgrading the VUV Beamlines (Dowbin)

There are five VUV beamlines available for experiments. The existing beamlines may be improved by simply increasing the entrance mirror solid angle collection and improving the exit spot focus at the sample. The benefit of increasing the solid angle of collection on beamlines attached to bending magnets rather than insertion devices is that such entrance mirrors while large, could be designed to handle the heat load far more effectively. These modifications would also impart considerable stability in flux and resolution.

Optimized beamline optics can deliver considerable performance improvements in photoemission experiments that are often not flux limited, but require high beam stability. Improvements to the beamline focus could be effected on some beamlines with little effort and would greatly enhance the experimental performance of some beamlines especially the highly desirable 3 m NIM (see Section III.B.2.a.). However, all the beamlines would benefit from such modest upgrades. Other improvements include better slit management in the beamlines, better computer control and calibration set points when sweeping the monochromator photon energy. Further improved performance can be obtained through grating replacement. Gratings can now be fabricated with better high order light suppression and increased resolution, even for small radius grating monochromators. These improvements open the door to high resolution constant initial state spectroscopy.



## Section V:

The Future: Working toward Achieving  
the LSU Flagship Agenda with a Light  
Source for the Southeast



## **V. The Future: A New Light Source for the Southeast**

### **V.A. Introduction**

As of May 2008 and probably for several years to come, CAMD is and will be the only synchrotron light facility in the southeastern USA. It has operated successfully as a regional facility since 1992 with a growing and diverse research program that has been described in Section II. The overwhelming number of CAMD's over 300 users comes from LSU, and Louisiana. About 50 users are from the rest of the United States with about a dozen coming from Europe.

During the course of time new technology emerges and the science horizon changes. Therefore, CAMD and LSU must consider how the user community will be served and developed in the short and long term future.

Significant improvement to CAMD's brightness has been achieved by adjusting the existing accelerator systems at a modest cost. But as was described in section IV, further investment in the existing accelerator and beamlines would allow substantial performance improvements to the facility's capability. These developments must be put into the context of the ultimate replacement of the source and should also be reconciled with the likely timescale, as well as the impact the current (2008) financial crisis will have on federal and state budgets.

Given that a 3<sup>rd</sup>/4<sup>th</sup> generation replacement for the existing CAMD is at least 5-10 years downstream and that the existing user community needs to be strengthened and to adapt to the techniques which exploit high brightness, there is a powerful case for investing in the CAMD accelerator system over the next several years. It will also be essential to invest in the beamlines so that the extra potential of the source can be efficiently exploited. Given an investment of about \$10 million dollars to upgrade the accelerator and install new insertion devices over the next 3 to 4 years the following benefits would result.

- Beam current increased to 500 mA,
- Brightness increased by a factor three,
- Beam lifetime doubled to 30 hours,
- High flux MPW for hard x-rays,
- High brightness/flux ID for the 1-4 keV region,
- Improved reliability from better infrastructure systems.

This would represent a powerful boost to the science research capability of Louisiana and the Southeast and would not necessarily require support outside the state of Louisiana.

In this section we will present several the possibilities but not define the parameters for the future light source at CAMD at this time.

The cost of a future CAMD source will range from about \$25,000,000 to something of order of a billion dollars, and thus the source characteristics will depend almost totally on obtainable funding. The search to define the next source and its funding is necessarily a task that the LSU Vice Chancellor of Research should direct.

CAMD held a workshop in November 2006 to consider the possibility of a 3<sup>rd</sup> generation light source. The report from this workshop is contained in Appendix C.1. In January 2008 another workshop was held, cosponsored by the Southeastern Universities Research Association (SURA); Florida State University, Office of the Vice President for Research; University of Tennessee, Office of the Vice Chancellor for Research; the Louisiana Board of Regents and the LSU Office of the Vice Chancellor of Research and Economic Development, to explore some of the possibilities for a fourth generation source. The report from this workshop is contained in Appendix C.2. Professor Eberhardt, the director of BESSY, was one of the participants at the January 2008 Workshop. He was invited to offer some comments relevant to source development at LSU and in the southeast. They include:

- A. As the ROSE report clearly states, the user community needs to be continuously developed to take full advantage of a new state of the art source.
- B. Continual interaction with the CAMD User community is essential to help CAMD staff work through the complex multidimensional space to arrive at the parameters of the next source to serve the south.
- C. Realistically, it takes about three years to design, build, and commission a state of the art insertion device and beamline. Given this timeframe and the resources required, whatever is constructed for CAMD now should actually be designed with the concept to transfer the equipment to the new source.
- D. Beamlines and endstations are getting more and more sophisticated --- ***there has to be adequate technical support for the users***. University professors with their graduate students can and should define the specifications required on the basis of the scientific program, the technical solutions, on the other hand, should be provided by the (permanent) staff of the facility.
- E. Microscopy is missing at CAMD. This is a very important aspect of high brightness sources and should be developed. Microfocus applications (tomography) have been developed and will definitely benefit from a brighter hard X-ray source.
- F. Protein crystallography and the life sciences program seems to be quite strong in comparison. A proposed crystal change robot would be a key addition for improving this facility. Successful experiments require literally hundreds of crystals to be characterized quickly in order to find the ones that give the best overall diffraction pattern. Often these are not the obvious choices by visual inspection.
- G. A state of the art ARPES photoemission setup is essential for the solid state physics – advanced materials efforts. This would be a SCIENTA R4000 with a helium cooled manipulator and an appropriate beamline delivering photon energies up to 100 eV with meV resolution and high flux.
- H. Full energy injection would help in many ways. The stability and reliability of the machine would improve greatly; top up injection would be possible, and this addition also would enable the installation of superbends.
- I. As the new source is being planned and later built, ***staffing and other resources will have to be increased substantially***. The exact levels are strongly dependent on the number of experimental stations to be operated by the facility. ***Every facility also needs an adequate capital fund to perform necessary upgrades and improvements at a steady, reliable, and consistent level***. In principle such funds have to be available at the director's discretion to be used in conjunction with proposals for other external funding.

The justifications of sources of greater brightness and intensity have been well documented in a series of workshops and websites. Representative ones can be found at the sites listed in the following paragraph and at the sites:

<http://www.science.doe.gov/bes/besac/Hemminger-02-2008.pdf>

<http://www.bnl.gov/nsls2/sciOps/LifeSci/default.asp>

<http://www.4gls.ac.uk/>

<http://cat.inist.fr/?aModele=afficheN&cpsidt=17833628>

<http://meetings.aps.org/Meeting/MAR08/Event/80418>

[http://www-ssrl.slac.stanford.edu/aboutssrl/documents/lbnl\\_slac\\_white\\_paper.pdf](http://www-ssrl.slac.stanford.edu/aboutssrl/documents/lbnl_slac_white_paper.pdf)

Worldwide there is a great interest in these advanced sources because of their high coherence and short pulse length. In fact, at least five different facilities in the United States are exploring the possibilities for different fourth generation sources. These sources have been described in various workshops and are based on a seeded-laser superconducting LINAC-undulator combination (proposed by the SRC (<http://www.wifel.wisc.edu/>) and the ALS (<http://www-als.lbl.gov/als/usermtg/talks2008/chu.pdf>)), and energy recovery LINAC's (ERL's) proposed by Cornell University, <http://erl.chess.cornell.edu/>, and by Florida State University, <http://www.magnet.fsu.edu/usershub/scientificdivisions/emr/facilities/fel.html> and as an upgrade at the APS. An operational THz ERL source is located at Jefferson National Laboratory (JLab, <http://www.jlab.org/fel/>) and an x-ray FEL (the LCLS, <http://www-ssrl.slac.stanford.edu/lcls/>) is under construction at Stanford University and will be operational in 2009. Therefore, CAMD is in good company as it ponders its future amid the diverse array of current possibilities.

The cost of a third generation source would be of order \$100M including a new building and the cost of a fourth generation source will range from several hundred million dollars to something of the order of one billion dollars depending on the design. Facilities of this magnitude will require a regional effort to obtain funding from state, federal and private sources. On the other hand the scientific benefits of such a source will drive cutting edge science and technology development for all the universities in the southeast.

It is clear that the future development of CAMD must be the subject of a parade of workshops that involve the user community, the LSU administration, and regional universities alike to chart the course of action.

The discussion in the following subsections provides an outline of a possible third generation source, and some ideas from the most recent workshop that outlines topics for consideration to develop a fourth generation source that can provide the ultimate in radiation to probe the science contained the "Grand Challenges." In Section V.d. the impact of the source and facility on work force development is described. In this section a strong argument is made that a "next" generation light source which should be university based rather than based at a national laboratory, because universities are key players in the drive to achieve the national mandate (The America COMPETES Act of 2007) to train new scientists to ensure that the United States is competitive in the 21<sup>st</sup> century.

## V.B . A Compact Third Generation Source: ROSE:

We will begin by considering the simplest new source that could be built at a relatively modest cost (\$90M). This source would supply our users with a high brightness beam and serve the community in the same way that the NSLS-II would serve their users through the availability of very bright high intensity light although with time structure and coherence properties that would be much less than 4<sup>th</sup> generation sources. However, the present third generation sources in the United States are highly productive and oversubscribed. A CAMD upgrade to a third generation source would serve the scientific community in the south for many years to come and would be the kernel for a fourth generation source.

The concept began several years ago with a study that considered the design of a new high performance third generation source which would cater to the increasing demand for synchrotron light in the region; (Ring of the South East- ROSE). In keeping with its role as a regional source, it would be economical to construct and operate, yet provide high brightness beams from its insertion devices (ID). For the expected research applications, the output must span both the soft x-ray region (0.1-4 keV) and the x-ray region up to at least 13 keV. A third generation storage ring at 2.5 GeV would be a suitable source satisfying all these requirements.

Modern 3<sup>rd</sup> generation light source designs, storing electrons in the energy range 2 to 2.5 GeV, achieve high beam brightness (emittance below about 10 nm.rad) generally with a circumference greater than 250 m. In order to produce comparable performance from a source with a circumference below 200m, that minimizes the capital cost, a very low emittance design is required. One such concept has recently been applied to the designs of both the Australian ([http://www.synchrotron.org.au/content.asp?Document\\_ID=1](http://www.synchrotron.org.au/content.asp?Document_ID=1)) and the Canadian Light Sources (<http://www.cls.usask.ca/>) with good results. It was decided to base the ROSE study on a similar design. An artist impression of the ROSE Facility is shown in Figure 1.

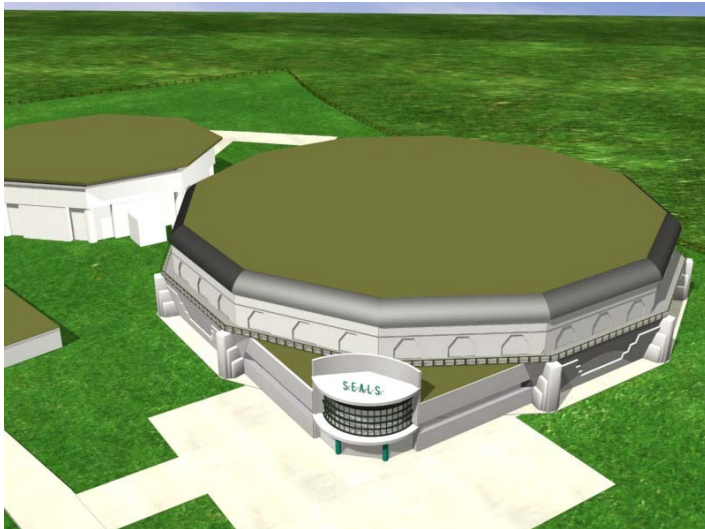


**Figure 1.** Artist's impression of the ROSE Facility on the CAMD site.



The outline design for ROSE has a circumference of 170 m with 12 long straight sections of length 5 m. A very economical structure for the storage ring is used so that costs are minimized by reducing the number of focusing magnets. Nevertheless, a very high performance can be expected (emittance about 8 nm.rad) from both the dipole magnets and the IDs. Allowing for some use of straight sections for accelerator systems (RF and injection) at least 10 IDs will be able to be accommodated and with the high brightness beam their performance will be world class. Figure 2 shows the spectral output which can confidently be expected from a superconducting undulator in ROSE.

Although many of the features of ROSE will follow the good practice established at other 3<sup>rd</sup> generation facilities, such as full energy, top-up injection; the emphasis will be on achieving high performance with economy. It is estimated after careful optimization that the facility could be constructed with an initial suite of 4 IDs with their beamlines, for under \$100 million.

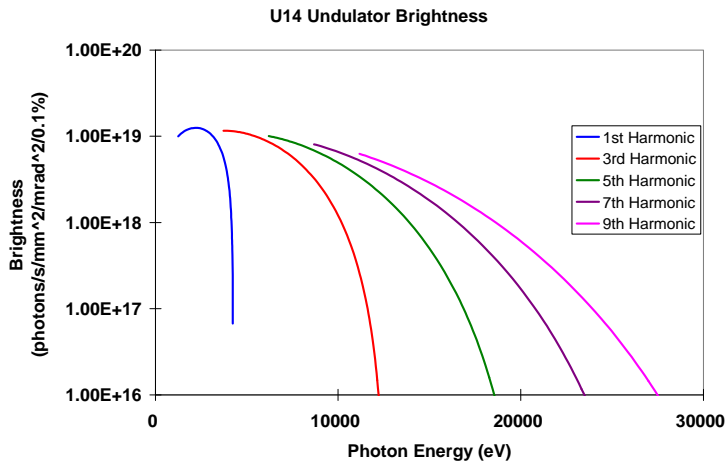


**Figure 2.** Output from a 14 mm superconducting undulator in ROSE

Energy (GeV)	2.5
Beam Current (mA)	400
Circumference (m)	169.2
Horizontal emittance (nm.rads)	7.74
Number of cells	12
Betatron tune (horiz; vert)	11.18; 3.15
Natural chromaticity (horiz; vert)	-19.5; -19.5
Length of straights (m)	5.0
Dipole field on orbit (T)	1.4
Dipole gradient (T/m)	-3.76
Radio frequency (MHz)	499.655

**Table 1.** Major parameters for ROSE

Machine	34.4 M\$
Buildings	24.7 M\$
4 beamlines with insertion devices	16.0 M\$
Personnel	11.3 M\$
Administrative cost	3.0 M\$
<b>Total</b>	<b>89.4 M\$</b>

**Table 2.** Cost estimate for ROSE in 2004 dollars.

**V.C. Defining the Road toward the Development of the “Light Source of the Future”: A report by the Source Breakout Group attending the workshop, Enabling Grand Challenge Science: The Light Source of the Future.** (M. Borland, J. Corbett, R. Falcone, G. Kraft, J. Lewellen, C. Steier, and V. Suller)

**V.C.1. Overview**

A clear theme emerging from discussions relating to Grand Challenge Science is the desire to develop an understanding of materials at a length scale of 1-100 nm, energy scales of 1-100 meV, and for processes with time scale of 1-1000 femtoseconds. This understanding will ultimately enable the creation of new materials with tailored properties for new technology applications.

Synchrotron Light Sources have contributed to these issues in the spatial and energy domain and storage rings can demonstrably deliver high average brightness with good reliability. Rings pushed to the ultimate limits seem feasible, if technically challenging, and would offer further brightness gains. However, they would fall short of delivering such brightness with femtosecond scale pulses. Linac based sources, in which the electron beam density has not been diluted by radiation emission, offer the combined possibility of high peak brightness with sub-picosecond pulses.

Linac based sources undoubtedly have the potential to meet many of the requirements of Grand Challenge Science, but significant technology development still needs to take place. For that reason our recommendation is to adopt a staged approach commencing with a conventional linac using a high brightness electron gun and feeding via a switchyard to a suite of undulator radiation sources. Later, technology development would allow the undulators to become true Free Electron Lasers (FELs) and the linac superconducting. Using energy recovery in the superconducting linac would allow much higher pulse repetition rates and thereby higher average brightness. Co-development of conventional lasers is another requisite, both for seeding the FELs and to act as the pump in pump-probe experiments.

These source issues are addressed in more detail in the following sections.

A highly schematic view of a fully developed 4<sup>th</sup> Generation Source is shown below.

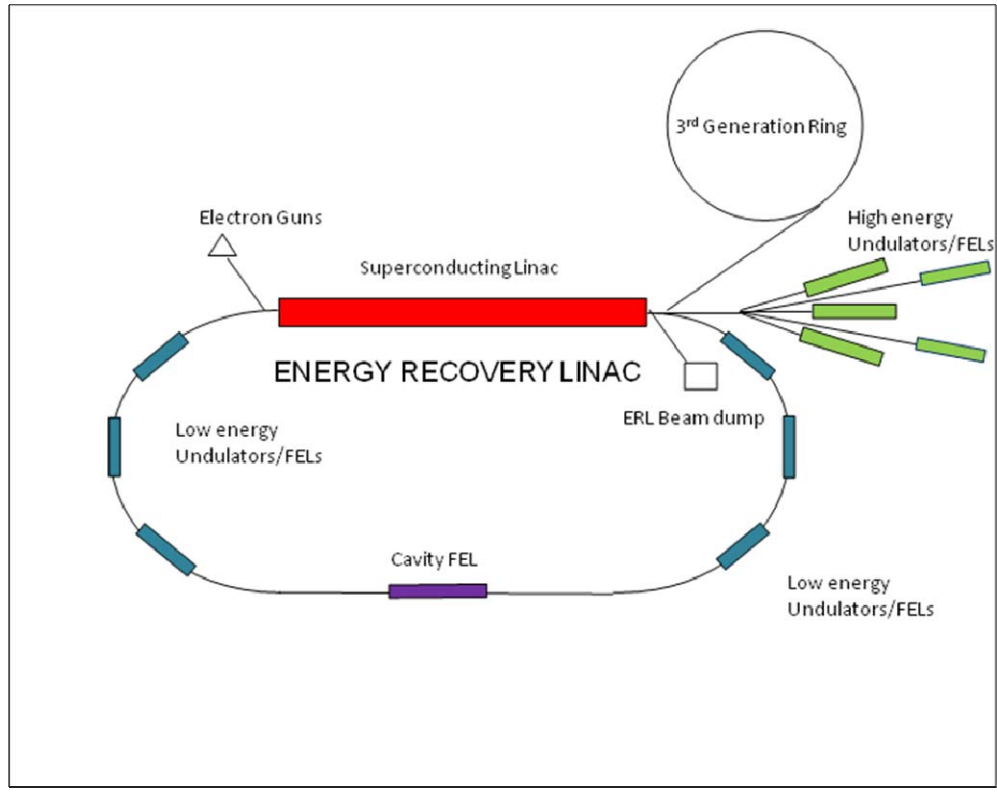


Fig.3 This scenario shows the final development of a staged 4<sup>th</sup> generation light source.

A complete 4<sup>th</sup> Generation light source has several modes of operation:-

- A. ERL with one accelerating pass and one recovery pass through the superconducting linac. Multiple lower photon energy undulator/FELs are located in the return arc, operating with high average beam current and high pulse repetition rate (MHz). A high rep rate electron gun with low emittance and moderate bunch charge (50 pC) is used.
- B. High energy with two accelerating passes through the superconducting linac with no energy recovery. Maximum pulse rep rate would be 1 kHz feeding a suite of high photon energy undulator/FELs. The electron gun delivers up to 1 nC per bunch.
- C. Intermittently the linac is used to fill a 3<sup>rd</sup> generation storage ring.

Not shown are the bunch compression systems which will be used to deliver bunch lengths of 100 – 200 femto seconds or the phase control adjustment of the returning beam to the linac.

Some key parameter goals for this source are:

- ✓ Electron bunch length ~100 - 500 fs
- ✓ Electron bunch charge (HE mode) 50 - 1000 pC
- ✓ Normalized electron beam emittance 1 μm radian
- ✓ Photons per pulse  $2 \cdot 10^{12}$  photons
- ✓ Peak brightness  $10^{31}$  photons/s/0.1%/mm<sup>2</sup>/mr<sup>2</sup>
- ✓ Average brightness (HE mode)  $3 \cdot 10^{23}$  " " " "
- ✓ Average brightness (ERL mode)  $5 \cdot 10^{22}$  " " " "

### **V.C.2. Electron Guns and Timing**

Over the years the technology of high brightness electron guns has made tremendous progress and can now deliver 6 dimensional phase space densities that cannot be matched by storage rings. However, nearly all existing low emittance guns (i.e. normalized emittance just above 1 mm mrad for 1 nC bunch charge) operate at low repetition rates (120 Hz). High average power guns (like the Boeing normal conducting gun) so far have only demonstrated emittances too large to be suitable to FEL applications. Similarly DC guns, which have demonstrated fairly sizeable average currents, so far deliver a charge per bunch that is generally too small for x-ray FEL applications. Therefore further gun development is necessary (and is ongoing at many places) to improve both emittance (below the best values achieved at low repetition rate guns) and repetition rate (or charge per bunch). Both would improve the performance of future FEL facilities and emittance improvements could allow to significantly reduce the length of the undulators. Several competing technologies (superconducting, DC, low frequency RF) are being pursued and in simulations all of them hold the promise of substantial performance improvements. However, the progress at all test facilities has been less than optimal over the past years.

Therefore the optimum injector-technology choice for high-repetition-rate FEL applications, cannot be made right now based on available experimental and theoretical work. Some of the fundamental issues to be resolved can be addressed by working with the leading groups in each of the relevant fields.

Complementing the further development of electron guns, many ideas exist to manipulate the phase space of the electron beam at some intermediate energy. This might allow trading the advantages and disadvantages of different gun designs and would make beam heaters, like those that might be employed at FERMI@ELETTRA, unnecessary. Those manipulations might include emittance exchange for improvement of transverse emittance, or optical manipulation to enhance peak current or to produce attosecond photon pulses.

Synchronization systems that have been developed recently will be employed at the LCLS to provide locking of remote lasers to several femtoseconds timing jitter. For the much more challenging demands of attosecond pump/probe experiments, which are mentioned as one science driver of a new facility, much more fundamental studies need to be carried out first to come up with ideas about the overall timing system. In this regime, ground motion and physical stability of machine and beamline components becomes extremely important, and new concepts need to be developed to gain control of timing systems to such a level.

### **V.C.3. Bunch Compression and Pulse Length**

The ability to produce femtosecond electron pulses is a highly desirable feature of the proposed source. To date, the most widely-used method of producing short electron pulses is magnetic bunch compression. In this scheme, a relatively long bunch is accelerated to an energy of typically several hundred MeV. Acceleration takes place “off crest,” so that an energy chirp is imparted to the individual electron bunches. The beam is then passed through a system of bending magnets called a chicane, which has an energy-dependent time of flight, resulting in a

reduction of the bunch length. This simultaneously increases the peak current inside the bunch, which is essential for obtaining FEL gain. Following this, additional off-crest acceleration is needed to both increase the beam energy and remove the chirp. In some cases, two stages of compression are employed.

Although the principle is simple, in practice magnetic bunch compression has challenging aspects. The number and location of the bunch compressors must be optimized to minimize error sensitivity and the overall length of the linac. Coherent synchrotron radiation (CSR) generated in the bunch compressor bending magnets increases the emittance and energy spread, both of which must be small in order to obtain large FEL gain. Additionally, CSR combined with longitudinal space charge in a long linac can lead to a high-gain microbunching instability, which can inflate the energy spread and modulate the bunch current profile. Both CSR and space charge effects are worst when one tries to produce high current or short bunches. Hence, R&D is required to determine reasonable beam parameters and make reliable predictions of performance.

To produce intense radiation pulses with duration below a few hundred femtoseconds, we must use other techniques in addition to bunch compression. One promising method in an unseeded FEL is “differential bunch spoiling [1],” in which a slotted foil is used in a chicane to impart a time-dependent emittance degradation to a bunch, allowing only a very narrow time slice to pass unaffected. Predictions for LCLS hold forth the promise of sub-femtosecond pulses from a 200-fs electron bunch.

In a seeded FEL, one can use a short seed pulse to begin the FEL process, as described in section V.C.4.

#### **V.C.4. Undulators and Free Electron Lasers**

Permanent-magnet based undulator design theory is fairly well-established, as are fabrication and tuning methods. Typically, storage ring undulators have periods in the 1 – 5 cm range, gaps of 1 – 3 cm, overall lengths of several meters, and K values up to 3. There has been significant work on the development of alternate undulator types and styles, including superconducting (for higher fields and smaller periods), in-vacuum (for higher fields via smaller gaps), and various arrangements intended to provide variable polarization ranging from linear through elliptical to circular. Undulators located along the return arc of the ERL should pose no special challenge compared to those presently in service, so long as the desired parameters are similar.

The advent of SASE-FEL sources has led to the development of techniques for designing, tuning and aligning long segmented undulators; the most recent example is the LCLS undulator, approximately 120 meters in length. An important aspect of SASE-FEL undulator systems is the placement of diagnostics (both e-beam and photon beam) along the undulator. These are used to both tune up the initial operation of the SASE-FEL, and to provide feedback to beam control systems. While the LCLS system has yet to be tested in practice, similar sorts of system were tested at the DESY and Argonne single-pass FEL experiments. While challenging to construct,

the undulators required for a fourth-generation light source appear to be within our current technical capabilities.

One concern for both return-path and SASE-FEL undulator design relates to the impedance of the undulator line. Compared to storage ring bunches, ERL bunches are very short. [Note that APS hybrid mode is 340 A peak current, while JLab ERL is 150 A, same as APS 24-bunch mode. Cornell x-ray ERL is even lower.]. This can lead to increased impact upon the beam from wakes, and also, for the ERL portion of the facility, to increased heating of the chambers and transitions compared to storage rings running the same average current. (This was noticed at the JLab ERL FEL.) Again, this does not appear to be an insurmountable challenge, but must be kept in mind during the design process.

The basic self-amplified spontaneous emission (SASE) process has been successfully demonstrated at several single-pass free-electron lasers (FELs), and is presently the method used to generate VUV radiation for users at the FLASH facility in Hamburg. In the SASE process, a single electron bunch amplifies its own spontaneous emission as it transits down a long undulator. The gain process is exponential, with most designs intending for the optical power to saturate just before the end of the undulator. The first X-ray FELs to come on-line, the LCLS project at Stanford and the X-FEL project at DESY, will use the basic SASE process.

The primary advantages of the SASE process are the need for neither a seed signal nor high-reflectivity optical cavity mirrors. An additional advantage is the requirement for only a single electron bunch, not a bunch train. Therefore, in principle, SASE-FELs can be designed to operate at any wavelength and have broad tunability, and the pulse repetition rate can be varied without regard to optical cavity round-trip times.

The disadvantages of the SASE process are inherent in the self-startup from noise. The SASE-FEL is intrinsically a high-gain, large-bandwidth amplifier. Therefore, even with identical incoming electron beams, shot-to-shot variation in output power, central wavelength, and bandwidth can be expected. Any variation in the electron beam properties from the driver accelerator will exacerbate these variations. Also, the current designs of most driver accelerators will result in a SASE optical pulse arrival time jitter on the order of 1 ps. This requires modifying the approaches to some types of experiments, as well as having available complete “post-mortem” diagnostics on the SASE-FEL light on a shot-to-shot basis.

There are however, many proposed methods to address the issues with the basic SASE-FEL process, several of which maintain the desirable features of arbitrary tunability and no resonator cavity. The efforts to date have focused on stabilization of the output central wavelength and bandwidth, and improving the temporal coherence of the optical pulse.

One class of method takes light from early on in the SASE process, filters it, and then reintroduces it as a seed signal. While not yet demonstrated experimentally, this approach is expected to deliver bandwidths approaching the transform limit and stable operating wavelengths [2]. Other approaches use a seed signal, generated by an external source, to modulate the beam in one undulator; subsequent undulators, tuned to a shorter wavelength, are used to radiate. Depending on the implementation, these approaches can either operate at closely

spaced but fixed harmonics of the seed signal, or at arbitrary wavelength [3]. The most straightforward of these techniques, high-gain harmonic generation, has been demonstrated for the second harmonic [4]. FERMI@Elettra, a VUV SASE-FEL facility currently in construction at Trieste, Italy [5], will incorporate some of these techniques to stabilize wavelength and bandwidth output, and should provide the first operational experience in a user-facility setting. The use of an external seeding scheme also allows controlling the length of the output pulse by changing the length of the seed pulse.

### **V.C.5. Superconducting LINACs**

In the new source it is desirable to deploy a continuous wave (CW) superconducting linac for a variety of reasons: (1) combined with a high repetition rate electron source, the possibility exists to provide separate beams to multiple users simultaneously, (2) the reduced beam impedance, by comparison to a normal conducting linac, allows the beam quality to be better preserved during the acceleration to high energy, and (3) a natural upgrade path to an energy recovered linac exists when a superconducting linac is complete.

Because of cavity heating, it is impossible to run a normal conducting linac CW at accelerating gradients more than a few MV/m, making them undesirable in CW applications. Recent progress in RF superconductivity allows CW accelerating gradients at the level of 20-30 MV/m in individual cavities, and around 160 MV each from 10 m cryomodules consisting of 8 x 1 m long cavities. Because the power lost in superconducting cavities is so small, the linacs are built from standing wave RF cavities, which allows acceleration in either direction through the linac. Approximately 20 such cryomodules are needed to achieve 3 GeV beam energy in a total length of 200 m in a single pass linac. Having a recirculation beamline at 1.5 GeV, combined with two pass acceleration of bunches with charge well under 1 nC, may allow the linac length to be halved without too serious consequences to the beam quality as the bending is done at a reasonably low energy. This would be one way of reducing the 20~30 MW wall-plug power requirements of the cryogenic system for a single-pass linac with high-gradient cavities. Another would be development of improved, high-efficiency helium refrigeration systems.

Because of their low beam impedance, superconducting linacs may be designed to be superior at accelerating and transporting the large bunch charges needed for Free Electron Laser operation. This feature can be further enhanced by choosing lower accelerating mode frequency for the cavities. Previously developed superconducting cavities employed by the Spallation Neutron Source have a frequency of 805 MHz, and could be beneficially employed in this project. Specially developed and optimized cavities in the frequency range 600-800 MHz could provide still better performance, at the cost of an expensive development program.

Since free-electron lasers induce large energy spreads on the electron beams used to drive them, FELs present some additional challenges for energy-recovered linac operation. This includes, for instance, the need for a large energy acceptance in the recovery loop. Still, operation of ERLs driving FELs has already been demonstrated [6][7] and it is likely that solutions can be found for single-pass FELs also.



### **V.C.6. Seed and Pump Lasers**

It is clear that future FEL facilities (whether seeded or SASE) will need to integrate lasers and accelerators to optimize the overall facility performance. Laser systems will be an integral part of all sections of the accelerators, timing systems and experiments. Applications include generating and shaping the electron beam at the photocathode, the ultra stable optical-timing systems for the accelerator, diagnostics systems throughout the machine and transport lines, seeds for the FELs, maybe optical manipulations of the electron beam, end-station pump-probe lasers, and finally the optical synchronization systems linking all lasers within the facility.

Recent developments in laser materials and techniques have yielded amplifiers with the required pulse energy and high repetition rates. However, the ongoing work in pulse shaping needs to make substantial progress to allow the stable generation of the temporal and spatial distributions, necessary to optimize the gun performance. In addition, the reliability of high performance laser systems is an issue that needs very significant progress before user facilities employing them can reach reliabilities approaching storage rings.

### **V.C.7. Inverse Compton Scatter Source**

The Inverse Compton Scatter source produces x-rays by back scattering an intense visible laser pulse brought into head on collision with a relatively low energy (50 MeV) electron beam [8]. The x-rays are monochromatic and although the intensity is not presently competitive with synchrotron radiation sources, development of high intensity lasers and high brightness/short pulse electron guns could result in source sizes of a few microns and sub picoseconds pulse lengths. Thus an Inverse Compton Scatter Source at a relatively modest cost could be a useful adjunct to a Southeast facility at a relatively modest price-tag.

### **V.C.8. Experimental Facilities**

The development of FEL-based soft x-ray sources will be necessary to address important questions in short-pulse nano-science research. Several design studies outline components of these high-tech facilities [9], and FLASH [10] has already opened the door to first experiments. Nevertheless, advanced hardware R&D is still needed prior to construction of a truly modern facility optimized for a broad range of applications with a wide user base. The areas of development run the entire length of the accelerator complex, through the insertion devices, and into the experimental hutches including sample manipulators, detectors and computing systems.

Depending on the top energy of the electron beam, a 4<sup>th</sup> generation light source is likely to be 300-500m long including accelerator systems, ID's and experimental hutches. The site needs to be stable against thermal variations (<0.1 C), ground vibration (few 10's of nm) and radiation hard. The site will likely require 10-20MW wall power (beam current dependent) with feeds delivering varying degrees of 'clean' power.

Starting from the gun, long-life, high-grade photocathode materials must be developed to operate in conjunction with very reliable laser systems featuring efficient frequency conversion and relay optics. The lasers will require accurate 3-D profile control, shot-to-shot intensity control, low

intensity jitter, and variable repetition rate. The laser system will be intimately connected to the master fiber-optic timing system.

The superconducting linac requires high-efficiency cryogenics and must maintain a stable longitudinal energy profile on a shot-to-shot basis independent of experimental target. Thus timing issues will be critical to successful operation. Both the linac and chicane sections will need advanced diagnostics to monitor electron beam properties in 6-D phase space. Visible, electro-optic and electron-beam based systems will be necessary.

The beam switchyard can be constructed with a series of pulsed deflection magnets to service a suite of ID's and associated end-stations. Development of very stable pulsed-power technology will be needed for the switchyard to deliver accurate and reproducible electron beam trajectories through the ID's.

Each of the ID's will likely be different to deliver photon beams of varying energy, bandwidth and pulse structure. Several of the concepts require advance R&D to demonstrate proof of principle. Examples of ID applications include:

- Incoherent radiation/SPPS (average flux, EPU-polarization)
- Low-gain FEL action (gain, coherence)
- Seeded FEL action (gain, coherence, pulse structure)
- eSASE, HGHG (gain, coherence, pulse structure)

The insertion device complex will require development of advanced laser systems and close integration with the site-wide timing system. Component drift, tunnel temperature, vacuum chamber development and vibration control are all critical for successful operation. Sophisticated beam steering, feedback and diagnostic systems are needed to monitor and control laser beam overlap with the e-beam. All systems need R&D.

The facility beamlines will require advanced beam optics to transmit short, yet intermittent high peak-power pulses spanning from VUV to soft x-ray spectral regions and associated high-resolution monochromators. The beamlines will also require sophisticated sample handling, detector and data processing systems.

The ultimate benefits of investing in a fourth generation source are shown in Figure 4.

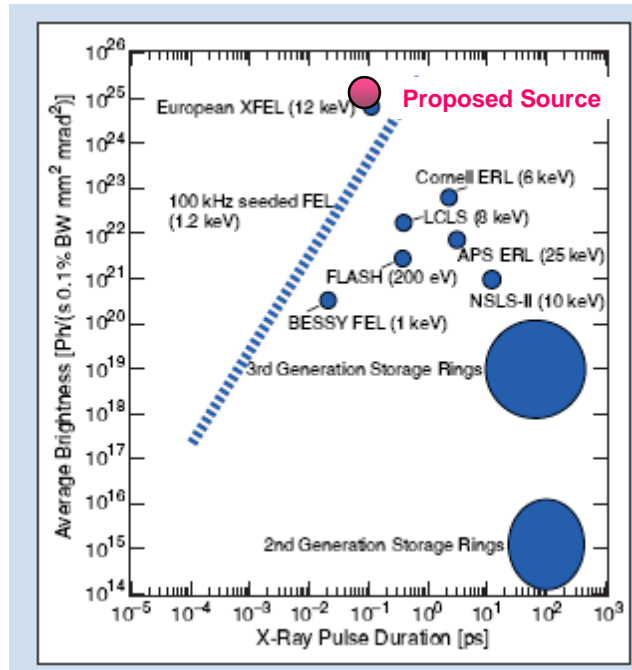


Figure 4: Parameters for light sources of various degrees of sophistication.

#### References:

- [1] P. Emma, Z. Huang, and M. Borland, "Attosecond X-ray Pulses in the LCLS Using the Slotted Foil Method," SLAC-PUB-10712.
- [2] J. Feldhaus et.al., Optics Communication 140 (1997) 341-352.
- [3] Biedron et.al., Nucl. Instr. Meth. A 475 (2001), pp. 401-406.
- [4] Doyuran et.al., Phys. Rev. Lett. 86 (2001), pp. 5902-5905.
- [5] <http://www.elettra.trieste.it/FERMI/>
- [6] G.R. Neil et.al., "The JLab high power ERL light source," Nucl. Instr. Meth. A (557), pp. 9-15 (2006).
- [7] S.V. Miginsky et.al., "Status of the Novosibirsk high power terahertz FEL," Proc. 2007 Asian Part. Accel. Conf, pp.616-618 (2007).
- [8] <http://www.camd.lsu.edu/SRI/Workshop3.pdf>.
- [9] Synchrotron Radiation News, Vol. 20, No. 6, Nov/Dec 2007.
- [10] [http://flash.desy.de/sites/site\\_vuvfel/content/e395/e2188/FLASH-Broschrefrs\\_web.pdf](http://flash.desy.de/sites/site_vuvfel/content/e395/e2188/FLASH-Broschrefrs_web.pdf)

## V.D. Work Force Development Implicit with the Development of an Advanced Light Source

### V.D.1. General Remarks, Nora Berrah (Western Michigan University)

Sustained investment in scientific research ensures critical national needs such as energy, economic competitiveness, and security. The latter can be achieved by aggressively investing in the production of the future scientific workforce. Recent statistics from the American Institute of Physics Statistical Research Center [1] showed alarming ratios of physics degrees to all bachelor degrees granted in the U.S. The ratio peaked at about 1.45 in the early 1960s but was about 0.4 in 2007. The number of physics majors dipped to about 3800 in 1999 and is now about 5400—still a very low number nationally.

The America COMPETES Act of 2007, signed into law, includes strengthening research but also educational programs. It provides incentives to increase the number of majors and teachers in the STEM fields such as science, technology, engineering, and mathematics. Future light sources should be seen as an opportunity not only to train majors in physics, chemistry, biology, and engineering but also to produce the next generation of scientists that will push forward the frontiers of science.

The fourth-generation light source, with source properties unattainable as of today, will allow some of the recently proposed DOE BESAC scientific grand challenges to be pursued and could also enable much-needed growth in our national scientific workforce. The future light sources will have several specific needs in terms of a workforce that is educated with the skills needed to make it a success. First, there will be a need for both *hardware and instrument development scientists*. Currently, the funding and support mechanisms in the U. S. do not train a sufficient number of these scientists. The demand for trained technical staff is critical enough that new light sources, such as NSLS-2 or LCLS, recruit their needed technical staff from other light sources or accelerator facilities. In addition to the technical staff that directly supports the facility, there is a need to train, fund, and engage young researchers and junior faculty to become the next-generation light source scientists. Furthermore, training *theorists* and hiring them in academia and national laboratories are also important because in order to make significant scientific advances, experimentalists and theorists need to work together.

The DOE has been a steward of major light-source facilities with construction, maintenance, upgrade, and operational leadership provided to various national laboratories. In recent years, DOE has also assumed stewardship for the operation of the experimental stations and other subfacilities at various light sources. This has successfully supported numerous research experiments proposed by the users from academia, industry, and national laboratories producing short-term returns for the investments by the funding agencies. However, in this operational paradigm, because the operational leadership is with the national laboratories, the traditional partners in these facilities—namely the academia, industry, and other agencies—have often disengaged in contributing to the scientific vision, future plans, and innovative design for developing next-generation scientific programs. *The consequence of this new funding strategy has severely precluded the academic institutions from developing a trained workforce.* This, in turn, limits the number of trained scientists with advanced science and technology skills that

could play a significant role at major facilities such as a light source, essential for U.S. scientific and technological competitiveness in the 21<sup>st</sup> century.

The National Academy of Sciences Report in 2003 based on the *Pan-Organizational Summit on the U.S. Science and Engineering Workforce* addressed key issues on the science and engineering (S&E) workforce needs in the U.S. for the 21<sup>st</sup> century and suggested various approaches to this noble goal. The key questions are: How will we capitalize on the growing opportunities for S&E discoveries in the 21<sup>st</sup> century? And, how will we keep pace with the growing competition in these areas with other countries? The simple and only answer to these questions is to develop a highly trained S&E workforce with all the means that we have at our disposal. Unfortunately, it is generally difficult for national laboratories, which currently operate the major light sources, to easily establish a *dedicated effort* to deliver a pipeline of S&E workforce. In our vision of a next-generation light source, this will be the foremost and natural priority for a university consortium that will operate the facility. It will include enhancing the existing programs such as Research Experience for Teachers (RET), teacher workshops, Historically Black Colleges and Universities (HBCU), Partnership for Research and Education in Materials (PREM), and graduate training within the university consortium. The light sources of the future provide an additional important component—the ability for large groups of trained students, undergraduates, graduates, scientists, and engineers from diverse and merging areas (of accelerator physics and technology, materials sciences, life sciences, chemical sciences, medical sciences, earth and planetary sciences, energy and environmental sciences, computational and informational sciences, etc.) to be able to work together as a team—a necessary ingredient for successful workforce development for the future. New inventions and innovations in health, defense, security, and technology, as well as in other areas, will greatly benefit from a qualified workforce capable of working in large teams that can be educated and trained at a next-generation light source.

1. Kerry G. Johnson, American Institute of Physics Statistical Research Center, Capitol Hill Quarterly, February 2008, v3, No 1. [www.aps.org/publications/capitolhillquarterly/index.cfm](http://www.aps.org/publications/capitolhillquarterly/index.cfm).

#### **V.D.2. Staffing Challenges to Develop the Accelerator, V. Suller, (CAMD)**

The Fourth Generation light source of the future will provide source properties which are unattainable as of today. Development of the necessary technologies is underway at several centers worldwide, including the USA, but no one center can supply all the critical R&D needed to credibly propose construction of such an advanced source. This includes high brightness electron guns, superconducting accelerators, lasers, insertion devices, optics, and related technologies. The team assembled to construct the new light source will initially need to interact and collaborate with these centers, and then instigate well-funded development programs of its own in the most critical areas. Undoubtedly this process would provide technology transfer into, and build up expertise in, the new project. More generic accelerator systems will be less demanding but will nevertheless require highly competent technical staff with the necessary expertise. To move in this direction will require an overall project team which could be constituted from collaborators who could be seconded from US National Labs and perhaps also from overseas centers. Additionally it would include a core group employed by the new facility, which could initially be relatively inexperienced, but visionary. They would gain expertise by being immersed in the build up phase of the project. Because what is envisioned is a national

flagship facility, there should be little difficulty in recruiting top quality staff where needed. Students and postdocs will additionally be drawn to this important frontier work.

### **V.D.3. Workforce Development through an Existing LSU Program.**

One avenue toward the future development of a 4<sup>th</sup> generation light source would be by expanding Professor Ken Schafer's ultra-fast laser-based program and by hiring accelerator physicists to develop design concepts and costs of new light source schemes. These schemes should include incorporation or upgrades to CAMD with possible relocation. In parallel, under careful guidance by the new CAMD director, science programs at CAMD should be developed, but be well integrated with programs on campus. The programs at CAMD and in ultra-fast laser science, also need to involve as many campuses in the SE as possible.

### **V.D.4. Workforce Development through a University-Federal and State Partnership,**

Herman Winick (Stanford), John Sutherland (East Carolina University), Harald Ade (North Carolina State University), John DiTusa (LSU), and Les Butler.

A unique opportunity exists for Government agencies to interact with academic institutions and a whole region outside the traditional national laboratory structure.

The main contact points whose interdigitation has to be considered and defined are:

- Education
- Research
- People: Faculty (Post docs, students)
- Facilities (land, etc.)
- Operation
- Outreach

**University Partnership:** It is felt that solid commitments from many universities in the southeast region are needed for the development of advanced research facilities such as light sources to provide the strong intellectual horsepower to make the facility succeed. These commitments are to (a) teaching, (b) on-going research funding, and (c) initial construction.

Workforce development at the 4<sup>th</sup> generation source (4G), and the teaching capacity of the partnering universities should be tightly coupled. If there is a target of 1,000 users/yr, then many, many workshops and graduate courses are needed. The new high-speed internets through the southeast will allow workshops and graduate courses to reach many students; the 4G is seen as the coordinator of workshop and course offerings.

**Joint Faculty Appointments:** Building upon the SSRL joint faculty appointment strategy, one envisions a policy of large scale joint faculty appointments across universities in the south. The driver for joint faculty appointments is the predicted large teaching load associated with the 4G: workshops and graduate courses.

To implement such a program the following joint faculty appointment strategy is proposed:

1. Joint faculty appointments, in pairs. That is, a university should split one position into two, with one person having majority appointment at the university (and tenure-track) and the other person sited at the 4G.
2. The appointments are fixed term: reviewed by the 4G and the university.
3. 4G courses and workshops are for both graduate, undergraduate.
4. 4G courses are internet based (see David Attwood's (Berkeley) course on VUV spectroscopy that reaches students and faculty worldwide ([Synchrotron Radiation for Material Science Applications \(http://www.coe.berkeley.edu/AST/srms\)](http://www.coe.berkeley.edu/AST/srms))).

**Joint Research Funding Support Strategy:** Beamline scientists, the facility, and faculty at the partnering universities will contribute to a yearly omnibus proposal. The proposal to be submitted for funding consideration by DOE. The DOE funds will be cost shared by the participating universities Offices of Research. In this arrangement the participating universities contribute operational facilities, and faculty positions.

## V.E. Conclusions

By now the reader has tired eyes, but I hope not a numbed mind! This report has been assembled by the committee of dedicated scientists listed on the cover page of this report.

Of the 40 sources listed at [http://www-als.lbl.gov/als/synchrotron\\_sources.html](http://www-als.lbl.gov/als/synchrotron_sources.html) seven are in the US. However, advanced sources are being considered worldwide, two have been funded in the US and twelve in Europe and Asia. There are two funded R&D programs in the US and four more in Europe. The US has seven concepts and proposals under way and there are seven more under consideration in Europe and Asia. This intense activity suggests how exciting the future is in high field and short pulse radiation research. These programs will be the cutting edge of research. It is time for CAMD to push ahead!





# Appendices



## Appendix A:

## Publications 2005-2001

**A fast-scanning, low- and variable-temperature scanning tunneling microscope**, L. Petersen, M. Schunack, B. Schaefer, T.R. Linderroth, P.B. Rasmussen, P.T. Sprunger, E. Lægsgaard, I. Stensgaard, and F. Besenbacher, *Rev. Sci. Instrum.* 72 (2001) 1438.

**A Giant Magnetoresistive (GMR) Sensor Array for Microfluidic Magnetocytometry**, N. S. Korivi and J.-W. Choi, *Proceedings of the 8th International Conference on Micro Total Analysis Systems (MTAS 2004)*, Malmo, Sweden, September 26-30, 2004, pp. 521-523.

**A Hybrid Approach for Fabrication of Polymeric BIOMEMS Devices**, V. Singh, Y. Desta, P. Datta, J. Guy, M. Clarke, D.L. Feedback, J. Weimert and J. Goettert; *Book of Abstracts, HARMST05*, June 10-13, 2005, Gyeongju, Korea, pp. 170-171, 2005, accepted for publication in *Microsystem Technologies*.

**A Microtomography Beamline at the LSU CAMD Synchrotron**, Kyungmin Ham, Hua Jin, Leslie G. Bulter, and Richard L. Kurtz, the proceedings of the 12<sup>th</sup> U.S. National Synchrotron Radiation Instrumentation Conference, Aug 22-24(2001), in press , Maddison, WI.

**A micro heat sink for cooling macro-scale conformal surfaces under the influence of thrust and frictional forces**, L. S. Stephens, K. W. Kelly, D. Kountouris, J. McClean, *Journal of MEMS*, Vol. 10, No. 2, June 2001.

**A Microtomography Beamline at the Louisiana State University Center for Advanced microstructures and Devices Synchrotron**, K. Ham, J. Hua, L.G. Bulter, and R.L. Kurtz , *Review of Scientific Instruments*, 73, 1521-1523 (2002).

**A new process to fabricate DXRL x-ray mask by direct pattern writing**, Z.G. Ling, K. Lian and S. Wen, *SPIE Vol. 4979*, pp. 501-507, 2003.

**A passive alignment method utilizing reference posts and its application in multi-level LIGA processing**, Z. Ling, K. Lian, J and Goettert, *Microsystem Technologies*, vol.9, 119-122, 2002.

**A passive alignment method utilizing reference posts and its application in multi-level LIGA processing**, Zhong-geng Ling, Kun Lian and Jost Goettert, *HARMST'01*, June 17-19, 2001, Baden-Baden, Germany.

**A Quantitative Study on the Adhesion Property of Cured SU-8 on Various Metallic Surfaces**, Wen Dai, Kun Lian and Wanjun Wang, *Microsystem Technologies*, Volume-1, Issue Online First page:46, June 23, 2005. DOI: 10.1007/s00542-005-0587-4.

**Adsorption of Water on the TiO<sub>2</sub> (011)-(2×1) Reconstructed Surface**, Cristiana Di Valentin, Antonio Tilocca<sup>4</sup> and Annabella Selloni, T. J. Beck, Andreas Klust, Matthias Batzill, Yaroslav Losovyj, Ulrike Diebold, *J. Am. Chem. Soc.* 127 (27) (2005) pp 9895-9903.

**Advanced Characterization of the Electronic Structure of MEH-PPV**, D. K. Chambers and S. Selmic, MRS Proceedings, Volume 871E, article I6.20, 2005.

**Amorphous hydrocarbon based thin films for high-aspect-ratio MEMS applications**, D. M. Cao, T. Wang, B. Feng, W. J. Meng, K. W. Kelly, Thin Solid Films 398/399, 553 (2001).

**Analytical considerations, design, and fabrication of a microfabricated fast GC x GC system for the DARPA Micro Gas Analyzer (MGA)**, E. B. Overton, J. Goettert, H. P. Dharmasena, A. Bhushan, D. Yemane, R. Simonson, D. Wheeler, D. Trudell, S. Dirke, 13th Intl. Conference On-Site Analysis, Arlington VA, January 2005.

**Angle-resolved Photoemission Spectroscopy**, P.T. Sprunger in: Synchrotron Radiation Applications to Materials Science (ed. P.T. Sprunger, CAMD/LSU Publishers, 2001) Chapt. 4:1-19.

**Angle-resolved photoemission study and first-principles calculation of the electronic structure of LaSb<sub>2</sub>**, A.I. Acatrinei, D Browne, Y B Losovyj, D P Young, M Moldovan, J.Y. Chan, P T Sprunger and R.L Kurtz, J. Phys.: Condens. Matter 15 (2003) L511-L517.

**Anomalous XANES spectra of octadecanethiol adsorbed on Ag(111)**, E.E. Doomes, P.N. Floriano, R.W. Tittsworth, R.L. McCarley, E.D. Poliakoff, Journal of Physical Chemistry B 107 (37): 10193-10197 (2003).

**Application of Scanning Acoustic Microscopy in Characterizing Metal Micro Gas Chromatograph Columns**, A. Bhushan, V. Challa, J. McKeon, D. Yemane, E. B. Overton, M. C. Murphy, J. Goettert, TMS Letters, 1 (7) (2004), pp. 145-146.

**Angle-resolved photoemission measurements of  $\pi$ -(n-pyrrolyl)alkanethiol self-assembled monolayers using *in-situ* sample preparation apparatus**, S. Hasegawa, T. Horigome, K. Yakushi, H. Inokuchi, K. K. Okudaira, N. Ueno, K. Seki, R. J. Willicut, R. L. McCarley, E. Morikawa, and V. Saile, J. of Electron Spectrosc. Relat. Phenom., 113, 101 (2001).

**Asymmetrical, Water-Soluble Phthalocyanine Dyes for Covalent Labeling of Oligonucleotides**, R.P. Hammer, C.V. Owens, S.H. Hwang, C.M. Sayes, and S.A. Soper, Bioconjugate Chem. 13, 1244-1252 (2002).

**Band structure symmetry effects in Gd multilayers grown on W(112)**, Ya. Losovyj, S.M. Zuber, and P.A. Dowben, Vacuum 74 (2004) 147-151.

**Beamline upgrade from PGM (SX700-type) to varied-line-space PGM at CAMD**, Maskai Ono, John D. Scott, and E. Morikawa, Eight International Conference on Synchrotron Radiation Instrumentation, AIP Conference Proceedings, 705, 360 (2004) (reviewed).

**BioMEMS using Electrophoresis for the Analysis of Genetic Mutations**, G.A. Thomas, H.D. Farquar, S. Sutton, R.P. Hammer, S.A. Soper, *Expert Rev. Mol. Diagn.* 2 (2002) 89.

**Borosilicate glass based x-ray masks for LIGA microfabrication**, Y. M. Desta, Y. Jin, J. Goettert, L. Jian, M. Bednarzik, B. Loechel, H. Scheunemann, D. Kim, S. Lee, M. D. Bryant, *Proc. SPIE Vol. 4979*, 2003, pp. 514-522.

**Bulk-defect Dependent Adsorption on a Metal Oxide Surface: S/TiO<sub>2</sub>(110)**, E. L. D. Hebenstreit, W. Hebenstreit, H. Geisler, C. A. Ventrice, Jr., P. T. Sprunger, and U. Diebold, *Surface Science Letters* 486 (2001) L467-L474.

**CAMD 6-m toroidal grating monochromator beamline**, K.D. Koch; C.V. Mohan; J.L. Erskine; P.T. Sprunger; J.D. Scott, *Nuclear Instruments & Methods in Physics Research Section A* 2002, Vol 483, Iss 3, pp 821-829.

**CAMD Six-meter Toroidal Grating Monochromator Beamline**, K. Koch, M. Chakka, J.L. Erskine, P.T. Sprunger, J. Scott, *Nucl. Instrum. & Meth. A*, 2001.

**Capillary and microelectrophoretic separations of ligase detection reaction products produced from low-abundant point mutations in genomic DNA**, Thomas, Gloria; Sinville, Rondedrick; Sutton, Shelby; Farquar, Hannah; Hammer, Robert P.; Soper, Steven A.; Cheng, Yu-Wei; Barany, Francis. *Electrophoresis* (2004), 25(10-11), 1668-1677.

**Catalytic CO oxidation on a dysprosium-promoted Pt(111) surface**, Ya. B. Losovyj, I.V. Ketsman, P. P. Kostrobij, and Yu. Suchorski, *Vacuum*, 63, 277 (2001).

**Cell transport via electromigration in polymer-based microfluidic devices**, Witek, Malgorzata A.; Wei, Suying; Vaidya, Bikas; Adams, Andre A.; Zhu, Li; Stryjewski, Wieslaw; McCarley, Robin L.; Soper, Steven A. *Lab on a Chip* (2004), 4(5), 464-472.

**Changes in Electronic Structure through a Disorder Transition in Gadolinium Adlayers on W(112)**, Ya. Losovyj, P.A. Dowben, *J Alloys Comp.* 401 (2005) 155-159.

**Changes in Electron-Phonon Coupling across a bulk phase transition in copolymer films of vinylidene fluoride (70%) with trifluoroethylene (30%)**, C.N. Borca, S. Adenwalla, J. Choi, Lee Robertson, H. You, V.M. Fridkin, S.P. Palto, N. Petukhova, and P.A. Dowben, *Applied Surface Science* 175-176 (2001) 265-269.

**Characterization and Application of PAG Diluted SU-8**, Z.G. Ling and K. Lian, *International Journal of Computational Engineering Science*, Vol.4 No.3, 533-536, 2003.

**Characterization and Application of PAG diluted SU-8**, Z.G. Ling, K. Lian and J. Zhang, *International Journal of Computational Engineering Science*, Vol. 4, No. 3 (2003) 529-532.

**Characterization of aluminum—organic-stabilized platinum-colloid network with electron and photon spectroscopies**, L. Beuermann, W. Maus-Friedrichs, S. Krischok, V.

Kempton, S. Bucher, H. Modrow, J. Hormes, N. Waldöfner, H. Bönemann, *Appl. Organometallic Chem.*, 17, 268, 2003.

**Characterization of microstructure and mechanical behavior of sputter deposited Ti-containing amorphous carbon coatings**, Feng B, Cao DM, Meng WJ, Xu J, Tittsworth RC, Rehn LE, Baldo PM, Doll GL *SURFACE & COATINGS TECHNOLOGY*148 (2-3): 153-162 DEC 3 2001.

**Characterization of size-dependent structural and electronic properties of CTAB-stabilized cobalt nanoparticles by X-ray absorption spectroscopy**, H. Modrow, N. Palina, C.S.S.R. Kumar, E.E. Doomes, M. Aghasyan, V.Palshin, R. Tittsworth, J.C. Jiang, J. Hormes, *Physica Scripta*, T115, 790-793, 2005.

**Characterization of sonochemically produced PdO nanoparticles by X-ray Absorption Near Edge Structure spectroscopy**, C.R. Kumar, H. Modrow, J. Hormes, *Particle and Particle Systems Characterization* 19, 336 (2002).

**Characterization of sulfur speciation in low molecular weight subunits of glutenin after reoxidation with potassium bromate at different pH values using X-ray absorption near-edge structure (XANES) spectroscopy**, A. Prange, B. Birzele, J. Krämer, H. Modrow, R. Chauvistre, J. Hormes, P. Köhler, *J. Agric. Food Chemistry*, 51, 7431, 2003.

**Characterization of the photo-irradiation effects on polystyrene ultrathin films with ultraviolet photoemission spectroscopy**, O. Kizilkaya, M. Ono, and E. Morikawa, *J. of Electron Spectrosc. Relat. Phenom*, 151, 34 (2005).

**Comment on "Spectral Identification of Thin Film Coated and Solid Form Semiconductor Neutron detectors" by McGregor and Shultis**, S. Hallbeck, A.N. Caruso, S. Adenwalla, J. Brand, Dongjin Byun, H.X. Jiang, J.Y. Lin, Ya.B. Losovyj, C. Lundstedt, D.N. McIlroy, W.K. Pitts, B.W. Robertson, and P.A. Dowben, *Nuclear Instruments and Methods in Physics Research A* 536 (2005) 228-231.

**Comparison of Crystalline Thin Poly(vinylidene (70%) - trifluoroethylene (30%)) Copolymer Films with Short Chain Poly(vinylidene fluoride) films**, Jaewu Choi, E. Morikawa, S. Ducharme and P.A. Dowben, *Matt. Lett.* 59 (2005) 3599-3603.

**Comparison of Simple Metal Doped Poly(vinylidene fluoride with trifluoroethylene) Copolymers by XPS**, B. Xu, Jaewu Choi, C. N. Borca, A. V. Sorokin, P. A. Dowben, S. P. Palto, N. Petukhova and S. G. Yudin, *Applied Physics Letters* 78 (2001) 448-450.

**Comparison of the  $\pi$ -Conjugated Ring Orientations in Polyaniline and Polypyrrole**, Jaewu Choi, Mircea Chipara, B. Xu, C.S. Yang, B. Doudin and P.A. Dowben, *Chem. Phys. Letters* 343 (2001) 193-200.

**Conformal deposition of Ti-C:H coatings over high-aspect-ratio micro-scale structures and tribological characteristics**, D. M. Cao, W. J. Meng, S. J. Simko, G. L. Doll, T. Wang, K. W. Kelly, *Thin Film Solids*, 429 (2003) 46-54.

**Contact Conductivity Detection in PMMA-Based Microfluidic Devices for the Transduction of Mono- and Polyionic Molecules**, M. Galloway, W. Stryjewski, D. Patterson, A. Henry, R.L. McCarley and S.A. Soper, *Anal. Chem.* 74 (2002) 2407.

**Contact Conductivity Detection of PCR Products Analyzed by Reverse-Phase Ion Pair Capillary Electrochromatography**, M. Galloway and S.A. Soper, *Electrophoresis* 23 (2002).

**Contact Voltage in Nanoparticle/Molecule Connections**, H. Modrow, S. Modrow, J. Hormes, N. Waldoefner, and H. Bönemann, *J. Phys. Chem. B*, Vol. 109, 900, 2005.

**Correlation between the atomic and electronic structures in Dy/Mo(112) and Gd/Mo(112) adsystems**, N.T. Dubyk, Ya.B. Losovyj, I.V. Ketsman and L.I. Ivankiv, *Vacuum*, 63, 67(2001).

**Correlations between heterocycle ring size and x-ray spectra**, E.E. Doomes, R.L. McCarley, E.D. Poliakoff, *Journal of Chemical Physics* 119 (8): 4399-4404 (2003).

**Cost Effective Masks for Deep X-ray Lithography**, H.-U. Scheunemann, B. Loechel, L. Jian, D. Schondelmaier, Y.M. Desta, J. Goettert; *Proc. SPIE* 5116, 2003.

**Cr-Diamondlike Carbon Nanocomposite Films: Synthesis, Characterization and Properties**, V. Singh, J.C. Jiang and E.I. Meletis; *Thin Solid Films*, Vol. 489 (1-2), 2005, 150-158.

**Cross Linking Behavior of Preceramic Polymers Effected by UV and Synchrotron Radiation**, M. Schulz, M. Boerner, J. Goettert, T. Hanemann, J. Hausselt, G. Motz; *Advanced Eng. Materials* 2004, 6, No. 8.

**Crystal structures of a multifunctional triterpene/flavonoid glycosyltransferase from *Medicago truncatula***, H. Shao, X. He, L. Achnine, J.W. Blount, R.A. Dixon, and X. Wang, *Plant Cell*, 17(11):3141-54, Nov. 2005.

**Crystalline Ice Grown on the Surface of the Ferroelectric Polymer Poly(vinylidene fluoride) (70%) and Trifluoroethylene (30%)**, Luis G. Rosa, Jie Xiao, Yaroslav B. Losovyj, Yi Gao, Ivan N. Yakovkin, Xiao C. Zeng, and Peter A. Dowben, *J. Am. Chem. Soc.* 127 (49) (2005) pp 17261 – 17265.

**Cu(0) Nanoclusters Derived from Poly(propylene imine) Dendrimer Complexes of Cu(II)**, P.N. Floriano, C.O. Noble, IV, J. M. Schoonmaker, E.D. Poliakoff, and R.L. McCarley, *J. Am. Chem. Soc.* 123, 10545-10553 (2001).

**Deep X-ray Lithography of SU-8 Photoresist: Influence of Process Parameters and Conditions on Microstructure Quality**, Y. Desta, H. Miller, J. Goettert, C. Stockhofe, V. Singh, O. Kizilkaya, Y. Jin, D. Johnson, W. Webber; *Book of Abstracts, HARMST05*, June 10-13, 2005, Gyeongju, Korea, pp. 70-71, 2005; June 2005.

**Deposition of highly hydrogenated carbon films by a modified plasma assisted chemical vapor deposition technique**, B. Shi, W. J. Meng, R. D. Evans, N. Hershkowitz, Surf. Coat. Technol. 200, 1543-1548 (2005).

**Design of a microfabricated device for ligase detection reaction (LDR)**, Barrett, Dwhyte O.; Maha, Amit; Wang, Yun; Soper, Steven A.; Nikitopoulos, Dimitris E.; Murphy, Michael C. Proceedings of SPIE-The International Society for Optical Engineering (2004), 5345(Microfluidics, BioMEMs, and Medical Microsystems II), 78-88.

**Detection of Low Abundant Mutations in DNA Using Single Molecule FRET and Ligase Detection Reactions**, M. Wabuyele, H. Farquar, R.P. Hammer, Y.-Wei Cheng, F. Barany and S.A. Soper, Proceedings of the Society of Photo-optical Instrumentation Engineers, 4962 (2003) 58-69.

**Differential Laterally Movable Gate FETs (LMGFETs) as a Position Sensor**, In-hyook Song and Pratul K. Ajmera, In Proc. of SPIE 11th Annual Intl. Symp. on Smart Structures and Materials, Vol.5389, pp 267-273, March 15-18, San Diego, CA, 2004.

**Dimensionality in the alloy-de-alloy phase transition of Ag/Cu(110)**, Kizilkaya O, Hite DA, Zhao W, Sprunger PT, Laegsgaard E, Besenbacher F, SURFACE SCIENCE 596, 242, 2005.

**Directed evolution of a ring-cleaving dioxygenase for polychlorinated biphenyl degradation**, Fortin, Pacal D., Ian Macpherson, David B. Neau, Jeffrey T. Bolin, and Lindsay D. Eltis, J Biol Chem. 2005 Dec 23;280(51):42307-14.

**Direct-LiGA service for prototyping – a status report**, B. Loechel, Y. Desta, J. Goettert; Book of Abstracts, HARMST05, June 10-13, 2005, Gyeongju, Korea, pp. 198-199, 2005; June 2005.

**Displacement synthesis of Cu shells surrounding Co nanoparticles**, Z.H. Guo, C.S.S.R. Kumar, L.L. Henry, E.E. Doomes, J. Hormes, E.J. Podlaha, J. Electrochem. Soc. 152(1), D1, 2005.

**Dopand concentration effect on NiO-doped sodium metaphosphate glasses: a combined X-ray absorption fine structure (XAFS) and UVNIS/NIR spectroscopic investigation**, B. Brendebach, R. Glaum, M. Funke, F. Reinauer, J. Hormes, H. Modrow, Z. Naturforschung Sect. A- A J. Physical Sci., 60(6), 449, 2005.

**Effect of substrate atomic structure on intersolubility and alloying in Pd/Nb adsorption system**, A. Ciszewski, J. Brona, S.M. Zuber, Z. Szczudlo, and Ya.B. Losovyj, Progress in Surface Science 74 (2003) 25.

**Effective Stabilization of Sulfate-Containing Soil: Mineralogical Evidence**, Wang, L., Roy, A., and Seals, R.K., Journal of the American Ceramic Society. Vol. 88, 1600-1606 (2005).



**Effects of MnO-doping on the structure of sodium metaphosphate glasses**, N. Zotov, H. Schlenz, B. Brendebach, H. Modrow, J. Hormes, F. Reinauer, R. Glaum, A. Kirfel, C. Paulmann, Z. Naturforschung, Section A-A J. Phys. Sciences, 58, 419, 2003.

**Efficacy of lytic peptide-bound magnetite nanoparticles in destroying breast cancer cells**, Kumar, Challa S. S. R.; Leuschner, Carola; Doomes, E. E.; Henry, Larry; Juban, Martha; Hormes, Josef, Journal of Nanoscience and Nanotechnology (2004), 4(3), 245-249.

**Electrochemical Micropump and Its Application in a DNA Mixing and Analysis**, D.E. Lee, H-P Chen, S.A. Soper, W. Wang, System Proceedings of the Society of Photo-optical Instrumentation Engineers, 4982 (2003) 264-271.

**Electronic Band Dispersion of Vertically Aligned Multiwall-Carbon Nanotubes**, Jaewu Choi, Seung Mi Lee, Young Chul Choi, Young Hee Lee, and J.C. Jiang, Chem. Phys. Lett. 349, 185 (2001)

**Electronic structure and metal-insulator transition in  $\text{SrTi}_{1-x}\text{Ru}_x\text{O}_3$** , M. Abbate, J.A. Guevara, S.L. Cuffini, Y.P. Mascarenhas, and E. Morikawa, Eur. Phys. J.B., 25, 203 (2002).

**Electronic Structure Modification of Multiwalled Carbon Nanotubes by Ion Bombardment and Thermal Treatment**, Jaewu Choi, Young Chul Choi, and Young Hee Lee, to be appeared ADC/FCT 2001 conference proceeding.

**Electronic structure of a surface quantum-wire array**, K. Yoo; S.J. Tang; P.T. Sprunger; I. Benito; J. Ortega; F. Flores; P.C. Snijders; M.C. Demeter; H.H. Weitering, Surface Science 2002, Vol 514, Iss 1-3, pp 100-107.

**Electronic, magnetic and geometric properties of functionalized magnetic nanoparticles**, J. Hormes, H. Modrow, H. Bonnemann and Challa S.S.R. Kumar, J. Appl. Phys. Lett (2005), 97(10), 10R102-10R102-6.

**Electron-phonon coupling and temperature-dependent shift of surface states on  $\text{Be}(10\bar{1}0)$** , S.J. Tang; Ismail; P.T. Sprunger; E.W. Plummer, Pys. Rev. B, 2002, Vol 65, Iss 23, art. no. 235428.

**Evidence for Multiple Polytypes of Semiconducting Boron Carbide ( $\text{C}_2\text{B}_{10}$ ) from Electronic Structure**, Petru Lunca-Popa, J.I. Brand, Snjezana Balaz, Luis G. Rosa, N.M. Boag, Mengjun Bai, B.W. Robertson, and P.A. Dowben, J. Physics D: Applied Physics 38 (2005) 1248-1252.

**Evidence for phonon effects in the electronic bands of granular  $\text{Fe}_3\text{O}_4$** , Ya.B. Losovyj and Jinke Tang, Materials Letters 59 (2005) 3828-3830.

**Evidence of possible band symmetry effects in STM studies of Gd overlayers**, Y.B. Losovyj, I.N. Yakovkin, S.D. Barrett, T. Komesu, P.A. Dowben, Surface Science 520, 43, 2002.

**Excitation of the symmetry forbidden bending mode in molecular photoionization**, J.S. Miller, E.D. Poliakoff, T.F. Miller, III, A.P.P. Natalense, and R.R. Lucchese, J. Chem. Phys. 114, 4496-4504 (2001).

**Expansion of SU-8 application scope by PAG concentration modification**, Z. Ling and K. Lian, Photonics West 2003: Micromachining and Microfabrication, 25-31 January 2003, San Jose, CA, USA, Proceedings of SPIE, vol.4979, 402-409, 2003.

**Experimental and full multiple scattering approaches to X-ray absorption near-edge structure spectra of chloronaphthalene in CH<sub>3</sub>I solvent**, K. Hayakawa, T. Fujikawa, K. Nakagawa, I. Shimoyama, R.C. Tittsworth, P.J. Schilling, V. Saile, CHEMICAL PHYSICS 289 (2-3): 281-289 APR 15 2003.

**Fabrication and Application of LIGA Microstructures**, Jost Goettert, Georg Aigeldinger, Yohannes Desta, Linke Jian, Kevin Kelly, Kun Lian, Zhong-geng Ling, Mike Murphy, Invited presentation at iMEMS 2001, Singapore, July 2001, Proc. of the Int. MEMS Workshop 2001, Singapore, July 2001, pp 62-72.

**Fabrication of an SU-8 based microfluidic reactor on a PEEK substrate sealed by a 'flexible semi-solid transfer' (FST) process**, Song, Yujun; Kumar, Challa S. S. R.; Hormes, Josef. Journal of Micromechanics and Microengineering (2004), 14(7), 932-940.

**Fabrication of DXRL and UDXRL masks by optical direct writing and x-ray lithography**, Z.G. Ling, K. Lian, Z. Peng, J. Kouba and J. Goettert, HARMST2003, Monterey, California, USA, Book of abstracts, pp. 47-48, 2003.

**Fabrication of micro-gas chromatograph columns for fast chromatography**, A. Bhushan, D. Yemane, D. Trudell, E. B. Overton, and J. Goettert, Book of Abstracts, HARMST05, June 10-13, 2005, Gyeongju, Korea, pp. 42-43, 2005, accepted for publication in Microsystem Technologies.

**Fabrication of Polymeric based Micro Fluidic Reactors Sealed by Semi-solid Transfer (FST) Process**, Yujun Song, Challa SSR Kumar and Josef Hormes, Journal of micromechanics and microengineering, 2004, 4, 932-940.

**Ferroelectric Polymer Langmuir-Blodgett Films**, S. Ducharme, S.P.Palto, V.M. Fridkin and L.M. Blinov, Book Chapter prepared for: Thin Film Handbook - Processing, Characterization and Properties, edited by H.S. Nalwa, (Academic Press), pp. 545-591.

**Ferroelectricity at Molecular Level**, L. Blinov, A. Bune, P. Dowben, S. Ducharme, V. Fridkin, S. Palto, K. Verkhovskaya, G. Vizdrik and S. Yudin, Phase Transitions 77 (2004)161-173.

**Field electron emission study of Ti and Hf adsorption layers on W**, Z. Szczudlo, A. Ciszewski, Ya. Losovyj, Appl. Surf. Sci., 174, 138(2001).

**Field Emission Properties of Vertically Aligned Carbon Nanotubes Driven by Polar and Non-Polar Gas Adsorption**, Youngsik Song, Brian Usner, Jaewu Choi, Seung-Chu Lim, and Young Hee Lee, to appear in 2001 Fall MRS Symp. Proceed.

**First results of digital topography applied to macromolecular crystals**, J.J. Lovelace, A.S. Soares, H.D. Bellamy, R.M. Sweet, E.H. Snell and G.E.O. Borgstahl. *J. Appl. Cryst.* (2004) 37, 481-485.

**Fluid-structure coupling analysis and simulation of a micromachined piezo microjet**, C. Liu, T. Cui, Z Zhou, K. Lian and J. Goettert, *Sensors and Actuators A*, 114 (2004) p.460-465.

**Fluid-structure coupling analysis and simulation of a micromachined piezo microjet**, C. Liu, T. Cui, Z. Zhou, K. Lian, and J. Goettert, *Transducers'03*, June 8-12, 2003, Boston, Vol. 2, 1271-1274.

**Fluorescence Multiplexing with Both Time-Resolved and Spectral Discrimination Capabilities using a Near-IR Microscope**, L. Zhu, W. Stryjewski, S. Lassiter, S.A. Soper, *Anal. Chem.* 75 (2003) 2280-2291.

**Formation and characterisation of Pt nanoparticle networks**, F. Wen, N. Waldofner, W. Schmidt, K. Angermund, H. Bönemann, S. Modrow, S. Zinoveva, H. Modrow, J. Hormes, L. Beuermann, S. Rudenkiy, W. Muas-Friedrichs, T. Vad, H.G. Haubold, *European J. Inorg. Chem.*, 18, 3625, 2005.

**Formation of aluminum oxide thin films on FeAl(110) studied by STM**, O. Kizilkaya, D. A. Hite, D. M. Zehner, P. T. Sprunger, *Surface Science*, 529, (2003), 223.

**Fracture toughness study on LIGA fabricated microstructures**, C. Oropeza, K. Lian and W. Wang, *Photonics West 2003: Micromachining and Microfabrication*, 25-31 January 2003, San Jose, CA. USA, *Proceedings of SPIE*, vol.4980, 183-191, 2003.

**Friction and wear characteristics of ceramic nanocomposite coatings: titanium carbide/amorphous hydrocarbon**, D. M. Cao, B. Feng, W. J. Meng, L. E. Rehn, P. M. Baldo, M. M. Khonsari, *Appl. Phys. Lett.* 79, 329 (2001).

**Functional microdevices using 'Nanoparticle-photoresist' composites**, G. Wiche, J.Goettert, Y.Song, J.Hormes and Ch.S.S.R.Kumar, *Int.J.Comp.Eng.Sci.*, 4(3), 525-528, (2003).

**Gas phase-dependent properties of SnO<sub>2</sub> (110), (100), and (101) single crystal surfaces: structure, composition, and electronic properties**, M. Batzill, K. Katsiev, J.M. Burst, U. Diebold, A.M. Chaka, B. Delley, *Phys. Rev. B* 72, 165414 (2005).

**Gold nanoparticles in polymer micro beads -one pot synthesis and XANES characterization**, Ch.S.S.R.Kumar, M.Aghasyan, H. Modrow, J. Hormes, and R. Tittsworth, *Journal of Metastable & Nanocrystalline Materials*, 23, 343-347, 2004.

**Graphite Membrane X-ray Masks for Rapid and Inexpensive - Prototyping of LIGA Structures**, Yohannes M. Desta, Jost Goettert, Linke Jian, Georg Aigeldinger, Michael C. Murphy, Phil Coane, Proc. HARMST 2001, June 2001, Baden-Baden, Germany.

**HARMST by means of SU-8 Based Optical Lithography and Deep X-ray Lithography**, L. Jian, Y. Desta, J. Goettert, K. Lian, M. Bednarzik, H.-U. Scheunemann, B. Loechel, H.O. Moser, O. Wilhelmi; Book of Abstracts, HARMST05, June 10-13, 2005, Gyeongju, Korea, pp. 76-77, 2005; June 2005.

**Heteroduplex Analysis of Mycobacterium Tuberculosis using High-Resolution Capillary Electrophoresis**, G. Thomas, L. Spring, V. Williams, and S.A. Soper, *Clin. Chem.* 47 (2001) 1195.

**High Aspect Ratio Microstructures Fabricated by X-Ray Lithography of Polymethylsilsequioxane-based Spin-on Glass Thick Films**, Y. Liu, T. Cui, P. Coane, M. Vasile and J. Goettert, presented at the HARMST 2001 Conference, June 2001.

**High Resolution X-ray Masks for High Aspect Ratio MEMS Applications**, L. Wang, T. Christenson, Y.M. Desta, R.K. Fettig and J. Goettert; *Journal of Micromechanics and Microengineering*, 14 (2004) S.722-26.

**High resolution x-ray masks for the application of high aspect ratio microelectromechanical systems (HARMS)**, L. Wang, Y. M. Desta, J. Goettert, Z. Ling, J. R. Kong, F. Aristone, Y. Jin, T. R. Christenson, K. Bradshaw, Proc. SPIE Vol. 4979, p. 508-513 (2003).

**High-aspect ratio neural probes for monolithic integration with ultra-low power CMOS operational amplifier circuit**, T. Xin, P. K. Ajmera, C. Zhang and A. Srivastava, In Proc. of SPIE 11th Annual Intl. Symp. on Smart Structures and Materials, Vol.5389, pp 20-25, March 15-18, San Diego, CA, 2004.

**High-energy X-ray diffraction study of Ni-doped sodium metaphosphate glasses**, H. Schlenz, F. Reinauer, R. Glaum, J. Neuefeind, B. Brendebach, J. Hormes, *J. Non-Crystalline Solids*, 351(12-13), 1014, 2005.

**Homogeneity of a supersaturated solid solution**, J.H. He, H.W. Sheng, J.S. Lin, P.J. Schilling, R.C. Tittsworth, E. Ma, *Phys. Rev. Lett.*, 89 (12): art. no. 125507 2002.

**Hot Embossing High-Aspect-Ratio Microstructures in Poly(Methylmethacrylate) for Constructing Microfluidic Devices with Integrated Components**, S. Qi, S. Ford, X. Liu, J. Barrows, G. Thomas, K. Kelly, A. McCandless, K. Lian, J. Goettert, S.A. Soper, *Lab-on-a-Chip* 2 (2002) 88.

**Imaging modulated reflections from a semi-crystalline state of profilin:actin crystals**, J.J. Lovelace, K. Narayan, J.K. Chik, H.D. Bellamy, E.H. Snell, U. Lindberg, C.E. Schutt and G.E.O. Borgstahl, *J. Appl. Cryst.* (2004) 37, 327-330.

**Implementation of an Ultra Deep X-ray Lithography System at CAMD**, Georg Aigeldinger, Jost Götttert; Timo Mappes, Franz-Josef Pantenburg, Louis Rupp, Proc. HARMST 2001, June 2001, Baden-Baden, Germany.

**In situ fabrication of SU-8 movable parts by using PAG diluted SU-8 as the sacrificial layer**, Z. Ling, K. Lian, Book of Abstracts, HARMST05, June 10-13, 2005, Gyeongju, Korea, pp. 153-154, 2005, accepted for publication in *Microsystem Technologies*.

**In situ study of the surface oxidation of FeCr alloys using grazing incidence X-ray absorption spectroscopy (GIXAS)**, J. Janssen, H. Rumpf, H. Modrow, R. Rablbauer, G. Frommeyer, J. Hormes, *Z. Anorg. Allg. Chemie*, 629, 1701, 2003.

**In situ study on the wet chemical synthesis of nanoscopic Pt colloids by "reductive stabilization"**, Angermund, M. Buhl, U. Endruschat, F.T. Mauschick, R. Mörtel, R. Mynott, B. Tesche, N. Waldofner, H. Bönemann, G. Köhl, H. Modrow, J. Hormes, E. Dinjus, F. Gassner, H.G. Haubold, T. Vad, M. Kaupp, *J. Phys. Chem. B* 107 (30): 7507, 2003.

**In situ sulfur K-edge X-ray absorption near edge structure of an embedded pyrite particle electrode in a non-aqueous Li<sup>+</sup>-based electrolyte solution**, D.A. Totir, M.R. Antonio, P. Schilling, R. Tittsworth, D.A. Scherson, *Electrochimica Acta*, 47 (19): 3195-3200, 2002.

**Industrial use of synchrotron radiation: a very subjective overview**, J. Hormes, H. Modrow, *Nucl. Instrum. Meth. A* 467, 1179, 2001.

**Influence of mycotoxin producing fungi (Fusarium, Aspergillus, Penicillium) on gluten proteins during suboptimal storage of wheat after harvest and competitive interactions between field and storage fungi**, A. Prange, H. Modrow, J. Hormes, J. Krämer, P. Kohler, *J. Agricultural and Food Chem.*, 53(17), 6930, 2005.

**Influence of Oxygen Plasma Treatment on the Microstructure of SnO<sub>x</sub> Thin Films**, J.C. Jiang, K. Lian and E.I. Meletis, *Thin Solid Film* 411, 203-210, 2002.

**Infrared Microspectroscopy Beamline at CAMD**, E. Morikawa, M. Ono, S. Kodukula, A. Bordelon, J. D. Scott, J. D. Garber, and R. S. Perkins, Eight International Conference on Synchrotron Radiation Instrumentation, AIP Conference Proceedings, 705, 364 (2004) (reviewed).

**Interaction between core and protection shell of N(butyl)<sub>4</sub>Cl<sup>-</sup> and N(octyl)<sub>4</sub>Cl<sup>-</sup>-stabilized Pd—colloids**, S. Bucher, J. Hormes, H. Modrow, R. Brinkmann, N. Waldöfner, H. Bönemann, L. Beuermann, S. Krischok, W. Maus-Friedrichs, V. Kempter, *Surface Science* 497, 321 (2002).

**Interconnected Multi-Level Microfluidic Channels Fabricated Using Low Temperature Bonding of SU-8 and Multilayer Lithography**, Z-C Peng, Z-G Ling, J. Goettert, J. Hormes, K. Lian; SPIE Photonics West 2005, Proceeding of SPIE Vol. 5718, 209-215.

**Interfacing a Polymer-based Micromachined Device to a Nanoelectrospray Ionization Fourier Transform Ion Cyclotron Resonance Mass Spectrometer**, Z. Meng, S. Qi, S.A. Soper, P.A. Limbach, *Anal. Chem.*, 73 (2001) 1286.

**Intrinsic stresses and mechanical properties of Ti-containing hydrocarbon coatings**, B. Shi, W. J. Meng, *J. Appl. Phys.* 94, 186 (2003).

**Investigation for the formation of polarization-induced two –dimensional electron gas in AlGaN/GaN heterostructure field effect transistors**, H.W. Jang, C.M. Jeon, K.H. Kim, J.K. Kim, S.B. Bae, J.H. Lee, Jaewu Choi, and J.L. Lee, *Phys. Stat. Sol. b*228, 621 (2001).

**Investigation of S-H bonds in biologically important compounds by Sulfur K-edge X-ray absorption spectroscopy**, A. Prange, C. Dahl, H.G: Trüper, M. Behnke, J. Hahn, H. Modrow, J. Hormes, *European Physical Journal D* 20, 489 (2002).

**Investigations into sulfobetaine-stabilized Cu nanoparticle formation: towards development of a microfluidic synthesis**, Y.J. Song, E.E. Doomes, J. Prindle, R. Tittsworth, J. Hormes, C.S.S.R. Kumar, *J. Phys. Chem. B* 109, 9330, 2005.

**Investigations of different human pathogenic and food contaminating bacteria and moulds Grown on selenite/selenate and tellurite/tellurate by X-ray absorption spectroscopy**, A. Prange, B. Birzele, J. Hormes, H. Modrow, *Food Control*, 16(8), 723, 2005.

**Investigations on the behaviour of C-60 as a resists in X-ray lithography**, H. Klesper, R. Baumann, J. Bargon, J. Hormes, H. Zumaque-Diaz, G.A. Kohring, *Applied Phys. A-Materials Science & Processing* 80(7), 1469, 2005.

**Iron and Manganese Minerals from South African Ironstone Deposits**, A. Roy, G.R. Byerly, D.R. Lowe, M.W. Walsh, and C. Bianchetti, *Physica Scripta*, in press (2003).

**Ironstone Pods in the Archean Barberton Greenstone Belt, South Africa: Earth's Oldest Seafloor Hydrothermal Vents Reinterpreted as Quarternary Subaeral Springs**, D.R. Lowe, and G. L. Byerly, *Geology* 31, 909-912 (2003).

**Is Magnetic Circular Dichroism Surface Sensitive In The Manganese Perovskites?**, C.N. Borca, R.H. Cheng, Shane Stadler, Y.U. Idzerda, Jaewu Choi, D.N. McIlroy, Q.L. Xu, S.H. Liou, Z.C. Zhong and P.A. Dowben, in: *Magnetoresistive Oxides and Related Materials*, Edited by: M. Rzchowski, M. Kawasaki, A.J. Millis, M. Rajeswari, S. von Molnár, *MRS Symp. Proc.* 602 (2001) 301-306.

**Ketones from Acid/Aldehyde Condensation Using Metal/CeO<sub>2</sub> Catalysts**, K.M. Dooley, A.K. Bhat, A.D. Roy and C.P. Plaisance, Proceedings, 19th North American Meeting, Catalysis Society, Philadelphia, 2005.

**Lattice-Stiffening Transition in Gadolinium Chains on Furrowed (112) Surfaces**, Ya.B. Losovyj, I.N. Yakovkin, Hae-Kyung Jeong, David Wisbey, and P.A. Dowben, J. Phys. Cond. Matter. 16 (2004) 4711-4724.

**Layer-by-layer nanoengineered magnetic encapsulation system for drug delivery**. Lu, Zonghuan; Prouty, Malcolm D.; Guo, Zhanhu; Kumar, Challa S. S. R.; Lvov, Yuri M., MSE Preprints (2005), 93, 656-657.

**LIGA fabricated high aspect ratio nickel gas chromatograph (GC) columns as a step towards a portable and fast GC instrument**, A. Bhushan, D. Yemane, J. Goettert, and E. B. Overton, The 5th Harsh-Environment Mass Spectrometry Workshop, Center for Ocean Technology, College of Marine Science /University of South Florida September 20-23 2005, Lido Beach Sarasota, Florida.

**LIGA Service at CAMD**, Jost Goettert, Georg Aigeldinger, Yohannes Desta, Josef Hormes, Linke Jian, Kun Lian, Zhong-Geng Ling, Shaloma Malveaux, Craig Stevens, Proc. 6<sup>th</sup> Commercialization of MEMS Conference (COMS2001), Oxford, September 2001.

**Local structure of composite Cr-containing diamond-like carbon thin films**, V. Singh, V. Palshin, R. Tittsworth and E.I. Meletis; Carbon In Press, Corrected Proof, Available online 9 December 2005.

**Low abundant biomarker screening in poly(methylmethacrylate) high aspect ratio microstructures using immunoaffinity-based molecular recognition**, Adams, Andre A.; Feng, Juan; Murphy, Michael C.; Soper, Steven A. Special Publication - Royal Society of Chemistry (2004), 296 (Micro Total Analysis Systems 2004, Volume 1), 132-134.

**Macrocycle-Derived Functional Xanthenes and Progress Towards Concurrent Detection of Glucose and Fructose**, O. Rusin, O. Alpturk, M. He, J. Escobedo, S. Jiang, F. Dawan, K. Lian, M. McCarroll, I. Warner, R. Strongin, Journal of Fluorescence, 14 (5) September 2004, p.611-615.

**Macromolecular Crystal Quality in Methods in Enzymology**, E. H. Snell, G.E.O. Borgstahl, and Bellamy, H.D. Macromolecular Crystallography Part C, Carter, C.W. and Sweet, R.M. Eds. Academic Press New York. 374:268-288 (2003).

**Magnetic Switch of Permeability for Polyelectrolyte Microcapsules Embedded with Co@Au Nanoparticles**, Zonghuan Lu, Malcolm D. Prouty, Zhanhu Gao, Vladimir O. Golub, Challa S.S.R. Kumar, Yuri M. Lvov, Langmuir, 21(5), 2042 -2050, 2005.

**Materials for LiGA and LiGA-based Microsystems**, J. Hormes, J. Gottert, K. Lian, Y. Desta, and L. Jian, Nuclear Instruments and Methods in Physics Research, B 199, 332-341, 2003.

**Measured Mechanical Properties of LIGA Ni Structures**, H.S. Cho, K.J. Hemker, K. Lian, J. Goettert and G. Dirras, *J. of Sensors and Actuators A*, 103 (2003) 59-63.

**Mechanical Property Evaluation and Failure Analysis of Cantilevered LIGA Nickel Microposts**, L. S. Stephens, S. Simhadri, A. B. McCandless, K. W. Kelly, E. I. Meletis, *Journal of MEMS*, Vol. 10, No. 3, Sept. 2001.

**MEMS-based piezoelectric array microjet**, S. Yuan, Z. Zhou, G. Wang, and C. Liu, *Microelectronic Engineering*, 66(2003), 767-772.

**Mercury and C2B10 Icosahedra Interaction**, Carolina C. Ilie, Petru Lunca-Popa, Jiandi Zhang, Bernard Doudin, Peter A. Dowben, *Mater. Res. Soc. Symp. Proc.* 848 (2005) FF6.5.1-FF6.5.6.

**Metal hybridization and electronic structure of Tris(8-hydroxyquinolato)aluminum (Alq3)**, A.N. Caruso, D.L. Schulz and P.A. Dowben, *Chem. Phys. Lett.* 413 (2005) 321.

**Methods for Polymer Hot Embossing Process Development**, P. Datta and J. Goettert; Book of Abstracts, HARMST05, June 10-13, 2005, Gyeongju, Korea, pp. 256-257, 2005; June 2005, accepted for publication in *Microsystem Technologies*.

**Micro Optical Fiber Display Switch Based on the Magnetohydrodynamic (MHD) Principle**, Kun Lian and Khee-hang Heng, *International Conference on Sensor Technology (ISTC2001)*, Proc. SPIE Vol 4414, 328-333, 2001.

**Microarrays Assembled in Microfluidic Chips Fabricated from Poly(methylmethacrylate) for the Detection of Low Abundant Mutations**, Y. Wang, B. Vaidya, Y.-Wei Cheng, F. Barany, H.D. Farquar, R.P. Hammer and S.A. Soper, *Anal. Chem.* 75 (2003) 1130-1140.

**Microfluidic devices fabricated in poly(methyl methacrylate) using hot-embossing with integrated sampling capillary and fiber optics for fluorescence Detection**, S. Qi, X. Liu, S. Ford, J. Barrows, G. Thomas. K. Kelly, A. McCandless, K. Lian, J. Goettert, and S. Soper, *Lab Chip*, vol.2, 88-95, 2002.

**Microfluidic Labware for Developing Biofunctional Surface on GMR Sensor**, M. Pease, V. Singh, P. Datta, O. Kizilkaya, E. Kornemann and J. Goettert; Book of Abstracts, HARMST05, June 10-13, 2005, Gyeongju, Korea, pp. 94-95, 2005; June 2005, submitted for publication to *Microsystem Technologies*.

**Micromolding of Pb and Zn with Surface Engineered LiGA Mold Inserts**, D. M. Cao, D. J. Guidry, W. J. Meng, K. W. Kelly, *Mat. Res. Soc. Symp. Proc.* 741, J10.5 (2003).

**Microstructure and Mechanical Properties of Ti-Si-N Coatings**, W. J. Meng, X. D. Zhang, B. Shi, R. C. Tittsworth, L. E. Rehn, P. M. Baldo, *J. Mater. Res.* 17(10), 2628 (2002).



**Microstructure and Microchemistry of Waste forms. Stabilization and Solidification of Hazardous, Radioactive and Mixed Wastes**, Book Chapter, Roy, A. and Cartledge, F.K, R. D. Spence and C. Shi. Boca Raton, Florida, CRC Press: 199-227, (2004).

**Microstructure and Tribological Behavior of Cr-DLC Nanocomposite films**, V. Singh, J.C. Jiang and E.I. Meletis, Mat. Res. Soc. Symp. **697**, (2002) 249-254.

**Microstructure Evolution and Surface Mechanical Properties of Electroplated Nickel as a Function of Processing Parameters**, Kun Lian, Jie Chao Jiang, Dean Guidry, Z-G Ling, Jost Goettert, E.I. Meletis, Proc. HARMST 2001, June 2001, Baden-Baden, Germany.

**Mineralogy of soil susceptible to sulfate attack after stabilization**, Wang, L., Roy, A., Tittsworth, R., and Seals, R.K., (2004), Journal of Materials in Civil Engineering - ASCE 16(4): 375-382.

**Mixed dissociated/molecular monolayer of water on the TiO<sub>2</sub>(011)-(2x1) surface**, T.J. Beck, A. Klust, M. Batzill, U. Diebold, C. Di Valentin, A. Tilocca, A. Selloni, Surf. Sci. Lett. 591, L267 (2005).

**Modal analysis of a unimorph piezoelectrical transducer**, C. Liu, T. Cui, and Z. Zhou, Journal of Microsystem Technologies, Vol. 9, No. 6-7(2003), 474-479.

**Model for chainlength-dependent core-surfactant interaction in N(Alkyl)<sub>4</sub>Cl-stabilized colloidal metal particles obtained from X-ray absorption spectroscopy**, H. Modrow, S. Bucher, J. Hormes, R. Brinkmann, H. Bönemann, J. Phys. Chem B, 107, 3684, 2003.

**Modeling and Validation of a Molded Polycarbonate Continuous-flow Polymerase Chain Reaction Device**, M.W. Mitchell, X. Liu, Y. Bejat, D.E. Nikitopoulos, S.A. Soper, M.C. Murphy, Proceedings of the Society of Photo-optical Instrumentation Engineers, 4982 (2003) 83-92.

**Molded multilevel modular microfluidic devices**, F. Aristone, P. Datta, Y.M. Desta, J. Goettert, Proc. SPIE Vol. 4982, pp. 65-72 (2003).

**Molding of Pb and Zn with microscale mold inserts**, D. M. Cao, D. Guidry, W. J. Meng, K. W. Kelly, Microsystem Technologies 9(8), 559 – 566 (2003).

**Monitoring thermal oxidation of sulfur crosslinks in SBR-elastomers by quantitative analysis of sulfur K-edge XANES spectra**, H. Modrow, F. Visel, R. Zimmer, J. Hormes, Rubber Chem. Technol. 74, 281, 2001.

**Multi-level Microstructures and Mold Inserts Fabricated with Planar and Oblique X-ray Lithography of SU-8 Negative Photoresist**, Linke K. Jian, Yohannes Desta, Jost Goettert, SPIE Proceedings Vol. 4557, San Francisco, 2001.

**Multiplexed fluorescence detection in microfabricated devices with both time-resolved and spectral-discrimination capabilities using near-infrared fluorescence**, Zhu, Li; Stryjewski, Wieslaw J.; Soper, Steven A., *Analytical Biochemistry* (2004), 330(2), 206-218.

**Nanocrystalline bulk and thin films of  $\text{La}_{1-x}\text{SrMnO}_3$  ( $0 \leq x \leq 0.3$ )**, Gnanasekar, X. Jiang, J.C. Jiang, M. Aghasyan, R. Tittsworth, J. Hormes, B. Rambabu, *Solid State Ionics*, 148, 575, 2002.

**Nanolithographic Manipulated Length of Aligned Metal Oxide Nanowires**, L.J. Campbell, Y.X. Chen, and W.L. Zhou, *Mat. Res. Soc. Symp. Proc.* 8, 23 (2004).

**Nanosopic Pt colloids in the embryonic state**, K. Angermund, M. Bühl, U. Endruschat, F.T. Mauschick, R. Mörtel, R. Mynott, B. Tesche, N. Waldöfner, H. Bönemann, G. Köhl, H. Modrow, J. Hormes, E. Dinjus, F. Gassner, H.-G. Haubold, T. Vad, *Angewandte Chemie International Edition* 41, 4041 (2002).

**Nanostructured Bulk and Thin Films of  $\text{LaSrMnO}_3$** , K.I. Gnanasekar, Xin Xiang, Josef Hormes, Roland Tittsworth, A. Mher and B. Rambabu, accepted for publication in the *Journal of Solid State Ionics* (June 2002), presented the paper in International Conference on Advanced Materials and Technologies (ICMAT 2001), July 1-6, 2001, National University of Singapore.

**Nanostructured  $\text{LiCoNiO}_2$  Cathode for Li ion Batteries**, K.I. Gnanasekar, Cathrino Henri, Anthony Narse, and B. Rambabu, accepted for publication in the *Journal of Solid State Ionics*, ICMAT 2001.

**Nanostructured Metal Clusters and Colloids**, U. Kreibitz, H. Bönemann, J. Hormes, In: H.S. Nalwa (ed.), *Handbook of Surfaces and Interfaces of Materials*, Vol. 3, 1-85, Academic Press, San Diego (2001).

**Near-infrared time-resolved fluorescence lifetime determinations in poly(methylmethacrylate) microchip electrophoresis devices**, Llopis, Shawn D.; Stryjewski, Wieslaw; Soper, Steven A. *Electrophoresis* (2004), 25(21-22), 3810-3819.

**Noncollinear spin states and competing interactions in half-metals and magnetic perovskites**, R. Skomski, J. Zhou, P.A. Dowben and D.J. Sellmyer, *Journal of Applied Physics* 97 (2005) 10C305.

**Noncovalent Functionalization of Single-Walled Carbon Nanotubes using Alternate Layer-by-Layer Polyelectrolyte Adsorption for Nanocomposite Fuel Cell Electrodes**, R.B. Dhullipudi, Y.M. Lvov, S. Adiddela, Z. Zheng, R.A. Gunasekaran, T.A. Dobbins, *Materials Research Society Symposium – Proceedings* 837, paper N3.27.1 (2005).

**Observation of filler-crosslink-interaction using XANES of the sulfur K-edge**, B. Brendebach, H. Modrow, *Kautschuk Gummi Kunststoffe* 55, 157 (2002).

**On the importance of defects in magnetic tunnel junctions**, P.A. Dowben and B. Doudin, in *Local Moment Ferromagnets: Unique Properties for Modern Applications*, Lecture Notes in Physics 678, Springer (2005), M. Donath and W. Nolting, editors, pp. 309-326, ISBN number 0075-8450.

**On the option of generating novel type surfaces with multiphilic ligands within the cavity of a giant metal-oxide based wheel type cluster: chemical reactions with well-defined nanoobjects**, A. Müller, S.K. Das, C. Kuhlmann, H. Boge, M. Schmidtman, E. Diemann, E. Krickemeyer, J. Hormes, H. Modrow, M. Schindler, *Chem. Commun. Z*, 655, 2001.

**Online CE-MALDI-TOF MS Using a Rotating Ball Interface**, Musyimi, Harrison K.; Narcisse, Damien A.; Zhang, Xia; Stryjewski, Wieslaw; Soper, Steven A.; Murray, Kermit K., *Analytical Chemistry* (2004), 76(19), 5968-5973.

**Orientation and bonding of 4,4'-biphenyldiisocyanide**, A.N. Caruso, R. Rajesh, G. Gallup, J. Redepenning and P. A. Dowben, *Journal of Physical Chemistry B* 108 (2004) 6910-6914.

**Orientation and bonding of biphenyldimethyldithiol**, A.N. Caruso, R. Rajesekaran, G. Gallup, J. Redepenning and P. A. Dowben, *Journal of Physics Condensed Matter* 16 (2004) 845-860.

**Overlapping solid solubility in mechanically alloyed Fe-Ni and Fe-Cu**, P.J. Schilling, V. Palshin, R.C. Tittsworth, J.H. He, E. Ma, *PHYSICAL REVIEW B* 68 (22): Art. No. 224204 DEC 2003.

**Patterning of surface-capture architectures in polymer-based microanalytical devices**, McCarley, Robin L.; Soper, Steven A.; Murphy, Michael C.; Wei, Suying; Smith, Alison F.; Vaidya, Bikas; Feng, Juan. *Special Publication - Royal Society of Chemistry* (2004), 297 (*Micro Total Analysis Systems* 2004, Volume 2), 130-132.

**Performance of the infrared microspectroscopy beamline at CAMD**, Kizilkaya O, Scott JD, Morikawa E, Garber JD, Perkins RS, *REVIEW OF SCIENTIFIC INSTRUMENTS* 76,13703, 2005

**Photohole Screening Effects in Polythiophenes with Pendant Groups**, D.-Q. Feng, A.N. Caruso, D. L. Shulz, Ya.B. Losovyj, and P. A. Dowben, *J. Phys. Chem. B*(2005) 109 (34) pp 16382-16389.

**Photoionization spectra of CH<sub>3</sub>I and C<sub>2</sub>H<sub>5</sub>I perturbed by CF<sub>4</sub> and c-C<sub>4</sub>F<sub>8</sub>: Electron scattering in halocarbon gases**, C. M. Evans, E. Morikawa and G. L. Findley, *J. Phys. B: At. Molec. Opt. Phys.*, 34, 3607 (2001).

**Physical and structural studies on the cryocooling of insulin crystals**, A. Vahedi-Faridi, J. Lovelace, H.D. Bellamy, E.H. Snell and G.E.O. Borgstahl, *Acta Cryst. D* 59:2169-2182 (2003).

**PLC Based Upgrades for the CAMD LINAC and Storage Ring Control System**, P. Jines and B. Craft, Proceedings of the 2001 ICALEPCS, 2001

**Polymer-based Microfluidic Systems for Biomedical Applications**, M.L. Hupert, M.A. Witek, Y. Wang, M.W. Mitchell, Y. Liu, Y. Bejat, D.E. Nikitopoulos, J. Goettert, M.C. Murphy and S.A. Soper, Proceedings of the Society of Photo-optical Instrumentation Engineers, 4982 (2003) 52-64.

**Polymer-Based Valves with Tunable Opening Pressures for Biomedical Applications**, C. Liu, Y. Qiu, K. Lian; SPIE Photonics West 2005, Proceeding of SPIE Vol. 5718, 179-185.

**Portable Coordinate Measuring Tool**, L. Jiang and M. Feldman, J. Vac. Sci. Technol. B 23, p. 3056, Nov./Dec. 2005.

**Possibility of the Fermi Level Control by VUV-induced Doping of an Organic Thin Film: polytetrafluoroethylene**, Masaki Ono, Hiroyuki Yamane, Hirohiko Fukagawa, Satoshi Kera, Daisuke Yoshimura, Eizi Morikawa, Kazuhiko Seki, and Nobuo Ueno, Proc. Int. Symp. Super-Functionality Organic Devices, IPAP Conf. Series 6, 27-30, (2005).

**Preparation of nanocrystalline BaTiO<sub>3</sub> characterized by in situ X-ray absorption spectroscopy**, H. Rumpf, H. Modrow, J. Hormes, H.-J. Gläsel, E. Hartmann, E. Erdem, R. Böttcher, K.H. Hallmeier, J. Chem. Phys. B105, 3415, 2001.

**Pressure studies of subthreshold photoionization: CH<sub>3</sub>I, C<sub>2</sub>H<sub>5</sub>I and C<sub>6</sub>H<sub>6</sub> perturbed by Ar and SF<sub>6</sub>**, C. M. Evans, E. Morikawa and G. L. Findley, Chem. Phys., 264, 419 (2001).

**Probing for mechanical and tribological anomalies in the TiC/amorphous hydrocarbon nanocomposite coating system**, B. Feng, D. M. Cao, W. J. Meng, L. E. Rehn, P. M. Baldo, G. L. Doll, Thin Solid Films 398/399, 210 (2001).

**Processing-Microstructures-Surface Modification and Resulting Materials Properties of LIGA Ni**, Kun Lian, J. Jiang, Z. Ling, J. Goettert, and J. Hormes; Book of Abstracts, HARMST05, June 10-13, 2005, Gyeongju, Korea, pp. 53-54, 2005; June 2005, accepted for publication in Microsystem Technologies.

**Quantitative speciation of sulfur in bacterial sulfur globules: X-ray absorption spectroscopy reveals at least three different speciations of sulfur**, Prange, R. Chauvistre, H. Modrow, J. Hormes, H.G. Trüper, C. Dahl, Microbiology -- UK 148, 267, (2002).

**Rapid PCR in a continuous flow device**, Hashimoto, Masahiko; Chen, Pin-Chuan; Mitchell, Michael W.; Nikitopoulos, Dimitris E.; Soper, Steven A.; Murphy, Michael C.. Lab on a Chip (2004), 4(6), 638-645.

**Rapid replication of polymeric and metallic high aspect ratio microstructures using PDMS and LIGA technology**, K. Kim, S. Park, J.-B. Lee, H. Manohara, Y. Desta, M. Murphy, C. H. Ahn, J. Microsystem Technologies, Volume 9, Issue 1-2, pp 5-10.

**Reaction mechanism of the exchange reaction between CuCl and BaO studied by time-resolved X-ray absorption spectroscopy**, H. Rumpf, J. Janssen, H. Modrow, K. Winkler, J. Hormes, J. Solid State Chemistry, 163, 158, 2002.

**Research and Service in LIGA Microfabrication at CAMD**, Jost Goettert, Georg Aigeldinger, Yohannes Desta, Linke Jian, Kun Lian, Zhong-Geng Ling, Shaloma Malveaux, Timo Mappes, Proc. HARMST 2001, June 2001, Baden-Baden, Germany.

**Resonantly amplified vibronic symmetry breaking**, G.J. Rathbone, E.D. Poliakoff, J.D. Bozek, and R.R. Lucchese, J. Chem. Phys. 114, 8240-8243 (2001) [Communication].

**Rotationally resolved photoionization: influence of the  $4\sigma \rightarrow k\sigma$  shape resonance on  $\text{CO}^+(\text{B}^2\Sigma^+)$  rotational distributions**, G. Farquar, J.S. Miller, E.D. Poliakoff, K. Wang, and V. McKoy, J. Chem. Phys., 115, 9764-9770 (2001).

**SEALS: A high brightness, low cost, light source proposal for the Southeastern USA**, V.P. Suller, M. Fedurin, J. Hormes, D. Einfeld, G. Vignola, Nuclear Instr. Methods in Phys. Research: Sect. A- Accelerators, Spectrometers, Detectors And Assoc. Equipment, 543(1), 23, 2005.

**Selective Deposition of Metals on Plastics Used in the Construction of Microanalytical Devices—Photo-Directed Formation of Metal Features on PMMA**, A.C. Henry and R.L. McCarley, *J. Phys. Chem. B* 2001, 105, 8755-8761.

**Sensing Interactions Between Vimentin Antibodies and Antigens for Early Cancer Detection**, C. Milburn, J. Zhou, O. Bravo, C. Kumar, and W. O. Soboyejo, *J. Biomed. Nanotech.* 1(1), 30-38, 2005.

**Simulation and design of micromixers for microfluidic devices**, Maha, Amit; Barrett, Dwhyte O.; Nikitopoulos, Dimitris E.; Soper, Steven A.; Murphy, Michael C. Proceedings of SPIE-The International Society for Optical Engineering (2004), 5345(Microfluidics, BioMEMs, and Medical Microsystems II), 183-193.

**Single crystal ice grown on the surface of the ferroelectric polymer poly(vinylidene fluoride) (70%) and trifluoroethylene (30%)**, Luis G. Rosa, Jie Xiao, Ya.B. Losovyj, Yi Gao, I.N. Yakovkin, Xiao C. Zeng and P.A. Dowben, *Journ. Am. Chem. Soc.* 127 (2005) 17261-17265.

**Single Molecule Analysis of dsDNA Molecules in Polymer Microfluidic Chips**, M. Wabuyeale and S.A. Soper, *Electrophoresis* 22 (2001) 3939.

**Single Pair FRET Generated from Molecular Beacon Probes for the Real-Time Analysis of Low Abundant Mutations**, M. Wabuyeale, W. Stryjewski, Y.-Wei Cheng, F. Barany, H. Farquar, R.P. Hammer and S.A. Soper, *JACS* 125 (2003) 6937-6945.

**Single photon-counting technology: for single-molecule detection applications in biotechnology**, Trotter, Claude; Davies, Murray; Dautet, Henri; Wabuyele, Musundi; Soper, Steven A.; Kapanidis, Achillefs N.; Lacoste, Thilo; Weiss, Shimon. *PharmaGenomics* (2004), 4(2), 24-26, 28-30, 32-34.

**Size-dependence of the Co-phase in nanocrystalline thin films “From the Atomic to the Nano-Scale” Proceedings of the International Workshop**, V.G. Palshin, R. Tittsworth, J. Hormes, E.I. Meletis, X.Nie, J. Jiang, H. Modrow, Old Dominion University Dec. 12th-14th 2002, (eds.: C.T. Whelan, J.H. McGuire), Old Dominion University, 2003, ISBN 0-9742874-0-7, p. 99 – 125.

**Solid Phase Reversible Immobilization in Microfluidic Chips for the Purification of Dye-Labeled DNA Sequencing Fragment**, Y. Zu, B. Vaidya, R.L. McCarley and S.A. Soper, *Anal. Chem.* 75 (2003) 2975-2984.

**Solid-phase immunoassay on polymer-based microanalytical devices**, Wei, Suying; Soper, Steven A.; McCarley, Robin L. *Polymer Preprints* (American Chemical Society, Division of Polymer Chemistry) (2004), 45(2), 434-435.

**Solid-state NMR and XANES studies of lithium and silver silicate gels synthesized by the gel-gel route**, A.A. Mrse, P.L. Bryant, F.J. Hormes, L.G. Butler, N. Satyanarayana, B. Rambabu, *J. Non-Crystalline Solids*, 318, 296, 2003.

**Some Applications of X-Ray Absorption Spectroscopy in the Study Cement and Concrete**, A. Roy, P.J. Schilling, R. Tittsworth, N. Moelders, and J.M. Schoonmaker, *The Cement Chemists' Science and Technology Newsletter*, Vol. 6, issue 1, June 2002, 5-11. (2002).

**Spatially resolved sulphur K-edge XANES spectroscopy for in situ characterization of the fungus-plant interaction Puccinia tritica and wheat leaves**, A. Prange, E.C. Oerke, U. Steiner, C.M. Bianchetti, J. Hormes, H. Modrow, *J. Phytopathology*, 153(10), 627, 2005.

**Status of the Center for Advanced Microstructures and Devices (CAMD) – 2001**, E. Morikawa, J. D. Scott, J. Goettert, G. Aigeldinger, Ch. S. S. R. Kumar, B. C. Craft, P. T. Sprunger, R. C. Tittsworth and F. J. Hormes, *Rev. Sci. Instrum.*, 73, 1680 (2002).

**STM observation of steps and terraces on tungsten (2 1 1) surface**, S. M. Zuber, Z. Szczudlo, A. Szczepkowicz, Ya. B. Losovyi and A. Ciszewski, *Ultramicroscopy* 95, (2003) 165-169. Available online 1 October 2002.

**Strain Induced half metal to semiconductor transition in GdN**, Chun-gang Duan, R.F. Sabiryanov, Jianjun Liu, W.N. Mei, P.A. Dowben and J.R. Hardy, *Physical Review Letters* 94 (2005) 237201.

**Structural characterization and transport studies of AgI-Ag<sub>2</sub>O-(MoO<sub>3</sub> + As<sub>2</sub>O<sub>5</sub>) glass system**, N. Satyanarayana, A. Karthikeyan, and B. Rambabu, *Phys. Chem. Glasses*, 2001, 42(1).

**Structural Characterization of a Novel Catalyst Obtained from Nanoscopic NiAl<sub>x</sub> by X-ray Absorption Spectroscopy**, H. Modrow, M.O. Rahman, R. Richards, J. Hormes, H. Bönnemann, *J. Phys. Chem. B*, 107, 2221, 2003.

**Structure analyses of Ba-silicate glasses**, H. Schlenz, A. Kirfel, K. Schulmeister, N. Wartner, W. Mader, W. Raberg, K. Wandelt, C. Oligschleger, S. Bender, R. Franke, J. Hormes, W. Hoffbauer, V. Lansmann, M. Jansen, N. Zotov, C. Marian, H. Putz, J. Neuefeind, *J. Non-Crystalline Solids*, 297, 37, 2002.

**Structure and Mechanical Properties of Ti-Si-N Ceramic Nanocomposite Coatings**, W. J. Meng, X. D. Zhang, B. Shi, J. C. Jiang, L. E. Rehn, P. M. Baldo, R. C. Tittsworth, *Surf. Coat. Technol.* 163/164, 251 (2003).

**Structure and mechanics of W-DLC coated spur gears**, J. C. Jiang, W. J. Meng, A. G. Evans, C. V. Cooper, *Surf. Coat. Technol.* 176, 50-56 (2003).

**Structure-property relationship of Si-DLC films**, Varma A., Palshin V., Meletis E.I., *Surface Coatings and Technology*, 148 (2-3): 305-314 DEC 3 2001.

**Study of ammonia-gas-induced irreversibility in polypyrrole films**, J. Choi, J. Hormes, P.K. Kahol, *Appl. Phys. Lett.*, 83, 2288, 2003.

**Studying Stacked Ultra Deep X-ray Lithography Exposures - Preliminary Results**, Georg Aigeldinger, Yohannes Desta, Jost Göttert, Franz-Josef Pantenburg, *SPIE Proceedings* Vol. 4557, San Francisco, 2001.

**SU-8 3D micro optic components fabricated by inclined UV lithography in water**, Z. Ling, K. Lian, *Book of Abstracts, HARMST05*, June 10-13, 2005, Gyeongju, Korea, pp. 94-95, 2005, accepted for publication in *Microsystem Technologies*.

**SU-8 as Negative Resist in Deep X-ray Lithography**, Linke Jian, Georg Aigeldinger, Yohannes M. Desta, Jost Goettert, *Proc. HARMST 2001*, June 2001, Baden-Baden, Germany.

**SU-8 based deep x-ray lithography/LIGA**, L. Jian, Y. M. Desta, G. Aigeldinger, M. Bednarzik, B. Loechel, J. Goettert, *Proc. SPIE* Vol. 4979, pp. 394-401 (2003).

**Sulfur in different chemical surroundings - S-K-XANES spectra of sulfur - containing heterocycles and their quantum - chemically supported interpretation**, B. Flemmig, H. Modrow, K.-H. Hallmeier, J. Hormes, J. Reinhold, R. Szargan, *Chem. Phys.* 270, 405, 2001.

**Sulfur in wheat gluten: In situ analysis by in-situ X-ray absorption near edge structure (XANES) spectroscopy**, A. Prange, N. Kühlsen, B. Birzele, I. Arzberger, J. Hormes, S. Antes, P. Köhler, *Eur. Food Res. Technol.* 212, 570, 2001.

**Sulfur on TiO<sub>2</sub>(110) studied with resonant photoemission**, E. L. D. Hebenstreit, W. Hebenstreit, H. Geisler, S. N. Thornburg, C. A. Ventrice, Jr., D. A. Hite, P. T. Sprunger, and U. Diebold, *Physical Review B* 6411 (2001) 5418.

**Surface Modification and Characterization of Microfabricated Poly(carbonate) Devices: Manipulation of Electroosmotic Flow**, B. Vaidya, S.A. Soper and R.L. McCarley, *Analyst* 127 (2002) 1289.

**Surface Modification of Polymer-based Microfluidic Devices**, S.A. Soper, M. Galloway, A.C. Henry, B. Vaidya, Y. Wang and R.L. McCarley, *Anal. Chim. Acta*, (2002) 1.

**Surface Modification of Silicon Containing Fluorocarbon Films Prepared by Plasma Enhanced Chemical Vapor Deposition**, Y. Jin, Y. Desta, J. Goettert, G. S. Lee and P. K. Ajmera, *J. Vac. Sci. Technol. A*, Vol. 23, No. 4, pp666-670, Jul/Aug (2005).

**Surface reconstruction of FeAl(110) studied by scanning tunnelling microscopy and angle-resolved photoemission spectroscopy**, O. Kizilkaya, D. A. Hite, D. M. Zehner, P.T. Sprunger, *Journal of Physics-Condensed Matter*, 16(30), 5395-5406 (2004)

**Surface resonances and reduced symmetry in the heteroepitaxial Ag/Cu(110) system**, D.A. Hite, O. Kizilkaya; P.T. Sprunger; E. Laegsgaard; F. Besenbacher, *Phys. Rev. B* 2002, Vol 65, Iss 11, art. no. 113411.

**Synthesis and characterization of S-Au interaction in gold nanoparticle bound polymeric beads**, Kumar, CSSR; Aghasyan, M; Modrow, H; Doomes, E; Henk, C; Hormes, J; Tittsworth, R, *JOURNAL OF NANOPARTICLE RESEARCH* AUG 2004, VOL 6, 4, 369-376.

**Synthesis of palladium nanoparticles using a continuous flow polymeric micro reactor**, Song, Yujun; Kumar, Challa S. S. R.; Hormes, Josef, *Journal of Nanoscience and Nanotechnology* (2004), 4(7), 788-793.

**Tapered LIGA HARMS**, R. Turner, Y. Desta, K. Kelly, J. Zhang, E. Geiger, S. Cortez, D. Mancini, *Journal of Micromechanics and Microengineering*, Volume 13, Issue 3 (May 2003), pp 367-372.

**Targeting breast cancer cells and their metastases through luteinizing hormone releasing hormone (LHRH) receptors using magnetic nanoparticles**, C. Leuschner, C.S.S.R. Kumar, W. Hansel, and J. Hormes, *J. Biomed. Nanotech.*, 1(2), 229-233, 2005.

**Temperature dependent induced spin polarization in Cr<sub>2</sub>O<sub>3</sub> on epitaxial CrO<sub>2</sub> film**, R.H. Cheng, T. Komesu, H.K. Jeong, L. Yuan, S.H. Liou, B. Doudin, P.A. Dowben, Y.B. Losovyj, *Physics Lett. A*, 302, 211, 2002.

**Temperature effects on microstructural evolution and resulting surface mechanical properties of Ni-based MEMS structures**, K. Lian, J. Jiang, Z. Ling, and E. Meletis, *Photonics West 2003: Micromachining and Microfabrication*, 25-31 January 2003, San Jose, CA. USA, *Proceedings of SPIE*, vol.4980, 192-199, 2003.



**Tensile, Creep and Fatigue Testing of LIGA-Ni Microsamples**, Kevin J. Hemker, H. S. Cho, Yohannes Desta, Kun Lian, Linke K. Jian, Jost Goettert, Proc. HARMST 2001, June 2001, Baden-Baden, Germany.

**The adsorption and decomposition of HS-(CH<sub>2</sub>)<sub>2</sub>-(CF<sub>2</sub>)<sub>7</sub>-CF<sub>3</sub> thin films on Au(111)**, A.N. Caruso, Ya.B. Losovyj, J. Choi, P.A. Dowben, Materials Letters 57 (2003) 3614-3617.

**The adsorption of chlorine on TiO<sub>2</sub>(110) studied with scanning tunneling microscopy and photoemission spectroscopy**, E.L.D. Hebenstreit; W. Hebenstreit; H. Geisler; C.A. Ventrice; D.A. Hite; P.T. Sprunger; U. Diebold, Surface Science 2002, Vol 505, Iss 1-3, pp 336-348.

**The Anomalous “Stiffness” of Biphenyldimethyldithiol**, D.Q. Feng, R. Rajesh, J. Redepenning and P.A. Dowben, Applied Physics Letters 87 (2005) 181918.

**The Band Offsets of Isomeric Boron Carbide Overlayers**, A.N. Caruso, P. Lunca-Popa, Y.B. Losovyj, A.S. Gunn, and J.I. Brand, Mater. Res. Soc. Symp. Proc. 836 (2005) L5.40.1.

**The Band Structure and Orientation of Molecular Adsorbates on Surfaces by Angle-resolved Electron Spectroscopies**, P.A. Dowben, J. Choi, E. Morikawa, and B. Xu, Chapter 2, Vol. 2 in “Thin Film Handbook”, Academic Press, H. S. Nalwa, Edt, (2001).

**The Coadsorption and Interaction of Molecular Icosahedra with Mercury**, Carolina C. Ilie, Snjezana Balaz, Luis G. Rosa, Jiandi Zhang, P. Lunca-Popa, Christopher Bianchetti, Roland Tittsworth, J.I. Brand, B. Doudin, P.A. Dowben, Applied Physics A 81 (2005) 1613-1618.

**The crystal structure of Escherichia coli heat shock protein YedU reveals three potential catalytic active sites**, Y. Zhao, D. Liu, W.D. Kaluarachchi, H.D. Bellamy, M.A. White, and R.O. Fox, Protein Science, 12:2303-2311 (2003).

**The Development of the Gadolinium Surface State**, Ya. Losovyj, I.N. Yakovkin, P.A. Dowben, Vacuum 74 (2004) 191-194.

**The Double-Tailed Normal-Incidence-Monochromator Beamline at CAMD**, E. Morikawa, C. M. Evans, and J. D. Scott, Rev. Sci. Instrum., 73, 1557 (2002).

**The effect of rock surface characteristics on reservoir wettability**, C.S. Vijapurapu, D.N. Rao and K.Lian, 13th Symposium on improved oil recovery, Tulsa, Oklahoma, 13-17 April 2002, SPE75211.

**The electronic structure and band hybridization of Co/Ti doped BaFe<sub>12</sub>O<sub>19</sub>**, Natalie Palina, H. Modrow, R. Müller, J. Hormes, P.A. Dowben and Ya.B. Losovyj, Materials Letters 60 (2006) 236-240.

**The electronic structure of metal/alkane thiol self-assembled monolayers/metal junctions for magnetoelectronics applications**, Y.A. Ovchenkov, H. Geisler, J.M. Burst, S.N. Thornburg, C.A. Ventrice Jr., C. Zhang, J. Redepenning, Y. Losovyj, L. Rosa, P.A. Dowben, B. Doudin, *Chemical Physics Letters* 381, 7-13 (2003).

**The Electronic Structure of Oriented poly(2-methoxy-5-(2'-ethyl-hexyloxy)-1,4-phenylenevinylene)**, David Keith Chambers, Srikanth Karanam, Difei Qi, Sandra Selmic, Ya.B. Losovyj, Luis G. Rosa and P.A. Dowben, *Applied Physics A* 80 (2005) 483-488.

**The Heteroisomeric Diode**, A.N. Caruso, Ravi B. Billa, Snjezana Balaz, Jennifer I. Brand and P.A. Dowben, *J. Physics Condensed Matter* 16 (2004) L139-L146.

**The influence of coordination geometry and valency on the K-edge absorption near edge spectra of selected chromium compounds**, A. Pantelouris, H. Modrow, M. Pantelouris, J. Hormes, D. Reinen, *Chemical Physics*, 300, 13, 2004.

**The influence of various coatings on the electronic, magnetic and geometric properties of Cobalt – nanoparticles**, J. Hormes, H. Modrow, H. Bönnemann, C.S.S.R. Kumar, *J. Appl. Physics*, 97(10), Art. No. 10R102 Part 3, 2005.

**The Limits to Spin-Polarization in Finite-Temperature Half-Metallic Ferromagnets**, P.A. Dowben and S.J. Jenkins. in *Frontiers in Magnetic Materials*, edited by Anant Narlikar, Springer Verlag (2005) 295-325.

**The New Normal-Incidence-Monochromator Facility at CAMD**, E. Morikawa, C. M. Evans, and J. D. Scott, J. D. Scott, *Proceedings of Application of Accelerators in Research and Industry: Sixteenth International Conference*, AIP Conference Proceedings, 576, 730 (2001).

**The photoemission from the gadolinium submonolayers on W(112)**, Ya. Losovyj, D. Wisbey, P.A. Dowben, *Synchrotron Radiation in Natural Science*, 3, N1-2, (2004) 76-77.

**The structure of coral allene oxide synthase reveals a catalase adapted for metabolism of a fatty acid hydroperoxide**, M.L. Oldham, A.R. Brash, & M.E. Newcomer, *Proc Natl Acad Sci U S A* 102, 297-302 (2005).

**The surface and materials science of tin oxide**, M. Batzill, U. Diebold, *Prog. Surf. Sci* 79, 47 (2005).

**The Surface Band Structure of W(112)**, Ya.B. Losovyj, I.N. Yakovkin, Hae-Kyung Jeong and P.A. Dowben, *Physica Status Solidi b*, 241 (2004) 829-839.

**The Surface Photovoltage Effects on the Isomeric Semiconductors of Boron-Carbide**, A.N. Caruso, Snjezana Balaz, Bo Xu, P.A. Dowben, A.S. McMullen-Gunn, J.I. Brand, Y.B. Losovyj, D.N. McIlroy, *Applied Physics Letters* 84 (2004) 1302-1304.

**The use of synchrotron microtomography for three-dimensional statistical characterization of non-aqueous phase liquids (NAPL) in porous media systems**, Willson, C.S. and R.I. Al-Raoush, 2001, Proceedings of the 2001 International Symposium on Environmental Hydraulics, Tempe, AZ, December 5-8, 2001.

**Theoretical study of the magnetic ordering in rare-earth compounds with face-centered-cubic structure**, Chun-gang Duan, R.F. Sabiryanov, Jianjun Liu, W.N. Mei, P.A. Dowben and J.R. Hardy, Journal of Applied Physics 97 (2005) 10A915.

**Thermal decomposition of  $(\text{NH}_4)_2[\text{PdCl}_6]$  studied by in situ X-ray absorption spectroscopy**, H. Rumpf, H. Modrow, J. Hormes, P. Amann, A. Möller, G. Meyer, J. Synchrotron Radiat. 8, 707, 2001.

**Thermal Stability and Resulting Surface Mechanical Properties of Electroplated Nanocrystalline Ni-Based MEMS Material**, K. Lian, J.C. Jiang, S. Wen, C.G. Liu and Z.G. Ling, International Journal of Computational Engineering Science, Vol.4 No.3, 529-532, 2003.

**Thermal stability and resulting surface mechanical properties of electroplated nanocrystalline Ni-based MEMS material**, K. Lian, J. Jiang, S. Wen, C. Liu, and Z.G. Ling, International Journal of Computational Engineering Science, Vol. 4, No. 3 (2003), 533-536.

**Thermal stability of SU-8 fabricated microstructures as a function of photo initiator and exposure doses**, K. Lian, Z. Ling, and C. Liu, Photonics West 2003: Micromachining and Microfabrication, 25-31 January 2003, San Jose, CA. USA, Proceedings of SPIE, vol.4980, 208-212, 2003.

**Thermal stability of SU-8 fabricated microstructures as a function of photo initiator and exposure doses**, K. Lian, Z.G. Ling, C. Liu, Proceedings of SPIE on Reliability, Testing, and Characterization of MEMS/MOEMS II, Jan. 27-29, 2003, San Jose, USA, Vol. 4980, 208-211.

**Three-Dimensional Chemical Analysis with Synchrotron Tomography at Multiple X-ray Energies: Brominated Aromatic Flame Retardant and Antimony Oxide in Polystyrene**, Ham, K. Hua, J., Al-Raoush, R.I., Xie, X, Willson, C.S., Byerly, G.R., Simeral, L.S., Rivers, M.L., Kurtz, R.L., Butler, L.G., 2004, J. Chemistry Materials 16 (21), 4032-4042.

**Tomography at the Louisiana State University CAMD synchrotron: applications to polymer blends**, L.G. Butler, K. Ham, H. Jin, R.L. Kurtz, Proceedings of SPIE-The International Society for Optical Engineering 2002, 4503, 54-61.

**Tomography at the LSU CAMD Synchrotron: Applications to Polymer Blends**, Butler, L. G.; Ham, K.; Jin, H.; Kurtz, R. L., in Proceedings of the SPIE, 2001, 4503, in press: Developments in X-Ray Tomography III, Aug 2-3 (2001) , San Diego, CA.

**Tuning surface properties of SnO<sub>2</sub>(101) by reduction**, M. Batzill, K. Katsiev, J.M. Burst, Y. Losvoyi, W. Bergermayer, I. Tanaka, and U. Diebold submitted to the Journal of Physics and Chemistry of Solids, as part of the Proceedings of the Third Meeting of the Study of Matter at Extreme Conditions (SMEC), May 2005.

**Tuning the oxide/organic interface: Benzene on SnO<sub>2</sub>(101)**, M. Batzill, K. Katsiev, U. Diebold, Appl. Phys. Lett. 85, 5766 (2004).

**Ultralow-k Silicon Containing Fluorocarbon Films Prepared by Plasma Enhanced Chemical Vapor Deposition**, Y. Jin, P. K. Ajmera, G. S. Lee, V. Singh, Journal of Electronic Materials, IEEE, Vol. 34, No. 9, pp1193-1205 (2005).

**Ultraviolet Photoelectron Spectroscopy Study of Synchrotron Radiation-Degraded Polyethylene Ultrathin Films**, Masaki Ono and Eizi Morikawa, J. Phys. Chem. B, 108, 1894 (2004).

**UPS Study of VUV-Photodegradation of Polytetrafluoroethylene (PTFE) Ultrathin Film by using Synchrotron Radiation**, Masaki Ono, Hiroyuki Yamane, Fumimasa Katagiri, Hirohiko Fukagawa, Satoshi Kera, Daisuke Yoshimura, Koji K. Okudaira, Eizi Morikawa, Kazuhiko Seki, and Nobuo Ueno, Nucl. Instr. and Meth., B236, 377 (2005).

**Using EDX/SEM to Study Heavy Metal Uptake and Elemental Composition in Plant Tissues**, Y. Qi, K. Lian, K.L. Chin, and R.L. Ford, Microsc Microanal 9 (Suppl 2), 1486-1487, 2003.

**Vibronic Coupling in the Valence Band Photoemission of the Ferroelectric Copolymer: poly(vinylidene fluoride) (70%) and trifluoroethylene (30%)**, Luis G. Rosa, Ya.B. Losovj, Jaewu Choi, and P.A. Dowben, J. Phys. Chem. B(2005) 109 (16) pp 7817-7820.

**Visual Detection of Cysteine and Homocysteine**, O. Rusin, N.N. St. Luce, R. A. Agbaria, J. O. Escobedo, S.Jiang, I. M. Warner, F. B. Dawan, K. Lian, and R. M. Strongin, J.Am. Chem. Soc. 126, 438-439, 2004.

**Welcome to the Journal of Biomedical Nanotechnology**, Kumar, Challa S. S. R., J. Biomed. Nanotech. (2005), 1(1), 1-2.

**X-ray absorption and photoemission electron spectroscopic investigation of crystalline and amorphous barium silicates**, S. Bender, R. Franke, E. Hartmann, V. Lansmann, M. Jansen, J. Hormes, J. Non-Crystalline Solids, 298, 99, 2002.

**X-ray absorption near edge structure (XANES) investigations of MnO<sub>y</sub>-doped sodium metaphosphate glasses and crystalline reference materials**, B. Brendebach, F. Reinauer, N. Zotov, M. Funke, R. Glaum, J. Hormes, H. Modrow, J. Non-Crystalline Solids, 251, 1072, 2005.

**X-ray absorption spectroscopy of bacterial sulfur globules: a detailed reply**, A. Prange, C. Dahl, H.G. Trüpper, R. Chauvistre, H. Modrow, J. Hormes, Microbiology-SGM, 148, 2268, 2002.

**X-ray Absorption Spectroscopy of Ti-doped NaAlH<sub>4</sub> at the Titanium K-edge**, E. Bruster, T.A. Dobbins, R. Tittsworth, D. Anton, Materials Research Society Symposium – Proceedings 837, paper N3.4.1 (2005).

**X-Ray Absorption Spectroscopy, Simulation and Modeling of Si-DLC Films**, V. Palshin, R.C. Tittsworth, E.I. Meletis, Journal of Materials Science, 37 (8): 1535-1539 APR 15 2002.



## Appendix B: User Report 2006





## Scientific Thrusts

### Life Sciences

#### ***Resisting Resistance: LSU-CAMD's Ongoing Battle to Keep Antibiotics Working***

Since the discovery of penicillin in 1928, the world has breathed a collective sigh of relief. Bacterial infections, once a slow and painful death sentence, could now be eradicated by something as simple as a small pill. It seemed that modern medicine had saved the day. But only four years after penicillin entered mass production, something strange happened. *Staphylococcus aureus*, more commonly known as staph, developed a resistance to the antibiotic. Other bacteria soon followed suit. Fast forward to today, and the problem has grown tremendously, threatening the efficacy of the drugs we depend on.

A general overuse of antibiotics has led to a dramatic increase in the growth of drug-resistant bacteria. The improper usage of these medications only fuels the already rapid spread of the problem. “We’re definitely seeing more resistant staph bacteria because of previous exposure to antibiotics,” said Dr. Waref Azmeh, an infectious disease specialist in Baton Rouge.

According to Dr. Azmeh, part of the issue is that patients are often capable of pressuring their physicians into prescribing antibiotics, even when the illness in question is viral and therefore not responsive to such medication. “Most viral infections get better on their own within three to four days and then the patient attributes that to the antibiotics. But it’s not so,” said Azmeh. “But patients expect a prescription, and it makes doctors feel like they’re doing something. And, often, once you have a bad habit, it sticks.”

Pharmaceutical companies are also partly to blame, as they diligently work to develop a constant barrage of new strategies for marketing antibiotics to physicians. “They’re getting smarter and smarter. They really know how to keep a product in your face constantly,” said Dr. Azmeh.

Several national health organizations, including the Infectious Diseases Society of America (IDSA), the Centers for Disease Control (CDC) and the Food and Drug Administration (FDA), among others, are engaged in long-term campaigns to educate the public about the dangers of improper antibiotic usage. But the numbers of resistant- bacteria continue to grow, and many scientists agree that we are perched on the brink of a world-wide health crisis.

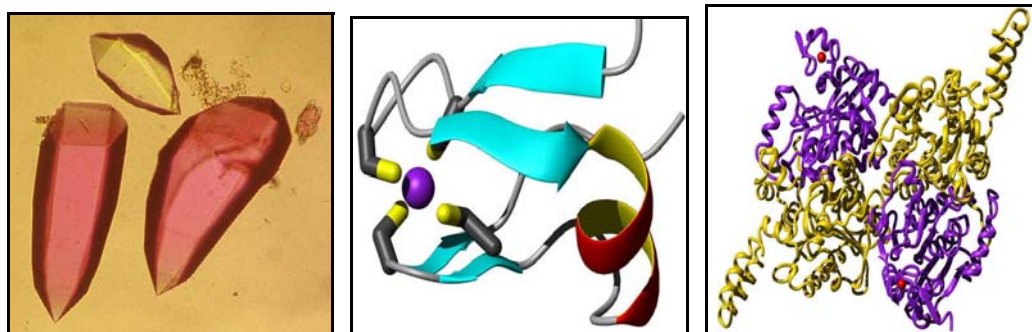
In 1974, 2% of staph bacteria showed resistance to antibiotics. That number jumped to 22% in 1995. Today we’re facing the astronomical figure of more than 60% of staph that are currently resistant to all forms of antibiotics except for one. And that last antibiotic is near-toxic and can cause serious side effects.

“It’s not a question of if, but when bacteria become completely resistant to existing antibiotics,” said Grover Waldrop, associate professor of biological sciences at LSU. “It’s happening as we speak. We are witnessing evolution in real-time.”

“It’s a significant problem,” agreed Azmeh. “For example, if staph is not treated within a few days, it can kill.”

Waldrop is currently waging war against these virulent strains of bacteria with the help of Pfizer Pharmaceuticals and LSU's Center for Advanced Microstructures and Devices (CAMD). As the only source of synchrotron radiation in the south, CAMD plays a pivotal role in providing Waldrop with the extremely intense X-rays necessary to design molecules that will inhibit resistance in bacteria. With luck, the molecules Waldrop is developing may be produced and distributed clinically to use as antibiotics that are essentially immune to bacterial resistance.

Basically, antibiotics work by targeting and destroying essential enzymes in the invading bacteria. Waldrop's research focuses on the inhibition of a particularly important enzyme called acetyl-CoA carboxylase (ACC), which is required to support bacterial growth.



**Left: Carboxyltransferase crystals; Center: Zn ribbon motif of carboxyltransferase; Right: Staphylococcus aureus carboxyltransferase.**

In order to find molecules that will bind and inhibit ACC, one must have an excruciatingly thorough knowledge of the three-dimensional structure of the enzyme. This approach, commonly known as structure-based design, is best understood through a simple analogy. “If the structure of the inside of a lock was understood in detail, then a key could be designed and manufactured to fit the lock,” said Waldrop. “In the case of enzymes, once the structure is known, a molecule that binds to it and prevents it from functioning can be designed and synthesized.”

The only way to determine these three-dimensional structures is through a process called X-ray crystallography, which is entirely dependent upon having access to the CAMD synchrotron's high-intensity X-rays. Because of this technology, Waldrop has already successfully determined the structure of ACC from several pathogenic bacteria, including staph. “It's only a step,” cautioned Waldrop, but it does bring them incrementally closer to finding a solution for this growing problem.

Drug discovery takes a minimum of 5-10 years and costs an average of \$500 million per drug. Because of the lag time between research and realization, it's that much more important to support studies like Waldrop's right now. However, according to Dr. Azmeh, pharmaceutical companies find little incentive in investing in antibiotic discovery. “A new antibiotic will most likely lose efficacy in 10-15 years. This is not a good investment. Bacteria are living organisms – they adapt.”

Azmeh says we are currently trapped in a situation where we're trying to get as much life as possible from a single drug before significant levels of resistance occur. “If no new drugs were to

be developed in the next five to ten years, the antibiotics we have now will lose effectiveness,” he said. “We will go back to the pre-antibiotic era, a time when infectious diseases were the number one killer in the population.”

For now, Waldrop is back in the lab, working hard to identify more ACC structures. “It’s not an exaggeration to say that we could not have succeeded to this point without CAMD. They’re playing a vital role in battling one of the most pressing health care problems currently facing our society.” And he’ll continue to work on the problem with CAMD and Pfizer as long as the pharmaceuticals company continues its support. “You can’t wait until the problem actually becomes an epidemic before you do something. Once it reaches that point,” he said, “it’s just too late.”

***Venezuelan Equine Encephalitis Virus Protease*** (Stanley Watowich, UTMB Galveston TX)

The CAMD Protein Crystallography beamline was used to determine the structure of a protein that the Venezuelan Equine Encephalitis (VEE) virus requires for replication. VEE is a mosquito-borne virus found in Central and South America, and southern Texas. Periodic outbreaks infect tens of thousands of people and kill hundreds of thousands of horses, donkeys and mules. The virus was developed into a biological weapon during the Cold War by both the United States and the Soviet Union. There is concern that terrorists could do likewise.

Dr. Andrew Russo in the lab of Prof. Stanley Watowich at the University of Texas Medical Branch at Galveston (UTMB) solved the structure of a protein called nsP2 protease. This protein is an enzyme that cuts a large viral protein into smaller segments at specific locations. Only the smaller segments are active for the replication of the virus. Therefore an inhibitor of nsP2 protease would prevent the virus from replicating and causing encephalitis.

Knowledge of the structure of nsP2 protease will enable vast data bases of known compounds to be screened by computers to find potential inhibitors of its function. The structure can also be used to design new compounds to test as inhibitors. Prof. Watowich says that potential inhibitors could be available for pre-clinical trials within two years.

The protein was isolated and crystallized at UTMB and initial data was collected there. The researchers then came to Baton Rouge to use the more powerful x-ray source provided by the CAMD beamline. The data from CAMD enabled them to see the structure in much greater detail which is essential for the design of inhibitors.

## Imaging

Tomography for 3D Chemical Analysis

Kyungmin Ham and Les Butler

CAMD, [kham1@lsu.edu](mailto:kham1@lsu.edu) and Department of Chemistry, LSU, [lbutler@lsu.edu](mailto:lbutler@lsu.edu);  
Chem-LB1206

Successful tomography requires efforts across a wide number of fronts, as evident by our activities of 2006.

Tomography is mathematically demanding. In a quest for more algorithms, we co-hosted a 120-person workshop entitled “3D Image Acquisition and Image Analysis Algorithms” at the Institute for Mathematics and Its Applications, University of Minnesota, Jan 9-12, 2006. Our co-hosts were Prof. Gestur Olafsson (LSU) and E. Todd Quinto (Tufts Univ.).

Tomography can be done with neutron, so as to yield information complementary to X-rays. We served on the international advisory committee for “Imaging and Neutrons 2006”, held at the Spallation Neutrons Source at Oak Ridge National Laboratory, Oct 23-25, 2006. The meeting registration reached 200 people, representing pulsed and reactor neutron sources as well as other imaging methods.

To address the need for more computational power, especially for “new” algorithms, we submitted this proposal to NSF: “CRI: IAD: Rapid Implementation of Mathematics into 3D Imaging Experiments via Parallel Computing”, Les Butler, Burak Aksoylu, Gabrielle D. Allen, Kyungmin Ham, Daniel S. Katz, NSF CISE-0708366, amount requested = \$135,491, submitted November, 2006.

We submitted for publication a description of the Greek golden ratio method of projection ordering [1] and a simulation of signal-to-noise issues in 3D chemical tomography [2].

The CAMD beamline was offline for experiments in much of 2006 for testing EXAFS experiments. We hope to have more tomography days in 2007. Our work is supported by an NSF grant: "Three-Dimensional Chemical Analysis and Molecular Dynamics Simulations: Application to Flame Retardants in Polymers", L. G. Butler and R. W. Hall, NSF CHE-0517326, \$450,000, 7/05 - 6/09.

[1] “Faster Tomography Data Acquisition based on the Greek Golden Ratio”, Rev. Sci. Instr., Ham, K.; Butler, L. G., submitted, Nov. 2006

[2] “Algorithms for three-dimensional chemical analysis via multi-energy synchrotron X-ray tomography”, Ham, K.; Butler, L. G., Nuclear Instruments & Methods in Physics Research Section B-Beam Interactions with Materials and Atoms, submitted, Dec. 2006

Recent applications of the beamline include biology, engineering, and chemistry. Tomography is revealing previously unknown structures in a cat claw [31]; the goal of this work is to better understand cornified tissues such as cat claws, bird beaks, and horse hooves, as shown in Figure 3 (Did you know that 15% of horses are afflicted by hoof diseases, leading to euthanasia for about 75%?).

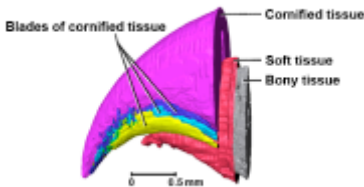


**Figure 3:** Composite image of a 3D reconstruction of tomography data, showing the relative positions of the basic tissues in the tip of the claw of the fifth digit of an adult cat (specimen #12, left paw) through synchrotron X-ray phase contrast tomography.

In environmental engineering, the fundamental aspects of hydrocarbon pollutant flow through aquifers is studied in 3D with tomography of synthetic and real aquifer materials and multiple fluids, as shown in Fig.4. These experiments are often performed as a function of a variable, such as pressure, raising the question, has the tomography sample stabilized at the new pressure setting? Mass transfer experiments as a function of time yield the distribution of hydrocarbons, water, and air in porous media. Rapid feedback regarding the temporally-varying hydrocarbon mass and distribution is crucial.

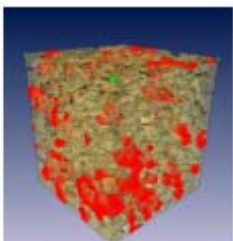


**Figure 4:** 3D rendering of sand (semi-transparent brown), entrapped oil (red), and water imaged at 12 micron voxel resolution with multi-energy synchrotron X-ray tomography.

Chemical applications include the analysis of polymer blends.[25, 38] Recently, a fiberglass-reinforced polymer blend with a new-generation flame retardant has been studied with multi-energy synchrotron X-ray tomography to assess the blend homogeneity.[28] Relative to other composite materials, this sample is difficult to image due to low contrast between fiberglass and the polymer blend. To investigate the chemical composition of this polymer blend, new procedures and algorithms were developed to produce, segment and analyze a chemical concentration distribution that assesses the flame retardant distribution throughout the blend. The

results show an extremely homogenous system to the level of the tomography resolution, 3.26  $\mu\text{m}$ . The processes and algorithms used herein include: (a) correction of reconstructed subvolumes absorption values, (b) model for chemical distribution, including the fiberglass matrix, (c) model for chemical distribution, excluding the fiberglass matrix, and (d) an algorithm for generating the radial concentration distribution about the glass fibers in the polymer matrix, Figure 5. Higher flux from the proposed MPW will enable faster acquisition and higher resolution experiments.

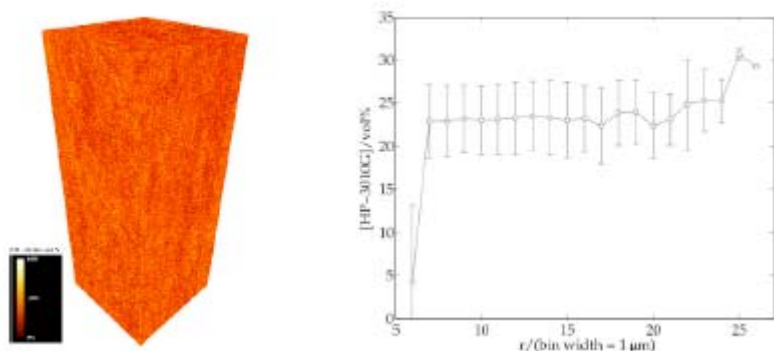


**Figure 5** Tomography results of a fiberglass-reinforced nylon (Albemarle Corp., Baton Rouge, LA) blended with a brominated flame retardant. (left) The 3D concentration in the  $200 \times 200 \times 500$  cuboid with 3.26  $\mu\text{m}$  voxels shows expected streaking due to exclusion by fiberglass and excellent blending in nylon (right). The radial concentration in the near vicinity of fiberglass (fiber radius = 5  $\mu\text{m}$ ).

Some examples of XAS research in Biological Sciences at CAMD are presented below.

The close proximity of CAMD to the laboratory of these researchers allowed great flexibility in sample preparations. All of these projects would benefit from the greater flux from the new wiggler because biological samples are generally very dilute.

- Dr. Marcia Newcomer (LSU Biological Sciences) is studying lipoxygenases and allene oxide synthases. The former are non-heme iron enzymes, and the latter, heme enzymes that structurally resemble catalase. Determination of the state of Fe in both types of enzymes is an essential step in this process.
- Dr. Huangen Ding (LSU Biological Sciences) is interested in identifying the nature of the ligand between iron and iron sulfur protein cluster A (IscA). The protein is suspected to transport iron in many biological processes.
- Drs. Thomas Gillis and Ramanuj Lahiri (National Hansen's Disease Program) are interested in iron transport in leprosy bacteria, *Mycobacterium leprae*, whose genome shows no siderophore-like proteins. Thus, the exact mechanism by which it transports iron is not understood. An Fe K-edge study may elucidate the iron-transport mechanism.

## Iron-binding site of IscA protein

Huangen Ding, Louisiana State University, [hding@lsu.edu](mailto:hding@lsu.edu); Katherine Buckalew, Louisiana State University, [kbucka2@lsu.edu](mailto:kbucka2@lsu.edu); PRN: BS-HD1206

This project is studying the bond between the protein IscA and iron. IscA is a protein believed to be involved in the formation of iron-sulfur clusters in biological systems. Besides storing iron and sulfur, these clusters have many purposes in cell functions, including participating in electron transport and controlling chemical reactions. Because these two elements do not bind spontaneously in concentrations that could be maintained by a living cell, it is believed a group of proteins must assist in the assembly. The formation of these clusters is still under investigation, although it is suspected that IscA facilitates iron transport. The understanding of IscA's part in the cluster forming process can be improved by discerning the bonds the molecule forms with iron. This can give information concerning how the metal attaches to the protein and is released to the iron-sulfur clusters. To further study IscA's role, the protein was synthesized and then allowed to bond with iron. By taking an X-ray spectrum of the molecule near the K-edges for iron and sulfur, the chemical bonds the protein makes with the metal can be determined. EXAFS and XANES theories provide methods to analyze the spectrum and determine the bonds on the iron atom.

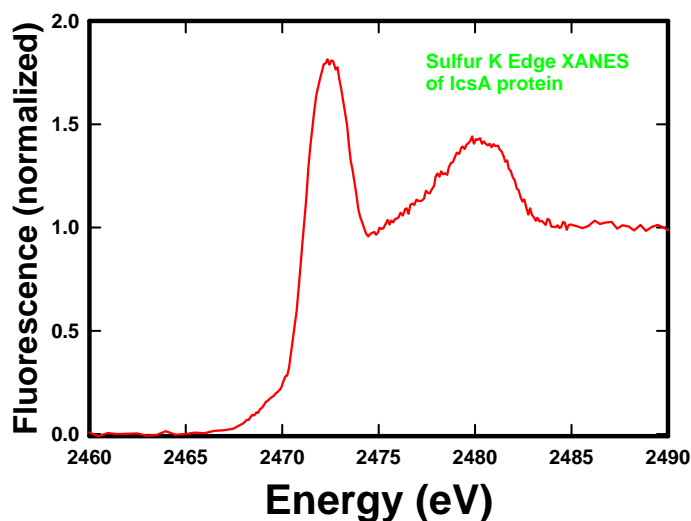


Figure 1. X-ray near edge absorption structure of sulfur in IcsA protein.

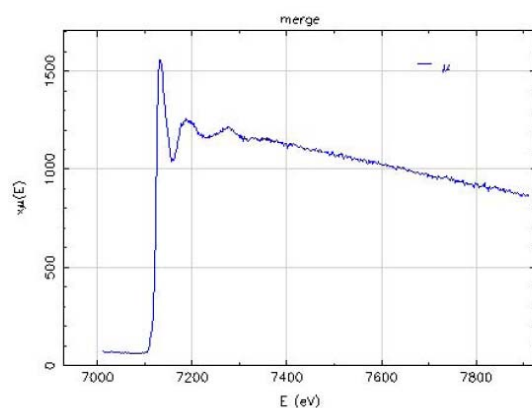
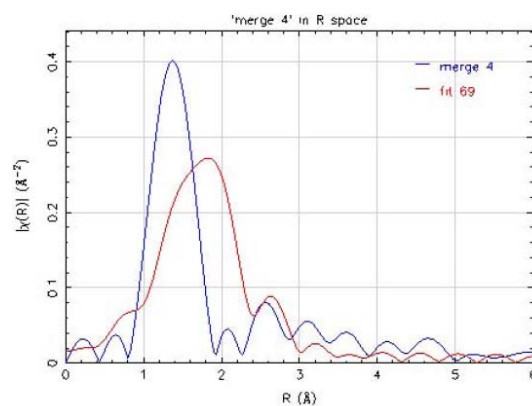


Figure 2. EXAFS spectrum of Fe K edge of iron in IcsA protein.

The scans made at the K-edge for iron can be analyzed using EXAFS theory, while scans made at the K-edge for sulfur can be analyzed using XANES theory. Fits were made using the program Artemis on the scans for the k-edge of iron comparing them to the bonds in iron sulfide.



XANES analysis of the sulfur scans will give information concerning the species of sulfur in the protein.

Further data analysis is in progress.



## Tomographic Imaging of Water Infiltration

David DiCarlo<sup>1</sup>, Larry Don Seale<sup>1</sup>, Kyungmin Ham<sup>2</sup>, and Clinton Willson<sup>2</sup>

<sup>1</sup>USDA Agricultural Research Service  
National Sedimentation Laboratory, Oxford, MS 38655.  
[ddicarlo@ars.usda.gov](mailto:ddicarlo@ars.usda.gov)

<sup>2</sup>Civil and Environmental Engineering, Louisiana State University  
Baton Rouge, LA 70803  
PRN# WPPRU-DD0607

The infiltration and drainage of water through the unsaturated zone plays an important role in the water cycling, aquifer recharge, pollutant transport as well as other processes. It is hypothesized that the pattern of the pores that are filled during infiltration can control the stability of large scale flows, with pore filling by collective mechanisms (piston-like filling) leading to preferential flow, and pore filling by individual mechanisms (snap-off filling) leading to stable flow. Thus micro-tomographic measurements of which pores are filled with water and which remain filled with air on infiltration are key to determining which pore filling processes take place. In particular, the images will provide definitive information on: (1) determining which pores are filled as a function of infiltration rate; (2) investigating the impact of the column walls on near-edge pores and throats; and (3) ascertaining whether or not wall effects have an impact on the flow and distribution of water.

From December 12-13, 2006, we completed a feasibility study using the tomographic beamline at The Center for Advanced Microstructures and Devices (CAMD) to non-destructively image columns of sand after infiltrations of varying rates have taken place. The feasibility study had several purposes. First, to determine whether the tomography could provide good images of our samples. Second, to determine the optimal doping of the water phase in order to maximize the contrast between the sand, water, and air phases within the tomographic image. Third, to determine the optimal scanning time for each sample (balancing the image quality with the speed of measurement). And fourth, to determine the optimal height of the sample to scan.

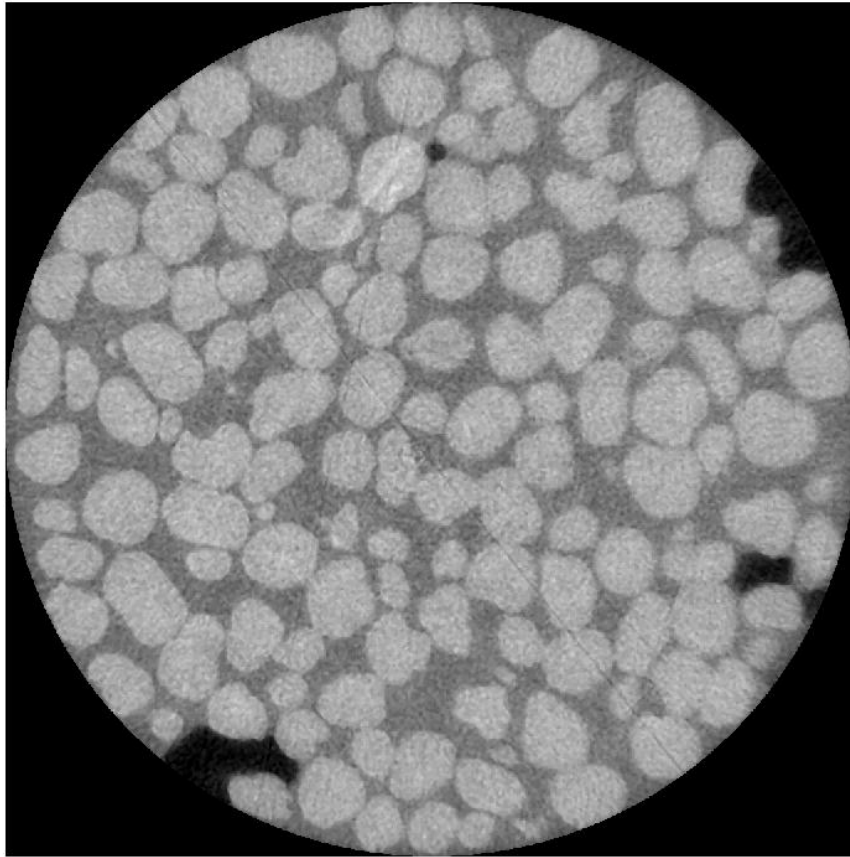


Figure 1: One tomographic slice through the experimental column. The sand (white), water (gray), and air (black) can be easily observed, and the occupancy of each pore recorded.

All of these goals were met. Figure 1 shows an example image obtained from such a tomographic scan within our sample. The image has a thickness of 9 microns, and the sand grains (white), the water (gray), and the air (black) can be easily delineated. This image was taken with a monochromatic beam of 35.3 KeV thus eliminating beam hardening in the image. Figure 2 shows a histogram of the CT values of the pixels within the sample tube, and there is very good separation of the CT values of sand, water, and air when the water is doped at 2% KI by weight. 10% and 0% KI solutions were also tried, but did not provide nearly as good a separation in CT values. This scan took 2 hours, and has close to the resolution of a 4 hour scan.

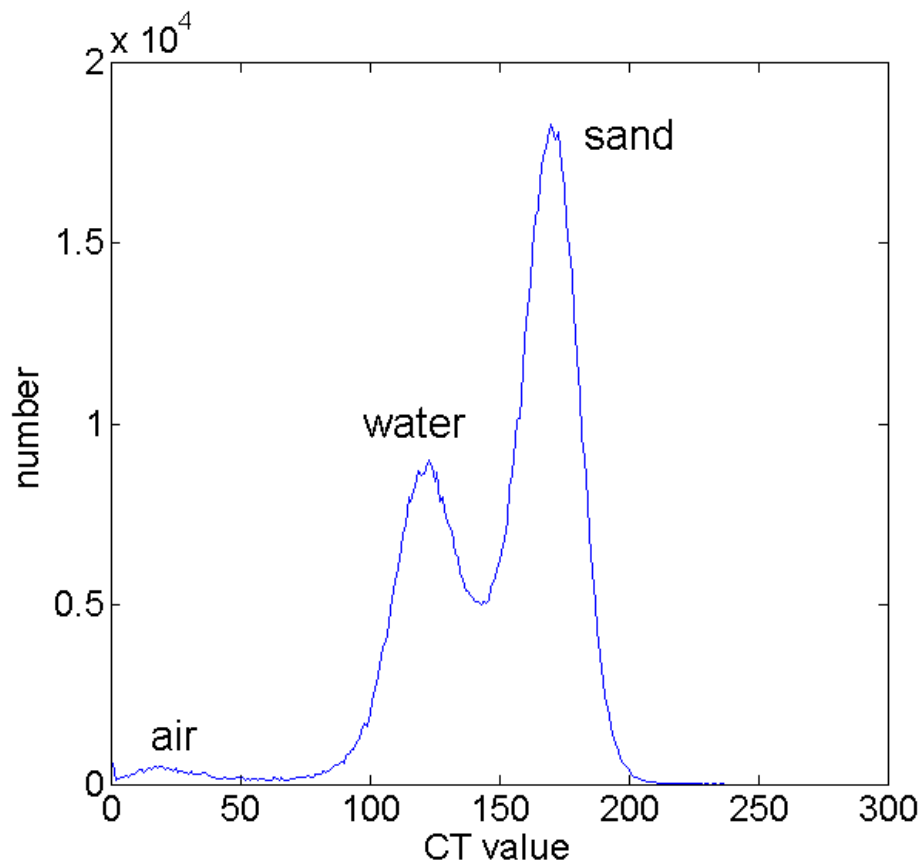


Figure 2: Histogram of the pixel values showing good separation in CT values between the air, water, and sand.

This feasibility study has shown that extremely good images can be obtained in less than 2 hours for the size of the sample that is necessary for our experiments. From these preliminary experiments we are already able to plot the water, sand and air fractions as a function of the distance from the center of the column. Figure 3 shows these data for one of our data sets. The tomography shows that there is large porous opening at the edge of the column, and a low porosity a small distance from the edge. The air filled porosity is preferentially at this edge. We are currently performing further analysis on these images taken in December 2006.

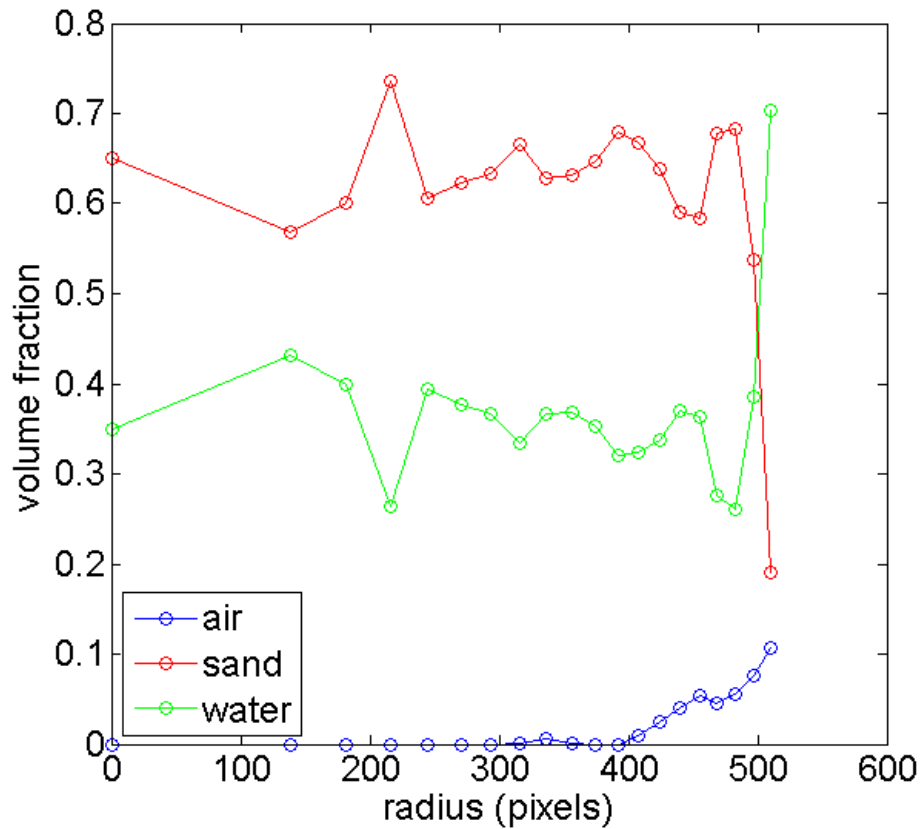


Figure 3: Radial dependence on the volume fraction of air, sand, and water. There is a big increase of porosity near the samples edge.

We plan to return to CAMD in the spring of 2007, to obtain an understanding of which pores are filled as a function of flow rate and grain size. These measurements will be a major data set to quantitatively compare models of pore filling, and provide physical insight to these processes.

**Characterization of the Iron Binding Site in IscA**  
Katherine Buckalew and Huangen Ding  
Department of Biological Sciences, Louisiana State University  
Baton Rouge, LA 70803  
E-mail: [hding@lsu.edu](mailto:hding@lsu.edu)  
PRN: BS-HD1206

The goal of this project is to explore the atomic structure of the iron binding site in IscA, a key member of the iron-sulfur cluster assembly machinery found in bacteria, yeast and humans. Undergraduate student Katherine Buckalew has been the driving force for this project. She has purified IscA from bacterium *E. coli*, reconstitute IscA with iron in the presence of the thioredoxin reductase system, and taken the EXAFS spectrum of the iron-loaded IscA. With the help from the members at CAMD, Katherine has finished the data collection and is now in the process of analyzing the data. A full publication on the iron binding site of IscA is anticipated in year 2007.

Undergraduate student: **Katherine Buckalew**

## Macromolecular Crystallography

### Crystal structure of the GAP-related domain of human IQGAP1

Jessica Ricks, Vinodh Kurella, Courtney Bryan, and David K. Worthylake

Department of Biochemistry and Molecular Biology, LSU Health Sciences Center, 1901

Perdido St., Room 7101, New Orleans, LA 70112 Phone (504) 568-5176

E-mail [dworth@lsuhsc.edu](mailto:dworth@lsuhsc.edu)

IQGAP1 is a widely expressed 190kD molecular scaffold that has an important role in cell adhesion and cell motility (for reviews see [1-6]). IQGAP1 possesses at least six distinct interaction domains including isoleucine and glutamine rich repeats (IQ) and a region of high sequence homology (16.9% identity, 45% similarity) to the GTPase-activating domain of p120RasGAP. IQGAP1 has been shown to bind to numerous proteins including F-actin, calmodulin, Erk2, CLIP-170,  $\beta$ -catenin, E-cadherin, APC, and the Rho-family small GTPases Cdc42 and Rac1. However, despite possessing a GAP-related domain (GRD), IQGAP1 has not been shown to accelerate the hydrolysis of GTP on any small GTPase. Instead, binding of Cdc42 or Rac1 to a region of IQGAP1 that includes the GRD significantly stabilizes the activated forms of Cdc42 and Rac1 *in vitro*. Furthermore, over-expression of IQGAP1 has been shown to increase the amount of activated Cdc42 *in vivo*. These results are consistent with a role for IQGAP1 as either a novel Cdc42 (or Rac1) effector, or as a newly discovered guanine nucleotide exchange factor (activator) for Cdc42 (or Rac1). To better understand the role of the GRD in IQGAP1 function, we have crystallized a 43kD fragment of IQGAP1 that encompasses the GRD.

Crystals of the GRD were initially characterized at the PX beamline in the summer of 2005. The crystals were shown to diffract to at least 2.5Å and belong to a primitive orthorhombic spacegroup ( $P2_12_12_1$  or  $P2_12_12$ ) with cell parameters  $a = 170.1\text{Å}$ ,  $b = 42.1\text{Å}$ ,  $c = 59.4\text{Å}$ . Volume considerations indicated unambiguously that just one GRD molecule occupied the crystal asymmetric unit. In the Fall of 2006, data extending to 2.2Å were collected (by Henry Bellamy) at the PX beamline at wavelengths corresponding to the minimum of dispersive differences, maximum of anomalous differences and a significant increase in dispersive differences for selenium atoms (incorporated as L-selenomethionine) within a single crystal of the GRD. The data were processed using HKL2000[7] and SHELXD[8] was used to locate all 10 selenium atoms in the  $P2_12_12$  asymmetric unit. A high quality experimental electron density map phased using MLPHARE and density modified using DM (CCP4 suite[9]) was used to guide model building with the program "O"[10] followed by cycles of refinement in CNS[11] using amplitudes and the maximum likelihood target with phase probability distribution (Hendrickson-Lattman coefficients from MLPHARE). Currently, the model includes 366 of the 383 residues in the GRD and has  $R_{\text{Free}} = 27.8$ ,  $R_{\text{Cyst}} = 24.8$  using data 25Å – 2.2Å and all  $|F|s > 0$ . The manuscript describing this structure is in preparation.

Information acquired during our visits to CAMD was utilized to secure Board of Regents funding (BOR 2006-09-RD-A-17) and has been included in a Centers of Biological Research Excellence (COBRE) application submitted in October 2006.

1. Briggs, M.W. and D.B. Sacks, *IQGAP proteins are integral components of cytoskeletal regulation*. EMBO Rep, 2003. 4(6): p. 571-4.
2. Briggs, M.W. and D.B. Sacks, *IQGAP1 as signal integrator: Ca<sup>2+</sup>, calmodulin, Cdc42 and the cytoskeleton*. FEBS Lett, 2003. 542(1-3): p. 7-11.
3. Brown, M.D. and D.B. Sacks, *IQGAP1 in cellular signaling: bridging the GAP*. Trends Cell Biol, 2006. 16(5): p. 242-9.
4. Noritake, J., et al., *IQGAP1: a key regulator of adhesion and migration*. J Cell Sci, 2005. 118(Pt 10): p. 2085-92.
5. Noritake, J., et al., *[Roles of IQGAP1 in E-cadherin-mediated cell-cell adhesion]*. Tanpakushitsu Kakusan Koso, 2006. 51(6 Suppl): p. 648-53.
6. Tirnauer, J.S., *A new cytoskeletal connection for APC: linked to actin through IQGAP*. Dev Cell, 2004. 7(6): p. 778-80.
7. Otwinowski, Z., *Data Collection and Processing*, ed. L. (Sawyer, N. Isaacs, and S. Bailey. 1993: Daresbury Laboratory, Warrington UK. 56-62.
8. Sheldrick, G.M.a.S., T.R., *SHELXL: High-resolution refinement*, in *Methods in Enzymology (Macromolecular Crystallography; Part B)*. 1997. p. 319-343.
9. CCP4, *CCP4*. Acta Crystallogr. Sec D, 1994. 50: p. 760-763.
10. Jones, T.A., et al., *Improved methods for building protein models in electron density maps and location of errors in these models*. Acta Crysta, 1991. A47: p. 110-119.
11. Brünger, A.T., et al., *Crystallography&NMR System: A New Software Suite for Macromolecular Structure Determination*. Acta Cryst., 1998. D54: p. 905-921.

## Crystallographic studies on mutant forms of Allene Oxide Synthase

Nathanial C. Gilbert and Marcia Newcomer

Department of Biological Sciences, Louisiana State University, Baton Rouge, LA 70803

A naturally occurring fusion protein consisting of an allene oxide synthase (AOS) domain and 8R-lipoxygenase (8R-LOX) domain has been discovered from a Caribbean soft coral, *Plexaura homomalla*. The combined sequential activities of 8R-LOX and AOS transform arachidonic acid into a water insoluble product, an allene oxide. AOS shares sequence, fold, and heme site similarities with catalases, but differs significantly in function as it lacks the proverbial catalase function of catalyzing the dismutation of hydrogen peroxide to water and molecular oxygen. AOS instead catalyzes the conversion of a hydrocarbon peroxide (8R-hydroperoxyeicosatetraenoic acid, the product of the 8R-LOX domain), into the epoxide. The structural basis for the difference in the functions of AOS and catalase is thought to reside in the heme environment. A valine residue in the active site is highly conserved in the catalase family, but the AOS has a threonine positioned in its place. The presence of the hydrogen bonding residue in AOS appears to confer the difference in function. Our collaborator performed site directed mutagenesis on AOS and changed the threonine to a valine. Catalase function was observed, albeit at a greatly reduced rate. Native AOS has an unusual planar heme which we perceive to directly correlate with lack of catalase activity. We wish to establish whether the heme environment is significantly altered in the mutant enzyme. These studies will provide insight into how heme geometry and environment affect function.



## The structures of heme enzymes of a newly described mini-catalase enzyme family

Svetlana Pakhomova, Alan Brash\*, Marcia Newcomer  
Department of Biological Sciences, LSU, Baton Rouge, LA 70803  
\*Vanderbilt School of Medicine

Our recently solved structure of an allene oxide synthase (AOS; Oldham, Brash, Newcomer, PNAS, 2005) from the soft coral *Plexaura Homomalla clearly* established a structural relationship between AOS and catalase: AOS resembles catalase both in terms of its overall fold (rmsd 1.65 Å for 225 of 373 Ca's) and heme environment, which is essentially completely conserved in a context of <15% sequence identity. Yet AOS and catalase have distinct enzymatic activities, and the basis for the different activities is not obvious from comparison of the structures. Differences in heme access, heme planarity and substrate recognition sites are proposed to contribute to the distinct functional properties of these enzymes. Other mini-catalases proposed to be involved in the metabolism of endogenous peroxides from *Fusarium graminearum*, *Anabaena*, *Mycobacterium avium* subsp. *paratuberculosis*, *Helicobacter pylori*, and *Pseudomonas aeruginosa* have been identified. These enzymes are associated with activities thought to be restricted to members of the P450 superfamily, heme enzymes with a Cys rather than Tyr as the proximal heme ligand. The identification of enzymes that are P450-like in activity, yet structurally dissimilar, is an important contribution towards understanding how protein environments tune heme activity. These enzymes, like AOS, are expected to promote the homolysis of the peroxide bound and generate a highly reactive free radical intermediate. Accordingly, the fate of the intermediate is determined by the shape of the binding pocket which constrains it. Thus the crystals structures will provide a framework with which to understand the chemical transformations catalyzed by "mini-catalases."

In 2005 we collected an Fe-MAD data set on the *Mycobacterium avium* subsp. *paratuberculosis* AOS-homologue and solved the structure to 2.4 Å resolution ( $R/R_{\text{free}}=0.194/0.231$ ) with Fe-MAD data collected at CAMD. In 2006 we collected data for another crystal form of this enzyme and solved the structure to 1.8 Å. These structures differ in heme planarity and ligation. The functional significance of these differences are under investigation.

## What features of the mini-catalase allene oxide-synthase (AOS) are essential for catalysis?

Nathan Gilbert, Alan Brash\*, Marcia Newcomer  
Department of Biological Sciences, LSU, Baton Rouge, LA 70803  
\*Vanderbilt School of Medicine

Modest differences in the heme environments of allene oxide synthase (AOS) and catalase lead to significantly different enzyme chemistries. There are three possible factors that may contribute to fundamental differences in catalytic mechanisms: the heme environment, heme conformation, and the nature of the substrate and its fit into the binding site. As part of an effort to understand how similar heme environments provide distinct catalytic activities, structural and functional studies on various mutant forms of AOS designed to test theories of catalytic mechanism are underway. We have initially focused on the fact that despite an open cavity that cannot exclude the approach of  $H_2O_2$  to the heme, AOS does not have catalase activity, nor is it rapidly deactivated by hydrogen peroxide. We have proposed that the fact that the distal His (H66) is H-bonded to both T66 (an invariant Val in catalase) and N137 protects an otherwise highly accessible heme. The prediction is then that a T66V mutation will open up the active site to pseudo-substrates. Indeed, a T66V mutation confers some catalase activity, albeit at a rate greatly reduced with respect to catalase. A structure of this mutation is necessary in order to fully understand its consequences and we have screened crystals for AOS:T66V at CAMD. In 2006 we collected a 1.8 Angstrom resolution data set of T66V:AOS in a novel crystal form. In contrast to what is seen for the wild type enzyme, the heme is not planar. Additional structures are being pursued to complete this work: a wild type enzyme in the same crystal form, as well as structures of the T66A and T66S mutants.

## **Structural studies on enzymes that confer resistance to the antibiotic fosfomycin**

Svetlana Pakhomova, Sue Bartlett, Marcia Newcomer  
Department of Biological Sciences, LSU, Baton Rouge, LA 70803

In an effort to elucidate the mechanism by which the enzymes FomA and FomB confer resistance to the common antibiotic fosfomycin, Svetlana Pakhomova has expressed, purified and crystallized the enzyme FomA. In 2006 she collected native data to 2.1 Angstroms resolution, as well as a potential derivative data set. She has now prepared crystals of the SeMet form of the enzyme and since December 2006 has been awaiting beam time for MAD data collection so that she can solve the structure. .

### **2006 Publications that cite CAMD**

Bilder, P., S. Lightle, et al. (2006). "The Structure of the Carboxyltransferase Component of Acetyl-CoA Carboxylase Reveals a Zinc-Binding Motif Unique to the Bacterial Enzyme(,)." Biochemistry **45**(6): 1712-1722.

Bordelon, T., S. P. Wilkinson, et al. (2006). "The crystal structure of the transcriptional regulator HucR from *Deinococcus radiodurans* reveals a repressor preconfigured for DNA binding." J Mol Biol **360**(1): 168-77.

Vander Kooi, C. W., M. D. Ohi, et al. (2006). "The Prp19 U-box Crystal Structure Suggests a Common Dimeric Architecture for a Class of Oligomeric E3 Ubiquitin Ligases(,)." Biochemistry **45**(1): 121-130.

## Structural Studies of U-box domain proteins

Craig W. Vander Kooi

Johns Hopkins School of Medicine - Dept. of Biophysics  
725 N Wolfe St, Hunterian 714  
Baltimore, MD 21205

and

Vanderbilt University - Center for Structural Biology  
5142 BIOSCI/Medical Research Building III  
Nashville, TN 37232-8725

(410)614-2533

Craig.Vanderkooi@jhmi.edu

Walter J. Chazin

Vanderbilt University - Center for Structural Biology  
5142 BIOSCI/Medical Research Building III  
Nashville, TN 37232-8725

(615)936-2210

walter.chazin@vanderbilt.edu

Daniel J. Leahy

Johns Hopkins School of Medicine - Dept. of Biophysics  
725 N Wolfe St, Hunterian 714  
Baltimore, MD 21205

(410)614-2533

dleahy@jhmi.edu

Post-translational modification of target proteins via covalent attachment of ubiquitin and other ubiquitin-like modifiers is a central biological regulatory mechanism. Addition of ubiquitin to target proteins is accomplished via an enzyme cascade consisting of activating (E1), conjugating (E2), and ligating (E3) enzymes. Our studies focus on E3 ligases, which have the critical task of bringing together the substrate and an activated ubiquitin-E2 conjugate, thereby catalyzing the formation of a covalent ubiquitin-substrate bond. In particular our studies focus on the most recently discovered family of E3 proteins, U-box domain E3 ligases.

Our structural studies have centered on the essential eukaryotic protein Prp19. A high-resolution structure of the homodimeric state of the Prp19 U-box was determined by X-ray crystallography to 1.5 Å with phases from three wavelength SeMet MAD. All data was collected at CamD. Combined with mutagenesis and biophysical characterization, these data allowed us to identify a common oligomeric architecture for E3 ubiquitin ligases.

### Publications:

Vander Kooi CW, Ohi MD, Rosenberg JA, Oldham ML, Newcomer ME, Gould KL, Chazin WJ. (2006) The Prp19 U-box crystal structure suggests a common dimeric architecture for a class of oligomeric E3 ubiquitin ligases. *Biochemistry*. 45, 121-130.

## The Structural Biology of Siderophore Production

Kathy Meneely, Jelena Zaitseva and Audrey Lamb

University of Kansas, Molecular Biosciences, 1200 Sunnyside Ave., Lawrence, KS 66049;  
[lamb@ku.edu](mailto:lamb@ku.edu); PX beamline

The long-term goal of this project is to understand in atomic detail the molecular mechanisms of siderophore production. Siderophores are frequently virulence factors for bacterial pathogens. If siderophore production is disrupted, the bacteria cannot acquire the iron required for survival in iron limiting environments such as the human host. *Pseudomonas aeruginosa* are notoriously antibiotic resistant and are able to colonize immuno-compromised patients and the lungs of patients with cystic fibrosis (CF). Other deadly bacteria use chemically similar siderophores in colonization of human tissues including *Yersinia spp.* Therefore, structural information about these biosynthetic enzymes may provide new anti-microbial targets for rational drug design of antibiotics for CF therapy, and secondary infections due to immunodepression in cancer, AIDS and burn patients, and also for the fight against bioterrorism.

We have sent seleno-methione crystals of two proteins to Dr. Henry Bellamy for multi-wavelength anomalous dispersion data collection: PchD, the salicylate adenylase from *P. aeruginosa*, and Irp3, the NADPH reductase from *Yersinia enterocolitica*. In both cases, we are still working to solve the phase problem for structure determination. We have not published any work related to these projects, nor have we submitted any grants based on this work. This ongoing work is being conducted by a post-doctoral fellow and a graduate student.

## Structural biology of interactions between Spy1294 and maltodextrins

Fang Han<sup>#</sup>, Sam Shelburne <sup>§</sup>, James Musser<sup>^</sup>, and Dar-Chone Chow<sup>\*#</sup>

From the <sup>\*</sup>Structural and Computational Biology and Molecular Biophysics Program, <sup>§</sup>Dept of Molecular Virology and Microbiology, and <sup>§</sup>Dept of Biochemistry and Molecular Biology, Baylor College of Medicine, Houston, Texas 77030, and <sup>^</sup>Methodist Hospital, Houston, Texas, and the <sup>#</sup>Department of Chemistry, University of Houston, 4800 Calhoun road, Houston, Texas 77204

Email: dchow@mail.uh.edu

This research project seeks to determine the chemical nature of the interactions between maltodextrins and the newly described maltodextrin-binding protein of group A Streptococcus, Spy1294 (GAS-spy1294) using x-ray protein crystallography and protein-maltodextrin binding kinetic methods. This Group A Streptococcus Spy1294 protein has quite different maltodextrin-binding characteristics, from specificity to binding thermodynamics, than that of the other better-known maltose-binding protein from Escherichia coli (Shelburne, S.A., Fang, H., Okorafor, N., Sumbly, P., Sitkiewicz, I., Keith, D., Patel, P., Austin, C., Graviss, E.A., Musser, J. M. and Chow, D.-C. 2007. MalE of Group A Streptococcus participates in the rapid transport of maltotriose and longer maltodextrins. Journal of Bacteriology. in press). These differences are providing insight into why GAS-spy1294 is essential for the pathogenic group A Streptococcus (GAS) bacteria to survive in human saliva to colonize the human throat, that in turn cause the pharyngitis, sore throat. The results of this investigation will further help us understand (1) the physical and chemical basis of the specificity of the maltodextrin-binding in GAS-spy1294, (2) the molecular basis for the maltodextrin-binding thermodynamics of GAS-spy1294, and (3) provide a relatively complete picture of the energetic landscape of the maltodextrin-binding and the structural details of chemical nature and physical configuration associated with the interaction.

We have successfully crystallized the complexes of Spy1294 with two different maltodextrins. The crystals of these two complexes show x-ray diffraction at a resolution better than 2 angstroms. We have collected x-ray diffraction data sets from these crystals at CAMD protein crystallography beamline. Currently, structural determination of the complexes is ongoing.

## Recognition of D-tyrosine by tyrosyl-tRNA synthetase

Eric A. First<sup>1</sup> and Gyanesh Sharma<sup>2</sup>

Department of Biochemistry and Molecular Biology, LSU Health Sciences Center in Shreveport,  
1501 Kings Highway, Shreveport, LA 71130, [efirst@lsuhsc.edu](mailto:efirst@lsuhsc.edu),  
PRN = LSUHS-EF1207

Tyrosyl-tRNA synthetase (TyrRS) plays an essential role in protein synthesis. Specifically, tyrosyl-tRNA synthetase catalyzes the attachment of tyrosine to the 3' end of tRNA<sup>Tyr</sup>. Understanding how tyrosyl-tRNA synthetase catalyzes this reaction is important because of both the central role that this process plays in protein synthesis and the potential for using this enzyme to introduce unnatural amino acids into proteins.

In contrast to other aminoacyl-tRNA synthetases, tyrosyl-tRNA synthetase is able to catalyze the attachment of both the L- and D-stereoisomers of its cognate amino acid to tRNA. Kinetic analysis indicates that (1) tyrosyl-tRNA synthetase binds the side chain of D-tyrosine in a manner similar to that of L-tyrosine, and (2) at least one of the carboxylate oxygen atoms in D-tyrosine is positioned for attack on the  $\alpha$ -phosphate of ATP. Preliminary structural analysis of the TyrRS•D-Tyr complex is in agreement with this model.

Surprisingly, in the presence of D-tyrosine, the binding of ATP is cooperative. This is in contrast to the binding of ATP to the TyrRS•L-Tyr complex, which exhibits hyperbolic kinetics. Replacement of Thr 234 by alanine in tyrosyl-tRNA synthetase results in an enzyme that displays hyperbolic kinetics with respect to the binding of ATP to the TyrRS•D-Tyr complex. This suggests that Thr 234 mediates the interaction between D-tyrosine and ATP. To understand the structural basis of this interaction, we have crystallized the wild type and T234A variants of tyrosyl-tRNA synthetase with either L- or D-tyrosine bound.

During the fourth quarter of 2006, we collected x-ray diffraction data at the Center for Advanced Microstructures and Devices (CAMD) synchrotron on the following tyrosyl-tRNA synthetase complexes: (1) wild type TyrRS•L-Tyr, (2) wild type TyrRS•D-Tyr, (3) T234A TyrRS•L-Tyr, and (4) T234A TyrRS•D-Tyr. We are currently determining the structures of these complexes using molecular replacement methods.

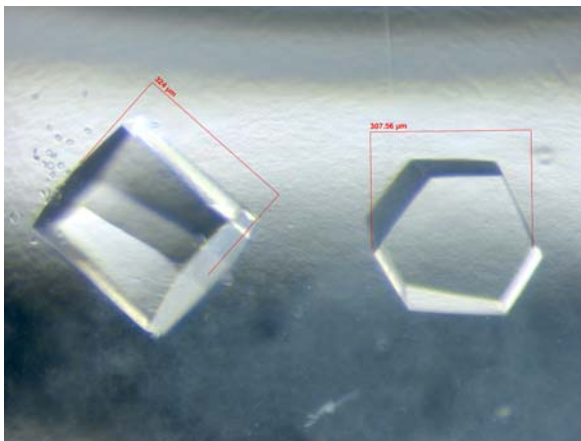


**Figure 1 – Crystals of the wild type TyrRS•D-Tyr complex.** The TyrRS•D-Tyr complex crystallized in the  $P3_121$  space group with unit cell dimensions of  $a = b = 63.765 \text{ \AA}$  and  $c = 234.29 \text{ \AA}$ .

ion (XAS) spectroscopy beamlines during the tions. During these years, experiments were magnet. The demands for XAS of higher-Z

elements have led to the plan to install a new beamline at the fourth port of the wavelength shifter. This will allow access to K edges up to 40 keV, but the flux will not be much increased.

The proposed MPW will produce much higher flux in the 3 to 40 keV range, comparable to the bending-magnet beamlines at medium-energy, third-generation rings. CAMD has three beamline scientists who oversee the XAS, small-angle scattering, and X-ray diffraction beamlines. These researchers work closely with the users and support them as needed. The XAS users come from diverse disciplines.

The Katrina flood waters were analyzed with traditional methods.[49] Dr. Amitiva Roy (USGS funding) studied metal (Cr, Fe, Cu, Zn) speciation in New Orleans soil samples.[50] Like many old cities, the soil in New Orleans has a very high Pb content which the new wiggler will allow us to characterize. • Dr. Annette Summers Engel (LSU Geology and Biological Sciences) is interested in the survivability of bacteria exposed to radiation at very high altitudes (which mimics conditions during Earth's early history). She has performed some exploratory work at CAMD related to sulfur and arsenic in bacteria and has received NSF funding to expand the arsenic work. • Several users at CAMD, including Dr. David Butcher from Western Carolina University, are interested in phytoremediation of toxic metals, As and Pb. XAS can provide information about speciation, and spatially-resolved measurements can be made with an X-ray microprobe. Since the 1990s, a large number of XAS studies related to phytoremediation have improved our understanding of the process.



## Environmental and Agricultural Science

### **Sifting Slush: Speciation of Heavy Metals in Katrina Sediments from New Orleans, Louisiana**

Amitava Roy, Christopher Bianchetti, Roland Tittsworth, and John Pardue

Hurricane Katrina, a Category 4 storm on the Saffir-Simpson scale, struck the Gulf Coast of Louisiana on August 29<sup>th</sup>, 2005. The storm surge resulted in breaches of the levee system in New Orleans at least at two locations, flooding up to 80% of the city. The floodwater also brought sediment which was left behind once the water receded after a few days.

The flood water was sampled in the Mid-City and Lakeview areas of New Orleans within five days by Dr. John Pardue and his co-workers from the Civil and Environmental Engineering Department of LSU. The concentrations of metals such as iron, zinc and copper in the flood water were often elevated compared to EPA drinking water standards, but rarely exceeded the limits. The metal concentrations conformed to those typically expected in urban storm water.

Dr. Pardue and his group went back to New Orleans after the flood water receded and collected sediment samples. Dr. Amitava Roy and his colleagues at CAMD collaborated with Dr. Pardue to investigate the speciation of metals in Katrina sediments.



Figure 1

Sediment samples were obtained from the Lakeview and Mid City areas of New Orleans (Figure 1). The sediments contained highly diverse materials, including broken Mardi Gras beads.



Iron oxide coated particle in the sediment from Lakeview neighborhood (left) and a clay mineral-rich particle.



Sediment samples from Mid City. There are particles of asphalt, quartz, and rounded glass. The reddish areas are coating of iron oxide.

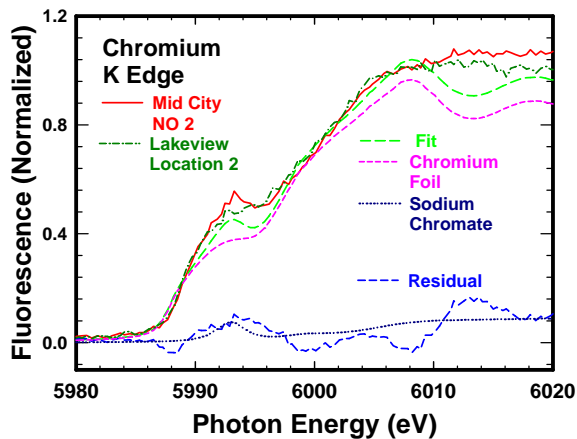


Figure 3

Chromium K edge spectra from specimens from two sites show a distinct pre-edge peak at around 5993 eV (Figure 3) due to hexavalent chromium. The peak is more prominent for the sample from Mid City New Orleans. Least squares fitting for these spectra showed the Mid City sample contained ca. 10% by weight of this toxic metal or a total of 3 ppm.

There is quite a bit of variation in speciation of the metals at the two sites and even within a single neighborhood. One sample from the Mid City region showed both copper and zinc in reduced (metallic) state but iron appeared in II+ oxidation state.

The variation in speciation to some extent represents the variation in the sources themselves. There is a wide variation in mineralogy and chemistry of the sediments in a neighborhood and between them. This suggests that there sources could be different and/or there is mixing of sediments coming from different sources. The floodwater not only entrained the local particulate matter but also brought in sediments from the surrounding water bodies, such as Lake Pontchartrain and the canals joining the Mississippi River with the Gulf of Mexico.

## Are microbes involved in the reducing of arsenate and chromate by *Nasturtium officinale*: An *in vitro* cultivation and X-ray absorption spectroscopy study

Anika N. S. Brünig<sup>1</sup>, Josef Hormes<sup>2,3</sup>, and Alexander Prange<sup>2,4</sup>

<sup>1</sup>Institute of Ornamental and Woody Plant Science, Leibniz University Hannover, Herrenhäuser Straße 2, D-30419- Germany

<sup>2</sup>Center for Advanced Microstructures and Devices, Louisiana State University, 6980 Jefferson Hwy., Baton Rouge, LA 70806, USA

<sup>3</sup>Institute of Physics, University of Bonn, Nussallee 12, D-53115 Bonn, Germany

<sup>4</sup>Microbiology and Food Hygiene, Niederrhein University of Applied Sciences, Rheydter Straße 277, D-41065 Mönchengladbach, Germany

Correspondence to: J. Hormes, e-mail: [hormes@lsu.edu](mailto:hormes@lsu.edu) (physical aspects) and A. Prange, e-mail: [A.Prange@gmx.de](mailto:A.Prange@gmx.de) (biological aspects)

### Introduction

The use of plants to remove or detoxify heavy metals from soil, surface waters or air is recently evolving the field of science. Often plants are used to convert elemental heavy metals and pollutants to a less toxic chemical species (i.e. transformation) [1]. Experiments are mostly performed in very complex plant-soil systems with complex compositions. Furthermore, in these complex systems a lot of (different) microbes are present. Therefore, it is an important topic to clarify whether the plants themselves remove or detoxify heavy metals or whether microbes are involved in the process. To investigate this topic, experiments have to be performed under sterile and -as far as possible- defined growth conditions like the so-called *in vitro* culture of plants. *In vitro* culture keeps the plants under completely sterile conditions and enables to adjust the organic and inorganic compounds added to the culture medium to the plants requirements and excludes other additions which might influence the experiment. In this “semi-closed system” only light, temperature and a small amount of air are coming into the culture system from the outside and can also be mostly controlled. It was the goal of this project to investigate the hyperaccumulation and reduction of arsenate and chromate by *Nasturtium officinale* under sterile *in vitro* conditions. This allows to verify that reduction takes place in the plant and not in accompanying microorganisms which one can assume.

### Material and Methods

**Growth experiments.** *Nasturtium officinale* seeds were surface sterilized for 30 seconds in ethanol (70%) and 5 minutes in NaOCl (1,2% active chlorine) and washed 3 times for 5 minutes in sterile deionized water. The seeds were aseptically sown on Gamborg’s B<sub>5</sub> basal medium containing 2% sucrose (Duchefa, The Netherlands [2]) and MS basal medium containing 3% sucrose [3] both solidified with 4g/L gelrite (Duchefa, The Netherlands). The media were adjusted to a pH of 5,6 to 5,7 (with KOH and HCl) and autoclaved in 50 mL aliquots in glass vessels with a filter sealed metal lid for 20 minutes at 120°C at 15psi (103.5 kPa). The seeds and the growing seedlings were cultivated at 22°C in a 16h/ 8h (light/dark) cycle at a light intensity of 31,5 to 47,7  $\mu\text{molm}^{-2}\text{s}^{-1}$  from

cool white fluorescence tubes (TLD 58W/865, 120cm Phillips, Germany). For 6 different experimental setups chromate (CrVI) and arsenate (AsV) were solubilized in liquid MS medium with 125, 250 and 500ppm concentrations. The pH of the medium were adjusted to 5,6 to 5,7 like described above and filter sterilized.

After the precultivation phase the plants about 8cm height were placed aseptically into sterile glass vessels with 2cm rubber foam stabilization at the bottom and 75mL liquid MS medium and the different concentrations of arsenate or chromate and a control without any additions except the MS compounds. The plants were cultivated additional two weeks prior the measurements. To assure that no contamination of microorganisms was in the culture system 1mL of the culture medium was plated on standard LB-Agar [4] etri dishes and incubated at room temperature.

**XANES-spectroscopy - Experimental.** XANES spectra were recorded at CAMD's DCM beamline, the monochromator was equipped with Ge (220) crystals. Chromium foil (Cr<sup>0</sup>) and arsenic (As<sup>0</sup>) were used for calibration of the fluorescence detector and energy calibration (in transmission mode). The *Nasturium officinale* samples were measured in fluorescence mode using a Canberra 13 element Germanium detector. Measurements (repeated twice) were performed under ambient air pressure and temperature conditions. Spectra were scanned with step widths of 2.0 eV in the pre-edge region between 5840-5980 eV, 0.3 eV between 5980-6020 eV, the main region of interest, and 1.0 eV between 6020-6140 eV with an integration time of 3 s per point in the case of chromium, with step widths of 2.0 eV in the pre-edge region between 11800-11855 eV, 0.5 eV between 11855-11900 eV, the main region of interest, and 1.0 eV between 11900-12050 eV with an integration time of 3 s per point in the case of chromium. Using the Origin program (Origin Lab Corporation, Northhampton, MA 01060, USA) a linear background determined in the pre-edge region was subtracted from the raw data to correct the spectra from contributions of higher shells and from supporting materials.

**Sample preparation.** For XANES spectroscopy measurements, leaves, roots and stems were prepared separately. The plant material was used as fresh material and as dried material (1h, 100°C), ground into a fine powder and put onto a self-adhesive kapton film.

### First Results and Remarks

XANES spectroscopy clearly showed that *Nasturium officinale* is able to reduce CrVI to CrIII and AsV to AsIII (spectra not shown; to be published). However, plants were strongly affected by the heavy metals resulting in colorless, white leaves. Spectra of plants not treated with chromate and arsenate, respectively, hardly showed any occurrence of chromium and arsenic, respectively. The As-K-edge and Cr-K-edge spectra from "fresh plants" and from dried plant are identical. The speciation of chromium (CrIII) and arsenic (AsIII) was almost identical in the stems, leaves and roots. Therefore, it is still an open question where exactly in the plant (or on roots surface?) the reduction takes place. As plant were cultivated using the *in vitro* culture technique, the involvement of microbes in these processes in the processes can be ruled out. This is a first important result and the basis for the next steps in our ongoing study on phytoremediation of heavy metals by *Nasturium officinale* investigating the localization of heavy metal reduction in/on the plant, the influence of pH, transport of heavy metals within the plant, the bonding partners of heavy metals within the plant and plants metabolism etc.

### **Acknowledgement**

We would like to thank T. Winkelmann (Leibniz University Hannover) for many helpful discussions on *in vitro* cultivation experiments.

### **References**

1. R. B. Meagher (2000). Phytoremediation of toxic elemental and organic pollutants. *Current Opinion Plant Bio.* **3**, 153-162.
2. O. L. Gamborg, R. Miller and K. Ojima (1968). Nutrient requirements of suspension cultures of soybean root cells. *Exp. Cell Res.* **50**, 151-158
3. T. Murashige and F. Skoog (1962). A revised medium for rapid growth and bioassays with tobacco tissue cultures. *Physiol. Plant.* **15**, 473-497.
4. Miller J.H. (ed) 1992 *Experiments in molecular genetics*. Cold Spring Harbour Laboratory. Cold Spring Harbour, New York

## Utilization of elemental sulfur by *Allochromatium vinosum*

Bettina Franz<sup>1,2</sup>, Henning Lichtenberg<sup>3</sup>, Josef Hormes<sup>3</sup>, Hartwig Modrow<sup>3</sup>,  
Christiane Dahl<sup>1</sup> and Alexander Prange<sup>2,4</sup>

<sup>1</sup>Institute for Microbiology & Biotechnology, University of Bonn,  
Meckenheimer Allee 168, D-53115, Germany

<sup>2</sup>Microbiology and Food Hygiene, Niederrhein University of Applied Sciences,  
Rheydter Straße 277, D-41065 Mönchengladbach, Germany

<sup>3</sup>Institute of Physics, University of Bonn, Nussallee 12, D-53115 Bonn, Germany

<sup>4</sup>Center for Advanced Microstructures and Devices, Louisiana State University,  
6980 Jefferson Hwy., Baton Rouge, LA 70806, USA

Correspondence to: A. Prange, e-mail: [A.Prange@gmx.de](mailto:A.Prange@gmx.de) or [prange@lsu.edu](mailto:prange@lsu.edu);  
PNR GMX-AP0507DCM

### Introduction

It is well known since a long time that the anoxygenic phototrophic sulfur bacterium *Allochromatium vinosum* and other photo- and chemotrophic sulfur oxidizing bacteria are able to take up externally added solid, virtually insoluble elemental sulfur [1,2]. Although this step is very important in the global sulfur cycle (e.g. [3]), the process of mobilization and the utilization of different sulfur species is hardly understood.

Commercially available elemental sulfur is mainly a mixture of cyclic, orthorhombic  $\alpha$ -sulfur (*cyclo*-octasulfur, S<sub>8</sub> rings) and polymeric sulfur consisting of chain-like macromolecules. The bonding energy between S-S bonds in polymeric sulfur is 2.4 kJ mol<sup>-1</sup> weaker than in *cyclo*-octasulfur (e.g. [4]), therefore, polymeric sulfur might be easier accessible for elemental sulfur uptake by sulfur oxidizing bacteria like *A. vinosum*. The purple sulfur bacterium *A. vinosum* uses reduced inorganic sulfur compounds (sulfide, thiosulfate) as electron donor for anoxygenic photosynthesis. During the oxidation of reduced sulfur compounds, sulfur globules surrounded by a protein envelope are accumulated as an intermediate inside the cells (e.g. [5]). The chemical nature of these sulfur globules has been determined by Prange *et al.* (2002) [6] as sulfur chains, most probably terminated by organic residues at one or both ends. The intracellularly stored sulfur is further oxidized to the final product sulfate.

Besides the reduced sulfur compounds sulfide and thiosulfate, *A. vinosum* is also able to take up solid elemental sulfur and oxidize it to sulfate (e.g. [7]). The main goal of the present study was to investigate whether *A. vinosum* uses or prefers *cyclo*-octasulfur and polymeric sulfur, respectively, for this process. Furthermore, it was the aim to analyze the sulfur speciation in the sulfur globules of *A. vinosum* after uptake of elemental sulfur.

### Material and Methods

**Growth experiments.** *Allochromatium vinosum* DSMZ 180<sup>T</sup> was cultivated as described previously by Hensen *et al.* (2006) [8]. Solid elemental sulfur (“S<sup>0</sup>”; 50 mM) was added as single sulfur source to the culture. Two different commercially available ‘elemental’ sulfur were purchased and used as received from Riedel de Haen (Seelze, Germany) (sulfur 1: S1) and from Merck (Darmstadt, Germany) (sulfur 2: S2), respectively, in the

fermenter experiments. Furthermore, small amounts of ‘pure’ polymeric sulfur (50 mM) were used for culture volumes of 100 mL. The protein content of the culture in different growth stages was determined using the Bradford reagent (Sigma, Taufkirchen) as specified by the manufacturer [9]. Sulfate, the final product of ‘elemental’ sulfur oxidation, was determined in culture supernatants by HPLC (High performance liquid chromatography) (Thermo Separation Products TSP, Egelsbach, Germany) using the methods of Rethmeier *et al.* (1997) [10].

**XANES-spectroscopy - Experimental.** XANES spectra were recorded at CAMD’s DCM beamline, the monochromator was equipped with InSb (111) crystals. The monochromatic flux rate per second on the sample was about  $5 \times 10^8$  photons (at 100 mA). Measurements (repeated twice) were performed in transmission mode with 60 mbar air pressure inside of the ionisation chambers. For energy calibration of the spectra, the spectrum of zinc sulfate was used as a “secondary standard” setting the maximum of the first resonance (white line) to an energy of  $2481.44 \pm 0.1$  eV. Spectra were scanned with step widths of 0.5 eV in the pre-edge region between 2440-2468 eV, 0.1 eV between 2468-2485 eV, the main region of interest, and 0.3 eV between 2490-2520 eV with an integration time of 1 s per point. Using the Origin program (Origin Lab Corporation, Northampton, MA 01060, USA) a linear background determined in the pre-edge region was subtracted from the raw data to correct the spectra from contributions of higher shells and from supporting materials. Spectra were normalized at 2510 eV.

**Quantitative analysis of spectra, reference compounds.** The interactive fitting and plotting packages Mn-Fit 4.04/15 (available at: [http://www-zeus.physik.uni-bonn.de/~brock/mn\\_fit.html](http://www-zeus.physik.uni-bonn.de/~brock/mn_fit.html)) and WINXAS [11] were used. A set of five reference spectra was used (reduced and oxidized glutathione, *cyclo*-octasulfur, polymeric sulfur and zinc sulfate) for fitting the bacterial spectra and a set of two reference spectra for fitting the ‘elemental’ sulfur (*cyclo*-octasulfur, polymeric sulfur), respectively. Reduced and oxidized glutathione and zinc sulfate were purchased and used as received from Sigma (Sigma, Deisenhofen, Germany) and pure *cyclo*-octasulfur and polymeric sulfur were kindly provided by R. Steudel, Berlin.

**Sample preparation.** For XANES spectroscopy measurements, the remaining sulfur platelets were separated from the culture by filtration. Sulfur platelets were put homogeneously as a thin layer on a sulfur-free self adhesive kapton<sup>®</sup> film topped by a polypropylene film. Bacterial cells were prepared as described previously [6]. The thickness and homogeneity of the samples was optimized in order to avoid possible thickness- as well as pinhole-effects.

## Results and Discussion

The aim was to clarify whether *A. vinosum* is able to use both S<sub>8</sub> rings and polymeric sulfur chains, or whether it prefers one of those species. For this purpose, *A. vinosum* was cultivated photolithoautotrophically with 50 mM of ‘elemental sulfur’ as single sulfur source. In the growth experiments, two different ‘elemental’ sulfur were used (S1 and S2). Their exact chemical speciation was analyzed to determine the ratios of S<sub>8</sub> rings and polymeric sulfur. Figure 1a, b shows the sulfur K-edge XANES spectra of pure *cyclo*-octasulfur and pure polymeric sulfur, Figure 2 the sulfur K-edge XANES spectra of the two ‘elemental’ sulfur and the corresponding fits. The quantitative analysis of the spectra



showed that the two 'elemental' sulfur differ significantly in their ratio of S<sub>8</sub> rings and polymeric sulfur (Tab. 1).

In the first set of growth experiments, S1 was added to the culture. *A. vinosum* took up 'elemental' sulfur and accumulated sulfur globules. Oxidation of intracellularly stored sulfur to sulfate started after 12 h. The sulfur globules were completely degraded and oxidized to sulfate after 132 h (Tab. 3). During that time, protein concentration of the culture increased (Tab. 2), indicating growth with elemental sulfur as single sulfur source. Further uptake and oxidation of elemental sulfur did not occur in the following 24 h and small sulfur platelets remained in the culture. Only 37 mM sulfate were formed

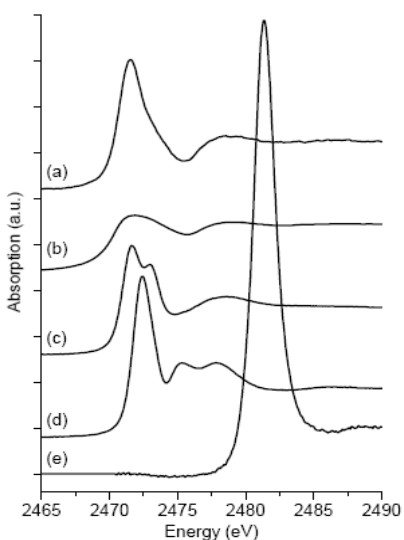


**Fig. 1:** Sulfur K-edge XANES spectra of the reference compounds which were used for fitting bacterial and sulfur spectra: polymeric sulfur (a), cyclo-octasulfur (S<sub>8</sub> rings) (b), oxidized glutathione (c), reduced glutathione (d) and zinc sulfate (e) (a.u. = arbitrary units).

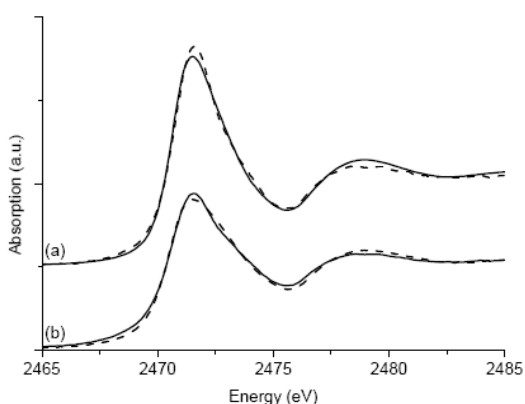


**Fig. 2:** Sulfur K-edge XANES spectra (solid lines) of the elemental sulfur (a) sulfur 1 (S1) and (b) sulfur 2 (S2) used in the growth experiments and accompanying fits (dashed lines) (a.u. = arbitrary units).

from 50 mM sulfur showing that only 74 % of the added elemental sulfur was taken up and oxidized to sulfate. Taking an error of  $\pm 10\%$  of the quantitative analysis into account, this result fits quite well to the 68 % polymeric sulfur fraction in S1 (Table 1). The protein concentration of the culture increased only marginally after oxidation of the intracellularly stored sulfur, also indicating that further sulfur oxidation did not occur in that time. XANES analysis of the remaining sulfur platelets showed, that they consisted almost completely ( $\sim 95\%$ ) of S<sub>8</sub> rings (Fig. 3a, Tab. 1). Only 3 % of polymeric chains were left in the remaining sulfur platelets compared to  $\sim 68\%$  at the beginning of the experiment.

In a second set of growth experiments, cultures of *A. vinosum* were fed with elemental sulfur with a different S<sub>8</sub> ring/ polymeric chain ratio (S2).

Quantitative analysis of the XANES spectra (Fig.2b) showed that the polymeric chain fraction was about 39 % (Table 1) and therefore significantly lower than that of S1. Formation of sulfur globules and beginning of sulfate production were comparable to the first experiment. Sulfur platelets also remained in the culture and were not taken up and oxidized by *A.*

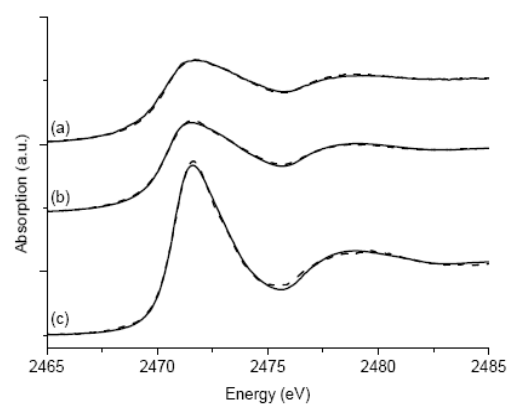


**Fig. 3:** Sulfur K-edge XANES spectra (solid lines) of remaining sulfur platelets in the cultures and accompanying fits (dashed lines): (a) sulfur 1 (S1) and (b) sulfur 2 (S2) and (c) *Allochromatium vinosum* cells containing sulfur globules after uptake of elemental sulfur (a.u. = arbitrary units).

*vinosum*. A constant amount of 22.6 mM sulfate was determined for 153 h corresponding to 45 % of the expected amount of sulfate. The added elemental sulfur contained ~ 39 % polymeric sulfur compared to 45 % sulfate and the remaining sulfur platelets mostly consisted of *cyclo*-octasulfur (Table 1,3).

Both experiments yielded evidence that *A. vinosum* can use only polymeric sulfur - or at least strongly prefers this sulfur species when growing on ‘elemental’ sulfur. This interpretation was supported by the observation that cultures of *A. vinosum* fed with “pure” polymeric sulfur (50 mM) completely took up the added sulfur, formed intracellular sulfur globules and completely oxidized the stored sulfur to 49 mM sulfate in the medium. Sulfur platelets did not appear after degradation of the sulfur globules. To make sure, that the speciation of the sulfur globules of *A. vinosum* grown on elemental sulfur is comparable to that of *A. vinosum* grown on sulfide, we investigated *A. vinosum* cells with internal sulfur globules

by XANES spectroscopy (Fig. 3c). Fitting the spectrum with five reference compounds (Fig. 1, Table 1) yielded a sulfur speciation very similar to that obtained for *A. vinosum* cells grown on sulfide [6].

Our observation that *A. vinosum* uses only or at least strongly prefers polymeric sulfur chains indicate, that the ability to take up elemental sulfur in the phototrophic bacterium *A. vinosum* seems to be completely dependent of the specific molecular composition of the elemental sulfur. Furthermore, sulfur globules of *A. vinosum* consists exclusively of sulfur chains (mono-bis-organyl sulfanes) [6]. Therefore, it appears that the organism is completely unable to deal with sulfur rings, the chemically more stable *cyclo*-octasulfur, neither inside nor outside the cell. On the basis of the results presented in this study for *A. vinosum*, one might speculate, that ‘sulfur chains’ are the “microbiologically preferred form of elemental, zero valent sulfur” also for other sulfur oxidizing bacteria.

**Table 1:** Results of fitting the sulfur K-edge XANES spectra of sulfur 1 (S1), sulfur 2 (S2), the remaining sulfur platelets and the intracellular sulfur globules of *A. vinosum* to the sum of the reference spectra.

sample	percentage contribution of sulfur species*	
	<i>cyclo</i> -octasulfur (S <sub>8</sub> rings)	polymeric sulfur
S1 (added)	30	68
S1 (remaining)	95	3
S2 (added)	62	39
S2 (remaining)	84	12

sample	percentage contribution of sulfur species*				
	glutathione (reduced)	glutathione (oxidized)	<i>cyclo</i> -octasulfur	polymeric sulfur	zinc sulfate
<i>A. vinosum</i> cells with sulfur globules after uptake of elemental sulfur S1	8	15	---	78	---

\*different sulfur species and their percentage contribution to the sulfur speciation; error: <math>\pm 10\%</math>; --- =

---

 contribution < 1 %;
 

---

**Table 2:** Protein determination of cultures fed with sulfur 1 (S1) and sulfur 2 (S2).

		time (h)							
fed with		0	3	12	84	114	132	156	267
protein-concentration (mg/mL)	S1	0.106	0.141	0.202	0.469	0.561	0.702	0.738	n.d.
	S2	0.048	0.059	0.062	0.263	0.265	0.245	0.252	0.229

**Table 3:** Sulfate determination and observation by light microscopy of sulfur globule formation in cultures fed with sulfur 1 (S1) and sulfur 2 (S2). The % values in parentheses show the relative amount of sulfur recovered as sulfate, compared to a total of 50 mM in the culture.

		time (h)							
fed with		0	3	12	84	114	132	156	267
S1	sulfate (mM)	0.0 (0%)	0.0 (0%)	0.2 (0.4%)	18.2 (36%)	27.9 (56%)	37.3 (74%)	37.3 (74%)	n.d.
	sulfur globules	---*	yes	yes	yes	yes	---*	---*	n.d.
	sulfate (mM)	0.0 (0%)	0.0 (0%)	0.1 (0.2%)	16.2 (32%)	22.6 (45%)	22.6 (45%)	22.6 (45%)	22.6 (45%)
S2	sulfur globules	---*	yes	yes	yes	---*	---*	---*	---*

\*sulfur globules were not observed

## References

1. H. H. Thiele, *Arch. Mikrobiol.* **60**, 124 (1968)
2. N. Pfennig and H. G. Trüper, In *Bergey's manual of determinative bacteriology*. 8<sup>th</sup> edn., p. 24. Edited by R.E. Buchanan & N.E. Gibbson. Baltimore: Williams & Wilkins (1974)
3. T. Brüser, P. N. Lens and H. G. Trüper, In *Environmental technologies to Treat Sulfur pollution*. p. 47. Edited by P. Lens & L. Hunshoff Pol. London: IWA Publishing (2002)
4. R. Steudel and B. Eckert, In *Elemental sulfur and sulfur-rich compounds I*. p. 1. Series Topics in current chemistry 230. Edited by R. Steudel. Berlin: Springer (2003)
5. C. Dahl and A. Prange, In *Bacterial Inclusions, chapter 2, Series Microbiology Monographs*, p. 21-51. Edited by J.M. Shivley. New York: Springer (2006)
6. A. Prange, R. Chauvistré, H. Modrow, J. Hormes, H. G. Trüper and C. Dahl, *Microbiology-UK* **148**, 267 (2002)
7. D. C. Brune, In *Anoxygenic photosynthetic bacteria*. p. 847. Edited by R.E. Blankenship, M.T. Madigan & C.E. Bauer. Dordrecht: Kluwer Academic Publishers (1995)
8. D. Hensen, D. Sperling, H. G. Trüper, D. C. Brune and C. Dahl, *Mol Microbiol* **62**, 794 (2006)

9. M. Bradford, *Anal. Biochem.* **72**, 248 (1976)
10. J. Rethmeier, A. Rabenstein, M. Langer and U. Fischer, *J Chromat. A* **760**, 295 (1997)
11. T. Ressler, *J. Synchr. Rad.* **5**, 118 (1998)

Publication from this project: Franz *et al.* (2007) Utilization of solid 'elemental' sulfur by the phototrophic purple sulfur bacterium *Allochromatium vinosum*: A sulfur K-edge X-ray absorption spectroscopy study. *Microbiology* (in press)

## **Filamentous microbial mats from sulfidic springs: Sulfur speciation in natural samples**

Alexander Prange<sup>1,2</sup>, Henning Lichtenberg<sup>1,3</sup>, Josef Hormes<sup>1,3</sup>  
and Annette Summers Engel<sup>4</sup>

<sup>1</sup> Center for Advanced Microstructures and Devices, Louisiana State University,  
6980 Jefferson Hwy., Baton Rouge, LA 70806, USA

<sup>2</sup>Niederrhein University of Applied Sciences, Rheydter Strasse 277,  
41065 Mönchengladbach, Germany

<sup>3</sup>Institute of Physics, University of Bonn, Nussallee 12, 53115 Bonn, Germany

<sup>4</sup>Department of Geology and Geophysics, Louisiana State University,  
LSU Campus, Baton Rouge, LA 70803, USA

Correspondence to: A. Prange, e-mail: A.Prange@gmx.de or prange@lsu.edu;

### **Introduction**

Geochemical and ecological changes that have occurred throughout Earth's history are recorded in accumulations of organic matter, minerals and rocks. In particular, materials with the reactive element sulfur have been used extensively to interpret past changes on Earth and might even be useful for understanding the Martian past. However, most transformations within the sulfur cycle are fundamentally controlled by biosphere processes, especially by the metabolisms of microorganisms. The oxidation of reduced inorganic sulfur compounds, such as hydrogen sulfide, is carried out by phylogenetically diverse microbes. However, the formation of sulfur globules and the assimilation of sulfur into biomolecules (e.g., proteins) result in temporarily stored sulfur within a microbial community, thereby creating an energetic imbalance. In many studies, the flux and transformation rates of sulfur in various systems have been determined by the use of stable sulfur isotope systematics has been done almost to the exclusion of any other method. Therefore, to truly understand what the isotope systematics of a system has recorded, processes affecting the speciation of sulfur need to be evaluated and more modern, "alive" samples need to be studied. The motivation for this study, which has "explorative character" was driven by the need to link complex sulfur bio-signature data to natural processes so that a better understanding of sulfur biosignatures from ancient, sulfur-rich deposits could be made. The primary goal was to characterize the dominant forms of sulfur within naturally-occurring microbial mats from aphotic (cave), sulfidic springs by XANES spectroscopy and to place the results into an ecological context.

### **Materials and Methods**

**Sample collection, habitat geochemistry, and stable isotope analysis.** Fresh microbial mat samples were aseptically acquired from terrestrial sulfidic springs that discharge into cave passages, including two springs (Fissure and Upper Spring; FS and US, respectively) from Lower Kane Cave, Wyoming (USA), and two spring-fed streams in the Frasassi Caves, Italy (Ramo Sulfureo, Pozzo di Cristalli, and Sala Calle; RS, PC, and SC respectively) (Fig. 1a, 1b).

Samples were maintained at 4°C prior to XANES analyses. Water from each sample location was collected for complete analyses of dissolved constituents, using standard field and analytical methods developed specifically for sulfidic cave systems. Dissolved hydrogen sulfide and oxygen levels were determined in the field spectrophotometrically using the methylene blue and rhodazine D colorimetric methods, respectively, with CHEMetrics chemistries (Calverton, VA). Aliquots of each mat sample (~2 mL) was homogenized by vortexing, freeze-drying, and powdering with a sterile mortar and pestle. Sulfur isotope ratio analyses and total sulfur content for the Frasassi Cave samples was done by Coastal Science Laboratories (Austin, Texas) on a VG (micromass) isotope ratio mass spectrometer; sulfur isotope ratio analyses and sulfur content for the Lower Kane Cave samples are described in Engel [1].

**XANES spectroscopy and Quantitative analysis.** XANES spectra at the sulfur K-edge were recorded at CAMDs DCM beamline equipped with a modified Lemonnier type double crystal X-ray monochromator and InSb (111) crystals. Measurements of most samples were performed in transmission mode using ionization chambers (60 mbar air pressure inside), as intensity monitor for I<sub>0</sub> in front of as detector for the transmitted intensity behind the sample. Measurements for four samples with low sulfur concentrations (LKC-04A04, LKC-05-201, ITY-05-005D, and ITY-05-011A) were done in fluorescence mode. For energy calibration of the spectra, the spectrum of zinc sulfate was used as a "secondary standard" setting the maximum of the first resonance (white line) to an energy of 2481.44 eV, which is reproducible to ±0.1 eV. Spectra were scanned (repeated twice) with step widths of 0.5 eV in the pre-edge region between 2450-2468 eV, 0.1 eV between 2468-2485 eV, the main region of interest, and 0.3 eV between 2490-2520 eV with an integration time of 1 s per point. Spectra were normalized at 2510 eV.

For a quantitative analysis, the fitting and plotting package WinXAS was used. The errors of the percentage contributions of sulfur species (Tab.1) can be estimated to be smaller than ± 10% (absolute value). A set of five reference spectra (*cyclo*-octasulfur, polymeric sulfur, methionine sulfone, cysteic acid, and zinc sulfate) was used (Tab. 1), as representatives of the atomic environment of the sulfur atom.

## Results

Microorganisms associated with sulfur metabolism dominated the mats, including members of the *Epsilonproteobacteria* and *Gammaproteobacteria*. These groups have not been examined previously by sulfur K-edge XANES. All of the mats consisted of elemental sulfur, with greater contributions of *cyclo*-octasulfur (S<sub>8</sub>) compared to polymeric sulfur (S<sub>n</sub>). While this could be a biological fingerprint for some bacteria, the signature may also indicate preferential oxidation of S<sub>n</sub> and S<sub>8</sub> accumulation. Higher sulfate content, possibly as the mineral gypsum, correlated to less S<sub>8</sub> content and the presence of *Epsilonproteobacteria*. The sulfur isotope systematics confirmed that various metabolic processes influenced sulfur content and speciation, including sulfur oxidation, sulfate reduction, and sulfur disproportionation. The results imply that interacting biogeochemical processes may inhibit confident interpretations of ancient, or even modern, sulfur records.

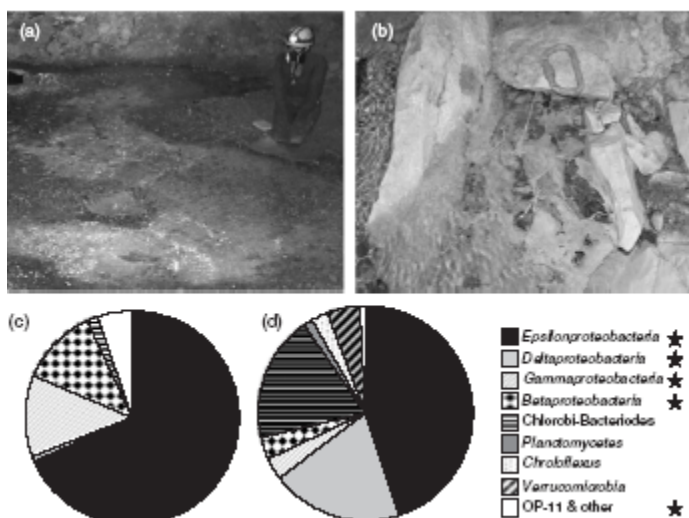


**Fig. 1:** (A) Microbial mats in sulfidic stream channel flowing from Upper Spring, Lower Kane Cave, WY. (B) Microbial mats from Ramo Sulfureo, Frassassi Caves, Italy; carabineer at center is approximately 10 cm long (photograph by M. Menichetti) (C) Summary of 16S rRNA gene sequences from clone libraries constructed from white filament bundles from Lower Kane Cave [2]. (D) Summary of 16S rRNA gene sequences from clone libraries constructed from white filaments from the Ramo Sulfuro, based on results from Reger, *et al.* (2006) [3]: Diversity comparisons between microbial mats and endosymbiont gut communities associated with the cave-dwelling *Androniscus dentiger* (Isopoda: Oniscidae) from the Frassasi Caves, Italy. Stars refer to microbial groups involved in cycling sulfur.

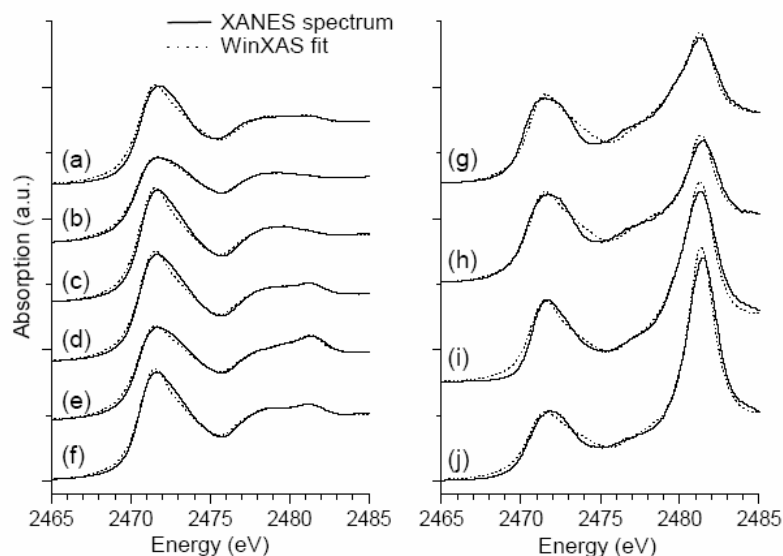


**Fig. 2:** (a) Sulfur K-edge XANES spectra of (a) LKC-04A-03, (b) LKC-05-203, (c) LKC-05-123, (d) ITY-05-010D, (e) ITY-05-005E, (f) ITY-05-013, (g) LKC-05-201, (h) LKC-04A04, (i) ITY-05-005D and (j) ITY-05-011A and corresponding WinXAS fits (cf. Table 1).

Sample Number	Description and prevalent microbial groups	Microbial Community Habitat Physicochemistry							Percentage Contribution of Sulfur Species from XANES				
		pH	Temp	Oxygen	Sulfide <sup>1</sup>	Sulfate <sup>1</sup>	$\delta^{34}\text{S}$	%S	S <sub>8</sub>	S <sub>μ</sub>	Met-O <sub>2</sub>	Cya	SO <sub>4</sub> <sup>2-</sup>
		°C	μmol L <sup>-1</sup>	μmol L <sup>-1</sup>	mmol L <sup>-1</sup>	‰		cyclo-octasulfur	polymeric sulfur	methionine sulfone	cysteic acid	zinc sulfate	
LKC-04A04 <sup>2</sup>	US; Gray; orifice sediment	7.4	21.3	<0.1	35	1.27	-23.5	<2	62	21	2	2	13
LKC-05-201	US; White-gray; thick mat and biofilms	7.4	21.5	19.4	18.5	1.31	-22.3	26	58	20	3	8	11
LKC-04A-03	US; White filaments; thick mat	7.3	21.6	26.6	18.5	1.33	-23.3	50	71	27	—	—	—
LKC-05-203	US; White filaments	7.3	21.6	24.7	18.5	1.33	-24.1	50	91	8	—	—	—
LKC-05-123	FS; White, thin webs	7.5	21.1	46.9	22.5	1.28	-22.1	18	63	34	—	—	—
ITY-05-013	SC; White-gray; thin film	7.3	13.8	10.2	153	1.03	N.D. <sub>3</sub>	N.D.	66	31	—	—	—
ITY-05-005D	RS; Gray filaments	7.4	13.7	6.9	201	1.27	-11.6	<5	35	28	2	15	20
ITY-05-005E	RS; White filaments	7.4	13.7	6.9	201	1.27	-12.4	>90	78	17	—	—	3
ITY-05-010D	PC; White-gray thick mat	7.3	13.5	12.5	345	2.03	-15.7	>90	60	36	2	—	2
ITY-05-011A	PC; White-gray thick mat, 5 m downstream	7.4	13.8	15	230	2.07	N.D.	<5	53	14	2	4	28

<sup>1</sup> Total dissolved ion concentration

<sup>2</sup> LKC samples from Lower Kane Cave (USA) and ITY samples from the Frasassi Caves (Italy); see methods for location name abbreviations.

<sup>3</sup> No detection, usually due to low sulfur content

**Table 1:** (a) Sulfur K-edge XANES spectra of (a) LKC-04A-03, (b) LKC-05-203, (c) LKC-05-123, (d) ITY-05-010D, (e) ITY-05-005E, (f) ITY-05-013, (g) LKC-05-201, (h) LKC-04A04, (i) ITY-05-005D and (j) ITY-05-011A and corresponding WinXAS fits (cf. Table 1).

## Summary

Sulfur K-edge X-ray absorption near edge structure (XANES) spectroscopy was done to examine sulfur speciation in natural microbial mats from two aphotic (cave) settings. Habitat geochemistry, microbial community compositions, and sulfur isotope systematics were also determined.

Organisms associated with sulfur metabolism dominated the mats, including members of the *Epsilonproteobacteria* and *Gammaproteobacteria*.

All of the mats consisted of elemental sulfur, with greater contributions of *cyclo*-octasulfur (S<sub>8</sub>) compared to polymeric sulfur (S<sub>μ</sub>). While this could be a biological fingerprint for some bacteria, the signature may also indicate preferential oxidation of S<sub>μ</sub> and S<sub>8</sub> accumulation. Higher sulfate content, possibly as the mineral gypsum, correlated to less S<sub>8</sub> content and the presence of *Epsilonproteobacteria*.

The sulfur isotope systematics confirmed that various metabolic processes influenced sulfur content and speciation.



### Acknowledgements

This work was partially supported for A.S.E. by the Board of Regents Support Fund (Contract NSF/LEQSF(2005)-Pfund-04) and the College of Basic Sciences at Louisiana State University, for A.P. by the Fonds der Chemischen Industrie (grant 661209) and CAMD at Louisiana State University . A.P. thanks the Heinrich-Hertz-Stiftung for a travel grant to stay at CAMD.

### References

1. A. S. Engel (2004). *Geomicrobiology of sulfuric acid speleogenesis: microbial diversity, nutrient cycling, and controls on cave formation*. PhD thesis, Dept. Geological Science, Austin, Texas.
2. A. S. Engel, M. L. Porter, L. A. Stern, S. Quinlan and P. C. Bennett (2004). *FEMS Microbiol. Ecol.* **51**, 31-53.
3. R. L. Reger, M. Porter, M. Menichetti and A. S. Engel (2006) Diversity comparisons between microbial mats and endosymbiont gut communities associated with the cave-dwelling *Androniscus dentiger* (Isopoda: Oniscidae) from the Frassasi Caves, Italy. National Speleological Society meeting, Bellingham, Washington.

Publication from this project:

Engel *et al.* (2007) Speciation of sulfur from naturally-occurring, filamentous microbial mats from sulfidic cave springs using X-ray absorption near edge spectroscopy. *FEMS Microbiology Letters* (in press).

## **Speciation of Phosphorus Compounds in Red Mud and Mixed Mineral Systems Using XANES**

J. J. Wang<sup>1</sup>, M.H.S. Stietiya<sup>1</sup>, and Amitava Roy<sup>2</sup>. <sup>1</sup>LSU Agriculture Center and LSU Department of Agronomy and Environmental Management, Sturgis Hall, Baton Rouge, LA, 70810, [jjwang@agctr.lsu.edu](mailto:jjwang@agctr.lsu.edu), [mstiet2@lsu.edu](mailto:mstiet2@lsu.edu) <sup>2</sup>LSU Center for Advanced Microstructures and Devices, 6980 Jefferson Hwy., Baton Rouge, LA 70806, [reroy@lsu.edu](mailto:reroy@lsu.edu). PRN: Agr-JW040.

Recent evidence from wet chemistry has showed that Fe oxides may play an equally important role in P retention in calcareous soils. The objective of this study is to use XANES techniques to identify P controlling minerals in some typical calcareous soils. In 2006, the P K-XANES spectra for sets of P-loaded samples of a mixed mineral and red mud at different pH levels along with different model compounds were collected using the Double Crystal Monochromator beamline (DCM) equipped with a InSb(111) crystal.

A pre-edge feature characteristic of Fe-phosphate minerals in the region from -5 to -2 eV was evident for the mixed mineral systems of pH 4.5 and 6.0. This pre-edge feature had disappeared for the mixed mineral system at pH 7.5. In addition, a shoulder on the higher energy side of the absorption edge which is characteristic of calcium phosphate minerals was evident for the mixed mineral system at pH 7.5. For the other mixed mineral systems at pH 4.5 and 6.0, such a shoulder was not evident. The results clearly demonstrated the effect of pH on phosphorus coordination with Ca and Fe constituents in these systems.

Using Principal Component Analysis (PCA), the number of probable species was determined to be two for the red mud samples (relative energy range from -10 to 15 eV). Four model compounds yielded a sufficient match upon target transformation: ferrihydrite, hematite, dicalcium phosphate, and octacalcium phosphate. Based on PCA results, linear combination fitting (LCF) was applied to determine the percentage of each probable constituent in the samples. The fitting results indicated that dicalcium phosphate dominated at high pH levels whereas P-Fe oxides were dominant at pH values of 4.5 and 6.0. Red mud with no pH adjustment showed that 84.5% of total P was dicalcium phosphate and 15% of total P was adsorbed to ferrihydrite ( $\chi^2=0.35$ ). At pH 4.5, LCF of red mud showed that 77.6% of P was adsorbed to ferrihydrite whereas 22.4% was present as dicalcium phosphate ( $\chi^2=0.62$ ). Finally, at pH 7.5, as much as half of P was adsorbed to ferrihydrite and the other half was in the form of dicalcium phosphate. Overall these spectroscopic evidences are consistent with current understanding of P chemistry as predicted by chemical equilibrium.

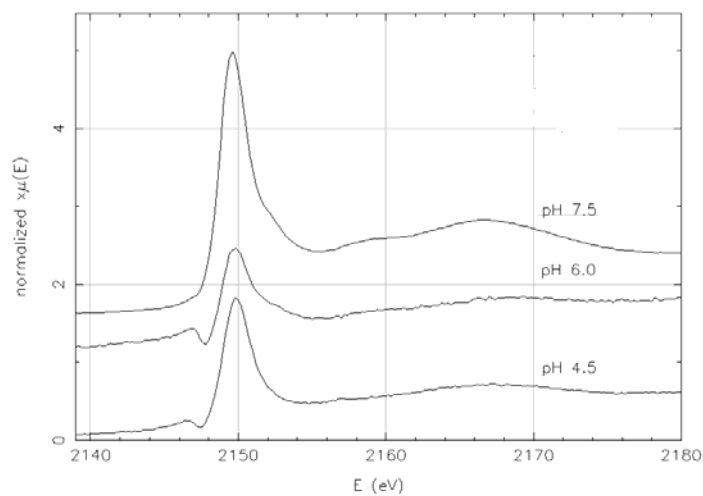


Figure1. Spectral comparison of mixed mineral systems at varying pH levels

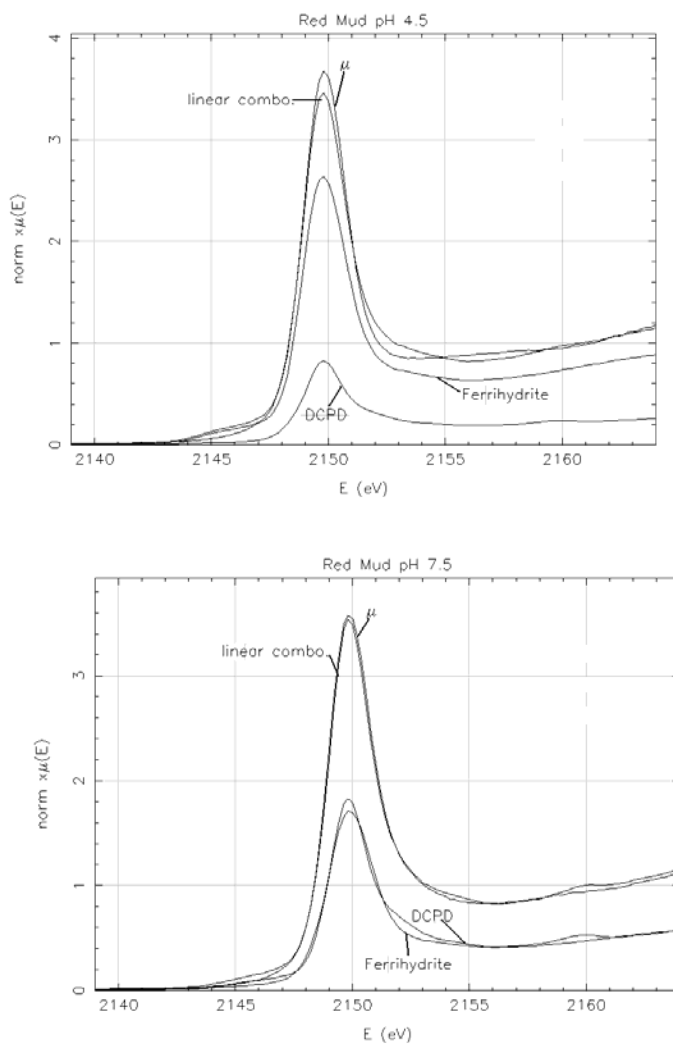


Figure2. LCF for red mud at pH 4.5 and 7.5

## **Pore-scale imaging of drainage in fractionally-wet unconsolidated porous media systems**

Zaydoun Abu-Salem, PhD candidate, LSU Department of Civil and Environmental Engineering, zabusal@lsu.edu

Clinton S. Willson, Ph.D., P.E., Associate Professor, LSU Department of Civil and Environmental Engineering, cwillson@lsu.edu

3513 CEBA, Department of Civil and Environmental Engineering, Louisiana State University, Baton Rouge, LA 70803, 225-578-8672

PRN ????

### **Motivation**

Water infiltration and drainage rates in the shallow subsurface following a rain or irrigation event and the distribution of water within the soil have an impact on crop growth, evapotranspiration, and aquifer recharge. Hydrologists typically use drainage and imbibition relationships to describe the relationship between the capillary driving forces and the volumetric water content (i.e., the fraction of a given volume occupied by water). These relationships, such as Van Genuchten and Brooks-Corey models, have been well-studied for wide variety of soils that are completely water wet (i.e., the water strongly wets the soil particles compared to air).

The Van Genuchten equation relating the volumetric water content to the capillary pressure head during drainage is:

$$\theta = \theta_r + \left[ (\theta_s - \theta_{ir}) / \left( 1 + (\alpha_d h_c)^{n_d} \right)^{m_d} \right]$$

where  $h_c$  is the capillary pressure head,  $(\theta)$  is the volumetric water content,  $(\theta_{ir})$  is the residual water content,  $(\theta_s)$  is the fully saturated water content,  $\alpha$ ,  $m$  and  $n$  are fitting parameters to account for the air entry value and pore size distribution of the porous media, and in most cases  $m=1-1/n$ . Subscript  $_d$  refers to the drainage process. Hereafter, we will refer to this equation as the  $h_c$ - $\Theta$  relationship.

Recent evidence points to the fact that many soils are not completely water-wet (here, we will call these fractionally-wet or water-repellent). Infiltration, drainage, and  $h_c$ - $\Theta$  experiments have demonstrated the impact of water repellency on the constitutive relations and how increased water repellency can lead to preferential flow in the unsaturated zone. Preferential flow can lead to higher rates of solute transport to the water table and increased variability in the water distribution in the vadose zone.

The imaging experiments we are conducting at the CAMD tomography beamline are directed at gaining insights in to the pore-scale processes that govern the drainage of water in fractionally-wet (or water-repellant) unconsolidated porous media. The high-resolution images that we are able to acquire provide us with the data to quantitatively characterize the granular packing, the pore network structure (i.e., the pore bodies,

throats, and connectivity), the distribution of the two fluids (e.g., water and air) within the pore space, and the correlation between the pore network structure and the fluid distribution.

## **Methods**

First, a series of capillary pressure – water content ( $hc-\Theta$ ) experiments were conducted in our laboratory in “large” columns (5 cm diameter, 20 cm in length) using standard procedures. Smaller aluminum columns (5 mm diameter, 10 cm in length) columns were used in the imaging experiments. Quartz sand (standard mesh size 40 to 50) was used in all the experiments. Water repellent sand was created by coating quartz sand with an organic chemical (OTS) that results in a water/air/solid contact angle of approximately 65 degrees. Fractionally-wet systems were created by packing the column with known fractions of the OTS-coated sand; in these experiments we used either 0% or 25% OTS-coated sand systems. Experimental procedures were identical in all columns.

Drainage experiments on the tomography columns were conducted while the column was mounted in the CAMD tomography beamline hutch. At various stages during the drainage experiments, the columns were imaged using a 35.3 keV monochromatic beam at 9 micron resolution. The resulting 1 mm high tomography images allow us to qualitatively and quantitatively examine the pore-scale drainage.

## **Results**

Results from the  $hc-\Theta$  experiments in both the 0% and 25% OTS systems (Figure 1) were compared to literature values and to verify that the drainage processes are similar in the large and tomography columns. Attempts to perform drainage experiments in 50% OTS systems were unsuccessful due to the small size of the tomography columns and the increasingly complex nature of the drainage processes in highly water repellent systems. Of note is that as the system becomes more water repellent, the drainage curve shift lower resulting in more drainage at lower capillary pressure.

The block symbols in Figure 1 show locations along the drainage curves where tomography images were acquired. Representative images are shown in Figure 2. These images show the solid (red), water (green) and air (phases) after the original images has been thresholded (i.e., the phase of each voxel has been uniquely identified). Of interest is that while the capillary pressure head conditions for both systems is approximately the same (28 cm for the 0% versus 27 cm for the 25%), the water content and distribution is different. This correlates well with theoretical studies and with the  $hc-\Theta$  relations shown in Figure 1.

Current and future work is directed at: (1) using algorithms developed by our group to quantitatively analyzing the grain and pore structure, the water and air phase distribution properties, and the correlation between the pore structure and fluids; (2) investigating systems with large grain size distributions; and (3) numerical modeling of the drainage processes in the various systems.

## Funding

This work has been partially supported by a grant from the American Chemical Society – Petroleum Research Fund (#41169-AC9).

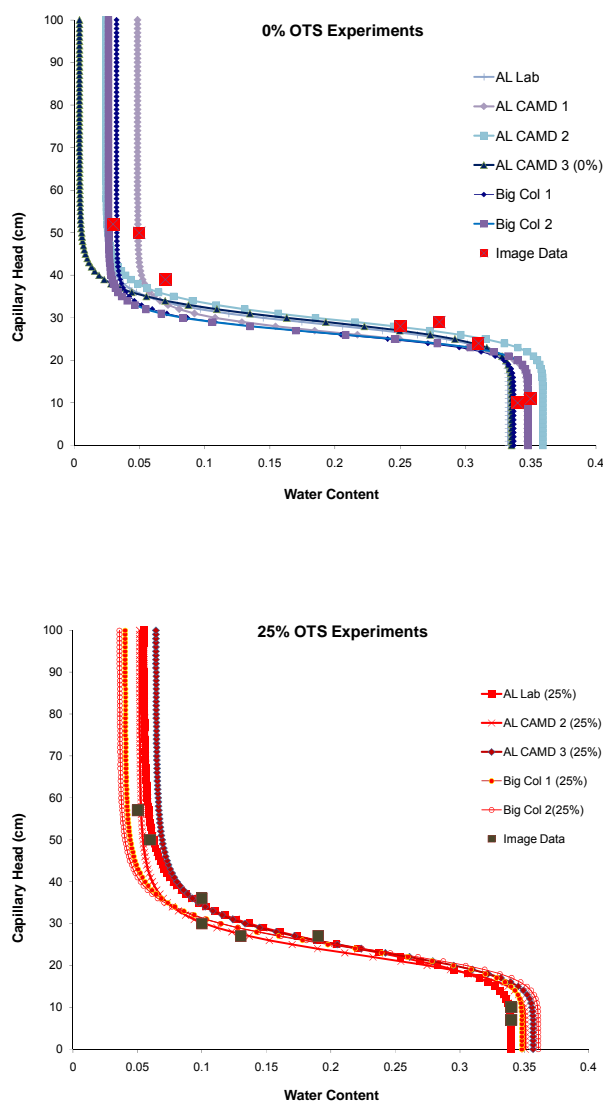


**Figure 1:**  $hc-\Theta$  curves for 0% (top) and 25% (bottom) OTS-coated systems. AL refers to experiments conducted in tomography column and “Big Col” refers to experiments conducted in larger columns. The block symbols denote points along the drainage curves where imaged were collected.

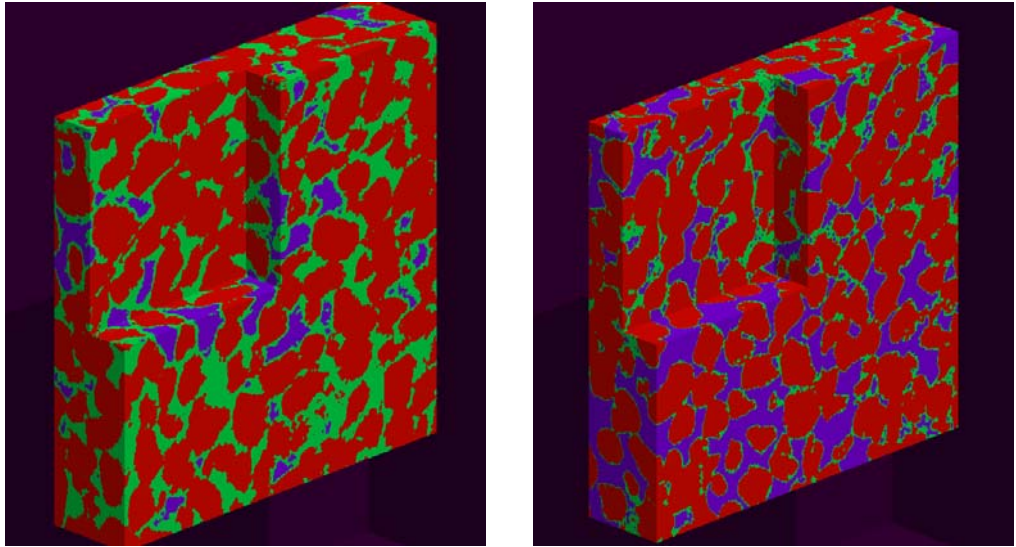


**Figure 2:** Thresholded images showing sand (red), water (green), and air (blue) in a 0% OTS system at 28 cm hc (left) and in a 25% OTS system at 27 cm hc (right).

## Species of Arsenic Accumulated in the Asparagus Fern, *Asparagus sprengeri*, and Perennial Ryegrass, *Lolium perenne*

LaShunda L. Anderson ([lander7@lsu.edu](mailto:lander7@lsu.edu)) and Maud Walsh ([evwals@lsu.edu](mailto:evwals@lsu.edu));  
Louisiana State University  
School of Plant, Environmental, & Soil Sciences  
Baton Rouge, Louisiana, 70803  
PRN # AGR-MW-1205

Environmental contamination by heavy metals such as arsenic can cause adverse effects on human health (Kos, 2002). Therefore, the public has become more concerned with the issue of arsenic pollution in soil and water systems (Association for the Environmental Health of Soils, 1998). Contamination of drinking water by arsenic is a severe health risk to millions of people worldwide (Huang et al., 2004). Prolonged arsenic exposure in humans can cause an increased risk of cancer development, reproductive abnormalities, and neurological abnormalities (O'Connor, 2002).

The remediation of toxic metals in the environment is challenging because metal cannot degrade (Kos et al., 2002). Phytoremediation is the use of plants to clean contaminated environments (Zynda, 2001). ladder brake fern, *Pteris vittata*, the first reported hyperaccumulator of arsenic, has shown great potential for application in phytoremediation (Ma et al., 2001; Tu, 2002). Certainly, there is a need for the identification of other plants with the ability to accumulate metals, such as arsenic, in high levels from contaminated areas and exhibit potential for application in phytoremediation (Lasat, 2002).

The focus of this study was to gain further insight into the behavior of arsenic during translocation and accumulation in *Asparagus sprengeri* (asparagus fern) and *Lolium perenne* (perennial ryegrass). This is one part of an assessment of these plant species for their potential for the phytoremediation of arsenic-contaminated soils. Asparagus fern and perennial ryegrass were chosen for this study because of their ease of cultivation, diverse habitats, and limited information in the literature pertaining to their abilities to accumulate and tolerate arsenic.

Asparagus fern and perennial ryegrass were cultivated under greenhouse conditions. Plants were potted in ½ gallon plastic pots containing a growth media mixture of medium grade vermiculite and Osmocote® extended time release fertilizer. Pots were lined with landscaping fabric to reduce loss of growth media. Individual hydroponic experiments for the asparagus fern and perennial ryegrass were performed. Each hydroponic experiment consisted of 12 plastic pans which contained one potted plant and hydroponic solution. The plastic pans were arranged into a randomized complete block design (RCB). Arsenic treatment levels for the asparagus fern hydroponic experiment were 0, 250, & 500 ug/l and arsenic treatment levels for perennial ryegrass hydroponic experiment were 0, 1800, and 2500 mg/l. An additional non-replicated hydroponic experiment consisting of two plastic pans containing one asparagus fern and ryegrass, respectively, was conducted to evaluate the species of arsenic in fresh plant



material. The arsenic treatment level for this experiment was 4500 ppm. This experiment was conducted at a higher concentration in order to better assess the species of arsenic contained in fresh samples. For all hydroponic experiments potassium arsenate ( $\text{KH}_2\text{AsO}_4$ ) was added to the hydroponic solution to achieve arsenic treatment levels.

XANES analysis was performed on freeze-dried and fresh samples of asparagus fern exposed to 500 ppb and 4500 ppm of arsenic, respectively. XANES analysis was also performed on freeze-dried and fresh samples of perennial ryegrass exposed to 2500 mg/l and 4500 mg/l of arsenic, respectively. Samples were placed between two layers of kapton tape and XANES spectra for the species of arsenic contained in each sample were produced using a synchrotron double-crystal monochromator beamline. XANES spectra of samples were then compared to the XANES spectra of arsenic standards using Athena® software Linear Combination Fit option. The linear combination (red line in figures 1-4) is the spectra to which the standard spectra are compared. The graph peaks under the linear combination line represent the species of arsenic contributing to the linear combination spectra.

Freeze-dried of asparagus fern were contained As (V) and As (0) arsenic species (Figure 1); while fresh asparagus fern samples contained arsenic species of As (V) and As (II) (Figure 2). Freeze-dried (Figure 3) and fresh samples (Figure 4) of ryegrass were both found to have As (V) as the dominant species of arsenic; however, in addition to As (V), both types of ryegrass samples were found to have small amounts of As (III) in association with sulfur.

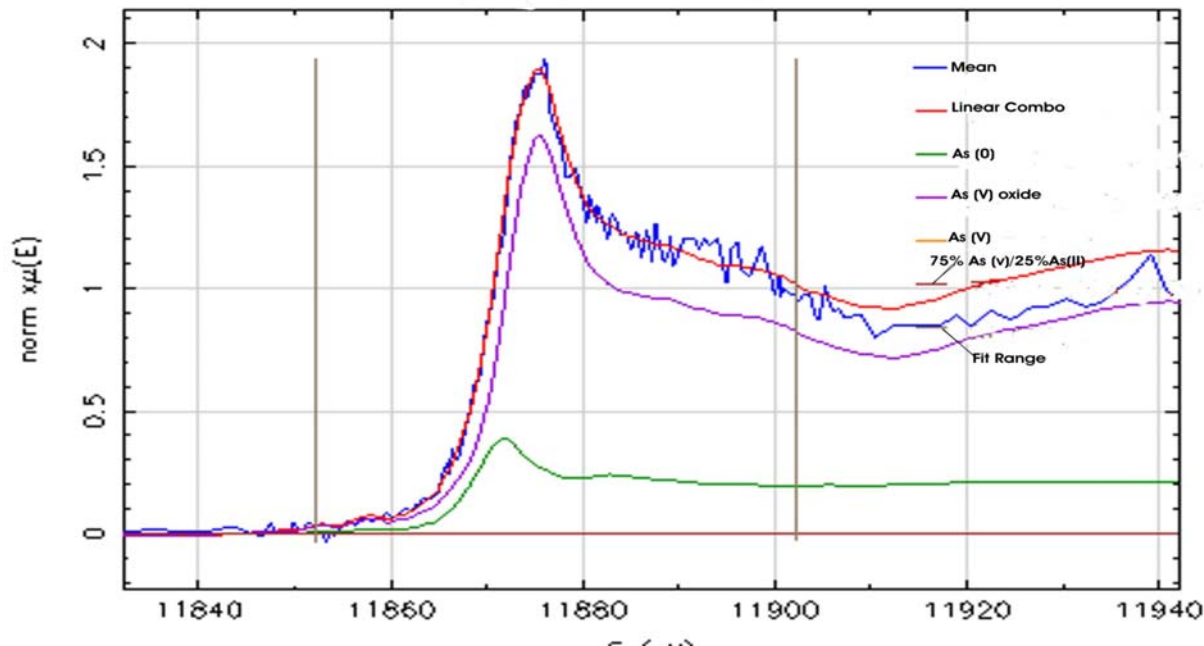


**Figure 1:** Arsenic species in freeze-dried asparagus fern exposed to 500 ug/l of arsenic.

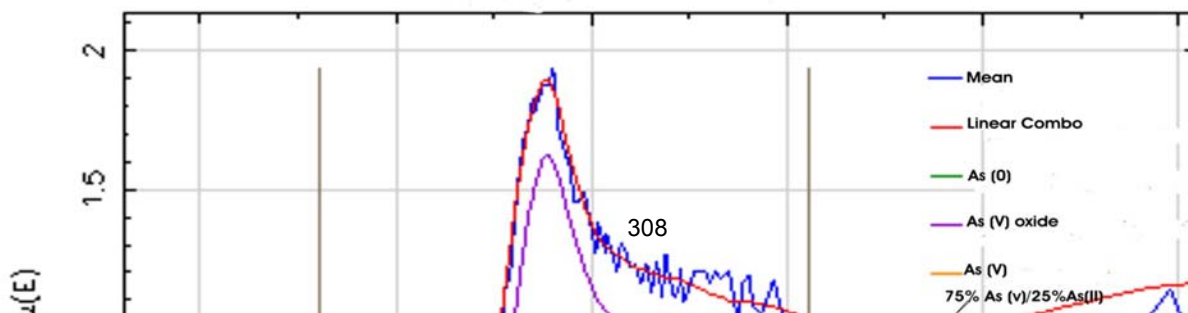


Figure 2: Arsenic species in fresh asparagus fern exposed to 4500 mg/l

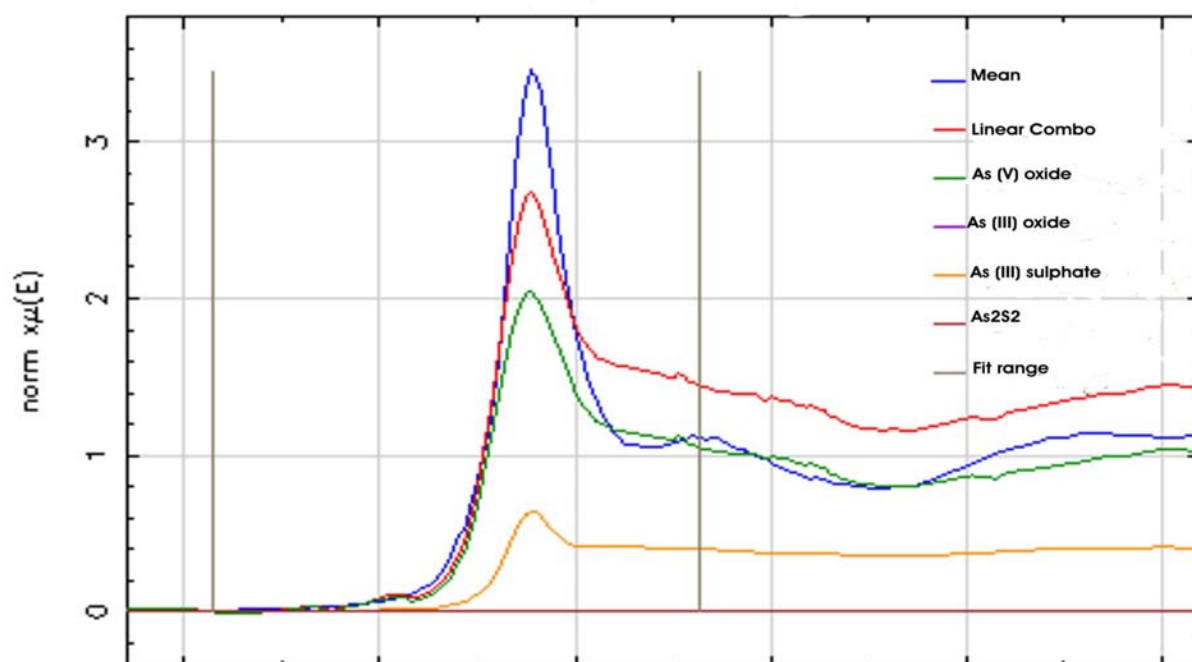
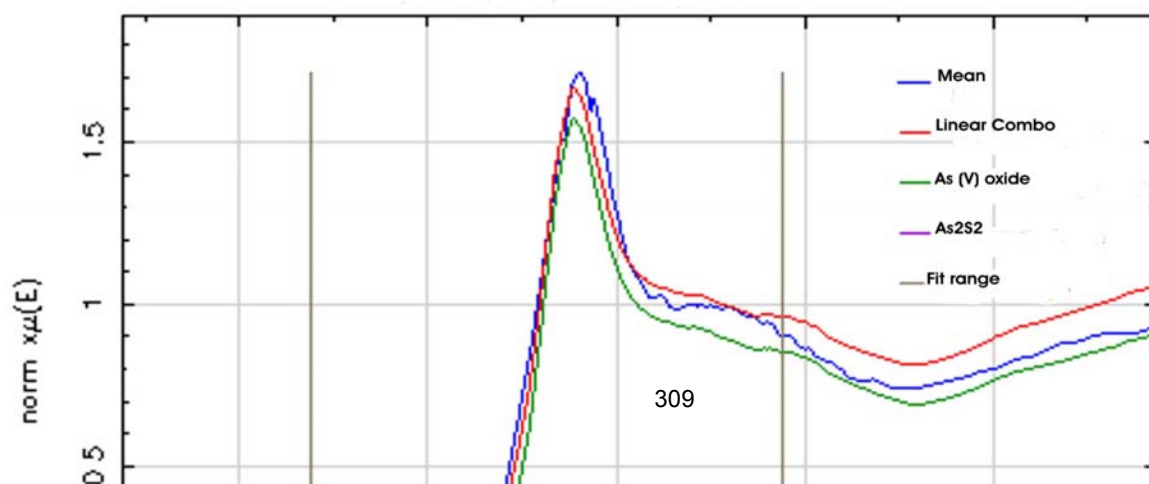


Figure 3: Arsenic species in perennial ryegrass exposed to 2500 ug/l of arsenic



**Figure 4:** Arsenic species in fresh perennial ryegrass exposed to 4500 mg/l of arsenic

#### **RELATED PRESENTATIONS**

**Anderson, L., & Walsh, M. M. (2006).** The Potential of the Common Marsh Fern, *Thelypteris palustris*, and Asparagus fern, *Asparagus sprengeri*, in the Phytoremediation of Arsenic. Oral presentation at the Minorities in Agriculture Natural Resources and Related Sciences Annual Career Fair and Training Conference, St. Louis, Missouri

**Anderson, L., & Walsh, M. W. (2006).** The Potential of the Common Marsh Fern, *Thelypteris palustris*, and Asparagus fern, *Asparagus sprengeri*, for Use in Phytoremediation. Poster presented at the Air and Waste Management National Conference, New Orleans, Louisiana

**Anderson, L., & Walsh, M. M. (2006).** The Uptake of Arsenic in the Common Marsh Fern, *Thelypteris palustris*, and the Asparagus Fern, *Asparagus sprengeri*. Oral presentation at the Louisiana State University Center for Advanced Microstructures and Devices Users Meeting, Baton Rouge, Louisiana.

## **The Use of Synchrotron Radiation to Produce Industrially Important Mutants**

M.L. Marceau-Day<sup>1</sup>; D.F. Day<sup>2</sup>; B. Prior<sup>3</sup>; D. Kim<sup>4</sup>,

1. LSU-CAMD; 2. LSU-Agricultural Center; Stellenbosch University, South Africa;

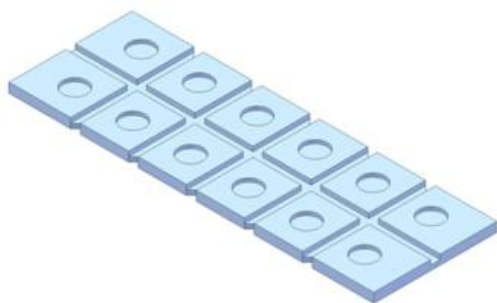
4. Chonnam University, Korea

### **Introduction:**

As part of the program to develop independence from foreign oil, the US Department of Energy is supporting work on alternative fuels. One of the major foci is the use of biomass to produce ethanol. Thus far, corn, which is mostly starch, has been shown to be readily convertible to ethanol. Today, ethanol is routinely added to gasoline in the corn growing areas such as Iowa and Nebraska. However, this non-food use of corn has caused a sharp spike in the price of the commodity which has already affected the price of corn for food in Mexico and Central America. Corn is a staple in the diet and the rising cost of corn has sparked riots in Mexico and a concern over the ability of the indigent poor of that country to get enough to eat. Research has now shifted to alternate biomass sources. Bagasse from sugar cane is routinely burned in boilers to make sugar which is an energy intensive process. However, excess is always available. The Audubon Sugar institute has been given research funds to design a cost-effective process to convert Bagasse to ethanol, in a manner that is economically competitive with the current gasoline producing refinery methods. Bagasse, like all biomass contains 3 main components: lignin, cellulose and hemicellulose. The lignin can be quite easily separated, but the similarity between the remaining carbohydrates, cellulose [glucose] and hemicellulose [xylose] makes it economically unfeasible to separate these precursors of ethanol. However, there is a major obstacle to fermenting xylose and glucose to ethanol. The presence of xylose feedback inhibits the conversion of glucose to ethanol; while the presence of glucose in the medium inhibits the fermentation of xylose to ethanol via a separate process. Genetically, this appears to be a control problem. If one can modify the "operon" that controls ethanol production from xylose or glucose, then one can develop a simultaneous process for the conversion of both sugars to ethanol. Further, the genetics of most industrially important microbial species have not been identified. Therefore, site-directed mutagenesis is not a viable option. Chemical mutagens cause multiple mutations, due to their non-selectivity.

We had previously used VUV mutagenesis at the Pohang Light Source to produce a dextran-sucrase mutant with 30 times more activity than the parent strain<sup>1</sup>. However, this was accomplished via an indirect process using backscatter at an angle from synchrotron radiation using an aluminum plate. LSU-CAMD, with its X-ray lithography scanners offered the chance to attempt a direct mutagenesis process.

Figure 1:



Microscope slide-sized exposure tool. The tool is molded in polycarbonate, then cut into final shape with a bandsaw. 12 holes each with a capacity of 10 microliters permits quadruple replicates of each of 3 samples for each exposure condition.

Methods:

Pichia cells were grown in liquid media at 30°C, with shaking at 200 rpm for 24 hours. Absorbance readings at 600 nm were converted to direct counts. 10 µl aliquots of known concentrations of cells were placed in specially designed, microfabricated holder [Figure 1]. Each sample was 10 µl in volume and the chosen material for the exposure sample holder was polycarbonate. Earlier prototypes made of PMMA were found to fail upon autoclaving and caused poor recovery of exposed or unexposed cells.

To increase the hardness of the SR spectrum and to determine a kill curve, varying thicknesses of aluminum foil were used, in parallel, to generate the best possible chance for mutants. Scanner travel above and below the sample holder was used from -50mm to +50mm and the number of full cycles were counted. Mutants were selected using selective medium containing 2-deoxyglucose and potato dextrose agar.

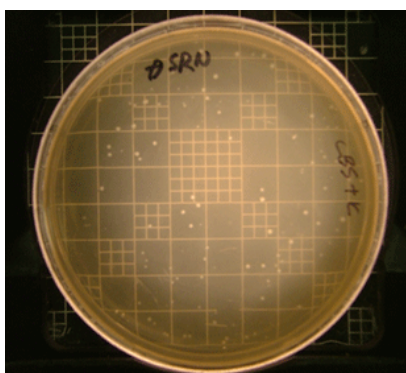
In a related experiment, supercoiled [non-replicating] DNA from a known plasmid was isolated and subjected to the same synchrotron radiation. SR was used to produce mutations in this plasmid DNA which was transduced into the cells following exposure to synchrotron radiation. Such DNA is extremely dry [free of associated water] and so the use of SR for such samples eliminates the secondary photolytic effects of X-rays on water with the consequent release of damaging radicals such as OH·.

### Results:

Preliminary results indicated that the use of synchrotron radiation is a viable alternative to chemical mutagenesis. Mutations were produced in both dried Pichia cells and in isolated DNA samples.

Figure 2

Production and isolation of Pichia mutants on selected media following the exposure of air-dried cells to synchrotron radiation.

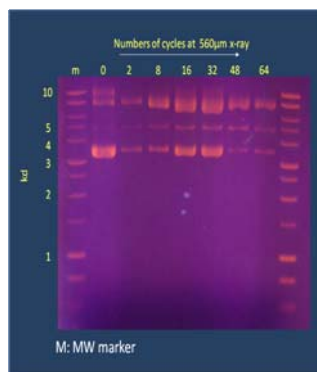


Though the precise mutation sought, has not yet been achieved, this novel method for the production of mutants has been demonstrated. The authors look forward to additional beam time and results this summer when Dr. Doman Kim will spend the summer at the LSU Audubon Sugar Institute as a visiting professor. Benchmarking of the procedure is also being carried out in tandem at the Pohang Light Source in Korea.

Mutations were produced in both the exposed dried yeast cells in a plasmid of supercoiled DNA containing non-expressed dextran-sucrase. Following

exposure and transduction into non-dextran-sucrase containing *Saccharomyces cerevisiae*, the enzyme was expressed and the supercoiled DNA was uncoiled as a result of Synchrotron radiation exposure.

Figure 3  
Uncoiling of supercoiled DNA as a consequence of exposure to SR.



### Conclusions:

SR is a viable tool for the development of mutants of industrial importance. Conditions need to be standardized, including energy and time discrimination as well as reproducibility and dose calculations. Future experiments will include the exposure of lyophilized cells from which all moisture has been removed to further decrease the potential for untoward reactions from the photolysis of bound water. Additionally, temperature should be monitored as another scurrilous reaction that needs to be avoided. Still, the initial results are indeed promising and represents the first use of synchrotron radiation for the production of mutagenesis in isolated DNA fractions.

### Literature Cited

1. Doman Kim, Do-Won Kim, Jin-Ha Lee, Kwan-Hwa Park, Lorraine M. Day and Donal F. Day (1997) *Biochemical Techniques*, 11: 319-321

*Acknowledgements: The authors wish to thank Proyag Datta and Prof. Jost Goettert for their micro-fabrication and exposure help.*

## Influence of Roasting on Sulfur Speciation in Coffee Beans

Henning Lichtenberg<sup>1</sup>, Alexander Prange<sup>2,3</sup>, Holger Hindorf<sup>4</sup>  
and Josef Hormes<sup>1,2</sup>

<sup>1</sup>Institute of Physics, University of Bonn, Nussallee 12, 53115 Bonn, Germany

<sup>2</sup>Center for Advanced Microstructures and Devices, Louisiana State University,  
6980 Jefferson Hwy., Baton Rouge, LA 70806, USA

<sup>3</sup>Niederrhein University of Applied Sciences, Rheydter Strasse 277,  
41065 Mönchengladbach, Germany

<sup>4</sup>INRES-Phytomedicine, University of Bonn, Nussallee 9, 53115 Bonn,  
Germany

Correspondence to: H. Lichtenberg, e-mail: [lichtenberg@physik.uni-bonn.de](mailto:lichtenberg@physik.uni-bonn.de);  
PNR GMX-AP0507XMP

### Introduction

Coffee is one of the most widely consumed beverages in the world. It is cultivated on a large scale in many countries and has enormous commercial relevance. A multitude of scientific publications has been dealing with the chemical composition of coffee, in particular with the identification of aroma and flavor compounds which are for the most part formed during roasting. Sulfur compounds play an important role for both coffee flavour and aroma [1].

Previous „explorative studies“ at CAMD [2] using XANES (X-ray absorption near edge structure) spectroscopy at the sulfur K-edge gave a first impression of how sulfur speciation in coffee beans is influenced by roasting - several differences between XANES spectra of green and roasted coffee beans could be observed.

### Materials and Methods

**Samples and sample preparation.** Five samples of commercially available green coffee beans were investigated: Harrar, Yirgacheffe, Sidamo dry process and Sidamo wet process (all of Ethiopian origin) and Colombian Huila. Moreover, green and hand-roasted Ethiopian wild coffee and green Mexican coffee beans (from Chiappas) were available. Apart from the hand-roasted Ethiopian wild coffee, roasted beans were prepared in a test roaster. Since the degree of roast depends largely on the size of beans, roasting time was adjusted 'individually' to each coffee in order to obtain beans of comparable degree of roast. After roasting, coffee beans were vacuum sealed (plastic bags) and kept in a refrigerator. Shortly before the XANES measurements, coffee beans were ground in a coffee grinder. Powder samples thus obtained were uniformly spread on adhesive sulfur free kapton tape and covered with polypropylene foil.

**XANES measurements.** XANES spectra at the sulfur K-edge were recorded at CAMD's DCM beamline [3]. The white X-ray beam was monochromatized with a modified Le-monnier type double crystal X-ray monochromator equipped with InSb(111)-crystals [4]. Measurements were performed in fluorescence mode using a 10 cm-long ionization chamber for monitoring the incident monochromatic X-ray intensity and a Germanium

detector for measuring the fluorescence intensity. Ionization chamber and sample chamber were flushed with Helium to minimize the attenuation of fluorescence radiation.

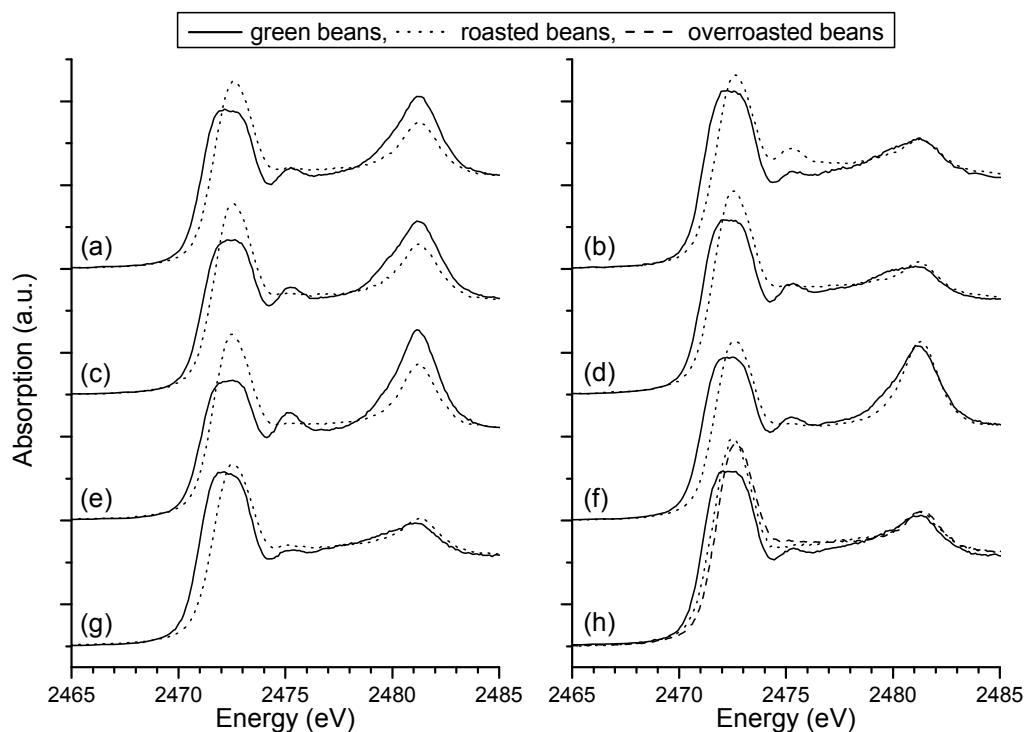


**Fig. 1:** Sulfur K-edge XANES spectra of green, roasted and overroasted coffee beans: (a) Ethiopian wild coffee, (b) green and hand-roasted Ethiopian wild coffee, (c) Ethiopian sidamo dry process, (d) Ethiopian sidamo wet process (e) Ethiopian Harrar, (f) Ethiopian Yirgacheffe, (g) Colombian Huila, (h) Mexican (Chiappas)

### Results and Discussion

XANES spectra of green and roasted coffee beans are shown in figure 1. All spectra show a first strong resonance with a maximum at approx. 2472.5 eV (“white line”), most probably resulting from a superposition of C-S, S-H and disulfide bonds, which is the typical environment of sulfur in biological systems, e.g. in the protein matrix resulting from the sulfur containing amino acids cysteine and methionine [5]. According to the literature, the vast majority of sulfurous molecules in green coffee beans are proteins [6]. For each coffee, roasting obviously leads to an increase in whiteline intensity and to a whiteline shift towards higher energies. This can be assigned to breaking of disulfide bonds; similar changes in the white line structure have been observed for the system “wheat gluten proteins”[7,8]. However, the chemical processes occurring in the course of the roasting process are considered to be more complex: upon thermal degradation of proteins and reactions of proteins (protein fragments) with other coffee compounds (esp.



carbohydrates) a wide variety of additional sulfur compounds is produced. Quantitative analysis of the measured spectra by fitting them to a linear combination of suitable reference spectra using a least square fitting routine is accordingly difficult. Identification of sulfur compounds formed during roasting (esp. cyclic thiols, e.g. furfurylthiol [1]), i.e. candidates for reference compounds, has not yet been achieved in this study, but is an objective of ongoing investigations.

Besides the white line peak, all spectra in figure 1 show a more or less pronounced structure at approx. 2481.3 eV, being evidence of the presence of a sulfate. Presence of sulfate in coffee beans – although not mentioned explicitly in the literature – is not surprising as for most plants uptake of sulfate is the major sulfur source for growth [9]. The contributions of hexavalent sulfur to the XANES spectra are either reduced (Fig. 1 (a), (c), (e)) or remain constant (Fig. 1 (b), (d), (f), (g), (h)) during roasting. Furthermore, in all XANES spectra of green beans a weak maximum at 2475.3 eV, which might be assigned to a Rydberg-state indicating the presence of S-H bonds [10] or the presence of a sulfoxide [8], can be observed. In the XANES spectra of the samples prepared in the test roaster this spectral feature disappears as a result of roasting (in the spectrum of roasted Huila coffee an extremely weak local maximum still remains), and the spectral region between whiteline and sulfate is homogeneously filled up. Solely in the spectrum of hand-roasted Ethiopian wild coffee this feature remains pronounced after roasting, suggesting that differences in roasting technique have a greater influence on XANES spectra than origin of beans.

### Acknowledgement

The authors would like to thank CAMD staff (especially Amitava Roy and Gregory Merchan) for their support, the State of Louisiana for providing the operating budget of CAMD and Mr. Carl Leonard (Community Coffee, Baton Rouge) for valuable advice.

### References

3. R. Tressl and R. Silwar, *J. Agric. Food Chem.* **29**, 1078-1082 (1981)
4. CAMD Annual Report 2004
5. J. Hormes, J. D. Scott and V. Suller, *Synchrotron Rad. News* **19**, 27-30 (2006)
4. M. Lemonnier, O. Collet, C. Depautex, J.-M. Esteva and D. Raoux, *Nucl. Instr. Meth.* **152**, 109-111 (1978)
5. D. Voet and J. G. Voet, *Biochemistry*, John Wiley, New York (1996)
6. J. R. Feldman, W. S. Ryder and J. T. Kung, *J. Agric. Food Chem.* **17**, no. 4, 733-739 (1969)
7. A. Prange, N. Kühlsen, B. Birzele, L. Arzberger, J. Hormes, S. Antes and P. Köhler, *Eur. Food Res. Technol.* **212**, 570-575 (2001)
8. A. Prange, B. Birzele, J. Krämer, H. Modrow, R. Chauvistré, J. Hormes and P. Köhler, *J. Agric. Food Chem.* **51**, 7431-7438 (2003)
9. H. Marschner, *Mineral nutrition of higher plants* (2<sup>nd</sup> edition), Academic Press, London, UK (1995)
10. A. Prange, C. Dahl, H.G. Trüper, M. Behnke, J. Hahn, H. Modrow and J. Hormes, *Eur. Phys. J. D* **20**, 589-596 (2002)

## Impact of H<sub>2</sub>S Exposure on the Sulfur Speciation in *Allium cepa*

Alexander Prange<sup>1,2</sup>, Henning Lichtenberg<sup>3</sup>, Mark Durenkamp<sup>4</sup>, Luit J. De Kok<sup>4</sup>  
and Josef Hormes<sup>1,3</sup>

<sup>1</sup>Center for Advanced Microstructures and Devices, Louisiana State University,  
6980 Jefferson Hwy., Baton Rouge, LA 70806, USA

<sup>2</sup>Niederrhein University of Applied Sciences, Rheydter Strasse 277,  
41065 Mönchengladbach, Germany

<sup>3</sup>Institute of Physics, University of Bonn, Nussallee 12, 53115 Bonn, Germany

<sup>4</sup>Laboratory of Plant Physiology, University of Groningen, Kerklaan 30,  
9751 Haren, The Netherlands

Correspondence to: A.Prange, e-mail: A. [Prange@gmx.de](mailto:Prange@gmx.de); PNR GMX-AP0507DCM

### 1. Introduction

Besides cysteine and methionine residues (present in the protein fraction) as well as thiols (e.g. glutathione) and sulfolipids, *Allium cepa* L. (onion) contains a variety of secondary sulfur compounds, e.g.  $\gamma$ -glutamyl peptides and alliin, which have potential value as phytopharmaceuticals [1]. Furthermore, alliin (supposedly predominantly synthesized in the leaves and then transferred to the bulb) and their breakdown products are important flavor precursors.

Under 'normal' (sulfate-sufficient) conditions, sulfate taken up by the root is the major sulfur source for plant growth. Sulfate has to be reduced to sulfite and subsequently further-reduced to sulfide, before it is incorporated into cysteine, the sulfur donor for most organic sulfur compounds in plants. Remaining sulfate is transferred to vacuoles for storage. Sulfate reduction and incorporation of sulfide into cysteine predominantly takes place in the shoot (chloroplast).

It has been shown by Durenkamp and De Kok [2] that onions are able to utilize absorbed atmospheric H<sub>2</sub>S as an 'alternative' sulfur source for growth. Foliarly absorbed H<sub>2</sub>S is then apparently directly incorporated into cysteine (regulation of the sulfate-uptake by the roots is then by-passed).

The regulation of sulfate uptake by the root, transport of sulfate to the shoot, subcellular sulfate distribution as well as the synthesis of secondary sulfur compounds strongly depends on the sulfur nutritional status of the plant. Investigating the interaction between pedospheric and atmospheric sulfur nutrition might help to gain an insight into regulation of sulfate uptake and sulfur assimilation, metabolism of H<sub>2</sub>S and synthesis of secondary sulfur compounds in *Allium cepa*.

It was the aim of this study to investigate whether the sulfur speciation differs in *Allium cepa* grown with sulfate and H<sub>2</sub>S, respectively, as sole sulfur source.

### 2. Materials and Methods

**Samples and sample preparation.** Powder samples of freeze-dried roots and shoots of *Allium cepa* L., grown under different conditions (sulfate-sufficient, sulfate-deprived,

H<sub>2</sub>S exposure) were uniformly spread on adhesive sulfur free kapton tape and covered with polypropylene foil. For further details see Durenkamp (2005)[3].

**XANES measurements.** XANES spectra at the sulfur K-edge were recorded at CAMD's DCM beamline [4]. The storage ring was operated at an energy of 1.3 GeV with electron currents between 200 and 80 mA. The X-ray beam was monochromatized with a modified Lemonnier type double crystal X-ray monochromator equipped with InSb(111)-crystals [5]. Measurements were performed in transmission mode. The incident monochromatic X-ray intensity and the transmitted intensity were measured with 10 cm-long ionization chambers (60 mbar air).

### 3. Results and Discussion

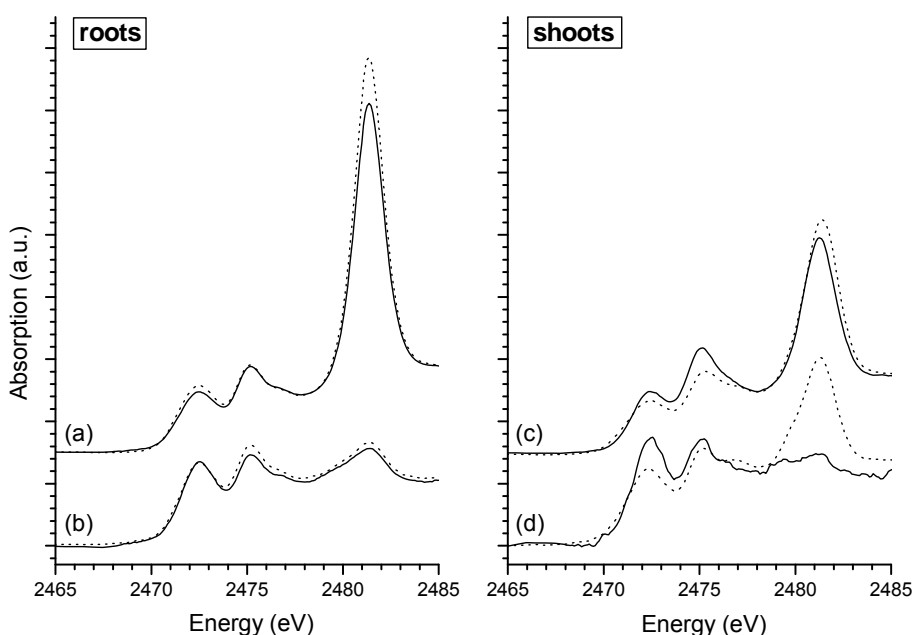


**Fig. 1:** Sulfur K-edge XANES spectra of freeze-dried roots and shoots of onion grown under different conditions (solid: 'normal' atmosphere, dots: H<sub>2</sub>S exposure): (a)/(c) sulfate-sufficient conditions, (b)/(d) sulfate-deprived conditions

In all measured XANES spectra spectra (Fig. 1) three local maxima are observable. The first strong resonance with a maximum at approx. 2472.4 eV ("white line") most probably results from a superposition of C-S, S-H (cysteine and methionine residues, thiols e.g. glutathione) and disulfide bonds (e.g. inter- and intra-protein crosslinks). The local absorption maximum at approx. 2475 eV might be assigned to compounds with a sulfoxide group, e.g. Alliins (S-alk(en)yl cysteine sulfoxides). The structure at approx. 2481.4 eV is a typical sulfate structure.

The results show that switching from pedospheric (sulfate-sufficient conditions) to atmospheric (H<sub>2</sub>S exposure) sulfur nutrition does not involve significant changes in the sulfur speciation in *Allium cepa*: neither formation of additional spectral features nor disappearance of existing structures could be observed in the measured XANES spectra.

Quantitative analysis of the spectra by fitting them to a linear combination of suitable reference spectra in order to interpret differences in the relative concentrations of sulfurous components between the measured samples is an objective of ongoing activities.

#### **Acknowledgement**

The authors would like to thank CAMD staff (especially Amitava Roy and Chris Bianchetti) for their support and the State of Louisiana for providing the operating budget of CAMD.

#### **References**

6. M. Keusgen, H. Schulz, J. Glodek, I. Krest, H. Krüger, N. Herchert and J. Keller, *J. Agric. Food Chem.* **50**, 2884-2890 (2002)
7. M. Durenkamp and L. J. de Kok, *Phyton* **42**, 55-63 (2002)
8. M. Durenkamp, Metabolism of atmospheric hydrogen sulfide in onion, PhD thesis, University of Groningen, 2005
4. J. Hormes, J. D. Scott and V. Suller, *Synchrotron Rad. News* **19**, 27-30 (2006)
5. M. Lemonnier, O. Collet, C. Depautex, J.-M. Esteva and D. Raoux, *Nucl. Instr. Meth.* **152**, 109-111 (1978)

#### **Poliakoff /Alderman Insert as PDF**

#### **Poliakoff XANES**

# An Infrared and X-ray Spectroscopic Study of the Reactions of 2-Chlorophenol, 1,2-Dichlorobenzene, and Chlorobenzene with Model CuO/Silica Fly Ash Surfaces

STEVEN L. ALDERMAN,<sup>†</sup>  
 GEORGE R. FARQUAR,<sup>‡</sup>  
 ERWIN D. POLIAKOFF, AND  
 BARRY DELLINGER\*

Department of Chemistry, Louisiana State University,  
 Baton Rouge, Louisiana 70803

The surface-mediated reactions of 2-chlorophenol, 1,2-dichlorobenzene, and chlorobenzene were studied using CuO/SiO<sub>2</sub> as a fly ash surrogate. These compounds served as model precursors that have been implicated in the formation of polychlorinated dibenzo-*p*-dioxins and polychlorinated dibenzofurans (PCDD/Fs). With FTIR, we determined that reactions of the model precursors with a substrate composed of CuO dispersed on silica result in the formation of a mixture of surface-bound phenolate and carboxylate partial oxidation products from 200 to 500 °C. Chemisorption of 2-chlorophenol and 1,2-dichlorobenzene resulted in the formation of identical surface-bound species. Using X-ray absorption near-edge structure spectroscopy, we measured the time- and temperature-dependent reduction of Cu(II) in a fly ash surrogate during reaction with each precursor. It was demonstrated that Cu<sub>2</sub>O is the major reduction product in each case. The rate of Cu(II) reduction could be described using pseudo-first-order reaction kinetics with Arrhenius activation energies for reduction of Cu(II) of 112, 101, and 88 kJ mol<sup>-1</sup> for 2-chlorophenol, 1,2-dichlorobenzene, and chlorobenzene, respectively. We demonstrate that chlorinated phenol and chlorinated benzene both chemisorb to form chlorophenolate. Although chlorinated phenols chemisorb at a faster rate, chlorinated benzenes are found at much higher concentrations in incinerator effluents. The implication is that chlorinated benzenes may form 10 times more chlorophenolate precursors to PCDD/Fs than chlorinated phenols in combustion systems.

## Introduction

Surface-mediated reactions are suspected of accounting for the majority of polychlorinated dibenzo-*p*-dioxin and polychlorinated dibenzofuran (PCDD/F or "dioxin") emissions from combustion sources (1–3). It is well established that transition-metal species found in native fly ash play a central role in PCDD/F formation, with copper oxides and chlorides having received the most attention to date. Two surface-

mediated pathways to PCDD/F formation have been developed, *de novo* and precursor. In both, PCDD/Fs are formed from approximately 250 to 450 °C, with a maximum occurring around 350 °C (1, 4, 5). PCDD/F formation may occur via the *de novo* pathway in which elemental (and possibly organic) carbon in the fly ash undergoes oxidation and chlorination reactions that result in the release of PCDD/F from the carbon matrix (1, 5). In the precursor pathway, PCDD/Fs are formed from chemically similar aromatic precursors such as chlorinated phenols and chlorinated benzenes that undergo surface-mediated coupling reactions to yield PCDD/Fs (4, 6). Additionally, some *de novo* research has shown that chlorinated phenols and chlorinated benzenes are formed from native carbon that reacts to yield primarily PCDDs (7). Regardless, low-temperature formation of PCDD/Fs in the postcombustion region of combustion systems requires the presence of a transition metal whether formation is from an aromatic precursor or carbonaceous material as in the *de novo* process.

Here, we present the results of two complementary studies to clarify some of the uncertainty regarding PCDD/F formation from aromatic precursors. Specifically, Fourier transform infrared (FTIR) spectroscopy and X-ray absorption near-edge structure (XANES) spectroscopy were used. FTIR was used to examine the nature of precursor chemisorption at potentially active surface sites, and XANES spectroscopy was used to investigate the role of Cu<sup>II</sup>O in promoting dioxin formation. A temperature-controlled dosing cell was used for *in situ* examination of the reactions of 2-chlorophenol (2-MCP), 1,2-dichlorobenzene (1,2-DCBz), and chlorobenzene (MCBz) with model fly ash surrogates composed of CuO and silica. 2-MCP is useful as a model chlorinated phenol precursor to PCDD/Fs (4, 8, 9), while the studies of MCB and 1,2-DCBz provide insight into the reactions and roles of chlorinated benzenes in the formation of PCDD/Fs.

The first step involved in the conversion of chlorophenols to PCDD/Fs must be adsorption at a catalytic surface site, where they subsequently react via Eley–Rideal- and/or Langmuir–Hinshelwood-type pathways to form PCDD/Fs (4, 6). In the Eley–Rideal pathway, a surface-bound chlorophenolate combines with a gas-phase chlorophenol to form PCDD/Fs, while the Langmuir–Hinshelwood pathway involves formation of PCDD/Fs from two surface-adsorbed molecules. Although chlorinated benzenes are often suggested PCDD/F precursors, they have not been studied extensively in this regard. Transition-metal species clearly promote PCDD/F formation after precursor adsorption (1, 4, 6), but the exact mechanism has not been elucidated. It has been proposed that these metals may promote the formation of surface-associated chlorophenoxy radicals that react to form PCDD/Fs through radical–radical and radical–molecule reactions similar to those detailed in gas-phase PCDD/F formation from chlorophenols (4, 10–12). This formation of a surface-associated radical likely invokes reduction of the metal center, but the reaction has not been studied extensively.

## Experimental Section

**FTIR Studies.** Time-dependent FTIR absorption spectra of 2-MCP, 1,2-DCBz, and MCBz reacting with a CuO/SiO<sub>2</sub> surface at 350 °C were collected *in situ* using a temperature-controlled dosing cell. Descriptions of the dosing cell and experimental procedure have been given elsewhere (13, 14). One significant feature of the dosing cell is the ability to rapidly heat and cool the sample, owing to the low heat capacity of the tungsten grid, which serves as a sample holder

\* To whom correspondence should be addressed. Phone: (225) 578-6759. Fax: (225) 578-3458. E-mail: barryd@lsu.edu.

<sup>†</sup> Current address: Diagnostic Instrumentation and Analysis Laboratory, Mississippi State University, Starkville, MS 39759.

<sup>‡</sup> Current address: Environmental Sciences Division, Oak Ridge National Laboratory, Oak Ridge, TN 37831.

and heating element. The sample can be heated or cooled (i.e., quenched) in less than 5 s. This permits the time-dependent spectral studies, as the reaction can be quenched so a spectrum can be acquired, and the reaction can be reinitiated by rapid heating.

Additionally, temperature-dependent spectra after 3 min of reaction with 2-MCP were obtained in the 200–500 °C range. FTIR spectra were collected in the absorbance mode from 4000 to 1100  $\text{cm}^{-1}$  with 2  $\text{cm}^{-1}$  resolution using a Midac M2000 Fourier transform infrared spectrometer. The region below 1200  $\text{cm}^{-1}$  could not be examined due to strong absorption by the silica.

The surrogate fly ash used for the FTIR study was composed of CuO (5 wt % Cu) supported on Cabosil that was prepared by the method of incipient wetness. Cabosil is a moderately high surface area (250  $\text{m}^2/\text{g}$ ) fumed silica. An aqueous solution of copper(II) nitrate hemipentahydrate ( $\text{Cu}(\text{NO}_3)_2 \cdot 2.5\text{H}_2\text{O}$ ) of the concentration necessary to yield 5% Cu was used for the active-phase precursor. The appropriate amount of Cabosil to achieve incipient wetness was added to this solution and the resulting solution allowed to stand for 2 h with occasional stirring. The substrate was dried for 7 h at 100 °C and then calcined at 450 °C for 12 h to convert the  $\text{Cu}(\text{NO}_3)_2$  to CuO.

The powder substrate was deposited on a tungsten grid that acts as the dosing cell's sample holder and heating element (13). The substrate was heated in air at 450 °C to remove any organic impurities before being pumped down to a base pressure of  $10^{-6}$  Torr. At the onset of each run, the surface temperature was brought to reaction temperature. Dosant vapor was introduced to the dosing cell from the liquid from an evacuated side arm dosing port. The concentration was that of the room temperature vapor pressure of the dosant. This corresponds to 1.4 Torr for 2-MCP, 1.5 Torr for 1,2-DCBz, and 11.9 Torr for MCBz. Because the dosant vapor was introduced to the cell from the bulk and the cell was evacuated and redosed before each spectrum was collected, the concentration of each dosant was essentially constant throughout any given run. At the end of the desired reaction interval, terminating the power supply across the tungsten grid quenched the reaction in less than 5 s due to rapid cooling of the grid. The cell was then evacuated to  $10^{-6}$  Torr to remove all free and physisorbed dosant so that the FTIR spectrum revealed only chemisorbed reaction products.

**XANES Studies.** XANES spectra were collected at the Cu K-edge using the double-crystal monochromator beam line at the synchrotron radiation source at the Center for Advanced Microstructures and Devices (CAMD), at Louisiana State University (15, 16). At injection, the electron storage ring operates with a beam current of ca. 150 mA and typically has a lifetime of 4–8 h. The photon flux after the monochromator is estimated to be approximately  $10^8 \text{ s}^{-1}$ . The photon bandwidth is 2 eV, and the step size in the region of the Cu K-edge is  $\sim 0.3$  eV.

For the XANES experiments, the surrogate fly ash was a mixture of Cabosil and  $<5 \mu\text{m}$  particle size CuO. The concentration of CuO is approximately 40%. While this value is higher than typical fly ash copper concentrations, the attenuation of the X-ray beam provides for high-quality XANES spectra, thereby permitting precise determinations of chemical speciation in the substrate. The time-dependent reduction of Cu(II) was monitored from 275 to 375 °C when 2-MCP, 1,2-DCBz, and MCBz were exposed to the substrate. In each case, the concentration of the dosant is in excess, allowing for pseudo-first-order kinetic analysis of  $\text{Cu}^{\text{II}}$ O reduction. The same temperature-controlled dosing cell used for the FTIR work was used for the XANES studies, with 100  $\mu\text{m}$  Kapton transmission windows in place of the IR windows.

We had previously demonstrated that consistent results are obtained when the copper oxide is cycled, i.e., reduction

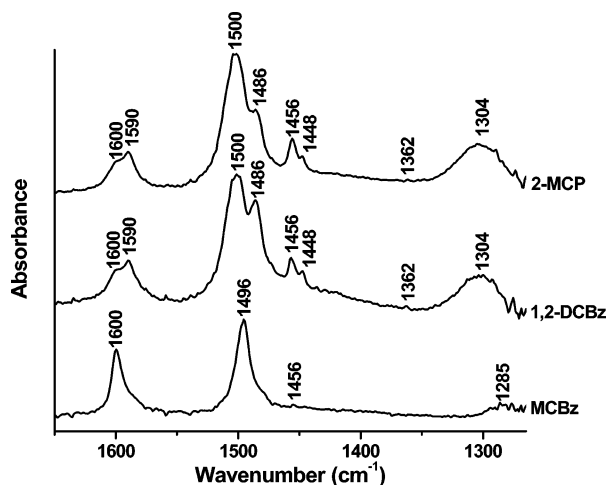


**FIGURE 1.** FTIR spectra comparing the chemisorbed reaction products after exposure of 2-chlorophenol, 1,2-dichlorobenzene, and chlorobenzene to  $\text{CuO}/\text{SiO}_2$  at 350 °C.

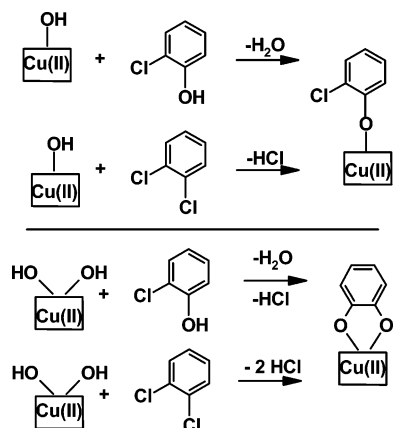
by exposure to the dosant, followed by reoxidizing it to Cu(II) (13). This cycling procedure was also used in this study. Over the course of the reaction, Cu(II), Cu(I), and Cu(0) each contribute to the experimental XANES spectra. The composition can be quantified with regard to copper speciation by fitting the experimental spectra to a superposition of standard spectra (CuO,  $\text{Cu}_2\text{O}$ , Cu metal foil). Best fits were determined by minimizing  $\chi^2$  values generated from the residual differences between experimental and simulated spectra, as discussed elsewhere (13).

## Results and Discussion

**FTIR.** Figure 1 compares FTIR spectra in the region between 1645 and 1265  $\text{cm}^{-1}$  resulting from the reaction of 2-MCP, 1,2-DCBz, and MCBz with the  $\text{CuO}/\text{SiO}_2$  surface at 350 °C. On the basis of the FTIR spectra, 2-MCP and 1,2-DCBz adsorb to the surface to produce identical species. Peaks at 1590, 1486, and 1448  $\text{cm}^{-1}$  are attributed to aromatic ring-breathing modes of 2-MCP and 1,2-DCBz adsorbed as a chlorophenolate. These bands are shifted 8–10  $\text{cm}^{-1}$  lower in energy than the analogous gas-phase bands of 2-MCP and 13–24  $\text{cm}^{-1}$  to lower energy than those of 1,2-DCBz. As will be demonstrated later in this discussion, infrared absorptions corresponding to surface hydroxyl groups of primarily silica and possibly those of CuO are removed from the surface during reaction, indicating that they are sites of adsorption. Absent from the 2-MCP spectrum is a peak at 1338  $\text{cm}^{-1}$  due to 2-MCP phenolic hydroxyl bending. This peak is present when 2-MCP is physically adsorbed at room temperature and indicates that 2-MCP adsorbs to surface hydroxyl sites through its phenolic O–H substituent. Although the C–Cl stretching bands of 1,2-DCBz could not be examined, it must chemisorb through its chlorine substituent since the phenolate species observed is identical to that formed from 2-MCP chemisorption. The chemisorption pathways of 2-MCP and 1,2-DCBz to yield chlorophenolate are depicted at isolated CuO hydroxyl sites in the upper half of Scheme 1.

In an earlier study, where 2-MCP was chemisorbed to Cabosil, but with no copper present, the phenolate ring breathing bands were in exact agreement with the present results (14). However, 1,2-DCBz did not chemisorb to the silica in the absence of CuO. A control experiment in which the silica was prepared by the method of incipient wetness, with the exception of the addition of the CuO precursor, revealed that the wetting, drying, and calcination steps alone involved in supporting CuO on silica did not alter the reactivity of surface silanol groups with regard to the uptake

**SCHEME 1. Chemisorption of 2-Chlorophenol and 1,2-Dichlorobenzene To Yield the Same Surface Species<sup>a</sup>**



<sup>a</sup> Adsorbed chlorophenolate, upper trace, was observed directly by FTIR, while the formation of the catecholic intermediate was inferred from the observation of carboxylate partial oxidation products.

of 1,2-DCBz. Therefore, the presence of CuO seems to be critical for 1,2-DCBz chemisorption to take place. Silica hydroxyl groups are, however, removed from the surface following 1,2-DCBz adsorption. This implies that 1,2-DCBz adsorption initially takes place at copper sites before migration across the surface to the less active silica hydroxyl sites. Although we depicted 2-MCP and 1,2-DCBz reacting at surface hydroxyl sites of CuO, it is possible that these compounds are ultimately adsorbed at other sites on CuO, such as oxygen vacancies.

Also evident in the 2-MCP and 1,2-DCBz spectra in Figure 1 is an absorption band centered around  $1304\text{ cm}^{-1}$ . This peak appears to be unresolved from an additional peak at  $1289\text{ cm}^{-1}$ . In the previous study of 2-MCP adsorption on pure Cabosil, a peak was observed at  $1287\text{ cm}^{-1}$  which was assigned to the C–O stretching vibration of phenolate adsorbed to a silica hydroxyl site (14). This is also the assignment for the peak at  $1289\text{ cm}^{-1}$ . Although not shown, peaks attributed to aromatic C–H stretching vibrations of the adsorbed phenolate are also present at  $3079$  and  $3046\text{ cm}^{-1}$  following 2-MCP and 1,2-DCBz adsorption.

Absorption bands at  $1600$ ,  $1511$ ,  $1505$ ,  $1500$ ,  $1456$ , and  $1362\text{ cm}^{-1}$  are also present in the 2-MCP and 1,2-DCBz spectra in Figure 1 and are attributed to the formation of surface-bound carboxylate partial oxidation products (formates and acetates). These assignments are in good agreement with multiple FTIR studies in the catalysis literature. Additionally, carboxylates have been detected upon adsorption and partial oxidation of 2-MCP and 1,2-DCBz (17–21). It has been proposed that the formation of surface carboxylates from chlorinated aromatics is preceded by the formation of a bidentate-adsorbed, catecholic-type intermediate (22), and we have previously reported the formation of catechols in similar systems (14). The lower half of Scheme 1 illustrates the proposed chemisorption pathways of 2-MCP (or 1,2-DCBz) to yield catecholic intermediates at geminal hydroxyl sites.

Reaction of MCBz yields absorption bands due to phenolate ring-breathing modes at  $1600$  and  $1496\text{ cm}^{-1}$ , shown in the lower trace of Figure 1. Peaks not shown at  $3080$  and  $3053\text{ cm}^{-1}$  are due to aromatic C–H stretching. When phenol is chemisorbed to pure silica at  $200\text{ }^\circ\text{C}$ , peaks appear that are in exact agreement with those shown for MCBz chemisorption in Figure 1, indicating a common surface-bound species following phenol and MCBz chemisorption. Thus, phenol and MCBz chemisorb in a manner analogous to that of 2-MCP and 1,2-DCBz, via  $\text{H}_2\text{O}$  and  $\text{HCl}$  elimination, respectively. As with 1,2-DCBz, MCBz did not

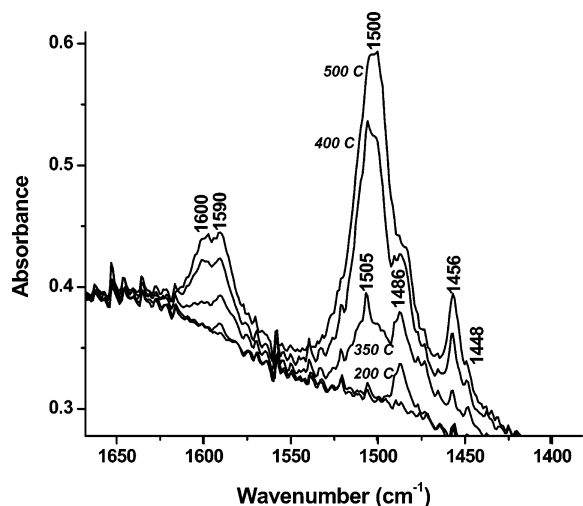


**FIGURE 2. Temperature-dependent FTIR spectra of 2-MCP chemisorption and oxidation after 3 min of reaction time. The reaction temperatures, in order of increasing absorbance are, baseline,  $200\text{ }^\circ\text{C}$ ,  $350\text{ }^\circ\text{C}$ ,  $400\text{ }^\circ\text{C}$ , and  $500\text{ }^\circ\text{C}$ .**

chemisorb to any appreciable extent in the absence of CuO. Surface-bound partial oxidation products make a very small contribution to the MCBz spectrum, with only a weak peak at  $1456\text{ cm}^{-1}$  due to acetate. However, it is possible that other oxidation products were formed but not chemically bound to the surface and were removed during the cell evacuation procedure.

Figure 2 illustrates the temperature dependence of 2-MCP chemisorption and oxidation after 3 min of exposure to the CuO/SiO<sub>2</sub> surface. At  $200\text{ }^\circ\text{C}$ , peaks due to adsorbed chlorophenolate at  $1486$  and  $1590\text{ cm}^{-1}$  are evident. A relatively small concentration of a surface-bound formate is also observed. By  $350\text{ }^\circ\text{C}$ , the relative absorbance due to partial oxidation products is greater than that of the chlorophenolate bands. The carboxylate-to-phenolate ratio continues to increase with increasing temperature. We also observed the formation of these surface carboxylates in our temperature-dependent investigation of 2-MCP chemisorption on pure Cabosil (14). The current study demonstrates that when CuO is dispersed on the silica, carboxylates are formed at approximately  $100\text{ }^\circ\text{C}$  lower temperature and with much higher carboxylate-to-phenolate ratios, illustrating the effectiveness of CuO in promoting the oxidation of 2-MCP.

Figure 3a depicts the time-dependent loss of surface hydroxyl groups due to the reaction of the surface with 2-MCP at  $350\text{ }^\circ\text{C}$ . The major feature is a loss in intensity of a band at  $3745\text{ cm}^{-1}$ , which is consistent with that of silica surface hydroxyl groups (23). As these are difference absorption spectra, the more negative the peak, the greater the extent of reaction with the surface hydroxyls. Also evident is the loss of absorption bands at  $3742$  and  $3737\text{ cm}^{-1}$ , indicating that more than one type of surface hydroxyl participates in the adsorption process. These latter absorption bands may be due to either vicinal or geminal surface hydroxyls of the silica, or possibly hydroxyl groups associated with CuO. For completeness, the time-dependent growth of chlorophenolate and partial oxidation products is illustrated by the FTIR spectra in Figure 3b. Spectra taken after the substrate samples were dosed to completion, and then oxidized at  $350\text{ }^\circ\text{C}$  in air for 5 min, revealed no evidence of adsorbed surface species and show that the surface hydroxyl groups have been replenished, indicating complete oxidation and desorption of surface species.

The time-dependent FTIR spectra for 1,2-DCBz adsorption and oxidation products are identical to those shown for 2-MCP in Figure 3b, but adsorption and oxidation occur at

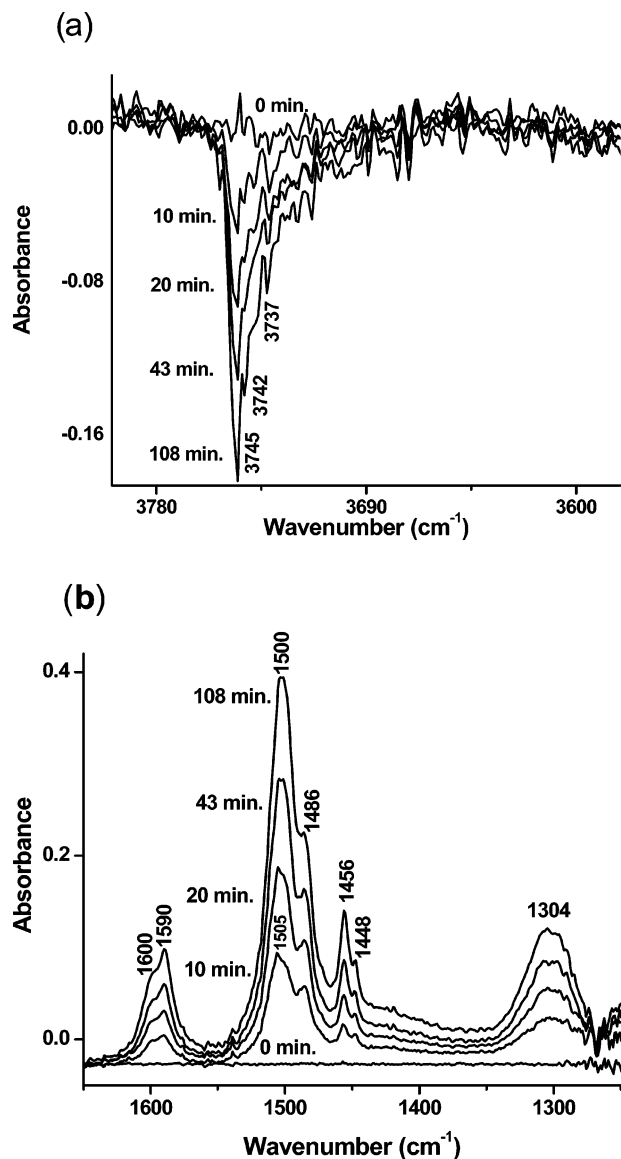


**FIGURE 3.** FTIR spectra depicting the time-dependent (a) loss of surface hydroxyl groups after reaction of 2-MCP at 350 °C [the peak becomes more negative (more -OH removed from the surface) as the reaction proceeds; reaction times are  $t = 0, 10, 20, 43,$  and 108 min] and (b) growth of adsorption and partial oxidation products after reaction of 2-MCP at 350 °C after  $t = 0, 2, 10, 20, 43,$  and 108 min.

a slower rate. The vapor pressures of 2-MCP and 1,2-DCBz are sufficiently close that the rates of adsorption and oxidation can be compared by plotting the peak height of one of the chlorophenolate ring-breathing modes and the peak height of a partial oxidation product vibration with respect to time, as shown in Figure 4. We chose to compare the chlorophenolate ring-breathing mode at 1486 cm<sup>-1</sup> and formate peaks at 1500 cm<sup>-1</sup>. The growth in intensity of these bands was fit to an exponential of the form  $I_t = I_\infty(1 - e^{-kt})$ , where  $I_t$  is the peak height at reaction time  $t$ ,  $I_\infty$  is the asymptotic value of the peak height, and  $k$  is the rate coefficient for chemisorption ( $k_{cs}$ ) and oxidation ( $k_{ox}$ ). The fit of the phenolate band resulting from 2-MCP adsorption gives  $I_\infty = 0.245$  and  $k_{cs} = 6.6 \times 10^{-4} \text{ s}^{-1}$ . For 1,2-DCBz,  $I_\infty = 0.304$  and  $k_{cs} = 6.0 \times 10^{-5} \text{ s}^{-1}$ . Fitting of the growth of the formate peak at 1500 cm<sup>-1</sup> results in  $I_\infty = 0.424$ ,  $k_{ox} = 5.5 \times 10^{-4} \text{ s}^{-1}$  and  $I_\infty = 0.269$ ,  $k_{ox} = 1.0 \times 10^{-4} \text{ s}^{-1}$  for 2-MCP and 1,2-DCBz, respectively. These analyses indicate that adsorption to form chlorophenolate is approximately 11 times faster for 2-MCP versus 1,2-DCBz. Partial

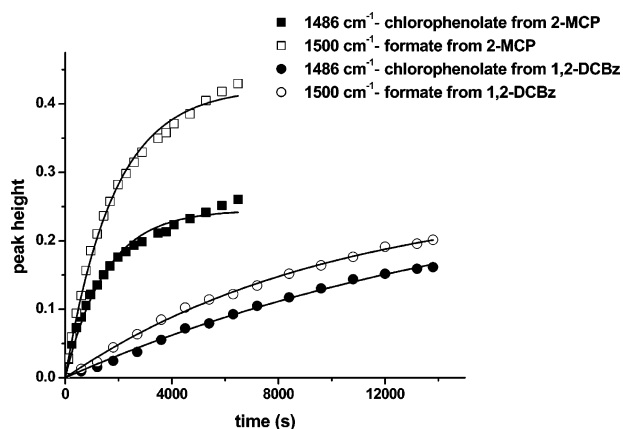


**FIGURE 4.** A comparison of the rates of chemisorption (cs) and oxidation (ox) of 2-MCP and 1,2-DCBz by fitting the increasing peak height of a common phenolate ring-breathing mode (1486 cm<sup>-1</sup>) and formate COO<sup>-</sup> stretch (1500 cm<sup>-1</sup>) to the form  $I_t = I_\infty(1 - e^{-kt})$ .  $I_t$  is the peak height, and  $k$  is the rate of precursor chemisorption ( $k_{cs}$ ) and oxidation ( $k_{ox}$ ).

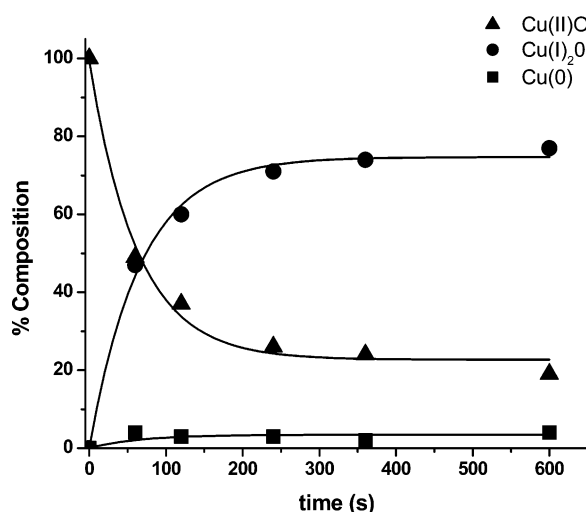


**FIGURE 5.** Time-dependent reduction of Cu<sup>II</sup>O and formation of Cu<sub>2</sub>O and Cu(0) for reaction of 2-MCP with CuO at 350 °C.

**TABLE 1.** Time-Dependent Copper Speciation for the Reaction of 2-MCP, 1,2-DCBz, and MCBz with CuO at 350 °C

time (s)	2-chlorophenol			1,2-dichlorobenzene			chlorobenzene		
	% CuO	% Cu <sub>2</sub> O	% Cu(0)	% CuO	% Cu <sub>2</sub> O	% Cu(0)	% CuO	% Cu <sub>2</sub> O	% Cu(0)
0	100	0	0	100	0	0	100	0	0
60	49	47	4	54	44	2	74	20	6
120	37	60	3	46	50	4	57	38	5
240	26	71	3	30	67	3	37	57	6
360	24	74	2	20	75	5	31	64	5
600	19	77	4	19	76	5	21	74	5

oxidation is approximately 6 times faster for 2-MCP. The more rapid reaction rate of 2-MCP reaction was expected since chemisorption requires breaking of the phenolic O-H bond, which has a bond dissociation energy of 82 kcal mol<sup>-1</sup> (24), compared to a bond dissociation energy of 97 kcal mol<sup>-1</sup> for the C-Cl bond in 1,2-DCBz (25).

**XANES.** Figure 5 illustrates the reduction of CuO and the formation of Cu<sub>2</sub>O and Cu(0) when the CuO/silica mixture is exposed to 2-MCP at 350 °C. Table 1 presents the copper speciation of the substrate after exposure to each dosant at 350 °C. In each case, the major reduction product is Cu<sub>2</sub>O,



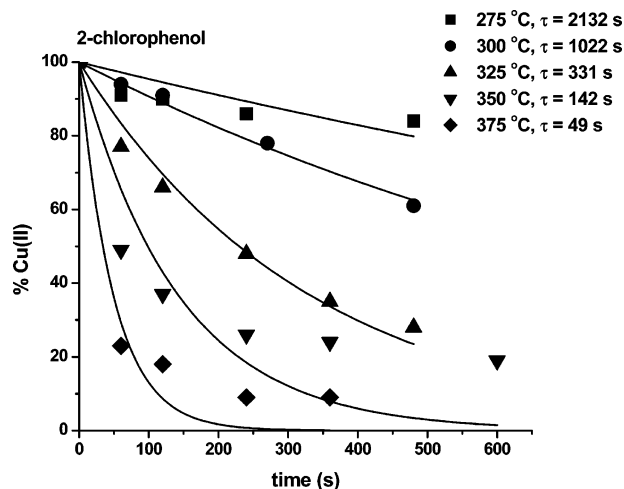
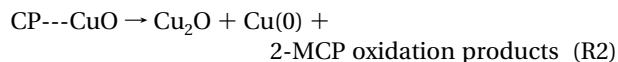
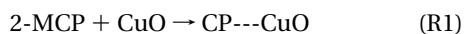


FIGURE 6. Reduction of Cu(II) due to reaction of 2-MCP with CuO from 275 to 375 °C.  $1/\tau = k'$ , the pseudo-first-order rate coefficient, where  $k' = D_0 k_{bi}$ .

i.e., copper in the Cu(I) oxidation state. We have determined this to be  $\text{Cu}_2\text{O}$  and not another Cu(I) species, as the  $\text{Cu}_2\text{O}$  reference standard resulted in qualitatively superior fits compared to other reference standards. Reduction to metallic copper is a negligible reaction product. Reduction of CuO to  $\text{Cu}_2\text{O}$  (and trace amounts of Cu(0)) was the result for each dosant at all temperatures measured.

2-MCP is adsorbed onto the copper oxide surface to form surface-bound chlorophenolate (CP---CuO) (cf. reaction R1), which is followed by reduction of Cu(II) to Cu(I) and Cu(0) and the formation of 2-MCP oxidation products (cf. reaction R2).



1,2-DCBz and MCBz react similarly. The rate of Cu(II) reduction can be measured using a pseudo-first-order kinetic reaction scheme, with the form of the rate law given in eq 1,

$$\ln f_r(\text{Cu(II)}) = -k_{bi} D_0 t \quad (1)$$

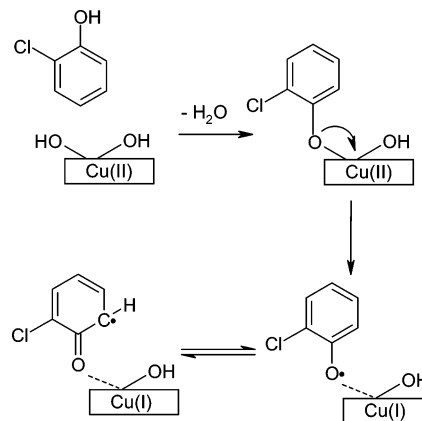
where  $f_r$  is the amount of Cu(II) remaining *unreacted* at time  $t$ ,  $D_0$  is the vapor-phase concentration of the chlorinated aromatic dosant, and  $k_{bi}$  is the true bimolecular reaction rate coefficient for reduction of  $\text{Cu}^{II}\text{O}$  by the dosant. The percent composition of Cu(II) vs time was fit to an exponential decay of the form  $[\text{Cu(II)}]_t = [\text{Cu(II)}]_\infty + (100 - [\text{Cu(II)}]_\infty) e^{-t/\tau}$ , where  $[\text{Cu(II)}]_t$  denotes the percent composition of Cu(II) in the substrate at reaction time  $t$  and  $[\text{Cu(II)}]_\infty$  denotes the asymptotic value of the decay curve. The inverse of the decay constant,  $\tau$ , yields a pseudo-first-order rate coefficient,  $k'$ , where  $k' = k_{bi} D_0$ . An example of this is shown for the reaction of 2-MCP in Figure 6. Fits are acceptable over the time interval measured at lower reaction temperatures but begin to degrade at higher temperatures and longer reaction times, probably due to competing reactions of secondary reaction products. This kinetic analysis was also performed for 1,2-DCBz and MCBz. The calculated values of  $k_{bi}$  for each dosant at each temperature are given in Table 2.

Arrhenius plots ( $\ln k_{bi}$  versus  $1/T$ ) yields the two-parameter Arrhenius activation energy ( $E_a$ ) and preexponential factor ( $A$ ). The activation energies of Cu(II) reduction were found to be  $112 \pm 6.4$ ,  $101 \pm 1.21$ , and  $88 \pm 3.3 \text{ kJ mol}^{-1}$  for 2-MCP, 1,2-DCBz, and MCBz, respectively. The  $A$  factors are  $9.7 \pm$

TABLE 2. Bimolecular Rate Coefficients for the Reduction of Cu(II) in CuO by 2-MCP, 1,2-DCBz, and MCBz

temp (°C)	2-MCP $k_{bi}$ ( $\text{atm}^{-1} \text{s}^{-1}$ )	1,2-DCBz $k_{bi}$ ( $\text{atm}^{-1} \text{s}^{-1}$ )	MCBz $k_{bi}$ ( $\text{atm}^{-1} \text{s}^{-1}$ )
275	0.251	0.125	0.022
300	0.524	0.573	0.048
325	1.62	1.25	0.096
350	3.77	2.93	0.24
375	10.93	2.73	0.415
$E_a$ ( $\text{kJ mol}^{-1}$ )	$112 \pm 6.4$	$101 \pm 1.21$	$88 \pm 3.3$
$A$ ( $\text{atm}^{-1} \text{s}^{-1}$ )	$(9.7 \pm 18.6) \times 10^9$	$(1.2 \pm 11.7) \times 10^9$	$(6.6 \pm 1.93) \times 10^6$

SCHEME 2. Adsorption of 2-Chlorophenol at a Surface Hydroxyl of CuO and Formation of the Chlorophenoxy Radical<sup>a</sup>



<sup>a</sup> Since this radical is resonance stabilized, spin density is located at both the carbon and oxygen.

$18.6 \times 10^9$ ,  $1.2 \pm 11.7 \times 10^9$ , and  $5.6 \pm 1.93 \times 10^6 \text{ atm}^{-1} \text{ s}^{-1}$ , respectively.

**Possible Implications for PCDD/F Formation.** A detailed packed-bed flow-reactor study was conducted by Lomnicki and Dellinger, who used 2-MCP as a model PCDD/F precursor and CuO supported on silica as a model fly ash (4). Their results suggested that PCDDs are formed through an Eley–Rideal mechanism and that PCDFs are formed via the Langmuir–Hinshelwood pathway. The main PCDD/F products formed from their experiments were the same products observed from gas-phase radical–molecule and/or radical–radical reactions of 2-MCP (8, 26). On the basis of this, it was suspected that surface-associated phenoxy radicals may form PCDD/Fs in a manner similar to that of gas-phase formation. Using EPR spectroscopy, they found convincing evidence for the existence of a carbon-centered phenoxy radical when 2-MCP is adsorbed onto CuO/SiO<sub>2</sub>. They went on to suggest that chlorophenol adsorbs to a Cu(II) site as chlorophenolate and a surface-associated radical is formed following electron transfer from chlorophenolate to the metal cation site, thus reducing Cu(II) to Cu(I), as illustrated in Scheme 2.

We have previously demonstrated that CuO is reduced to primarily  $\text{Cu}_2\text{O}$  in the presence of 2-MCP vapor at 375 °C (13). We have now shown that 1,2-DCBz and MCBz also reduce CuO to  $\text{Cu}_2\text{O}$ , and that these reactions occur over a temperature range of 275–375 °C, which is the temperature range of cool-zone, surface-mediated formation of PCDD/Fs in combustion systems. These results are consistent with the proposal that phenoxy radical forms following a one-electron transfer to Cu(II) sites. Although most of the adsorbed aromatics will be completely oxidized to their thermodynamic end products, incomplete oxidation processes that yield PCDD/F compounds involve the same initial steps, i.e., adsorption and partial oxidation.

The results of our FTIR study demonstrate that 1,2-DCBz chemisorbs to the surface to produce the same species as 2-MCP. If reactions of adsorbed phenolate (phenoxyl radicals) are responsible for PCDD/F formation, it stands to reason that chlorinated benzenes will make a contribution to total yields, especially PCDF formation, which is proposed to take place by coupling of adsorbed chlorophenoxyl radicals. Our measurements indicate that the rate of chemisorption of 1,2-DCBz is  $\sim 10\times$  slower than that of 2-MCP. This suggests that since the concentrations of chlorinated benzenes observed in incinerator effluent are  $100\times$  greater (27) than those of chlorinated phenols, the number of surface-bound PCDD/F phenolate precursors that result from chlorinated benzenes is approximately  $10\times$  greater than the number of those that result from chlorinated phenols. Additional research on the role of chlorinated benzenes as precursors in PCDD/F formation is clearly indicated.

## Acknowledgments

We acknowledge the support of this work under NSF Grant CTS-9996085 and the Patrick F. Taylor Chair. We regret the recent passing of Mr. Patrick F. Taylor, who founded the TOPS tuition remission program for qualified students at Louisiana universities and who established the Patrick F. Taylor Chair of the Environmental Impact of Treatment of Hazardous Wastes held by B.D.

## Literature Cited

- (1) Fiedler, H. Thermal formation of PCDD/PCDF: a survey. *Environ. Eng. Sci.* **1998**, *15*, 49.
- (2) Altwicker, E. R.; Schonberg, J. S.; Konduri, R. K. N. V.; Milligan, M. S. Polychlorinated dioxin/furan formation in incinerators. *Hazard. Waste Hazard. Mater.* **1990**, *7*, 73.
- (3) Taylor, P. H.; Dellinger, B. Pyrolysis and molecular growth of chlorinated hydrocarbons. *J. Anal. Appl. Pyrolysis* **1999**, *49*, 9.
- (4) Lomnicki, S.; Dellinger, B. A detailed mechanism of the surface-mediated formation of PCDD/F from the oxidation of 2-chlorophenol on a CuO/Silica Surface. *J. Phys. Chem. A* **2003**, *107*, 4387.
- (5) Pekarek, V.; Grabic, R.; Marklund, S.; Puncocar, M.; Ullrich, J. Effects of oxygen on formation of PCB and PCDD/F on extracted fly ash in the presence of carbon and cupric salt. *Chemosphere* **2001**, *43*, 777.
- (6) Milligan, M. S.; Altwicker, E. R. Chlorophenol reactions on fly ash. 2. equilibrium surface coverage and global kinetics. *Environ. Sci. Technol.* **1996**, *30*, 230.
- (7) Hell, K.; Stieglitz, L.; Dinjus, E. Mechanistic aspects of the *de-novo* synthesis PCDD/PCDF on model mixtures and MSWI fly ashes using amorphous  $^{12}\text{C}$ - and  $^{13}\text{C}$ -labeled carbon. *Environ. Sci. Technol.* **2001**, *35*, 3892.
- (8) Weber, R.; Hagenmaier, H. Mechanism of the formation of polychlorinated dibenzo-p-dioxins and dibenzofurans from chlorophenols in gas-phase reactions. *Chemosphere* **1999**, *38*, 529.
- (9) Evans, C. S.; Dellinger, B. Mechanisms of dioxin formation from the high-temperature Pyrolysis of 2-chlorophenol. *Environ. Sci. Technol.* **2003**, *37*, 1325.
- (10) Tuppurainen, K.; Ruuskanen, J. A plausible mechanism for copper-catalyzed oxidative chlorophenol coupling reaction. Semi-empirical AM1 and *ab initio* 3-21G molecular orbital studies. *Chemosphere* **1999**, *38*, 1825.

- (11) Voncina, E.; Solmajer, T. Thermolysis of 2,4,6-trichlorophenol chemisorbed on aluminum oxides as example of fly ash mediated surface catalysis in PCDD/PCDF formation. *Chemosphere* **2002**, *46*, 1279.
- (12) Boyd, S. A.; Mortland, M. M. Radical formation and polymerization of chlorophenols and chloroanisole on copper(II)-smectite. *Environ. Sci. Technol.* **1986**, *20*, 1056.
- (13) Farquar, G. R.; Alderman, S. L.; Poliakoff, E. D.; Dellinger, B. X-ray spectroscopic studies of the high-temperature reduction of Cu(II)O by 2-chlorophenol on a simulated fly ash surface. *Environ. Sci. Technol.* **2003**, *37*, 931.
- (14) Alderman, S. L.; Dellinger, B. FTIR investigation of 2-chlorophenol chemisorption on a silica surface from 200-500 °C. *J. Phys. Chem.*, in press.
- (15) Schilling, P.; Morikawa, E.; Tolentino, H.; Tamura, E.; Kurtz, R. L.; Cusatis, C. Installation and operation of the LNLS double-crystal monochromator at CAMD. *Rev. Sci. Instrum.* **1995**, *66*, 2214.
- (16) Stockbauer, R. L.; Ajmera, P.; Poliakoff, E. D.; Craft, B. C.; Saile, V. A new synchrotron light source at Louisiana State University's Center for Advanced Microstructures and Devices. *Nucl. Instrum. Methods Phys. Res.* **1990**, *291*, 505.
- (17) Bandara, J.; Mielczarski, J. A.; Kiwi, J. Adsorption mechanisms of chlorophenol on iron oxides, titanium oxide and aluminum oxide as detected by infrared spectroscopy. *Appl. Catal., B* **2001**, *34*, 307.
- (18) Larrubia, M. A.; Busca, G. An FT-IR study of the conversion of 2-chloropropane, *o*-dichlorobenzene, and dibenzofuran on  $\text{V}_2\text{O}_5$ - $\text{MoO}_3$ - $\text{TiO}_2$  SCR- $\text{DeNO}_x$  catalysts. *Appl. Catal., B* **2002**, *39*, 343.
- (19) Krishnamoorthy, S.; Rivas, J. A.; Amiridis, M. D. Catalytic oxidation of 1,2-dichlorobenzene over supported transition metal oxides. *J. Catal.* **2000**, *193*, 264.
- (20) Angevaere, P. A. J. M.; Grootendorst, E. J.; Zuur, A. P.; Ponc, V. In *New Developments in Selective Oxidation*; Centri, G., Trifiro, F., Eds.; Elsevier: Amsterdam, 1990; p 861.
- (21) Busca, G. Infrared studies of the reactive adsorption of organic molecules over metal Oxides and of the mechanisms of their heterogeneously-catalyzed oxidation. *Catal. Today* **1996**, *27*, 457.
- (22) Lichtenberger, J.; Amiridis, M. D. Catalytic oxidation of chlorinated benzenes over  $\text{V}_2\text{O}_5/\text{TiO}_2$  catalysts. *J. Catal.* **2004**, *223*, 296.
- (23) Hair, M. L.; Hertl, W. Reactions of chlorosilanes with silica surfaces. *J. Phys. Chem.* **1969**, *73*, 2372.
- (24) Khachatryan, L.; Asatryan, R.; Dellinger, B. Development of expanded and core kinetic models for the gas-phase formation of dioxins from chlorinated phenols. *Chemosphere* **2003**, *52*, 695.
- (25) Tsang, W. Mechanisms for the formation and destruction of chlorinated organic products of incomplete combustion. *Combust. Sci. Technol.* **1990**, *74*, 99.
- (26) Sidhu, S.; Maqsood, L.; Dellinger, B.; Mascolo, G. The homogeneous, gas-phase formation of chlorinated and brominated dibenzo-p-dioxin from 2,4,6-trichloro- and 2,4,6-tribromophenols. *Combust. Flame* **1995**, *100*, 11.
- (27) Blumenstock, M.; Zimmermann, R.; Schramm, K. W.; Kaune, A.; Nikolai, U.; Lenoir, D.; Ketttrup, A. Estimation of the dioxin emissions (PCDD/F I-TEQ) from the concentration of low chlorinated aromatic compounds in the flue and stack gas of a hazardous waste incinerator. *J. Anal. Appl. Pyrolysis* **1999**, *49*, 179.

Received for review January 12, 2005. Revised manuscript received July 25, 2005. Accepted July 27, 2005.

ES050063N

# X-ray Spectroscopic Studies of the High Temperature Reduction of Cu(II)O by 2-Chlorophenol on a Simulated Fly Ash Surface

GEORGE R. FARQUAR, S. L. ALDERMAN, E. D. POLIAKOFF,\* AND B. DELLINGER

Department of Chemistry, Louisiana State University, Baton Rouge, Louisiana 70803

The reaction of 2-chlorophenol on Cu(II)O at 375 °C is studied using X-ray absorption near edge structure (XANES) spectroscopy. A mixture of copper(II) oxide and silica is prepared to serve as a surrogate for fly ash in combustion systems. 2-Chlorophenol is utilized as a model precursor for formation of polychlorinated dibenzo-*p*-dioxins and polychlorinated dibenzofurans (PCDD/F). The Cu K-edge spectra shift to lower binding energy, reflecting the reduction of the copper. The substrate is found to form a mixture of Cu(II), Cu(I), and Cu(0), with the dominant species being Cu(I). The data are fitted well with a first-order reaction scheme, with a time constant at 375 °C of 76 s. This is the first application of XANES spectroscopy for studying the kinetics and mechanism of heterogeneous reactions relevant to combustion processes, and the results demonstrate the utility and desirability of such X-ray spectroscopic studies.

## I. Introduction

In recent years, there has been a growing recognition within the combustion research community that surface-mediated reactions are responsible for a significant fraction of toxic air pollutants emitted from combustion and thermal processes (1, 2). Research in this area has been driven by the discovery that emissions of polychlorinated dibenzo-*p*-dioxins and polychlorinated dibenzofurans (PCDD/F or "dioxins") are nearly ubiquitous and that their formation is largely due to surface-mediated reactions involving transition metals, hydrocarbons, and a chlorine source (2–12).

Pathways of formation of PCDD/F have been proposed that involve gas-phase formation from precursors such as chlorinated phenols (3, 13), so-called de novo formation from reaction of chlorine and oxygen with carbon in soot and char (10–12), and transition metal mediated reactions of precursors, such as chlorinated phenols/benzenes on the surfaces of combustion-generated particulate matter (3, 13–18). It is generally felt that gas-phase formation contributes no more than 30% of the total PCDD/F emissions (19–21). Under the original de novo theory it was suggested that PCDD/F-like species were contained in fly ash/soot/char and were liberated after heating and further reaction under appropriate conditions, whereas the precursor theory focused on reaction of specific precursors such as chlorinated phenols and benzenes with transition metals. It is now recognized that the de novo and surface precursor pathways probably

involve many of the same reaction intermediates, specifically the reactions of chlorinated phenols on transition metal surfaces.

Various studies presented in the literature presume that the catalytic transition metals are reduced or oxidized as chlorophenols are converted to PCDD/F (22). However, the change in oxidation state has not been studied directly nor confirmed by experimental observation. This is largely due to the unavailability of techniques and methods to study the metal oxidation/reduction reactions in situ.

In this paper, we describe an X-ray spectroscopic study of the high-temperature chemisorption of a known dioxin precursor, 2-chlorophenol, and the reduction of Cu(II)O on a simulated fly ash surface consisting of a mixture of CuO and silica. The study has two related goals. First, we wish to study the fate of the copper using an in situ probe when pollutant precursors react on the surface. Second, this study is intended to demonstrate the utility of XANES spectroscopy for mechanistic and kinetic studies of heterogeneous reactions involved in pollutant formation. Both of these goals are based on the expectation that X-ray spectroscopy data can provide element-specific data. Thus, one can study an element of interest in a complex mixture. This feature has been utilized extensively in the catalysis literature, but has not been exploited previously for the types of studies discussed here for research problems in air pollution formation. The results of this study demonstrate that X-ray spectroscopy is a powerful probe of surface reactions relevant to combustion problems. More specifically, the results are consistent with the contention that copper is reduced by chlorinated phenols, and reactive surface-bound species are formed that can react further to form PCDD/F.

## II. Experimental Section

The XANES spectra were collected using the double crystal monochromator beam line (23) at the synchrotron radiation source at the Center for Advanced Microstructures and Devices (CAMD), at Louisiana State University (24). The time-dependent reduction of Cu(II)O by 2-chlorophenol was monitored at 375 °C by X-ray absorption spectroscopy using a temperature-controlled dosing cell. The electron storage ring was operated with ca. 150 mA of beam current at injection, and the beam decayed over time with lifetimes of 4–8 h. The monochromator provided photon fluxes of  $\sim 10^8$  s<sup>-1</sup>. The photon bandwidth is 2 eV, and the step size in the region of the K-edge is approximately 0.3 eV.

**A. Dosing Cell.** The temperature-controlled dosing cell is shown in Figure 1(25). The cell consists of a stainless steel cube with six ports that accept 2.75 in. Conflat flanges at each face. In the center of the cell is a 6 cm<sup>2</sup> tungsten mesh (Buckbee-Mears) fastened between two copper posts that extend from the high-current electrical feedthroughs. The mesh is composed of 0.05-mm diameter wire spaced in 0.22-mm intervals, with an optical transmission of approximately 80%. Substrate samples are supported on the grid and resistively heated. The surface temperature is measured with a 0.08-mm type K thermocouple spot-welded to the top center of the grid. A 22 A variable transformer generates the current for resistive heating and is regulated by a temperature controller (Love Controls, Series 16 A) and a solid-state relay. Surface temperatures from ambient to 900 °C can be achieved. The transmission windows are 100 μm-thick Kapton film sealed between flat Viton gaskets. The 2-chlorophenol dosant is introduced to the substrate via a septum-capped dosing port. The base pressure of the cell is 10<sup>-6</sup> Torr. One significant feature of this apparatus is the ability to rapidly heat and

\* Corresponding author phone: 225-578-2933; fax: 225-578-3458; e-mail: epoliak@lsu.edu.

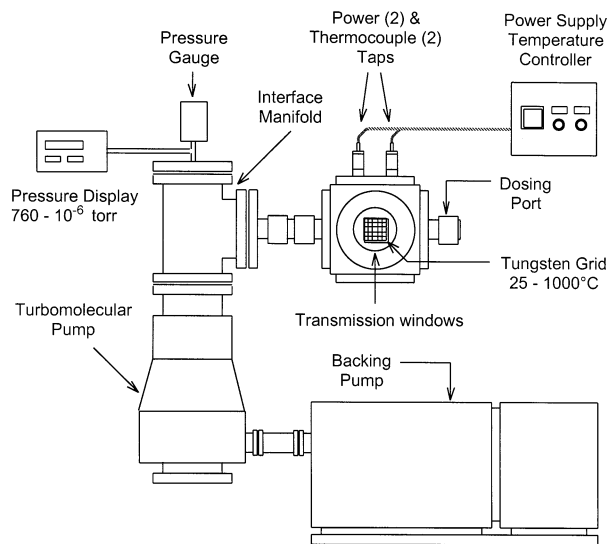


FIGURE 1. Experimental schematic of the endstation used at the end of the X-ray monochromator beam line.

cool the sample, owing to the low heat capacity of the tungsten grid. The sample can be heated or cooled (i.e., quenched) in less than 5 s. This permits the time-dependent spectral studies as the reaction can be quenched so a spectrum can be acquired, and the reaction can be reinitiated by rapid heating.

**B. Sample Preparation.** The surrogate fly ash substrate was composed of a mixture of Cab-O-Sil (Cole-Parmer) and  $<5\text{-}\mu\text{m}$  particle size copper oxide (Aldrich). Cab-O-Sil is a high purity, fumed silica with a surface area of approximately  $250\text{ m}^2/\text{g}$ . An acetone slurry containing  $0.17\text{ g}$  of each component was prepared using an ultrasonic bath. An atomizer was then used to evenly coat the entire tungsten mesh with a fine mist of the suspension. By heating the grid surface to  $\sim 70\text{ }^\circ\text{C}$  the solvent is flash-evaporated leaving behind a uniform layer of the substrate over the voids in the grid (25). The total amount of powder deposited on the grid is typically  $20\text{--}25\text{ mg}$ . This procedure results in a sample of approximately  $40\text{ wt } \%$  copper in silica. Although this value is higher than typical fly ash copper concentrations, the attenuation of the X-ray beam provides for high quality XANES spectra, thereby permitting precise determinations of chemical speciation in the substrate.

To ensure pseudo-first-order kinetics of adsorption with respect to the reactant, an excess of gas-phase 2-chlorophenol was used (ca. 1 Torr). Before acquiring spectra, the substrate was heated in air at  $375\text{ }^\circ\text{C}$  for 20 min to remove any remaining solvent and organic impurities in the material. It was determined that consistent data resulted if the substrate was first exposed to 2-chlorophenol at  $375\text{ }^\circ\text{C}$  for 20 min, then subjected to another surface cleaning cycle by heating in air at  $350\text{ }^\circ\text{C}$  for an additional 20 min, thus removing any chemisorbed reactant. The cell was evacuated to  $10^{-5}$  Torr after each 20-min exposure step. The effects of this 2-chlorophenol pretreatment are not known, and we are currently investigating how the substrate is affected by such a procedure. However, it is clear that the experimental protocol described above results in consistent and reproducible data.

After completion of the substrate pretreatment procedure, the cell was evacuated to  $10^{-5}$  Torr and a XANES spectrum was taken of the unreacted Cu(II)O. Then,  $60\text{ }\mu\text{L}$  of 2-chlorophenol was introduced through the dosing port. The sample temperature was rapidly raised to  $375\text{ }^\circ\text{C}$  and held for 2 min. The sample was then quickly cooled (i.e.,  $<5\text{ s}$ ) and a XANES spectrum taken. The heating, cooling, spectral acquisition cycle was repeated in 2-minute intervals until no further

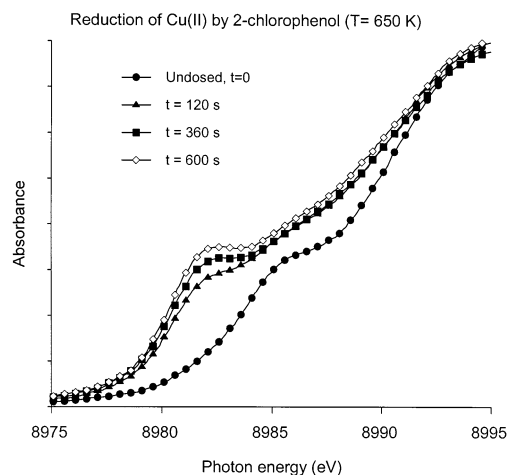


FIGURE 2. Absorption spectra of the CuO/Cab-O-Sil/2-chlorophenol mixture acquired at the Cu K-edge as a function of time following exposure to 2-chlorophenol.

reduction in copper was observed (10 min). Prior to performing duplicate experimental measurements, the sample chamber was evacuated to  $10^{-5}$  Torr to remove excess 2-chlorophenol and any volatile reaction products. The substrate sample was then exposed to air and held at  $350\text{ }^\circ\text{C}$  for 20 min in order to clean the surface of any adsorbed reaction products and to reoxidize the reduced copper back to Cu(II). Subsequent XANES spectra revealed that this treatment was sufficient to return the copper to its original, undosed state.

**C. Acquisition of XANES Spectra.** A series of three ion chambers was used to monitor the incident and absorbed photon flux (26). The experimental chamber was placed between the first and second chamber with the sample mesh normal to the incident beam. The internal standard, a Cu metal foil, was placed between the second and third ion chambers. All of the ion chamber currents were collected using electrometers (Keithley model 428) and recorded with an analog-to-digital interface. For these experiments, the synchrotron radiation was monochromatized using a pair of Ge(220) crystals.

**D. Data Analysis.** The analysis procedures were performed using standard X-ray absorption methods included in the commercial analysis program WinXAS (27). A standard spectrum (metallic Cu, binding energy of  $8979\text{ eV}$ ) was obtained simultaneously with the desired spectrum using a 3-ion chamber arrangement, permitting precise calibration of the sample spectra. Small shifts could exert considerable leverage on the fitted spectra, so calibrations were important for obtaining meaningful data. The spectra were corrected for variations in photon flux that occur over time and as a function of energy. Background subtraction and normalization were also performed using WinXAS. The spectra were found to include contributions of Cu(II), Cu(I), and Cu(0), and the concentrations of the components were determined by taking linear combinations of the component spectra, and minimizing the residual differences between the experimental and simulated spectra. The optimized fits were determined by minimizing  $\chi^2$ . The standards used for purposes of fitting were CuO, Cu<sub>2</sub>O, and Cu (metal foil). The quality of the fits depended strongly on the choice of the standard used for fitting the Cu(I) component, and the Cu<sub>2</sub>O gave qualitatively superior fits to other candidates that were tested, e.g., CuCl.

### III. Results

Figure 2 depicts representative transmission spectra taken at  $T = 375\text{ }^\circ\text{C}$  for various times during the course of reaction.

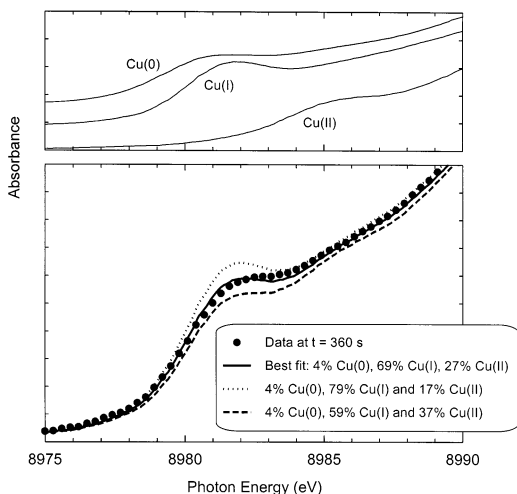


FIGURE 3. Top frame: Absorption spectra of standards (Cu metal, Cu(I)<sub>2</sub>O, and Cu(II)O). Bottom frame: a typical spectrum with different fits. It is clear that we can estimate the composition to within a few percent with good accuracy. Fits such as those shown in the bottom frame are performed for each time in the reaction and are plotted to chart the course of the reaction.

These data are acquired at the Cu K-edge, which illustrates a key point, i.e., X-ray spectroscopy allows one to obtain element-specific information even under conditions where the element of interest is present in a complex mixture. The X-ray absorption edges of the other elements in the reaction mixture (i.e., C, O, Cl) are sufficiently distant in energy that they do not influence the spectra at the Cu K-edge. Only a few of the spectra are shown in Figure 2 to illustrate the trend. The data indicate a shift in the binding energy toward lower values as the reaction proceeds. This reflects the reduction of the Cu, and the extent of the reaction can be quantified. Moreover, the data quality is excellent, and we will show that the data can provide the desired information on the substrate composition. It is possible to acquire data even more efficiently using rapid scanning methods described elsewhere (28, 29).

The spectrum obtained for each time in the course of reaction can be fitted to a superposition of spectra for Cu in three oxidation states (cf. Figure 3). At each time in the reaction that a spectrum is obtained, the spectrum is fitted as shown in Figure 3, and the composition for each Cu species is plotted as a function of time in Figure 4.

#### IV. Discussion

**Mechanisms of Chemisorption and Reduction of Cu(II).** Reasonable models for the chemisorption of 2-chlorophenol on Cu(II)O/silica are depicted in Figure 5. We know from FTIR studies of phenol and 2-chlorophenol on Cu(II)O/silica that phenols chemisorb at surface hydroxide sites through elimination of water to form surface-bound phenoxylates (30). On the basis of packed bed flow reactor studies, we also suspect that PCDFs are formed by a Langmuir–Hinshelwood (LH) mechanism involving two surface-bound species, while PCDDs are formed by an Eley–Rideal (ER) mechanism in which only one species is surface bound (22, 31). The LH pathway implies that reactions of two phenolates occur at geminal or vicinal copper sites. EPR studies also demonstrate the existence of a surface-bound phenoxyl radical (31). The existence of the radical implies electron-transfer resulting in reduction of the copper.

If two molecules of 2-chlorophenol are chemisorbed to the same geminal copper site and two phenoxyl radicals are formed, then Cu(II)O is reduced to Cu(0) (viz. pathway a in Figure 5). If only one 2-chlorophenol is chemisorbed to each

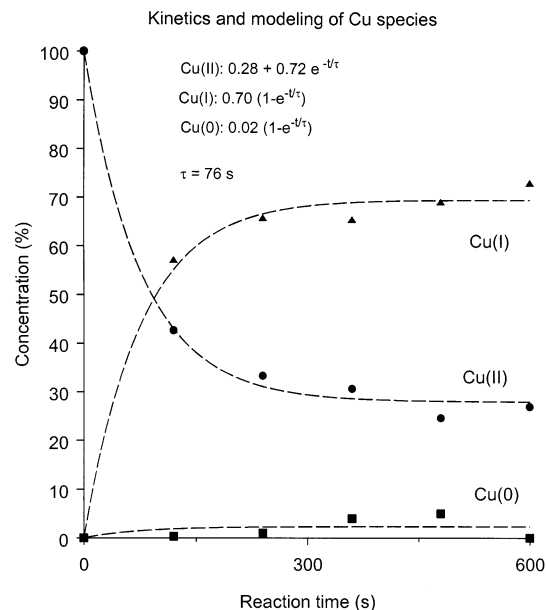


FIGURE 4. Experimental compositions as a function of time following exposure of Cu(II)O to 2-chlorophenol. The fits are also shown and are discussed in the text.

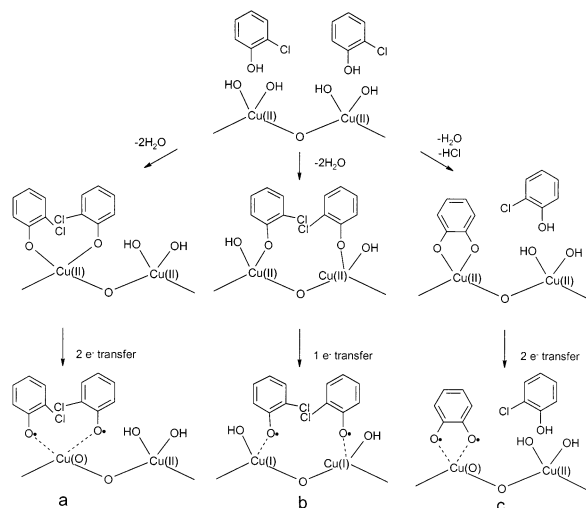


FIGURE 5. Possible mechanisms for the adsorption of 2-chlorophenol and reduction of Cu(II)O in a silica matrix. Pathway a invokes geminal chemisorption of two 2-chlorophenols and 2e<sup>-</sup> transfer to form Cu(0). In pathway b, two 2-chlorophenols are chemisorbed at vicinal sites and result in formation of Cu(I) by a 1e<sup>-</sup> transfer reaction at each site. In pathway c, a single 2-chlorophenol forms a bidentate ligand with copper by eliminating H<sub>2</sub>O and HCl. 2e<sup>-</sup> transfer results in the formation of Cu(0).

copper, then reduction to Cu(I) is implied (viz. Pathway b in Figure 5). An Eley–Rideal mechanism that results in the reduction to Cu(0) requires desorption of the 2-chlorophenoxyl radical and subsequent adsorption of a second 2-chlorophenol to continue the reduction in a second cycle, or the formation of a quinone-type intermediate as shown in pathway c of Figure 5. The ultimate yield of PCDD/F is partially dependent upon the number of copper sites that are available for reaction as well as the number of geminal and vicinal adsorptions. Most of the 2-chlorophenol is oxidized; however, oxidation still requires chemisorption and formation of reaction intermediates such as those depicted in Figure 5.

A first-order kinetic model that is consistent with the data in Figure 4 is fitted with the following equations.

$$f_2(t) = (1 - f^{\text{reac}}) + f^{\text{reac}} \exp[-t/\tau]$$

$$f_1(t) = f^{\text{reac}} f^{12} [1 - \exp[-t/\tau]]$$

$$f_0(t) = f^{\text{reac}} (1 - f^{12}) [1 - \exp[-t/\tau]]$$

where  $f_2(t)$  = fraction of Cu present as Cu(II) at time  $t$ ,  $f_1(t)$  = fraction of Cu present as Cu(I) at time  $t$ ,  $f_0(t)$  = fraction of Cu present as Cu(0) at time  $t$ ,  $f^{\text{reac}}$  = fraction of Cu(II) that is available for reaction =  $0.72 \pm 0.02$ ,  $f^{12}$  = fraction of the available Cu(II) that reacts to form Cu(I) =  $0.97 \pm 0.02$ , and  $\tau$  = time constant for depletion of Cu(II) =  $76 \pm 12$  s.

The data were fitted with a commercial least-squares fitting program, and the errors are reported to two standard deviations. There are 3 adjustable parameters in this model:  $f^{\text{reac}}$  (fraction of Cu available to react), branching ratio ( $f^{12}$ ), and the time constant for reaction,  $\tau$ .

First, it appears that most, but not all, of the copper is reacting. This is evident from the observation that some Cu(II) remains unreduced even after the reaction has proceeded to apparent completion. In the case of the samples studied here, 72% of the Cu(II) was converted to Cu(I) or Cu(0) with 28% left unreacted. The large extent of reaction implies that as 2-chlorophenol reacts at surface oxide sites, additional oxides migrate from the interior to replenish the reactive surface oxide sites. Larger grains of oxide have interiors that may prevent oxide migration and limit the extent of reaction. Further tests are warranted to determine why the extent of reaction was so large, but still incomplete.

Second, it appears that there are 2 reaction pathways involving electron transfer to copper, as the Cu(II) is being reduced to both Cu(I) and Cu(0). It is clear that most of the reacted copper is forming Cu(I) rather than Cu(0). The percentage of Cu(0) is small, and consequently, is not precisely determined. As a result, it is unclear if the rates of formation of the Cu(I) and Cu(0) are characterized by the same time constant. Since the simplest kinetic model assumes the same time constant (i.e., parallel reactions) and this

reduces the number of adjustable parameters, we have chosen this approach for purposes of data reduction. The point is that not too much significance should be ascribed to the use of a single time constant.

Third, the data indicate that the dominant surface-mediated mechanism is consistent with a single electron-transfer mechanism, rather than a 2- $e^-$  pathway, as 2- $e^-$  pathways would result in reduction to Cu(0). Thus the proposed pathway that is most consistent with the observed data is pathway **b** in Figure 5.

#### Implications for the Pathways of PCDD/F Formation.

To our knowledge, this application of XANES has provided the first in situ demonstration of the reduction of copper by a PCDD/F precursor. Although the current data do not definitively prove a particular mechanism, they do provide useful guideposts for informed speculation regarding likely reaction pathways. For example, the reduction of Cu(II) to Cu(I) is consistent with the mechanism involving the conversion of a surface-bound chlorophenolate to a surface-associated chlorophenoxy species. The chlorophenoxy species can undergo further reaction, such as elimination of CO to form a chlorocyclopentadienyl radical. Cyclopentadienyls are a known intermediate in the oxidation of benzenes and possible intermediates in the formation of polycyclic aromatic hydrocarbons (PAHs) (32–36). Because yields of PCDD/F from reactions of chlorophenols on fly ash are less than 1%, this is the likely dominant fate of the surface-associated chlorophenoxy (37).

However, the surface-associated chlorophenoxy can also react to form PCDD/F. If the reaction is with another vicinal chlorophenoxy via an LH pathway, it can form 4,6-dichlorodibenzofuran via reaction involving the keto-mesomer (cf. Pathway **a** in Figure 6). 1-Monochlorodibenzo-*p*-dioxin can be formed by reaction with a gas-phase 2-chlorophenol via an ER pathway (cf. Pathway **b** in Figure 6), while a surface bound unchlorinated dibenzo-*p*-dioxin can also be formed via an ER pathway (cf. Pathway **c** in Figure 6).

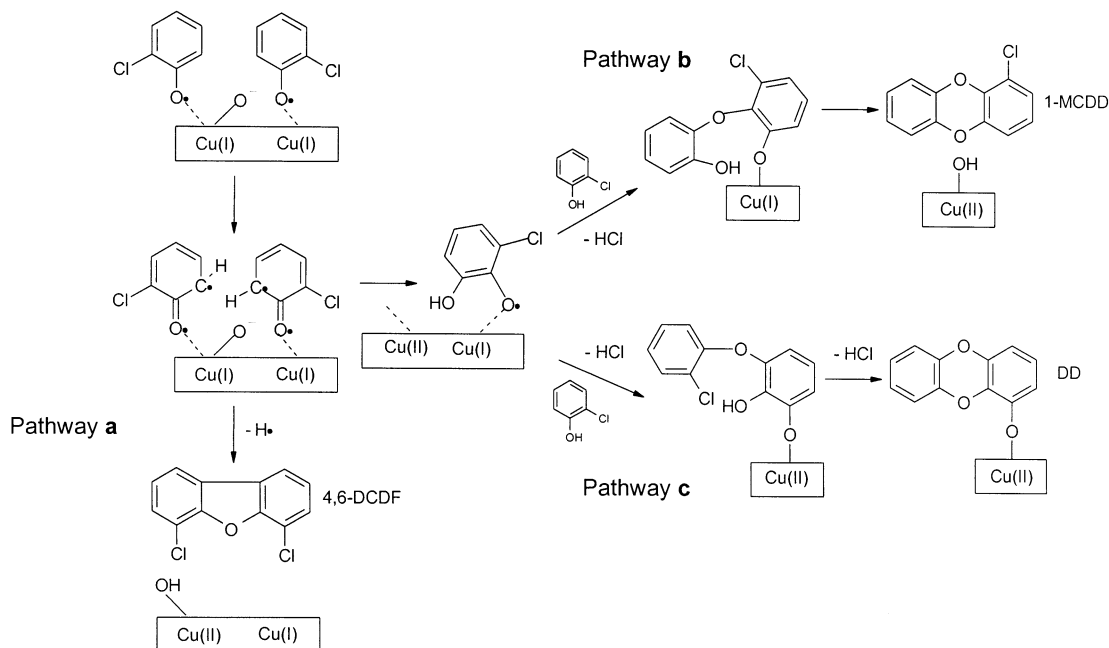


FIGURE 6. Pathways to formation of 4,6-dichlorodibenzofuran (pathway a), 1-monochlorodibenzo-*p*-dioxin (pathway b), and dibenzo-*p*-dioxin (pathway c) following chemisorption of 2-chlorophenol on a Cu(II)/silica matrix. Pathway a involves reaction of two keto-phenoxy mesomers (resonance structures) in a Langmuir–Hinshelwood reaction. In pathways b and c, the surface-bound phenoxy first reacts with a vicinal oxylyate to form a surface-associated hydroxy phenoxy. In pathways b and c, either a desorbed 1-monochlorodibenzo-*p*-dioxin or a chemisorbed (unchlorinated) dibenzo-*p*-dioxin are formed depending upon whether the elimination of HCl involves a hydroxyl group of the gas-phase 2-chlorophenol or the surface-associated 2-chloro, 6-hydroxy phenoxy, respectively.

In summary, these XANES data provide critical information and can help in understanding the detailed microscopic mechanism of PCDD/F formation via surface-mediated processes. This is expected, as the analogous literature on methanol-induced reduction of CuO provided clear and useful information on related catalytic mechanisms (38). We have shown that 2-chlorophenol reacts with Cu(II)O/silica under conditions that are known to be favorable to formation of PCDD/F. Cu(II) is reduced primarily to Cu(I), which, in conjunction with information from other reported studies (22, 30, 31), implicates the formation of a surface-associated phenoxy species that can react to form PCDDs or PCDFs depending upon whether the reaction is with a gas-phase chlorophenol or another surface-associated phenoxy species, respectively. Additional XANES and EXAFS studies of these surfaces are needed to better understand the nature of the binding and local environment of PCDD/F precursors. The properties and origins of surface-associated radicals are important in their own right, as it has been previously demonstrated that persistent radicals associated with fine particles can induce lesions in DNA (39–42). The demonstration project described here will be extended to temperature-dependent measurements, as well as studies of other precursors, other substrates, and related X-ray absorption methods, including EXAFS spectroscopy to provide detailed structural information.

### Acknowledgments

This work is partially supported by the National Science Foundation (DMR-0119672). E.D.P. acknowledges support by the Chemical Sciences, Geosciences and Biosciences Division, Office of Basic Energy Sciences, Office of Science, U.S. Department of Energy. B.D. acknowledges the support of the Thermal Systems Division of NSF (CTS-9996085). We also wish to thank Roland Tittsworth and Mike Schoonmaker at CAMD for their invaluable assistance.

### Literature Cited

- (1) Wehrmeier, A.; Lenoir, D.; Sidhu, S. S.; Taylor, P. H.; Rubey, W. A.; Kettrup, A.; Dellinger, B. *Environ. Sci. Technol.* **1998**, *32*, 2741.
- (2) Taylor, P. H.; Dellinger, B. *J. Anal. Appl. Pyrolysis* **1999**, *49*, 9.
- (3) Dellinger, B.; Taylor, P. H. *Cent. Eur. J. Public Health* **1998**, *6*, 79.
- (4) Fiedler, H. *Environ. Eng. Sci.* **1998**, *15*, 49.
- (5) Altwicker, E. R. *Chemosphere* **1996**, *33*, 1897.
- (6) Huang, H.; Buekens, A. *Chemosphere* **1995**, *31*, 4099.
- (7) Altwicker, E. R.; Schonberg, J. S.; Konduri, R. K. N. V.; Milligan, M. S. *Hazard. Waste Hazard. Mater.* **1990**, *7*, 73.
- (8) Hagenmaier, H.; Kraft, M.; Brunner, H.; Haag, R. *Environ. Sci. Technol.* **1987**, *21*, 1080.
- (9) Addink, R.; Altwicker, E. R. *Environ. Eng. Sci.* **1998**, *15*, 19.
- (10) Stieglitz, L. *Environ. Eng. Sci.* **1998**, *15*, 5.
- (11) Vogg, H.; Stieglitz, L. *Chemosphere* **1986**, *15*, 1373.
- (12) Stieglitz, L.; Zwick, G.; Beck, J.; Roth, W.; Vogg, H. *Chemosphere* **1989**, *18*, 1219.
- (13) Taylor, P. H.; Sidhu, S. S.; Rubey, W. A.; Dellinger, B.; Wehrmeier, A.; Lenoir, D.; Schramm, K. W. *Proc. Combust. Inst.* **1998**, *27*, 1769.
- (14) Addink, R.; Olie, K. *Environ. Sci. Technol.* **1995**, *29*, 1425.
- (15) Karasek, F. W.; Dickson, L. C. *Science* **1987**, *237*, 754.
- (16) Dickson, L. C.; Lenoir, D.; Hutzinger, O. *Environ. Sci. Technol.* **1992**, *26*, 1822.
- (17) Milligan, M. S.; Altwicker, E. R. *Environ. Sci. Technol.* **1995**, *30*, 225.
- (18) Altwicker, E. R.; Milligan, M. S. *Chemosphere* **1993**, *27*, 301.
- (19) Shaub, W. M.; Tsang, W. Overview of dioxin formation in gas phases under municipal incinerator conditions. In *Chlorinated Dibenzodioxins and Dibenzofurans in the Total Environment II*; Butterworth: Boston, MA, 1985; p 469.
- (20) Bruce, K. R.; Beach, L. O.; Gullett, B. K. *Waste Manage.* **1991**, *11*, 97.
- (21) Sidhu, S. S.; Maqsood, L.; Dellinger, B.; Mascolo, G. *Combust. Flame* **1995**, *100*, 11.
- (22) Lomnicki, S.; Dellinger, B. *Proc. Combust. Inst.* (in press).
- (23) Schilling, P.; Morikawa, E.; Tolentino, H.; Tamura, E.; Kurtz, R. L.; Cusatis, C. *Rev. Sci. Instrum.* **1995**, *66*, 2214.
- (24) Stockbauer, R. L.; Ajmera, P.; Poliakov, E. D.; Craft, B. C.; Saile, V. *Nucl. Instrum. Methods Phys. Res.* **1990**, *291*, 505.
- (25) Basu, P.; Ballinger, T. H.; Yates, J. T. *Rev. Sci. Instrum.* **1988**, *59*, 1321.
- (26) West, J. B. *Vacuum Ultraviolet Spectroscopy II*; Academic Press: San Diego, CA, 1998; Vol. II.
- (27) Ressler, T. *J. Synchrotron Radiat.* **1998**, *5*, 118.
- (28) Frahm, R. *Nucl. Instrum. Methods Phys. Res., Sect. A* **1998**, *270*, 578.
- (29) Floriano, P. N.; Noble, C. O.; Schoonmaker, J. M.; Poliakov, E. D.; McCarley, R. L. *J. Am. Chem. Soc.* **2001**, *123*, 10545.
- (30) Alderman, S. L.; Dellinger, B. *Environ. Sci. Technol.* **2002**, submitted for publication.
- (31) Lomnicki, S.; Dellinger, B. *J. Phys. Chem.* (submitted for publication).
- (32) Roy, K.; Horn, C.; Slutsky, V. G.; Just, T. *Proc. Combust. Inst.* **1998**, *27*, 329.
- (33) Breninsky, K.; Butler, R. G.; Glassman, I. *Prepr.-Am. Chem. Soc., Div. Pet. Chem.* **1992**, 1467.
- (34) Tregrossi, A. C. A.; Barbella, R. *Combust. Flame* **1999**, *117*, 553.
- (35) Mulholland, J. A.; Lu, M.; Kim, D. H. *Proc. Combust. Inst.* **2000**, *28*, 2593.
- (36) Melius, C. F.; Colvin, M. E.; Marinov, N. M.; Pitz, W. J.; Senkan, S. M. *Proc. Combust. Inst.* **1996**, *26*, 685.
- (37) Weber, R.; Hagenmaier, H. *Chemosphere* **1999**, *38*, 2643.
- (38) Gunter, M. M.; Ressler, T.; Jentoft, R. E.; Bems, B. *J. Catal.* **2001**, *203*, 133.
- (39) Squadrito, G. L.; Cueto, R.; Dellinger, B.; Pryor, W. A. *Free Radical Biol. Med.* **2001**, *31*, 1132.
- (40) Dellinger, B.; Pryor, W. A.; Cueto, R.; Squadrito, G. L.; Hedge, V.; Deutsch, W. A. *Chem. Res. Toxicol.* **2001**, *14*, 1371.
- (41) Dellinger, B.; Pryor, W. A.; Cueto, R.; Squadrito, G. L.; Deutsch, W. A. *Proc. Combust. Inst.* **2000**, *28*, 2675.
- (42) Dellinger, B.; Pryor, W. A.; Cueto, R.; Squadrito, G. L.; Deutsch, W. A. *Organohalogen Compd.* **2000**, *16*, 302.

Received for review July 16, 2002. Revised manuscript received December 9, 2002. Accepted December 16, 2002.

ES020838H

## Speciation of Phosphorus Compounds in Red Mud and Mixed Mineral Systems Using XANES

J. J. Wang<sup>1</sup>, M.H.S. Stietiya<sup>1</sup>, and Amitava Roy<sup>2</sup>. <sup>1</sup>LSU Agriculture Center and LSU Department of Agronomy and Environmental Management, Sturgis Hall, Baton Rouge, LA, 70810, [jjwang@agctr.lsu.edu](mailto:jjwang@agctr.lsu.edu), [mstiet2@lsu.edu](mailto:mstiet2@lsu.edu) <sup>2</sup>LSU Center for Advanced Microstructures and Devices, 6980 Jefferson Hwy., Baton Rouge, LA 70806, [reroy@lsu.edu](mailto:reroy@lsu.edu). PRN: Agr-JW040.

Recent evidence from wet chemistry has showed that Fe oxides may play an equally important role in P retention in calcareous soils. The objective of this study is to use XANES techniques to identify P controlling minerals in some typical calcareous soils. In 2006, the P K-XANES spectra for sets of P-loaded samples of a mixed mineral and red mud at different pH levels along with different model compounds were collected using the Double Crystal Monochromator beamline (DCM) equipped with a InSb(111) crystal.

A pre-edge feature characteristic of Fe-phosphate minerals in the region from -5 to -2 eV was evident for the mixed mineral systems of pH 4.5 and 6.0. This pre-edge feature had disappeared for the mixed mineral system at pH 7.5. In addition, a shoulder on the higher energy side of the absorption edge which is characteristic of calcium phosphate minerals was evident for the mixed mineral system at pH 7.5. For the other mixed mineral systems at pH 4.5 and 6.0, such a shoulder was not evident. The results clearly demonstrated the effect of pH on phosphorus coordination with Ca and Fe constituents in these systems.

Using Principal Component Analysis (PCA), the number of probable species was determined to be two for the red mud samples (relative energy range from -10 to 15 eV). Four model compounds yielded a sufficient match upon target transformation: ferrihydrite, hematite, dicalcium phosphate, and octacalcium phosphate. Based on PCA results, linear combination fitting (LCF) was applied to determine the percentage of each probable constituent in the samples. The fitting results indicated that dicalcium phosphate dominated at high pH levels whereas P-Fe oxides were dominant at pH values of 4.5 and 6.0. Red mud with no pH adjustment showed that 84.5% of total P was dicalcium phosphate and 15% of total P was adsorbed to ferrihydrite ( $\chi^2=0.35$ ). At pH 4.5, LCF of red mud showed that 77.6% of P was adsorbed to ferrihydrite whereas 22.4% was present as dicalcium phosphate ( $\chi^2=0.62$ ). Finally, at pH 7.5, as much as half of P was adsorbed to ferrihydrite and the other half was in the form of dicalcium phosphate. Overall these spectroscopic evidences are consistent with current understanding of P chemistry as predicted by chemical equilibrium.



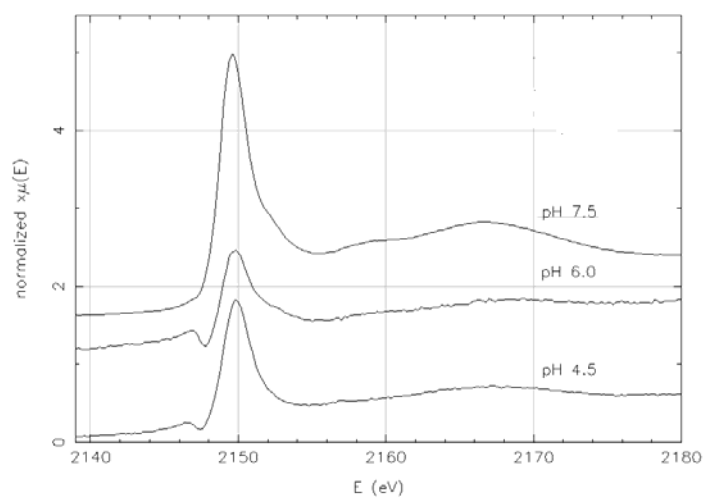


Figure1. Spectral comparison of mixed mineral systems at varying pH levels

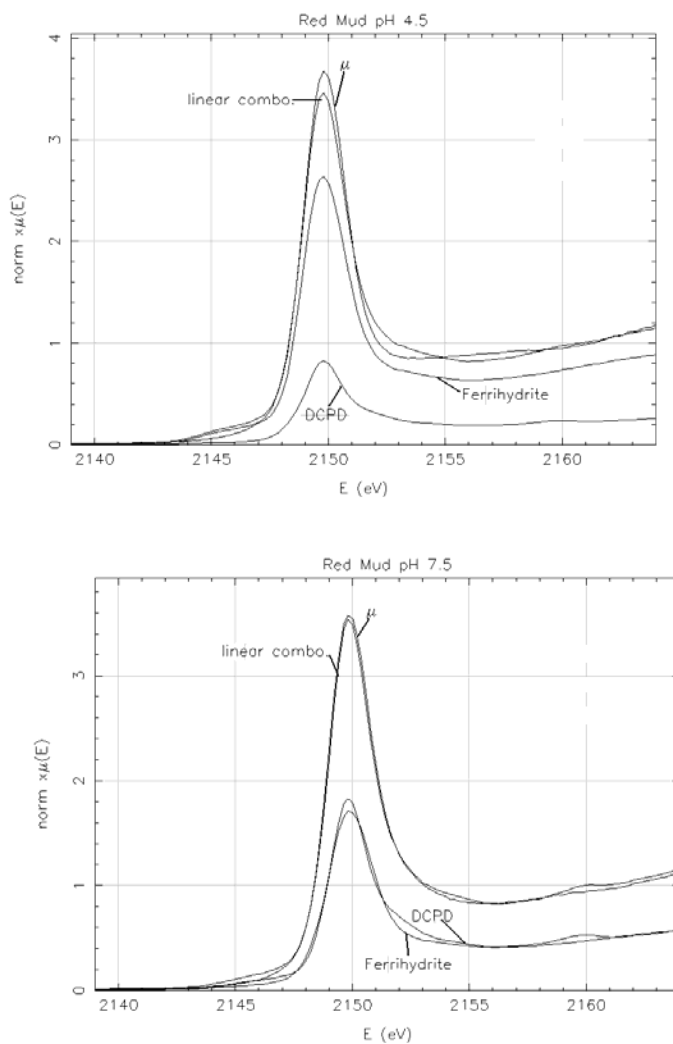


Figure2. LCF for red mud at pH 4.5 and 7.5

## Arsenic speciation in *Pteris cretica cv Mayii* (Moonlight Ferns) using X-ray Absorption and X-ray Fluorescence Spectrometry

Youngsoo Cho<sup>1</sup>, James Bolick<sup>1</sup>, Amitava Roy<sup>2</sup>, and David J. Butcher<sup>1\*</sup>

<sup>1</sup>Department of Chemistry and Physics  
Western Carolina University  
Cullowhee, NC 28723

<sup>2</sup>Center for Advanced Microstructures and Devices (CAMD)  
Louisiana State University  
6980 Jefferson Hwy., Baton Rouge, LA 70806

\*Author to whom correspondence should be addressed.  
Email: butcher@email.wcu.edu  
Phone: (828) 227-7646

PRN: WCU-DB0106

### Abstract

*Pteris cretica cv Mayii* (moonlight fern) has been demonstrated to be an efficient arsenic hyperaccumulating plant, suitable for phytoremediation of this toxic element. In this work, moonlight ferns were grown hydroponically in solutions containing various arsenic compounds. The arsenic species present in the foliage were characterized by x-ray absorption and x-ray fluorescence spectrometries. In freshly-cut leaves, arsenic was present as arsenic (III), while drying induced oxidation to arsenic (V) (Figure 1). The concentration of arsenic in foliage exposed to different chemical forms of arsenic was measured by inductively coupled plasma – optical emission spectrometry. These data indicate that arsenic (III) and arsenic (V) are accumulated preferentially to monomethyl arsenate.

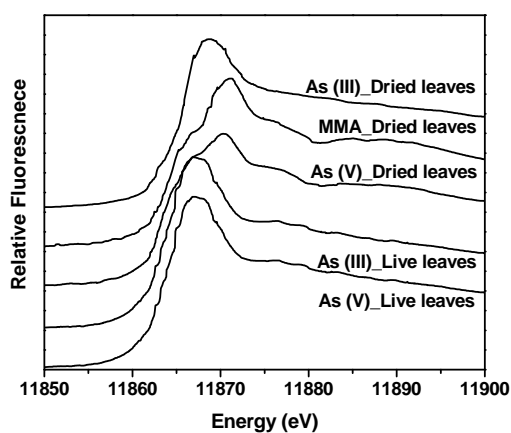


Figure 1. Comparison of As K-edge XFS between live leaves and dried leaves exposed to arsenic (III), arsenic (V), and MMA.

**(1) Publications and Presentations**

We currently are developing a manuscript to be submitted later this year for publication. This work will be presented at the 2007 FACSS Conference October 14-18 in Memphis, TN.

**(2) Grants which involved CAMD Research**

None.

**(3) Graduate Student Involvement**

Two M.S. students have contributed to this project, Youngsoo Cho and James Bolick. Both are scheduled to graduate in August, 2007.

## **Nanoscience Structures and Research with Nanoparticles**

The Nanofabrication group collaboration at CAMD has specialized in working closely with the Pennington Center in the use of nanoparticles to target cancer cells. Their work has made extensive use of the CAMD microfabrication, x-ray and i.r. facilities. The following papers are a representative example of their work during the past year 2006.

## Investigation of the Influence of Organometallic Precursors on the Formation of Cobalt Nanoparticles

Rohini M. de Silva, Vadim Palshin, Josef Hormes, Frank R Fronczek<sup>#</sup> and Challa S. S. R. Kumar\*

Centre for Advanced Microstructures and Devices, Louisiana State University, 6980 Jefferson Hwy, Baton Rouge, LA 70806; <sup>#</sup>Department of Chemistry, Louisiana State University, LA 70803

A great deal of research continues to be focused on nanometer sized materials in general and cobalt-based magnetic materials in particular due to their potential applications in the field of electronics,<sup>1</sup> high density data storage media,<sup>2</sup> catalysis,<sup>3</sup> and bio medical sciences.<sup>4</sup> Numerous physical and chemical methods such as sputtering,<sup>5</sup> chemical vapor deposition,<sup>6</sup> reverse micelle synthesis,<sup>7</sup> mechanical milling,<sup>8</sup> solution phase metal salt reduction<sup>9-13</sup> and decomposition of neutral organometallic precursors<sup>14</sup> have already been well established to produce cobalt nanoparticles. Of these, high temperature wet-chemical reactions, as compared to other techniques, are particularly attractive as they are known to offer better control over size, size distribution, shape, and crystal structure of cobalt nanoparticles. The effect of reaction conditions such as temperature,<sup>18</sup> time of addition of reagents<sup>16</sup> solvents,<sup>19</sup> utilization of surfactants,<sup>9-10,20</sup> polymeric stabilizers<sup>21</sup> and type of reaction vessels, for example, utilization of micro reactors<sup>22</sup> for control of cobalt nanoparticle formation is well documented. However, the influence of different precursors has not been examined systematically. Such an investigation assumes more importance as it is well established that properties of cobalt nanoparticles are extremely sensitive to the presence of even minute surface impurities.<sup>7</sup> In order to initiate investigations in this direction, we have identified two organometallic cobalt complexes, alkyne-bridged dicobalthexacarbonyl  $[(Co_2(\mu-HC\equiv CH)(CO)_6]$  and the well known dicobalt octacarbonyl. The two precursors were decomposed under identical reaction conditions and the mechanism of their decomposition was monitored (Figure 1). The cobalt nanoparticles were characterized, their properties were compared and correlated to the starting precursors and the reaction intermediates.

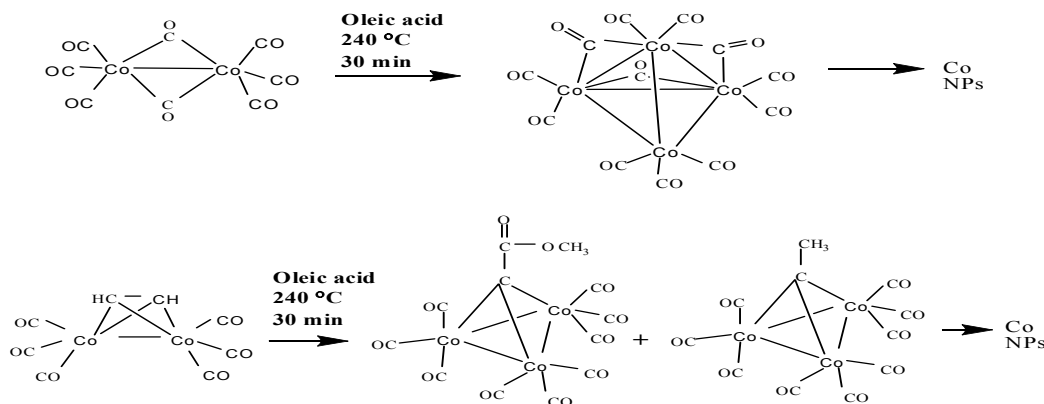


**Figure 1.** Schematic representation of the decomposition of two organometallic cobalt complexes under identical reaction conditions.

The investigations carried out so far demonstrate that the nature of precursors strongly influences the formation of cobalt nanoparticles synthesized wet-chemically. The precursors not only influence the formation of cobalt nanoparticles but also their physical properties such as particle size, crystal structure and oxidative stability. It is difficult to pin point, based on the data we have generated so far, exactly how the precursors are influencing the formation of cobalt nanoparticles. However, two possible scenarios can be envisaged. First, the presence of different reaction intermediates from the precursors interacting differently with the surfaces of nuclei could be influencing the formation of cobalt nanoparticles differently. Second, different nucleation and growth kinetics arising due to different decomposition rates of precursors and the reaction intermediates could also be responsible. The differences in particle size, size distribution and crystal structure can be explained based on the differences in nucleation and growth rates. However, the differences in the oxidative stability can only be explained based on the differences in surface coatings arising either from different precursors/intermediates during the cobalt nanoparticle formation or from different binding modes of the surfactants on the final particle. Further work is in progress in order to investigate which of the two scenarios are predominant and how they influence the properties of cobalt nanoparticles. It is anticipated that investigations in this directions will lead to elucidation of comprehensive relationship between the structures of organometallic cobalt precursors versus properties of cobalt nanoparticles obtained.

### References

- (1) (a) Alivisatos, A. P. *Science* **1996**, *271*, 933. (b) Heath, J. R. *Acc. Chem. Res.* **1999**, *32*, 388.
- (2) Charap, S. H.; Lu, P. L.; He, Y. *IEEE Trans. Magn.* **1997**, *33*, 978.
- (3) (a) Klingelhöfer, S.; Heitz, W.; Greiner, A.; Oestreich, S.; Foster, S.; Antonietti, M. *J. Am. Chem. Soc.* **1997**, *119*, 10116. (b) Kim, S. W.; Son, S. U.; Lee, S. S.; Hyeon T.; Chung, Y. K. *Chem. Commun.* **2000**, 2212.
- (4) (a) Bao, Y.; Krishnan, K. M.; *J Magn. Magn. Mater.* **2005**, *293*, 15. (b) Cao, Y. C.; Jin, R.; Mirkin, C. A.; *Science*, **2002**, *297*, 1536.
- (5) (a) Kitakami, O.; Sato, H.; Shimada, Y.; Sato, F.; Tanaka, M. *Phys. Rev. B*, **1997**, *21*, 13849. (b) Sato, H.; Kitkami, O.; Sakurai, T.; Shimada, Y.; Otani, Y.; Fukamichi, K. *J Appl. Phys.* **1997**, *81*, 1858.
- (6) Billas, I. M. L.; Châtelain, A.; de Heer, W. A. *J Magn. Magn. Mater.* **1997**, *168*, 64.
- (7) (a) Petit, C.; Pilen, M. P. *J Magn. Magn. Mater.* **1997**, *166*, 82. (b) Connolly, J.; Pierre T.G.; Rutnakornpituk, M. Riffle J. S. *J Phys. D: Appl. Phys.* **2004**, *37*, 2475. (c) Chen, J. P.; Sorensen, C. M.; Klabunde, K. J.; Hadjipanayis, G. C. *J. Appl. Phys.* **1994**, *76*, 6316.
- (8) Huang, J. Y.; Wu, Y. K.; Ye, H. Q. *Acta Mater.* **1996**, *44*, 1201.
- (9) Murray, C. B.; Sun, S.; Gaschler, W.; Doyle, H.; Betley, T. A.; Kagan, C. R.; *IBM J. Res. Dev.* **2001**, *45*, 47.
- (10) Sun, S.; Murray, C. B.; *J. Appl. Phys.* **1999**, *85*, 4325.
- (11) Pelecky, D. L. L.; Bonder, M.; Martin, T.; Kirkpatrick E. M.; Liu, Y.; Zhang, X. Q.; Kim, S. H.; Rieke, R. D. *Chem. Mater.* **1998**, *10*, 3732.
- (12) Wu, N.; Fu, L.; Su, M.; Aslam, M.; Wong, K. C.; Dravid, V. P. *Nano Lett.* **2004**, *4*, 383.
- (13) Cha, S. I.; Chan, B. M.; Kim, K. T.; Hong, S. H. *J mater. Res.* **2005**, *20*, 2148.
- (14) (a) Masala, O.; Seshadri, R. *Annu. Rev. Mater. Res.* **2004**, *34*, 41. (b) Green, M. *Chem commun*, **2005**, 3002. and ref, therein
- (15) Holzwarth, A.; Lou, J.; Hatton, A. T.; Laibinis P. E. *Ind. Eng. Chem. Res.* **1998**, *37*, 2701.

- (16) (a) Puentes, V. F.; Zanchet, D.; Erdonmez, C. K.; Alivisatos, A. P. *J. Am. Chem. Soc.* **2002**, 124, 12874. (b) Wuhn, M.; Weckesser, J.; Woll, Ch. *Langmuir*, **2001**, 17, 7605.
- (17) Pelecky-L, D. L.; Zhang, X. Q.; Rieke, R. D. *J. Appl. Phys.* **1996**, 79, 5312.
- (18) Puentes, V. F.; Krishnan, K. M.; Alivisatos, A. P. *Appl. Phys. Lett.* **2001**, 78, 2187.
- (19) (a) Abes, J. I.; Cohen, R. E.; Ross, C. A. *Chem. Mater.* **2003**, 15, 1131. and references therein.. (b) Tadd, E. H.; Bradley, J.; Tannenbaum, R. *Langmuir* **2002**, 18, 2378. (c) Wojciechowska-W, D.; Jeszka, J. K.; Amiens, C.; Chaudret, B.; Lecante, P. *J. Coll. Inter. Sci.* **2005**, 287, 107.
- (20) Song, Y.; Hartwig, M.; Henry, L. L.; Saw, C. K.; Doomes, E. E.; Palshin, V.; Kumar, C. S. S. R. *Chem. Mater.* **2006**, 18, 2817.
- (21) Respaud, M.; Broto, J. M.; Rakoto, H.; Fert, A. R.; Thomas, L.; Barbara, B.; Verelst, M.; Snoeck, E.; Lecante, P.; Mosset, A.; Osuna, J.; Ely, T. O.; Amiens, C.; Chaudret, B. *Phys. Rev. B* **1998**, 57, 2925.
- (22) Hormes, J.; Modrow, H.; Bonnemann, H.; Kumar, C. S. S. R. *J. Appl. Phys.* **2005**, 97, (10, pt. 3)

## LHRH-Functionalized Magnetite Nanoparticles for Contrast Enhancement in Breast Tumor MRI

<sup>1</sup>J. Meng, <sup>2</sup>G. Galiana, <sup>2</sup>T. Branca, <sup>1</sup>J. Zhou, <sup>3</sup>C. Leuschner\*, <sup>4</sup>C. S. S. R. Kumar, <sup>4</sup>J. Hormes, <sup>5</sup>T. Otiti, <sup>6</sup>A. Beye, <sup>2</sup>W. Warren\* and <sup>1</sup>W. O. Soboyejo\*

<sup>1</sup>Princeton Institute of Science and Technology of Materials and the Department of Mechanical and Aerospace Engineering, Princeton University, Princeton, NJ 08544; <sup>2</sup>Department of Chemistry, Duke University, Durham, NC 27708-0354; <sup>3</sup>Pennington Biomedical Research Center, 6400 Perkins Road, Baton Rouge, LA 70808, USA; <sup>4</sup>Center for Advanced Microstructures and Devices, Louisiana State University, 6980 Jefferson Hwy, Baton Rouge, LA 70806, USA; <sup>5</sup>Department of Physics, Makerere University, Kampala, Uganda; <sup>6</sup>Department of Physics, Cheikh Anta Diop University, Dakar, Senegal.

Ligand conjugated superparamagnetic iron oxide nanoparticles (SPIONs) offer an alternative to existing gadolinium contrast agents as they can be used to overcome some of the following limitations. First, the attachment of specific ligands to such nanoparticles offers the potential for the design of systems that can target specific tumors. In the case of breast cancer, prior work has shown that luteinizing hormone releasing hormone (LHRH) receptors are over-expressed. This stimulated Kumar et al.<sup>6,7</sup> and Leuschner et al.<sup>6,7,8,9,10,11</sup> to design superparamagnetic iron oxide nanoparticles conjugated to LHRH that can be used to target breast tumor sites leading to potential applications in cancer drug delivery and cancer diagnosis.<sup>12,13</sup> These fabricated nanoparticles are subsequently named LHRH-SPIONs.

Transmission electron microscopy work by Zhou et al.<sup>14</sup> later showed that the LHRH-SPIONs accumulate specifically in breast cancer xenografts. Shannon et al.<sup>15</sup> have also shown that the LHRH-SPIONs enhance the MULTI-CRAZED MRI images of breast cancer xenografts from experiments with tumors in the same experiment with human breast cancer xenograft bearing female mice used in the TEM experiments by Zhou et al.<sup>14</sup>

This investigation extends the work by Shannon et al.<sup>15</sup>, where preliminary results of MRI on tumor tissue samples from the laboratory of Leuschner were utilized by presenting additional evidence of MRI contrast enhancement in female mouse breast tumor tissue injected with LHRH-conjugated superparamagnetic iron oxide nanoparticles (LHRH-SPIONs). The intracellular LHRH-SPIONs provide significant contrast enhancement in conventional T2 images of breast cancer xenografts, and bulk T2 measurements. The possible implications of these images are then discussed for the early detection and treatment of breast cancer.

This work presents evidence of MRI contrast enhancement in tumor tissue. The results suggest that specially intracellular accumulated LHRH-SPIONs provide contrast enhancement that could lead to sub-millimeter spatial resolution in MRI by classical T2 imaging. Such sub-millimeter detection could be very significant for the early detection of cancer. However, further work is needed to explore the use of LHRH-SPIONs in live mice (not just tissue) and larger animals. The potential conjugation of cancer drugs to



LHRH-SPIONs also offers the potential for the design of specific targets that can be used to detect and treat breast cancer.

## References

- [1]. A. Jemal, T Murray, E. Ward, A. Samuels, R. C. Tiwari, A. Ghafoor, E. J. Feuer and M. J. Thun, *CA Cancer J Clin* **55**, 10-30 (2005).
- [2]. D.G.Gadien, *NMR and Its Applications to Living Systems*. Oxford University Press. New York. (2000).
- [3]. A. E. Merbach, E. To'th, *The Chemistry of Contrast Agents in Medical Magnetic Resonance Imaging*, Wiley, Chichester, United Kingdom, (2001).
- [4]. P. Tartaj, M. P. Morales, S. Veintemillas-Verdaguer, T. Gonz'alez-Carre ~no and C. Serna, *J. Phys. D: Appl. Phys.* **36** R182–R197. (2003).
- [5]. G. Molema, D. K. F. Meijer: *Drug targeting*. WILEY-VCH, (2001).
- [6]. C. Leuschner, C. S. S. R. Kumar, W. Hansel, J. Hormes. *Journal of Biomedical Nanotechnology*, **Vol. 2**, p 229-233. (2005).
- [7]. C. S. S. R. Kumar, C. Leuschner, E.E. Doomes, L. Henry, M. Juban and J. Hormes, *Journal of Nanoscience and Nanotechnology*, Vol. 4, pp. 245-249, (2004).
- [8]. C. Leuschner, F. Enright, P. Melrose, W. Hansel, *Prostate*, **46(2)**, 116-125. (2001).
- [9]. B. Gawronska, C. Leuschner, F. Enright, W. Hansel, *Gynecologic Oncology* **85**, 45-52 (2002).
- [10]. C. Leuschner, F. Enright, B. Gawronska, W. Hansel, *Breast Cancer Research and Treatment* **78**, 17-27. (2003).
- [11]. C. Leuschner, F. Enright, B. Gawronska, W. Hansel, *Prostate*, **56(4)**, 239-249. (2003)
- [12]. C. S. S. R. Kumar, C. Leuschner, J. Hormes and W. Hansel, Patent application No : 10/816,732, (2004).
- [13]. C. Leuschner, C. S. S. R. Kumar, J. Hormes and W. Hansel, Patent application Nos : 60/706,800 and 60/735,523, (2005).
- [14]. J. Zhou, C. Leuschner, C. S. S. R. Kumar, J. F. Hormes, W. O. Soboyejo, *Biomaterials*, **27**, 2001-2008, (2006).
- [15]. K. L. Shannon, R.T Branca, G. Galiana, S. Cenzano, L. S. Bouchard, W. O. Soboyejo and W. S. Warren, *Magnetic Resonance Imaging*, **Vol. 22**, p.1407-1412, (2004).
- [16]. C. Leuschner, C. S. S. R. Kumar, W. Hansel, J. Zhou, W. Soboyejo, J. Hormes: *Breast Cancer Research and Treatment*, in press. (2006).
- [17]. M. S. O'Reilly, L. Holmgren, Y. Shing, C. Chen, R. A. Rosenthal, M. Moses, W. S. Lane, Y. Cao, E. H. Sage, J. Folkman . *Cell* **79**, 315-328 (1994).

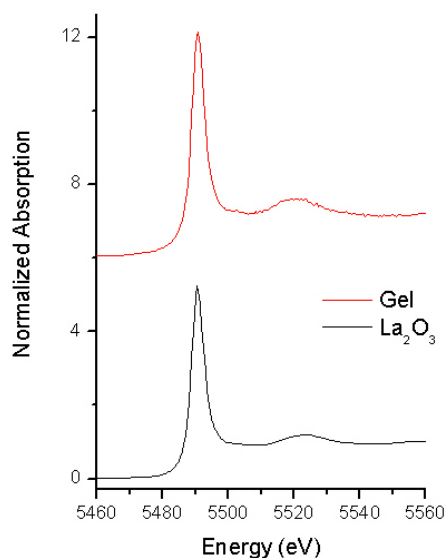
## XAS of doped Lanthanum Oxide and Strontium Oxide Nanoparticles

E.E. Doomes and E.H. Walker, Jr.; Southern University and A&M College, Baton Rouge, Department of Physics, P.O. Box 10554, Baton Rouge, LA 70813; [edward\\_doomes@subr.edu](mailto:edward_doomes@subr.edu). Southern University and A&M College, Baton Rouge, Department of Chemistry, [edwin\\_walker@cxs.subr.edu](mailto:edwin_walker@cxs.subr.edu).  
PRN: SU-ED1206LOSON

This experimental work is preliminary and exploratory in nature. Lanthanum Oxide and Strontium Oxide nanoparticles have applications in fuel cell materials. A large amount of empirical data has been assembled on these systems, but the mechanisms remain poorly understood.

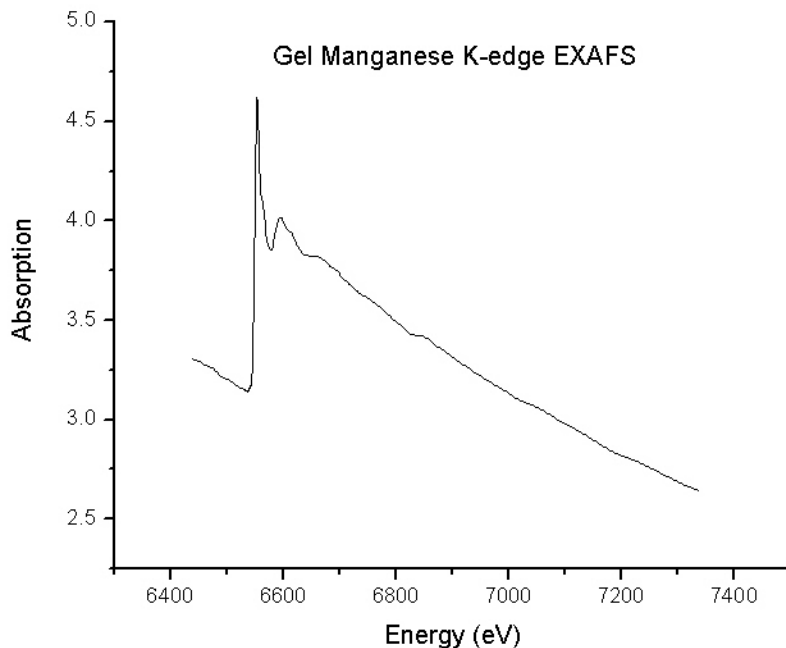
X-ray absorption spectra were recorded at the Double Crystal Monochromator beamline at the J. Bennett Johnston Center for Microstructures and Devices. X-ray spectra were obtained at the Manganese K-edge and Lanthanum L<sub>III</sub>-edge in fluorescence mode as well as in transmission. The incident beam intensity and transmitted beam intensity were measured using an ion-chambers filled with air. Samples and the detector were placed in the standard 45° geometry for fluorescence measurements. The detector was a liquid nitrogen cooled Canberra 13-element Germanium detector was used to record the fluorescence data. While recording fluorescence spectra, the multichannel analyzer was windowed (~200 eV) about the Manganese K (1s) and Lanthanum L<sub>α1</sub> ( $2p^{3/2}$ ) fluorescence lines.

Data was smoothed and analyzed with standard procedures (Teo 1986) using the Ifeffit EXAFS analysis package (Newville 2001) which employs the Autobk algorithm (Newville, Livins et al. 1993)



The previous figure displays the lanthanum L<sub>III</sub>-edge spectra of the gel and a Lanthanum oxide standard (+3 oxidation state). The similarity between the spectra indicates that the lanthanum in the gel is also in the +3 oxidation state.

We have also obtained preliminary EXAFS data at the Manganese K-edge; analysis of this data is ongoing and will allow for determination of the bond distances, identity and number of Mn nearest neighbor atoms.



## References

- Newville, M. (2001). "IFEFFIT: interactive XAFS analysis and FEFF fitting." *Journal of Synchrotron Radiation* 8: 322-324.
- Newville, M., P. Livins, et al. (1993). "Near-edge x-ray absorption fine structure of Pb: A comparison of theory and experiment." *Phys. Rev. B* 47(21): 14126-14131.
- Teo, B. K. (1986). *EXAFS : Basic principles and data analysis*. New York, Springer-Verlag.

## Glutaric Acid as a Spacer facilitates Improved Intracellular uptake of LHRH-SPION into Human Breast Cancer Cells

Challa S. R. Kumar<sup>a</sup>, Carola Leuschner,<sup>a,c</sup> Michelle Urbina,<sup>a,b</sup> Tevhida Ozkaya<sup>a,d</sup>, and Josef Hormes,<sup>a</sup>

<sup>a</sup>Center for Advanced Microstructures and Devices, Louisiana State University, 6980 Jefferson Hwy, Baton Rouge, Louisiana 70806, USA; <sup>b</sup>Biological and agricultural engineering, Louisiana State University, Baton Rouge, Louisiana 70803; <sup>c</sup>Pennington Biomedical Research Center, Louisiana State University System, 6400 Perkins Road, Baton Rouge, Louisiana 70808, USA; <sup>d</sup>Chemistry Department, Fatih University, Istanbul, Turkey

There is a growing interest in developing superparamagnetic nanoparticle-based materials that are biocompatible, biodegradable and efficient in intracellular uptake to cancer cells for applications in cancer therapy and diagnosis.<sup>1</sup> While there is a continuous progress in this direction in terms of excellent experimental and theoretical work, there are several challenges that need to be addressed.<sup>2</sup> One of the most important challenges is to prevent uptake of nanoparticles by the reticuloendothelial system (RES) and enhance their circulation times so that they can navigate through irregularities of tumoral vasculature leading to efficient intracellular uptake preferably via endocytosis. The efficacy of a nanoparticulate system is determined by their ability for intracellular uptake in *in vitro* studies. Experimental studies, mathematical models and computer simulations have already demonstrated that rapid intracellular uptake can be improved through suitable surface modifications, especially coating of SPIONs with hydrophilic polymers and surfactants.<sup>3</sup> Several studies have demonstrated that polyethylene glycol (PEG) coatings, due to their biocompatibility, resistance to proteins and nonantigenicity, are the most widely utilized for increasing circulation times and enhancing intracellular uptake of SPIONs in cancer cells. Dextran coated SPIONs also have been demonstrated to improve intracellular uptake. In addition to simple coatings such as PEG and Dextran, there are also investigations related to more complex coatings involving multi-step synthetic procedures to prevent RES uptake and improved cellular uptake.<sup>4</sup> However, to improve production and *in vivo* applications, it is important to avoid complicated and lengthy chemical procedures for SPION coatings. We recently demonstrated that ligands such as LHRH (Luteinizing Hormone Releasing Hormone) act as targeting agents for breast cancer cells that express receptors for LHRH.<sup>5</sup> We have also demonstrated that intracellular accumulation of LHRH-bound SPIONs (without any PEG or dextran coating on SPIONs) in MDA-MB-435S.luc cells *in vitro* was 12-fold higher than the corresponding free SPIONs uptake.<sup>6</sup> The results are not very surprising as LHRH is a decapeptide and can function as coating (in addition to being a targeting agent) thus preventing macrophage recognition, RES uptake and enhance circulation time and facilitates cellular uptake. In addition to demonstrating the concept of utilizing a targeting agent itself acting as a coating for improved intracellular uptake, we are also currently investigating the introduction of a small spacer in-between SPION and LHRH in order to engineer SPION conjugates for further improvements in intracellular uptake. In this study, we have synthesized SPIONs and covalently bound to it glutaric acid followed by LHRH using carbodiimide chemistry. The intracellular uptake and cytotoxicity of newly engineered SPIONs were investigated and compare with the data obtained with that of free SPIONs and SPION-LHRH. The results obtained, so far, indicates that incorporation of a small spacer molecule such as glutaric acid between LHRH and

SPION shows significant enhancement in intracellular uptake without causing toxicity to the breast cancer cells.

### References

1. Alexiou, Christoph; Schmid, Roswitha J.; Jurgons, Roland; Kremer, Marcus; Wanner, Gerhard; Bergemann, Christian; Huenges, Ernst; Nawroth, Thomas; Arnold, Wolfgang; Parak, Fritz G. Targeting cancer cells: magnetic nanoparticles as drug carriers. *European Biophysics Journal* (2006), 35(5), 446-450.
2. Gabizon, A., Shmeeda, H., Horowitz, A.T., Zalipsky, S. Tumor cell targeting of liposome-entrapped drugs with phospholipid-anchored folic acid-PEG conjugates. *Advanced Drug Delivery Review*, 2004, 56, 1177-92.
3. (a) Reference 1, (b) Torchilin, V.P., Omelyanenko, V.G., Papisov, M.I., Bogdanov, Jr., A.A., Trubetskoy, V.S., Herron, J.N., Gentry, C.A. Poly(ethylene glycol) on the liposome surface: on the mechanism of polymer-coated liposome longevity. *Biochimica et Biophysica Acta*, 1994, 1195, 11-20.
4. (a) Koeseoglu, Yueksel. Effect of surfactant coating on magnetic properties of Fe<sub>3</sub>O<sub>4</sub> nanoparticles: ESR study. *Journal of Magnetism and Magnetic Materials* (2006), 300(1), e327-e330.
5. Leuschner, C., Enright, F., Gawronska, B., Hansel, W. (2003), Membrane disrupting lytic peptide conjugates destroy hormone dependent and independent breast cancer cells in vitro and in vivo. *Breast Cancer Research and Treatment* 78: 17-27.
6. (a) Carola Leuschner, Challa SSR Kumar, William Hansel, and Josef Hormes, Targeting breast cancer cells and their metastases through luteinizing hormone releasing hormone (LHRH) receptors using magnetic nanoparticles, *J.Biomed.Nanotech.*, 1(2), 229-233, 2005. (b) Carola Leuschner, Challa SSR Kumar, Zhou, Jikou, Soboyejo, Winston O, William Hansel, and Josef Hormes, LHRH-conjugated magnetic iron oxide nanoparticles for detection of breast cancer metastases, *Breast Cancer Research and Treatment* (2006) (c) Zhou, Jikou; Leuschner, Carola; Kumar, Challa; Hormes, Josef F.; Soboyejo, Winston O., Sub-cellular accumulation of magnetic nanoparticles in breast tumors and metastases., *Biomaterials* (2006), 27(9), 2001-2008.

## Non-Conventional MRI : Intermolecular Multiple Quantum Coherence Imaging of tumors after injection with LHRH-SPIONs

Warren Warren's Group, Duke University  
 Carola Leuschner's Group, Pennington Biomedical Research Center  
 Challa Kumar's Group, LSU-CAMD.

Intermolecular multiple quantum coherence (iMQC) imaging is a new advanced technique that provides information not available from conventional MR imaging<sup>1-3</sup>: this technique can enhance regions of anisotropy in structured samples<sup>4-8</sup> and visualize local dipole fields created by super paramagnetic iron oxide nanoparticles (SPION)<sup>9</sup>. Though iMQC images generally have a very poor signal to noise ratio (SNR), our *in vivo* results demonstrate that we can get very clean images that highlight only regions of high anisotropy, most likely related to the regions of maximum loading of the nanoparticles.

In this study mice were inoculated with human breast cancer cells. After the tumor vascularization the mice received an injection of a new kind of contrast agent, LHRH-SPION (luteinising hormone-releasing hormone-conjugated superparamagnetic nanoparticles)<sup>10,11</sup>. In the LHRH-SPION contrast agent the cellular uptake of the SPIONs is improved by coating the magnetic core with luteinizing hormone releasing hormone (LHRH), which has receptor sites in breast cancer cells.

Standard spin echo and a series of three intermolecular double quantum images (iDQC) were acquired *in vivo* and *post mortem*. The combination of three different iDQC images (with the correlation gradient pointing in three orthogonal directions) gave us the anisotropy map.

Figure 1 shows *in vivo* standard spin echo and the iDQC anisotropy map images. The iDQC anisotropy image shows an interesting new feature: tumor region highlighting. From theoretical derivations regions of high intensity signal correspond to regions of high anisotropy. An example of high anisotropy region is tumor masses which will be emphasized using this methodology, therefore improving MRI soft tissue characterization.

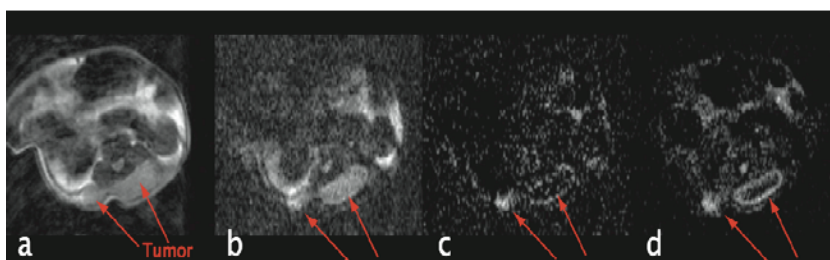


Figure 1: a) *in vivo* axial spin echo image of the mice breast tumor; b) *in vivo* iDQC image; c) *in vivo* iDQC anisotropy map image; d) *post mortem* iDQC anisotropy map image

**References**

- [1] Richter W, Sanghyuk L, Warren WS, Qihong He. "Imaging with intermolecular Multiple-Quantum Coherences in Solution Nuclear Magnetic Resonance". *Science* **1995**;267:654-657.
- [2] Warren WS, Ahn S, Mescher M, Garwood M, Ugurbil K, Richter W, Rizi RR, Hopkins J, Leigh JS. "MR imaging contrast enhancement based on intermolecular zero quantum coherences". *Science* **1998**;281:247-252.
- [3] Rizi RR, Ahn S, Alsop DC, Garret Roe S, Schnall MC, Leigh JS, Warren WS. "Intermolecular zero-quantum coherence imaging of the human brain". *Magn Reson Med* **2000**;43:627-632.
- [4] Bowtell R and Robyr P. "Structural investigations with the dipolar demagnetizing field in solution NMR". *Phys. Rev. Lett.* **1996**;76:4971-4974.
- [5] Bowtell R, Gutteridge S and Ramanathan C. "Imaging the long-range dipolar field in structured liquid state samples". *J. Magn. Reson.* **2001**;150:147155.
- [6] Bouchard LS, Rizi RR and Warren WS. "Magnetization structure contrast based on intermolecular multiple-quantum coherences". *Magn. Reson. Med.* **2002**;48:973-979.
- [7] Bouchard LS, Wehrli FW, Chin CL and Warren WS. "Structural anisotropy and internal magnetic fields in trabecular bone: coupling solution and solid dipolar interactions". *J. Magn. Reson.* **2005**;176:27-36.
- [8] Ramanathan C, Bowtell R. "NMR imaging and structure measurements using the long-range dipolar field in liquids". *Phys. Rev. E* **2002**;66: 1-10.
- [9] Faber C, Heila C, Zahneisen B, Ballaa DZ and Bowtell R. "Sensitivity to local dipole fields in the CRAZED experiment: An approach to bright spot MRI". *J Magn. Reson.* **2006** ;315-324.
- [10] Leuschner C, Kumar C, Hansel W, Soboyejo W, Zhou J, Hormes JF."LHRH-conjugated Magnetic Iron Oxide Nanoparticles for detection of breast cancer metastases". *Breast Cancer Res Treat* **2006**; 99(2):163-176.
- [11] Zhou J, Leuschner C, Kumar C, Hormes JF, Soboyejo WO."Sub-cellular accumulation of magnetite nanoparticles in breast tumor metastases". *Biomaterials* **2006**; 27(9):2001-2008.

## Synthesis of PLGA-Magnetite Nanoparticles by Emulsion Evaporation Technique

Carlos Astete<sup>1</sup>, Challa S.S.R.Kumar<sup>2</sup>, and Cristina Sabliov<sup>1\*</sup>

<sup>1</sup>Louisiana State University, Agricultural Center, Biological & Agricultural Engineering Department; <sup>2</sup>Louisiana State University, CAMD.

The emulsion evaporation is one of the oldest methods used with preformed polymers, and it has been extensively used to entrap numerous drugs, albeit with different degrees of success [1, 2, 3, 4]. However, magnetite entrapment has not been reported so far with this method. The versatility of emulsion evaporation method permits entrapment of magnetite in the PLGA matrix by double-emulsion method due to the hydrophilic behavior of magnetite. Important drawbacks of double-emulsion are the bigger nanoparticle size obtained, and lower entrapment efficiencies of the hydrophilic active components entrapped as compared with single emulsion. Hydrophilic compounds (i.e. magnetite) can be tailored to be solubilized in organic solvents by addition of a surfactant layer (oleic acid) to the particle surface. We hypothesized that increasing the hydrophobicity of the magnetite is likely to allow its entrapment in the PLGA matrix by a single emulsion process, which is a faster process and leads to a smaller nanoparticle size as compared to double-emulsion. This magnetite surface modification ensures its entrapment in the PLGA (hydrophobic polymer) matrix by emulsion evaporation method because magnetite can be solubilized in the organic phase. In order to test this hypothesis, we have developed a single emulsion evaporation method for the entrapment of surface modified magnetite with oleic acid (MOA). The nanoparticles were characterized in terms of size and size distribution with dynamic light scattering (DLS). The magnetite entrapment efficiency was measured by colorimetric method for free iron ( $\text{Fe}^{3+}$ ) detection. The sodium dodecyl sulfate remaining in the nanospheres after dialysis was calculated by thermogravimetric analysis (TGA), and the morphology of the particles was visualized with Transmission Electron Microscopy (TEM).

Based on these investigations it can be concluded that Surface modification of magnetite with oleic acid was a useful approach to ensure the entrapment of magnetite into a hydrophobic polymer (PLGA) with high entrapment efficiency by single emulsion evaporation method. M-P NPs with a final mean size less than 100 nm were obtained at 4% w/w MOA theoretical loading. When MOA theoretical loading was increased to 8% w/w, the nanoparticle size was less than 120 nm. The entrapment efficiency was highly different for the low (57.4%) and high PLGA molecular weight (91.9%).

The emulsion evaporation method was a suitable synthesis method for the formation of nanoparticles with a mean size under 100 nm. The SDS concentration played a critical role in controlling the nanoparticle size. With the method proposed, it was possible to increase the PLGA concentration by at least three times without increasing the empty PLGA nanoparticle size over 100 nm.

Another important factor that affected M-P NPs' size was MOA size and size distribution, which can be controlled by sonication; the stronger the sonication of MOA suspension prior to its addition to the process, the lower the size and the better the PI of the M-P NPs formed. The size and uniformity of the MOA suspension was found critical in forming small and uniform M-P NPs.



Stability of M-P NPs was improved by applying a purification step quickly after synthesis. Dialysis was used as a purification step to remove the excess of SDS and avoid aggregation.

### **References**

1. Mu L, Feng SS. A novel controlled release formulation for anticancer drug paclitaxel (Taxol®): PLGA nanoparticles containing vitamin E. TPGS. *Journal of Controlled Release*. 2003; 86:33-48.
2. Panyam J, Labhasetwar V. Dynamics of endocytosis and exocytosis of poly(D,L-lactide-co-glycolide) nanoparticles in vascular smooth muscle cells. *Pharmaceutical Research*. 2003; **20**:212-220.
3. Yan P, Huiying Z, Hui X, Gang W, Jinsong H, Junming Z. Effect of experimental parameters on the encapsulation of insulin-loaded poly(lactide-co-glycolide) nanoparticles prepared by a double emulsion method. *Journal of Chinese Pharmaceutical Science*. 2002; 11:38-40.
4. Song CX, Labhasetwar V, Murphy H, Qu X, Humphrey WR, Shebuski RJ, Levy RJ. Formulation and characterization of biodegradable nanoparticles for intravascular local drug delivery. *Journal of Controlled Release*. 1997; 43:197-212.

## VIABLE LIGA FABRICATION TO ENHANCE BOILING HEAT TRANSFER FOR PRESSURIZED WATER REACTORS (PWRs)

Kun Lian<sup>a</sup>, Min Zhang<sup>a</sup>, Guoqiang Li<sup>b</sup>, Su-Seng Pang<sup>b</sup>, Zhong-Geng Ling<sup>a</sup>, Chang-Geng Liu<sup>a</sup>, Samuel Ibekwe<sup>c</sup>

<sup>a</sup> Louisiana State University, Center for Advanced Microstructures and Devices (CAMD), [klian@lsu.edu](mailto:klian@lsu.edu).

6980 Jefferson Hwy, Baton Rouge, Louisiana 70806, USA

<sup>b</sup> Louisiana State University, Mechanical Engineering Department, Baton Rouge, LA70803, USA

<sup>c</sup> Southern University, Mechanical Engineering Department, Baton Rouge, LA70813, USA

This project is designed to look for novel routes of fabricating microstructures on the heat exchangers of pressurized water reactors used in navel propulsion systems.

In a nuclear power plant, the power generating capability is practically limited by the boiling heat transfer efficiency of the pressurized water reactor (PWR). One of the major factors that prevent PWR from producing more steam is the boiler pipe overheating caused by inadequate heat transmitted from pipe to the water during the steam generation. The heat transfer inside a boiler is a complex combination of different physical phenomena, which, besides the traditional convection, conduction, and radiation, include liquid to vapor phase change, vapor nucleation and evolution, surface tension between the liquid and heating element, etc. Chyu et al [1] presented that the presence of a pin-fin array on the surface of heating channel enhances the heat transfer significantly. Several fundamental researches have been done in studying effects of geometrical parameters: fin array orientation [1], fin shape [2], lateral flow ejection in pinfinned channels [3], and gap atop an array of pin fins [4, 5].

The experiments were performed to obtain results of adding microstructures on the surface of heating elements to enhance the boiling process and so the heat exchange efficiency of pressurized water reactor (PWR). The micro-pin finned samples (figure 1) were fabricated by KOH etching. Each testing sample is a 10mm × 80mm silicon strip, on which are trapezoid-shaped micro-pin-finned structures with square top of 200μm, height of 35μm, and different spacing values of 200, 400, 600, 800, 1000μm and infinite (no poles on the surface, named *plain* here). The micro-pin fins were examined by SEM (figure 2a-e) and WYKO NT3300 surface optical profiler (figure 2f). The experimental setup is shown in figure 3. The heater was emerged in a pool of de-ionized water at atmospheric pressure. The data acquisition devices are linked to a PC, allowing raw data to be directly recorded to an Excel spreadsheet for further analyses. The input power, weight loss, temperature, and boiling phenomena were continuously recorded. The results were also compared with an un-etched silicon strip of same dimensions but a much smoother surface. Simulation was performed in collaboration with the Department of Mechanical Engineering in the Louisiana State University.

The current results suggest that the main factors leading to the enhanced boiling process are the surface morphology and configuration of microstructures, which provide enhanced vapor nucleation sites (figure 4), affect bubble departing frequency and

retention time, and achieve a higher boiling heat transfer efficiency. Figure 5 shows the testing results between the input power and the heater temperature changes during the boiling process. It is clear that the *plain* sample has the highest temperature increasing slope, and the heater with the highest pin-fin density has the lowest temperature increase rate. These results suggest that LIGA or LIGA-like processes may play a significant roles in the future enhanced PWR fabrication.

**Acknowledgements**

This study was sponsored by a grant from U.S. Department of Energy, Award No. DE-FG52-05N27041. The authors also acknowledge the State of Louisiana for the financial support.

**References**

- [1] M.K. Chyu, Y.C. Hsing, T.I-P. Shih, V. Natarajan, Journal of Turbomachinery, 1999, 121, p257-263.
- [2] M.K. Chyu, C.H. Yen, W. Ma, T. I-P. Shih, Presented at the International Gas Turbine & Aeroengine Congress & Exhibition, Indianapolis, 1999, June 7-10.
- [3] S.C. Lau, J.C. Han, Y.S. Kim, Journal of Heat Transfer, 1989, 111, p51-58.
- [4] S.C. Arora and W. Abdel-Messeh, 1990, Journal of Turbomachinery, 112, p559-565.
- [5] J.J. Wei and H. Honda, International Journal of Heat and Mass Transfer, 2003, 46, p4059 – 4070.

**Figures**

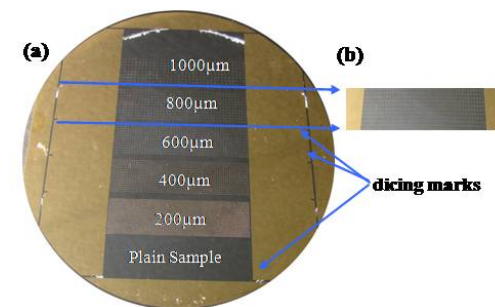


**Figure 1**

(a) One KOH etched silicon wafer with 7 strips of different spacing values as marked; (b) One diced silicon heater.

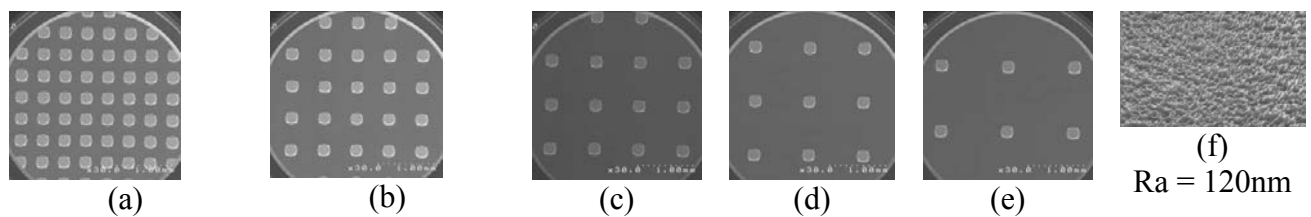


**Figure 2** SEM micrographics of 200µm square micro-pin fins of spacings (µm) (a) 200 (b) 400 (c) 600 (d) 800 and (e) 1000. (f) 3D image of etched surface.

**Figure 3** Experimental setup (not proportional): (a) computer, (b) DAC and serial interface, (c) voltage and temperature measurement, (d) boiler made of a beaker and a heater strip, (e) applied heating power.

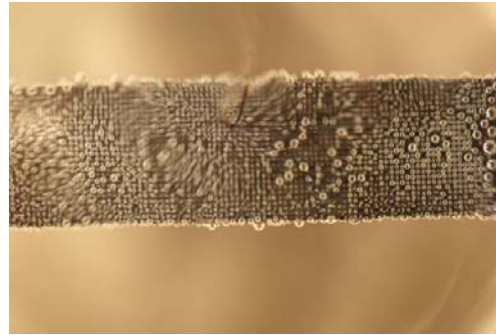
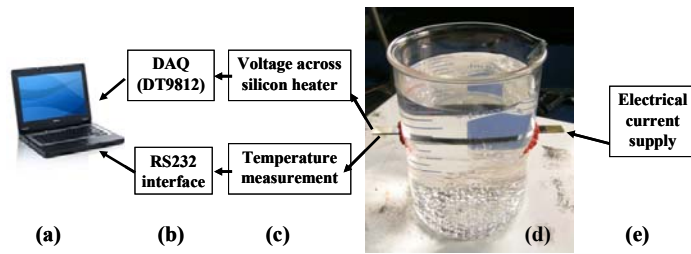


**Figure 4** Close-up view of vapor nucleation sites located on the micro-pin fins.

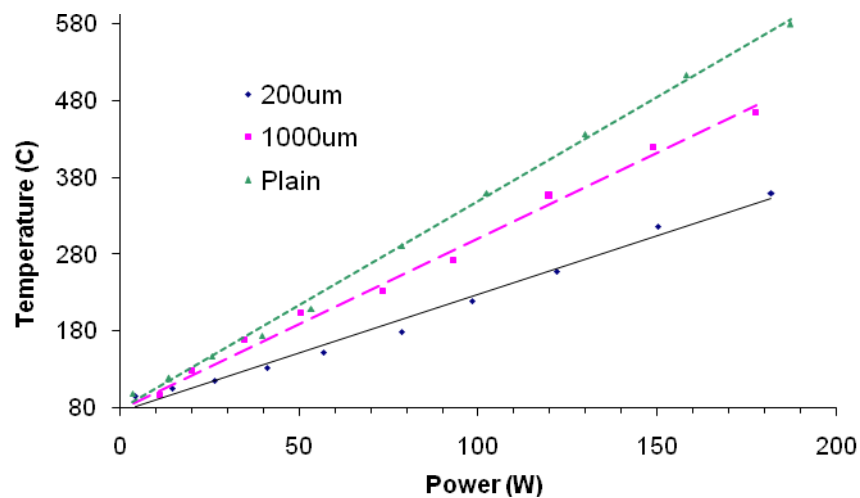


**Figure 5** Temperature vs. Power for different micro-pole structures.

#### 1. CAMD-research-related publications during 2006

(1) M. Zhang, K. Lian, G.Q. Li, S. Ibekwe, S.S. Pang, The study of LIGA microstructures for enhancing the performance of pressurized water reactors (PWRs), 7th LMET Conference, Baton Rouge, LA, October 23 – 24, 2006.

(2) M. Zhang, S. Ibekwe, G.Q. Li, S.S. Pang, K. Lian, Using LIGA based microfabrication to improve overall heat transfer efficiency of pressurized water reactor, 14th International Conference on Composites/Nano Engineering (ICCE-14), Boulder, Colorado, USA, July 2 – 8, 2006.

2. Grants

“Towards Miniaturization of the Naval Nuclear Propulsion Reactors: Novel Processing Routes of Fabricating Microstructures on Pressurized Water Reactors”, DOE/NNSA

Project # DE-PS62-05NA26772

Co-PI : Dr. Kun Lian

3. Nine undergraduate students from the Southern University took part in this research during the 2006 calendar year, including two REU students from the Southern University.

## Microfluidic Synthesis of Cobalt Nanoparticles

Yujun Song,<sup>1†</sup> Hartwig Modrow,<sup>2</sup> Laurence L. Henry,<sup>3</sup> Cheng K. Saw,<sup>4</sup> Ed E. Doomes,<sup>1</sup> Vadim Palshin,<sup>1</sup> Josef Hormes<sup>1</sup> and Challa S S R Kumar<sup>1\*</sup>

<sup>1</sup>Center for Advanced Microstructures and Devices, Louisiana State University, 6980 Jefferson Hwy, Baton Rouge, LA 70806; <sup>2</sup>Physikalisches Institut, University of Bonn, Nußallee 12, D-53115, Bonn, Germany; <sup>3</sup>Department of Physics of Southern University and A&M College, Baton Rouge, LA 70813; <sup>4</sup>Lawrence Livermore National Laboratory, Livermore, CA 94550.

<sup>1†</sup> Current address: Applied Research Centre at Old Dominion University, Newport News, VA 23606.

Engineering of nanomaterials is the primary focus of numerous research groups as nanomaterials find extensive industrial applications in the field of catalysis, electronics, high-density magnetic recording media, sensors, nanobiotechnology and biomedical nanotechnology.<sup>1</sup> Several synthesis methodologies, both “top-down” and “bottom-up” approaches, have been developed to obtain a broad variety of nanomaterials of different sizes and shapes.<sup>2</sup> Amongst the bottom-up approaches, a wet-chemical approach appears to be most promising for industrial applications due to its intrinsic scale-up potential. Wet-chemical synthesis methods can be broadly classified into co-precipitation and chemical reduction, which can be carried out either in traditional “flask” techniques or micro fluidic processes. However, the challenge continues to be the control of the size, the size distribution, shape, crystal structure and surface modifications of the nanoparticles. Our group has been involved in the synthesis of metal nanoparticles, more specifically magnetic nanoparticles, using traditional wet-chemical as well as microfluidic processes.<sup>1(e), 10(a,b), 22</sup> Amongst the metallic nanoparticles, cobalt is most well studied due to its unique properties and potential applications. Cobalt nanoparticles are known to exist in three polymorphs, face centered cubic (fcc), hexagonally close packed (hcp) and the epsilon ( $\epsilon$ ) phase. While microfluidic processes for size and shape control synthesis of nanoparticles are known, there is no report of crystal structure controlled synthesis..<sup>25</sup>

We hypothesized that kinetic energies of the reactants can be controlled better in a microfluidic environment through appropriate design of micro mixtures and manipulation of flow rates which in turn lead to controlling the crystal structure of the nanoparticles. We report here for the first time a microfluidic process for obtaining all the three phases of cobalt nanoparticles (Figure 1). The micro fluidic synthesis results reported here, in conjunction with analysis based on Selected Area Electron Diffraction (SAED), X-Ray Diffraction and *in-situ* liquid Co K-edge X-ray Absorption Near Edge Structure (XANES) spectroscopy, demonstrate that hcp ( $\alpha$ ), fcc ( $\beta$ ) and epsilon ( $\epsilon$ ) crystal structures of cobalt nanoparticles can be obtained by controlling the reaction times, the flow rates and quenching procedures. Cobalt nanoparticles of fcc ( $\beta$ ) phase were obtained from a high flow rate of the reactants followed by *in-situ* quenching of the reaction. Hcp and  $\epsilon$ -cobalt nanoparticles were obtained at a low flow rate of the reactants followed by *in-situ* quenching and delayed quenching, respectively. In-situ XANES measurements on Co nanoparticles coming out of the outlet of the micro fluidic reactor at different flow rates seem to indicate that the difference in flow rate influences the nucleation process in

a critical way and that particle growth occurs mainly outside the reactor. The magnetic properties of the cobalt nanoparticles, measured using a SQUID magnetometer system, showed significant differences between the three different crystal structures.

The results from these investigations are published in the ACS journal, Chemistry of Materials, last year.

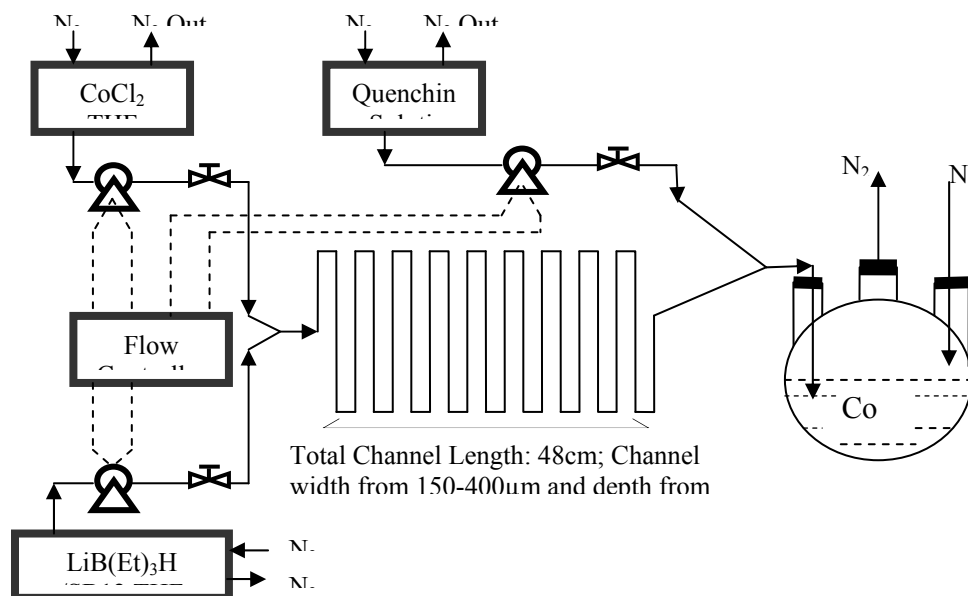


**Figure 1.** Schematic of the micro fluidic reactor process for phase-controlled synthesis of cobalt nanoparticles.

## References

- (a) Lisiecki, I. *J.Phys.Chem. B* **2005**, 109, 12231. (b) Green, M. *Chem. Commun.*, **2005**, 3002 (c) Liu, Y.; Majetich, S. A.; Tilton, R. D.; Sholl, D. S.; Lowry, G. V.; *Environ.Sci.Technol.* **2005**; 39(5); 1338. (d) Farrell, D.; Cheng, Y.; McCallum, R. W.; Sachan, M.; Majetich, S. A.; *J. Phys. Chem. B.* ; **2005**; 109(28); 13409. (e) Catherine, B.; *J. Mater. Chem.* **2005**, 15(5), 543. (f) Kumar, C.S.S.R., Hormes, J., Leuschner, C. (Eds), Nanofabrication towards biomedical applications, Wiley-VCH, **2004** (g) Kumar, C.S.S.R.. (Ed) Biofunctionalization of nanomaterials, Wiley-VCH, **2005**. (h) Cheng, C.; Romero, D.; Fraser, G.T.; Walker, A.R.H. *Langmuir*, **2005**, 21(26), 12055.
- [a] Richards, R.M.; Bönnemann, H., Nanofabrication Towards Biomedical Applications: Techniques, Tools, Applications, and Impact, Kumar, C.S.S.R., Hormes, J., Leuschner, C. (Eds), Wiley-Vch, **2004**, 3-32 (b) B.L. Cushing; V.L. Kolesnichenko, C.J. O'Connor, *Chem. Rev.* **2004**, 104, 3893.
- (a) Popov, A. K.; Brummer, J.; Tanke, R. S.; Taft, G.; Wruck, A.; Loth, M.; Langlois, R.; Schmitz, R. Los Alamos National Laboratory, Preprint Archive, Physics **2005**, 1-15, arXiv:physics/0511147. (b) de Dios, M.; Barroso, F.; Tojo, C.; Blanco, M. C.; Lopez-Quintela, M. A., *Coll. Surf., A: Physicochem. Eng. Aspects* **2005**, 270-271(Complete), 83-87. (c) Frenkel, A. I.; Nemzer, S.; Pister, I.; Soussan, L.; Harris, T.; Sun, Y.; Rafailovich, M. H., *J. Chem. Phys.* **2005**, 123(18), 184701/1-184701/6. (d) Hussain, Irshad; Graham, Susan; Wang, Zhenxin; Tan, Bien; Sherrington, David C.; Rannard, Steven P.; Cooper, Andrew I.; Brust, Mathias., *J. Am. Chem. Soc.* **2005**, 127(47), 6398-16399.
- (a) Edel, E.B.; Fortt, R.; deMello, J.C.; deMello, A.; *J. Chem. Comm.* 2002, 1136. (b) Chan, M.E.; Mathies, R.A.; Alivisatos, A.P. *Nano Lett.* **2003**, 3, 199. (c) Kawa, M.; Morii, H.; Ioku, A.; Saita, S.; Okuyama, K.; *J. Nanoparticle Res.* **2003**, 5, 81. (d) Ayon, A.A.; Braff, R.A.; Bayt, R.; Sawin, H.H.; Schmidt, M.A. *J. Electrochem. Soc.* , **1999**, 146, 2730. (e) Jongen, N.; Donnet, M.; Bowen, P.; Lemaitre, J.; Hofmann, H.; Schenk, R.; Hofmann, C.; Aoun-Habbache, M.; Guillemet-Fritsch, S.; Sarrias, S.; Rousset, A.; Viviani, M.; Buscaglia,



M.T.; Buscaglia, V.; Nanni, P.; Testino, A.; Herguijuela, J.R. *Chem. Eng. & Tech.* **2003**, 26, 303. (f) Buscaglia, M.T.; Buscaglia, V.; Viviani, M.; Testino, A.; Nanni, P.; Bowen, P.; Donnet, M.; Natalie, J.; Rainer, S.; Hofmann, C.; Hessel, V.; Schonfeld, F. *Adv. Sci. Tech.* (Faenza, Italy) 30 (10<sup>th</sup> International Ceramics Congress, 2002, Part A), **2003**, 535. (g) Wei, G.; Huang, H.Y.; Xiong, R.C.; *Chinese Chem. Lett.*, **2003**, 14(8), 877. (h) He, S.; Kohira, T.; Uehara, M.; Kitamura, T.; Nakamura, H.; Miyazaki, M.; Maeda, H., *Chem. Lett.*, **2005**, 34(6), 748. (i) Kim, K. D.; Kim, H. T. *Mat. Letts* **2003**, 57(21), 3211.

## UNIQUE COPPER/CARBON CORE/SHELL NANOPARTICLES MADE BY USING BIOMASS AS TEMPLATES AND THEIR APPLICATIONS

Kun Lian<sup>1</sup>

Qinglin Wu<sup>2</sup>

<sup>1</sup>Louisiana State University, Center for Advanced Microstructures and Devices, Jefferson Hwy. Baton Rouge, Louisiana 70806, USA.  
Phone: 225-578-9341, Email: [klian@lsu.edu](mailto:klian@lsu.edu)

<sup>2</sup>Louisiana State University Ag Center, School of Renewable Natural Resources, AgCenter, Baton Rouge, Louisiana 70806, USA.  
Phone: 225-578-8369, E-mail: [wuqing@lsu.edu](mailto:wuqing@lsu.edu)

### ABSTRACT

Core-shell nanoparticles have attracted much research attention in recent years because of the great potential in protection, modification, and functionalization of the core particles with suitable shell materials to achieve specific physical, chemical, and biological performance [1,2]. Pure copper nanoparticles are unstable in the air. By coating the copper nanoparticle surface with a stable carbon layer, these copper nanoparticles are protected from the oxidation and retain most of the favorable properties. The carbon out-shell on the copper nanoparticles provides a stable and common chemical base for future functionalization and surface modification. Such modification has brought about interesting physical and chemical properties of the nano-structured materials that have shown important technological applications in catalyst, fuel cell, drug delivery, and other industries [3,4].

Many methods have been tried to synthesize core-shell structure nanoparticles. Among them, the Layer-by-Layer assembly, Microemulsion, Kratschmer-Huffman Carbon Arc Methods are most commonly used. The copper/carbon core/shell nanoparticles made from this method are expensive and carbon coating layer is not good enough for long time exposure in ambient environment (the protection usually last few hours).

In this paper, the authors present the characterization results of copper/carbon core/shell nanoparticles made from a proprietary manufacturing technology (patent filled by LSU with application No: 60/772.325). The metrology information, stability testing results, wood preservation applications, and results from termite, mold, and decay tests will be discussed.

### EXPERIMENTAL AND RESULTS

The copper/carbon core/shell nanoparticles used in this work have the particle size distribution around 100 nanometers (figure 1). The particles have continuous carbon shells of about 4nm in thickness around the copper cores (Fig. 2). This kind of nanoparticles can be exposed in water at ambient environment for more than 6 months and still keep the pure copper core composition (Fig.3). Two very important physical properties of

the copper/carbon core/shell nanoparticles are: (1) it has the original copper yellow color comparing to the dark black color that commercially available copper nanoparticles on the market; (2) the nanoparticles can be easily dispersed in both polarized solvents, such as acetone; water, as well as depolarized organic solvents, such as hexane; oil, without any further surface treatment (figure 4). This unique property will bring tremendous potential for different treatment applications.

Because of the low cost, this kind of core/shell copper/carbon nanoparticle has been studied as commercial wood preservation chemical. The carbon shell will help prevent the copper core from oxidation and not releasing toxic copper ions under normal conditions. Once the nanoparticles are attacked by insects, bacteria or fungi, toxic copper ions will be released to stop the attacks. This may provide a solution for next generation environmental friendly wood preservation chemicals to replace currently ones that have detrimental impacts on environment.

The water solution of copper/carbon core/shell nanoparticle compound at 1% concentration level was used to treat wood samples through a vacuum and pressure treatment, which is a standard processing procedure for current wood treatment plants. The treated samples were subsequently tested against Formosan Subterranean Termites using the American Wood Preservation Association (AWPA) E1-jar test standard. The preliminary testing results show a complete elimination of termite attacks on the copper/carbon core/shell nanoparticle treated samples (Fig.5 and Fig. 6). Figure 7 shows results of the 18-week decay test following the AWPA E10 standard with white rot fungus (*T. Versicolor*). Wood groups (A to H) treated by the copper/carbon core/shell nanoparticles showed strong decay resistance in comparison with untreated controls and ACQ-treated wood.

### ACKNOWLEDGEMENTS

This study was sponsored in part by the LEQSF Industrial Tie Grant [LEQSF(2006-08)-RD-B-01]. The authors also acknowledge the financial support of the State of Louisiana.

REFERENCES

- [1] F. Banhart, N. Grobert, M. Terrones, J. -C. Charlier and P. M. Ajayan, 2001, "Metal atoms in carbon nanotubes and related nanoparticles", International Journal of Modern Physics B, 15, p. 4037.
- [2] S. Subramoney, 1998, "Noel Nanocarbons-Structure, Properties, and Potential Applications", Advanced Materials, V10, pp 1157-1171.
- [3] Delafosse, D. 1986. J. Chim. Phys. Phys.-Chim. Biol., 83, p.791.
- [4] B.C.Gates, L. Guzzi, and H. Knozinger, 1986, "Metal Clusters in Catalysis", Stud Surf. Sci. Catal. p.29.

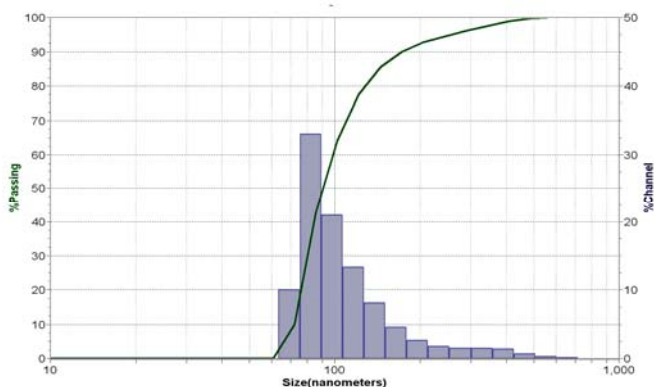


Figure 1. Laser scattering measurement result of copper/carbon core/shell nanoparticles size distribution.

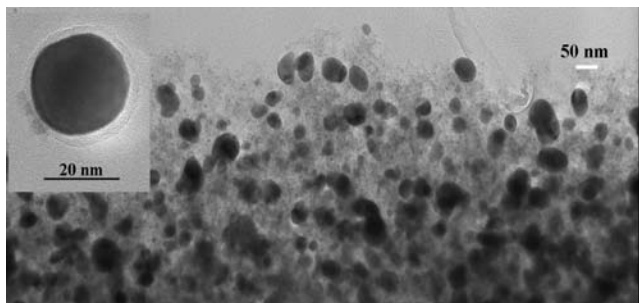


Figure 2. The TEM pictures show the copper man-sized copper particles and insert shows the copper/carbon core/shell structure.

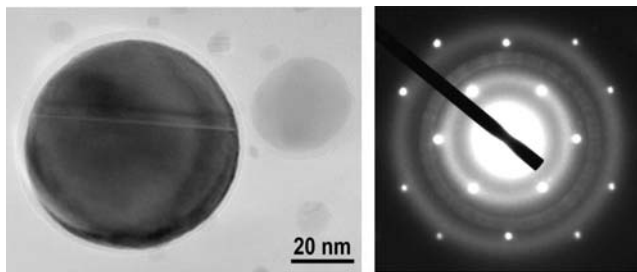


Figure 3. The TEM picture shows copper/carbon core/shell nano particles after 6 months immersion in water and diffraction pattern from a nanoparticles core show a pure copper core.

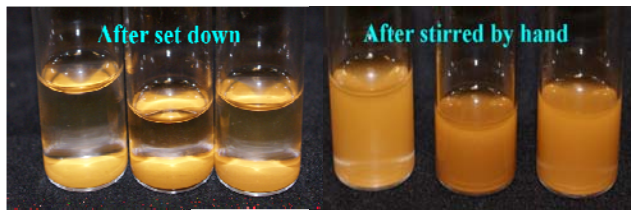


Figure 4. The color of the copper/carbon core/shell nanoparticles after 6 months in air and 6 months in water.

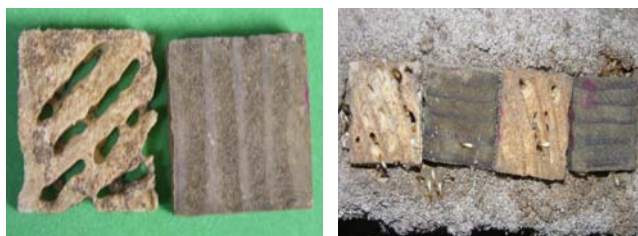


Figure 5. Pictures show the results of copper/carbon core/shell nanoparticle treated wood against Formosan subterranean termites. The results of treated wood (dark color no damage) versus untreated controls (light color – significant termite damage) show a complete elimination of termite attacks on the treated samples.

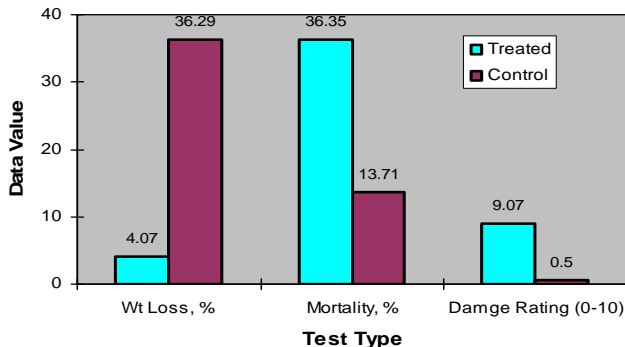


Figure 6. Weight loss, mortality, and damage rating from termite tests of NCCCS treated wood in comparison untreated controls.

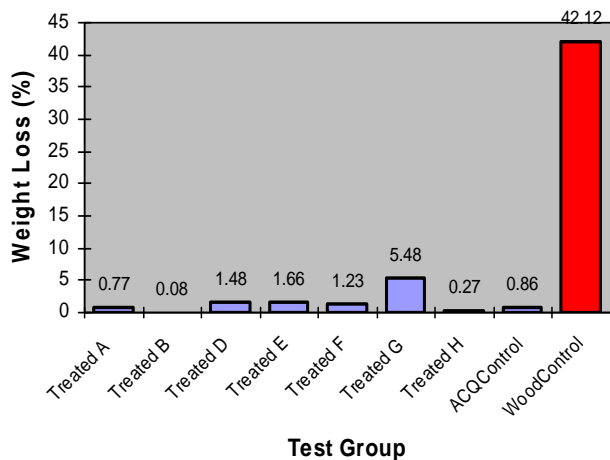


Figure 7. Weight loss from decay tests of NCCCS treated wood in comparison untreated controls.

## Time resolved observation of the wet-chemical synthesis of nanoparticles.

Svetlana Zinoveva<sup>\*</sup>, Rohini DeSilva, Russell D Louis, Proyag Datta, Challa SSR Kumar and Josef Hormes<sup>\*</sup>,

Center for Advanced Microstructures and Devices (CAMD), Louisiana State University, 6980 Jefferson Hwy., Baton Rouge, LA 70806, USA

<sup>\*</sup> Institute of Physics, University of Bonn, Nussallee 12, D-53115 Bonn, Germany

**Correspondence to: S.Zinoveva, e-mail: zinoveva@physik.uni-bonn.de**

### Introduction

Wet chemical synthesis of metal nanoparticles with enhanced compared to bulk materials magnetic, electronic and catalytic properties has attracted a lot of efforts in the last decades<sup>i</sup>. However, there is still seems to be a challenge to have a control over size, shape and structure of resulting nanoparticles, as well as on the reproducibility of synthesis which would give us an opportunity to scale up the process for industrial applications.

Among others our group has been involved in synthesis and characterization of cobalt nanoparticles, due to their remarkable magnetic properties and potential applications in ferro-fluids<sup>ii</sup>, medical diagnostic and therapy<sup>iii</sup>. Commonly nanoparticles are formed spontaneously via decomposition of organometallic complexes (precursor) in the presence of stabilizing agent (surfactant). Cobalt nanoparticles were prepared through thermal decomposition at 110 °C of either dicobalt octacarbonyl (DCO) or alkyne-bridged dicobalt hexacarbonyl (ADH) precursors in the presence of aluminum alkyl. While it was previously shown that reaction conditions such as temperature, time, surfactant, length of alkyl chain play a crucial role on the properties of resulting nanoparticles<sup>iv</sup>, there is no study of entire mechanism of cobalt nanoparticles formation from those syntheses.

Here we report experiments to gain a predictive understanding of the mechanism of cobalt nanoparticles formation and ability to tailor products with desired properties. Reduction of DCO and ADH organometallic cobalt complexes has been studied using a combination of structural techniques- time dependent X-ray absorption spectroscopy (XAS) and Transmission Electron Microscopy (TEM). To follow structural and electronic changes in the pass of nanoparticles formation X-ray absorption spectroscopy is one of the premiere tools.

### Synthesis and Characterization Methods

Co nanoparticles were prepared by thermolysis of  $\text{Co}_2(\text{CO})_8$  in the presence of  $\text{Al}(\text{C}_8\text{H}_{17})_3$  as described elsewhere<sup>v</sup>. Briefly, 17.1 g  $\text{Co}_2(\text{CO})_8$  were introduced to 88 ml  $\text{Al}(\text{C}_8\text{H}_{17})_3$  in 3000 ml of toluene at 90 °C gradually heated up to 110 °C and was kept so for 18 hours. In between, namely, after 2 minutes, 3 hours, 6 hours, 9 hours, 12 and 18 hours samples solutions were taken out from the flask without any interruption of stirring and under higher nitrogen flow. The contents were cooled to 20 °C. Identical synthesis

was repeated for ADH precursor. From both synthesis samples were prepared for TEM and XAS analysis.

XAS data collection was performed at the at the XMP beamline at the 1.3 GeV electron storage ring at the Center for Advanced Microstructures and Devices (CAMD, LA)<sup>vi</sup>. Details of the experiment you can find in the reference<sup>vii</sup>

## Results and Discussion

Co K-edge time dependent XANES spectra of the synthesis with DCO and ADH precursors are present in the Fig.1 and Fig.2, respectively along with Co foil and DCO, ADH complexes spectra for comparison at the bottom of the graphs. The observed changes in the spectra belong to different points of time of the synthesis allow us to follow a path of particles formation. Looking at the samples taken after 2 minutes DCO reaction started, 2 minutes and 3 hours for ADH reaction it turns out that nucleation is not an instant process and we are still dealing with cobalt organometallic complexes. Should be mentioned here, that different kinetic behavior observed at ADH compare to DCO (“2 minutes DCO” spectra plotted together with “3 hours ADH” coincide very well) are rising from different decomposition rates of ADH and DCO precursors. The general features of the shape resonance “2 minutes DCO” spectra (two maxima at 7749 eV and at 7798 eV) can be assigned to the shape resonance of the starting material spectra or possibly to one of the intermediate products:  $\text{Co}(\text{CO})_4$ -known radical<sup>viii</sup> of decomposition of dicobalt octacarbonyl, through the brake of the Co-Co bond or  $\text{Co}_4(\text{CO})_{12}$  as a result of decarbonylative dimerisation of  $\text{Co}_2(\text{CO})_8$ , that takes place rapidly above 50<sup>0</sup>C.<sup>ix</sup>

Spectra of “3 hours DCO” sample starts to exhibit properties of metallic phase of cobalt. The maxima located at 7757 eV and 7808 eV are almost the same positions as for bulk cobalt. This phase is also present at “6 hours ADH” sample.

For the sake of curiosity and desire for precise definition of nucleation phase, we tried to study products in between that time frame (2min- 3h). Once more was confirmed that decomposition of the dicobalt octacarbonyl goes in a non trivial way via formation of several intermediate compounds, spectra of those are not included in this work, but none of them (10 min, 30 min, 1 hour, 2 hours samples) does show any metallic features as “3 hours DCO” sample does. That implies that existing model of nanoparticles formation consisting of nucleation and growth phases in their used terms cannot be applicable to the carbonyl precursor reduction mechanism discussed here. The chemical growth of particles on the atom-by-atom basis from super saturated solution was not observed in this study.

The next pair of outstanding spectra in this model are spectra after 6 and 9 hours of DCO synthesis and “9 hours ADH” respectively. For which we see refinement of energy positions towards bulk cobalt and sharpness of the shape resonances. The intensity of the 1s-3d transition (height of pre-edge shoulder) gradually increases through 3 hours to 9 hours spectra, obviously that corresponds to the growth of nanoparticles. There are full

grown nanoparticles by 9 hours; growth process is complete as the pre-edge intensity rich maximum there.

Spectra of “12 and –“18 hours DCO” and “18 hours ADH” are somewhat different from those of full grown particles. The double peak shape resonance indicates that we are still dealing with a cobalt metal phase; however there is an increase of the white line intensity together with decrease of pre-edge shoulder. This is a result of surface effect, suggesting that we obtained core-shell nanoparticles. The most probable candidate for this metal core- surface interaction would be a CoO shell as a certain percentage of oxygen is possible in the system and cobalt is very sensitive to it.

Unexpectedly, from TEM analysis we found that overall particle size decreases for 12 and 18 hours samples resulting from both precursors. Indeed, the particle size decrease after 9 hours of synthesis lowers the amplitude of EXAFS oscillations (EXAFS analysis are not present here). Besides, contribution of the surface energy term caused a complete or partial phase transition from hcp to fcc- from 9 hours to 18 hours samples.

We could see that some of these reaction steps are very fast and time dependent experiments using batch processes were not able to follow all details, therefore real “*in-situ*” experiments using a newly developed microreactor technology for wet-chemical synthesis of metallic nanoparticles in combination with “spatially” resolved X-ray absorption spectroscopy (XAS) are currently in progress. This combination of microreactor technology and spatially resolved XAS allows the detailed study of the reaction steps as a function of the reaction time with unprecedented time resolution as “reaction time” is here “transformed” into a position along the channel of the microreactor.

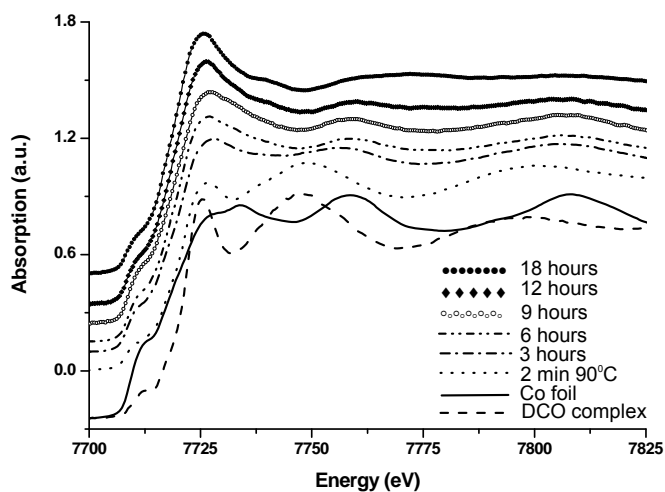


**Figure 1.** Co K-edge time resolved XANES spectra of cobalt nanoparticles resulting from DCO precursor (inert gas, 110<sup>0</sup>C) with reference spectra of Co foil and DCO complex.

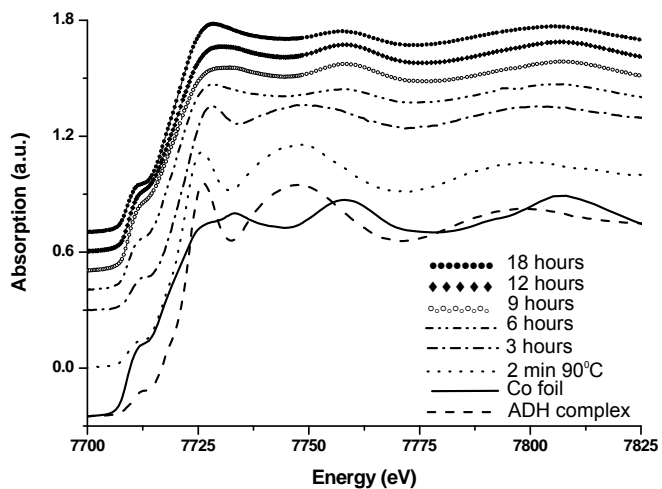


**Figure 2.** Co K-edge time resolved XANES spectra of cobalt nanoparticles resulting from ADH precursor (inert gas, 110<sup>0</sup>C) with reference spectra of Co foil and ADH complex.

#### Acknowledgements

We would like to thank CAMD operating machine group for the opportunity to conduct this work in outstanding conditions.

**Materials and Chemical Sciences**  
**Growth and Processing of Advanced Materials**

**Infrared Characterization of Localized Corrosion Products**  
**Richard S. Perkins<sup>1</sup>, James D. Garber<sup>1</sup>, Alexis Lee<sup>1</sup>, Byron Hills<sup>1</sup>, Khoa Ky<sup>1</sup>, John Hartsfield<sup>1</sup>, O. Kizilkaya<sup>2</sup>, E. Morikawa<sup>2</sup>, J. Scott<sup>2</sup>**

<sup>1</sup>UL Lafayette Corrosion Center, Lafayette, LA 70504-4370

<sup>2</sup>The J. Bennett Johnston, Sr., Center for Advanced Microstructures and Devices,  
Louisiana State University, Baton Rouge, LA 70806  
(PRN=ULL-RP0107)

Failure of devices due to corrosion often comes about because of localized corrosion, or pitting. Though general corrosion may occur across a metal surface, pitting corrosion occurs at a faster rate at certain locations. A better understanding of the pitting process should lead to better ways to predict and control it. One important aspect of localized corrosion is the corrosion products that form. The nature of these products has a bearing on the progress of the corrosion reaction.

During the past year four undergraduates have done student projects involving infrared study of corrosion products in the system composed of iron foil in an aqueous carbonate/bicarbonate buffer through which gaseous carbon dioxide is bubbled. This system is an important one in the oil industry. By adjusting the buffer components and the partial pressure of carbon dioxide, the pH can be controlled. The students obtained infrared spectra under ex-situ conditions. This was done to familiarize the students with the equipment for sample preparation as well as the infrared microscope at CAMD. It was also done to corroborate and extend the ex-situ data set that we have collected.

Our ultimate aim is to obtain infrared spectra of the products of general corrosion and pitting corrosion under in-situ conditions. Two of the students helped to initially construct and further modify sample holders (electrochemical cells) suitable for in-situ measurements.

Preliminary in-situ measurements have been made. These are guided by the many ex-situ spectra that we now have. For ex-situ measurements, samples were prepared, stored in nitrogen, and within 24 hours studied with the infrared beamline and microscope. The samples were prepared either by spontaneous corrosion or by anodic electrolysis at fixed potentials. The fixed potentials are chosen with the help of Pourbaix diagrams of the system and cyclic voltammograms obtained by us. Ex-situ measurements are relatively straightforward. But in-situ measurements require transport of our electrochemical and gasification equipment to CAMD. They also require an electrochemical cell consisting of three electrodes and enough electrolyte to support enough reaction so as to produce enough product to be detected. Yet the cell has to be small enough to operate with the space constraints of the microscope stage. The cell must also be adjustable during spectroscopic operation so that the iron electrode can react unrestricted in solution but also under conditions of a thin film of electrolyte. These requirements and constraints



have made cell construction a challenge. It is hoped that the current version of the cell, or something close to it, will make the collection of spectra routine.

A strong collaboration between CAMD scientists and the LSU physics department resulted in a new understanding of the behavior of silver on copper single crystal surfaces. To obtain these results the scientists used the very soft x-rays in the 10 – 100 eV spectral region to study the kinetic energy distribution of the photoemitted electrons ejected from the silver nanowires.

## Electronic Structure of Silver Nanowires on Cu(110)

*Phil Sprunger and Richard Kurtz, LSU Physics Department*

Self-assembled nanomaterials with reduced dimensionality, or at least one dimension that is on the nanoscale, such as one-dimensional nanowires, have been studied intensively in recent years. The nanostructured materials are promising building blocks for manufacturing devices of nanoelectronics and photonics from a bottom-up approach. STM results (see Fig.1) show that the Ag nanowires grown on Cu(110) are approximately 2 nm (~12 nm) in height (width). However, the nanowires orientate with the long axis parallel to the  $[\bar{1}10]$  substrate direction and possess an anisotropic morphology with aspect ratio up to 20:1. The strong anisotropic shape of the self-organized nanowires suggests a strong difference between the Ag band structure along, and perpendicular, to the nanowires. To investigate this idea, CAMD-LSU researchers, Richard Kurtz, Phil Sprunger, and Wei Chang Zhao performed angle-resolved photoemission spectroscopy (ARPES) on Ag nanowires grown on Cu(110) at the 3m NIM beamline at the CAMD synchrotron-radiation facility.

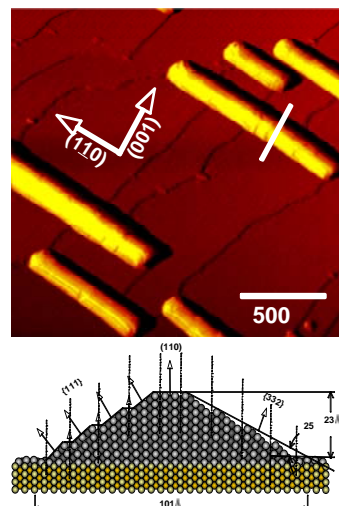
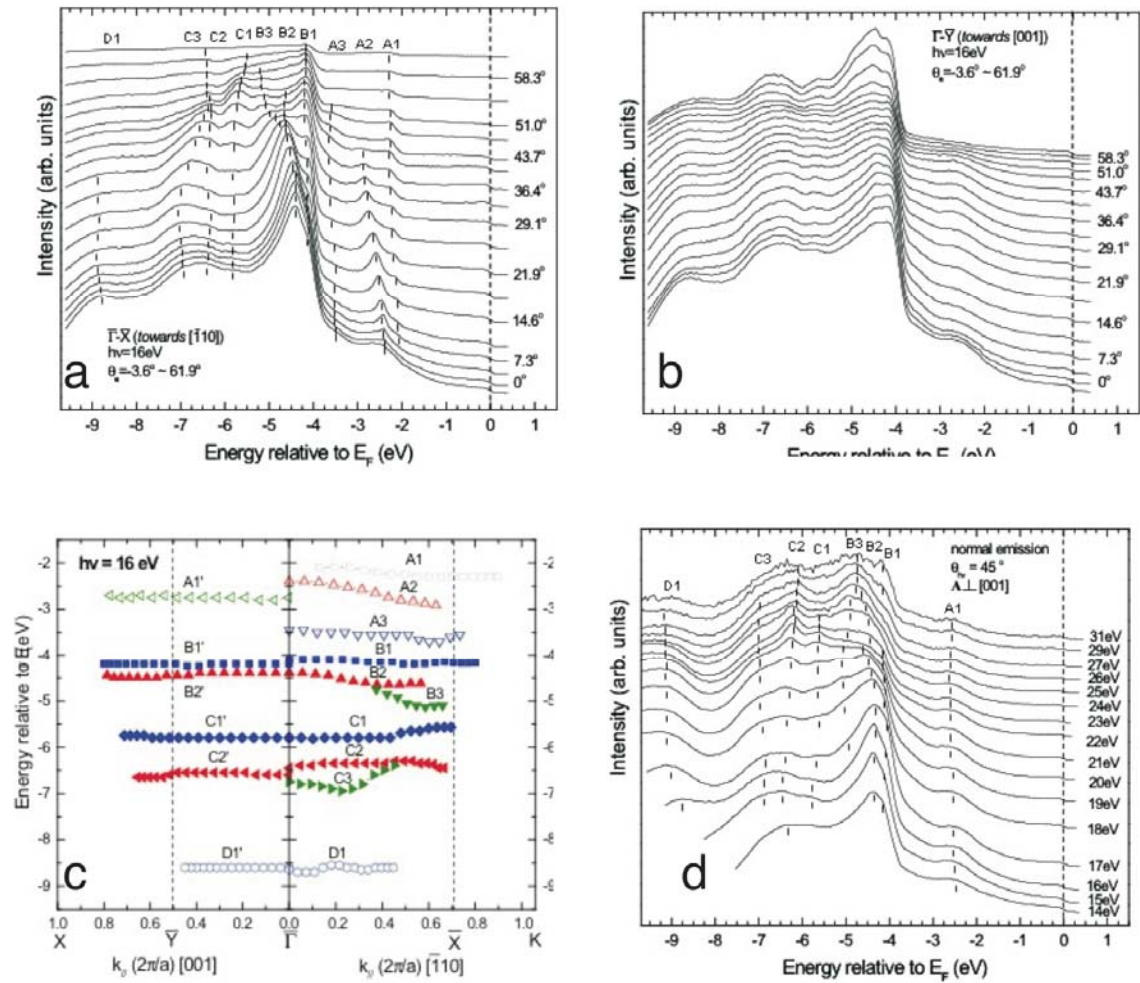


**Fig.1** Previous STM results (top) show the overall morphology of Ag nano-wires (bright protrusions). The model (bottom) shows details nanowire's proposed structure.

Consistent with the STM results, our ARPES results (see Fig. 2 ) show that the valence bands within the Ag nanowire are strongly anisotropic with a clear band dispersion in the along-wire direction, but no dispersion in the across-wire direction. This strongly suggests that the valence electrons of Ag behave one-dimensionally in the lateral plane (along the wire) and have little interaction with the lattice along the across-wire direction (perpendicular to the wire).

The ARPES studies of this system demonstrate that the electronic structure of the Ag(110) nanowire on Cu(110) considerably deviates from that of bulk Ag band structure in energy dispersion behavior and even in increased energy band number. The most obvious dispersion behavior deviation is that while the photoelectron spectra show dispersion in the vertical (or (110)) and the lateral  $[\bar{1}10]$  (or along-wire) direction (see Fig. 2. (a) and (b)), they show no dispersion in the lateral [001] (or across-wire) direction because of the limited dimension of the nanowire width (~ 12 nm in average; see Fig. 2. (c) and (d)). Therefore, the dimensionality of the band structure of the Ag(110) nanowire crystal is reduced in the vertical plane formed by the cross lines parallel to the vertical [110] and the lateral  $[\bar{1}10]$  directions. This result is in accordance with the STM results.

The results were presented at the Physical Electronics Conference at Princeton University  
 1996

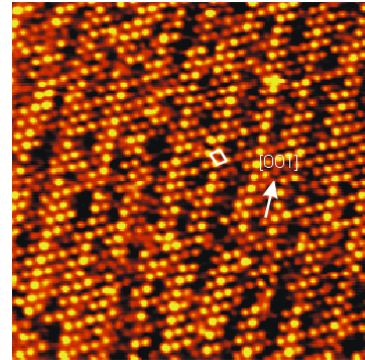


the along-wire direction; **(c)** Band structure map for the two high-symmetry directions across the (110) surface Brillouin zone, indicating band dispersion in the along-wire direction and absence of dispersion in the across-wire direction. **(d)** Normal emission photoelectron spectra from the same Ag/Cu(110) nanowires with photon beam towards the along-wire direction (A  $[001]$ ) at photon energy of 14 eV ~ 31 eV

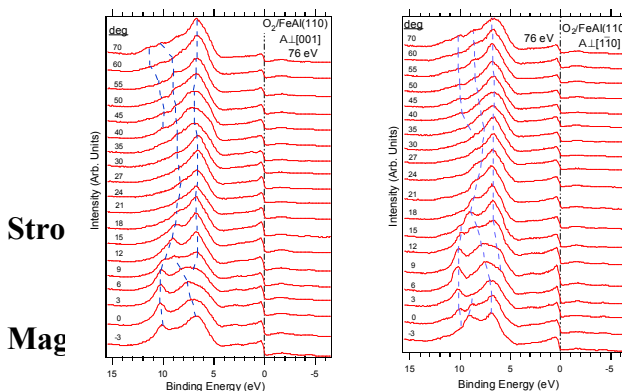
## The Electronic Structure of Ultra-thin Aluminum Oxide Film Grown on FeAl(110): A Photoemission Spectroscopy Study

A primary goal of this NSF award is to successfully grow and characterize reduced dimensional metals (1D nanowires and 2D sheets). A strong complementary requisite to realizing this goal is to judiciously develop substrates which, electronically, are relatively inert. The goal of CAMD-LSU researchers, Phil Sprunger and Orhan Kizilkaya, was to grow the proposed nanometals on ultra-thin oxides, wherein, because of the large bandgap, the hybridization/overlap with the underlying substrate band structure is minimized. Ultra-thin oxides serve as excellent templates because they provide a unique “insulating” substrate. Due to the nano-thickness of the oxide, electron spectroscopies (ARPES, STM, EELS) can be used without the problems associated with charging. In order to enable the subsequent growth of reduced-dimensional metals, it is necessary to probe the atomic and electronic structures of the proposed ultra-thin film oxide.

Over this last year, the electronic structure of ultra-thin aluminum oxide, grown on the FeAl(110) surface, has been investigated with angle-resolved photoemission spectroscopy. As shown on the right, our scanning tunneling microscopy studies have revealed that exposing the clean FeAl(110) surface to 1000 L of oxygen at 850° C, forms a homogeneous hexagonal oxide film with a thickness of approximately 10 Å. Core levels photoemission spectra of FeAl constituents indicate that Al is the only metal species present in the oxide film. As shown below, the measured band dispersion of oxide thin film indicates a 2-D electronic structure parallel to a plane of thin film due to the limited thickness of the oxide thin films. The appearance of a peak in the anticipated band gap of bulk oxide film suggests the unique electronic structure of the 2-D oxide film. This latter observation is correlated with previous scanning tunneling microscopy results to elucidate the structure of the ultra-thin alumina film grown on FeAl(110). The results of this research will appear in the forthcoming issue of Applied Physics Journal (2007).



STM image (70x70 nm<sup>2</sup>) of oxidized FeAl(110) surface. The surface exposed to 1000 L of O<sub>2</sub> at 850 °C. A unit mesh of oxide structure (18.6x19.6 Å) is shown with solid line.



EDCs of Al<sub>2</sub>O<sub>3</sub>/FeAl(110) collected along high-symmetry directions of the substrate surface Brillouin zone. Dispersion of the oxide-induced states in both directions indicate a two dimensional electronic structure.

ials -

## Reactive Multilayer Foils for Silicon Wafer Bonding

Xiaotun Qiu and Jiaping Wang

Department of Mechanical Engineering

Louisiana State University, Baton Rouge, LA 70808

jiaping@me.lsu.edu, PRN: ME-JW0020

### ABSTRACT

In this study silicon wafers were bonded using Al/Ni reactive multilayer foils as local heat sources for melting solder layers. Exothermic reactions in Al/Ni reactive multilayer foils were investigated by XRD and DSC. XRD measurements showed that dominant product after exothermic reaction was ordered B2 AlNi compound. The heat of reaction was calculated to be -57.9 KJ/mol by DSC. With Al/Ni reactive multilayer foil, localized heating can be achieved during bonding process. Both experimental measurements and numerical simulation showed that the heat exposure to the wafers was highly limited and localized. Moreover, leakage test showed that this bonding approach possessed a good hermeticity.

### INTRODUCTION

Wafer bonding techniques, such as anodic bonding and fusion bonding, have been reported for the silicon wafer-to-wafer bonding processes [1]. However, these bonding techniques are conducted at high temperature, 1000°C for the conventional fusion bonding and 300-500°C for anodic bonding. These high temperature processes may cause thermal damage to components. Dissimilar materials may debond on cooling due to the CTE (coefficient of thermal expansion) mismatch. Another disadvantage of these processes is that they require the bonding surfaces to be polished and thoroughly cleaned to achieve uniform bonding. Instead of bonding wafers directly, intermediate layer bonding methods, which employ thin films on one or both component surfaces as the bonding media, can be used to lower the bonding temperature. Intermediate layer bonding methods such as solder bonding and adhesive bonding also have their own shortcomings: the out-gassing of the flux and solvent in the solder paste during solder reflow can form voids in the bonding area [2], while the disadvantages of adhesive bonding are long-term instability, a limited working temperature range, low bonding strength, and non-hermeticity of the package [3]. In this regard, a special low temperature wafer bonding technique needs to be further researched for various wafer level packaging applications.

In this report, we describe a novel room temperature bonding technique using reactive multilayer Al/Ni foils as local heat sources to melt solder layers and thus bond silicon wafers. Reactive multilayer foils contain hundreds of nanoscale Al and Ni bilayers. Self-propagating formation reactions in such foils are driven by a reduction in chemical bond energy. This local reduction of chemical bond energy produces a large quantity of heat that is conducted down the foil and facilitates more atomic mixing and compound formation. Self-propagating reactions can be ignited in these foils at room temperature with a small thermal pulse. Such reactions in multilayer foils can be used as local heat sources to melt solders or brazes and thus bond components in a variety of applications [4-8]. With localized heating, temperature sensitive components such as microelectronic

devices can be joined without thermal damage. Such bonding can be performed in many environments, and can be completed in a second or less. The properties of the reactive foils were characterized using X-ray diffraction (XRD) and differential scanning calorimetry (DSC). The bond strength was tested. Temperature distributions on silicon wafer specimens during the bonding process were monitored by an infrared camera and compared with the simulation results. The leakage test was also performed on the bonded wafers.

## EXPERIMENTAL METHODS

Al/Ni reactive multilayer foils with Incusil coating were used as local heat sources for melting solder layers and joining silicon wafers in this study. The thickness of the Al/Ni foil is  $80\mu\text{m}$  with bilayer thickness of  $40\text{ nm}$ . The composition of the as-deposited Al/Ni multilayer foils and the reaction products was investigated by a Rigaku MiniFlex X-ray diffractometer (XRD) using Cu  $K\alpha$  radiation. The heat of reaction was measured by a Perkin Elmer differential scanning calorimeter (DSC7). In each DSC run, 7-10mg foil was heated from  $50^\circ\text{C}$  to  $720^\circ\text{C}$  at a rate of  $40^\circ\text{C}/\text{min}$  in flowing Ar. A base line was obtained by repeating the heating cycle, which was then subtracted from the heat flow in the first run. By integrating the net heat flow with respect to time, the heat of reaction was obtained.

Silicon wafer bonds were fabricated by stacking two sheets of AuSn solder (80 wt% Au-20 wt% Sn, Williams Advanced Materials) with thickness of  $25\mu\text{m}$  and one reactive foil between two silicon wafers, as shown schematically in Figure 1. The dimensions of the silicon wafers are 5.08 cm in diameter and  $300\mu\text{m}$  in thickness and were coated with Cr and Au by Electron Beam (e-beam) evaporation to enhance wetting. These silicon wafers were bonded at room temperature in air by igniting the reactive foil under an applied pressure. Heat released from the reaction melted the solder layers and thus bonded the silicon wafers together.

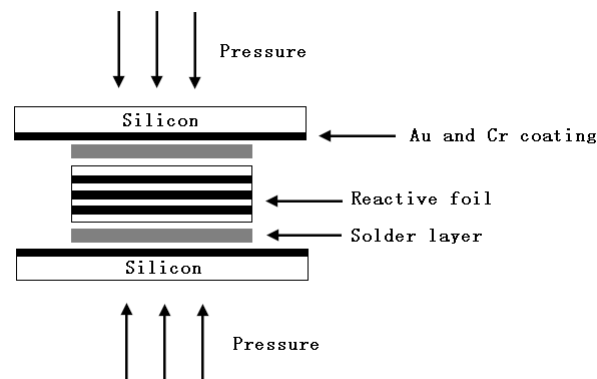


Figure.1 Schematic showing the reactive bonding of two silicon wafers using a reactive foil and two solder layers under an applied pressure.

Three different tests, including temperature distribution, bonding strength, and leakage test, has been conducted in this study to evaluate the performance and feasibility of the bonding process. The temperature distribution on silicon wafers during the bonding process was monitored by an infrared camera with temperature resolution of  $0.1^\circ\text{C}$  and compared with simulation. A numerical study was performed to predict the temperature

distribution on silicon wafers using a commercial software Fluent. After reactive bonding, the silicon wafer joints were tested in tension. In addition, leakage test was performed by immersing bonded wafers in red ink.

## RESULTS AND DISCUSSION

The composition of the as-deposited Al/Ni multilayer foils and the reaction products was investigated by XRD, and the XRD traces are shown in Figure 2. Before the reaction, all major peaks correspond to Al and Ni. While after the reaction, all major peaks correspond to the ordered B2 AlNi compound. Thus, during the bonding process, the B2 AlNi compound is expected to be the dominant product for the foil.

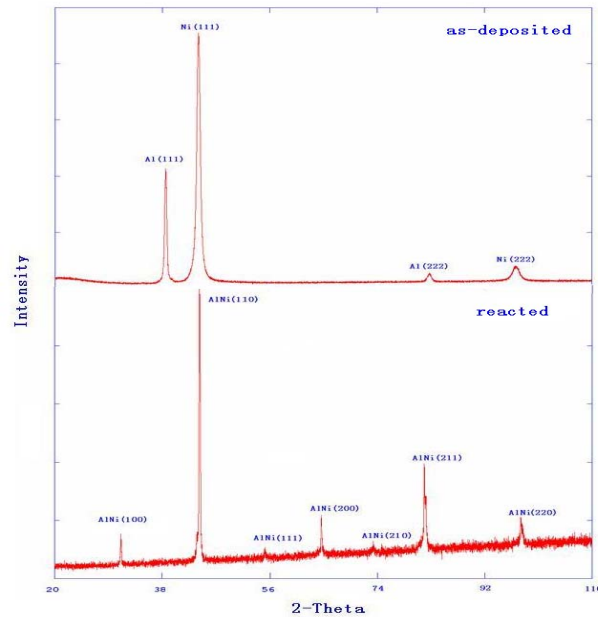


Figure.2 XRD patterns for Al/Ni reactive multilayer foils (both as-deposited and reacted).

In the DSC experiment of the Al/Ni reactive multilayer foil, three peaks can be identified in the constant-heating-rate curve, as shown in Figure 3. By integrating the heat flows with respect to time, the heat of reaction was obtained for Al/Ni reactive multilayer foil with the bilayer thickness of 40 nm, which was calculated to be -57.9 KJ/mol. It is in good agreement with the formation enthalpy of AlNi (-59 KJ/mol) [9]. This result was used as input for the numerical study of the temperature distribution on silicon wafers during the bonding process.

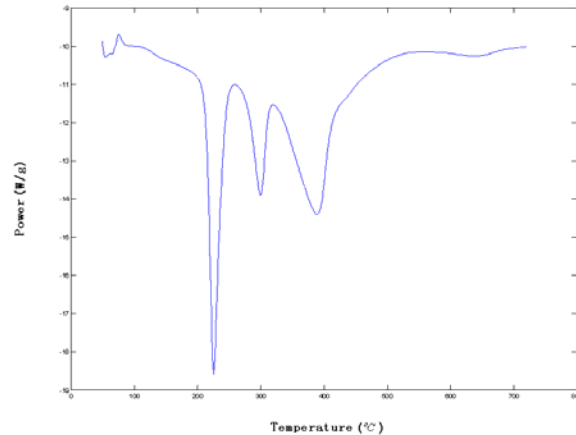


Figure.3 DSC curve for an Al/Ni reactive multilayer foil.

The temperature distribution on silicon wafers during the bonding process was monitored by an infrared camera with temperature resolution of  $0.1^{\circ}\text{C}$ . The bonding geometry is shown in Figure 4. The dimension of the reactive foil is 5.08 cm by 1.27 cm. Three locations A, B, and C were selected to measure the temperature distribution during the bonding process. Location A is at the center of the foil, B and C are further away from the foil. The distance between two adjacent points was 1.27 cm. A numerical simulation of the temperature distribution during bonding was conducted by a commercial software Fluent. The temperature evolutions at these three locations obtained both from experimental measurement and numerical simulation are shown in Figure 5. The simulation results are in good agreement with the experiment. The highest temperature of point A during bonding was  $221.4^{\circ}\text{C}$ . The highest temperature for point B was  $110.3^{\circ}\text{C}$ , while for point C was only  $59.9^{\circ}\text{C}$ . Thus, heating only influenced a limited area. It can be concluded from Figure 5 that the heating is highly localized. Meanwhile, the cooling rate for silicon wafer bonding by reactive multilayer foils is very high. In seven seconds, the wafer temperature dropped below  $60^{\circ}\text{C}$ . The localized heating and rapid cooling made reactive foil joining an ideal method for silicon wafer bonding.

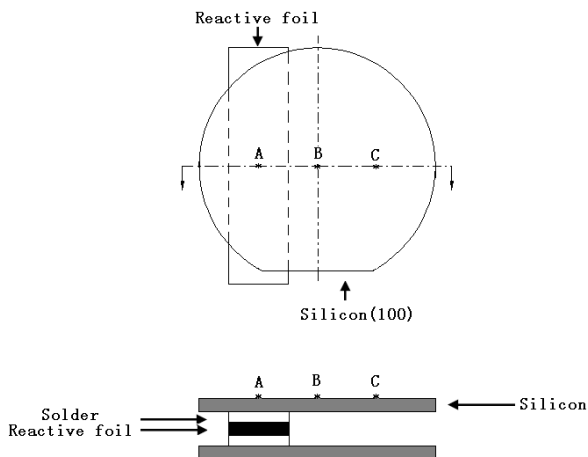


Figure.4 Geometry of silicon wafers bonding during thermal distribution test.



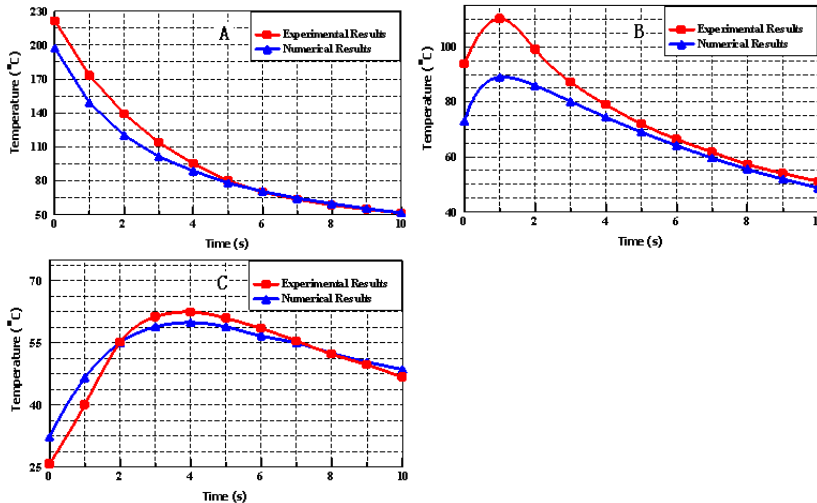


Figure.5 Temperature evolutions at point A, B, and C from experimental measurement and numerical simulation.

Simulation was also performed for the condition where the width of the reactive foil reduced to 1mm. The results are shown in Figure 6. The heating area became more localized. Most areas on silicon wafers remained unaffected. The wafer temperature decreased to room temperature in less than one second.

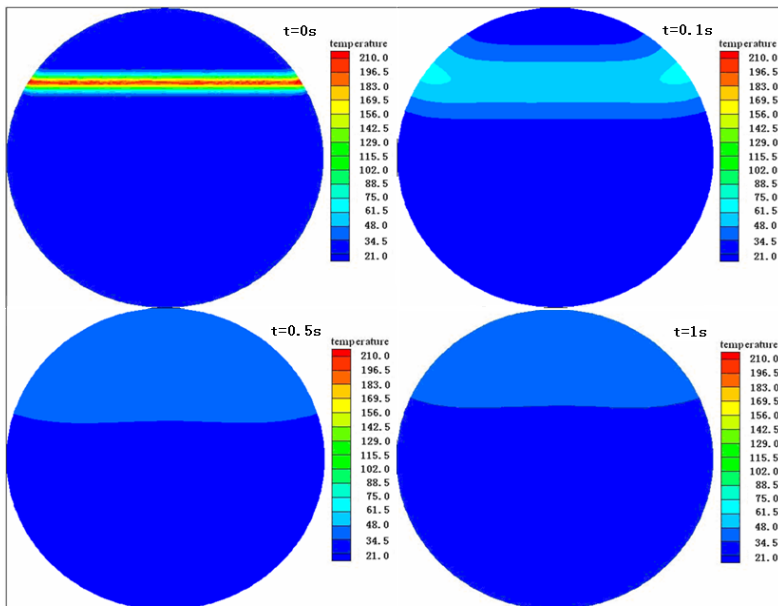


Figure.6 Numerical prediction of temperature distribution during bonding using 1mm wide reactive foil.

The strength of the bonded specimen was tested in tension. The fracture occurred at the interface between Si and Cr undercoat layer. The coating layer was peeled off from the wafer during the test. The weaker Si/Cr undercoat interface might be due to poor adhesion between Si surface and Cr in e-beam evaporation. Improvement on

metallization method for silicon wafer will be further pursued in order to obtain the strength of the bond.

A bonded wafer package was immersed in red ink to conduct the leakage test of liquid. The bonding geometry of this wafer package is shown in Figure 7. No leakage occurred after one hour's immersion of the wafer package in red ink. The test result indicated that this bonding approach can be exploited to protect the structures enclosed in the package from humidity. A helium leakage test will be performed to further demonstrate the hermeticity of this bonding method.

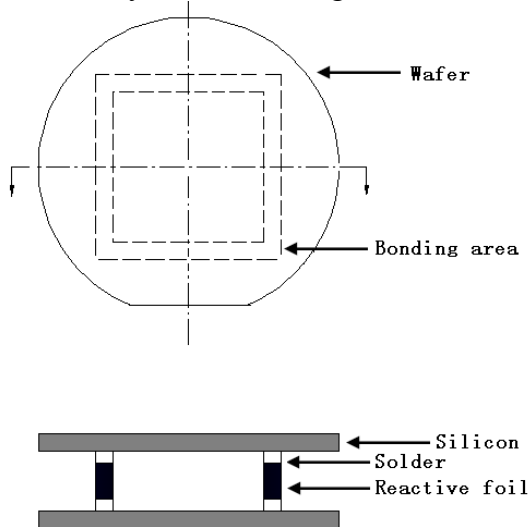


Figure.7 Geometry of silicon wafers bonding for leakage test.

## CONCLUSIONS

Exothermic reactions in Al/Ni reactive multilayer foils were investigated by XRD and DSC. The dominant product after exothermic reaction was ordered B2 AlNi compound. The heat of reaction was calculated to be -57.9 KJ/mol. The localized heating with Al/Ni reactive multilayer foil has been successfully used in silicon wafer bonding. The experimental measurement and simulation results showed that the thermal exposure to silicon wafers was highly limited and localized. The wafer temperature decreased to room temperature within several seconds after reactive multilayer foil bonding. This can effectively avoid the thermal damage to components during bonding and makes reactive foil an ideal bonding method for wafer level packaging. Moreover, leakage test showed that this bonding approach possessed a good hermeticity.

## REFERENCES

1. M. A. Schmidt, Proc. IEEE. 86, 1575 (1998).
2. D. Sparks, G. Queen, R. Weston, G. Woodward, M. Putty, L. Jordan, S. Zarabadi, K. Jayakar, J. Micromech. Microeng. 11, 630 (2001).
3. F. Sarvar, D. A. Hunt, D. C. Whalley, Proc. IEEE Polytronic. 22 (2002).
4. J. Wang, E. Besnoin, A. Duckham, S. J. Spey, M. E. Reiss, O. M. Knio, T. P. Weihs, J. Appl. Phys. 95, 248 (2004).
5. J. Wang, E. Besnoin, O. M. Knio, T. P. Weihs, J. Appl. Phys. 97, 4307 (2005).

6. A. Duckham, S. J. Spey, J. Wang, M. E. Reiss, T. P. Weihs, *J. Appl. Phys.* 96, 2336 (2004).
7. J. Wang, E. Besnoin, A. Duckham, S. J. Spey, M. Reiss, O. M. Knio, M. Powers, M. Whitener, T. P. Weihs, *Appl. Phys. Lett.* 83, 3987 (2003).
8. A. J. Swiston, Jr, T. C. Hufnagel, T. P. Weihs, *Scripta. Mater.* 48, 1575 (2003).
9. R. Pretorius, A. M. Vredenberg, F. W. Saris, R. de Reus, *J. Appl. Phys.* 70, 3636 (1991).

List of publications

“Fabrication and Characterization of Cold Rolling Al/Ni Multilayer Foils”, accepted by MRS proceedings, Boston, 2006

List of presentations

“Reactive Multilayer Foils for Silicon Wafer Bonding”, MRS annual meeting, Boston, 2006

“Fabrication and Characterization of Cold Rolling Al/Ni Multilayer Foils”, MRS annual meeting, Boston, 2006

List of grants

“Fabrication of and thermal testing in enclosed metal microchannels”, PI: W. J. Meng, Co-PIs: J. Wang, S. Ekkad, National Science Foundation - DMI Award 0556100, \$ 330,429, 05/01/2006 – 04/30/2009.

Students

Xiaotun Qiu

## Development of Ti-Al Phases during High Energy Ball Milling of 2 mol % TiCl<sub>3</sub> into NaAlH<sub>4</sub>

Tabbatha A. Dobbins<sup>1</sup>, Vimal Kamineni<sup>1</sup>, Amitava Roy<sup>2</sup>

<sup>1</sup>Louisiana Tech University, Institute for Micromanufacturing; 911 Hergot Avenue;  
Ruston, LA, 71272, USA

[tdobbins@latech.edu](mailto:tdobbins@latech.edu) and [ykk001@latech.edu](mailto:ykk001@latech.edu)

<sup>2</sup>Louisiana State University, Center for Advanced Microstructures and Devices (CAMD);  
6980 Jefferson Hwy.; Baton Rouge, LA, 60804, USA

[reroy@latech.edu](mailto:reroy@latech.edu)

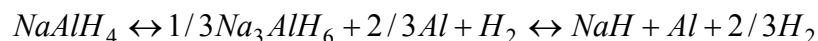
PRN: LaTech-TD0505

### Abstract

The present study explores chemical transitions of the 1.8 mol % Ti<sup>3+</sup> dopant ion added to NaAlH<sub>4</sub> powders during high energy ball milling using extended x-ray absorption fine structure (EXAFS) spectra. EXAFS spectra were analyzed for samples milled for various times (0 minutes, 1 minute, 5 minutes, 25 minutes, and 125 minutes). The occurrence of two transformations is revealed. The first transformation takes place during the first 5 minutes of ball milling whereby the dopant shifts from Ti<sup>3+</sup> (in TiCl<sub>3</sub>) to a transitional state Ti<sup>0</sup> (in TiAl). The second transformation occurs after an additional 20 minutes of high energy milling from Ti<sup>0</sup> (in TiAl) to Ti<sup>0</sup> (in TiAl<sub>3</sub>). The first Ti<sup>0</sup> state which appears is a disordered TiAl phase with bond lengths shorter than the crystalline TiAl phase. This phase exists for mill times up to 25 minutes. After 25 minutes of high energy milling, the stable TiAl<sub>3</sub> remains. This study reports, for the first time, the appearance of a TiAl phase as an intermediate between Ti<sup>3+</sup> (in TiCl<sub>3</sub>) and TiAl<sub>3</sub>. After a single desorption/absorption cycle, the Ti in *all* milled samples (i.e. those milled for 1 minute, 5 minutes, and 25 minutes) either underwent the transformation to a stable TiAl<sub>3</sub> phase or remained in the stable TiAl<sub>3</sub> phase had the transformation occurred before milling. Those samples milled for 1 minute form a disordered TiAl<sub>3</sub> phase with a slightly longer average bond length than the crystalline TiAl<sub>3</sub> phase. These titanium containing phases are formed in quantities which are below the detection limits for x-ray diffraction.

### Introduction

Dopant effects and hydrogenation desorption rates in sodium alanate (NaAlH<sub>4</sub>) have been studied extensively, making this system well suited to a focused investigation using synchrotron extended x-ray absorption fine structure (EXAFS) characterization. The work of Bogdanovic and Schwickardi<sup>1</sup> (in 1997) first established ability for NaAlH<sub>4</sub> to undergo reversible hydrogen desorption with improved kinetics in the two-step reaction,



after milling with titanium chloride.<sup>1</sup> Subsequently, Anton reported the comparative kinetic enhancements results for various transition metals—and demonstrated that Ti<sup>2+</sup>,

Ti<sup>3+</sup>, and Ti<sup>4+</sup> provide the highest desorption reaction rates.<sup>2</sup> However, a study by Sandrock, et al. shows decrease in reversible hydrogen capacities associated with increasing Ti-dopant content—suggesting detrimental effects associated with excess dopant.<sup>3</sup> In studies which have explored the role of Ti dopants using x-ray absorption spectroscopy at the Ti K-edge<sup>4-10</sup>, it has been realized that an amorphous TiAl<sub>3</sub> phase appears after dehydrogenation and that as-milled systems lead to the formation of nm-Ti or TiAl<sub>3</sub> metallic phases. Aluminum deficiency on the NaAlH<sub>4</sub> lattice (due to TiAl<sub>3</sub> intermetallic formation) is ultimately responsible for controlling hydrogen absorption capacity. Understanding consumption of Al by the Ti dopant to form Ti-Al intermetallic phases is important to controlling the reversible storage capacity in the alanates.

## Results and Discussion

Comparisons of the normalized absorption data of TiAl and TiAl<sub>3</sub> standards along with samples milled for various times are shown in Figure 1. After extracting the EXAFS ( $\chi(k)$ ) signal (using Athena Software), the Fourier transform of the EXAFS signal is used to indicate the distance to the first coordination sphere relative to the absorber atom.<sup>8</sup> The distance to the first coordination sphere around the Ti<sup>0</sup> (after a single desorption/absorption cycle) is shown in Figure 1. The sample milled for 1 minute shows a longer distance to the first coordination shell (at 2.50 Angstroms) relative to those milled for longer times (at ~2.26 Angstroms). Others report distances for Ti-Ti at 2.98 Angstroms<sup>6</sup> and Ti-Al at 2.80 Angstroms<sup>9</sup>. We believe that the longer distance revealed by XAS is strong evidence that metallic Ti<sup>0</sup> clusters form after the single desorption/absorption cycle in the sample milled for 1 minute. That is, the formation of Ti<sup>0</sup> clusters occurs for “undermilled” samples (i.e. samples milled for times below which Ti<sup>3+</sup> shifts to Ti<sup>0</sup> oxidation state). For samples milled for longer times, the shorter distance observed by XAS suggest the formation of the TiAl<sub>3</sub> intermetallic phase after the single desorption/absorption cycle. It remains to be explored as to whether the Ti<sup>0</sup> remains situated at the surface of the NaAlH<sub>4</sub> powder—as reported by others for samples milled for longer times.<sup>3,7,9,10</sup> These results are significant in that they suggest that there may be a brief period of time (or “induction period”) during which the dopant may be chemically altered by reactants in order to bypass Ti-Al formation—while permitting the Ti to attach at the NaAlH<sub>4</sub> particle surface for facilitating the Al-H bond weakening—a mechanism for the role of the dopant suggested by Iniguez et al.<sup>9,10</sup>

## Acknowledgments

This work is supported by the Dept. of Energy under grant # DE-FG02-05ER46246. Partial support for this research comes from the National Science Foundation under grant #DMR-0508560 and Louisiana State Board of Regents Research and Development Program under grant # LEQSF(2005-08)RD-A-20). We thank Dr. Joachim Schneibel and Dr. Scott Speakman (Oak Ridge National Laboratory) for their contributions to this work.

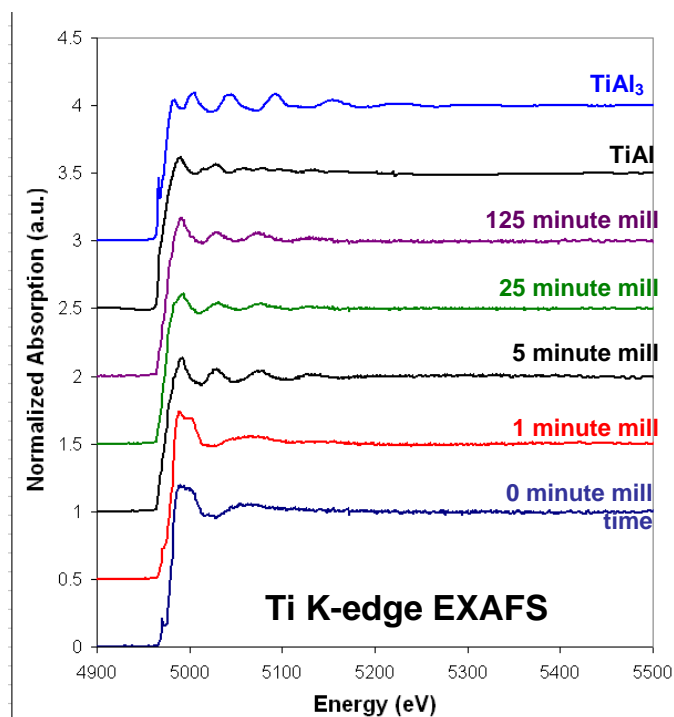


**Figure 1.** EXAFS XANES and EXAFS spectra reveal that structure changes from  $Ti^{3+}$  (milled with  $TiCl_3$ ) to  $Ti^0$ . This structural transition occurs after 5 minute mill time.

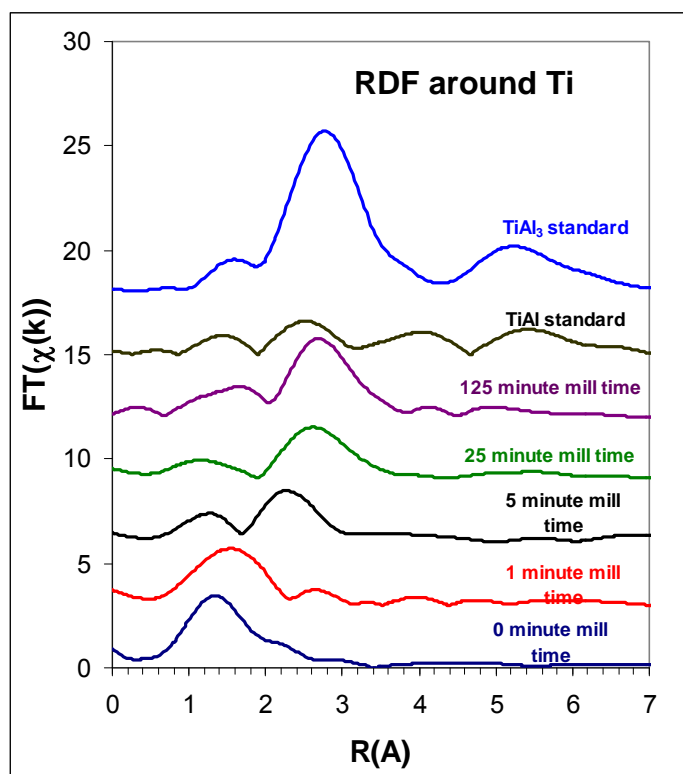


**Figure 2.** Radial Distribution Function (RDF) obtain from EXAFS spectra reveals the 2nd structure change occurring after 25 minute mill time.  $TiAl$  forms initially during mill. Local structure transitions from  $TiAl$  into  $TiAl_3$  after 25 minute mill time.

## References

1. Bogdanovic B., Schwickardi M., "Ti-doped Alkali Metal Aluminum Hydrides as Potential Novel Reversible Hydrogen Storage Materials". *Journal of Alloys and Compounds* 1997, 253-254[1-2], 1-9.
2. Anton D.L., "Hydrogen Desorption Kinetics in Transition Metal Modified NaAlH<sub>4</sub>". *Journal of Alloys and Compounds* 2003, 356, 400-404.
3. Sandrock G., Gross K., Thomas G. Effect of Ti-catalyst Content on the Reversible Hydrogen Storage Properties of the Sodium Aluminates, *Journal of Alloys and Compounds* 2002 339, 299-308.
4. Fichtner M., Kircher O., Rothe J., "Small Ti Clusters for Catalysis of Hydrogen Exchange in NaAlH<sub>4</sub>", *Nanotechnology* 2003 14 778-785.
5. Graetz J., Reilly J.J., Johnson J., Ignatov A., Yu A., Tyson T.A., "X-ray Absorption Study of Ti-Activated Sodium Aluminum Hydride", *Appl. Phys. Lett.* 2004, 85, 500-502.
6. Leon A., Rothe J., Kircher O., Fichtner M., "Chemical State and Local Structure Around Titanium Atoms in NaAlH<sub>4</sub> Doped with TiCl<sub>3</sub> Using X-ray Absorption Spectroscopy", *J. Phys. Chem B* 2004 108, 16372.
7. Leon A., Schild R.J., Fichtner M., "Comparative Study of NaAlH<sub>4</sub> Doped with TiCl<sub>3</sub> or Ti<sub>13</sub>.6THF by Ball Milling Using XAS and XPS", *Chem. Eng. Trans.* 2005 8 171-176.
8. Bruster E., Dobbins T.A., Tittsworth R., Anton D., "Decomposition Behavior of Ti-doped NaAlH<sub>4</sub> Studied using X-ray Absorption Spectroscopy at the Titanium K-edge", *Mater. Res. Soc Symp. Proc.* 2005 837 N3.4.1.
9. Leon A. Kircher O., Fichtner M., Rothe J., Study of the Evolution of the Local Structure around Ti Atoms in NaAlH<sub>4</sub> Doped with TiCl<sub>3</sub> or Ti<sub>13</sub>.6THF by Ball Milling Using XAS and XPS Spectroscopy", *J. Phys. Chem. B* 2006 110, 1192-1200.
10. Dobbins T.A., Tittsworth R., Speakman S.A., Schneibel J., "Synchrotron X-ray Absorption Spectroscopy (XAS) for Understanding Dopant Effects in Ti-doped NaAlH<sub>4</sub>", *Advanced Materials for Energy Conversion III, A Symposium in Honor of Drs. Gary Sandrock, Louis Schlapbach, and Seijirau Suda – ed. D. Chandra, J.J. Petrovic, R. Bautista, A. Imam*, 2006 263-70.
11. B. Teo, *EXAFS: Basic Principles and Data Analysis*. 1986.
12. Sayers D.E., S. E. A., Lytle F.W., New Technique for Investigating Noncrystalline Structures: Fourier Analysis of the Extended X-ray Absorption Fine Structure. *Physical Review Letters* 1971, 27, (18), 1204-1207.

**Publications**

1. Tabbetha A. Dobbins, Roland Tittsworth, Scott Speakman, Joachim Schneibel, “Synchrotron X-ray Absorption Spectroscopy (XAS) for Understanding Dopant Effects in Ti-doped NaAlH<sub>4</sub>”, *Advanced Materials for Energy Conversion Proceedings*, pg 263 (2006).

**Presentations**

1. Tabbetha A. Dobbins, “Synchrotron X-ray Studies Applied to Emerging Energy Applications”, Dept. of Materials Science and Engineering at University of Alabama, Tuscaloosa. October 19, 2006.
2. Tabbetha A. Dobbins, “Synchrotron X-ray Studies Applied to Emerging Energy Applications”, Synchrotron Radiation Center (SRC) at University of Wisconsin, Madison. April 18, 2006.
3. Tabbetha A. Dobbins, Roland Tittsworth, Scott Speakman, Joachim Schneibel, “Synchrotron X-ray Absorption Spectroscopy (XAS) for Understanding Dopant Effects in Ti-doped NaAlH<sub>4</sub>”, TMS Annual Meeting: Advanced Materials for Energy Conversion Symposium, Oral Presentation. March 12-16, 2006.
4. Tabbetha A. Dobbins, “Synchrotron X-ray Studies Applied to Emerging Energy Applications”, University of Arkansas at Little Rock (UALR), Invited Presentation. March 3, 2006.



## XAS of multilayer mirror coatings for LIGO mirrors

E.E. Doomes and S.C. McGuire.; Southern University and A&M College, Baton Rouge,  
Department of Physics, P.O. Box 10554, Baton Rouge, LA 70813;  
[edward\\_doomes@subr.edu](mailto:edward_doomes@subr.edu), [scmcguire1@cox.net](mailto:scmcguire1@cox.net).  
PRN: SU-ED1206LIGO

X-ray absorption spectroscopy relying upon high resolution energy dispersive detectors have been used to obtain detailed chemical composition and structure of titania ( $\text{TiO}_2$ )-doped tantalum ( $\text{Ta}_2\text{O}_5$ ) multilayers fabricated via ion beam sputtering on  $\text{SiO}_2$  substrates. These dielectric multilayers play a major role as mirror coatings in high power laser applications such as laser interferometric gravity-wave detectors where noise in the mirrors must be kept to a minimum. At present, exactly how the microscopic features of the coatings influence their macroscopic mechanical loss properties is poorly understood. The goal of our work is to obtain correlations between chemical impurities and/or dopants and the optical absorption and mechanical loss characteristics of these multilayer coatings. To this end we are employing synchrotron-based X-ray absorption Spectroscopy (XAS) techniques including Extended X-ray Absorption Fine Structure (EXAFS), X-ray Absorption Near Edge Structure (XANES) and X-ray Fluorescence (XRF) to examine our samples. In the current study several samples having varying multilayer composition have been investigated. The measurements were performed at the CAMD Double Crystal Monochromator (DCM) beamline. Fluorescent X-rays were detected with a 13-element liquid nitrogen cooled Ge detector array. We obtained chemical and structural data obtained at the titanium K-edge and tantalum  $L_{III}$ -edge as well as relative elemental (Ti/Ta, Fe/Ta, Cr/Ta) distribution information obtained via XRF. Stimulated by these results, we have prepared an experimental strategy that employs grazing incidence XRF measurements to further correlate the structure of these systems with their optical loss characteristics.

In the XRF experiments conducted thus far, clear signals are observable for the primary elements of interest, Ti and Ta. We have obtained data with excellent energy resolution and counting statistics at both of these edges. Relatively minor amounts Fe and Cr appear in a constant ratio for all samples which suggests that these elements are in the bulk, not in the coating. Our preliminary experiments indicate that grazing incidence beam measurements are required for XANES and EXAFS studies so as to minimize signals from the substrate. Complementary microbeam experiments are planned to determine spatial (x-y) uniformity of the element distributions.

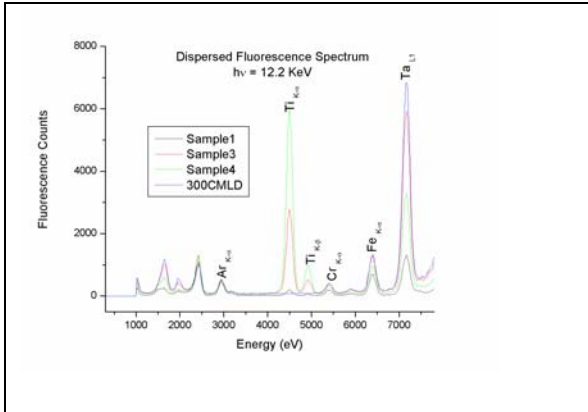


Figure 1, Dispersed fluorescence spectra of optical coating samples

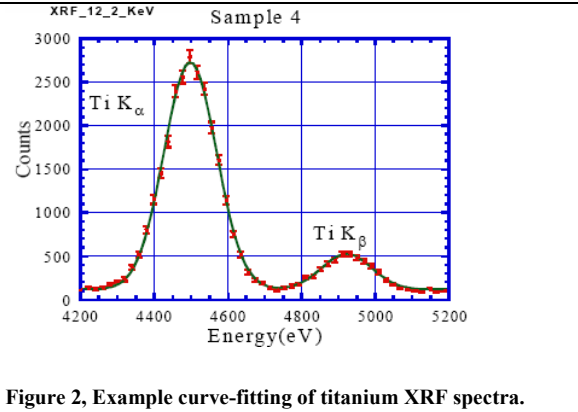


Figure 2, Example curve-fitting of titanium XRF spectra.

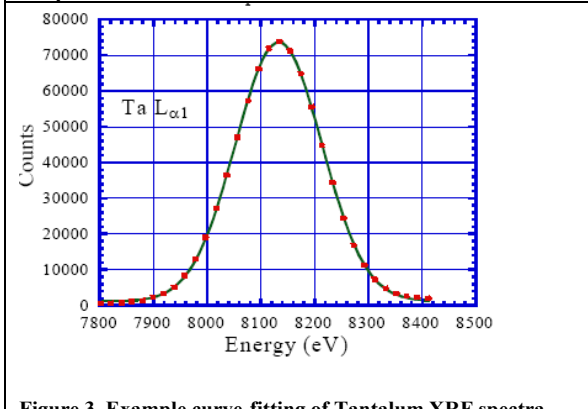


Figure 3, Example curve-fitting of Tantalum XRF spectra.

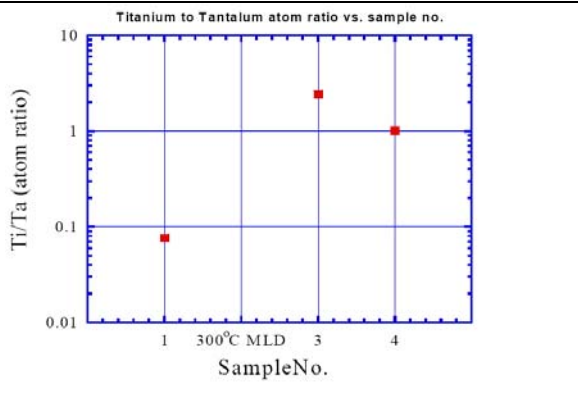


Figure 4, Titanium/tantalum ratio (corrected for cross-section)

**Presentation:** LIGO Mirror Coatings X-ray Absorption Measurements; E.E. Doomes and S.C. McGuire; LIGO Physics Group, Southern University and A&M College, Baton Rouge, Louisiana 70813. Presented at the LIGO Scientific Collaboration (LSC) Meeting, Louisiana State University, August 14-17 2006.  
LIGO Document number G060456-00-Z

*Work supported by NSF Grant No. PHY-0101177.*

## Soft Matter

### **Investigating the Effects of Near Net Shape Manufacturing (NNSM) on Solid-state Polymer Blending via Synchrotron Infrared Spectroscopy**

Ryan J. Schexnaydre, Graduate Student, Tulane University Chemical and Biomolecular Engineering, 135 Ormond Meadows Dr., Destrehan, LA 70047 email: [rschexna@tulane.edu](mailto:rschexna@tulane.edu)

Brian S. Mitchell, Associate Provost, Tulane University, 2125 Olvey Drive, Mandeville, LA 70448, email: [brian@tulane.edu](mailto:brian@tulane.edu)  
PRN TU-BM0507

The blending of immiscible polymers by conventional processing often results in a final product that is phase-separated at the macroscale due to thermal degradation, equilibrium-related composition fluctuations, inadequate mixing, undesirable chemical reactions with solvents, and kinetic-diffusional barriers for chemical compatibilizers [1]. One form of near net-shape manufacturing (NNSM) comprises mechanical attrition with subsequent hot isostatic pressing (HIP), all in the solid state while combining simultaneous particle size and crystallinity reduction [2]. NNSM combines intimate mixing at the microscale and nanoscale – a process dictated by interfacial, rather than bulk, thermodynamics – with an efficient consolidation of milled powders. The various factors that affect the compatibility of immiscible polymers, such as differences in crystallinity, glass transition temperature ( $T_g$ ), and molecular weight, are to be better understood. The goal of my research, therefore, is to both blend immiscible polymers via NNSM and investigate the compatibility of these solid-state blends by comparative post-processing annealing in order to explain the effects of various process parameters on final blend morphologies.

Typical characterization techniques used for these investigations are transmission electron microscopy and scanning electron microscopy (TEM and SEM, respectively). SEM shows cross-sections of bulk morphology, while TEM shows a 2D projection of a thin section about 50-100 nm thick and provides additional information about the possible nanostructure of the particles and/or the dispersed phase within the matrix [3]. There is no doubt that these techniques are needed for my investigations. However, chemical identification of the phases is difficult unless staining or selective leaching is done prior to imaging. Sample preparation is indeed an issue for both characterization routes and involves many steps and precautions. For instance, TEM specimens must be less than a micron thick, preferably less than 100 nm thick for the high detail investigation – below the thickness of commercially important self-supporting polymers and less than that of most polymer coatings [4]. Issues with SEM include specimen charging (even with conductive coatings, there is still some charge leaking) and structural damage caused by the beam when it impinges on the specimen.

Global Fourier-transform infrared spectroscopy (FT-IR) is often used to probe chemical changes in samples. The chemical structure (bonding arrangement, elements, etc) of the polymer determines which transitions can occur at specific wavenumbers for that polymer. Thus, it is useful in detecting crosslinking or radical-induced changes due to mechanical milling. However, its resolution is poor and cannot access information about dispersed-phase size or distribution in a polymer blend sample. Synchrotron IR, however, offers a unique set of advantages over global (thermal) IR. The brightness (photon flux emitted from unit source area and unit solid angle) is 100-1000 times greater than that of global sources – a phenomenon that allows for microspectroscopic (i.e., vibration-mode-selected mapping) investigations of both small and large size samples with heterogeneous regions [5]. The focused beam produced by synchrotron radiation is thus much smaller in size and more intense than the global source and also provides a better signal-to-noise ratio.

The basic approach of this technique is as follows: blend polymers via NNSM, prepare these samples prior to investigation by embedding and microtomy, and use the synchrotron IR microspectroscopy to obtain information about heterogeneity in these blends as well as identification of domains and interfacial regions. The use of KBr windows allows for a background. The spectral range of importance is 4000 to 1000 wavenumbers since the diffraction limit becomes important in the low energy region. The resolution, although it is not as good as that of TEM or SEM, should be eventually to the level of a few microns.

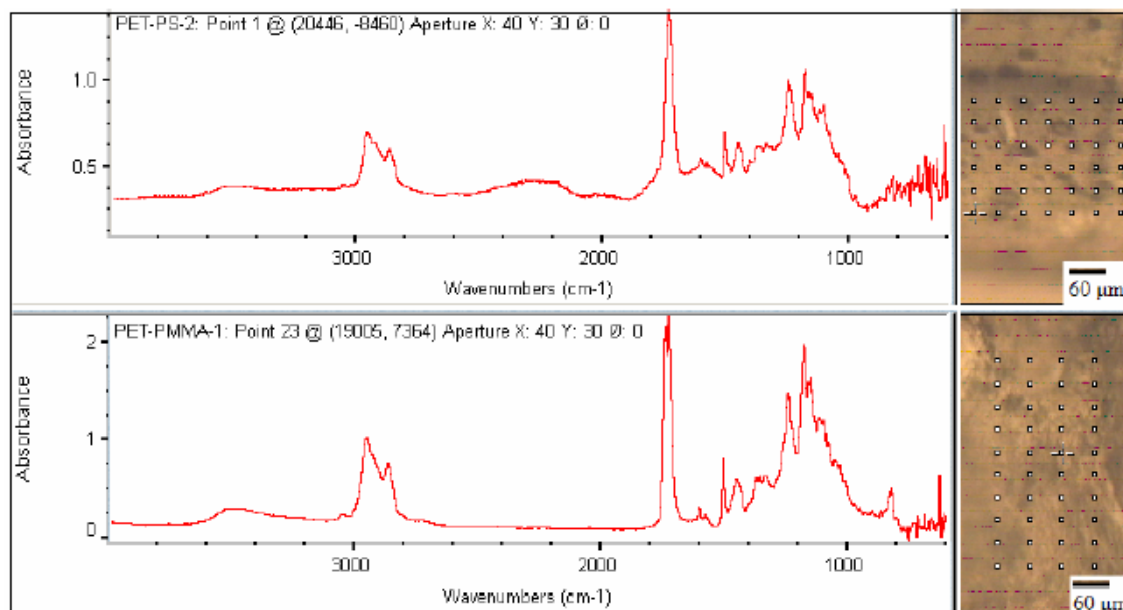


**Figure 1: Optical micrographs of blends of PET/PS (top) and PET/PMMA (bottom) with arbitrary area grids superimposed on the images. The FT-IR spectra for the blends' respective crosshaired points are shown at left.**

Preliminary results have shown that the technique is viable. Initial attempts with polyethylene oxide and polyvinylpyrrolidone were crude because I the samples were

mechanically pressed milled powders and were too thick. Later investigations of more immiscible blends like polystyrene (PS)/polymethylmethacrylate (PMMA), PS/polyethylene terephthalate (PET), and PET/PMMA showed great promise. Figure 1 shows spectra taken at arbitrary points within area grids constructed over optical microscope images of PET/PS and PET/PMMA blends. In a row-by-row fashion, a spectrum is taken at each point in the grid. A characteristic peak is chosen for one of the polymers (typically the dispersed or minor phase), and the intensity of this peak is correlated to a color code such that maximum peak intensity is blue and nil is white.

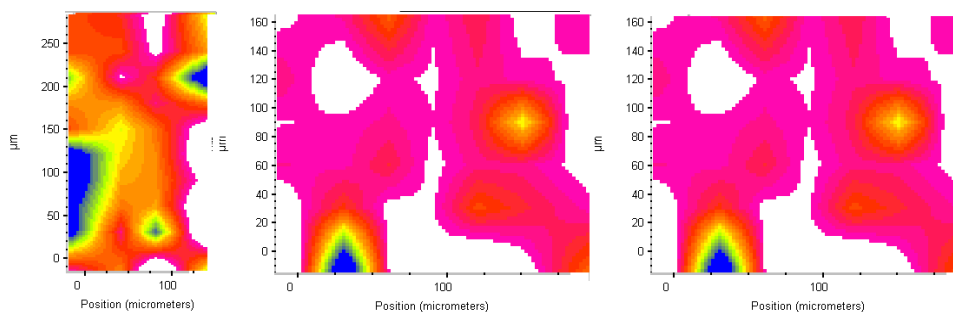


**Figure 2: PET/PMMA (left) and PET/PS (middle and right) compositional area maps (blue = high, white = low) of dispersed phase (PET and PS with two different choices for characteristic PS peaks in middle and right maps)**

Thus, compositional area maps of these blends in Figure 2 illustrate the ability of synchrotron FT-IR microspectroscopy to chemically map solid-state blends. The choices for the dispersed-phase characteristic peak were the aromatic C=C stretching frequency at  $1508\text{ cm}^{-1}$  specific to para-substitution on the aromatic ring for PET and the C-H aromatic stretching transitions at both  $3031\text{ cm}^{-1}$  and  $3061\text{ cm}^{-1}$  for PS. The reproducibility of this technique is also evidenced by the fact that identical area maps were generated for both PS peak selections.

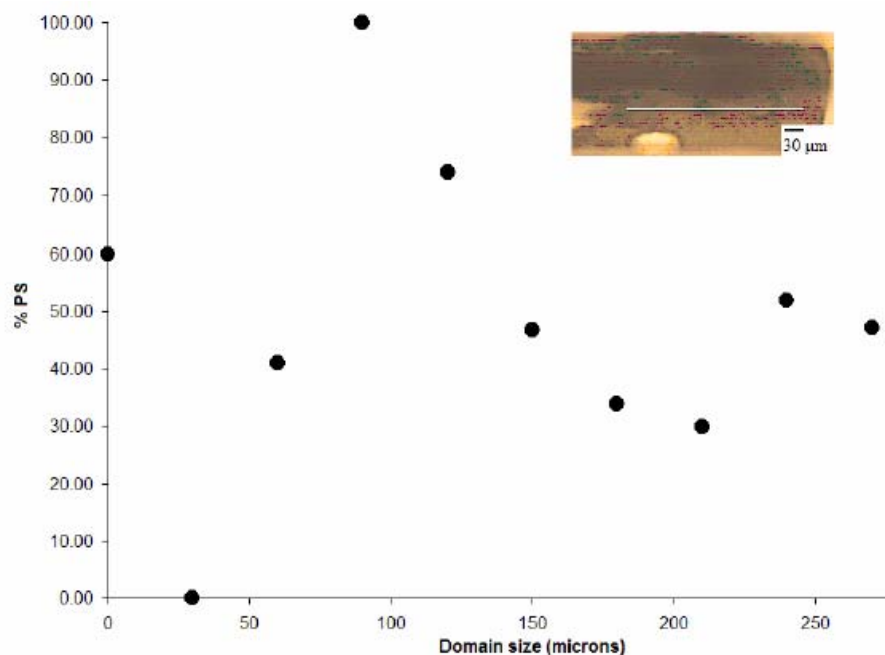


**Figure 3: Optical micrograph of 50/50 PS/PMMA blend with horizontal line arbitrarily drawn across a microtomed section and the corresponding line map**

It is often useful to determine specific concentration gradients in one direction using a process known as line mapping and giving a more quantitative insight into solid state blend phase separation. Figure 3 provides an example of how a concentration gradient across a polymer blend reveals how heterogeneous the domains are sized. In a similar fashion to area mapping, a color code corresponds to peak intensities, and a characteristic peak of the dispersed phase is chosen. Peak intensity ratios are calculated based on comparison to the pure dispersed phase polymer's peak signal, and composition in terms of weight percent is calculated. A quick way to verify the nominal 'bulk' composition of the blend is to 'line-average', i.e., average the composition across the line. For the sample shown in Figure 3, which used the same  $3061\text{ cm}^{-1}$  C-H aromatic stretching mode for PS, the  $1600\text{ cm}^{-1}$  in-plane aromatic ring stretching transition for PS was also used to obtain a similar profile, and both line-averages came out to 49 weight % PS – very close to the known nominal composition of 50 weight % PS.

Both qualitative and quantitative evidence of blend domain heterogeneity have been shown with FT-IR microspectroscopy with synchrotron radiation. The reproducibility and accuracy of these results is only limited by the spatial resolution of the instrument. Although this technique cannot probe interfaces on the order of nanometers, improved features such as better diamond windows and improving signal-to-noise ratios further at smaller apertures will continuously upgrade the resolution. Further studies will include comparative area and line maps between melt-blended and NNSM-blended samples. The use of this technique will complement several other characterization methods used in my investigation of polymer blending.

## References

1. Lebovitz, Andrew H. et al. *Polymer*, **44** (2003)
2. De Castro, C.L., Ph.D. Thesis, Tulane University (2005)
3. Corte, Laurent et al. *Polymer*, **46** (2005)
4. *Polymer Characterization: Physical Techniques*. D. Campbell et al. 2<sup>nd</sup> ed. Stanley Thornes Publishers Ltd. (2000)
5. Kizilkaya, Orhan et al. *Review of Scientific Instruments*, **76** (2005)

## Publications and Conference Presentations

Schexnaydre, Ryan J. and Brian S. Mitchell. "Synchrotron Infrared Microspectroscopy Characterization of Heterogeneities in Solid-State Blended Polymers," *Materials Letters*. Accepted for publication 13 August 2006

"Polymer Blending via Near Net-Shape Manufacturing (NNSM)." Eastern Regional Chemical and Materials Engineering Graduate Symposium (ERCGS), University of Kentucky in Lexington, KY, October 14<sup>th</sup>, 2006 (presentation)

"Solid State Polymer Blending via Near Net-Shape Manufacturing." 7<sup>th</sup> Annual Louisiana Materials and Emerging Technologies Conference, Louisiana State University in Baton Rouge, LA, October 22<sup>nd</sup>, 2006 (presentation and poster)

"Solid State Polymer Blending via Near Net-Shape Manufacturing." The 2006 AIChE Annual Meeting, Structures and Properties of Polymers 1: Polymer Blends, San Francisco, CA, November 15<sup>th</sup>, 2006 (presentation).

## Proposals

NSF/DMI "Solid State Blending of Polymers via Near Net-Shape Manufacturing," \$494,229 (unsuccessful).

## Grants (PI or co-PI)

## Students who worked on 2006 CAMD-related research

- (1) Ryan Schexnaydre (graduate, Ph.D.)



## EXAFS Study of Transition Metal Cationic (Mn<sup>2+</sup>) Dopant in Polymer Films during Layer-by-Layer Nanoassembly

Vimal Kamineni, Yuri Lvov, Pedro Derosa, Amitava Roy, Tabbetha A. Dobbins

Louisiana Tech University, Institute for Micromanufacturing, P.O. Box 10137, Ruston, LA 71272, U.S.A.

Contact: vkk001@latech.edu  
PRN: LaTech-TD0505

### INTRODUCTION

Layer-by-Layer (LbL) assembled polyelectrolyte films on planar or colloidal supports have advanced markedly in the past decade since their inception. Today, polyelectrolytes have been incorporated into microelectronics and microfluidics for sensor applications<sup>x,xi</sup> and are being fabricated onto colloidal particles<sup>xii</sup> for controlled delivery and release of drugs<sup>xiii,xiv</sup> using the LbL approach. Still, many questions surrounding the composition, kinetics of decomposition, film permeability and interaction between electrolyte layers are unanswered. Fundamental studies toward the physical structure—and its influence on the kinetic behavior—of these films assembled and under various conditions will advance their reliability in the semi-permeable membrane market.

The objective of this work is to identify the role of cationic additions to the polyelectrolyte solutions during film preparation. We have used extended x-ray absorption fine structure (EXAFS) and ab-initio density functional theory (DFT) simulations to examine the salient features of conventional polyion assemblies. Using samples prepared by alternately adsorbed polyanion—poly(styrenesulfonate) (PSS)—and polycation—poly(allylamine) (PAH), we examine the role of metal cations, to the polyanionic bath.

### EXPERIMENTAL

Quartz crystal microbalance (QCM) measurements record the LbL self assembly growth of the nanofilms on the piezoelectric quartz crystal. For these measurements two solutions of Polystyrene sulfonate (PSS) and polyallylamine hydrochloride (PAH) - each comprised of 2mg/ml concentration in water - were used. After the first 3 bilayers three different concentrations of MnCl<sub>2</sub> 0.5M, 0.3M and 0.15M are added to the polyelectrolyte solution. The growth of the films was measured using quartz crystal microbalance. The silver QCMs (9 MHz resonators) used to measure the thickness, underwent a change in resonant frequency during the deposition of alternate layers. The relationship  $\Delta M$  (g) = -0.87  $\Delta F$  (Hz) was used to relate the adsorbed mass to resonance frequency shift, by taking the characteristics of the resonators used. The thickness of a film is then

calculated from its mass. The adsorbed film thickness at both faces of the electrodes ( $d$ ) is obtainable from the density of the polyion film (ca  $1.3 \text{ g/cm}^3$ ) and the real film area:  $d(\text{nm}) = -(0.016 \pm 0.02) \Delta F (\text{Hz})$ . Figure 1 clearly shows the change in thickness of the films due to change in concentration of  $\text{MnCl}_2$  in the solution. The films thickness grows from 0.15M concentration to 0.3M concentration and the thickness decreases from 0.3M to 0.5M. The increase in the film growth from 0.15M to 0.3M can be attributed to metal cation addition is known to improve adsorption, by inducing polymer coil formation, and therefore, increasing the film growth step. The decrease in the film growth from 0.3M to 0.5M can be attributed to the decrease in the availability of a large number of electrostatically charged polyelectrolytes, due to the formation of (metal + polyelectrolyte) complexes.

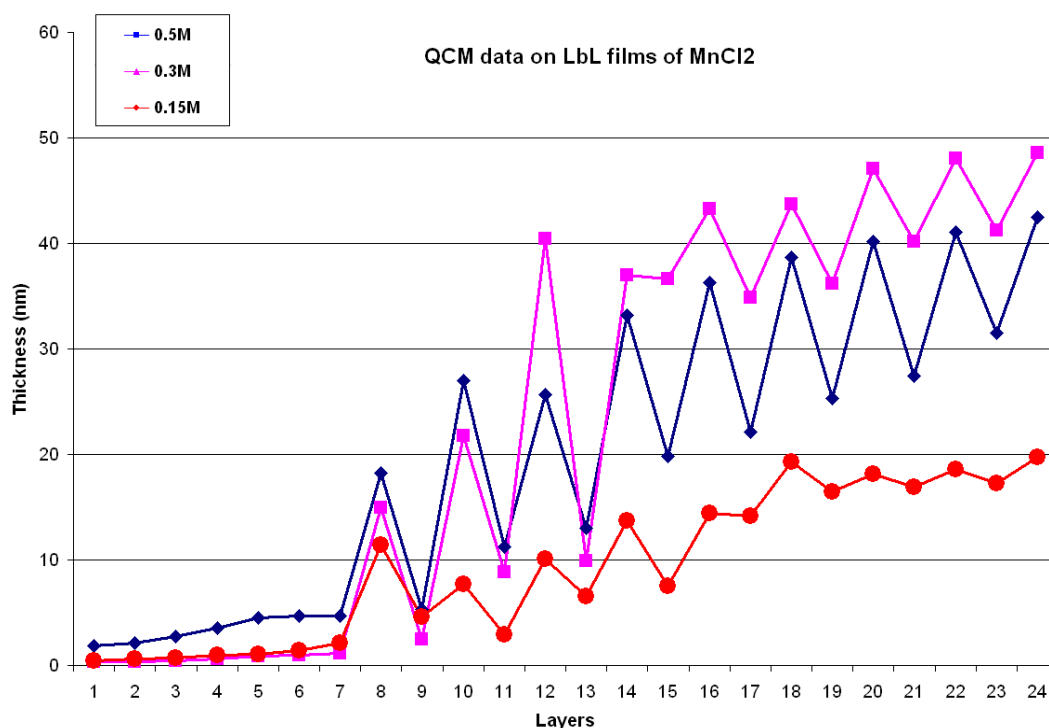


**Figure 1:** QCM data showing the thickness of  $\text{MnCl}_2_{0.5}$ ,  $\text{MnCl}_2_{0.15}$  and  $\text{MnCl}_2_{0.3}$  films.

## EXAFS MEASUREMENT AND ANALYSIS

The EXAFS data was collected using a double crystal monochromator beamline at CAMD (Port 5B - Energy range 1 - 15 KeV, with resolution from 0.5 eV (low energy) to 2 eV (high energy)). The raw data of the XAFS (X-ray absorption fine structure) is converted using Athena software and from the absorption edge, the oxidation state of the element can be determined.<sup>6</sup> FindIT software is used to search inorganic crystal structure database (ICSD).<sup>7</sup> This database is used to generate the atoms file, which is fed into the TkAtoms<sup>8</sup> software to give Feff<sup>9</sup> input file. The processed data from Athena is fitted to the Feff input files (TkAtoms) by using Artemis (Figure 2). Once a proper fit of the data

is achieved, the coordination number & the nearest neighbor distance of the central atom can be found.

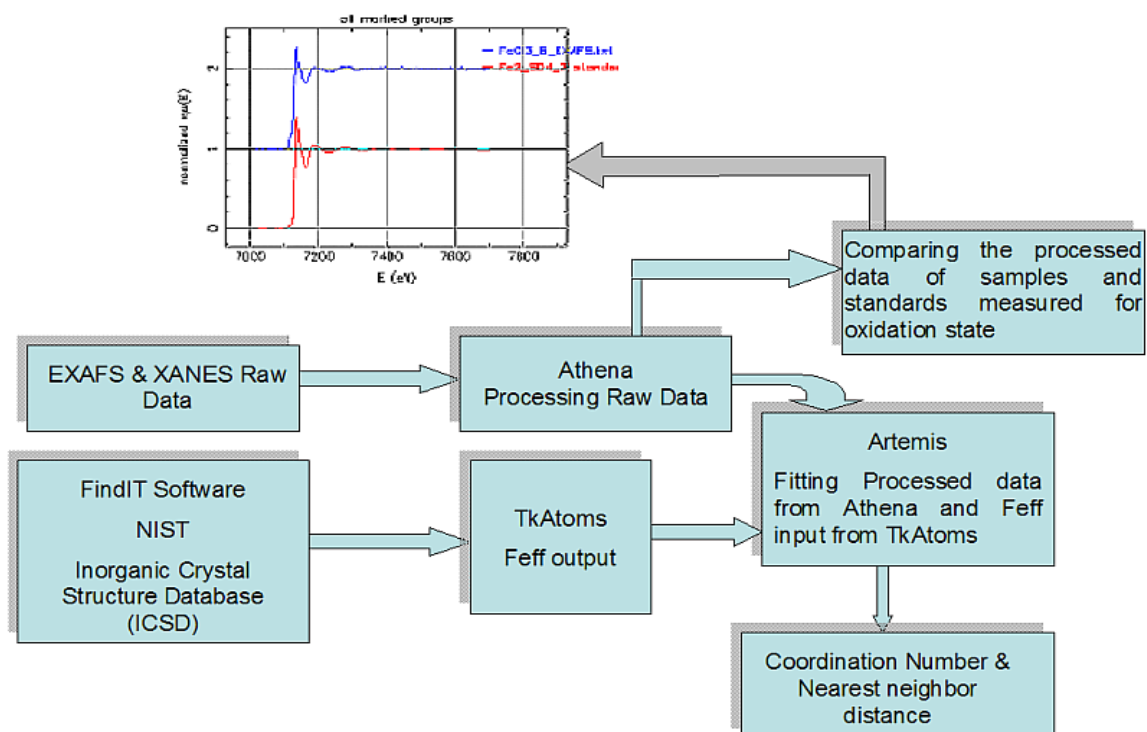


Fig. 2: The flowchart to be followed for processing data.

## RESULTS AND DISCUSSION

The DFT calculations show the final geometry of a system consisting on 2 PSS monomer attached to a  $Mn^{2+}$  atom (Figure 3). Using the coordinates of the atoms from the DFT calculations the feff input file has been created. From the feff input file the scattering paths are calculated.

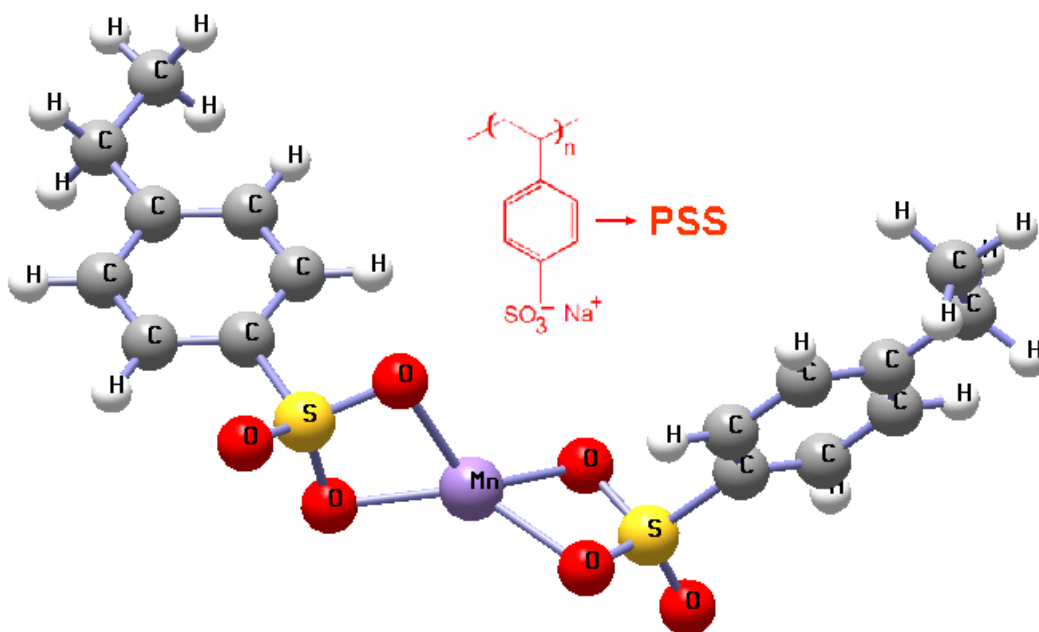


Figure 3: Final geometry of the system from DFT calculations

Using the first 10 scattering paths the data was fitted to the  $\text{MnCl}_2$  EXAFS data. A close fit was achieved as show in figure 4. Further analysis is required for a good fit of the data to find the coordination number and nearest neighbour distance of the central atom. One of the methods that can be adapted in our further studies is to get the normalized  $\chi\mu(E)$  Vs  $E(\text{eV})$  data from the DFT feff input files and compare it with the XANES(X-ray Absorption Near Edge Structure) data of  $\text{MnCl}_2$  Layer-by-layer nanofilms. Once a good fit is achieved that model could be used for the various cation species ( $\text{Fe}^{3+}$ ,  $\text{Mn}^{2+}$  and  $\text{Ti}^{3+}$ ) that will be added in our further studies on the Layer-by-layer nanofilms.

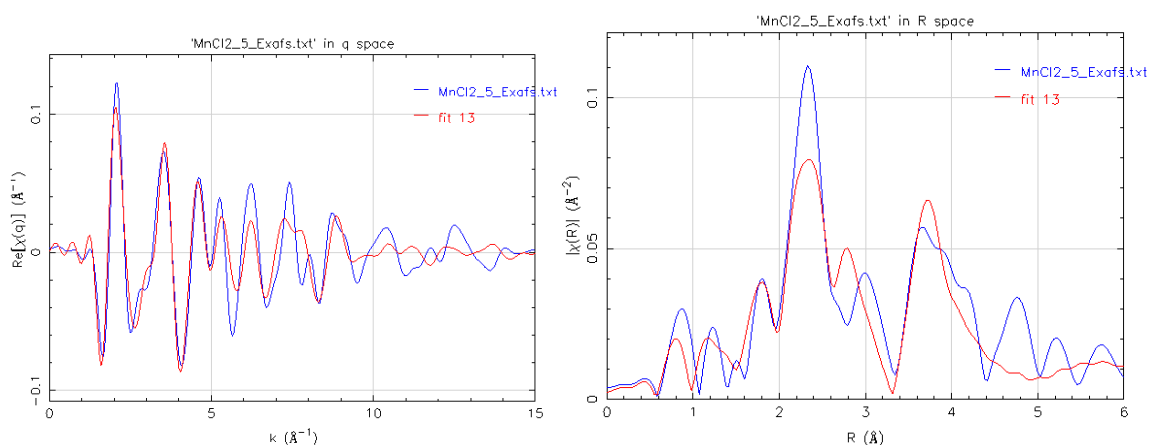


Figure 4: The  $\text{MnCl}_2$  and the DFT data fitted in the q & R space

### ACKNOWLEDGMENTS

We thank Dr. Amitava Roy (CAMD) and Mr. Christopher Bianchetti (CAMD) for kind help in our XAS measurements. Funding for this project is provided by the National

Science Foundation, Division of Materials Research (Contract No.: DMR-0508560). Partial support is provided by the Department of Energy, Office of Basic Energy Sciences (Contract No.: DE-FG02-05ER46246) and the Louisiana State Board of Regents Office of Sponsored Research (Contract No.: LEQSF(2005-08)RD-A-20).

**KEYWORDS**

Polyelectrolytes, layer by layer, nanoassembly, EXAFS.

**REFERENCES**

## Investigations of metal and free-base porphyrin thin films using AFM and VUV photoemission spectroscopy

F. Wang, F. Womack, J.T. Runnels, B.M. Watson, Z.M. LeJeune,<sup>1</sup> J. Fitzgerald,<sup>1</sup> J.C. Garno<sup>1</sup>, Y. Losovyi<sup>3</sup>, R.L. Kurtz,<sup>2</sup> P.T. Sprunger<sup>2</sup>

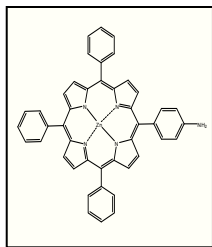
<sup>1</sup>Department of Chemistry, Louisiana State University, Baton Rouge, LA 70803

<sup>2</sup>Department of Physics, Louisiana State University, Baton Rouge, LA 70803

<sup>3</sup>CAMD, Louisiana State University, Baton Rouge, LA 70806

Porphyrins have practical applications in molecular electronic devices as light harvesting complexes, sensors, and photonic devices. The structural motif of the macrocycle, its peripheral groups and the addition of chelated metal ions result in the differences in their electrical, photophysical, magnetic and photo-electrical properties. The porphyrin backbone can be synthesized to contain a wide range of substituents, for

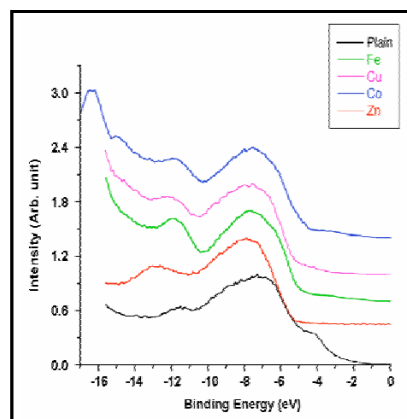
Zn(II) 4-(10,15,20 -  
Triphenyl-porphyrin  
-5-yl)-phenylamine



example to enable directing the orientation in a side-on assembly or co-planar configuration. The organization of porphyrin molecule on surfaces as well as the attached substituents and/or coordinated metals dictate the resulting function, properties and efficiency in molecular devices. This research applies atomic force microscopy (AFM) and synchrotron-based photoemission spectroscopy, at the 3mTGM beamline, to elucidate the assembly and electronic properties of metallated (FeIII, Co, Zn, Cu) and freebase porphyrin thin films on various surfaces (an example of the ZnII structure is shown above).

Of critical importance is elucidating the role and balance between inter- and intra-molecular interactions play in the overall electronic/transport properties of the porphyrin-based heterostructures. In the present experiment, these variables intended to be probed by selective synthesis (intramolecular) and subsequent deposition (intermolecular) techniques.

The information regarding valence/band structure differences, particularly about the LDOS near  $E_F$ , provides insight for maximizing transport and photonic properties. The photoemission data of the prepared porphyrins on Si substrates is shown in the figure above. From the present data, there appears to be subtle differences in the HOMO-LUMO gap. To understand these differences, calculations are on-going. Moreover, AFM results indicate that there may be inhomogeneities in the porphyrin films.



The PES data of metallated (Fe(III), Co, Zn, Cu) and free-base porphyrin systems, acquired with a photon energy of 24 eV,

*The authors gratefully acknowledge Professor Graca Vicente and Erhong Hao for synthesis of porphyrins. We also thank the LSU Council on Research Faculty Research Seed Grant, the Louisiana State Board of Regents RCS subprogram and the Petroleum Research Fund for financial support. Results presented at American Chemical Society 62nd Southwest Regional Meeting, Houston, TX (October, 2006).*

## Effect of polymerization on the shape of fluid interfaces

Pradeep Bhattad<sup>1</sup>, Karsten Thompson<sup>2</sup>, Clinton Willson<sup>3</sup>, Kyungmin Ham<sup>4</sup>

[pradeep@lsu.edu](mailto:pradeep@lsu.edu)

<sup>1</sup>Department of Chemical engineering, Louisiana state university, Baton rouge, LA 70802

<sup>2</sup>Department of Chemical engineering, Louisiana state university, Baton rouge, LA 70802

<sup>3</sup>Department of Civil and Environmental engineering, Louisiana state university, Baton rouge, LA 70802

<sup>4</sup>Center for Advanced Microstructure and Devices (CAMD), Baton rouge, LA 70806

### ChemE-KT1007

## Introduction

The objective of this work is to study the structure of fluid interfaces during primary spontaneous imbibition. However, the wetting fluid is susceptible to movement during transport and sample stage rotation during X-ray Computed Tomography (XCT) analysis. To avoid this problem, we replace water with Poly ethylene glycol dicarylate (PEGDA) as the wetting fluid, which can be UV polymerized into a solid at any point during the experiment to freeze the phase configuration in place. To study the change in the shape of interface upon polymerization, a simple capillary rise experiment was performed and the fluid interface was analyzed before and after polymerization using XCT.

## Experimental

### Sample Preparation:

The wetting fluid was prepared consisting of 1(wt%) Irgacure 2959 (initiator) mixed with PEGDA in a vortex mixer. A simple capillary rise experiment was performed in a glass capillary tube of 1.1-1.2mm ID. Upon equilibrium, the bottom of the capillary tube was sealed with Citrosol capillary sealant. Two similar samples were created and one was exposed to UV radiation for polymerization into solid and second one was left unchanged in liquid state. The samples were analyzed at the CAMD tomography station with X-Ray energy of 13.5keV and sample resolution of 4.5 micron/voxel.

### Image Analysis:

The volumetric grey scale image thus obtained was first converted to the grey-scale values of 0-255. The image was segmented using a simple thresholding technique followed by majority filtering of width 5 for the removal of speckled noise. Border detection algorithm was used to identify the interface voxels.

## Results

Figure-1 shows slices of un-polymerized and polymerized volumetric image. In the un-polymerized sample, the movement due to the rotation can be seen. Upon segmentation,

the interface voxels were identified on the slice of an image and plotted as shown in Figure-2.

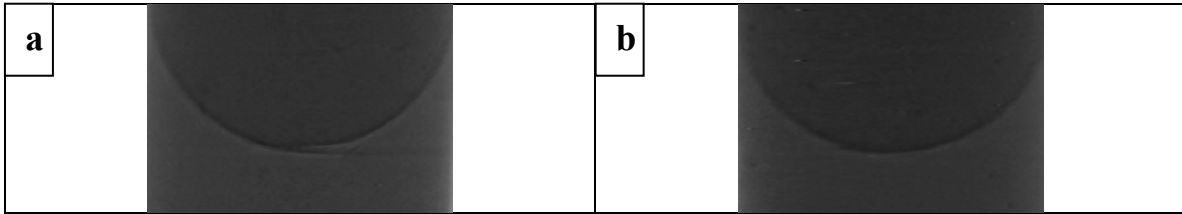


Figure-1: X-Ray tomography image at 13.5keV and 4.5 $\mu$ m resolution. PEGDA with 1% (wt) Irgacure 2959 (initiator). (a) Unpolymerized (b) Polymerized for 60 seconds in UV light.

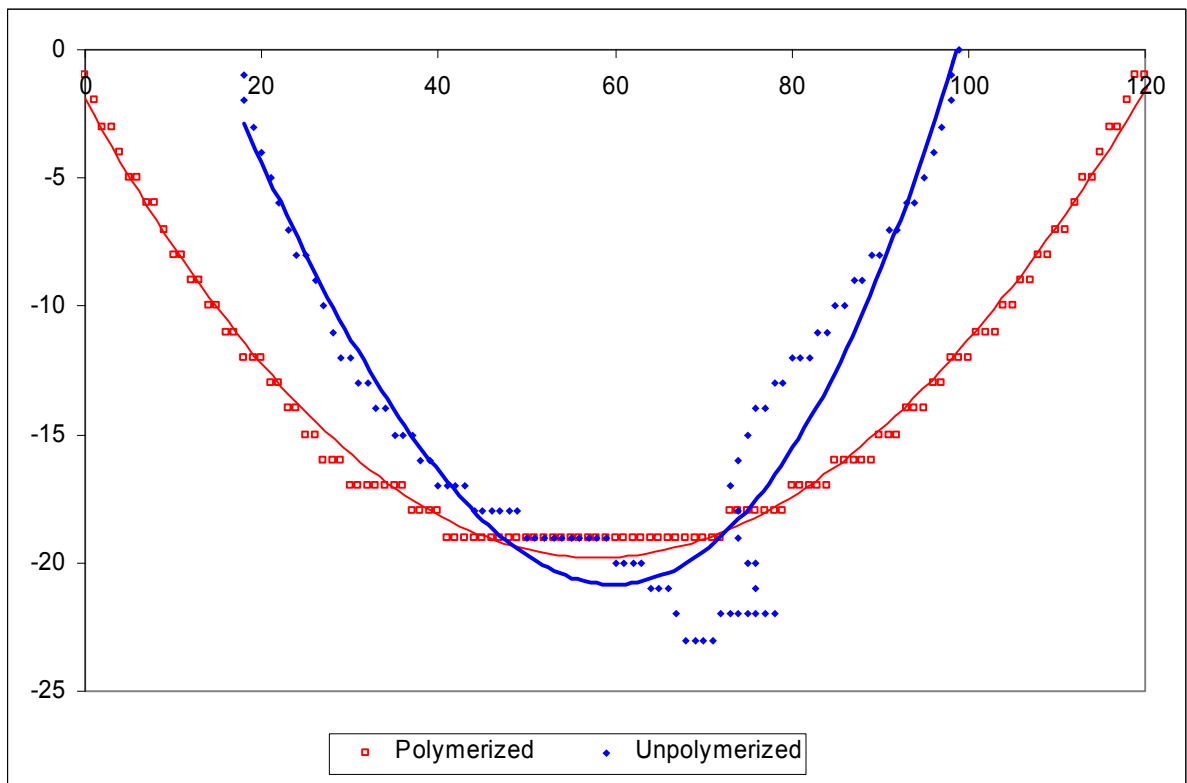


Figure-2: Plot of interface voxels from the slices of volumetric image showing the change in the shape of the interface upon polymerization

### Conclusion

As it can be seen from the plot, shape of the interface changes upon polymerization. Hence we need to account for the change in the shape of the interface when the wetting fluid is polymerized.



## X-ray Absorption Spectroscopy of Mixed Metal Iron-Based Fischer-Tropsch Catalysts

A. Roy<sup>1</sup>, A. Ignatov<sup>1</sup>, C. Bianchetti<sup>1</sup>, G. Merchan<sup>1</sup>, R. Louis<sup>1</sup>, A. Campos<sup>2</sup>, J.J. Spivey<sup>2</sup>,  
N. Lohitharn<sup>3</sup>, J. Goodwin<sup>3</sup>; <sup>1</sup>Center for Advanced Microstructures and Devices,  
Louisiana State University, Baton Rouge, Louisiana 70806; <sup>2</sup>Department of Chemical  
Engineering, Louisiana State University, Baton Rouge, LA 70803; <sup>3</sup>Department of  
Chemical and Biomolecular Engineering, Clemson University, 127 Earle Hall, Clemson,  
SC 29634-0909; E-mail: [acampo2@lsu.edu](mailto:acampo2@lsu.edu); PRN Number: ChemE-JS-1206

An ongoing collaborative effort between Clemson University and Louisiana State University to give a “birth-to-death” study of various mixed metal iron-based Fischer-Tropsch catalysts that began in December of 2005. The goal of the study is to correlate catalyst activity/stability studies obtained from Clemson University with structural studies at CAMD in order to give a unique understanding of the evolution of the catalysts. Research in CAMD in 2006 included *ex situ* studies of various central atoms (Fe, Cu, Mo, etc.) in each of the catalysts (Table I).

<b>Catalyst tested in parts by weight (synthesized in Clemson University laboratories):</b>
100 Fe / 5 Cu / 17 Si (calcined 300°C 5h)
100 Fe / 5 Cu / 17 Si pretreat in CO @ 280 °C 12 h & passivate in O <sub>2</sub>
100 Fe / 5 Cu / 4.2 K / 11 SiO <sub>2</sub> (calcined)
100 Fe / 5 Cu / 4.2 K / 11 SiO <sub>2</sub> (calcined) CO pretreat @ 280 °C 12h & passivate in O <sub>2</sub> for 1 h
90 Fe / 10 Mo / 5 Cu / 17 Si (calcined 300 °C 5h)
90 Fe / 10 Mo / 5 Cu / 17 Si (calcined) CO pretreat @ 280 °C + O <sub>2</sub> passivate
95 Fe / 5 Cr / 5 Cu / 17 Si sieved < 45 μm calcined @ 300 °C 5h
90 Fe / 10 Cr / 5 Cu / 17 Si CO pretreat @ 280 °C 12h & passivate in O <sub>2</sub> for 1h
90 Fe / 10 Cr / 5 Cu / 17 Si (calcined 300 °C 5h)
90 Fe / 10 W / 5 Cu / 17 Si calcined + CO pretreat
90 Fe / 10 W / 5 Cu / 17 Si calcined @ 300°C 5h
90 Fe / 10 W / 5 Cu / 17 Si (calcined) CO pretreat @ 280 °C 12 h + O <sub>2</sub> passivate
90 Fe / 10 W / 5 Cu / 17 Si prepared from WCl calcined @ 300 °C 5h *
95 Fe / 5 Zr / 5 Cu / 17 Si sieved < 90 μm calcine @ 300 °C 5h *
95 Fe / 5 Mn / 5 Cu / 17 Si calcined in air 300 °C 5h 45-90 μm *
* denotes newly synthesized (not tested yet)

Table I – Catalysts synthesized in Clemson University

Tests run on March 20-23 were electron yield experiments on the k-edge of Fe that have surface specific information of the catalysts. Figure 1 demonstrates that qualitative information in the XANES data in which two identical catalysts (except for the preparation techniques) have different oxidation states. The figure illustrates that a passivated sample has a lower oxidation state than the calcined sample (which is to be expected). In addition, semi-quantitative information can be obtained using a linear combination fit of known standards to evaluate the relative percentages of phases present in the sample using the XAFS software Athena [5]. Transmission experiments on March

23-24 transmission experiments will give bulk structural information on the k-edge of Fe to learn about the bulk structure of the catalyst, which is expected to be different from the surface, therefore future data analysis will be made comparing the surface structure to the bulk structure.

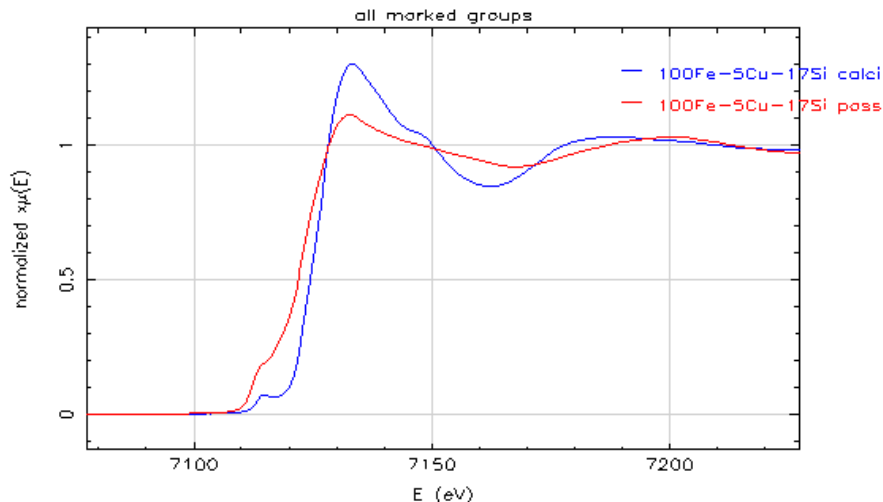


Figure 1 – Normalized XANES electron yield data in Athena for the Fe k-edge

Electron yield data for Cu (Figure 2) is interesting since it was desirable to have Cu not on the surface, therefore a low signal-to-noise ratio means that the Cu catalyst is mainly in the bulk of the catalyst since transmission tests of the Cu had a sufficient signal-to-noise ratio.

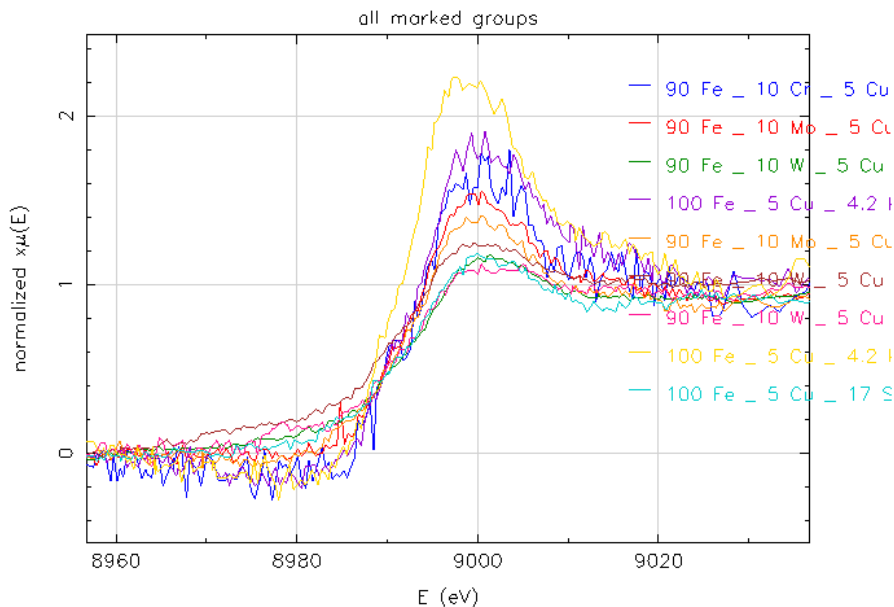


Figure 2 – Normalized XANES electron yield data in Athena for the Cu k-edge

Data analysis is still in progress for these spectra, and it will be very interesting to see the results since qualitative XANES spectra show that there are differences among the catalysts. The EXAFS region of the catalysts will give coordination numbers, Debye-Waller factors, and bond distances for at least the first shell in the Fourier transform [1, 3-4]. The *ex situ* studies of the catalysts will also give insight as to the time-evolution of catalysts when *in situ* studies occur since the active phase in Fe-based Fischer-Tropsch Synthesis is believed to be the carbide phase [2].

#### References

- [1] Chao, K.-j. and A. C. Wei (2001). "Characterization of heterogeneous catalysts by X-ray absorption spectroscopy." Journal of Electron Spectroscopy and Related Phenomena **119**(2-3): 175-184.
- [2] Jin, Y. and A. K. Datye (2000). "Phase Transformations in Iron Fischer-Tropsch Catalysts during Temperature-Programmed Reduction." Journal of Catalysis **196**(1): 8-17.
- [3] Greaves, G. N. (1988). "EXAFS and the structure of catalysts." Catalysis Today **2**(5): 581-584.
- [4] Gurman, S. (1995). "Interpretation of EXAFS Data." Journal of Synchrotron Radiation **2**(1): 56-63.
- [5] Ravel, B. and M. Newville (2005). ATHENA, ARTEMIS, HEPHAESTUS: data analysis for X-ray absorption spectroscopy using IFEFFIT. Journal of Synchrotron Radiation. **12**: 537-541.

## Characterization of Hexaluminates by X-ray Absorption Spectroscopy

A. Roy<sup>1</sup>, A. Ignatov<sup>1</sup>, G. Merchan<sup>1</sup>, A. Campos<sup>2</sup>, J.J. Spivey<sup>2</sup>, E. Kugler<sup>3</sup>

<sup>1</sup>Center for Advanced Microstructures and Devices, Louisiana State University, Baton Rouge, Louisiana 70806; <sup>2</sup>Department of Chemical Engineering, Louisiana State University, Baton Rouge, LA 70803; <sup>3</sup>Chemical Engineering; West Virginia University; PO Box 6102; Morgantown, WV 26506-6102; E-mail: [acampo2@lsu.edu](mailto:acampo2@lsu.edu); PRN Number: ChemE-JS-0707

Nickel k-edge XANES in fluorescence: Data that represents the XANES region best is actually the EXAFS of which ten scans for samples 115, 117, 119 a, b were taken at the DCM beamline in CAMD and averaged in XAS data reduction software Athena [3]. There is a (small bump) pre-edge feature on all samples at approximately 8332 eV, which the standards may be used in order to do a fingerprint analysis to identify the phases in each sample.

The Ni data normalized  $\mu(E)$  data in Figure 1 has (except for 117a) an isosbestic point at energy of  $\sim 8360$  eV, implying that there is definitively one component that is the same for these materials [1].

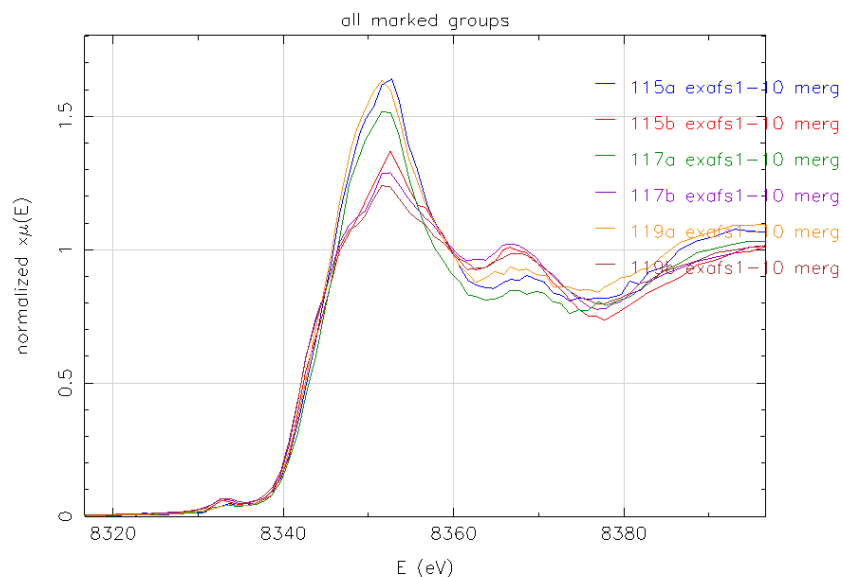


Figure 1 – XANES [normalized  $\mu(E)$ ] of hexaaluminate nickel samples

Nickel k-edge EXAFS in fluorescence: The EXAFS region for the Ni k-edge was taken during the same runs of the XANES region. After glitches were removed, the ten spectra were averaged in  $\mu(E)$  in Athena. Minimal data reduction of background removal was performed and the Fourier Transform of  $\chi(k)$  transforms the data from energy space into a pseudo-radial distribution in Figures 2-4. Until data modeling takes place in XAS modeling software Artemis, information from the pseudo-radial distribution function cannot be extracted from the data [2].

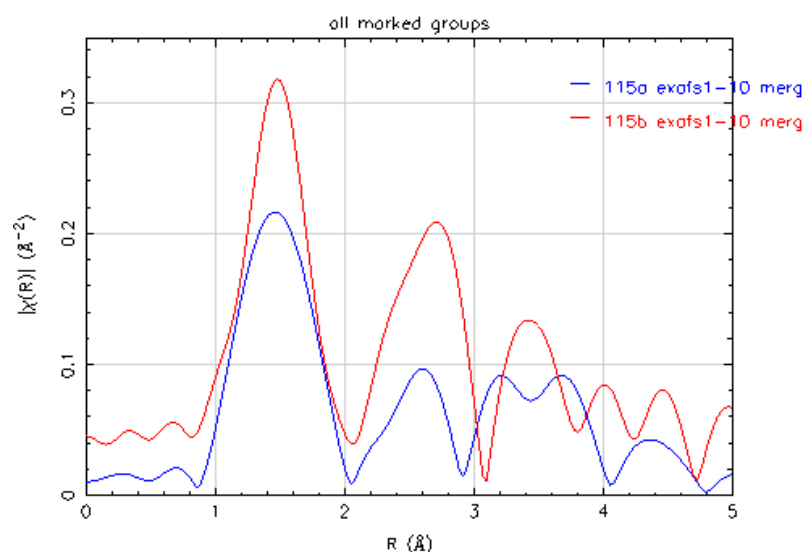


Figure 2 – Fourier transform (pseudo-radial distribution) of EXAFS data for 115a, 115b

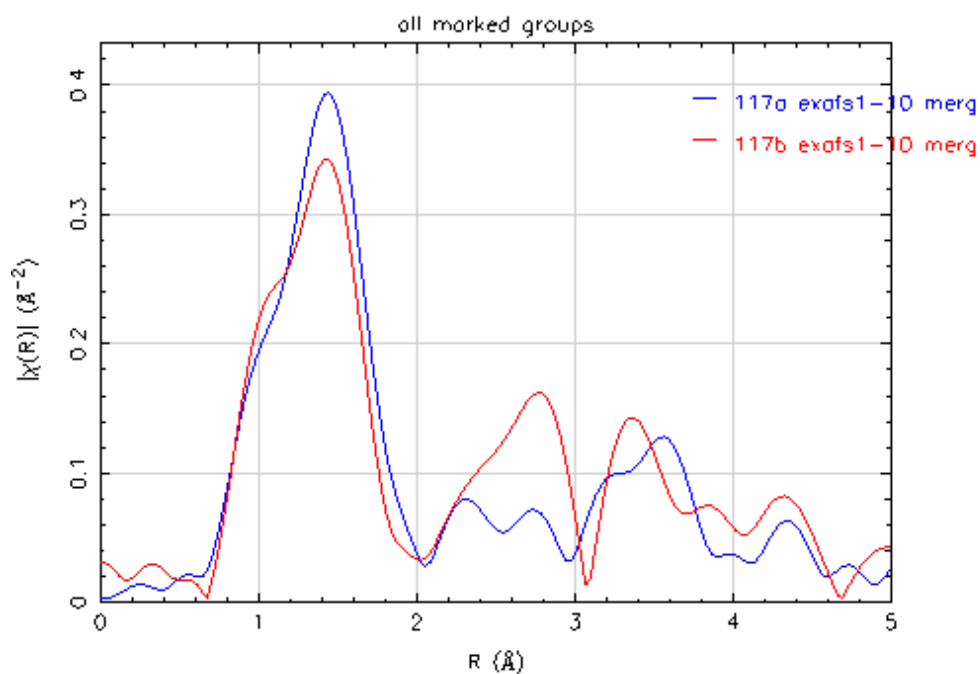


Figure 3 – Fourier transform (pseudo-radial distribution) of EXAFS data for 117a, 117b

Barium L3-edge XANES in fluorescence: Tests were also run on the XANES L3 edge of Barium in fluorescence on all received as-prepared samples (115-119 a, b). Two scans of the data were merged using normalized  $\mu(E)$ . A preliminary observation of double peaks in some of the spectra, as well as a higher normalized absorption for lower weight percentages of Ba in the samples and for samples prepared with technique ‘a’.

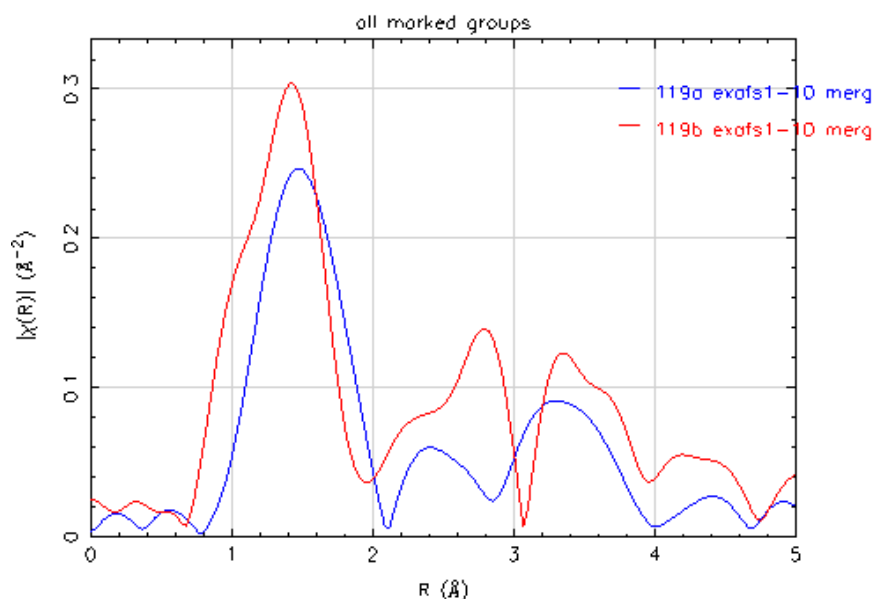


Figure 4 – Fourier transform (pseudo-radial distribution) of EXAFS data for 119a, 119b

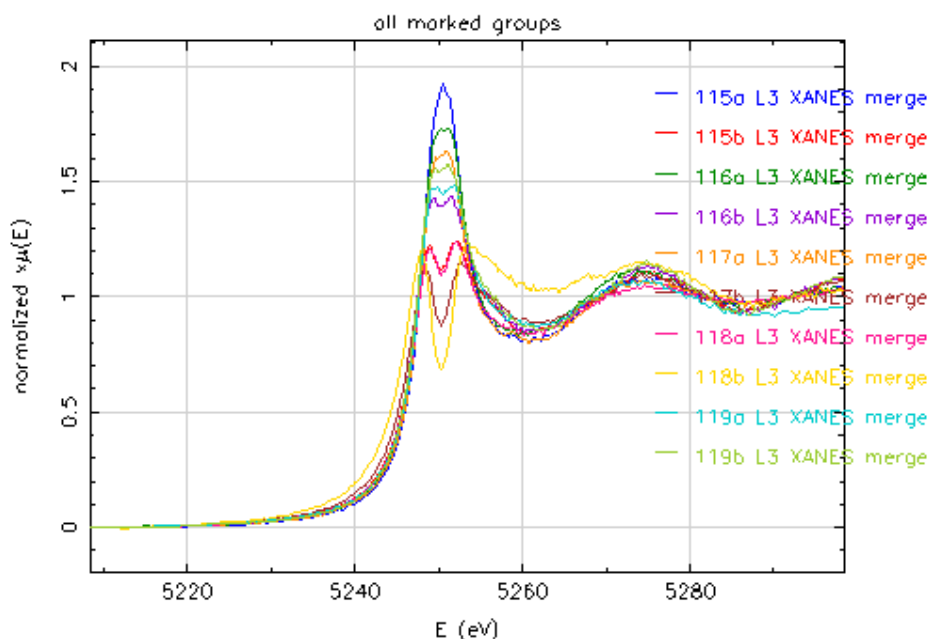


Figure 5 – Normalized  $\mu(E)$  (XANES spectra) for Ba

Data analysis status: The XRD results from Brookhaven National Laboratories by Kugler et. al. will be used in the EXAFS analysis for the Ni data. Two trends can be observed from the data analysis for Ni, the two different preparation techniques can be compared at three different weight percentages of Ni, as well as the trend of increasing weight percentages Ni for both preparation techniques.

The barium XANES can be used to do a fingerprint analysis on the data to determine the percentages of phases present in the each of the catalysts. Trends of both weight percentages and preparation techniques can be extracted from the data analysis. Literature will be used to determine what phases would cause the interesting double peak observed in several Barium samples.

Future tests to be performed by the LSU group: The EXAFS for the barium L3 edge will be interesting due to the vast differences in the XANES spectra of the different samples. Information that can be obtained from the EXAFS includes bond distances, nearest neighbors, Debye Waller factor (bond disorder), and coordination numbers [2].

The as-prepared samples are similar to that of the active catalysts, therefore testing the samples in liquid nitrogen temperature, an intermediate temperature, and room temperature will enable the extraction of the Debye Waller factor, which will allow for improved results for the coordination number since they are difficult to decouple from the EXAFS equation.

References:

- [1] Desrochers, P.J., et al., *A Stable Monomeric Nickel Borohydride*. 2003. p. 7945-7950.
- [2] Gurman, S. (1995). "Interpretation of EXAFS Data." Journal of Synchrotron Radiation **2**(1): 56-63.
- [3] Ravel, B. and M. Newville. *ATHENA, ARTEMIS, HEPHAESTUS: data analysis for X-ray absorption spectroscopy using IFEFFIT*, in *Journal of Synchrotron Radiation*. 2005. p. 537-541.

**Insert Spivey pdf**

## Strongly Correlated Electron Systems

### Enhanced spin polarization in polystyrene coated $\text{Fe}_3\text{O}_4$ granular materials and the investigation of the magnetic properties of doped/undoped $\text{HfO}_2$ and $\text{SnO}_2$

Jinke Tang

Department of Physics, University of New Orleans, New Orleans, LA 70148,

[jtang@uno.edu](mailto:jtang@uno.edu)

PRN: UNO-JT1205

Previously, Yaroslav Lozovyy and I reported the enhanced nonmetal-metal Verwey transition in high quality nanogranular  $\text{Fe}_3\text{O}_4$ , which is an evidence for phonon effects in the electronic bands of this material. We continued with the work on nanogranular  $\text{Fe}_3\text{O}_4$ . This time, the emphasis was placed on the surface engineering of the  $\text{Fe}_3\text{O}_4$  nanoparticles in order to preserve the spin polarization at its surfaces. Polystyrene coated  $\text{Fe}_3\text{O}_4$  nanoparticles exhibit intergranular tunneling magnetoresistance (MR) ratio of 22.8% at room temperature and a maximum MR of 40.9% at 110 K. The drastic enhancement of the MR ratio clearly suggests that there is high degree of spin polarization even at room temperature for half metallic  $\text{Fe}_3\text{O}_4$ . The derived spin polarization  $P$  is about 54% and 83% at room temperature and 110 K, respectively. Our work suggests further increase in the spin polarization can be achieved by preventing the oxidation of the surface of  $\text{Fe}_3\text{O}_4$  by a protective coating.

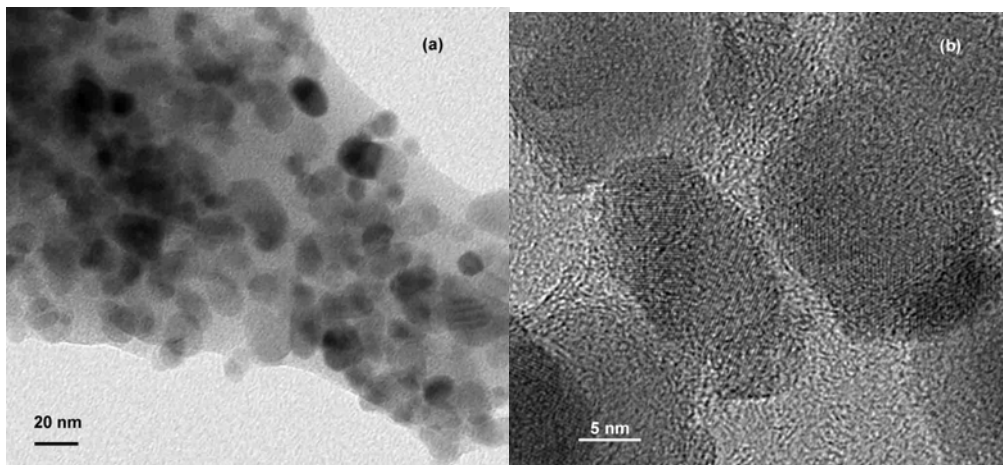


**Fig. 1** (a) TEM image for the Polystyrene coated  $\text{Fe}_3\text{O}_4$  sample indicating that  $\text{Fe}_3\text{O}_4$  nanoparticles are embedded in polymer matrix. (b) High resolution TEM image showing that the  $\text{Fe}_3\text{O}_4$  particles are separated by a thin polymer layer of a few nanometers, forming tunnel barrier for electron transport.



We have also investigated the magnetic properties of HfO<sub>2</sub> films. In view of the experimental report of unexpected ferromagnetism and theoretical investigation on the magnetic order in HfO<sub>2</sub> thin films, we have carried out a series experiments based on different target materials purity, substrates, and doping for the purpose of investigating the structure and magnetic properties of HfO<sub>2</sub>. Pure HfO<sub>2</sub> and Gd -doped HfO<sub>2</sub> thin films have been grown on different single crystal substrates (silicon, R-Al<sub>2</sub>O<sub>3</sub> and LaAlO<sub>3</sub>) by pulse laser deposition at substrate temperature of approximate 700 °C, with base vacuum  $5 \times 10^{-7}$  torr, and growth rate of about 0.15Å/s followed occasionally by annealing. The deposition targets were sintered by 99.95% and 99.995% pure HfO<sub>2</sub> powders. Some film samples were annealed in air at 700, 900 and 1100 °C. X-ray diffraction (XRD) patterns show that the pure HfO<sub>2</sub> thin films are single monoclinic phase with texture. Gd -doped HfO<sub>2</sub> thin film has the same XRD pattern except that its diffraction peaks have a small shift towards lower angles, which indicates that Gd dissolves in HfO<sub>2</sub>. Transmission electron microscopy images exhibit columnar crystallites in the films and film thickness is typically in the range of 100-200 nm. This is also confirmed by Rutherford backscattering spectrometry. Very weak ferromagnetism is observed in pure and Gd-doped HfO<sub>2</sub> films on different substrates at 300 K and 5 K, which is attributed to either impure target materials or signals from the substrates. The magnetic property does not change significantly with post deposition annealing for the HfO<sub>2</sub> films. In addition to films, HfO<sub>2</sub> powders were annealed at different temperatures (700, 900 and 1100°C) in pure hydrogen flow. There is no significant magnetic signal after the annealing. Our investigation casts doubt on the previously reported ferromagnetism in this material.

Cr and Fe-doped SnO<sub>2</sub> films, related to the system above, were deposited on Al<sub>2</sub>O<sub>3</sub> substrates by pulsed laser deposition. X-ray diffraction patterns show that the films have rutile structure and grow epitaxially along (101) plane. The diffraction peaks of Cr-doped samples exhibit a systematic shift toward higher angles with increasing Cr concentration. This indicates that Cr dissolves in SnO<sub>2</sub>. On the other hand, there is no obvious shift of the diffraction peaks of the Fe-doped samples. The magnetization curves indicate that the Cr-doped SnO<sub>2</sub> films are paramagnetic at 300 and 5 K. The Fe-doped SnO<sub>2</sub> samples exhibit ferromagnetic behavior at 300 and 5 K. Zero-field-cooled (ZFC) and field-cooled (FC) curves indicate superparamagnetic behavior above the blocking temperature of 100 K, suggesting that it is possible there are ferromagnetic particles in the Fe-doped films. The anisotropic magnetoresistance (AMR) was not observed in any of the samples. We are currently looking at the effect of oxygen content on the magnetic properties of Cr doped SnO<sub>2</sub>.

**Publications:**

\*\* Enhanced tunneling magnetoresistance and high spin polarization in polystyrene coated Fe<sub>3</sub>O<sub>4</sub> granular system, W. Wang, M. Yu, M. Batzill, J. He, U. Diebold and J. Tang, *Phys. Rev. B*, 73, (2006) 134412, 5 pages.

\*\* 4f-5d hybridization in a high k dielectric, Ya.B. Losovyj, J. Tang, W. Wang, Y. Hong, V. Palshin and R. Tittsworth, *Phys. Lett. A*, 357, (2006) 240, 5 pages.

\*\* Large room temperature spin-dependent tunneling magnetoresistance in a Fe<sub>3</sub>O<sub>4</sub>-polymer composite system, W. Wang, M. Yu, Y. Chen and J. Tang, *J. Appl. Phys*, 99, (2006) 08J108, 3 pages.

\*\* The structure and magnetic properties of Cr/Fe-doped SnO<sub>2</sub> thin films, W. Wang, Z. Wang, Y. Hong, J. Tang and M. Yu, *J. Appl. Phys*, 99, (2006) 08M115, 3 pages.

\*\* Structure and magnetic properties of pure and Gd-doped HfO<sub>2</sub> thin films, W. Wang, Y. Hong, M. Yu, B. Rout, G. A. Glass and J. Tang, *J. Appl. Phys*, 99, (2006) 08M117, 3 pages.

**Presentations:**

Is Magnetite a Half-Metal? at Clemson University and University of Wyoming, March/November 2006.

**Grants:**

Title: Spintronic Application of Room Temperature Ferromagnetic Semiconductor Fe/Mn-doped TiO<sub>2-δ</sub>

PI: J. Tang

Agency: BoRSF

Period: June 2004 through June 2007

Amount: \$180,000

**Student receiving degree:**

Student name: Yuanjia Hong

Ph.D. dissert. title: Magnetic Semiconductor Films by Pulsed Laser Deposition

Completion date: May 2007 (expected)

Undergraduate student: Ed Durant

## The electronic structure and polymerization of a self-assembled monolayer with multiple arene rings (UN-PD1206OR)

D.-Q. Feng<sup>1</sup>, D. Wisbey<sup>1</sup>, Ya. B. Losovyj<sup>2</sup>, Y. Tai<sup>3</sup>, M. Zharnikov<sup>3</sup> and P.A. Dowben<sup>1\*</sup>

1) Dept. of Physics and Astronomy and the Nebraska Center for Materials and Nanoscience, University of Nebraska-Lincoln, Lincoln, NE 68588-0111

2) Center for Advanced Microstructures and Devices, Louisiana State University, 6980 Jefferson Highway, Baton Rouge, LA 70806

3) Angewandte Physikalische Chemie, Universität Heidelberg, Im Neuenheimer Feld 253, D-69120 Heidelberg, Germany

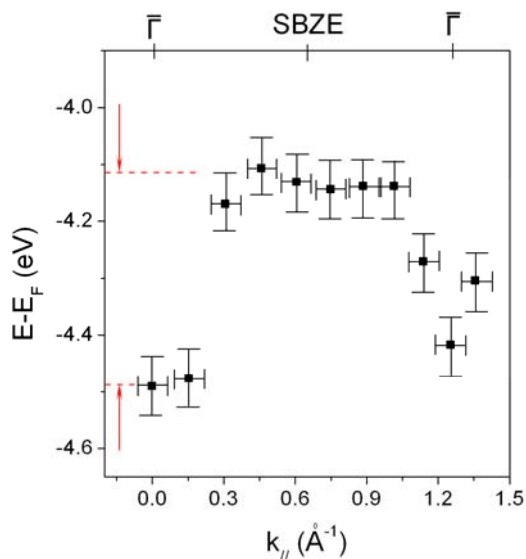


**Figure 1.** Inter-molecular dispersion of a band originating from the sulfur weighted  $\pi$  molecular orbitals of [1,1';4',1''-terphenyl]-4,4''-dimethanethiol (TPDMT) molecules assembled on Au(111) in the reduced zone scheme, determined from high resolution photoemission spectra taken with unpolarized He I (21.2 eV) light.

responsible for the easily observed dispersion of the lowest unoccupied molecular orbitals [1].

The electronic structure is also seen to be dependent upon temperature, and cross-linking between the neighbor molecules, indicating that the electronic structure may be subtly altered by changes in molecular conformation and packing. We found that the irradiated TPDMT films have a smaller HOMO-LUMO gap as compared to the pristine

We have found evidence of intermolecular interactions for a self-assembled monolayer (SAM) formed from a large molecular adsorbate,

[1,1';4',1''-terphenyl]-4,4''-dimethanethiol (TPDMT), from the dispersion of the molecular orbitals with changing the wave vector  $k$  (Figure 1). With the formation self assembled molecular (SAM) layer, the molecular orbitals hybridize to electronic bands, with indications of significant band dispersion of the unoccupied molecular orbitals [1]. The TPDMT films, on gold substrates, are very well ordered molecular assemblies as illustrated in by the evidence of band dispersion (Figure 1). Such in-plane ordering may be indicative of strong lateral interactions within the organic film, as has been suggested for other thiol-derived SAMs. The strong intermolecular interaction is most likely

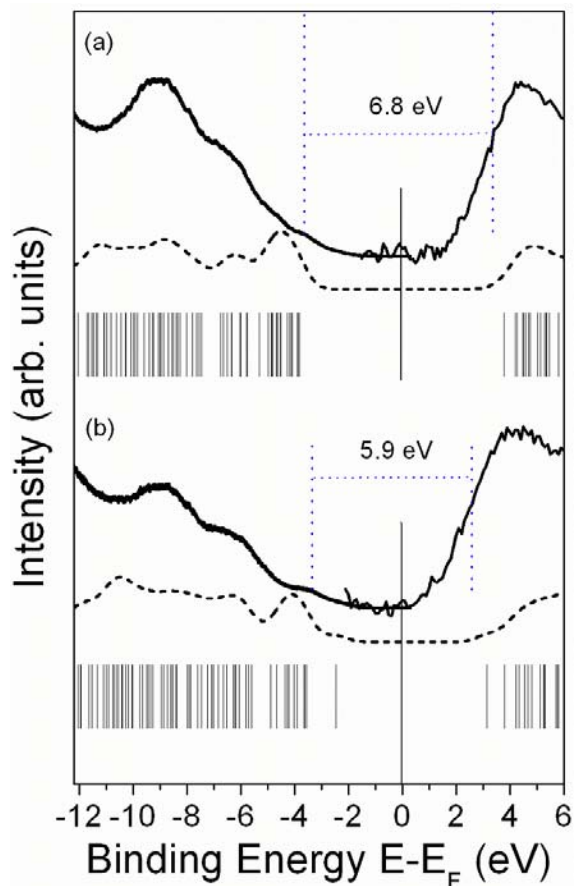


**Figure 2.** Combined photoemission (left) and inverse photoemission (right) spectra (solid line) of pristine (a) and irradiated (b) terphenyldimethanethiol on Au, along with the calculated density-of-states (dashed line) for a pair of the separate and cross-linked terphenyldimethanethiol molecules. The experimental HOMO-LUMO gaps are indicated. The photoemission spectra were taken with unpolarized He I (21.2 eV) light..

TPDMT films (Figure 2), which is consistent with theoretical calculation. The Fermi level placement, within the HOMO-LUMO gap suggests that strongly irradiated TPDMT films are more n-type insulating systems than the pristine TPDMT SAMs, and both molecular films have an electron structure consistent with a wide band gap insulator. The 2 dimensional quasi-polymerization of TPDMT forms a dielectric barrier that can be better characterized than a polymerized benzene barrier layer [2].

#### References:

- [1] D.-Q. Feng, D. Wisbey, Ya. B. Losovyj, Y. Tai, M. Zharnikov, P.A. Dowben, *Phys. Rev. B* **74** (2006) 165425; November 13, 2006 issue of *Virtual Journal of Nanoscale Science & Technology*
- [2] D.-Q. Feng, Ya.B. Losovyj, Y.Tai, M. Zharnikov, and P.A. Dowben, *J. Materials Chemistry* **16** (2006) 4343-434

## Valence structure of V[TCNE]

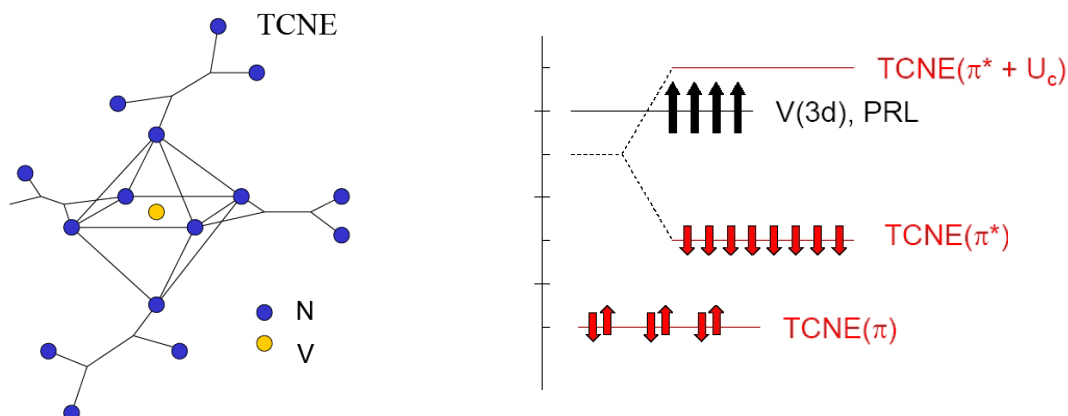
**A.N. Caruso<sup>1</sup>, Konstantin I. Pokhodnya and Joel S. Miller**

<sup>1</sup>Center for Nanoscale Science and Engineering, North Dakota State University,  
Fargo, ND 58102 (NDSU-AC0707) [anthony.caruso@ndsu.edu](mailto:anthony.caruso@ndsu.edu)

<sup>2</sup>Department of Chemistry, University of Utah, Salt Lake City, UT 84112

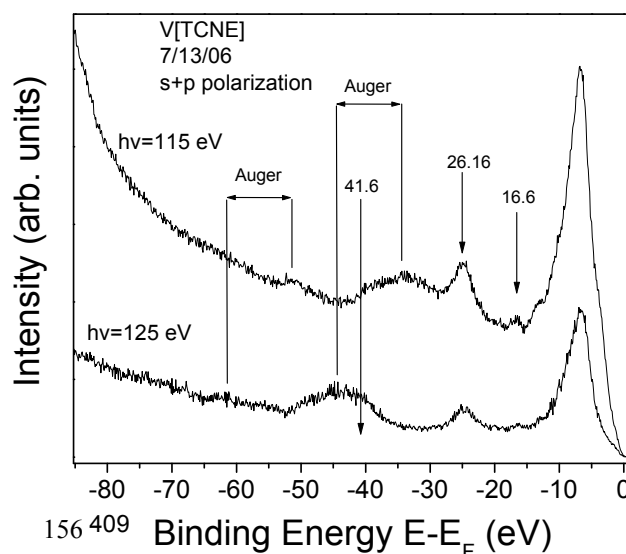
Room temperature remnant moments in thin film metal-organic materials (albeit few) is now reproducible. The use of such films in functional magnetic and spintronic devices have been limited due not only to the difficulty in fabricating the films and their atmospheric stability, but further, in the lack of understanding of their magnetic origin and determination of spin polarization. In order to progress in the development and utilization of organic and metal-organic materials in magnetic and spintronic devices, basic studies (i.e. spin polarized photoemission) must be completed to help reveal: (1) the mechanism(s) responsible for exchange; (2) where in binding energy the exchange occurs; and, (3) the raw polarization at the Fermi level.

In analogy with the importance of organic materials (i.e. conducting polymers, self-assembled monolayers) toward classical electronic applications are those organic and metal-organic materials being developed for magnetic and spintronic applications. The organic nature signifies the synthetic flexibility to easily tune the material, low density, typically inexpensive and efficient with regard to spin polarized electron transfer due to low hyperfine and small spin-orbit interaction. From a basic view there is a lack of understanding with regard to the exchange between metal centers through free radical or neutral organic ligands. Specifically there is a lack of understanding regarding the role of: (1) orbital orthogonality; (2) electron-phonon coupling; (3) conjugation; and, (4) degree of localization. Temperature dependent valence band spin polarized photoemission will indeed help understand, guide and corroborate theoretical predictions regarding the above questions, which ultimately hold the key to further development of this tremendously important and significant area in both the basic and applied communities.



**Figure 1.** (LEFT) Octahedrally coordinated vanadium(II) with TCNE linkages which support stable polarons. (RIGHT) Antiferromagnetic exchange leading to ferrimagnetism with fully spin polarized V band crossing  $E_F$ .

study of vanadium tetracyanoethylene or V[TCNE]. V[TCNE] was the first organic-based magnet to demonstrate a remnant moment above room temperature, as completed by the Miller group in 1991 [1] and provided in thin film form in 2000 [2]. For the V[TCNE], the mechanisms of both superexchange and double exchange have been reported wherein a free radical on the TCNE exists as the medium of exchange between vanadium centers (Figure 1). Due to the antiferromagnetic exchange between the carbon polarons and V(II), a distinct splitting should exist that is resolvable by photoemission. Such a simple study, prior to spin polarized photoemission is important as it provides the pragmatic tools such as photon energy, polarization and mounting procedures; especially for V[TCNE] which is pyrophoric and must be transferred under <1ppm of oxygen and water. Below (Figure 2) are shallow core photoemission demonstrating the oxygen free transfer of the thin films (no peak at -41.6 eV and no oxide shoulder on the V 3p) along with other photoemission lines which we have yet to account for. The V 3p binding energy position is roughly 2 eV higher in binding energy than expected for atomic V 3p indicating a very strong bond (increased binding energy) with the coordinating TCNE which helps further corroborate the superexchange mechanism. An LDA calculation demonstrating the orbitals, their delocalization and respective binding energy positions, backed up with resonant photoemission at the carbon and nitrogen edge, would be a great next step to further the superexchange understanding.



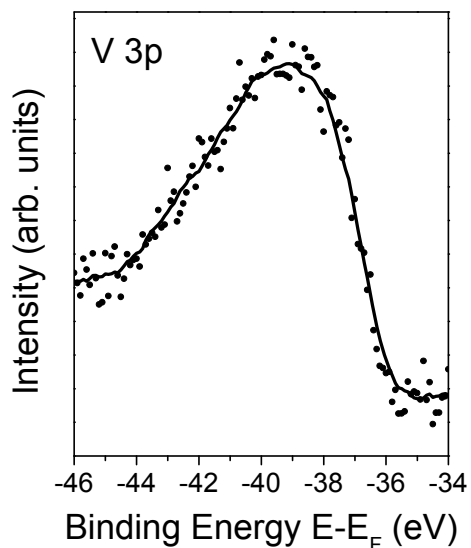


**Figure 2.** Shallow core photoemission of V[TCNE] on evaporated Au completed with normally collected photoelectrons and incident s+p polarization.

While measuring the valence band spectra, it was reproducibly apparent that the beam was not only causing decomposition, but also some charging. Future experiments will include thinner films grown in situ so as to eliminate both the charging and any oxidation.

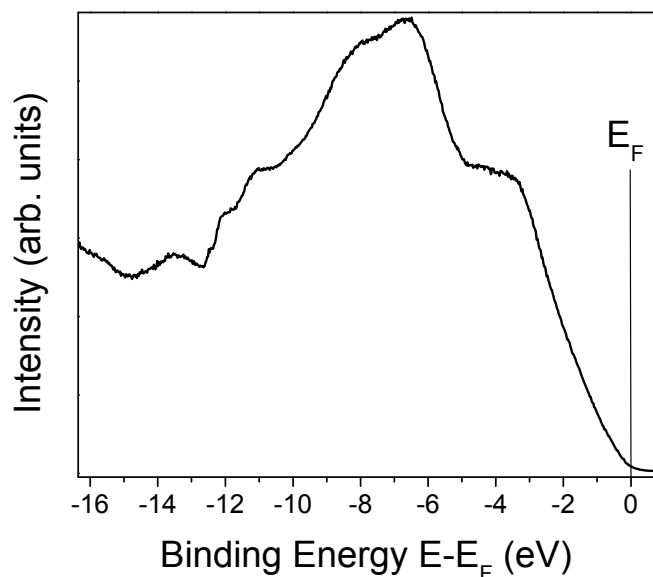


**Figure 3.** Valence band photoemission completed with s+p incident light at 32 eV and 300 K.

[1] Juan M. Manriquez, Gordon T. Yee, R. Scott McLean, Arthur J. Epstein and Joel S. Miller, *Science* **252** (1991) 1415

[2] Konstantin I. Pokhodnya, Arthur J. Epstein and Joel S. Miller, *Adv. Mat.* **12** (2000) 410

The above data was collected at the Center for Advanced Microstructures and Devices synchrotron radiation facility in Baton Rouge, LA on beamline 6B1. This work was supported by the Defense Microelectronics Activity (DMEA) under agreement DMEA90-02-2-0218 and the NSF through ND EPSCoR grant EPS-0447679.



## The Electronic Band Structure of CoS<sub>2</sub> (UN-PD1205-1 and UM-CL-1206)

Ning Wu<sup>1</sup>, Ya. B. Losovyj<sup>1,2</sup>, David Wisbey<sup>1</sup>, K. Belashchenko<sup>1</sup>, M. Manno<sup>3</sup>, L. Wang<sup>3</sup>,  
C. Leighton<sup>3</sup>, and P.A. Dowben<sup>1</sup>

1) Dept. of Physics and Astronomy and the Nebraska Center for Materials and  
Nanoscience, University of Nebraska-Lincoln, Lincoln, NE 68588-0111

2) Center for Advanced Microstructures and Devices, Louisiana State University, 6980  
Jefferson Highway, Baton Rouge, LA 70806

3) Department of Chemical Engineering and Materials Science,  
University of Minnesota, Minneapolis, MN55455

The experimental electronic structure of nominally ground state half metallic systems remains of considerable interest as a platform for studying the interplay between high spin polarization and band structure. This attraction remains in spite of the growing recognition that true half metallic character may not be possible at finite temperatures due to magnons as well as zero temperature interactions. The experimental band structure of very few nominally half metallic systems have been investigated. These studies have been largely limited by experimental difficulties in preparing a surface suitable for photoemission. The pyrite-type transition metal compound CoS<sub>2</sub> is an itinerant electron

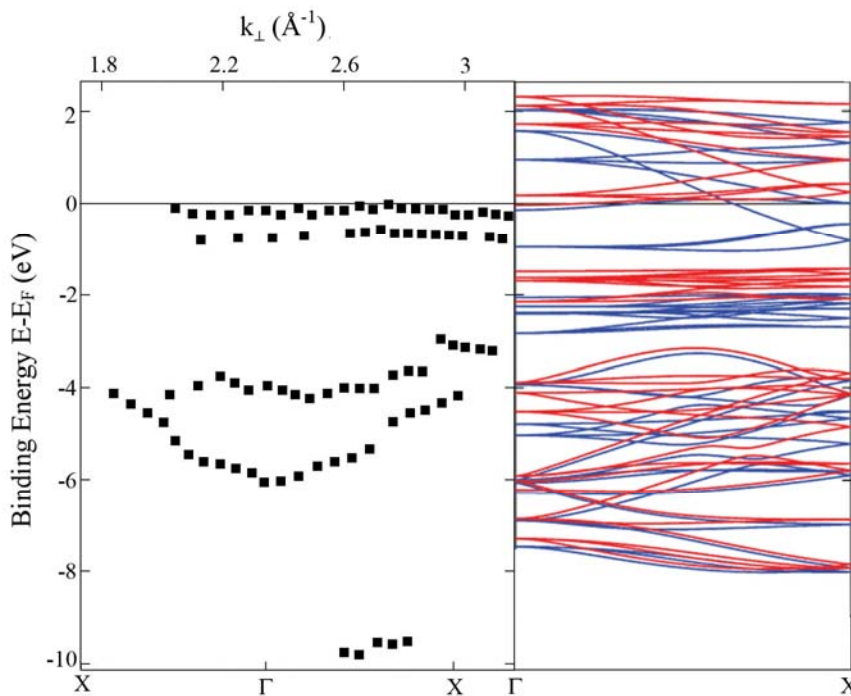


**Figure 1.** Experimental bulk band structure of CoS<sub>2</sub> along the <100> direction (left). The calculated bulk band structure (right). The blue curves are spin up (majority) bands and the red curves are the corresponding spin down (minority) states. For the experimental data, both critical points and the experimental wave vectors are identified.

ferromagnet. In ground state band structure calculations,  $\text{CoS}_2$  is predicted to be highly spin polarized and be at least close to existing as a half-metallic ferromagnet: i.e. a ferromagnet possessing only one spin channel for conduction.

We have identified a strong dispersing band of  $\text{CoS}_2(100)$ , with both sulfur and cobalt weight, along the  $\Gamma$ -X direction of the bulk Brillouin zone, from photon energy dependent angle resolved photoemission studies. From the critical points of the experimental band structure, the inner potential is estimated at about 4 to 5 eV, indicating that  $\text{CoS}_2$  has a narrow band width, consistent with the theoretical expectations [1].

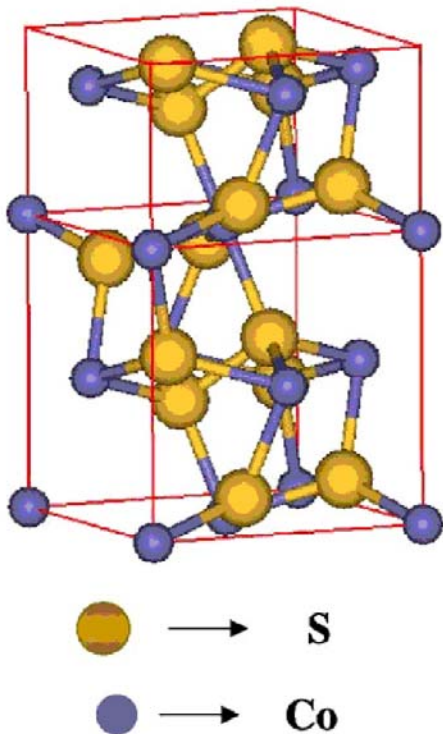


**Figure 2.** The cubic  $\text{CoS}_2(100)$ - $(1\times 1)$  surface.

Quantitative low-energy electron diffraction (LEED) has been used to determine the structure of the cubic  $\text{CoS}_2(100)$ - $(1\times 1)$  surface [2]. The clearly favored structural model from the LEED analysis is the 1S - terminated  $(1\times 1)$  surface, in which the S-S dimer is intact and the terminal surface layer retains a complete S-Co-S sandwich structure (Figure 2). The surface S atoms move outwards towards the vacuum while the subsurface Co atoms move towards the bulk, by approximately 0.03 and 0.11 Å, respectively. In addition, the S atoms in the third sublayer relax outwards by about 0.12 Å, thus providing an indication of a stronger S-S dimer bond and a denser surface region.

#### References:

- [1] Ning Wu, Ya. B. Losovyj, David Wisbey, K. Belashchenko, M. Manno, L. Wang, C. Leighton, and P.A. Dowben, "The Electronic Band Structure of  $\text{CoS}_2$ ", submitted to *J. Phys. Cond. Matter*
- [2] Z. X. Yu, M. A. Van Hove, S. Y. Tong, David Wisbey, Ya. B. Losovyj, Ning Wu, M. Manno, L. Wang, C. Leighton, W. N. Mei, and P.A. Dowben, "The structure of the  $\text{CoS}_2(100)$ - $(1\times 1)$  surface", submitted to *J. Phys. Cond. Matter*

## The stability and structure of adsorbed molecular spin 1/2 organometallic and metal organic complexes (UN-PD1206OR and NDSU-AC1205)

Jaewu Choi<sup>1,4</sup>, Jing Liu<sup>1</sup>, Jie Xiao<sup>1</sup>, Seok-Bong Choi<sup>2</sup>, P. Jeppson,<sup>1,2</sup> L. Jarabek<sup>2</sup>, Ya.B. Losovyj<sup>3</sup>, A.N. Caruso<sup>2\*</sup> and P.A. Dowben<sup>1\*</sup>

<sup>1</sup> Department of Physics and Astronomy and the Nebraska Center for Materials and Nanoscience, Behlen Laboratory of Physics, University of Nebraska-Lincoln, Lincoln, Nebraska, USA 68588-0111

<sup>2</sup> Center for Nanoscale Science and Engineering, North Dakota State University, Fargo, ND, USA 58102

<sup>3</sup> Center for Advanced Microstructures and Devices, Louisiana State University, 6980 Jefferson Highway, Baton Rouge, LA 70806

<sup>4</sup> Wayne State University, R3133 Engineering Bldg., Dept. of Electrical & Computer Engineering, 5050 Anthony Wayne Dr. #3100, Detroit, MI 48202

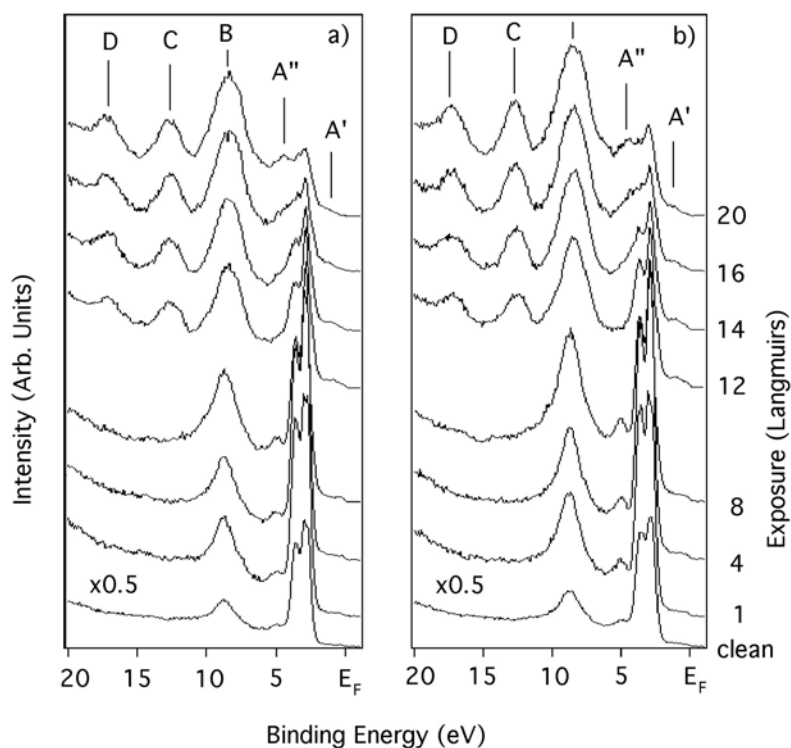


**Figure 1.** Coverage dependent angle-resolved photoemission spectra of cobaltocene on Cu(111) at 150 K. The photon energy of 36 eV and the photoelectrons are collected along the surface normal. The photoemission spectra were taken with s+p-polarized light (a) and more p-polarized light (b). The cobaltocene exposures are provided in units of Langmuirs (1L =  $1.0 \times 10^{-6}$  Torr.sec).

The stability and structure of adsorbed molecular spin 1/2 organometallic and metal organic complexes are seen to be either less stable, or adopt a lower point group symmetry. When comparing initial cobaltocene adsorption on Cu(111) with other adsorbed metallocenes, it seems fairly clear that cobaltocene is far less stable as a molecule on surfaces than ferrocene (Z-1) or nickelocene (Z+1). Unlike the other metallocenes, initial adsorption is dissociative (see the

Figure). Overall the big difference among these three metallocenes appears to be that the “nineteen electron” cobaltocene has a single unpaired electron resulting in a low ionization potential and facile decomposition [1]. With absorption other than end-on, nickelocene MUST adopt a singlet state as the off normal adsorption orientation has reduced the molecular symmetry to such an extent that a triplet state is simply not possible.

Similarly, while both Co(II) ( $s=1/2$ ) and Ni(II) ( $s=0$ ) tetramethyldibenzo-tetraazaannulene molecular electronic structures are very similar, when the molecules are adsorbed on Au(111), the Ni(II) adopts a high symmetry molecular configuration upon adsorption, with a strong preferential orientation [2].

References:

[1] Jaewu Choi and P.A. Dowben, *Surface Science* **600** (2006) 2997-3002

[2] Jing Liu, Jie Xiao, Seok-Bong Choi, P. Jeppson, L. Jarabek, Ya.B. Losovyj, A.N. Caruso and P.A. Dowben, *Journal of Physical Chemistry B* **110** (2006) 26180-26184

**The Electronic Structure of 1,7-PCB10H11 Molecular Films  
(UNL-SB1205, UNBD1203 and UNJB1203)**

Snjezana Balaz,<sup>1,2</sup> N.P. Platt,<sup>3</sup> Dimtcho I. Dimov,<sup>3</sup> N.M. Boag,<sup>1,3</sup> J.I. Brand,<sup>2</sup> Ya. B. Losovyj<sup>1,4</sup> and P.A. Dowben<sup>1</sup>

<sup>1</sup> Department of Physics and Astronomy and the Nebraska Center for Materials and Nanoscience, Behlen Laboratory of Physics, University of Nebraska, P.O. Box 880111, Lincoln, NE 68588-0111 U.S.A.

<sup>2</sup> College of Engineering and Technology, N245 Walter Scott Engineering Center, 17<sup>th</sup> & Vine Streets, University of Nebraska-Lincoln, Lincoln, Nebraska 68588-0511

<sup>3</sup> Functional Materials, Institute for Materials Research, Cockcroft Building, University of Salford, Salford M5 4WT, United Kingdom

<sup>4</sup> Center for Advanced Microstructures and Devices, Louisiana State University, 6980 Jefferson Highway, Baton Rouge, LA 70806

The electronic structure of the 1,7-PCB<sub>10</sub>H<sub>11</sub> molecular film is similar to that observed for adsorbed 1,2-PCB<sub>10</sub>H<sub>11</sub> [1]. Yet electronic structure (the increased HOMO-LUMO gap), sticking coefficient, and thermal stability of the film indicate the 1,7-PCB<sub>10</sub>H<sub>11</sub> molecular film is more stable than that of adsorbed 1,2-PCB<sub>10</sub>H<sub>11</sub> [2]. In spite of the fact that both molecules are isomers, when adsorbed these subtle differences indicating that the bonding within the molecular film different, and is most evident in the adoption of a Stranski-Krastanov growth mode for the 1,7-PCB<sub>10</sub>H<sub>11</sub> molecular film.

Given the closer distances of C-C, B-B and B-C bonds, identifying unique positions for carbon from the crystallographic data of orthocarborane (1,2-C<sub>2</sub>B<sub>10</sub>H<sub>12</sub>), metacarborane (1,7-C<sub>2</sub>B<sub>10</sub>H<sub>12</sub>), or paracarborane (1,12-C<sub>2</sub>B<sub>10</sub>H<sub>12</sub>) would present an even greater challenge than for 1,7-PCB<sub>10</sub>H<sub>11</sub>. Although the bulk crystal structure may differ from that found in thin films of 1,7-PCB<sub>10</sub>H<sub>11</sub>, we do have evidence of preferential orientation from light polarization dependent photoemission and strong evidence of band structure from angle-resolved photon energy dependent photoemission, with critical points that appear to be in agreement with the Figure.

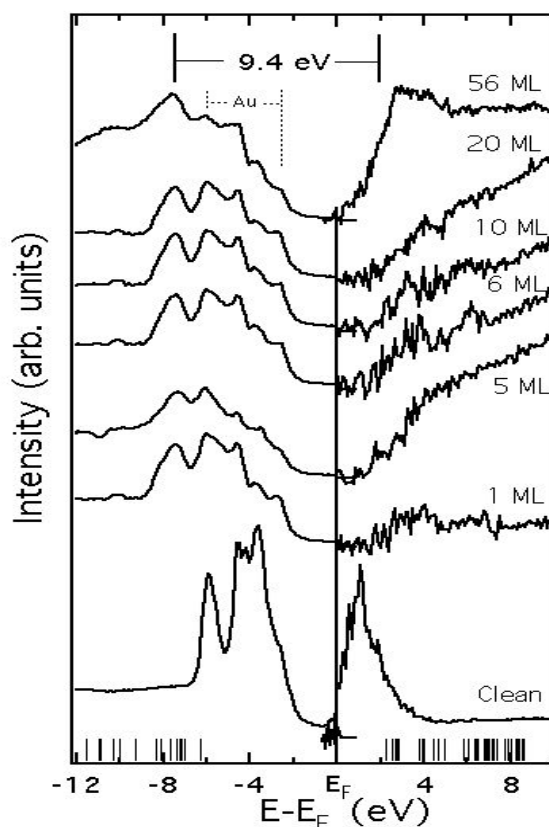
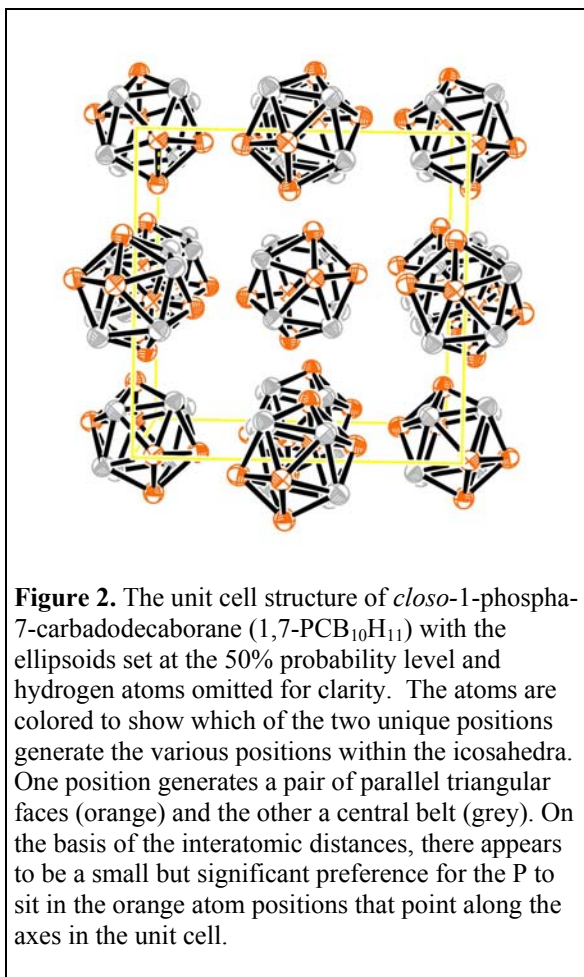


**Figure 1.** Normal emission photoemission (left) and normal incidence inverse photoemission (right) spectra of 1,7-PCB<sub>10</sub>H<sub>11</sub> on Au (111), as a function of coverage, in molecular monolayers (ML). The photoemission spectra were acquired with photon energy of 21.5 eV. Vertical lines, at the bottom of the figure, represent the theoretical molecular orbital binding energies and provide a HOMO-LUMO gap of 8.5 eV compared to the experimental HOMO-LUMO gap of 9.4 eV, as indicated.



## References:

[1] Snjezana Balaz, Dimtcho I. Dimov, N.M. Boag, Kyle Nelson, Benjamin Montag, J.I. Brand, and P.A. Dowben, *Appl. Phys. A* **84** (2006) 149-159

[2] Balaz, S.; Boag, N. M.; Platt, N. P.; Dimov, D. I.; Brand, J. I.; Dowben, P. A. *Mater. Res. Soc. Symp. Proc.* **2007**, in press.

## Comparison of the electronic structure of two polymers with strong dipole ordering (UN-PD1206PVDF)

Jie Xiao,<sup>1</sup> Luis G. Rosa,<sup>1</sup> Matt Poulsen,<sup>1</sup> D.-Q. Feng,<sup>1</sup> Sahadeva Reddy,<sup>2</sup> J.M. Takacs,<sup>2</sup>

Lei Cai,<sup>3</sup> Jiandi Zhang,<sup>3</sup> Stephen Ducharme<sup>1</sup> and P.A. Dowben<sup>1</sup>

1) Department of Physics and Astronomy and the Center for Materials Research and Analysis, Behlen Laboratory of Physics, University of Nebraska-Lincoln, Nebraska 68588-0111

2) Department of Chemistry, 316 Hamilton Hall, University of Nebraska-Lincoln, Nebraska 68588-0304

3) Department of Physics, Florida International University, Miami, Florida 33199

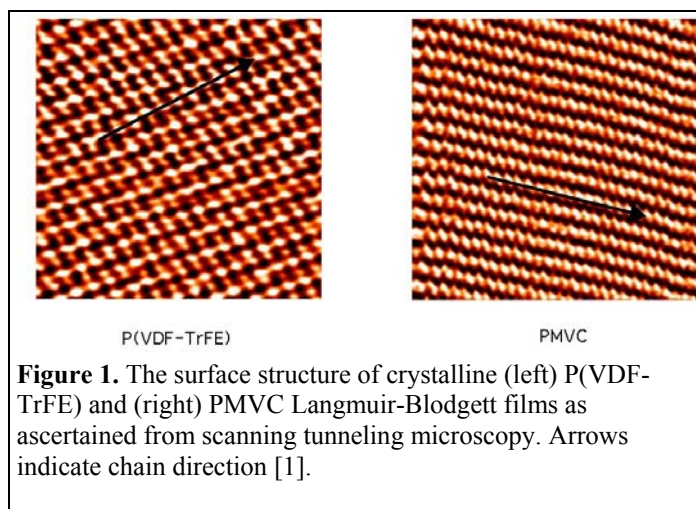


**Figure 1.** The surface structure of crystalline (left) P(VDF-TrFE) and (right) PMVC Langmuir-Blodgett films as ascertained from scanning tunneling microscopy. Arrows indicate chain direction [1].

Two different polymers, with large local electric dipoles, have been compared: copolymers of polyvinylidene fluoride with trifluoroethylene P(VDF-TrFE, 70%:30%) and polymethylvinylidenecyanide (PMVC). Poly(vinylidene fluoride) [PVDF,  $-(\text{CH}_2\text{-CF}_2)_n-$ ] copolymers with trifluoroethylene [TrFE,  $-(\text{CHF-CF}_2)-$ ] can form highly ordered crystalline ferroelectric polymer ultrathin films as has been demonstrated by x-ray and

neutron scattering, scanning tunneling microscopy (Figure 1), low energy electron diffraction and band mapping (Figure 2). Although not always evident in scanning tunneling microscopy, the band structure shows a characteristic super-periodicity dominated by  $-(\text{CH}_2\text{-CF}_2)_2-$  or  $-(\text{CH}_2\text{-CF}_2)-(\text{CHF-CF}_2)-$  “dimer” pairs in the ferroelectric phase. The copolymer P(VDF-TrFE, 70:30), in spite of the low overall symmetry does show all the characteristics of high local symmetry and symmetry selection rules. The effects are quite significant in photoemission and electron energy loss spectroscopy. By comparing the copolymer P(VDF-TrFE, 70:30) to the highly dipole-ordered polymer polymethylvinylidenecyanide (PMVC), we can see the influence of local point group symmetry on the intra-molecular band structure. The results summarized here show that PMVC  $-(\text{CH}(\text{CH}_3)\text{-C}(\text{CN})_2)_n-$  has a much lower local point group symmetry than poly(vinylidene fluoride), although not a copolymer system. While the different local point group symmetries play a key role, both crystalline polymers exhibit intra-molecular band structure, though the Brillouin zone critical points differ (Figure 2) [1].



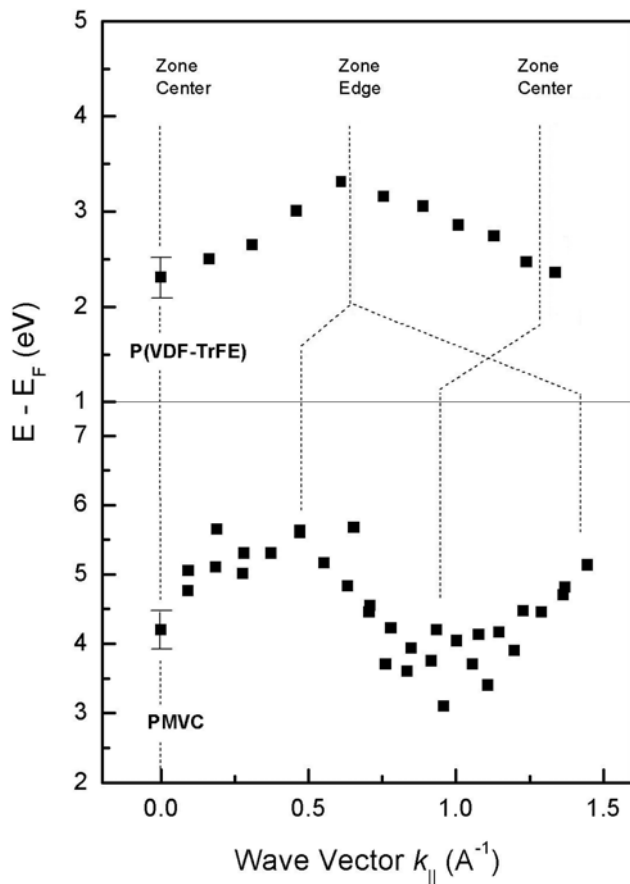


**Figure 2.** The band dispersion, from angle-resolved inverse photoemission, of the unoccupied feature closest to the Fermi level, along the polymer chains. The dashed lines indicate the different positions of the Brillouin zone centers and Brillouin zone edges between P(VDF-TrFE) copolymer and PMVC.

## References:

1. Jie Xiao, Luis G. Rosa, Matt Poulsen, D.-Q. Feng, Sahadeva Reddy, J.M. Takacs, Lei Cai, Jiandi Zhang, Stephen Ducharme and P.A. Dowben, *J. Phys. Cond. Matter* **18** (2006) L155-L161
2. Luis G. Rosa, P.A. Jacobson, and P.A. Dowben, *J. Phys. Chem. B* **110** (2006) 7944-7950

# The Influence of the Molecular Dipole on the Electronic Structure of Isomeric Icosahedral Dicarbadodecaborane and Phosphacarbadodecaborane Molecular Films

(UNL-SB1205, UNBD1203 and UNJB1203)

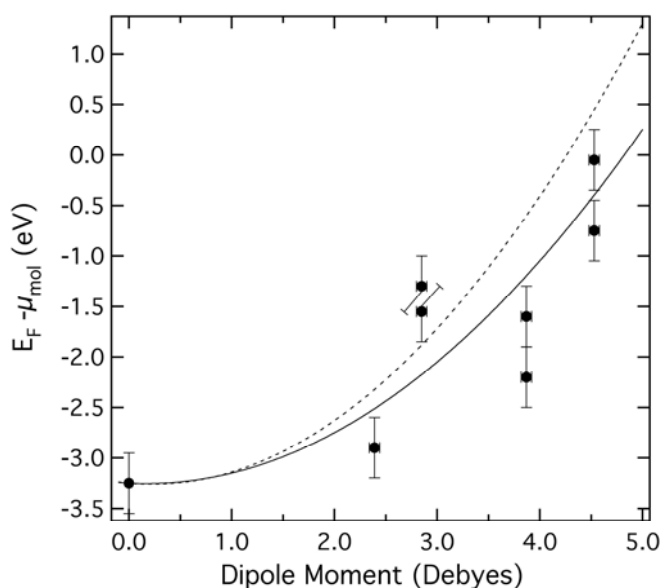
Snjezana Balaz,<sup>1,2</sup> A.N. Caruso,<sup>1</sup> N.P. Platt,<sup>3</sup> Dimtcho I. Dimov,<sup>3</sup> N.M. Boag,<sup>1,3</sup> J.I. Brand,<sup>2</sup> Ya. B. Losovyj,<sup>1,4</sup> and P.A. Dowben<sup>1</sup>

<sup>1</sup> Department of Physics and Astronomy and the Nebraska Center for Materials and Nanoscience, Behlen Laboratory of Physics, University of Nebraska, P.O. Box 880111, Lincoln, NE 68588-0111 U.S.A.

<sup>2</sup> College of Engineering and Technology, N245 Walter Scott Engineering Center, 17<sup>th</sup> & Vine Streets, University of Nebraska-Lincoln, Lincoln, Nebraska 68588-0511

<sup>3</sup> Functional Materials, Institute for Materials Research, Cockcroft Building, University of Salford, Salford M5 4WT, United Kingdom

<sup>4</sup> Center for Advanced Microstructures and Devices, Louisiana State University, 6980 Jefferson Highway, Baton Rouge, LA 70806



Chemical potential shift (experimental HOMO-LUMO midgap points) of each carborane with respect to the Fermi level of the substrate as a function of the experimental molecular dipole moment.

While the experimental electronic structure from combined photoemission and inverse photoemission studies of the molecular films are in good agreement with semi-empirical calculations for the isolated molecule, there is a shift in the chemical potential for each molecule (see Figure). The experimental position of the molecular chemical potential implicates an influence of both interface and adsorbate dipole.

The smaller the adsorbate dipole of each *closo*-carborane, the closer the placement of the substrate Fermi level to the lowest unoccupied adsorbate molecular

We have compared the molecular films of three different isomers of *closo*-dicarbadodecaborane (orthocarborane (1,2-C<sub>2</sub>B<sub>10</sub>H<sub>12</sub>), metacarborane (1,7-C<sub>2</sub>B<sub>10</sub>H<sub>12</sub>), paracarborane (1,12-C<sub>2</sub>B<sub>10</sub>H<sub>12</sub>)) and two related icosahedral cage molecules, 1-phospha-2-carbadodecaborane (1,2-PCB<sub>10</sub>H<sub>11</sub>) and 1-phospha-7-carbadodecaborane (1,7-PCB<sub>10</sub>H<sub>11</sub>) adsorbed on a variety of substrates. While the experimental electronic structure from combined photoemission and inverse photoemission studies of the molecular films are in good agreement with semi-empirical calculations for the isolated

orbital. By plotting the center of the adsorbate HOMO-LUMO gap with respect to the substrate Fermi level, we see that this energy shift generally follows the permanent dipole moment of the adsorbate. In other words, the molecular chemical potential is altered by different interactions upon adsorption, and this interaction leads to differences in the energy level alignment with respect to the Fermi energy of the substrate (Figure). This has been predicted in other molecular adsorbates and should follow the potential shift due to dipolar interactions i.e.

$$E_{\text{int}}^{\text{dip}}(R) = k \frac{\mu^2}{R^3} \quad (1)$$

where  $\mu^2$  is the dipole moment. Deviations from this  $\mu^2$  relationship can occur because of a dipole cant away from the surface normal, difference in intermolecular interaction, strong substrate interactions (chemisorption) and the interface dipole caused by the different substrates. In spite of the complications, there is general agreement with expectations based on dipole interactions for adsorbates on conducting substrates. The agreement with the dipole model is imperfect because of dipole misorientation with respect to the surface normal, for which we have some additional indications.

## Catalysis and Energy Research

### X-ray Absorption Spectroscopy of Mixed Metal Iron-Based Fischer-Tropsch Catalysts

A. Roy<sup>1</sup>, A. Ignatov<sup>1</sup>, C. Bianchetti<sup>1</sup>, G. Merchan<sup>1</sup>, R. Louis<sup>1</sup>, A. Campos<sup>2</sup>, J.J. Spivey<sup>2</sup>, N. Lohitharn<sup>3</sup>, J. Goodwin<sup>3</sup>; <sup>1</sup>Center for Advanced Microstructures and Devices, Louisiana State University, Baton Rouge, Louisiana 70806; <sup>2</sup>Department of Chemical Engineering, Louisiana State University, Baton Rouge, LA 70803; <sup>3</sup>Department of Chemical and Biomolecular Engineering, Clemson University, 127 Earle Hall, Clemson, SC 29634-0909; E-mail: acampo2@lsu.edu; PRN Number: ChemE-JS-1206

An ongoing collaborative effort between Clemson University and Louisiana State University to give a “birth-to-death” study of various mixed metal iron-based Fischer-Tropsch catalysts that began in December of 2005. The goal of the study is to correlate catalyst activity/stability studies obtained from Clemson University with structural studies at CAMD in order to give a unique understanding of the evolution of the catalysts. Research in CAMD in 2006 included *ex situ* studies of various central atoms (Fe, Cu, Mo, etc.) in each of the catalysts (Table I).

<b>Catalyst tested in parts by weight (synthesized in Clemson University laboratories):</b>
100 Fe / 5 Cu / 17 Si (calcined 300°C 5h)
100 Fe / 5 Cu / 17 Si pretreat in CO @ 280 °C 12 h & passivate in O <sub>2</sub>
100 Fe / 5 Cu / 4.2 K / 11 SiO <sub>2</sub> (calcined)
100 Fe / 5 Cu / 4.2 K / 11 SiO <sub>2</sub> (calcined) CO pretreat @ 280 °C 12h & passivate in O <sub>2</sub> for 1 h
90 Fe / 10 Mo / 5 Cu / 17 Si (calcined 300 °C 5h)
90 Fe / 10 Mo / 5 Cu / 17 Si (calcined) CO pretreat @ 280 °C + O <sub>2</sub> passivate
95 Fe / 5 Cr / 5 Cu / 17 Si sieved < 45 μm calcined @ 300 °C 5h
90 Fe / 10 Cr / 5 Cu / 17 Si CO pretreat @ 280 °C 12h & passivate in O <sub>2</sub> for 1h
90 Fe / 10 Cr / 5 Cu / 17 Si (calcined 300 °C 5h)
90 Fe / 10 W / 5 Cu / 17 Si calcined + CO pretreat
90 Fe / 10 W / 5 Cu / 17 Si calcined @ 300°C 5h
90 Fe / 10 W / 5 Cu / 17 Si (calcined) CO pretreat @ 280 °C 12 h + O <sub>2</sub> passivate
90 Fe / 10 W / 5 Cu / 17 Si prepared from WCl calcined @ 300 °C 5h *
95 Fe / 5 Zr / 5 Cu / 17 Si sieved < 90 μm calcine @ 300 °C 5h *
95 Fe / 5 Mn / 5 Cu / 17 Si calcined in air 300 °C 5h 45-90 μm *
* denotes newly synthesized (not tested yet)

Table I – Catalysts synthesized in Clemson University

Tests run on March 20-23 were electron yield experiments on the k-edge of Fe that have surface specific information of the catalysts. Figure 1 demonstrates that qualitative information in the XANES data in which two identical catalysts (except for the preparation techniques) have different oxidation states. The figure illustrates that a passivated sample has a lower oxidation state than the calcined sample (which is to be expected). In addition, semi-quantitative information can be obtained using a linear combination fit of known standards to evaluate the relative percentages of phases present in the sample using the XAFS software Athena [5]. Transmission experiments on March 23-24 transmission experiments will give bulk structural information on the k-edge of Fe

to learn about the bulk structure of the catalyst, which is expected to be different from the surface, therefore future data analysis will be made comparing the surface structure to the bulk structure.

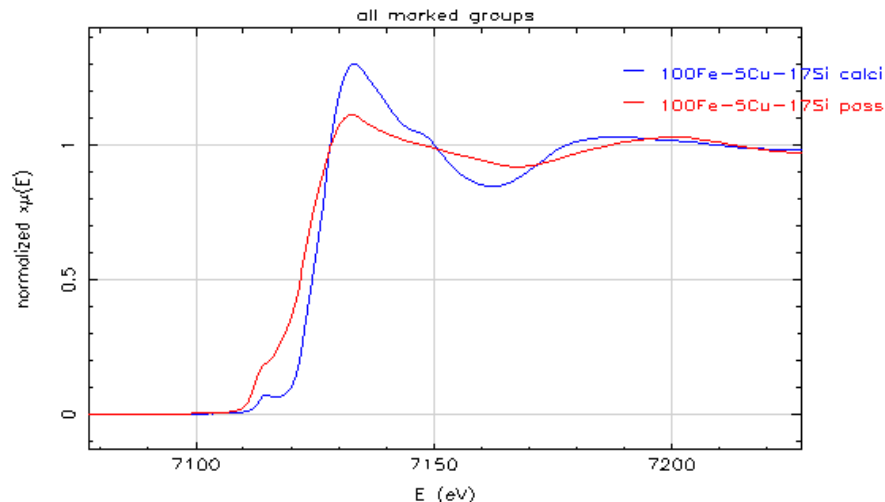


Figure 1 – Normalized XANES electron yield data in Athena for the Fe k-edge

Electron yield data for Cu (Figure 2) is interesting since it was desirable to have Cu not on the surface, therefore a low signal-to-noise ratio means that the Cu catalyst is mainly in the bulk of the catalyst since transmission tests of the Cu had a sufficient signal-to-noise ratio.

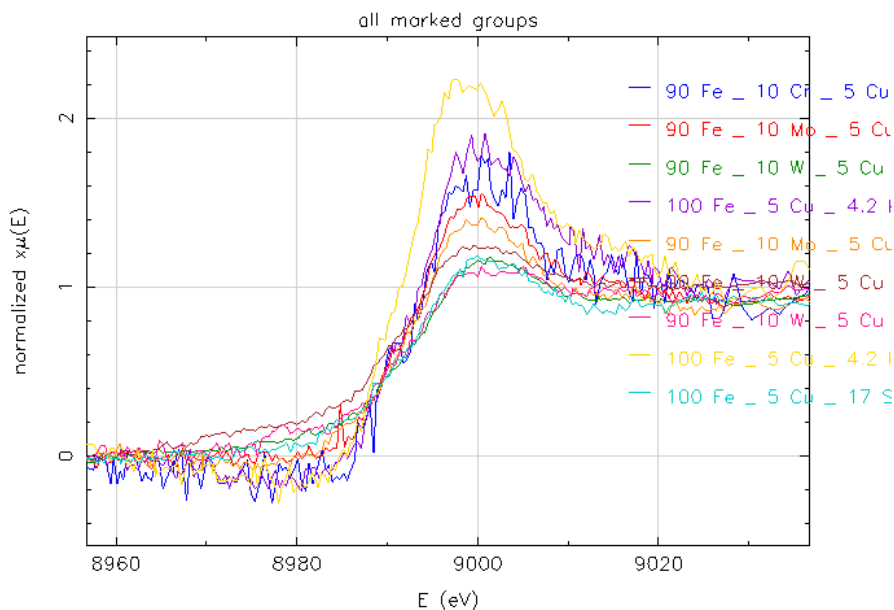


Figure 2 – Normalized XANES electron yield data in Athena for the Cu k-edge

Data analysis is still in progress for these spectra, and it will be very interesting to see the results since qualitative XANES spectra show that there are differences among the catalysts. The EXAFS region of the catalysts will give coordination numbers, Debye-Waller factors, and bond distances for at least the first shell in the Fourier transform [1, 3-4]. The *ex situ* studies of the catalysts will also give insight as to the time-evolution of catalysts when *in situ* studies occur since the active phase in Fe-based Fischer-Tropsch Synthesis is believed to be the carbide phase [2].

#### References

- [1] Chao, K.-j. and A. C. Wei (2001). "Characterization of heterogeneous catalysts by X-ray absorption spectroscopy." Journal of Electron Spectroscopy and Related Phenomena **119**(2-3): 175-184.
- [2] Jin, Y. and A. K. Datye (2000). "Phase Transformations in Iron Fischer-Tropsch Catalysts during Temperature-Programmed Reduction." Journal of Catalysis **196**(1): 8-17.
- [3] Greaves, G. N. (1988). "EXAFS and the structure of catalysts." Catalysis Today **2**(5): 581-584.
- [4] Gurman, S. (1995). "Interpretation of EXAFS Data." Journal of Synchrotron Radiation **2**(1): 56-63.
- [5] Ravel, B. and M. Newville (2005). ATHENA, ARTEMIS, HEPHAESTUS: data analysis for X-ray absorption spectroscopy using IFEFFIT. Journal of Synchrotron Radiation. **12**: 537-541.

## X-ray Absorption Spectroscopy of $\text{Zn}_2\text{TiO}_4$

A. Roy<sup>1</sup>, A. Ignatov<sup>1</sup>, G. Merchan<sup>1</sup>, A. Campos<sup>2</sup>, J.J. Spivey<sup>2</sup>, R. Rees<sup>3</sup>, H. Tian<sup>3</sup>;  
<sup>1</sup>Center for Advanced Microstructures and Devices, Louisiana State University, Baton Rouge, Louisiana 70806; <sup>2</sup>Department of Chemical Engineering, Louisiana State University, Baton Rouge, LA 70803; <sup>3</sup>Department of Chemical and Petroleum Engineering; Room 1249 Benedum Hall; University of Pittsburgh; Pittsburgh, PA 15261;  
 E-mail: acampo2@lsu.edu; PRN Number: ChemE-JS-????

Where the project stands: Catalysts synthesized by the University of Pittsburgh are being structurally studied by the bulk structure of zinc orthotitanate (ZTO or  $\text{Zn}_2\text{TiO}_4$ ) by using multiple methods including DFT calculations (U. of Pitt.), high resolution XRD (U. of Pitt.), and EXAFS in transmission (LSU). The LSU group has completed the scans of the k-edges of Zn and Ti, which are in Figures 1 and 2, respectively. In the XAFS reduction software Athena [1] the data was normalized in  $\mu(E)$ , which shows that both samples are similar in chemical structure from the similarities in the XANES spectra.

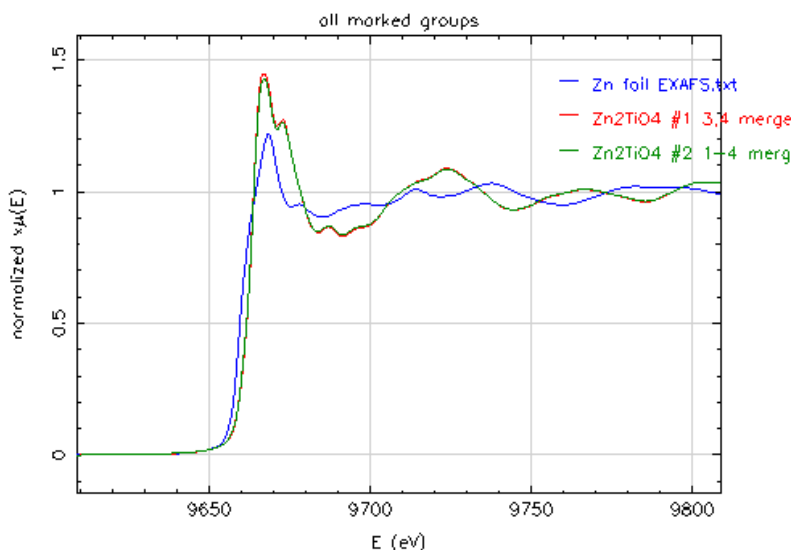


Figure 1 – Zn k-edge XANES scan for  $\text{Zn}_2\text{TiO}_4$  samples

What's next: The three main questions to be answered from the EXAFS analysis are: 1) The bulk atomic distribution of nearest and next nearest neighbor distances for the following pairs of species: Zn-Zn, Zn-Ti, and Ti-Ti. 2) The distribution of coordination types by species (how many different coordinations of Zn-Ti, Zn-O, Ti-O are there and what are their relative percentages) for each species in the material. 3) How many different oxygen bonds exist, how do they connect with Zn and Ti, as well as the coordination structure of oxygen.

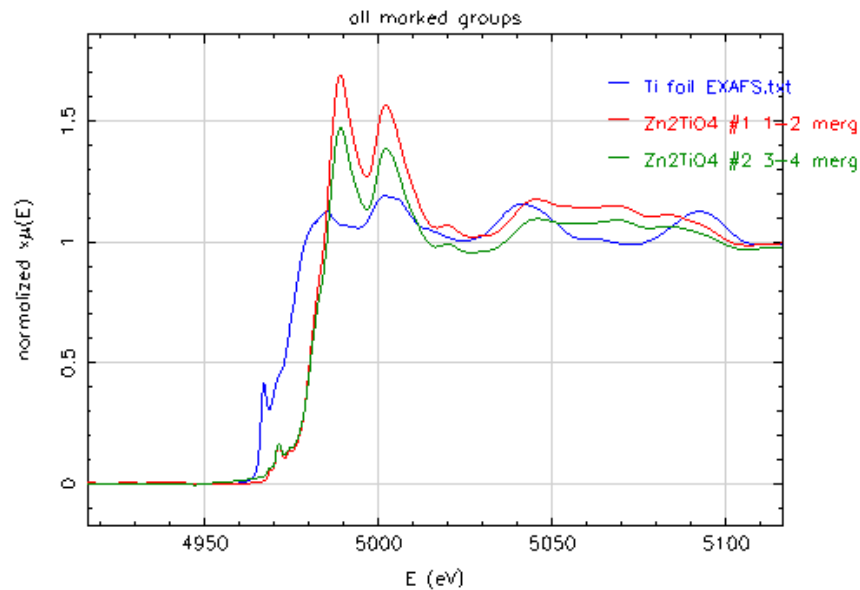


Figure 2 – Ti k-edge XANES scan for  $\text{Zn}_2\text{TiO}_4$  samples

The current goal is to complete the EXAFS data analysis. With careful data analysis, the EXAFS data will answer these questions. Proposing a model for the data fitting in Artemis will take careful planning and will be refined based on fitting results due the complexity of the spinel structure [2, 4-5]. Millard et. al. used x-ray diffraction and  $^{17}\text{O}$  MAS NMR to propose a structure for  $\text{Zn}_2\text{TiO}_4$  which be used as the first model for fitting (Figure 3) [4]. Researchers from the University of Pittsburgh will use EXAFS results to compare and supplement the DFT calculations.

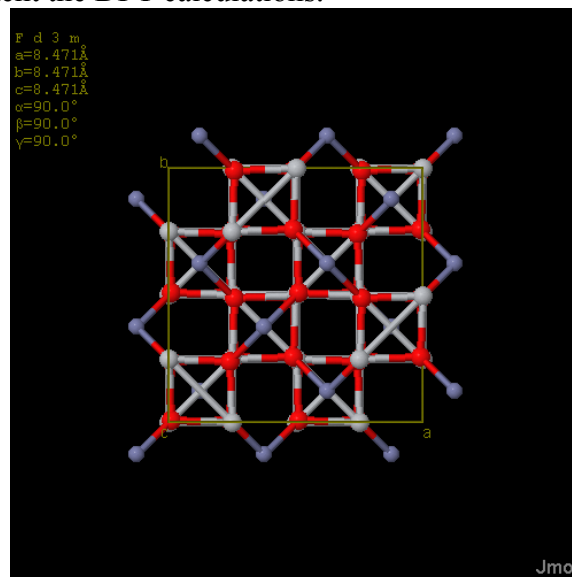


Figure 3 – Proposed preliminary structure for ZTO structures fitting in Artemis [3]

References:

- [1] Ravel, B. and M. Newville, *ATHENA, ARTEMIS, HEPHAESTUS: data analysis for X-ray absorption spectroscopy using IFEFFIT*, in *Journal of Synchrotron Radiation*. 2005. p. 537-541.



- [2] Bartram, S. and R. Slepetyts, *Compound Formation and Crystal Structure in the System ZnO-TiO<sub>2</sub>*. Journal of the American Ceramic Society, 1961. 44(10): p. 493-499.
- [3] Non-specified, *Spinel*. 2006, American Mineralogist Crystal Structure Database.
- [4] Millard, R. and R. Peterson, *Study of the cubic to tetragonal transition in Mg<sub>2</sub>TiO<sub>4</sub> and Zn<sub>2</sub>TiO<sub>4</sub> spinels by <sup>17</sup>O NMR and Rietveld refinement of X-ray diffraction data*. American Mineralogist, 1995. 80: p. 885-896.
- [5] Verwy, E.J.W. and E.L. Heilmann, *Physical Properties and Cation Arrangement of Oxides with Spinel Structures*. The Journal of Chemical Physics, 1947. 15(4): p. 174-180.

## New Catalysts for Methylketone Manufacture

Kerry Dooley<sup>1</sup>, Amitava Roy\*, Craig Plaisance

Louisiana State University, Gordon A & Mary Cain Department of Chemical Engineering, Baton Rouge, LA 70808 USA and \*Center for Advanced Microstructures & Devices 6980 Jefferson Hwy., Baton Rouge, LA 70806 USA

E-mail: [dooley@lsu.edu](mailto:dooley@lsu.edu); PRN - ChE-KD0306

### INTRODUCTION

The aim of this work is the determination of electronic structure and coordination environment of Ce and dopant atoms in pure and doped (K, Co, Pd) mixed metal oxide catalysts used for the manufacture of methylketones by acid/acid and acid/aldehyde condensations. XANES and EXAFS spectra were collected at room temperature and at 420°C (a typical reaction temperature), in both inert and reducing environments.

X-ray absorption spectroscopy is a very useful technique for determining both the electronic structure and the structural environment of the absorbing atom. By tuning the X-ray energy it is possible to determine the fine structure at and above the absorption edges of the selected atom. The XANES (X-ray Absorption Near Edge Structure) region contains information about the energy levels and occupation of bands and local orbitals near the Fermi surface, and the EXAFS (Extended X-ray Absorption Fine structure) region gives information about the structure of the coordination shells.

We are also in the process of synthesizing mixed metal rare-earth oxides with mesopore structure that can serve as future supports in reforming catalysis. For example, biomass reforming will require larger average pore sizes than conventional reforming catalysts, and if the reforming is to be “autothermal”, higher temperatures. We are developing CeO<sub>2</sub>/other REO/Al<sub>2</sub>O<sub>3</sub> (other REO = La<sub>2</sub>O<sub>3</sub>, e.g.) mixed oxides with mesoporous structure and better hydrolytic stability at typical autothermal reforming temperatures (e.g., 1000-1200 K). One test of interest is simultaneous DSC/TGA at these high temperatures; we are currently performing such measurements at CAMD although we have yet to fully analyze the results.

### EXPERIMENTAL

XAS (X-ray Absorption Spectroscopy) measurements were conducted using beamlines of the electron storage ring (operating at 1.3 GeV and 100-200 mA) at the LSU Center for Advanced Microstructures and Devices (CAMD). Measurements were done at the Ce L<sub>III</sub>-edge and Co K-edge in transmission mode and at the Co K-edge and Pd L<sub>III</sub>-edge in fluorescence mode. Spectra in transmission mode were obtained using ionization chambers measuring the incident beam intensity before and the transmitted beam intensity after the sample cell; fluorescence spectra were taken using a 13-element Ge

detector array. A Si (111) monochromator was used to obtain Pd L<sub>III</sub>-edge spectra, while a Si (311) monochromator was used for Ce L<sub>III</sub>-edge and Co K-edge spectra.

Catalyst samples were mixed with boron nitride and pressed into wafers giving a baseline absorbance of 4–5. The wafers were placed into an XAS cell and heated to 420°C in N<sub>2</sub>, then scanned. A mixture of 10% H<sub>2</sub>/N<sub>2</sub> was then introduced into the cell for 15 min followed by another scan. Some samples were reduced for longer times. For Co-containing samples, the cell was then cooled to room temperature in N<sub>2</sub> for Co K-edge EXAFS. A XANES scan was taken in fluorescence mode at room temperature of the Pd L<sub>III</sub> edge for the Pd-containing samples (undiluted), supported on Kapton tape.

The Ce L<sub>III</sub> XANES reference was CeO<sub>2</sub> (Aldrich, 99.9%), calcined at 400°C. Other reference materials included Ce(III) acetate (Aldrich, 99.9%), Co foil, Co(II) oxide, Co(II, III) oxide (Aldrich, 99.8%), Pd foil and KCl. The energies were calibrated from references as follows: Ce L<sub>III</sub>, from the calcined CeO<sub>2</sub>, E<sub>0</sub> = 5730 eV [1]; Co K, from Co foil; Pd L<sub>III</sub>, from Pd foil.

## RESULTS AND INTERPRETATION

The coordination environment of Ce was explored using XANES. A 10% H<sub>2</sub>/N<sub>2</sub> mixture simulated the reducing atmosphere of hydrocarbon reactants. XANES spectra for the standards Ce(III) acetate and CeO<sub>2</sub> are shown in Figure 1. A comprehensive review of the XANES is given by Fernandez-Garcia [2]. For Ce(III) acetate the spectrum is dominated by one white line at 5726 eV; for CeO<sub>2</sub> the white line is split into two peaks ca. 5730 and 5738 eV (formally 2p<sub>3/2</sub> to 5d excitation), with a shoulder at 5726 eV. For Ce(IV), the intensity of the lower energy peak is about 50% lower compared to Ce(III). The height of the second peak increases proportionally with CeO<sub>2</sub> content [3].

While the shoulder at 5726 eV in CeO<sub>2</sub> has sometimes been assigned to oxygen vacancies [4], in oxidized CeO<sub>2</sub> it is more likely due to crystal-field splitting of Ce 5d states [5,6]. The two white lines reflect a mixed valence final state of Ce(IV) [6,7]. In the lower energy state, labeled in Fig. 1 as 2p<sub>5</sub>4f<sub>1</sub>5d<sub>1v</sub>, an electron occupies the 4f orbital and a hole is present in the valence band. The other higher energy state, 2p<sub>5</sub>4f<sub>0</sub>5d<sub>1</sub> arises from an empty 4f orbital and an additional electron in the valence band. When an oxygen vacancy exists in CeO<sub>2</sub>, an electron occupies the 4f orbital on two neighboring Ce atoms. The 4f orbital dehybridizes and its electron excites to the valence band. The final state of Ce is no longer of mixed valence, so only one white line (2p<sup>5</sup>4f<sup>1</sup>5d<sup>1</sup>) is present (Fig. 1).

Normalized Ce L<sub>III</sub> XANES spectra of the CeO<sub>2</sub>/Al<sub>2</sub>O<sub>3</sub> catalysts are shown in Figure 2. The catalyst containing 0.8% Pd has a higher intensity peak corresponding to Ce(III) than does the undoped sample, while the catalyst containing 2.4% Co has a lower intensity peak; for 0.8% Co the change in peak height is small. For the K-containing samples (not shown here), the peak heights corresponding to Ce(III) were lower.

Two methods were used to estimate the number of oxygen vacancies from the XANES data: (1) the method of Takahashi et al.[8]; (2) linear fits using the WinXAS package [9]. Takahashi et al. derived a linear correlation between relative peak areas and relative amount of Ce(III) in Ce(III)/Ce(IV) physical mixtures. Following normalization

and background removal [9], each white line was fitted with a Lorentzian and an arctangent as shown in Fig. 1. Three parameters were fitted, the edge position and the amplitudes of Ce(III) and Ce(IV). It is assumed that the XANES spectrum of a Ce(III) atom (oxygen vacancy) and that of Ce(IV) are both similar to salt standards. But the shoulder present in CeO<sub>2</sub> due to the crystal field is not present in the Ce(IV) salt, so the amount of Ce(III) in supported CeO<sub>x</sub> will be overestimated by this method.

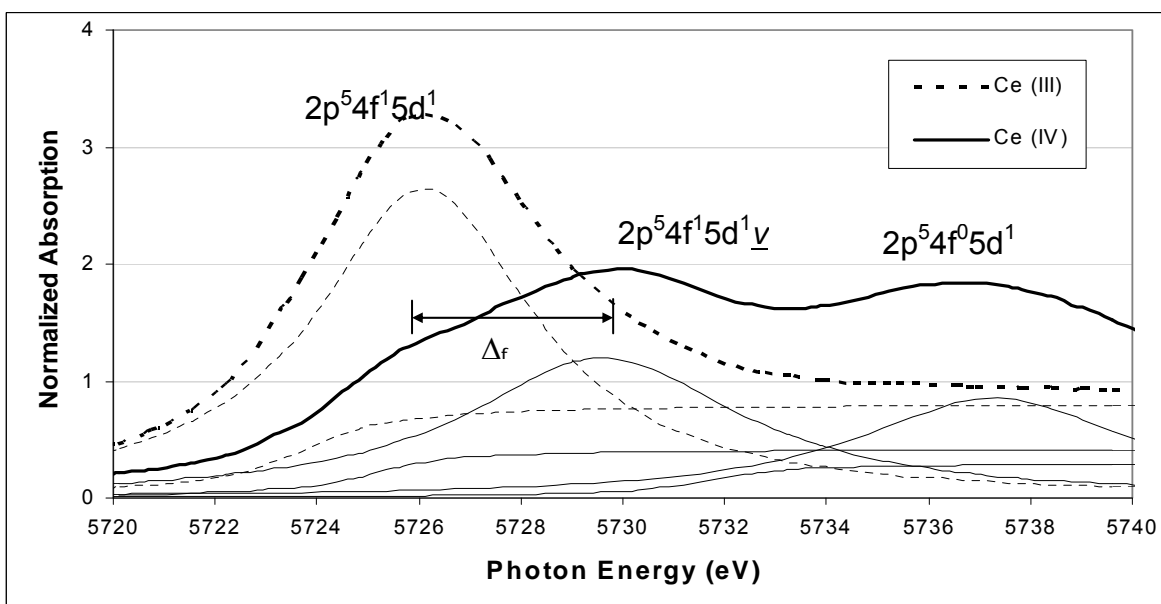


**Figure 1.** Ce L<sub>III</sub> XANES spectra of CeO<sub>2</sub> and Ce<sub>III</sub> acetate. The peaks are labeled with the corresponding excitation, and the crystal field splitting of the d orbitals is shown as  $\Delta_f$ . The Lorentzian and arctangent functions used in the Takahashi method are also shown for each peak.

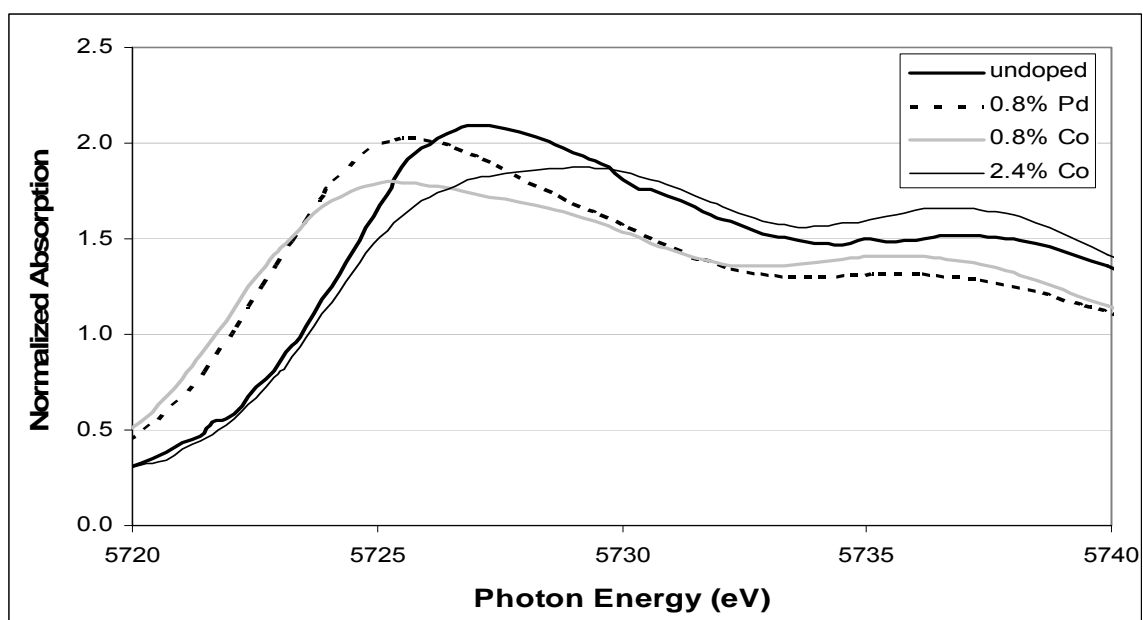


**Figure 2.** Normalized Ce L<sub>III</sub> XANES of CeO<sub>2</sub>/Al<sub>2</sub>O<sub>3</sub> catalysts reduced in 10% H<sub>2</sub>/N<sub>2</sub> at 420°C for 15 min.

WinXAS was also used to calculate the relative amounts of the valence states by matching XANES spectra to linear combinations of spectra for CeO<sub>2</sub> and Ce(III) acetate. The assumption for Ce(III) here is the same as Takahashi et al. The second assumption is that Ce(IV) gives the same spectrum as bulk CeO<sub>2</sub>. Since the shoulder and the lower energy white line are slightly more intense in larger crystals [10], and since these features are at energies close to the Ce(III) white line, this method will underestimate Ce(III) in the catalyst (the catalyst gives a spectrum similar to that of smaller crystals, because the CeO<sub>2</sub> is monolayer). Therefore, the number of oxygen vacancies predicted by the Takahashi et al. and WinXAS methods should bound the actual number of vacancies.

The trends in average number of oxygen vacancies in the coordination shell adjacent to each Ce atom (8 oxygen atoms maximum) are shown in Figure 3. The WinXAS method always predicts the smaller number of vacancies. Treatment with H<sub>2</sub> increased the number of vacancies; under the reducing reaction conditions, supported CeO<sub>2</sub> is quite defective. The number of vacancies for reduced CeO<sub>2</sub>/Al<sub>2</sub>O<sub>3</sub> (corresponding to ~40% reduction of CeO<sub>2</sub> to Ce<sub>2</sub>O<sub>3</sub>) and for reduced 0.8% Pd catalyst (~46-48% reduction of CeO<sub>2</sub>) are both similar to measured values from previous work [11], for reduced Ce<sub>x</sub>Zr<sub>1-x</sub>O<sub>2</sub> and Pd/Ce<sub>x</sub>Zr<sub>1-x</sub>O<sub>2</sub>. The number of vacancies for used, reduced Pd- and Co-containing catalysts were similar, 1.3-1.4 per Ce atom.

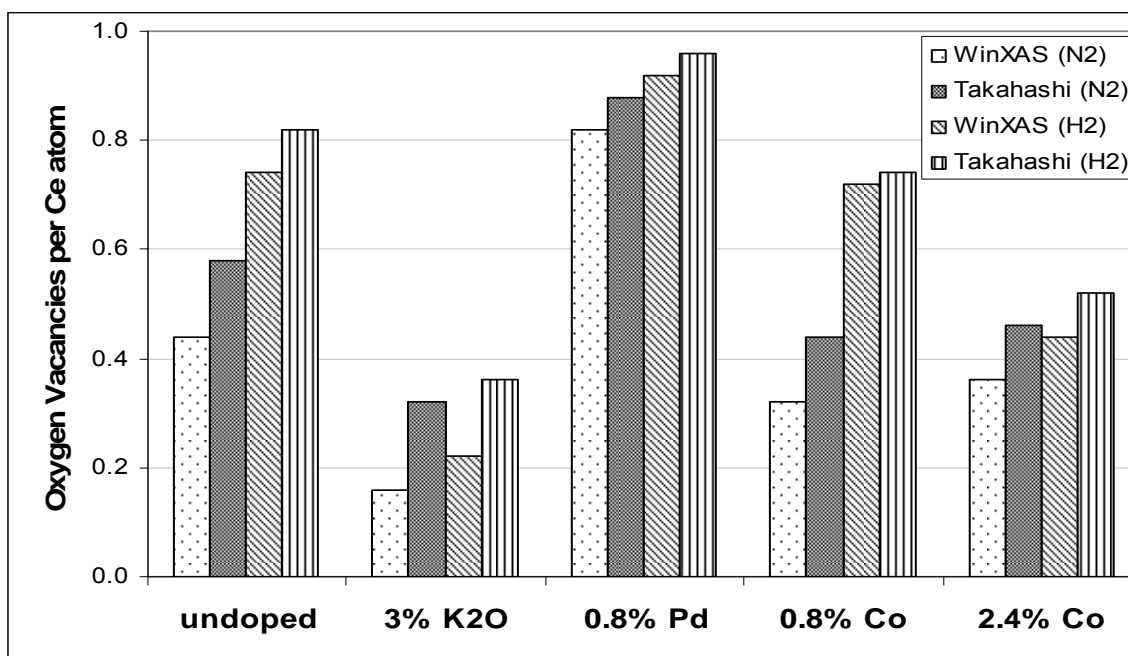
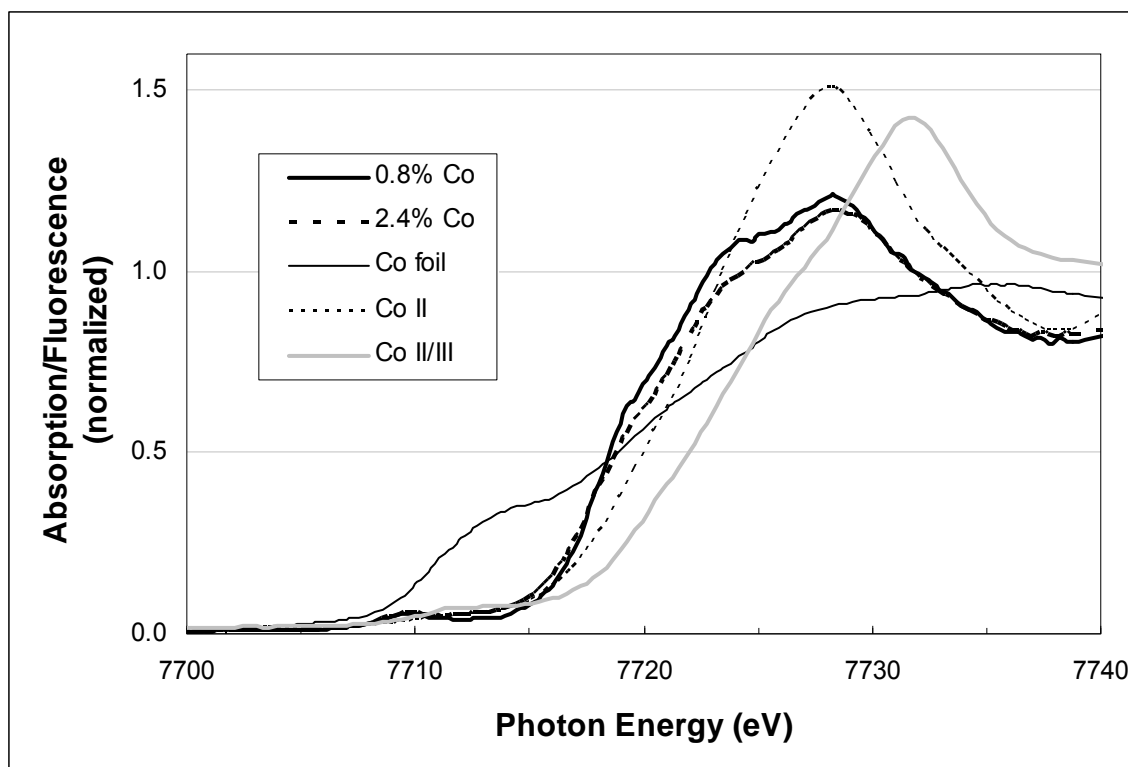


**Figure 3.** Average number of oxygen vacancies around each Ce atom in CeO<sub>2</sub>/Al<sub>2</sub>O<sub>3</sub> catalysts as determined by XANES using the Takahashi and WinXAS methods. In the



legend, N2 means heated in N<sub>2</sub> at 420°C, H2 means additional reduction in 10% H<sub>2</sub>/N<sub>2</sub> at 420°C for 15 min.

**Figure 4.** XANES spectra at Co K-edge for Co/CeO<sub>2</sub>/Al<sub>2</sub>O<sub>3</sub> catalysts and standards at 25°C.

XANES taken at the Co K-edge for both the 0.8 wt.% (14 at.% of M/CeO<sub>2</sub>) and 2.4 wt.% Co (41 at.% of M/CeO<sub>2</sub>) catalysts are shown in Figure 4. There is a main peak at 7728 eV, a shoulder about 4 eV lower and another about 8 eV lower. The main peak corresponding to the 1s → 4p white line in CoO [12] is less intense in the spectra of the catalysts. These deviations indicate that Co is in a different electronic state from CoO in the catalyst, due to substitution of Co into CeO<sub>2</sub>. The XANES of the 2.4% Co catalyst was fitted using the least-squares method to spectra of CoO, Co<sub>3</sub>O<sub>4</sub>, and metallic Co standards. The edge positions of all standard spectra were allowed to shift independently, thus only the shape of the catalyst spectrum was fit. Fitting results show that the Co<sub>3</sub>O<sub>4</sub> spectrum most closely matches that of the catalyst. Since some of the cobalt atoms in Co<sub>3</sub>O<sub>4</sub> have tetrahedral oxygen coordination, while in CoO all Co atoms are octahedrally coordinated, these results suggest that more Co in the catalysts is tetrahedrally coordinated by oxygen as a solid solution with CeO<sub>2</sub>. Analysis of the EXAFS (below) rules out the possibility that most of the cobalt is in a separate oxidic or metallic phase; also, these samples are X-ray amorphous in the reduced state and show no peaks characteristic of cobalt metal or its oxides even prior to reduction.

We estimated the oxidation state of the Co in both the 0.8% and 2.4% samples to be ~1.6 based on the method of Capehart et al. [13], which relates the Co K-edge shift to

the amount of charge transfer in rare earth – transition metal compounds. The XANES of  $\text{Co}_3\text{O}_4$  was also modeled using FEFF8 [14]; the  $\text{Co}_3\text{O}_4$  lattice consists of Co in octahedral and tetrahedral positions in 2:1 ratio. The spectrum was then broken down into separate contributions from the two positions; in the contribution corresponding to tetrahedral Co, the intensity of the white line is reduced and spread out towards lower energy, resembling the spectra of the actual Co-containing catalysts (Fig. 4).

EXAFS data for the Co K-edge were fitted using WinXAS and Artemis [15], to theoretical spectra for a Co atom substituted into  $\text{CeO}_2$ , generated by FEFF6 [16]. Data were fitted in the R-space range of 0.9 – 4.8 Å, derived from the Fourier-transformed region of k-space from 3.0 – 9.4 Å<sup>-1</sup>. Data in k-space were obtained by subtracting background Fourier components of less than 1.0 Å. The k, k<sup>2</sup> and k<sup>3</sup> weighted spectra of each set were simultaneously fit to reduce correlation between coordination number and Debye-Waller factors. The model included parameters for the radial distances and Debye-Waller factors of the first five shells and the coordination numbers of the first oxygen shell. Other details of the regression may be found in a thesis [17].

The Co EXAFS spectra in R-space for the  $\text{Co/CeO}_2/\text{Al}_2\text{O}_3$  catalysts are shown in Figure 5; the fitting parameters obtained using Artemis are given in Table 1. The first five coordination shells expected for Co added to a  $\text{CeO}_2$  lattice appear in the spectra. It was found that at least half of the Ce atoms in the second shell are substituted by Co, indicating that dispersion of Co within the lattice is not homogeneous, and is less so for the 2.4% Co catalyst, as might be expected. There are roughly four oxygen atoms in the first coordination shell of Co, compared to six for CoO. The results suggest that for both samples there is intimate association of the Co with a  $\text{CeO}_x$  phase.

Finally, XANES spectra for the Pd L<sub>III</sub> edge (not shown) suggest that most Pd in 0.8%  $\text{Pd/CeO}_2/\text{Al}_2\text{O}_3$  is in the II formal valence state. Since the catalyst had been previously calcined at 420°C where PdO would reduce to the metal, the Pd(II) must be associated with the  $\text{CeO}_2$  lattice. The white line due to the 2p → 4d transition [18] was much more intense for this catalyst than for a PdO standard, arising from an increased density of unoccupied d-states, therefore less hybridization of these states with the valence band [2].

## CONCLUSIONS

Doping of a supported  $\text{CeO}_2$  catalyst with a transition metal such as Co, Mn or Pd had different effects, but there is apparently little relationship between the number of oxygen vacancies and the reaction rate for ketonization reactions. Cobalt proved to be a useful additive for ketonization catalysis. In concentrations of <15 at.% in  $\text{CeO}_2$ , Co inserts into the rare earth oxide, increases the number of oxygen vacancies, and increases the reaction rate. In much higher concentrations some Co exists as separate reduced oxide domains, but with less tendency to catalyze dehydrogenation (undesired reaction) than, e.g., Pd.

REFERENCES

1. R. Cousin, S. Capelle, E. Abi-Aad, D. Courcot, A. Aboukais, *Chem. Mater.* 13 (2001) 3862-3870.
2. M. Fernandez-Garcia, *Catal. Rev.* 44 (2002) 59-121.
3. J. Wan, G.E. Thompson, K.Q. Lu, C.J.E. Smith, *J. Phys. IV* 7 (1997) C2-1181-C1182-1182.
4. G. Kaindl, G.K. Wertheim, G. Schmiester, E.V. Sampathkumaran, *Phys. Rev. Lett.* 58 (1987) 606-609.
5. J.E. Fallah., S. Boujana, H. Dexpert, A. Kiennemann, J. Majerus, O. Touret, F. Villain, F.L. Normand, *J. Phys. Chem.* 98 (1994) 5522-5533.
6. A.V. Soldatov, T.S. Ivanchenko, S.D. Longa, A. Kotani, Y. Iwamoto, A. Bianconi, *Phys. Rev. B: Condens. Matter* 50 (1994) 5074-5080.
7. A. Bianconi, A. Marcelli, H. Dexpert, R. Karnatak, A. Kotani, T. Jo, J. Petiau, *Phys. Rev. B: Condens. Matter* 35 (1987) 806-812.
8. Y. Takahashi, H. Sakami, M. Nomura, *Anal. Chim. Acta* 468 (2002) 345-354.
9. T. Ressler, *WinXAS* 97. 1998.
10. P. Nachimuthu, W.C. Shih, R.S. Liu, L.Y. Jang, J.M. Chen, *J. Solid State Chem.* 149 (2000) 408-413.
11. A. Norman, V. Perrichon, A. Bensaddik, S. Lemaux, H. Bitter, D. Koningsberger, *Top. Catal.* 16-17 (2001) 363-368.
12. G.P. Huffman, N. Shah, J. Zhao, F.E. Huggins, T.E. Hoost, S. Halvorsen, J.G.G. Jr., *J. Catal.* 151 (1995) 17-25.
13. T.W. Capehart, J.F. Herbst, R.K. Mishra, F.E. Pinkerton, *Phys. Rev. B: Condens. Matter* 52 (1995) 7907-7914.
14. A.L. Ankudinov, B. Ravel, J.J. Rehr, S.D. Conradson, *Phys. Rev. B: Condens. Matter* 58 (1998) 7565-7576.
15. B. Ravel, M. Newville, *J. Synchrotron Radiat.* 12 (2005) 537-541.
16. S.I. Zabinski, J. J., Rehr, A. Ankudinov, R.C. Albers, M.J. Eller, *Phys. Rev. B: Condens. Matter* 52 (1995) 2995-3009.
17. C. Plaisance, Zeolite and metal oxide catalysts for the production of dimethyl sulfide and methanethiol, M.S. Thesis, Louisiana State University: Baton Rouge, 2005.
18. K.R. Priolkar, P. Bera, P.R. Sarode, M.S. Hegde, S. Emura, R. Kumashiro, N.P. Lalla, *Chem. Mater.* 14 (2002) 2120-2128.



## **Publications, Grants, and Students Associated with this Work**

**(2005-07 only)**

### **Publications -**

K.M. Dooley, A.K. Bhat, C.P. Plaisance and A.D. Roy, "Methylketones from Acid Condensation Using Metal/CeO<sub>2</sub> Catalysts", in press, Appl. Catal. A (2007).

K.M. Dooley, A.K. Bhat, A.D. Roy and C.P. Plaisance, "Ketones from Acid/Aldehyde Condensation Using Metal/CeO<sub>2</sub> Catalysts," Proceedings, 19<sup>th</sup> North American Meeting, Catalysis Society, Philadelphia, 2005.

**Grants** - EagleView Technologies/MGK Co., "Catalyst Development and Reactor Study for Asymmetric Ketone and Amide Production," 2002-05 (\$90,000).

NASA, "Applied Polymer Technology Extension Cooperative", co-PI with P. Russo (PI), D. Spivak and L. Butler, 2005-06 (\$99,800).

**Students** – Craig Plaisance, "Catalyst Development and Reactor Study for Dimethyl Sulfide Production," M.S., August 2005. Current employer: Ph.D., Univ. of Virginia.

Landon Marchand (undergraduate), "Mesoporous Mixed Rare Earth Oxides".

## Characterization of Hexaluminates by X-ray Absorption Spectroscopy

A. Roy<sup>1</sup>, A. Ignatov<sup>1</sup>, G. Merchan<sup>1</sup>, A. Campos<sup>2</sup>, J.J. Spivey<sup>2</sup>, E. Kugler<sup>3</sup>

<sup>1</sup>Center for Advanced Microstructures and Devices, Louisiana State University, Baton Rouge, Louisiana 70806; <sup>2</sup>Department of Chemical Engineering, Louisiana State University, Baton Rouge, LA 70803; <sup>3</sup>Chemical Engineering; West Virginia University; PO Box 6102; Morgantown, WV 26506-6102; E-mail: acampo2@lsu.edu; PRN Number: ChemE-JS-0707

Nickel k-edge XANES in fluorescence: Data that represents the XANES region best is actually the EXAFS of which ten scans for samples 115, 117, 119 a, b were taken at the DCM beamline in CAMD and averaged in XAS data reduction software Athena [3]. There is a (small bump) pre-edge feature on all samples at approximately 8332 eV, which the standards may be used in order to do a fingerprint analysis to identify the phases in each sample.

The Ni data normalized  $\mu(E)$  data in Figure 1 has (except for 117a) an isosbestic point at energy of  $\sim 8360$  eV, implying that there is definitively one component that is the same for these materials [1].

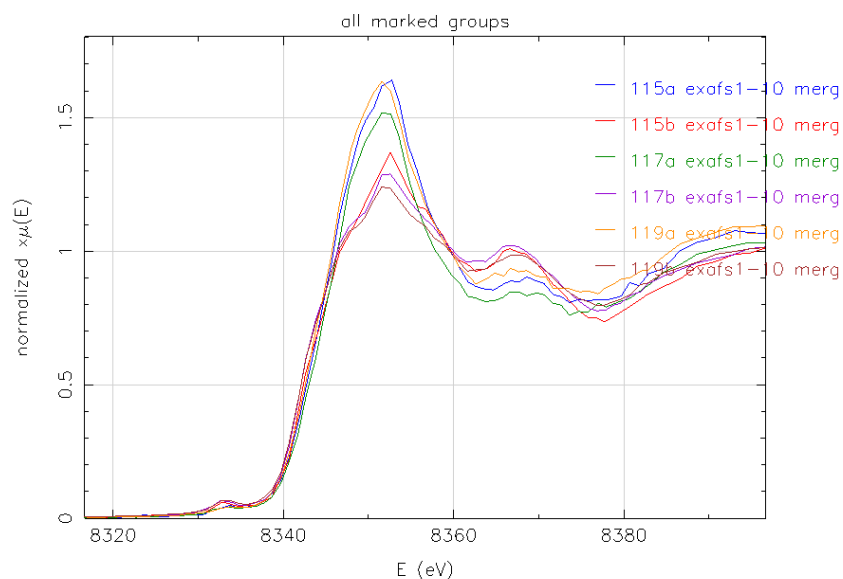


Figure 1 – XANES [normalized  $\mu(E)$ ] of hexaaluminate nickel samples

Nickel k-edge EXAFS in fluorescence: The EXAFS region for the Ni k-edge was taken during the same runs of the XANES region. After glitches were removed, the ten spectra were averaged in  $\mu(E)$  in Athena. Minimal data reduction of background removal was performed and the Fourier Transform of  $\chi(k)$  transforms the data from energy space into a pseudo-radial distribution in Figures 2-4. Until data modeling takes place in XAS modeling software Artemis, information from the pseudo-radial distribution function cannot be extracted from the data [2].

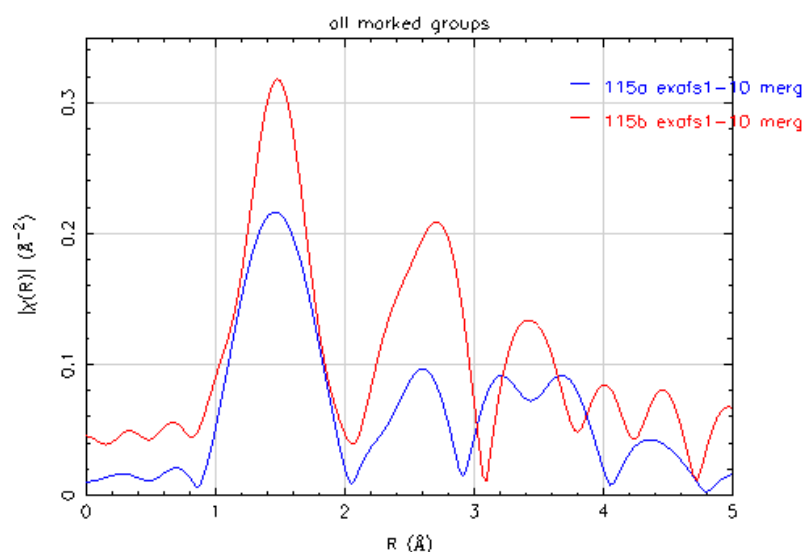


Figure 2 – Fourier transform (pseudo-radial distribution) of EXAFS data for 115a, 115b

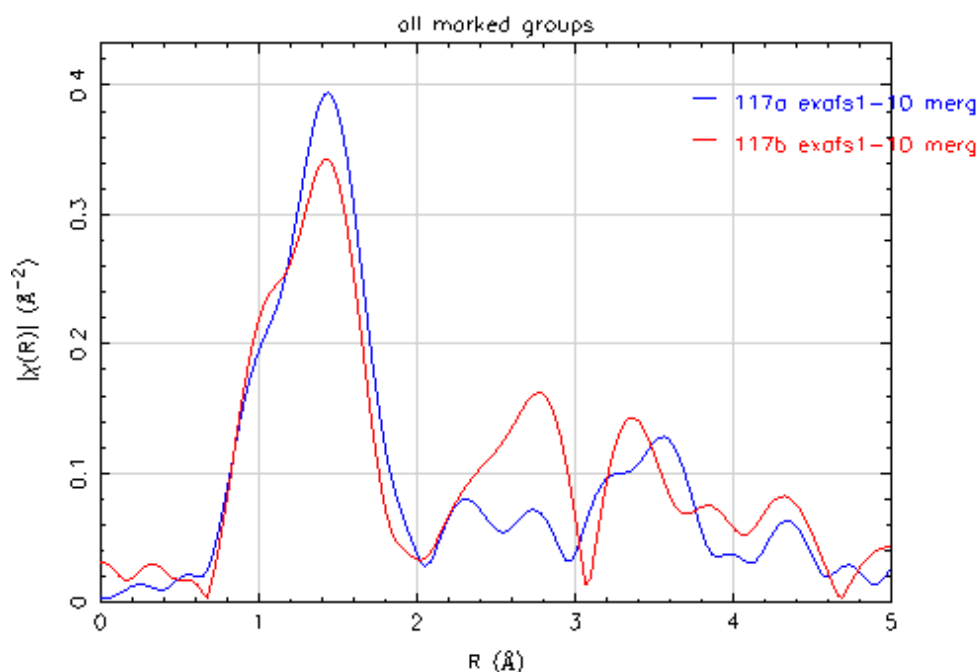


Figure 3 – Fourier transform (pseudo-radial distribution) of EXAFS data for 117a, 117b

Barium L3-edge XANES in fluorescence: Tests were also run on the XANES L3 edge of Barium in fluorescence on all received as-prepared samples (115-119 a, b). Two scans of the data were merged using normalized  $\mu(E)$ . A preliminary observation of double peaks in some of the spectra, as well as a higher normalized absorption for lower weight percentages of Ba in the samples and for samples prepared with technique ‘a’.

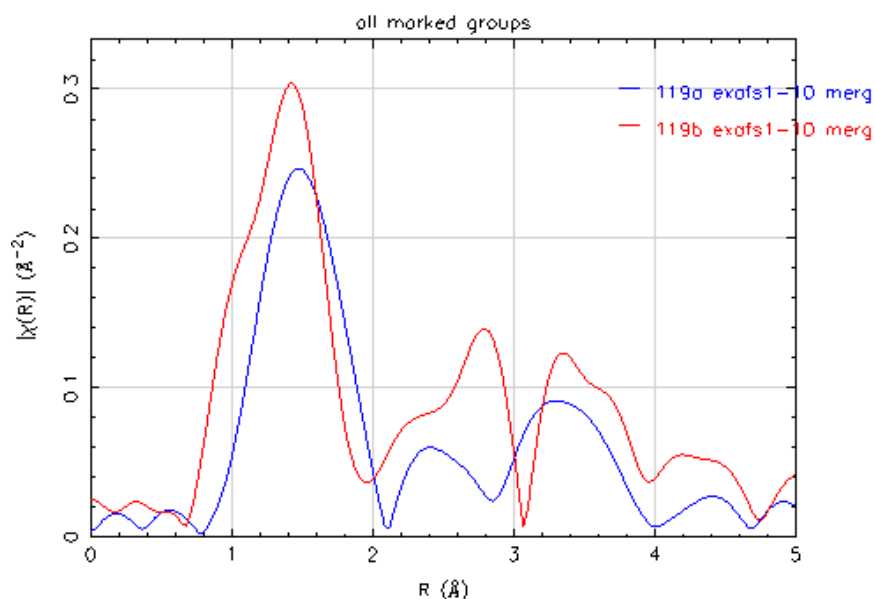


Figure 4 – Fourier transform (pseudo-radial distribution) of EXAFS data for 119a, 119b

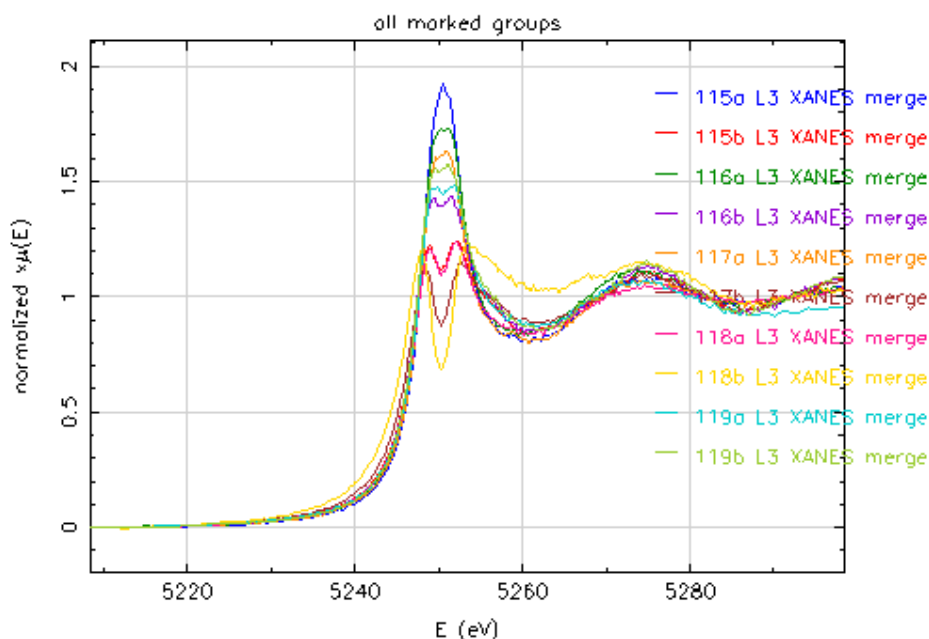


Figure 5 – Normalized  $\mu(E)$  (XANES spectra) for Ba

Data analysis status: The XRD results from Brookhaven National Laboratories by Kugler et. al. will be used in the EXAFS analysis for the Ni data. Two trends can be observed from the data analysis for Ni, the two different preparation techniques can be compared at three different weight percentages of Ni, as well as the trend of increasing weight percentages Ni for both preparation techniques.

The barium XANES can be used to do a fingerprint analysis on the data to determine the percentages of phases present in each of the catalysts. Trends of both weight percentages and preparation techniques can be extracted from the data analysis. Literature will be used to determine what phases would cause the interesting double peak observed in several Barium samples.

Future tests to be performed by the LSU group: The EXAFS for the barium L3 edge will be interesting due to the vast differences in the XANES spectra of the different samples. Information that can be obtained from the EXAFS includes bond distances, nearest neighbors, Debye Waller factor (bond disorder), and coordination numbers [2].

The as-prepared samples are similar to that of the active catalysts, therefore testing the samples in liquid nitrogen temperature, an intermediate temperature, and room temperature will enable the extraction of the Debye Waller factor, which will allow for improved results for the coordination number since they are difficult to decouple from the EXAFS equation.

References:

- [1] Desrochers, P.J., et al., *A Stable Monomeric Nickel Borohydride*. 2003. p. 7945-7950.
- [2] Gurman, S. (1995). "Interpretation of EXAFS Data." Journal of Synchrotron Radiation **2**(1): 56-63.
- [3] Ravel, B. and M. Newville. *ATHENA, ARTEMIS, HEPHAESTUS: data analysis for X-ray absorption spectroscopy using IFEFFIT*, in *Journal of Synchrotron Radiation*. 2005. p. 537-541.

**X-ray spectroscopic characterization of heterogeneous processes relevant to combustion, Erwin Poliakoff, *LSU Chemistry***

Combustion processes frequently produce persistent organic pollutants via reactions on metal oxide surfaces. However, the processes responsible for the production of such pollutants are not well understood. It is difficult to interrogate the interactions for real systems under conditions that are of interest in combustion science, as the systems are typically at high temperatures with many components present. However, it is possible to use straightforward x-ray spectroscopic methods for probing such systems. The x-ray absorption process can focus on a specific element in a complex mixture, permitting the acquisition of unambiguous electronic and structural information. This is particularly useful to heterogeneous processes that occur at metal oxide surfaces. For example, it is well known that phenols and related aromatic compounds react on copper oxide surfaces at elevated temperatures to form pollutants such as dioxins. In our work, we have studied the mechanism and kinetics of this process by studying the evolution of the Cu K-edge absorption spectrum as a function of time after the pollutant precursor adsorbs to the surface. Similarly, we are able to probe the oxidation state of metal oxide nanoparticles that have been implicated in soot formation in industrial combustion processes. Both structural and electronic information are extractable from such studies, enabling the acquisition of important information that is inaccessible otherwise.

## X-ray Absorption Spectroscopy of $\text{Zn}_2\text{TiO}_4$

A. Roy<sup>1</sup>, A. Ignatov<sup>1</sup>, G. Merchan<sup>1</sup>, A. Campos<sup>2</sup>, J.J. Spivey<sup>2</sup>, R. Rees<sup>3</sup>, H. Tian<sup>3</sup>;  
<sup>1</sup>Center for Advanced Microstructures and Devices, Louisiana State University, Baton Rouge, Louisiana 70806; <sup>2</sup>Department of Chemical Engineering, Louisiana State University, Baton Rouge, LA 70803; <sup>3</sup>Department of Chemical and Petroleum Engineering; Room 1249 Benedum Hall; University of Pittsburgh; Pittsburgh, PA 15261;  
E-mail: acampo2@lsu.edu; PRN Number: ChemE-JS-????

Where the project stands: Catalysts synthesized by the University of Pittsburgh are being structurally studied by the bulk structure of zinc orthotitanate (ZTO or  $\text{Zn}_2\text{TiO}_4$ ) by using multiple methods including DFT calculations (U. of Pitt.), high resolution XRD (U. of Pitt.), and EXAFS in transmission (LSU). The LSU group has completed the scans of the k-edges of Zn and Ti, which are in Figures 1 and 2, respectively. In the XAFS reduction software Athena [1] the data was normalized in  $\mu(E)$ , which shows that both samples are similar in chemical structure from the similarities in the XANES spectra.

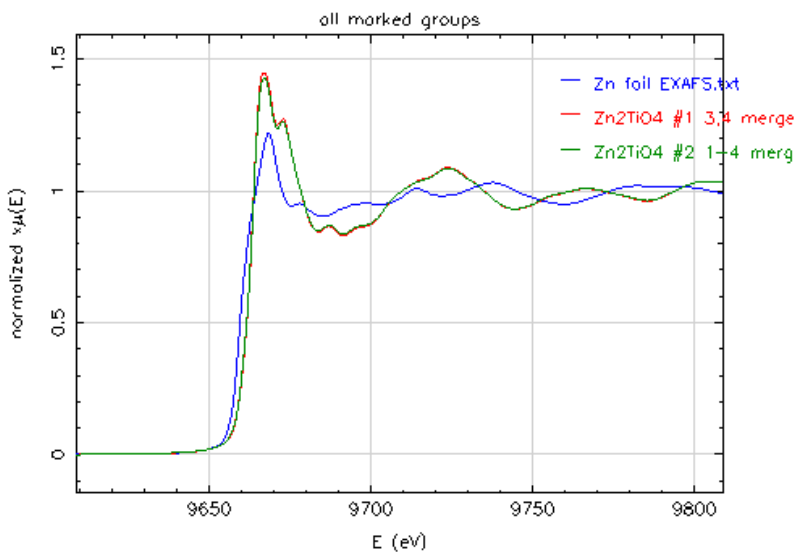


Figure 1 – Zn k-edge XANES scan for  $\text{Zn}_2\text{TiO}_4$  samples

What's next: The three main questions to be answered from the EXAFS analysis are: 1) The bulk atomic distribution of nearest and next nearest neighbor distances for the following pairs of species: Zn-Zn, Zn-Ti, and Ti-Ti. 2) The distribution of coordination types by species (how many different coordinations of Zn-Ti, Zn-O, Ti-O are there and what are their relative percentages) for each species in the material. 3) How many different oxygen bonds exist, how do they connect with Zn and Ti, as well as the coordination structure of oxygen.

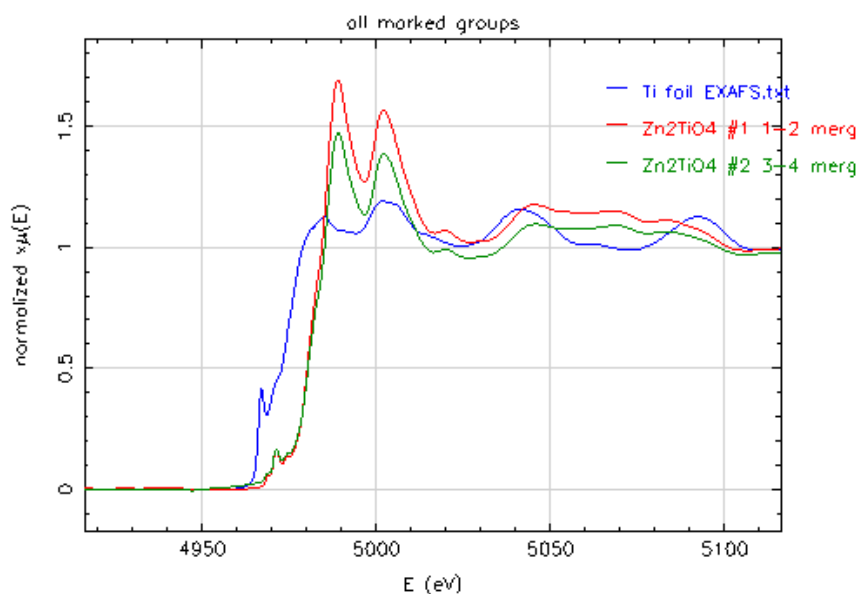


Figure 2 – Ti k-edge XANES scan for  $Zn_2TiO_4$  samples

The current goal is to complete the EXAFS data analysis. With careful data analysis, the EXAFS data will answer these questions. Proposing a model for the data fitting in Artemis will take careful planning and will be refined based on fitting results due the complexity of the spinel structure [2, 4-5]. Millard et. al. used x-ray diffraction and  $^{17}O$  MAS NMR to propose a structure for  $Zn_2TiO_4$  which be used as the first model for fitting (Figure 3) [4]. Researchers from the University of Pittsburgh will use EXAFS results to compare and supplement the DFT calculations.

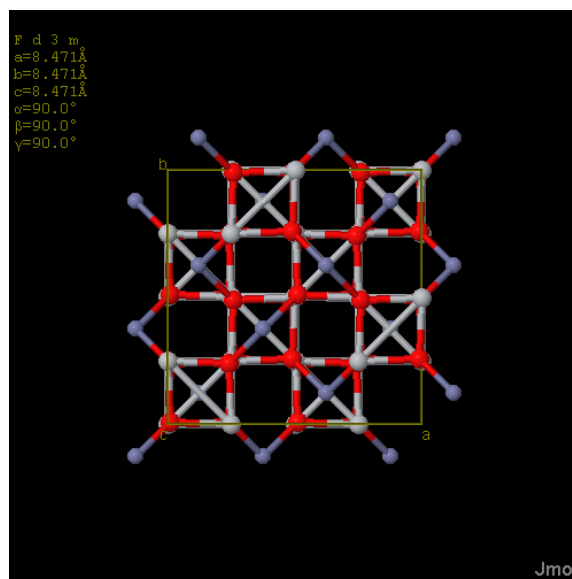


Figure 3 – Proposed preliminary structure for ZTO structures fitting in Artemis [3]



References:

- [1] Ravel, B. and M. Newville, *ATHENA, ARTEMIS, HEPHAESTUS: data analysis for X-ray absorption spectroscopy using IFEFFIT*, in *Journal of Synchrotron Radiation*. 2005. p. 537-541.
- [2] Bartram, S. and R. Slepety's, *Compound Formation and Crystal Structure in the System ZnO-TiO<sub>2</sub>*. *Journal of the American Ceramic Society*, 1961. 44(10): p. 493-499.
- [3] Non-specified, *Spinel*. 2006, American Mineralogist Crystal Structure Database.
- [4] Millard, R. and R. Peterson, *Study of the cubic to tetragonal transition in Mg<sub>2</sub>TiO<sub>4</sub> and Zn<sub>2</sub>TiO<sub>4</sub> spinels by <sup>17</sup>O NMR and Rietveld refinement of X-ray diffraction data*. *American Mineralogist*, 1995. 80: p. 885-896.
- [5] Verwy, E.J.W. and E.L. Heilmann, *Physical Properties and Cation Arrangement of Oxides with Spinel Structures*. *The Journal of Chemical Physics*, 1947. 15(4): p. 174-180.

## Characterization of Hexaluminates by X-ray Absorption Spectroscopy

A. Roy<sup>1</sup>, A. Ignatov<sup>1</sup>, G. Merchan<sup>1</sup>, A. Campos<sup>2</sup>, J.J. Spivey<sup>2</sup>, E. Kugler<sup>3</sup>

<sup>1</sup>Center for Advanced Microstructures and Devices, Louisiana State University, Baton Rouge, Louisiana 70806; <sup>2</sup>Department of Chemical Engineering, Louisiana State University, Baton Rouge, LA 70803; <sup>3</sup>Chemical Engineering; West Virginia University; PO Box 6102; Morgantown, WV 26506-6102; E-mail: acampo2@lsu.edu; PRN Number: ChemE-JS-0707

Nickel k-edge XANES in fluorescence: Data that represents the XANES region best is actually the EXAFS of which ten scans for samples 115, 117, 119 a, b were taken at the DCM beamline in CAMD and averaged in XAS data reduction software Athena [3]. There is a (small bump) pre-edge feature on all samples at approximately 8332 eV, which the standards may be used in order to do a fingerprint analysis to identify the phases in each sample.

The Ni data normalized  $\mu(E)$  data in Figure 1 has (except for 117a) an isosbestic point at energy of ~8360 eV, implying that there is definitively one component that is the same for these materials [1].

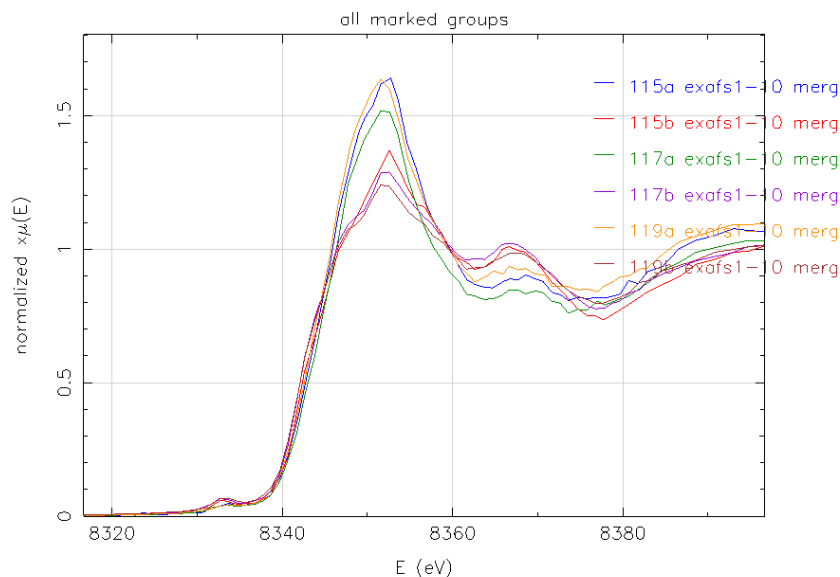


Figure 1 – XANES [normalized  $\mu(E)$ ] of hexaaluminate nickel samples

Nickel k-edge EXAFS in fluorescence: The EXAFS region for the Ni k-edge was taken during the same runs of the XANES region. After glitches were removed, the ten spectra were averaged in  $\mu(E)$  in Athena. Minimal data reduction of background removal was performed and the Fourier Transform of  $\chi(k)$  transforms the data from energy space into a pseudo-radial distribution in Figures 2-4. Until data modeling takes place in XAS modeling software Artemis, information from the pseudo-radial distribution function cannot be extracted from the data [2].

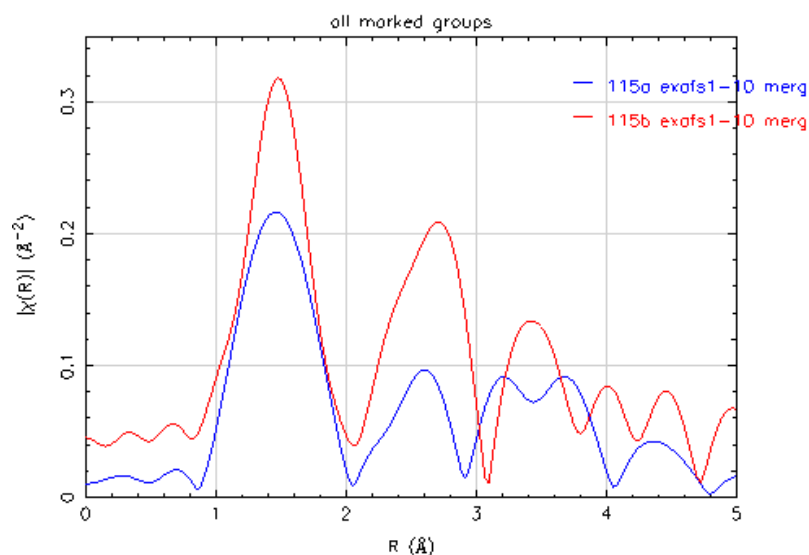


Figure 2 – Fourier transform (pseudo-radial distribution) of EXAFS data for 115a, 115b

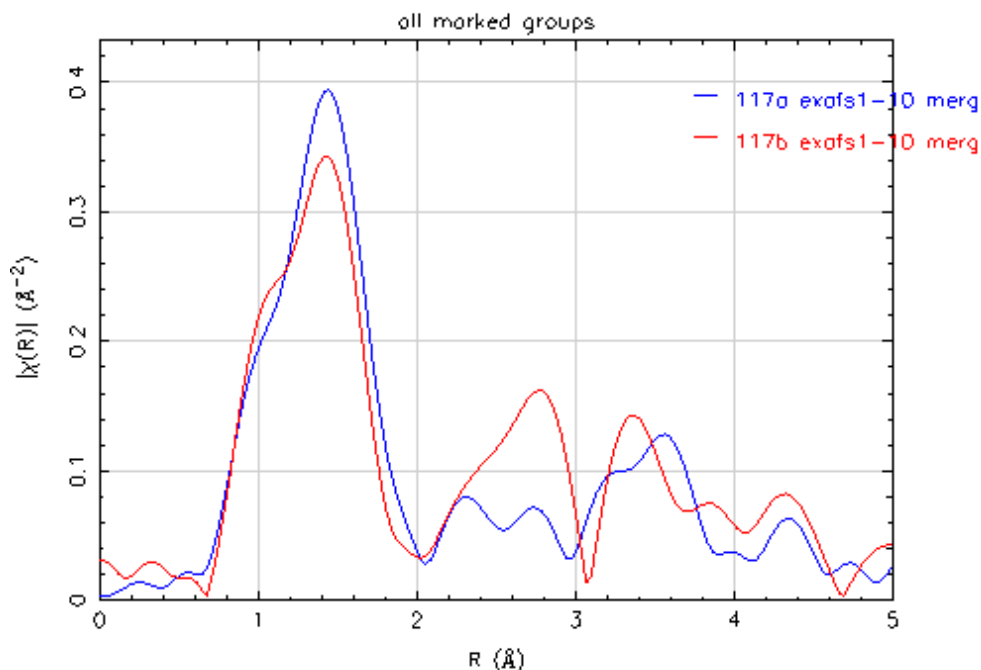


Figure 3 – Fourier transform (pseudo-radial distribution) of EXAFS data for 117a, 117b

Barium L3-edge XANES in fluorescence: Tests were also run on the XANES L3 edge of Barium in fluorescence on all received as-prepared samples (115-119 a, b). Two scans of the data were merged using normalized  $\mu(E)$ . A preliminary observation of double peaks in some of the spectra, as well as a higher normalized absorption for lower weight percentages of Ba in the samples and for samples prepared with technique ‘a’.

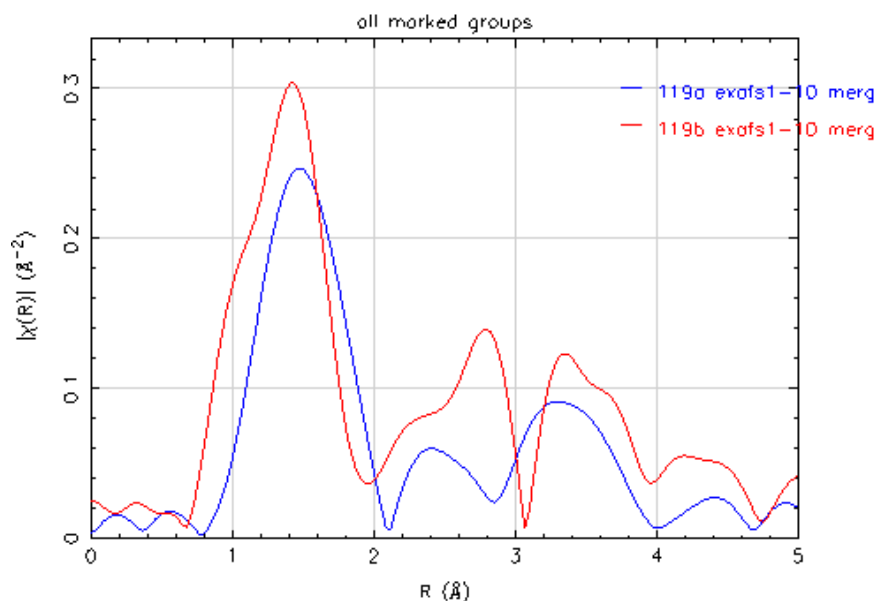


Figure 4 – Fourier transform (pseudo-radial distribution) of EXAFS data for 119a, 119b

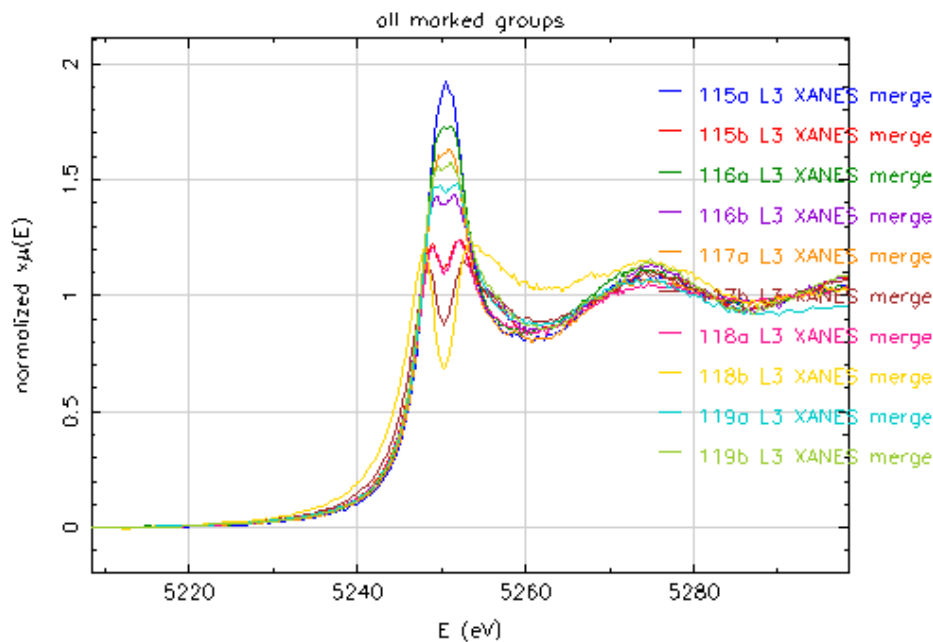


Figure 5 – Normalized  $\mu(E)$  (XANES spectra) for Ba

Data analysis status: The XRD results from Brookhaven National Laboratories by Kugler et. al. will be used in the EXAFS analysis for the Ni data. Two trends can be observed from the data analysis for Ni, the two different preparation techniques can be compared at three different weight percentages of Ni, as well as the trend of increasing weight percentages Ni for both preparation techniques.

The barium XANES can be used to do a fingerprint analysis on the data to determine the percentages of phases present in the each of the catalysts. Trends of both weight percentages and preparation techniques can be extracted from the data analysis. Literature will be used to determine what phases would cause the interesting double peak observed in several Barium samples.

Future tests to be performed by the LSU group: The EXAFS for the barium L3 edge will be interesting due to the vast differences in the XANES spectra of the different samples. Information that can be obtained from the EXAFS includes bond distances, nearest neighbors, Debye Waller factor (bond disorder), and coordination numbers [2].

The as-prepared samples are similar to that of the active catalysts, therefore testing the samples in liquid nitrogen temperature, an intermediate temperature, and room temperature will enable the extraction of the Debye Waller factor, which will allow for improved results for the coordination number since they are difficult to decouple from the EXAFS equation.

References:

- [1] Desrochers, P.J., et al., *A Stable Monomeric Nickel Borohydride*. 2003. p. 7945-7950.
- [2] Gurman, S. (1995). "Interpretation of EXAFS Data." Journal of Synchrotron Radiation **2**(1): 56-63.
- [3] Ravel, B. and M. Newville. *ATHENA, ARTEMIS, HEPHAESTUS: data analysis for X-ray absorption spectroscopy using IFEFFIT*, in *Journal of Synchrotron Radiation*. 2005. p. 537-541.

**The electronic structure and polymerization of a self-assembled  
monolayer with multiple arene rings**  
(UN-PD1206OR)

**D.-Q. Feng<sup>1</sup>, D. Wisbey<sup>1</sup>, Ya. B. Losovyj<sup>2</sup>, Y. Tai<sup>3</sup>, M. Zharnikov<sup>3</sup> and P.A.  
Dowben<sup>1\*</sup>**

**1) Dept. of Physics and Astronomy and the Nebraska Center for Materials and  
Nanoscience, University of Nebraska-Lincoln, Lincoln, NE 68588-0111**

2) Center for Advanced Microstructures and Devices, Louisiana State University, 6980  
Jefferson Highway, Baton Rouge, LA 70806

3) Angewandte Physikalische Chemie, Universität Heidelberg, Im Neuenheimer Feld  
253, D-69120 Heidelberg, Germany

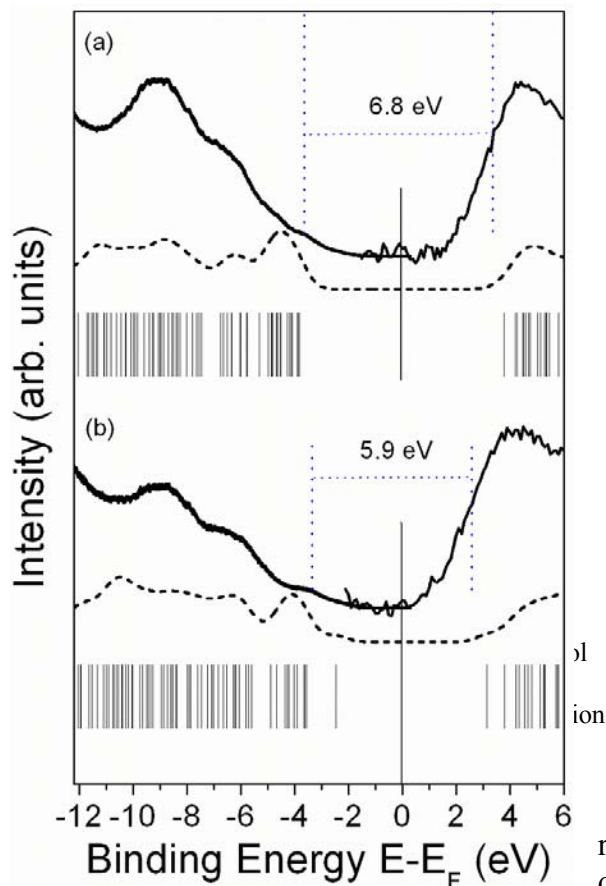


**Figure 2.** Combined photoemission (left) and inverse photoemission (right) spectra (solid line) of pristine (a) and irradiated (b) terphenyldimethanethiol on Au, along with the calculated density-of-states (dashed line) for a pair of the separate and cross-linked terphenyldimethanethiol molecules. The experimental HOMO-LUMO gaps are indicated. The photoemission spectra were taken with unpolarized He I (21.2 eV) light.

compared to the pristine TPDMT films (Figure 2), which is consistent with theoretical calculation. The Fermi level placement, within the HOMO-LUMO gap suggests that strongly irradiated TPDMT films are more n-type insulating systems than the pristine TPDMT SAMs, and both molecular films have an electron structure consistent with a wide band gap insulator. The 2 dimensional quasi-polymerization of TPDMT forms a dielectric barrier that can be better characterized than a polymerized benzene barrier layer [2].

References:

We have found evidence of intermolecular interactions for a self-assembled monolayer (SAM) formed from a large molecular adsorbate, [1,1';4',1''-terphenyl]-4,4''-dimethanethiol (TPDMT), from the dispersion of the molecular orbitals with changing the wave vector  $k$  (Figure 1). With the formation self assembled molecular (SAM) layer, the molecular orbitals hybridize to electronic bands, with indications of significant band dispersion of the unoccupied molecular orbitals [1]. The TPDMT films, on gold substrates, are very well ordered molecular assemblies as illustrated in by the evidence of band dispersion (Figure 1). Such in-plane ordering may be indicative of strong lateral interactions within the organic film, as has been suggested for other thiol-derived SAMs. The strong intermolecular interaction is most likely responsible for the easily observed dispersion of the lowest unoccupied molecular orbitals [1].

The electronic structure is also seen to be dependent upon temperature, and cross-linking between the neighbor molecules, indicating that the electronic structure may be subtly altered by changes in molecular conformation and packing. We found that the irradiated TPDMT films have a smaller HOMO-LUMO gap as

- [1] D.-Q. Feng , D. Wisbey, Ya. B. Losovyj, Y. Tai, M. Zharnikov, P.A. Dowben, *Phys. Rev. B* **74** (2006) 165425; November 13, 2006 issue of *Virtual Journal of Nanoscale Science & Technology*
- [2] D.-Q. Feng, Ya.B. Losovyj, Y.Tai, M. Zharnikov, and P.A. Dowben, *J. Materials Chemistry* **16** (2006) 4343-434



## Microfabrication

### Center for Bio-Modular Microsystems: Devices

P.-C. Chen<sup>1,3</sup>, N. Elmadjoub<sup>1,3</sup>, T.Y. Lee<sup>1,3</sup>, V. Palaparthi<sup>1,3</sup>, M. Witek<sup>2</sup>, J. Guy<sup>1</sup>, P. Datta<sup>4</sup>, D. E. Nikitopoulos<sup>1,3</sup>, S. A. Soper<sup>1,2</sup>, and M. C. Murphy<sup>1,3</sup>  
<sup>1</sup>Center for BioModular Multi-Scale Systems, <sup>2</sup>Department of Chemistry, <sup>3</sup>Department of Mechanical Engineering, <sup>4</sup>Center for Advanced Microstructures and Devices  
 Louisiana State University, Baton Rouge, LA 70803  
 E-mail: murphy@me.lsu.edu, PRN: ME-MM4100DEV

### Polymerase Chain Reaction Device Development

Participants: P.-C. Chen, J. Guy, P. Datta, D.E. Nikitopoulos, S.A. Soper, M.C. Murphy

**Objectives:** The original LSU-CFPCR was microfabricated using the LIGA process and the layout is shown in Figure 1. This device delivered rapid DNA amplification; a 500 bp DNA fragment was replicated as fast as 1.7 min (5.2 s/cycle) and the 997 bp fragments were amplified in 3.2 min (9.7 s/cycle) [1]. However the best amplification yield was 23% of a commercial thermal cycler with the same inputs and cycle sequence. Modifications were made to improve the performance of the LSU-CFPCR.

**Results:** The polymerase chain reaction (PCR) is a powerful technique for exponentially amplifying DNA sequences of specific interest using repetitive temperature cycling [1]. The temperatures that are typically used in the PCR reaction include 90 °C–95 °C for denaturation of the double-stranded (ds) DNA molecule, 50 °C–70 °C for hybridization of the primers to the single-stranded (ss) DNA template, and 70 °C–75 °C for enzymatic polymerization (extension) of the primers. The speed of thermal cycling is usually instrument limited. For example, some commercial PCR machines are based on a temperature-controlled metal block holding tubes containing the PCR cocktail. Standard protocols for 30 thermal cycles require 1-2 h of processing time. A large fraction of that time is needed to heat and cool the cocktail. Time is required both to bring the metal block to the cycle equilibrium temperature and to transfer heat to the cocktail through the microfuge tubes. The response time of these conventional systems is limited due to high thermal capacitance of the metal block and low heat transfer through the plastic microfuge tubes. Microfabricated PCR devices have the potential for much faster heating and cooling of the PCR cocktail due to the reduced sample volume and the to the lower thermal capacitance of the components. Continuous flow PCR (CFPCR) eliminates the heating and cooling of the reactor at each cycle step by defining constant temperature zones along a microfluidic channel and driving the analyte through the different zones to obtain the PCR thermal cycle.

Modifications, including decreasing the thickness of device, using copper plates as heating stages, and milling grooves to separate each temperature zone, improved the uniformity of temperature distribution. The changes to the thermal design increased the amplification efficiency to 74% of the commercial thermal cycler while maintaining the rapid amplification of the original CFPCR [2].

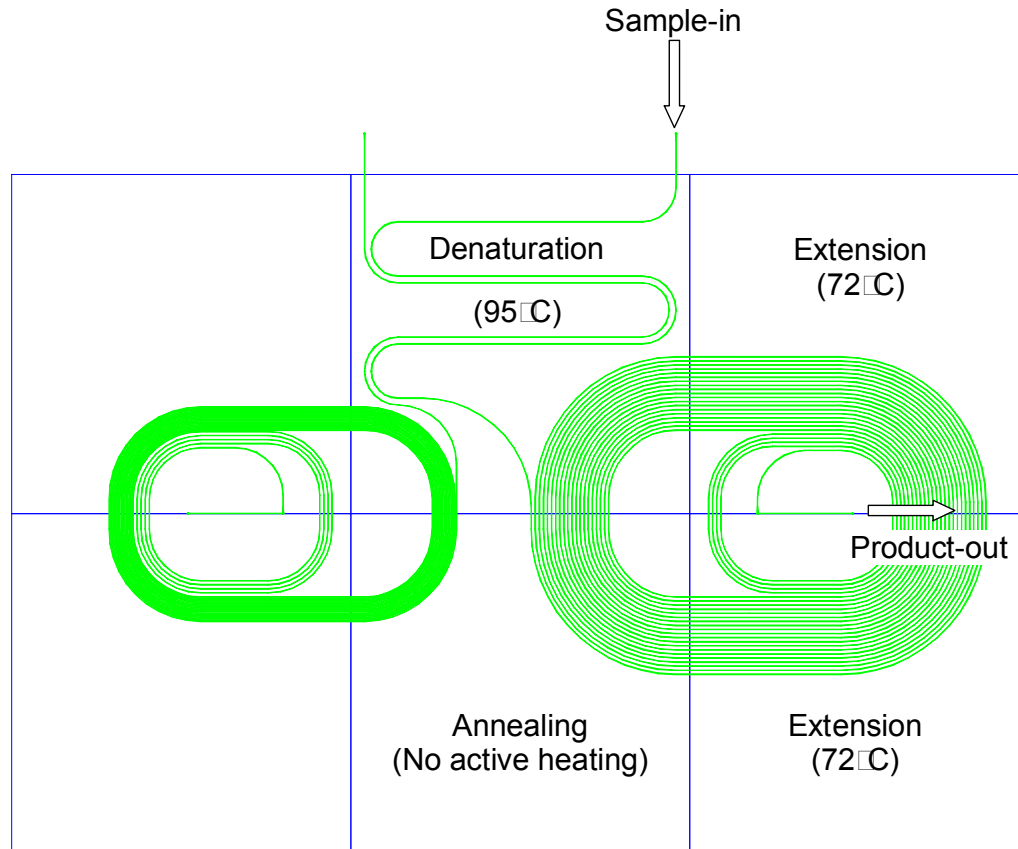


Figure 1: The layout of the LSU CFPCR.

## Ligase Detection Reaction Device Development

Participants: T.Y. Lee, J. Guy, P. Datta, D.E. Nikitopoulos, S.A. Soper, M.C. Murphy

**Objectives:** A double spiral, Continuous-Flow Ligase Detection Reaction (CFLDR) device with an integrated passive micromixer was designed, fabricated, and tested. Prior work on micro-LDR designs had focused on thermal isolation and relative speed of the ligation and denaturations steps [3].

**Results:** The devices consisted of a passive mixer, an incubator channel (95°C) for preheating, and a thermal-cycler spiral channel where the LDR. The onboard mixer was necessary since the LDR will usually be used in a modular format following amplification, so the Polymerization Chain Reaction (PCR) output, a cocktail of primers, and an enzyme of DNA – ligase, need to be mixed before the LDR can occur. In LDR, the thermal cycler performs cycles between 95°C for denaturation and 65°C for both annealing and ligation.

The device was laid out as a double spiral in order to ensure that all ports, both inlets and outlets, were located at the center of the chip to accommodate a universal interconnect. In the LDR the residence time necessary for the denaturation zone is typically much shorter than that required for the annealing/ligation zone (in this case 1:4). In order to avoid extreme lengths of the cycler channel, a large footprint and high pressure drop, the part of the spiral channel where annealing/ligation takes place was designed appropriately wider (4 times in this case). This also ensured that the two thermal zones were of equal surface

area, which contributed to more consistent thermal management, and a standard, more compact, footprint for the heater-elements. The mixer integrated into the chip was designed for an optimum flow ratio of 2. Therefore, the total flow ratio of the mixer was 1:2:6 to mix three different reagents.

A mold insert, containing representative test devices, was micro-milled in brass. Replica's were produced by hot-embossing into PC substrates. A groove was micromilled on the back side of the device to inhibit heat dispersion in the horizontal direction with holes for the inlet and outlet ports laser-drilled. Each device was covered with a thin sheet of polycarbonate by thermal bonding. Three inlet ports and one outlet port were sealed by customized tubing adapters with PEEK tubing, and then tested with BSA solution which was absorbed onto the PC surface to reduce the absorption of the DNA ligase enzyme into the surface.

The preliminary results showed that mixing occurred in the integrated passive micromixer without the formation of air bubbles under suction. Three different colors of food dye passed through the mixer and the mixture entered the preheating channel with the different color food dyes blended. However, when pushing the streams with syringe pumps, the mixing was interrupted by the formation of air bubbles in the passive micromixer. The balancing and timing of the micromixer were disrupted by the formation of the air bubbles, leading to insufficient or incomplete mixing.

Additional tests are underway.

### **Electrokinetic Thermal Cycler – Modified Electrophoretion**

Participants: N. Elmajdoub, M. Witek, D.E. Nikitopoulos, J. Guy, P. Datta, S.A. Soper, M.C. Murphy

**Objectives:** Proof of concept of an electrokinetically driven thermal-cycler, which can be used for PCR or LDR was carried out computationally with combined electro-osmotic and electrophoretic flow as appropriate for DNAs in aqueous buffer.

**Results:** The electrokinetically driven thermal-cycler achieves continuous cycling in a closed loop using only two electrodes and does not require high voltages. Conditions for optimum performance and associated tolerances for achieving the desired cycling performance under non-optimal conditions were identified. Feasibility was established both theoretically and through numerical simulations.

To be implemented the chip material needs to be surface-modified to control electroosmotic mobility and selectively reverse its sign. Experiments were conducted to determine the extent of electroosmotic mobility control through a combination of UV and chemical treatment. The experiments successfully demonstrated modification of the electroosmotic mobility in PMMA (verification) as well as PC (original) using an amination process. The modification included electroosmotic mobility reversal, which is critical to the application.

A Provisional Patent application was filed on the concept.

A chip is being designed based on the completed theoretical and numerical work and will be manufactured, surface modified and tested for a benchmark PCR reaction.

## References

1. M. Hashimoto, P.C. Chen, M.W. Mitchell, D.E. Nikitopoulos, S.A. Soper, M.C. Murphy, *Lab on a Chip*, 4, 638 (2004).
2. Pin-Chuan Chen, Michael W. Mitchell, Dimitris E. Nikitopoulos, Steven A. Soper, Michael C. Murphy, (2007) *Biomedical Microdevices*, In Preparation.
3. Barrett, D.O., Maha, A., Wang, Y., Soper, S.A., Nikitopoulos, D.E., and Murphy, M.C. (2004), *Proceedings of the ASME IMECE 2004, Anaheim, CA, November 15-20, 2004*, IMECE2004-62111.

## Center for Bio-Modular Microsystems: Large Area Mold Inserts (LAMI)

D. Park<sup>1</sup>, M. Hupert<sup>1</sup>, M. Witek<sup>2</sup>, B. H. You<sup>3</sup>, J. Guy<sup>1</sup>, P. Datta<sup>4</sup>, J.-B. Lee<sup>5</sup>, S. A. Soper<sup>1,2</sup>, D. E. Nikitopoulos<sup>1,3</sup> and M. C. Murphy<sup>1,3</sup>

<sup>1</sup>Center for BioModular Multi-Scale Systems, <sup>2</sup>Department of Chemistry, <sup>3</sup>Department of Mechanical Engineering, <sup>4</sup>Center for Advanced Microstructures and Devices, Louisiana State University, Baton Rouge, LA 70803

<sup>5</sup>Erik Jonsson School of Engineering and Computer Science, University of Texas at Dallas, Richardson, TX 75083

E-mail: [murphy@me.lsu.edu](mailto:murphy@me.lsu.edu), **PRN:** ME-MM4100LAMI

**Objectives:** A 96-well solid-phase reversible immobilization (SPRI) reactor for a microtiter plate-based microfluidic platform in micro molded, photo-activated polycarbonate (PPC) was designed, fabricated, and used to purify genomic DNA (gDNA).

**Results:** The PPC-SPRI reactor is a simple flow-through type reactor in a standard microtiter plate footprint [1] consisting of two microfluidic control ports, 96 immobilization beds for DNA capture, and reservoirs in microchannel network (Figure 1). The arrays of microposts (20  $\mu\text{m}$  by 20  $\mu\text{m}$  squares with spacing of 20  $\mu\text{m}$ ) were distributed in 96 immobilization beds for gDNA capture media upon UV surface modification [2]. Once a syringe or a syringe pump is connected to the port P1 and a vacuum pump to the port P2, there are two preferential flow paths at each well, from the port P1 to the reservoirs or from the reservoirs to the port P2 (Figure 1(b)). This allows for effective gDNA purification in a high throughput, automated format with a closed architecture to eliminate contamination effects.

UV lithography of SU-8 over 150 mm Si substrates was used to make 50  $\mu\text{m}$  thick patterns with feature dimensions as small as 20  $\mu\text{m}$  (Figure 2 (a)). The patterns were filled and overplated by nickel electroplating to obtain a large area mold insert (LAMI), following removal of the Si substrate in KOH solution, planarization of the over-plated nickel surface, complete removal of the SU-8 using microwave plasma ashing (Fig. 2(b)) [3]. The nickel mold insert was mounted in a stainless steel hot embossing fixture using laser welding (Fig. 3(a)).

Micro molding in polycarbonate (PC) was done using hot embossing, with nearly 100% replication results over the entire mold insert surface area (Figure 3(b)). Once additional reservoirs for effective sample handling were made at hot-embossed 96 reservoirs using micro-milling and laser-drilling (Figure 4), the surface of the molded PC chips was modified by UV radiation. After modification, thin PC cover plates (500  $\mu\text{m}$  thick) were used to seal the PC chips using thermal fusion bonding.

Whole cell lysates of several bacterial species (*Bacillus subtilis*, *Staphylococcus aureus*, and *Escherichia coli*) in 3% PEG, 0.4 M NaCl were introduced into the 96 sample reservoirs and immobilized to the capture beds by pulling out cell lysates to the port P2 using a vacuum pump (Figure 5(b)) [4]. Upon completion of sample immobilization, ethanol was pushed through from the port P1 to the sample reservoirs using a syringe and pulled out to the port P2 using a vacuum pump to remove salts and cell debris into a flask. Purified DNA was released from the polymer surface by pushing DI water from the port P1 to the sample reservoirs, and collected into 96 micro-tubes. One  $\mu\text{L}$  ( $\sim 10$  ng) of collected DNA was introduced to a PCR mixture and amplified. The PCR products were electrophoresed on a 3% agarose gel (5 V/cm) containing ethidium bromide, and were indexed against a DNA sizing ladder. Figure 6 shows the fluorescence image of the PCR amplicons generated during amplification reaction with 100 % gDNA purification capability at all 96 capture beds. The PCR primers were designed to produce a 159, 204, and 600 bp amplicons for the *B. subtilis*, *S. aureus*, and *E. coli*, respectively. The 96-well PPC-SPRI reactor developed in this work will open up new avenues for low cost, disposable DNA sample purification in high throughput applications and many other options for high throughput analysis once other micro-analytical systems are implemented in the multi-well format.

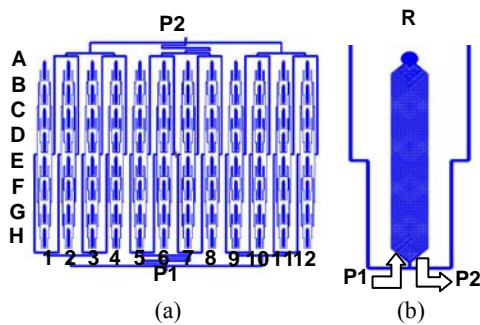


Figure 1: Layout of a 96-well SPRI reactor: (a) an overall view showing microfluidic control ports, P1 and P2; and (b) an individual capture bed with R representing the sample inlet/outlet reservoirs.

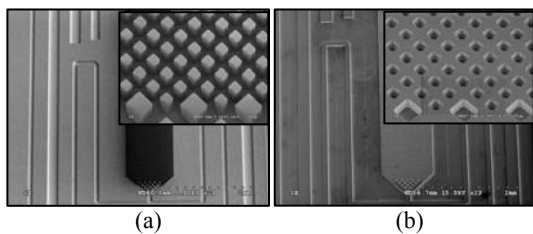


Figure 2: SEM images for (a) SU-8 UV lithography: an overall view of an individual capture bed and close-up view (inset); and (b) nickel LAMI after SU-8 removal and a close-up view of the micro recesses (inset).



Figure 3: (a) Photomicrograph of the 6-inch LAMI in a stainless steel fixture; and (b) SEM images of hot embossing results: an overall view of a capture bed and a close-up view (inset).

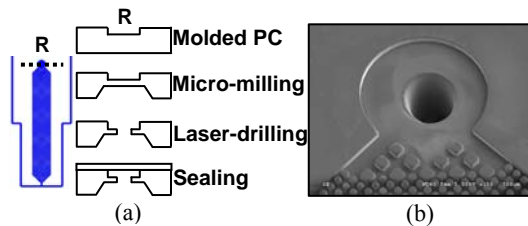


Figure 4: (a) Post-processing of a molded PC chip with R designating the reservoir; and (b) SEM image of a laser-drilled hole.

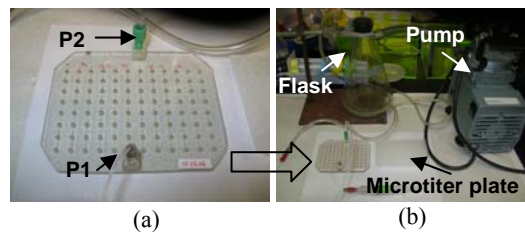


Figure 5: (a) Photomicrograph of a post-processed PC chip; and (b) 96-well gDNA purification setup using a PPC-SPRI chip (P1 and P2: microfluidic control ports).

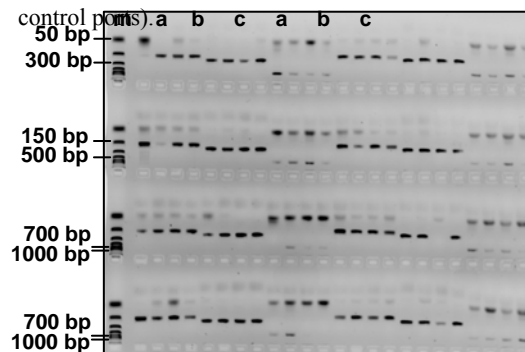


Figure 6: Agarose gel electrophoresis images of the products generated from 96 amplification reactions with purified (a) *B. subtilis*, (b) *S. aureus*, and (c) *E. coli* gDNA using the UV-LIGA PPC-SPRI microchip. Lane m represents DNA sizing ladder (50, 150, 300, 500, 750, 1000 bp).

## REFERENCES

- [1] Microplate Standards Development Committee (2004) *For Microplates – Footprint Dimensions – ANSI/SBS 1-2004*, eds. Secretariat Society for Biomolecular Screening. Danbury, CT.
- [2] M. A. Witek, S. D. Llopis, A. Wheatley, R. L. McCarley, and S. A. Soper, *Nucleic Acids Research*, vol. 34, no. 10, (2006) e74.
- [3] D. Park, M. Hupert, J. Guy, P. Datta, J.-B. Lee, M. Witek, B. H. You, S. A. Soper, D. E. Nikitopoulos, and M. C. Murphy, “Microtiter Plate-based Microfluidic Platforms: Sealing, Leakage Testing, and Performance of a 96-well SPRI Device,” in 2006 ASME International Mechanical Engineering Congress & Exposition (IMECE), Chicago, IL, USA, Nov. 5-10, 2006, IMECE2006-15275.
- [4] D. Park, M. Hupert, M. Witek, J. Guy, P. Datta, B. H. You, S. A. Soper, and M. C. Murphy, “A 96-well SPRI Reactor in Photo-Activated Polycarbonate (PPC) Microfluidic Chip,” in the 20th International Conference on Micro Electro Mechanical Systems (MEMS 2007), Kobe, Japan, Jan. 21-25, 2007, pp. 433-436.

## Center for Bio-Modular Microsystems: Reagent Delivery

N. Kim<sup>1,2</sup>, E. Evans<sup>1</sup>, D.S. Park<sup>2</sup>, D.E. Nikitopoulos<sup>1,2</sup>, S.A. Soper<sup>2,3</sup>, and M.C. Murphy<sup>1,2</sup>

<sup>1</sup>Department of Mechanical Engineering, <sup>2</sup>Center for BioModular Multi-Scale Systems,  
<sup>3</sup>Department of Chemistry, Louisiana State University, Baton Rouge, LA 70803

E-mail: [murphy@me.lsu.edu](mailto:murphy@me.lsu.edu), PRN: ME-MM4100RDE

**Objectives:** Continuous delivery of segmented reagents to microchannel is one of the fundamental operations necessary for high throughput bioassay in microfluidic systems. Segmented flow spaced by gas plugs would decrease the amount of reagents consumed in assays and reduce process time significantly. Application of gas-liquid two-phase flow for controlled reagent delivery is being developed for rectangular microchannels in low cost polymer-based chips.

**Results:** Mold inserts with test devices encompassing several different channel sizes (widths of 50  $\mu\text{m}$ , 100  $\mu\text{m}$  and 200  $\mu\text{m}$  with a height of 220  $\mu\text{m}$ ) were fabricated using the X-ray LIGA process and by micro milling of brass. For the LIGA masks, two types of X-ray masks, with graphite and polyimide membranes, were used to assess the effect of the sidewall roughness on segmented flow stability. Polymer microfluidic chips were thermoformed by hot embossing polycarbonate (PC) and poly(methylmethacrylate) (PMMA) using the mold inserts. Polymer microfluidic chips made by direct micro-machining of the polymer were also fabricated to compare the characteristics of devices made with each fabrication method and the resulting two-phase flow patterns in each type of polymer chip. Cover plates of the same polymer materials were thermally bonded to seal the microchannels in the polymer chips.

An experimental study was performed on gas-liquid two-phase flow in a 200  $\mu\text{m}$  wide by 220  $\mu\text{m}$  deep rectangular microchannel. Dry air and deionized water were injected into the rectangular microchannels at gas superficial velocities ( $j_G$ ) of 0.008 – 12 m/s and liquid superficial velocities ( $j_L$ ) of 0.002 – 0.028 m/s to generate two-phase flow. Two-phase flow patterns were determined by image processing of images captured with a CCD camera. With different liquid fractions ( $\alpha_L$ ), bubbly, plug, slug, annular and dry flow patterns were obtained and compared with previous work. Frictional pressure drops of single and two-phase flow in rectangular microchannel were measured.



## Detection of Very Rare Breast Cancer Cells in Whole Blood

T. Park<sup>1</sup>, J. Guy<sup>3</sup>, P. Datta<sup>4</sup>, S.A. Soper<sup>2,3</sup>, and M.C. Murphy<sup>1,3</sup>

<sup>1</sup> Department of Mechanical Engineering

<sup>2</sup> Department of Chemistry

<sup>3</sup>Center for Biomodular Multi-Scale Systems

<sup>4</sup>Center for Advanced Microstructures and Devices

Louisiana State University, Baton Rouge, LA, 70803

E-mail: [murphy@me.lsu.edu](mailto:murphy@me.lsu.edu), PRN: ME-MM5172

**Objectives:** The most important factor in successfully treating human breast cancer is detection at the earliest stages. Currently, a combination of mammogram screening and biopsy are used for breast cancer detection and diagnosis, but only highly developed calcified tumors can be reliably detected. A microfluidic device for detecting very rare (1-10 mL) cancer cells in whole blood in less than 10 minutes would provide a new foundation for early treatment.

**Results:** Feng [1][2][3] applied mathematical models developed by Chang and Hammer [4] to estimate the optimal flow velocity for antigen/antibody binding of the epithelial cell adhesion molecule (EpCAM), which is over-expressed on breast cancer cells. The capture of MCF-7 breast cancer cells in a functionalized PMMA microfluidic device at the optimal velocity of 2 mm/s was demonstrated in different width channels.

A device for evaluating velocity and channel size effects on the capture efficiency is illustrated in the schematics and micrographs of Figure 1. The core of the system is a 100  $\mu\text{m}$  width, 25  $\mu\text{m}$  height PMMA channel. Assembly of two chips, a cover chip and a channel chip, and alignment of a capillary tube was done using passive alignment to minimize the dead volume and to avoid unexpected trapping of cancer cells along the flow path.

Channel and cover mold inserts were micro-milled (Kern MMP, Germany) and parts hot embossed using the Jenoptik HEX 02 system at the Center for Advanced Microstructures and Devices (CAMD). Sealing of the channel was completed by thermoplastic fusion bonding method without any damage or deformation of microstructures. Thermoplastic fusion bonding for UV-modified PMMA was optimized at 103°C for 35 min under minimal pressure. The cross-section of the fusion bonded device is shown in Figure 2.

NH<sub>2</sub>-modified and anti-EpCAM functionalized PMMA channels were obtained by UV exposure and EDC coupling.[1][2][3][5] The required PMMA exposure time was determined to be 8 min at 254 nm light with 15 mW/cm<sup>2</sup> intensity which was determined through a combination of maximizing the water contact angle on the modified PMMA, minimizing the physical surface damage, and maximizing the FITC intensity on the anti-EpCAM functionalized PMMA surface with different conditions, materials, and doses. A novel protocol was established to collect single or precise small numbers of MCF-7 cells in the capillary tube, After flaking off a polyimide coated silica capillary tube by over

600°C flame, the capillary was visible and movable in the hemacytometer (see Figure 3). Transferring the collected MCF-7 cells from inside of capillary to micro channel was achieved without cell loss. MCF-7 cells were stained with DAPI and trypan blue to mark as target cell and delivered at a 2 mm/s flow velocity. Captured and retained MCF-7 cells after over 10mm/s PBS rinse are shown in Figure 4.

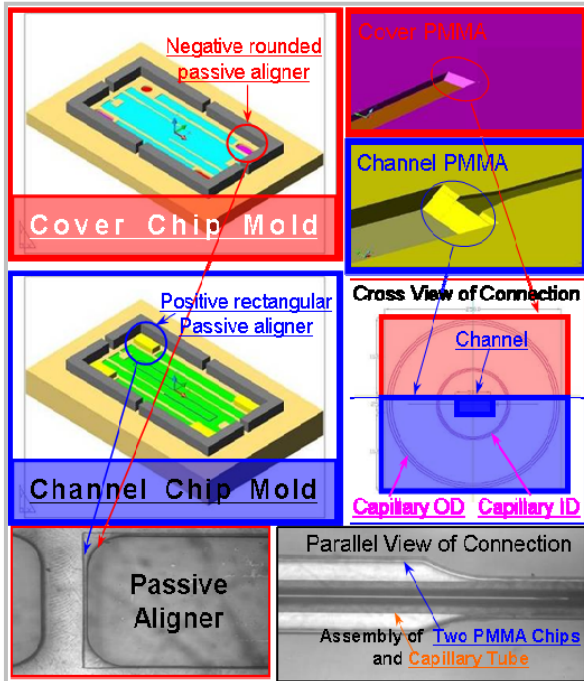


Figure 1. Connector and passive align design

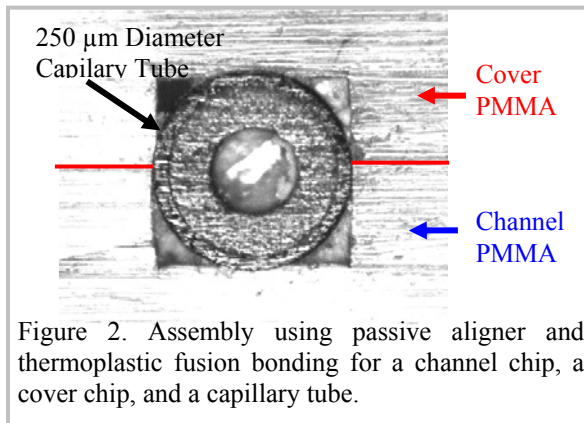


Figure 2. Assembly using passive aligner and thermoplastic fusion bonding for a channel chip, a cover chip, and a capillary tube.

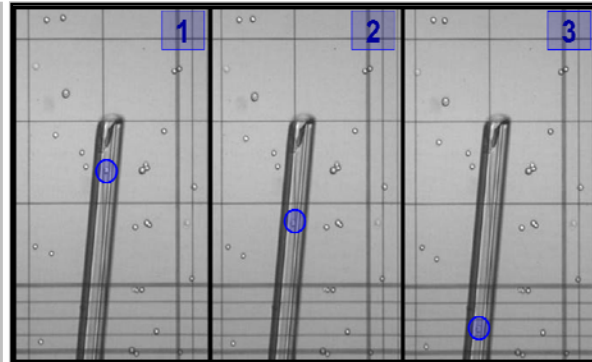


Figure 3. Collection of single cell using a silica capillary (OD =105 μm, top) and syringe (25 μl) in a hemacytometer. The blue circles indicate the single target MCF-7 cell. The capillary was clearly visible and easily movable since the polyimide was removed.

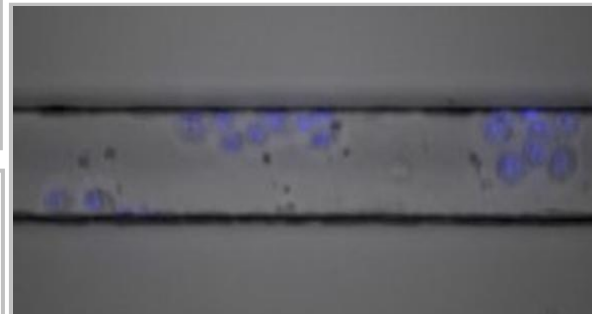


Figure 4. DAPI stained MCF-7 cell capture in the anti-EpCAM functionalized channel.

## REFERENCES

1. Feng, J., *A Microfluidic Device for Trapping Rare Cells in Whole Blood*, M.S. Thesis, Department of Mechanical Engineering, LSU, May 2004.
2. McCarley, R. L., Vaidya, B., Wei, S., Smith, A. F., Patel, A. B., Feng, J., Murphy, M. C., and Soper, S. A. (2005) "Resist-Free Patterning of Surface Architectures in Polymer-Based Microanalytical Devices," *J. Am. Chem. Soc. (Communication)*; 127(3):842-843.
3. Feng, J., Soper, S.A., McCarley, R.L., and Murphy, M.C. (2004) "Separation of breast cancer cells from peripherally circulating blood using antibodies fixed in micro-channels," in *Lasers in Surgery: Advanced Characterization, Therapeutics, and Systems XIV*, eds. D.S. Robinson and K.D. Paulsen, Society of Photo-optical Instrumentation Engineers (SPIE), Volume 5312, 278-293.
4. Chang, K.C. and Hammer, D.A. , (1999) "The forward rate of binding of surface-tethered reactants: effect of relative motion between two surfaces", *Biophysical Journal*, 76:1280-1292.
5. Henry, A.C. et al. (2000) "Surface modification of poly(methyl methacrylate) used in the fabrication of microanalytical devices," *Anal. Chem*, 72:5331-5337.

## Design and Fabrication of a Recurve Bimorph Thermosensor

R. Simmons<sup>1</sup>, D. Gonzales<sup>1</sup>, E.J. Podlaha-Murphy<sup>2</sup>, W.M. Goh<sup>3</sup>, and M. C. Murphy<sup>1</sup>

<sup>1</sup>Department of Mechanical Engineering  
Louisiana State University, Baton Rouge, LA 70803, U.S.

<sup>2</sup>Department of Chemical Engineering  
Northeastern University, Boston, MA , U.S.

<sup>3</sup>Schlumberger Technology, Inc.  
Sugarland, TX, U.S.

E-mail: [murphy@me.lsu.edu](mailto:murphy@me.lsu.edu), PRN: ME-MM4188

**Objectives:** A bimetallic recurve thermosensor was designed to replace current Mercury in glass thermometers used to monitor downhole temperatures during oil exploration. Requirements for the sensor were to be compact, shock resistant, cost effective to manufacture, and capable of passively recording maximum temperatures up to 300°C. Resolution for the sensor was to be 2°C. Initial efforts focused on reproducing previous bimorph structures [1][2] for test and characterization of the bimorph elements and fabrication process.

**Results:** The simplified two mask process demonstrated by Sathe [3], was adopted to fabricate test structures for evaluating the performance of the bimorphs. CAD files containing a selection of different bimorph designs initially used by Datta [1][2], were modified to incorporate alignment marks and a set of two UV masks purchased. Two X-ray masks were made, one for each layer of the bimetallic strip. Graphite was used as the substrate and SU-8 as the resist. After development, the masks were electroplated with gold and mounted on a NIST ring.

Several first layer X-ray exposures were then performed on PMMA samples on titanium wafers. Currently, the electroplating of the first layer of Invar-like FeNi is in progress.

### REFERENCES

1. Datta, P., "Design and Fabrication of a Thermomechanical Micro-actuator", (2001), Master's Thesis, LSU, Department of Mechanical Engineering.
2. Datta, P., Sathe, M., Namburi, L., Podlaha, E.J., Acharya, S. and Murphy, M.C. (2003) "Microfabricated bimetallic actuator," in *MEMS Components and Applications for Industry, Automobiles, Aerospace, and Communication II*, ed. S.W. Janson, Society of Photo-optical Instrumentation Engineers (SPIE), Volume 4981, pp. 83-94.
3. Sathe, M., "Design, Fabrication and Thermomechanical Testing of a Vertical Bimorph Sensor in the Wafer Plane", (2004), Master's Thesis, LSU, Department of Mechanical Engineering)

## **MEMS/LIGA Services at CAMD in 2006**

Editor: Jost Goettert

Service Group Members: Proyag Datta, Fareed Dawan, Yoonyoung Jin, Zhong-Geng Ling, Shaloma Malveaux, Tracy Morris, Varshni Singh

Student Worker: Sitanshu Gurung, Sanjay Kalakheti, Kyung-Nam Kang, Abhilash Krishna, Philip Smith, Sital Towari, Gurda Venkatramana

### **Summary**

In 2006 the MEMS/LIGA Service Group at CAMD has continued to provide a multitude of MEMS related services to the MEMS community primarily at LSU but also the wider LIGA community in the world. Besides well-established routine services including thin film deposition, X-ray masks, optical and X-ray lithography (print-shop), electroplating of Ni, Ni-Fe, Cu, and Au, mold insert fabrication, and hot embossing also novel capabilities including thick SU-8 patterning, UDXRL patterning at the CAMD wiggler, nano-composite materials, and nano-size lithographic patterning have been explored and further improved. These R&D efforts were inspired by interaction with customers and understanding their process and application requirements as well as the desire to establish internal R&D projects with focus to meet requirements of future applications, and generating new funding opportunities.

In addition the service group focused on writing proposals to enhance the existing process equipment and microfabrication infrastructure to expand process capabilities and better meet future R&D demands.

The following contributions briefly summarize service and beamline statistics, the enhancement activities, and some of the ongoing R&D efforts.

Executive summary describing the clean room and beamline situation and conclude with a need to drive R&D in the x-ray lithography program and partner more aggressively (including PR) with customers promoting the commercial use of the technology.

### Overview of currently provided microfabrication services

**Tables I and II** summarize the base processes and process modules offered by the MEMS/LiGA Services Group at CAMD. All services are offered to customers on a pay basis. These services are mostly comparable to the ones offered in 2004 and 2005<sup>1</sup> with some minor adjustments marked at the bottom of each table.

**Table I**  
Services provided by the CAMD Service Group in 2006

Service Type	Materials	Specifications	Contact person
<b>E-beam deposition</b>	Cr, Au, Cu, Ni, Ti	0-2000 Å	Yoonyoung Jin
<b>Surface modification</b>	Ti oxidation	2 µm	Yoonyoung Jin
<b>Printshop (X-ray exposure)</b>	PMMA SU-8 <sup>(1)</sup>	1-2000 µm 1-3000 µm	Zhong-Geng Ling
<b>Electroplating</b>	Ni Cu Au Ni-Fe	1-5000 µm 1-500 µm 1-100 µm 1-500 µm	Varshni Singh Varshni Singh Varshni Singh Varshni Singh
<b>Hot-embossing</b>	PMMA, PC	CD > 10 µm Aspect-ratio 10:1	Proyag Datta
<b>Flycutting</b>	PMMA, SU-8	50 µm – any	Varshni Singh
<b>Metrology: SEM EDAX WYKO</b>	Any Any Any	< 4" DIA Any	Varshni Singh Varshni Singh Varshni Singh

<sup>(1)</sup>SU-8 substrates are to be provided by customer, CAMD is not offering application of thick (>500µm) SU-8 resists at this time.

**Table II**  
Process modules offered by the CAMD Service Group in 2006

Module Type	Materials	Specifications	Contact person
<b>UDXRL Substrates</b>	PMMA	100-2000 µm	Varshni Singh
<b>X-ray masks</b>	Au on Be, C, SiNx, or Kapton	5-40 µm Au thickness, 5 µm CD	Yoonyoung Jin
<b>Mold inserts</b>	Nickel Brass (machined) <sup>(1)</sup>	5 µm CD, 4"-6" DIA 20 µm CD	Jost Goettert, Varshni Singh, Proyag Datta, Jason Guy

<sup>(1)</sup>Machined mold inserts made from Brass is a rapid prototyping service provided through CBM2/Jason Guy; while evaluating the customer's design and specification CAMD staff is recommending the most suitable fabrication approach to make a mold insert. Precision machined

<sup>1</sup> Y. Desta et al: 'MEMS/LIGA Services at CAMD in 2004', CAMD Annual Report 2004. J. Goettert et al: 'MEMS/LIGA Services at CAMD in 2005', CAMD Annual Report 2005.

mold inserts are especially attractive for microfluidic applications and design iteration but are typically limited to Aspect Ratios (AR) <4.

**Table III**

Summary of service jobs completed in 2006 and compared with service jobs in 2005

Service type	Customers	Number of Jobs 2006	Number of Jobs 2005
Thin film deposition	LSU, Industrial	389 (993 substrates)	519 (1591 substrates)
Surface modification	LSU, Industrial	258	NA
UDXRL Substrates	Industrial	5 (116)	5(27 substrates)
X-ray masks	LSU, Industrial	12	21
Mold inserts	LSU, Industrial	75 (2 LiGA)	4
Electroplating	LSU, Industrial	12 (211)	46 (112 substrates)
X-ray Exposure	LSU, Industrial	592 substrates	598 (661 substrates)
Hot embossing	LSU, Industrial	75 (950)	57(930)
Metrology	LSU, Industrial	10 (71 samples)	30 (105 samples)
Fly cutting	Industrial	20 (162 substrates)	22 (191 substrates)
Polishing	Industrial	4 (20 substrates)	4 (16 substrates)

Overall the number of service jobs remains constant indicating a stable demand for MEMS services provided by CAMD. It should be noted that new customers for microfluidic applications could be attracted through collaboration with CBMM. Most of their current needs can be satisfied by micromachining and molding and do not need (at least initially) lithography based services. This accounts partly for the dramatic increase in mold insert fabrication.

### User statistic – X-ray lithography exposures

The two charts in Fig. 1 represent the distribution of exposed substrates (left) and exposure dose (right) from different user groups (CAMD, External, LSU) at all four beamlines for 2006. The user groups include CAMD with currently one major project (accounting for approx. 60% of the CAMD substrates and funded through DARPA-MTO, MGA project; for details see contribution from A. Bhushan and D. Yemane in this annual report) and 4 smaller projects, while external print-shop users include HT Micro, Mezzo, and Creatv Inc and LSU users are from Mechanical (2 professors) and Chemical (1 professor) Engineering at LSU.

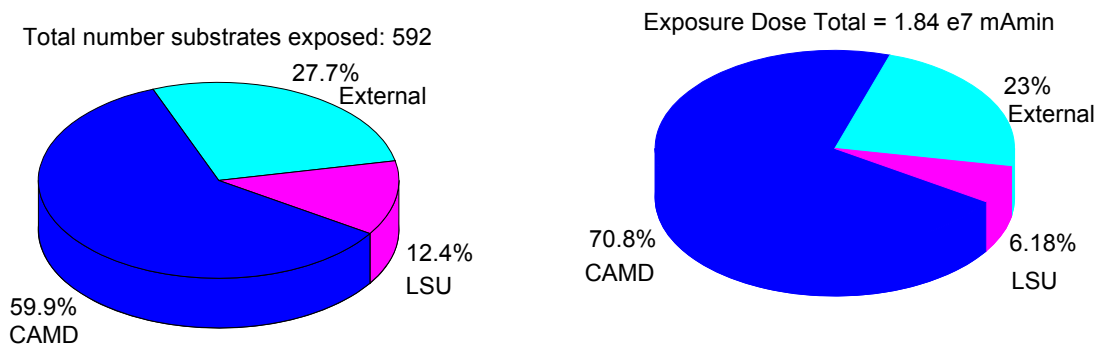


Fig. 1: Distribution of total number of substrates (left) and exposure dose (right) for all beamlines among the three main user groups – CAMD, LSU professors and students, and external, industrial customers. The total number of substrates was 592.

When comparing these numbers with previous years (Figs. 2 and 3) the following observations can be made:

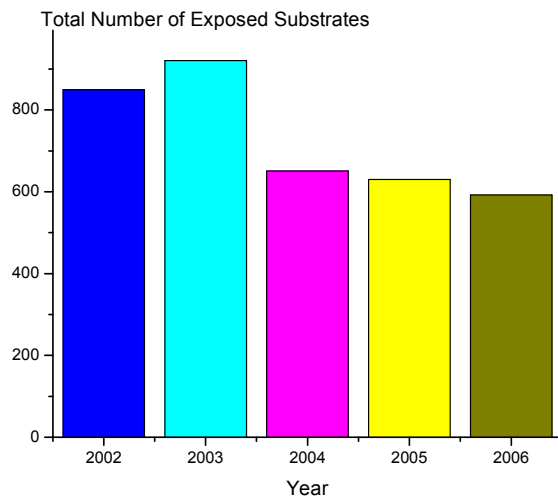


Fig. 2: Total numbers of substrates exposed in the last 5 years at all beamlines.

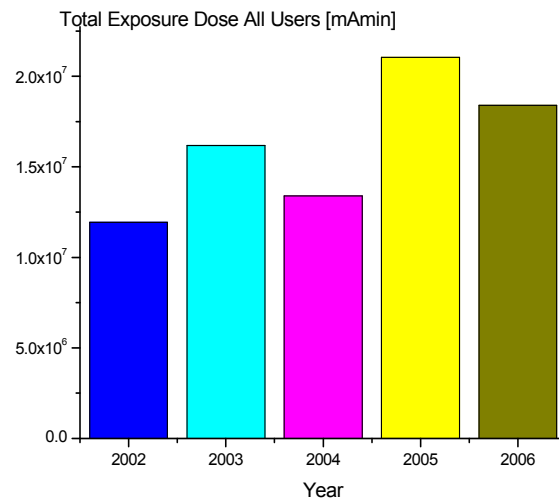


Fig. 3: Total exposure dose in the last 5 years accumulated at all beamlines.

- The higher numbers of exposed substrates in 2002 and 2003 was stimulated through CAMD research projects funded through DARPA. On from 2004 the number stabilized around 600 substrates per year.
- The trend for total exposure dose is somewhat increasing over time. This indicates a desire for longer exposures per substrate caused by thicker resists/taller structures and larger mask areas/larger scanning distance. This also reflects an improvement in technology as we are now able to fabricate X-ray masks with large open areas (80mm) as well as patterning thick resist layers beyond 500µm thickness.

While these overall trends demonstrate a certain stability of operation and a reasonable interest in using LIGA technology a closer look at the three main user groups shown in Figs. 4 and 5 leads to the following observations:



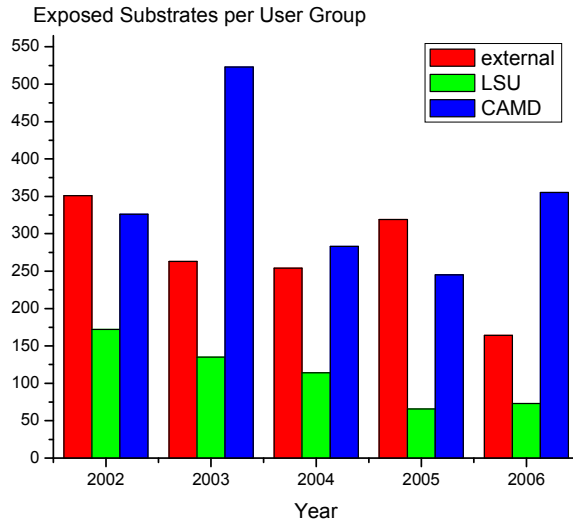


Fig. 4: Number of substrates exposed by the main user groups over the past 5 years.

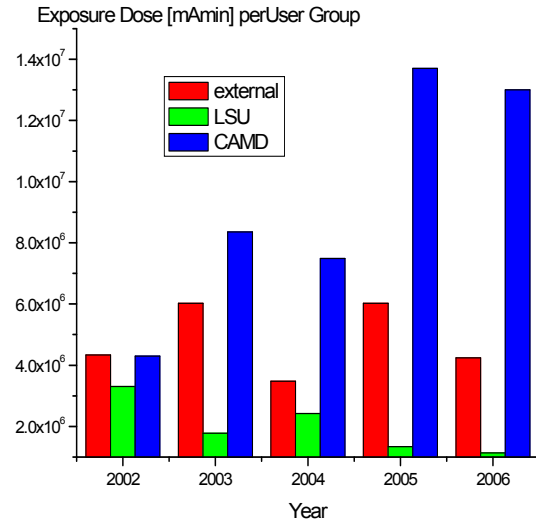


Fig. 5: Exposure dose accumulated by the main user groups over the past 5 years.

- The number of substrates from LSU users is decreasing somewhat continuously over the past 5 years; there is mainly one active user (E. Podlaha, Chem Eng) who uses X-ray lithography to pattern templates for plating tests; all other users choose alternative approaches (micromachining, optical lithography) and only turn to x-ray lithography when in need for highest quality.
- The external users experienced a dramatic dip (~50%) last year mainly because HT Micro – the leading customer in 2005 – had significant fewer substrates to expose. However, the exposure dose didn't decrease at the same rate indicating the need for thicker substrates to expose.
- The CAMD portion increased primarily because of the demand for GC samples needed for column coating and chromatography tests; however, due to process optimization the exposure dose for these samples could be reduced.

In conclusion, x-ray lithography capabilities are under-utilized and find fewer and fewer users. Especially the LSU community seems to shy away from this technology and favor alternative options, namely micromachining and molding. This approach is certainly appropriate for many microfluidic applications, a focus of researchers at LSU's CBMM center. CAMD researchers become the main user group and strong efforts and good progress are developing when funding is available. Smaller research efforts (see contribution by Jost Goettert et al. in this annual report) are ongoing and are stimulated by customer interest but cannot be pursued with high priority due to a lack of funding.

Taking a closer look at the use of different beamlines and how they are used data from Figs. 6 and 7 provide the following information:

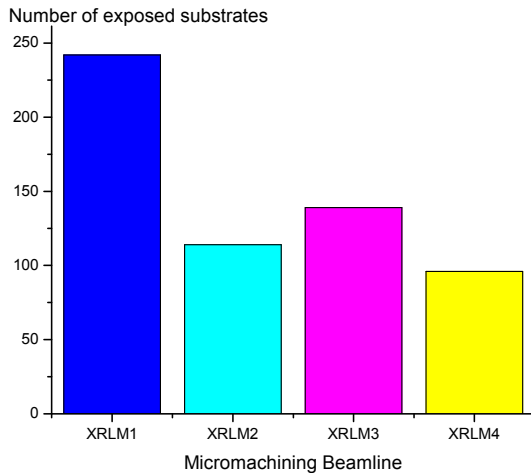


Fig. 6: Number of substrates exposed at the different CAMD micromachining beamlines.

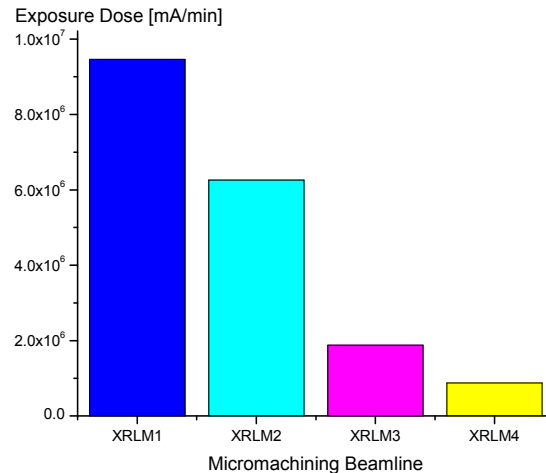


Fig. 7: Accumulated exposure dose at the different CAMD micromachining beamlines.

- XRLM1 exposes the majority of substrates as well as the highest dose; this is mainly due to the versatility of this beamline allowing to switch between a soft x-ray spectrum and the regular bending magnet spectrum by inserting two mirrors into the beam; demand for the soft x-ray photons arose from projects associated with micrometer down to sub-micrometer structures.
- XRLM 2 and 3 expose approx. the same number of substrates; however the exposure dose at XRLM 2 is ~3x higher as this beamline is used for thicker substrates (longer exposure times) and larger scan range (larger mask areas); it should be noted that XRLM 2 could easily accommodate all exposure requests for both beamlines.
- There is an increasing interest in hard x-ray radiation for UDXRL samples which are now available at the DEX 3 scanner (modification of the substrate fixture and cooling circuit resulted in stable, reliable exposure conditions); however, despite the increased resist thickness (typ. 1-1.5mm) exposure dose is low as the wiggler spectrum is harder and overall power output is significantly higher. There is certainly opportunity to provide more print-shop services at this beamline in the future.

In conclusion, CAMD microfabrication group should consider reducing the number of operating micromachining beamlines from 4 to 3 (XRLM 1 and 4 and either XRLM 2 or 3). There is a need for a versatile exposure spectrum using the mirror option or the wiggler source. There is a growing interest for smaller (sub-micrometer) structures requiring soft x-ray lithography (applications include for example photonic crystals, RF MEMS devices, and filter structures for microfluidic applications) and an interest in very tall structures patterned by hard x-rays from the wiggler beamline. It should also be noted that process improvements (meaning R&D) is needed to establish a standard service in these areas. For example, patterning of ultra-thick resist structures needs systematic studies on dose and development parameters to ensure the desired structure quality for PMMA and there is always the interest of reducing exposure dose by replacing PMMA with the more sensitive SU-8 resist (see contribution J. Goettert et al in this report).

### **Enhancement proposals**

The Louisiana Board of Regents (BoR) provides annual funding opportunities for enhancement of infrastructure. The CAMD microfabrication group regularly submits proposals for equipment that is of interest to a larger user community and allows the microfabrication community to stay on the cutting edge of R&D infrastructure and capabilities.

The following proposals have been submitted in 2006. The abstract for each proposal is included and further details can be requested from the PI directly.

#### **Enhancement of Thin-Film and Surface Process Capabilities at the CAMD Cleanroom**

**(PI Y. Jin, funds requested: \$ 145,882)**

The goal of this proposal is to upgrade and add process equipment for advanced MEMS and NEMS processing capabilities in the CAMD cleanroom. A significant upgrade is requested for the existing Temescal E-beam evaporator. Three new components/features will be added to the current system resulting in higher quality films (replacing the oil-based vacuum pumps with dry pumps that also achieve a better vacuum) made from alloys and a number of other, novel materials and material layer combinations significantly expanding the current single and multi-layer metal deposition capability.

New spin-coating and surface cleaning and modification equipment is required to meet the more stringent demands of nano-size structures. Spin-coating equipment with high rpm and programmable spin-protocols will guarantee high quality, uniform films with heights ranging from 100 nm to several 100 $\mu$ m. A special Edge Bead Removal feature explicitly improves thick resist film coating critical for many research projects at CAMD. Surface cleanliness and modification using a dedicated UV/ozone cleaner will allow to establish defined surface conditions critical for high yield, low defect processing.

#### **Electronic Post Processing Equipment for Micro and Nano Technology**

**(PI J. Goettert, funds requested: \$ 112,455)**

In the recent years more and more projects conducted by CAMD staff as well as 60-70 external CAMD academic users require equipment and processes that exceed the pure microfabrication needs and expand to system design, fabrication and testing. MEMS systems typically consist of discrete microfabricated components and modules performing mechanical, fluidic, or optical functions that have to be combined with basic electronic circuitry for data acquisition, signal processing, system control, and user interface.

The goal of this proposal is to add fundamental electronic equipment for an 'Electronic Laboratory' to the already existing MEMS CAMD infrastructure. This new equipment will be partly installed inside the CAMD clean room (bonding equipment), and partly in a dedicated area with controlled access for trained users. The new

equipment will directly impact basic electronic fabrication and MEMS assembly and integration capabilities. The printed circuit board machining equipment consisting of a rapid prototyping, precision milling machine and an electroplating bath for through-hole plating will be the workhorse for many customer-specific electronic solutions needed by the MEMS researcher community and the CAMD machine and beam-line engineers. A set of bonding tools including wedge, ball and die bonder will provide technical solutions for many interconnect and assembly tasks combining MEMS modules for fluidic, optical, and mechanical functions with electronic modules for control, data acquisition and processing, and user interface. The stand-alone cutting and grinding tool is essential separating batch fabricated MEMS components and prepare them for the assembly and integration process.

### **Biocompatible Coating (Parylene) Deposition System**

**(PI V. Singh, funds requested: \$98,690)**

Biocompatibility and miniaturization are extremely critical for biosciences and micro-electro-mechanical systems (MEMS) researcher and its user community in medical and health sciences. It is essential for the devices fabricated by them to have a biocompatible and inert surface, to be functional and work at a high level repeatedly for extended period of time even in a harsh environment such as inside our body. However, it is extremely difficult to fabricate devices by employing only such materials that are truly biocompatible and inert. This is undesirable and/or a limitation to researchers with bio applications. This limitation can be addressed by a thin, biocompatible, conformal, transparent, chemically inert and free from pinholes, 'perfect' coating, which gives a uniform surface to the whole device and is crucial to ensure reliable functionality and performance. One of the most desired among the few available solutions is Parylene, a polymer coating that possess all the required properties and additionally possess excellent adhesion and autoclavable property. The funds are requested to purchase a biocoating (Parylene) deposition system. This unique equipment will enhance/improve a great number of research and development projects at LSU and other LA universities in the area of Bio-MEMS, MEMS and nano-electro-mechanical systems as is indicative by the large and diverse group of PI and Co-PIs.

### **Analytical equipment for in-situ detection in MEMS and NEMS systems**

**(PI C. Kumar, funds requested: \$ 134,686)**

Two different analytical probes - a React IR4000 (Mettler Toledo Auto Chem ReactIR) with silicon probe and a UV-VIS optical spectrometer with fiber probing capability – are proposed to enhance the in-situ analysis of nanoparticle formation during wet chemical synthesis in traditional flask as well as micro fluidic reactor systems. CAMD researchers combined their efforts with colleagues at LSU ChemEng and Pennington Biomedical Research Center to develop new and advanced methods of wet-chemical synthesis of custom-made nanoparticles with biofunctionalized shell. A major enhancement towards complete process control is provided through spectroscopic in-situ analysis as an immediate control and feedback mechanism to regulate the reaction. The

IR4000 will be utilized to investigate the presence of possible reaction intermediates during the formation of magnetic nanoparticles such as cobalt and iron oxide and their bioconjugates through in-situ measurements. The UV-VIS analysis utilizing miniaturized fiber-optic spectrometers such as the Ocean Optics QE65000 uses special fiber probes as well as transmission setups to monitor the spectral changes and/or specific reaction changes (pH-value, O<sub>2</sub> content) allowing easy, in-situ control of the synthesis. Having these monitoring capabilities will ensure repeatable results of nanoparticle synthesis and the systematic optimization of reaction conditions in order to achieve well-controlled particle properties.

### **Acknowledgements**

The members of the services group would like to thank all customers and users for their interest and support of their activities. Special thanks are given to our 'active' users for their interest in working at CAMD and sharing their expertise and knowledge, which ultimately helps to enhance CAMD's service capabilities.

## Fabrication of perforated polymer membranes using hot embossing technology

Anish Roychowdhury and Sungook Park

Department of Mechanical Engineering and Centre for Bio-Modular Multiscale Systems  
Louisiana State University, Baton Rouge, LA 70803,  
PRN: ME- SP1205, email: sungook@me.lsu.edu

**Objectives:** To develop a process for the production of perforated polymer membranes using thermal imprinting technology. The realization of such membrane architectures would provide a future platform for various fundamental research activities, e.g. transport behavior in cell biology, protein patterning, separation of substances and polymer optics.

A single step imprinting process was used to realize the membranes combined with semiconductor micromachining processes. The several technical challenges in this project included developing and optimizing a series of processes starting from stamp design to materials choice, imprinting of high aspect ratio patterns, and post- processing.

**Experimental procedures:** Fig 1 presents a proposed process scheme for the fabrication of polymer membranes. The process consists of patterning of desired structures, followed by pattern transfer and removal of sacrificial layer.

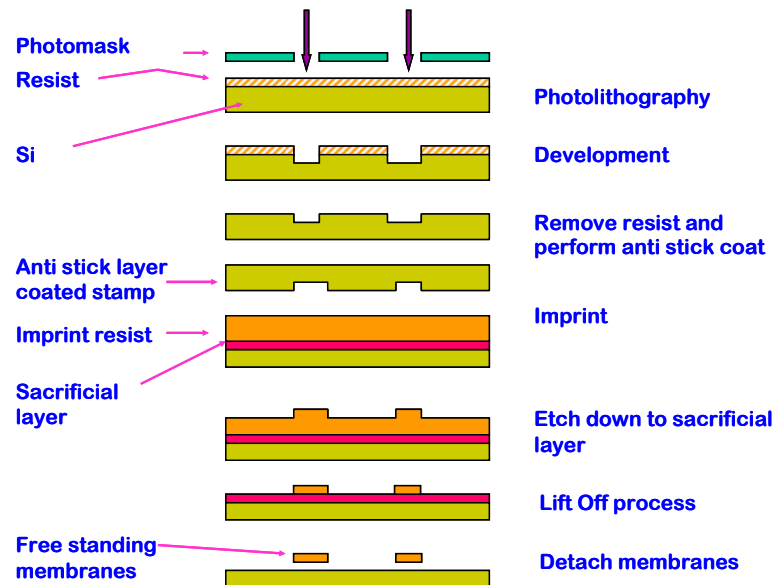


Fig 1 – Schematic of proposed process

Taking advantage of the existing micro fabrication facilities at CAMD, a UV lithography based approach was used to make pattern on a photo resist coated silicon wafer in order to fabricate microscale stamps for imprinting. S1813 photo resist was spin coated and baked on the wafer. The Quintel UV exposure station at CAMD was used to pattern the photo resist, a subsequent deep reactive ion etching (DRIE) was done (at Georgia Tech) on the exposed and developed wafer to complete micro scale stamps.

These stamps were used in a thermal imprint process using an NIL imprinter (Obducat, Sweden) to transfer pattern unto PMMA sheets as a first step towards optimizing the imprinting process.

**Required Facilities:** CAMD Cleanroom: for UV lithography (Quintel), substrate preparation (spin coat + bake) and developing. Preparing photomask for back side etch (Pattern generator)

**CBM2:** Imprint and post processing

**Life Sciences:** for Gold coating for SEM metrology

**MCC at ME department:** SEM metrology

**MiRC at Georgia Institute of Technology:** DRIE tool,

**AMRI at University of New Orleans:** Ebeam tool for nanoscale patterning.

**Results:** SEM images were taken at MCC at Mechanical Engineering Department at LSU to verify the membrane structures. Refer Fig- (2a,b)

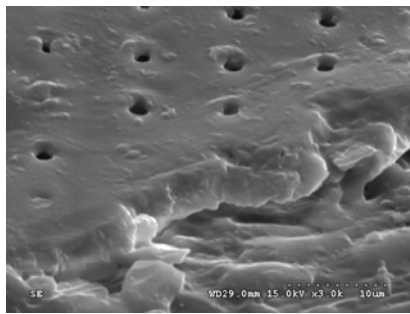


Fig 2a – SEM of 1.5 $\mu$  dia ,Su-8 membrane supported on Si with PMMA sacrificial layer

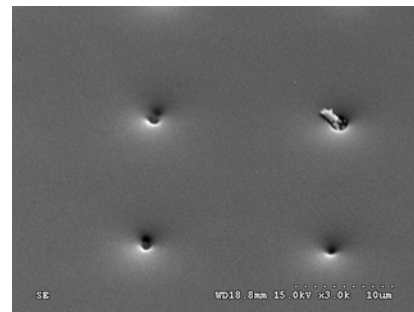


Fig 2b – SEM of 500 nm diameter holes in Su-8 using LOR as sacrificial layer

**Future work:** The effort will be given to reduce the size of holes in the polymer membranes down to sub-200 nm level. The formation of perforated membranes will be used as architecture to study transport behavior through lipid bilayer.

## Current Thrusts in Microfabrication

### Fabrication of High Aspect Ratio Nanostructures Using Soft X-Ray Lithography

PI's: Yoonyoung Jin, Fareed Dawan, Jost Goettert, V. Singh

Fabrication and development of submicron/nanostructures with high aspect ratios using soft x-ray LIGA has been revived in order to prepare mold insert fabrication for Nano-Imprint-Lithography (NIL) efforts associated with CBM<sup>2</sup> (Prof. Sunggook Park). Novel methods and advances in nanotechnology have generated an ever increasing desire and necessity for such fabrication ability, highly relevant in nearly all fields of actual research. Examples include biomimetry, or the artificial mimicking of natural biological submicron and nanostructures such as gecko foot hairs<sup>1</sup> or the Lotus effect<sup>2</sup>; environmental engineering, such as using fabricated photonic nanocrystals in thin polymeric films for the construction of photovoltaic cells to harness solar energy<sup>3</sup>; nanoelectromechanical systems or NEMS, an exciting new field innately derived from the popular microelectromechanical systems (MEMS) field.

One approach to make nanosize structures is using soft X-ray lithography initially developed to fabricate the next generation microelectronic chips<sup>4</sup>. While structure height for microelectronics is typically a few 100 nanometer the aforementioned applications require high aspect ratio submicron and/or nanosize structures. There are a number of ways of making these structures. For example nano-embossing of the fine probe tip of an AFM or STM is used to produce nano-scaled indentations into soft, impressionable<sup>1</sup>. As with any embossing or molding method, difficulty in fabrication arises in the releasing of the molds without structural loss and without compromising structural precision, particularly when dealing with high aspect ratio features. Electron or E-beam lithography is another method. Though shown to produce very precise nanostructures in the lateral dimension, this approach has limitations regarding high aspect ratio structures requiring high electron energies (100keV) and feature broadening because of scattering. X-ray LIGA either used in a conventional shadow printing setup<sup>5</sup> or as interference lithography<sup>6</sup> method is another technique capable of achieving high precision submicron/nanostructures, and also may provide a cost effective solution for nanoscale patterning by copying many structures in parallel.

High aspect ratio submicron/nanoscale patterning of PMMA was carried out using X-rays emitted from synchrotron radiation at the Center for Advanced Microstructures and Devices (CAMD). The XRLM1 microfabrication beamline is equipped with a double-mirror system which provides soft x-rays<sup>7</sup>. The patterning process utilized a silicon nitride membrane mask with gold absorber structures (posts) of 750 nm diameter fabricated by E-beam lithography<sup>5</sup>. The substrate for exposure was PMMA spin coated to approximately 4  $\mu\text{m}$  on a gold coated silicon wafer. The resulting PMMA structures are cylindrical posts with a diameter of 750 nm and a height of  $\sim 4 \mu\text{m}$  giving a high aspect ratio of 5. Wet development of the structures from unexposed PMMA may be problematic due to the tendency to stick together. In order to avoid this, a method was devised to develop without the use of liquids which will be further discussed. Subsequently, nickel electroplating around the post structures was done and as a final



step the PMMA posts were dissolved. Figure 1 shows the top view of the LIGA structures. The diameter of each hole is 750 nm with a depth of 4  $\mu\text{m}$ .

In addition to the method of fabrication, the evaluation of various factors for high-aspect ratio nanostructure fabrication will be discussed. Specifically, these factors include 1) exposure doses using the XRLM1 in mirror system operation, 2) the development of the structures and preventing the sticking problems, and 3) nickel electroplating to achieve high uniformity and ease of handling of the fragile structures.

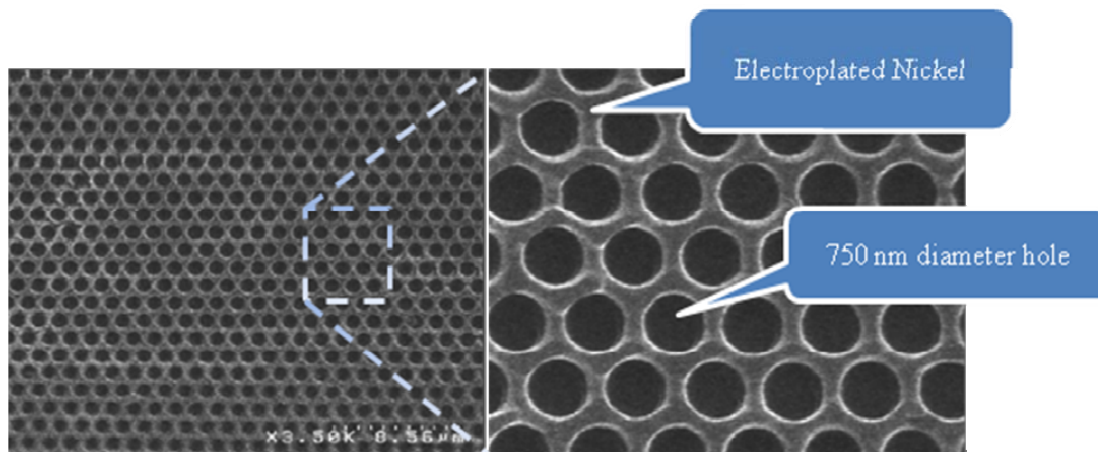


**Figure 1.** SEM images of a wide view (left), and magnified view (right) of the x-ray LIGA fabricated high aspect ratio nanostructures. As indicated, surrounded with electroplated Ni, the holes have a diameter of 750 nm at a depth of 4  $\mu\text{m}$ .

## References:

1. Sitti, M. "High Aspect Ratio Poly Mico/Nano-structure Manufacturing using Nanoembossing, Nanomolding and Directed Self-Assembly", Proceedings of the 2003 IEEE/ASME International Conference on Advanced Intelligent Mechatronics (AIM), 2003.
2. *Blossey, R. (2003): Self-cleaning surfaces - virtual realities ; Nature materials 2: 301-306*
3. Sinkkonen, J, Novikov, S, Ovchinnikov, V, Toivola, T. "Light Emission From Si/SiO<sub>2</sub> Nanostructures", 3<sup>rd</sup> World Conference on Photovoltaic Energy Conversion, May 11-18, 2003.
4. Cerrina, F. ; *X-ray Lithography* ; in : Rai-Choudhury, P. (Ed.) SPIE Handbook of Microlithography. Micromachining, and Microfabrication, Vol. 1 (1997), 251-320.
5. L. Wang, T. Christenson, Y.M. Desta, R.K. Fettig and *J. Goettert*; "High Resolution X-ray Masks for High Aspect Ratio MEMS Applications" Journal of Micromechanics and Microengineering, 14 (2004) S.722-26.
6. For more details on x-ray interference lithography check the PSI-Laboratory for Micro- and Nanotechnology webpage at <http://lmn.web.psi.ch/xil/intro.htm>.
7. For details see <http://www.camd.lsu.edu/beamlines.htm>

## Sweat/Saliva Stick Volume Meter December 2006 Report for CAMD/LSU

Varshni Singh and Jost Goettert

### Body Fluid Collection Biocompatible, Non-invasive, Small Device

The R&D work started in second half of 2003 [<sup>xv</sup>] was continued by the CAMD group in 2004 to modify and build the sweatstick demonstrator devices for preliminary testing to be conducted at University of Houston [<sup>xvi</sup>]. The design of the device was further modified in 2005 to make it more versatile and this modified device was designed to collect both sweat or saliva from human body [<sup>xvii</sup>]. The work was further continued by the CAMD group in 2006. The results from previous work [**Error! Bookmark not defined.**] showed that the design needs to be modified to improve its saliva (relatively more viscous fluid than sweat) collection efficiency without the help of trained personnel. Therefore, 5 saliva sticks with a modified design were fabricated and assembled to perform the preliminary testing to compare the results with other saliva collecting techniques. Further, the work on fabricating a portable device was also continued [<sup>xviii</sup>] and a presentation at the COMS2006 conference sparked some interest in commercialization of the sweat stick device for health monitoring [5].

Fig.1 shows the schematic of the modified saliva collection device. The device has 1 mm diameter channels all around it at an angle of 20°. Saliva is collected in these channels and it flows into the tube connected to the device, which is spun at high speed in centrifuge. Two vent channels on the right side ensure free flow of saliva by preventing any vacuum. Preliminary results show that the volume of saliva collected is much smaller than expected. Therefore, this was not the optimum design and work is under progress for modifying it further.

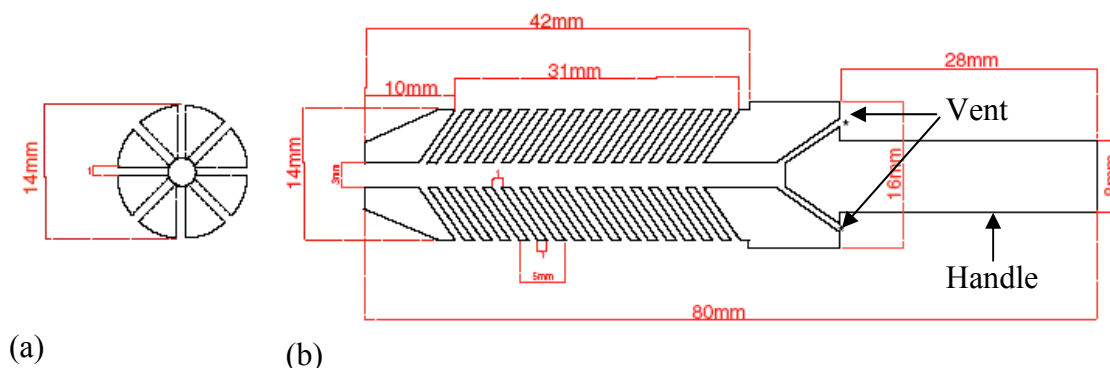
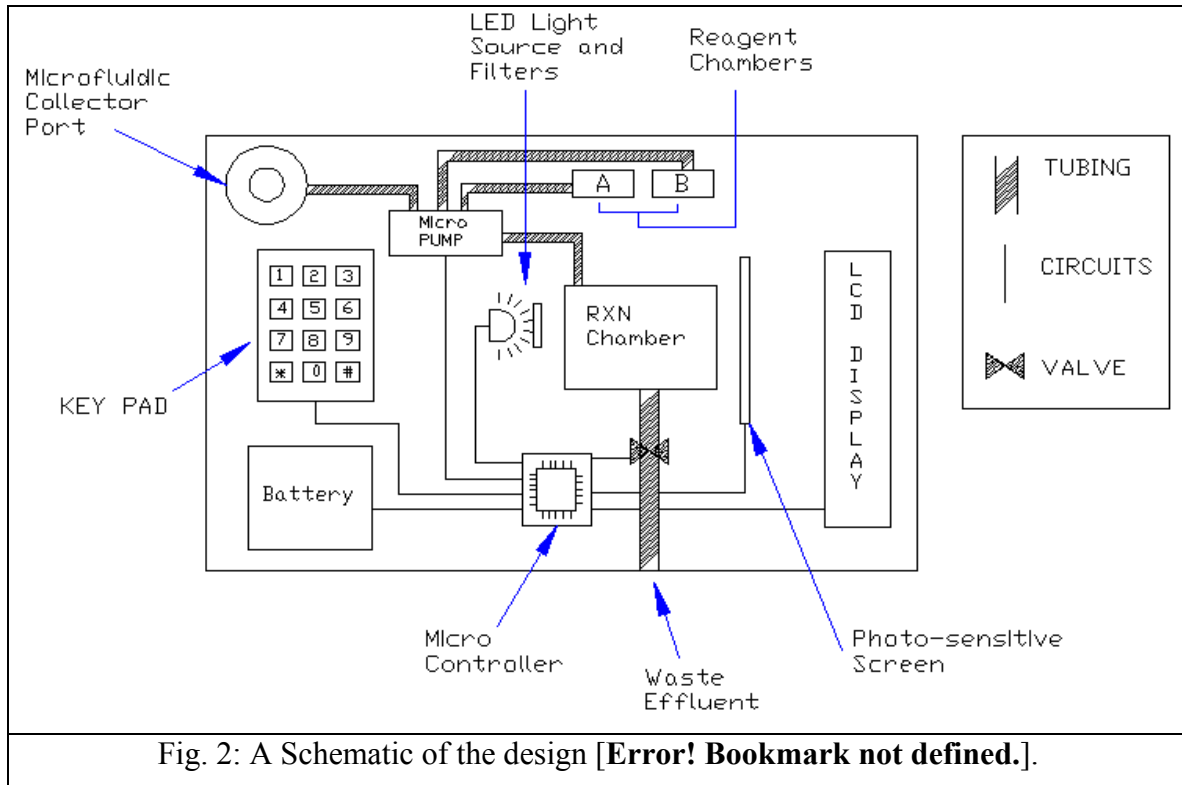


Fig. 1: Schematic view of the device (a) Top (X-section), (b) Longitudinal (X-section).

Fig.2 shows the schematic of the point-of-care, non-invasive, diagnostic device. A proposal was written for an undergraduate research grant to partially fund the senior

design project and it was approved for an amount of \$1300. The work is under progress to fabricate and test the design.



### Conclusions

The project has progressed further but has not reached the point where tests can be performed routinely that will allow evaluation of sweat/saliva stick device to enter the medical market as a new product

### Issues and Future Work

*(All this work requires additional funding. Work and discussions are under progress to submit a white paper/proposal to obtain a funding.)*

- A porous mesh made of biocompatible material (PMMA or Polypropylene) with pore size of  $\sim 10 \mu\text{m}$  to replace the membrane. This will make device more robust along with solving the problem of residual liquid trapped in membrane and need of trained personnel for saliva collection. This is planned for the advanced version of the device.
- Redesign mesh to further improve the performance of salivastick.
- Fabrication of PMMA/ PP mesh using injection molding technique. However, a feasibility study is required to manufacture the tapered mold inserts required as found in the present study.
- New mask for SU-8 with appropriate bias and testing the compatibility of SU-8 with body fluids.
- Identify other applications and eventually modify design as per the requirement. A good example can be tear collection device.
- Develop next generation device by integrating analysis (detection system) of sample, with an aim to obtain Lab-on-a- CD device.

Acknowledgments:

The authors would like to thank Jason Guy and Basic Science machine shop for helping with fabricating the Saliva Stick.



## Developing Molding Replication Technology for Metal-based High-Aspect-Ratio Microscale Structures (HARMS)

W.J. Meng, J. Jiang, Fanghua Mei

Mechanical Engineering Department, Louisiana State University  
Baton Rouge, Louisiana 70803, USA, wmeng@me.lsu.edu, PRN: ME-WM4172

We continued our research on replication-based microfabrication of metallic high-aspect-ratio microscale structures (HARMS).

In 2006, we demonstrated the use of micro-electrical-discharge-machining ( $\mu$ EDM) to fabricate HARMS mold inserts out of refractory metals and alloys, such as Ta and the Ni-based superalloy Inconel X750 [1]. Parallel transfer of complex micropatterns was demonstrated [2]. We have studied the fabrication of multilevel mold inserts [3], and performed further experimentation aimed at understanding the mechanics of micromolding [4].

In addition, we have demonstrated successful bonding of Al-based HARMS with an eutectic bonding technique [5]. The effect of strain rate on the mechanics of micromolding was also studied [6].

### References:

1. D. M. Cao, J. Jiang, W. J. Meng, J. C. Jiang, W. Wang, "Fabrication of high-aspect-ratio microscale Ta mold inserts with micro-electrical-discharge-machining", *Microsystem Technologies*, s00542-006-0198-8 (2006).
2. D. M. Cao, J. Jiang, R. Yang, W. J. Meng, "Fabrication of high-aspect-ratio microscale mold inserts by parallel  $\mu$ EDM", *Microsystem Technologies* 12, 839-845, s00542-006-0131-1 (2006).
3. R. Yang, J. Jiang, W. Wang, W. J. Meng, "Numerical simulation and fabrication of microscale, multilevel, tapered mold inserts using UV-Lithographie, Galvanoformung, Abformung (LIGA) technology", *Microsystem Technologies* 12, 545-553, s00542-005-0073-z (2006).
4. D. M. Cao, J. Jiang, W. J. Meng, G. B. Sinclair, "Metal micromolding: further experiments and preliminary finite element analysis", *Microsystem Technologies*, s00542-006-0200-5 (2006).
5. Fanghua Mei, J. Jiang, W. J. Meng, "Eutectic bonding of Al-based high aspect ratio microscale structures", *Microsystem Technologies*, s00542-006-0352-3 (2007).
6. J. Jiang, W. J. Meng, G. B. Sinclair, E. Lara-Curzio, "Further experiments and modeling for microscale compression molding of metals at elevated temperatures", *J. Mater. Res.*, submitted JMR-2006-0898 (2007).

**Insert Soper pdf.**

## Radiology

### Auger Electron Radiotherapy and Dosimetry

Joseph P. Dugas<sup>1</sup>, Scott Oves<sup>1</sup>, Erno Sajo<sup>1</sup>, Marie E. Varnes<sup>1</sup>, Frank Carroll<sup>2,3</sup>,  
and Kenneth R. Hogstrom<sup>1,4</sup>

[jpugas@lsu.edu](mailto:jpugas@lsu.edu); [soves1@lsu.edu](mailto:soves1@lsu.edu); [mvarnes@lsu.edu](mailto:mvarnes@lsu.edu); [nserno@lsu.edu](mailto:nserno@lsu.edu);  
[frank.carroll@vanderbilt.edu](mailto:frank.carroll@vanderbilt.edu); [hogstrom@lsu.edu](mailto:hogstrom@lsu.edu)

1. Louisiana State University, Department of Physics and Astronomy, 202 Nicholson Hall, Baton Rouge, LA, 70803
2. Department of Radiology and Radiological Sciences, Vanderbilt University Medical Center, 1221 21<sup>st</sup> Ave. S., Nashville, TN 37235-2675
3. MXISystems Inc., 7226 White Oak Drive, Fairview, TN, 37062
4. Mary Bird Perkins Cancer Center, 4950 Essen Lane, Baton Rouge, LA, 70809

PRN: Phy-KH0606

**Overview.** The collaboration of LSU Medical Physics, MXISystems (Fairview, TN), and CAMD personnel begun in 2005 continues to study: (1) monochromatic Auger electron radiotherapy, dosimetry, and treatment planning; and (2) monochromatic x-ray imaging in medicine. Specific aims under examination at CAMD in 2006 were:

*Aim 1: Beam Characterization.* Determination of monochromatic x-ray beam properties to provide physical data for theoretical calculations and designing future experiments. Beam data include beam intensity (# x-rays·s<sup>-1</sup>), mean energy (keV), spatial (x-y) distribution, and beam divergence.

*Aim 2: X-ray Dosimetry.* (a) Measurement of the central-axis dose versus depth for a broad beam (3×3 cm<sup>2</sup>) in a homogeneous plastic phantom (PMMA) and in inhomogeneous phantoms (PMMA, bone-equivalent plastic, and lung-equivalent plastic) for dose intercomparisons between measurements (ion chamber, radiochromic film) and Monte Carlo calculations. (b) Verification of dose distributions in phantom simulations of small animals as preparation for future animal trials.

*Aim 3: Radiation Biology.* Measurement of the dose-response of Chinese hamster ovary (CHO) cells with and without DNA-incorporated IUdR as a validation of the potential dose enhancement resulting from Auger electron radiotherapy.

**Administrative Progress.** Results from specific aim 1 of this research were presented by Joseph P. Dugas in August 2006 at the AAPM 48<sup>th</sup> Annual Meeting in Orlando, FL. In November 2006, the collaboration was represented at the CAMD Autumn users meeting workshop through both a presentation by Dr. Frank Carroll, M.D. (President, CEO, and Chief Medical Officer of MXISystems, Inc.) and by Kenneth Hogstrom leading the Medical Radiology breakout session. The collaboration has been active in developing and submitting research proposals: (1) Board of Regents grant, "Treatment

Planning System for Monochromatic X-ray Auger Electron Therapy” (Erno Sajo, PI) and (2) contribution to the medical radiology sections of a NSF MRI grant for a new multipole wiggler at CAMD (Kenneth Hogstrom, Co-PI).

**Research Progress.** Aim specific progress is detailed below.

*Aim 1: Beam Characterization.* We have utilized two independent methods to measure the mean energy of the beam: Compton spectroscopy and powder diffraction (crystallography). At several monochromator settings between 15-40 keV, results from both methods and the monochromator specified setting were measured to be within  $\pm 0.5$  keV (Figure 1) verifying both the accuracy of the monochromator setting and our ability to measure the beam’s mean energy.

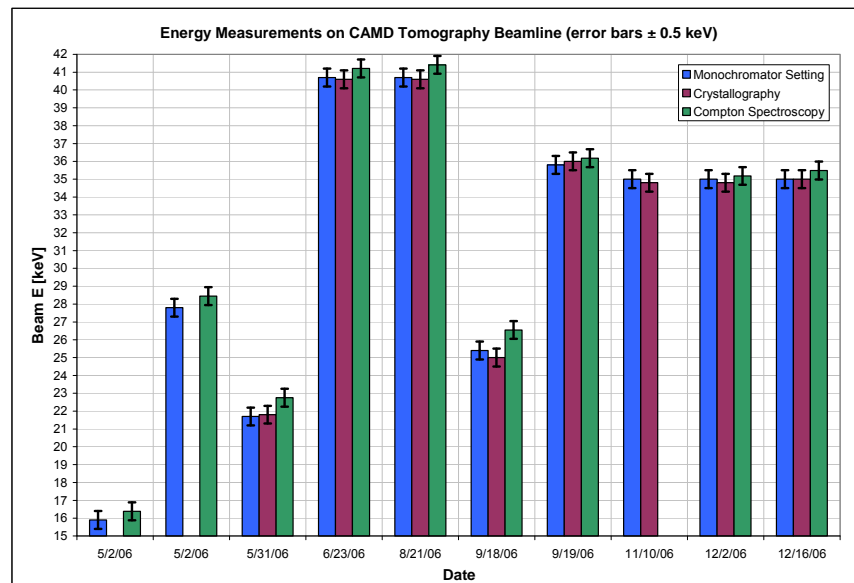


**Figure 1:** Mean energy measurements from Compton spectroscopy and crystallography methods as compared to the monochromator setting (k-edge absorption calibration).

Spatial distribution and angular divergence were measured using GAFCHROMIC<sup>®</sup> film. Spatial distribution of beam intensity (pixel values) was shown to decrease by an average of  $7.2 \pm 1.1\%$  from left to right (looking downstream) across the full 3 cm beam width and remain relatively constant across the approximately 1 mm, well-collimated beam height. Beam divergence, measured from films spaced a known distance apart, was shown to be less than  $2.5 \times 10^{-3}$  horizontally and less than  $5 \times 10^{-4}$  vertically.

Beam intensity and fluence rate were calculated from Compton scattering data, ion chamber measurements, and film measurements for narrow and broad x-ray beams. Table 1 shows the Compton scattering results for the average of multiple measurements made at scattering angles from  $15-60^\circ$ . The incident fluence was calculated from the number of photons scattered into our detector and the Klein-Nishina collisional cross section for polarized incident radiation. Ion chamber results were calculated using the ideal narrow beam relationship between fluence and dose from extrapolated phantom surface doses on measured depth versus dose curves. Measurements showed the photon



fluence rate in the beam ranged from  $1 \times 10^{11}$  photons $\cdot$ cm $^{-2}\cdot$ s $^{-1}$  to  $2 \times 10^{11}$  photons $\cdot$ cm $^{-2}\cdot$ s $^{-1}$  per 100 mA of ring current at beam energies near 35 keV (suitable for reaching the iodine k-edge in DNA-incorporated IUdR to initiate Auger electron cascades).

FLUENCE (PHOTONS $\cdot$ CM $^{-2}\cdot$ S $^{-1}$ ) PER 100 MILLIAMPS BEAM CURRENT			
Experiment Date	Energy [keV]	Compton Spectroscopy	Ion Chamber
August 21, 2006	40.7 $\pm$ 0.5	1.37 $\pm$ 0.2 $\times 10^{11}$	1.82 $\times 10^{11}$
September 18, 2006	25.4 $\pm$ 0.5	1.56 $\pm$ 0.2 $\times 10^{11}$	1.30 $\times 10^{11}$
September 19, 2006	35.8 $\pm$ 0.5	1.73 $\pm$ 0.2 $\times 10^{11}$	1.97 $\times 10^{11}$
November 11, 2006	35.0 $\pm$ 0.5	N/A	1.96 $\times 10^{11}$
December 2, 2006	35.0 $\pm$ 0.5	1.19 $\pm$ 0.1 $\times 10^{11}$	N/A

**Table 1:** Results for narrow beam fluence measurements.

*Aim 2: X-ray Dosimetry.* A broad beam was created by vertically oscillating the irradiation target through a well collimated, 0.9-mm height beam using a motorized screw-drive stage controlled via a PC and LabVIEW software. Placement of external vertical collimation jaws limits the useable beam width to 2.75 cm. Radiochromic film measurements showed that spatial and dose distributions are uniform within the broad beam generated in this fashion with the expected horizontal falloff noted in Aim 1. Broad-beam, central-axis depth-dose measurements were made in a homogeneous plastic phantom (PMMA) and inhomogeneous phantoms (PMMA and bone plastic, PMMA and lung plastic) using radiochromic film and ion chamber dosimetry. Results comparing ion chamber and film depth-dose curves are shown in Figure 2.

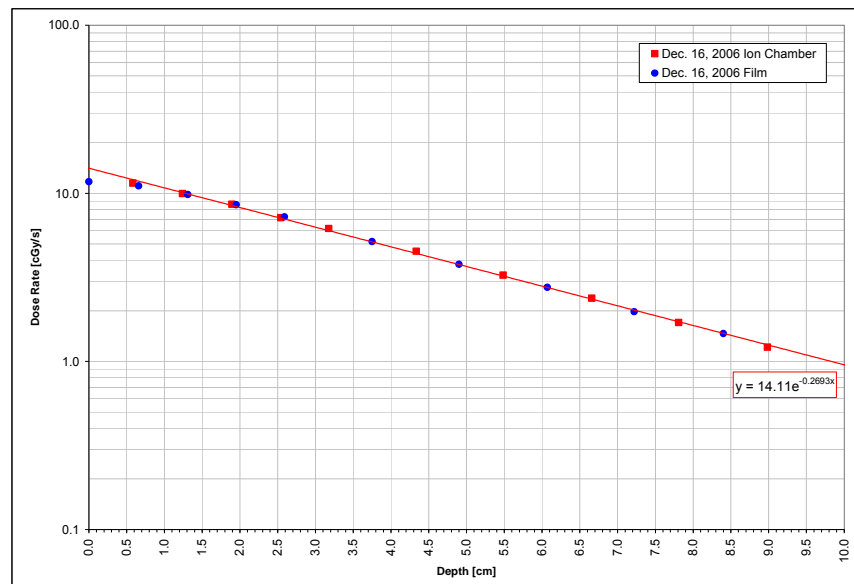


**Figure 2:** Depth dose measurements with film and ion chamber for broad beam geometries. Dose rates are given for within the narrow beam used to create the irradiated area.

Additionally, using the beam properties measured in Aim 1, the beam specifications and phantom geometry have been modeled using the MCNP5 Monte Carlo. Comparisons between Monte Carlo generated and measured dose distributions are currently being performed.

*Aim 3: Radiation Biology.* The dose-response of Chinese hamster ovary (CHO) cells was measured by irradiating monolayers of log-phase cells at doses from 1 to 8 Gy using 35 keV x-rays. Clonogenic assays were performed at the Pennington Biomedical Research Center by Marie Varnes in collaboration with Carola Leuschner's laboratory. Irradiated cells were plated, incubated, and allowed to grow for 1 week. Cells were then fixed and stained with crystal violet (Figure 3); colonies of 50 or more cells were scored as survivors. Survival curves, (cf. Figure 4) are consistent with previously published data.

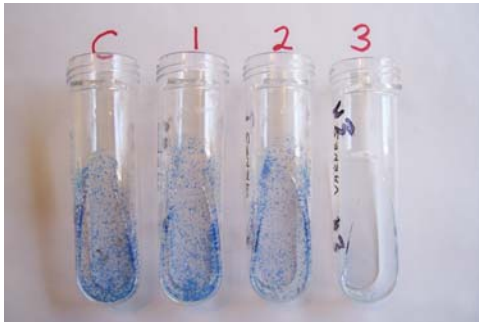


**Figure 3:** Growth of cell colonies after 1 week of incubation from cells irradiated to 0 Gy (C), 1 Gy (1), 2 Gy (2), and 4 Gy (3).

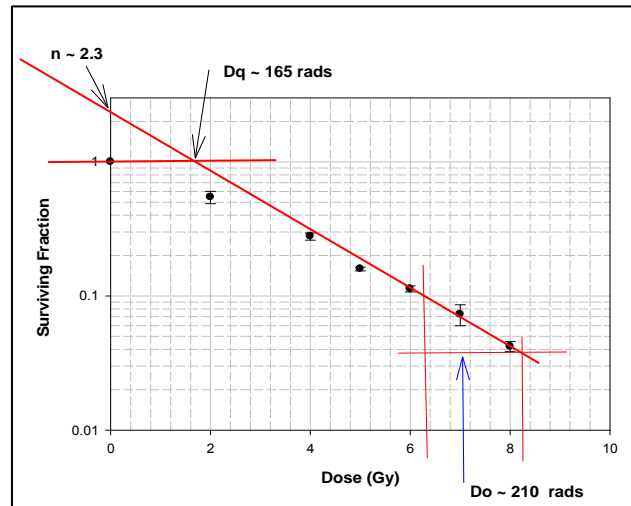


**Figure 4:** CHO dose-response from December.

This result indicates that we should soon be ready to commence experiments incorporating IUdR into the growth medium of the cells prior to irradiation in order to evaluate the amount of iodine uptake into the DNA and the attainable dose enhancement resulting from Auger electron radiotherapy.

**CAMD User Report 2006**

**Prof. Steve Soper**

**William L. & Patricia Senn, Jr. Professor of  
Chemistry**

**Professor, Mechanical Engineering  
Director, Center for BioModular Multi-Scale  
Systems**

## LIST OF PUBLICATIONS AND PRESENTATIONS

### **Isolation and Enumeration of Circulating Tumor Cells from Peripheral Blood Using Antibody Immobilized Polymer-Based High Throughput Microsampling Units**

#### **Presentations:**

2006 NSF/EPSCoR National Conference, Circulating Tumor Cell Capture from Peripheral Blood Using PMMA Microdevices

2006 CBM<sup>2</sup> Colloquium, Isolation and Enumeration of Circulating Tumor Cells from Peripheral Blood Using Antibody Immobilized Polymer-Based High Throughput Microsampling Units

### **96-well Microfluidic Titer Plate for High-throughput Purification of Nucleic Acids**

#### **Publications:**

Witek, M.A.; Llopis S.D.; Wheatley, A.; McCarley, R.L.; Soper, S.A. *NAR*, **2006**, *34*, e74

Park, D. S.; Hupert, M.; Guy, J.; Datta, P.; Lee, J.-B.; Witek, M.; You, B. H.; Soper, S. A.; Nikitopoulos, D. E.; and Murphy, M. C.; *Proceedings of ASME IMECE*, **2006**, 15275

#### **Presentations:**

Witek et al., “Purification of Genomic DNA from Whole Cell Lysates Using Photoactivated Polycarbonate (PPC) Microfluidic Devices”; Pittcon 2006; March 12-16, 2006, Orlando, FL

Hupert, et al. “96-well Microfluidic Titer Plate for High-throughput Purification of Nucleic Acids” 7<sup>th</sup> Louisiana Materials & Emerging Technologies Conference; October 23-24, 2006 Baton Rouge, LA

Park, et al.; “Microtiter Plate-Based Microfluidic Platforms: Sealing, Leakage Testing, and Performance of a 96-Well SPRI Device”; 2006 ASME International Mechanical Engineering Congress & Expo; November 5-10, 2006, Chicago, IL

### **PMMA Waveguides and Microarray Integrated to Microfluidics for Low Abundance Mutation Detection of Breast Cancers**

#### **Publications:**

Datta, P.; Xu, F.; Gurung, S., Soper, S.A.; and Goettert, J.; *Proceedings of SPIE-The International Society for Optical Engineering* **2006**, vol. 6112 (Microfluidics, BioMEMS, and Medical Microsystems IV), 61120B/1-61120B/12

#### **Presentations:**

Datta, P.; Xu, F.; Gurung, S., Soper, S.A.; and Goettert, J. “Polymeric Waveguides for Orthogonal Near Surface Fluorescent Excitation” SPIE Photonics West, San Jose, CA, Jan. 2006

## 96-well Microfluidic Titer Plate for High-throughput Purification of Nucleic Acids

Mateusz L. Hupert<sup>a,b</sup>, Malgorzata A. Witek<sup>a,b</sup>, Daniel Park<sup>a</sup>, Michael C. Murphy<sup>a,c</sup>,  
and Steven A. Soper<sup>a,b,c,\*</sup>

<sup>a</sup> *Center for Bio-Modular Multi-Scale Systems, Louisiana State University, 8000 GSRI Rd  
Baton Rouge, LA 70820*

<sup>b</sup> *Department of Chemistry, Louisiana State University, 232 Choppin Hall,  
Baton Rouge, LA 70803*

<sup>c</sup> *Department of Mechanical Engineering, Louisiana State University, 2508 CEBA Bldg.,  
Baton Rouge, LA 70803*

\*[chsoper@lsu.edu](mailto:chsoper@lsu.edu);

PRN: .....

A purification and pre-concentration of DNA from complex biological samples is of extreme importance in many DNA-based bioassays. A typical isolation protocol of genomic DNA (gDNA) involves organic extractions, dialysis or precipitations using ethanol, phenol or 2-propanol, and ultracentrifugation. These procedures are labor intensive and time consuming. A much gentler and efficient way of DNA purification is provided by group of methods based on solid-phase reversible immobilization (SPRI). In SPRI, DNA from a crude sample is first selectively immobilized on a solid support, washed, and subsequently released in purified form.

We have developed fast, simple, and effective way for the direct purification of the gDNA from cell lysates and whole blood samples using SPRI in photoactivated polycarbonate (PPC) microfluidic chip. The incorporation of a purification platform for nucleic acids into a microfluidic chip is very appealing because it offers the ability to handle and preconcentrate nucleic acids in a high throughput, automated format and in a closed architecture to minimize contamination effects. The process of DNA purification consists of precipitation of DNA on UV-photoactivated (i.e., carboxylated) surface of polycarbonate in the presence of immobilization buffer (a mixture of polyethylene glycol, NaCl, and ethanol). Captured DNA is then washed with ethanol to remove the excess of salts, proteins and cell debris. In the final step purified DNA is released from the polymer surface using water (see Figure 1). The capture efficiencies for this process are as high as 85%.

In order to achieve high-throughput purification of DNA samples, 96 capture beds were fabricated into the surface of single polycarbonate sheet using hot-embossing of metal masters fabricated either via high-precision micromilling or LiGA. The capture beds were arranged according to the standardized format of 96-well titer plate (Figure 2). This allowed for loading of the reservoirs with standard 8-channel pipetter. All capture beds were interconnected through microfluidic network and could be operated simultaneously with a use of a single vacuum pump and two syringes for delivery of ethanol and water. The unique operating procedure prevented the possibility of cross-contamination between samples. The performance of the device was validated by capture

of DNA fragments from 4 different samples, performing the PCR on eluted different size DNA template, and confirming the presence of PCR products via gel electrophoresis (Figure 3). The 96-well PPC-SPRI chip was also successfully used for the purification of gDNA from whole bacteria cell lysates (e.g.: *S. aureus*, *B. subtilis*, *M. luteus*, *E. aerogenes*, and *E. coli*)

The specific advantages of our high-throughput DNA purification device include very low cost of the device achievable through use of polymer as the substrate material and replication from the master as fabrication procedure (e.g.: hot-embossing or injection molding). Low cost of the device allows for its single time, disposable use which is extremely important in the processing of medical and forensic samples. The purification process is also very fast (<20 min), easy to automate, and uses very inexpensive equipment and chemicals. Also, the design of the device is in accordance with existing standards and provides its complete compatibility with instrumentation and laboratory protocols already present and implemented in both academia and industry without a need for new, expensive handling equipment.

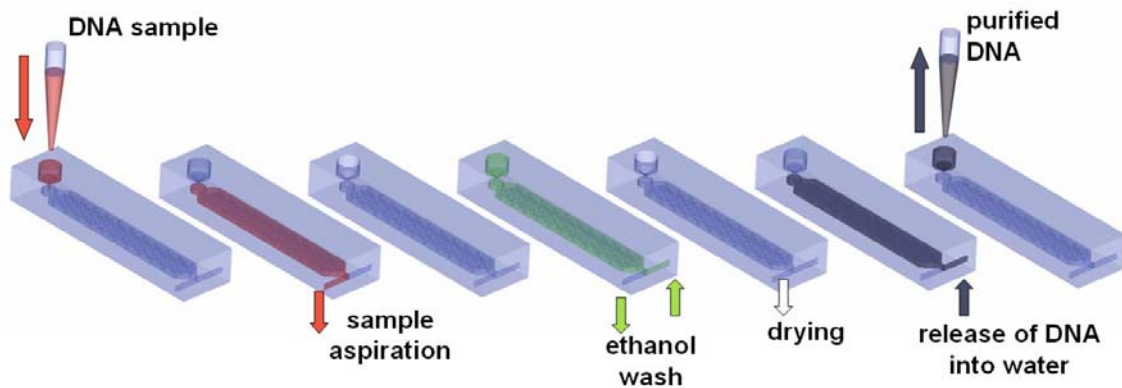


**Figure 1.** Schematic operation of PPC-SPRI microfluidic chip.

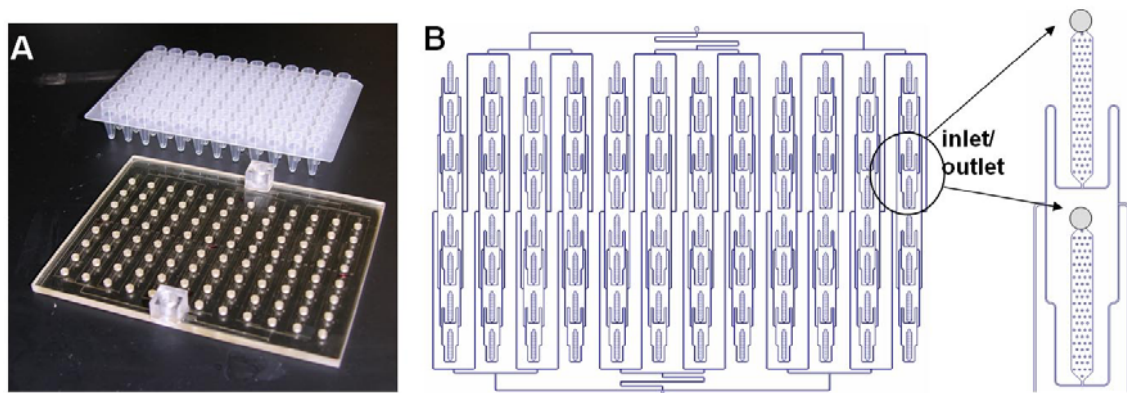


**Figure 2.** (A) 96-well PPC-SPRI microfluidic chip and a commercial 96-well titer plate. (B) The schematics of the microfluidic network of 96-well PPC-SPRI chip.

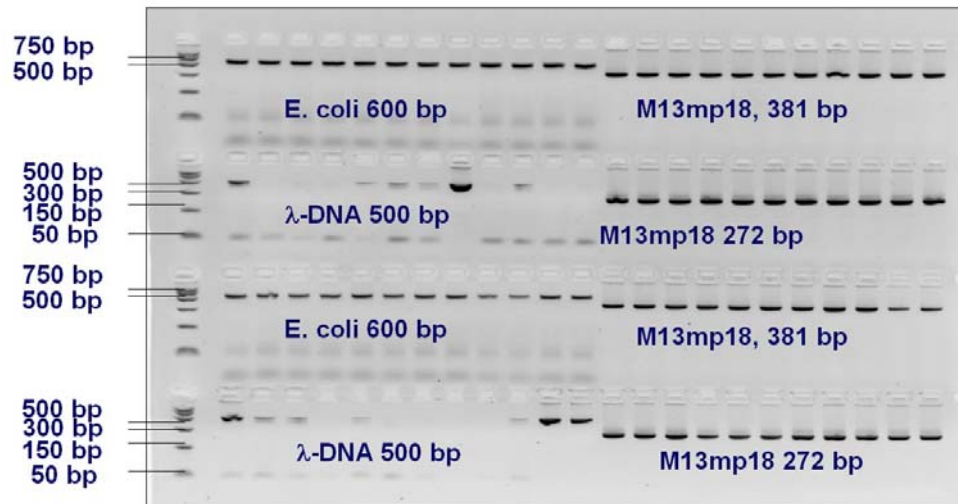


**Figure 3.** Gel electrophoresis of DNA samples purified with 96-well PPC-SPRI microfluidic chip.

## PMMA Waveguides and Microarray Integrated to Microfluidics for Low Abundance Mutation Detection of Breast Cancers

Feng Xu,<sup>a,b</sup> Proyag Datta,<sup>c</sup> Sitanshu Gurung,<sup>c</sup> Jost Goettert,<sup>a,c</sup> Steven A. Soper<sup>a,b,\*</sup>

<sup>a</sup> Center for BioModular Multi-Scale Systems, Louisiana State University,  
Blg. 3100, 8000 GSRI Road, Baton Rouge, LA 70820

<sup>b</sup> Department of Chemistry, Louisiana State University,  
232 Choppin Hall, Baton Rouge, LA 70803

<sup>c</sup> Center for Advanced Microstructure and Devices, Louisiana State University,  
6980 Jefferson Hwy, Baton Rouge, LA 70806

\*[chsope@lsu.edu](mailto:chsope@lsu.edu);

PRN: .....

In this study, a waveguide was assembled into a microfluidic chip in a sole material of poly(methyl methacrylate) (PMMA), and the channel floor of the chip acted as both the waveguide surface and the microarray surface. The microchannel was fabricated through a single-step double-side hot embossing using two brass mold masters produced via high precision micromilling. A home-built evanescent fluorescence microscopy system was used to detect mutation of DNA specimen in the waveguide-based microchips. The microscopy system could provide either high resolution (2  $\mu\text{m}$  using a 10 $\times$  objective) or wide field-of-view (20 mm diameter circle area using a 1.25 $\times$  objective). Hence, it was easy to detect a large slide area sensitively without scanning. An equilateral triangular prism was used to effectively couple a laser beam (675 nm) to waveguides with a coupling efficiency of 64%. The waveguide design could excite a wide range of probe area. The solution in the channel acted as an upper cladding layer and the air as a lower cladding layer. A mild, simple and efficient surface activation protocol was developed to convert the waveguide-embedded PMMA microchannels to biochip platforms for DNA probe immobilization and target detection. In the first step the surface of PMMA microchannel was exposed to oxygen plasma for 2 min, it was then activated by using 1-(3-dimethylaminopropyl)-3-ethylcarbodiimide (EDC) to produce surface carboxyl groups which served as an anchoring site for amine-terminated universal zip-code oligonucleotide probes. The application of the waveguide was demonstrated by detecting low abundance DNA mutations in BRCA1 gene fragments that carry insertion C mutations and have high clinical relevance in diagnosing breast cancers. Covalent immobilization of universal zip-code oligonucleotide probes inside the channels was performed using a PiezorrayIR non-contact microarraying spotter. Mutant and wide-type genomic DNAs of breast cancer gene were PCR amplified, mixed at a certain concentration ratio to undergo ligation detection reaction (LDR). Herein suitably-designed allele-specific LDR primers (discriminating primers) covalently ligate to a common primer with an Alexa Fluor 660 dye tag, if a complementary match exists between the LDR product and the PCR amplified product. On their 5'-terminus, the discriminating primer contains zip-code complements that are used to direct LDR products to specific zip-code addresses tethered previously onto the surface of PMMA waveguides (microchannels). After the LDR products flowed through the waveguide-



based microchannel and hybridized with the tethered zip-code probes for 5 min, BRCA1 insertion C mutation present at less than 1% ratio in the bulk wild-type DNA concentration was selectively and sensitively distinguished, which shows the promising application of high-throughput screening of low abundance mutation by using waveguide-based microchip platforms.

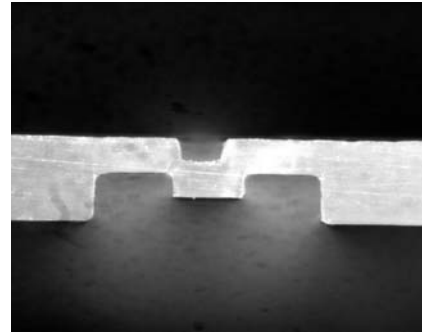
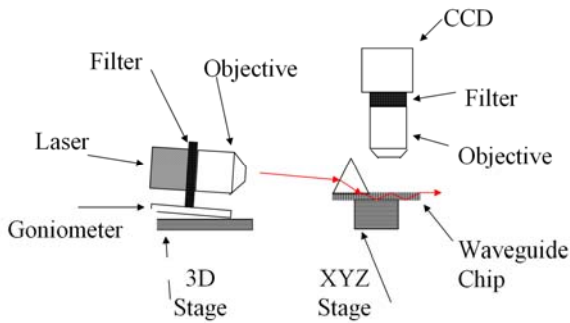


Figure 1. Schematic of the home-built evanescent fluorescent microscopy setup for measuring fluorescence in waveguide-assembled microchannels. The laser beam is incident on the coupling prism.

Figure 2. Image of cross section of a waveguide-assembled microfluidic channel.

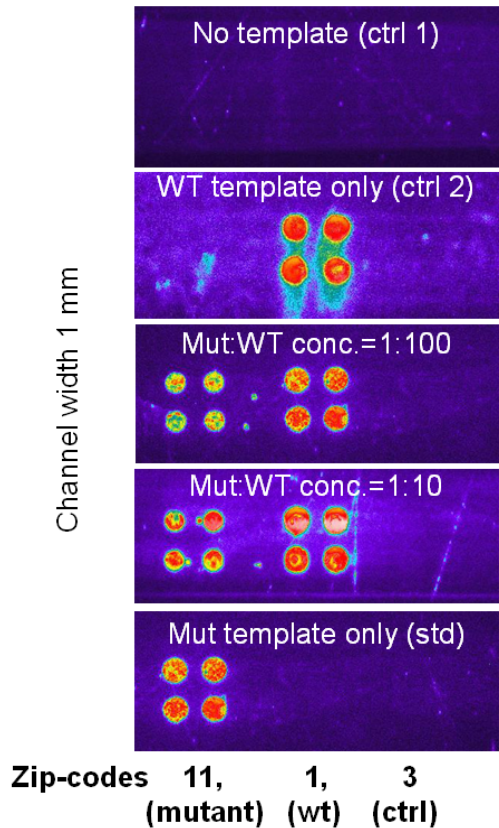


Figure 3. Detection of point mutation (insertion C) in BRCA1 gene using the waveguide-assembled zip-code array microchip (1 mm wide) assembly. The probes tethered in each channel were zip-codes 11, 1, and 3, respectively. The spot size is 150  $\mu\text{m}$ , and the center to center spacing is 300  $\mu\text{m}$ . The LDR cocktail was pumped through the assembly using a flow rate of 2  $\mu\text{L}/\text{min}$  for 5 min at 37°C hybridization temperature.

# Isolation and Enumeration of Circulating Tumor Cells from Peripheral Blood Using Antibody Immobilized Polymer-Based High Throughput Microsampling Units

André A. Adams,<sup>a,b</sup> Mateusz L. Hupert,<sup>a,b</sup> Paul Okagbare,<sup>b</sup> Michael C. Murphy,<sup>a,c</sup>  
Robin L. McCarley,<sup>a,b</sup> and Steven A. Soper<sup>a,b,c,\*</sup>

<sup>a</sup> Center for BioModular Multi-Scale Systems, Louisiana State University,  
8000 GSRI Road, Blg. 3100, Baton Rouge, LA 70820

<sup>b</sup> Department of Chemistry, Louisiana State University,  
232 Choppin Hall, Baton Rouge, LA 70803

<sup>c</sup> Department of Mechanical Engineering, Louisiana State University,  
2508 CEBA Blg., Baton Rouge, LA 70803

\*[chsope@lsu.edu](mailto:chsope@lsu.edu);

PRN: .....

Micrometastatic breast cancer is characterized by tumor cells in the circulatory system originating at the primary tumor site. These cells are typically low frequency (1:10<sup>7</sup>) relative to normal haematopoietic cells and are often referred to as circulating tumor cells (CTC) when found in the peripheral blood. CTCs are of particular interest because they provide both diagnostic and prognostic information on disease state for a variety of adenocarcinomas. The presence and frequency of CTCs in peripheral blood is indicative of the existence of a neoplasm, characteristic of the cancer stage, and can also provide probative information about the degree of success of a prior excision. MCF-7 cells are of particular interest due to their close association with micrometastatic breast cancer. The MCF-7 cell is also of importance due to the commercial availability of monoclonal antibodies specific for a heavily over-expressed MCF-7 cell membrane protein termed the epithelial cell adhesion molecule. As such, MCF-7 cells are regarded as excellent biomarkers for the existence of micrometastatic adenocarcinomas attributable to breast cancer.

To that end, novel high throughput curvilinear 37-channel microsampling units (37MSU) (shown in figure 1) consisting of high aspect ratio microstructures were designed and fabricated to facilitate the capture of low abundant CTCs from peripheral blood. The devices were hot embossed in poly (methylmethacrylate) (PMMA) using a brass mould insert fabricated by high precision micromilling. The 37MSU was designed with 37 parallel channels that served as capture beds for pre-concentrating CTCs from peripheral blood or other matrices. The MSU walls were selectively carboxylated through an aluminum mask via irradiation with a 10 min dose of 254 nm ultraviolet light (15 mW/cm<sup>2</sup>) prior to device assembly via thermal annealing. Subsequently, a solution containing 4.0 mg/mL 1-ethyl-3-[3-dimethylaminopropyl] carbodiimide hydrochloride (EDC) and 6.0 mg/mL N-hydroxysuccinimide (NHS) was introduced to the MSU prior to adding a solution containing 1.0 mg/mL anti-EpCAM antibodies resulting in covalent antibody immobilization on the MSU channel walls in only the UV modified regions.

Prior to being seeded into whole blood CTCs were labeled with FITC (membrane). Captured CTCs were imaged with a Carl Zeiss Axiovert 200M by scanning the MSU microchannels using a programmable motorized stage in conjunction with fluorescence real-time video microscopy at 30 fps. These conditions were applied to undiluted citrated whole blood samples (1.0 mL) that were spiked with 2500, 1000, 250, and 25 MCF-7 cells ( $\pm 8.0\%$ ). Recovery rates of the spiked CTCs from the whole blood matrix were consistently  $> 90\%$ . Large volumes of spiked whole blood samples ( $\sim 1.0$  mL) were also processed through the MSUs without any device failures due to clogging at 1.0, 2.0, 4.0, and 7.5 mm/s. Captured MCF-7 cells shown in figure 2 were retained on the MSU walls when exposed to bulk suspension linear velocities in excess of 100 mm/s. In addition, post capture MSU rinses resulted in  $< 500$  residual RBCs and no WBCs being observed in the 37MSU.

In an effort to further automate the cell counting process a conductance based measurement system was developed and incorporated into the 37MSUs on the devices effluent side. Captured MCF-7 cells were removed from the 37MSU walls using a tryptic digest sufficient to digest the EpCAM - anti-EpCAM complexes thereby terminating the cell-wall adhesion. The CTCs were then rinsed from the device and swept through the detection zone where they were counted based on perturbations of the baseline conductance exhibited by the releasing agent. Wild-type cells caused no perturbations due to their inherently low amino acid and low to non-existent nucleic acid content relative to CTCs. A typical plot of conductance vs. time is shown in figure 3 where 22 cells were eluted from a 37MSU used to process 1.0 mL of whole blood spiked with 25 MCF-7 cells. No statistical difference exists between the conductance and fluorescence based cell enumeration protocols, and  $\sim 90\%$  CTC recovery was demonstrated using both counting techniques as indicated in figure 3.

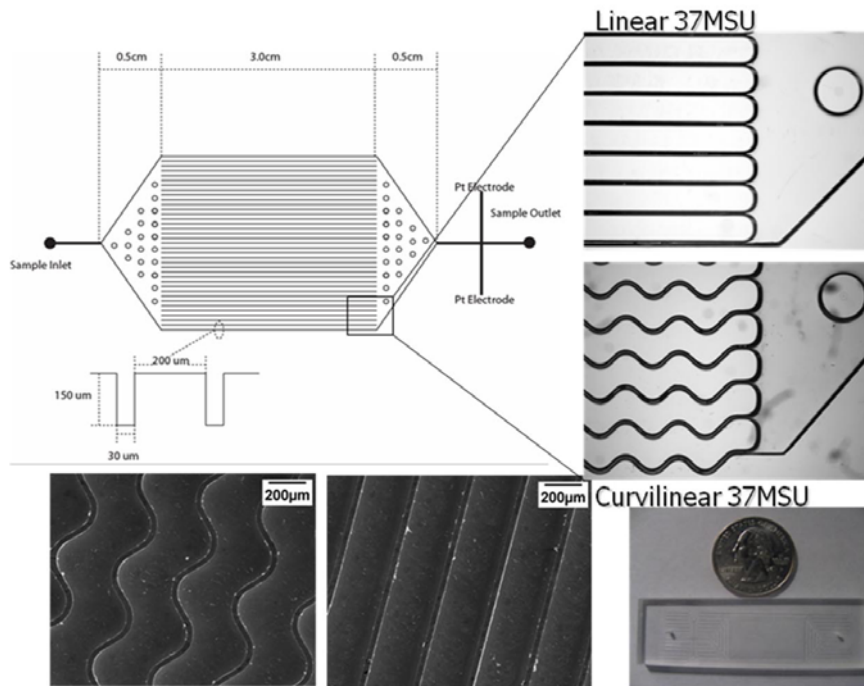


Figure 1.

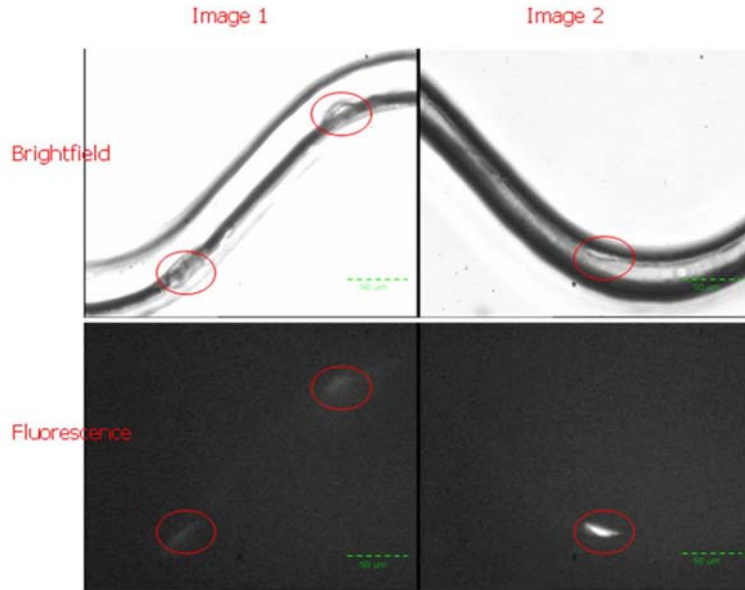


Figure 2.

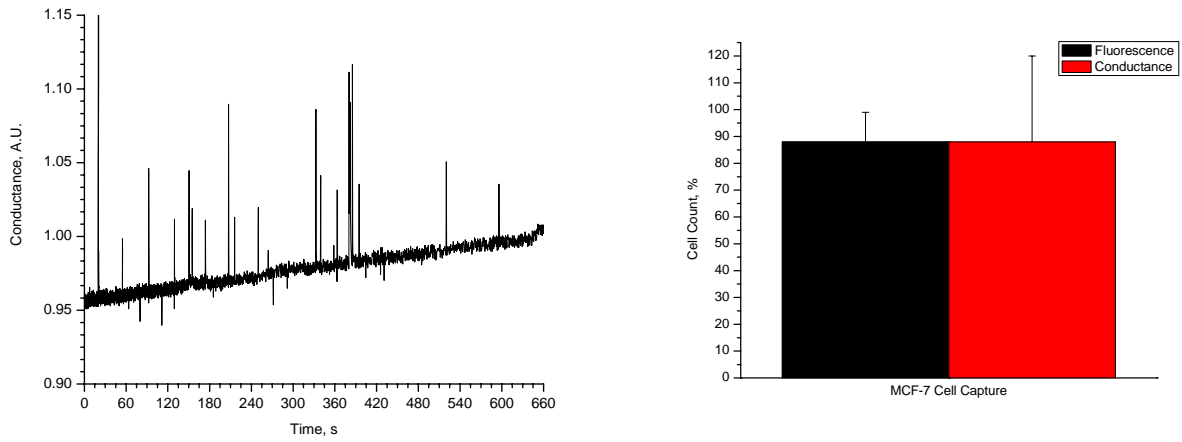


Figure 3.

## Appendix C: Workshop Reports



Appendix.C.1. First Workshop to Evaluate a New Advanced Light  
Source 2006

## **CAMD Autumn User Meeting Workshop Schedule *November 19–21, 2006***

***Sunday, November 19, 2006 - CAMD Conference Room***

**3:00–4:30pm - Registration and reception**

**4:30–5:00pm - Motivation for the Workshop, *Dave Ederer*,  
Director, CAMD**

**5:00–5:30pm - CAMD and Its Role in Commercial Ventures,  
*Kevin Kelly*, LSU Mechanical Engineering and  
International Mezzo Technologies.**

**5:30pm - Formal Session adjourns**

***Monday, November 20, 2006 - Energy, Coast, and Environment  
Building, LSU, Rotunda and Auditorium***

**8:00–8:30am - Registration and Continental Breakfast**

***8:30–11:45am - Morning Session***

**8:30–8:45am - Welcome, *Brooks Keel*, LSU Vice Chancellor  
for Research and Economic Development**

**8:45–9:00am - CAMD Director's Welcome *David Ederer*,  
Director CAMD**

**9:00–9:45am - SEALS/ROSE: A Regional Third Generation  
Synchrotron Light Source for the Southeast- *Vic Suller*,  
CAMD**

**9:45–10:15am - Coffee Break**

**10:15–10:45am - New Frontiers in Tomography from High Brightness Sources, *Carolyn A Larabell*, Dept of Anatomy, University of California, San Francisco, and LBL Berkeley**

**10:45–11:15am - The Inverse Compton Effect X-ray Source, *Frank Carroll*, Vanderbilt University, Physics and Astronomy**

**11:15–11:45am - What High Brightness and Source Proximity means to Protein Crystallography, *Jim Sacchetti*, Chemistry, Texas A&M University**

**11:45am–1:00pm - Break for lunch**

**1:00–5:30pm - Afternoon Session**

**1:00–1:30pm - Coherence and Microscopy at Third Generation Light Sources. *Ian McNulty*, APS**

**1:30–2:00pm - Chemical Dynamics at a Third Generation Light Source, *Erwin Poliakoff*, LSU Chemistry**

**2:00–2:30pm - Energy-related Applications, *Tabbatha Dobbins*, Louisiana Tech, and Grambling University**

**2:30–3:00pm - Case for Environmental Science at Third Generation Light Sources, *Amitava Roy*, LSU CAMD**

**3:00–3:30pm - Coffee Break**

**3:30–4:00pm - The case for XMCD and XMLD at a High Brightness Synchrotron Radiation Source, *Tony Caruso*, University of North Dakota, Physics**

**4:00–4:30 pm - Bioscience and Cancer Identification with Nanoparticules, *Challa Kumar*, LSU CAMD**

**4:30–5:00pm - Industrial Applications for Microtechnology, *Steve***



**Soper, LSU Chemistry, Jost Goettert, LSU CAMD**

**5:00–5:30 pm - X-ray Tomography and the Multipole Wiggler, Les Butler, LSU Chemistry**

**Tuesday, November 21, 2006 - Energy, Coast, and Environment Building, LSU, Rotunda and Auditorium**

**8:00–8:30am - Registration and Continental Breakfast**

**8:30–9:00am - Nanoscience with Photoelectron Spectroscopy, Franz Himpsel, University of Wisconsin**

**9:00–9:15am - Instructions for the Breakout Sessions -Les Butler**

**9:15–9:30am - Coffee Break**

**9:30–10:30am - Breakout Session I**

- **Soft Materials - Paul Russo, LSU Chemistry, Tabbetha Dobbins, Louisiana Tech, and Grambling University**
- **Chemical Physics and Nano Science - Erwin Poliakoff, LSU Chemistry**
- **Microfabrication and Industrial Collaborations- Steve Soper, LSU Chemistry, Jost Goettert, LSU CAMD**

**10:30–10:50am - Coffee Break**

**10:50–11:50am - Breakout Session II**

- **Hard and Dilute Materials - Phil Sprunger, LSU Physics**
- **Medical Radiology - Ken Hogstrom, LSU Physics**

**12:00–12:30pm - Summary of Breakout I & II**

**End of workshop**

## **Appendix.C.1.a. First Workshop to Evaluate a New Advanced Light Source 2006**

The outcome of the workshop can be broken into two pieces.

1. CAMD (Microfabrication and radiation source) is a valuable resource and should be nurtured and integrated into the Flagship Agenda and developed as a part of the strategy for creating a technical center of excellence at LSU.
2. Steve Soper and Jost Goettert work very well together, and facilities under their immediate control are productive and are recognized by their peers as making important contributions. LSU should give them both the resources to continue to make progress together and give them the charge to work out a plan to continue to develop the excellence of LSU's of advanced technologies.

### 3. Should CAMD significantly expand/enhance its external user function?

**David:** The general consensus is yes. CAMD can do that through work shops, meetings and publicity. Increased services will also require increased staff. In particular we are short on staff focusing on capabilities related to IT, and in the area of the accelerator development and maintenance.

**Les:** High-speed internet, simple video conferencing. Director or Science Advisor attends some academic dept meetings. Need to maintain target numbers: For example, how many LSU chemistry faculty should have tight CAMD connections, loose CAMD connections? As chemistry faculty retire/move, CAMD should seek to regain that target number. Ditto for other science & engineering departments.

**Jost:** The term ‘user facility’ was never clearly defined and is certainly one reason why there is not a well-**defined** role for CAMD’s role within the LSU R&D community. Before we volunteer to do more we may want to learn what the expectations are? Harold conducted a survey and the responses were widely scattered. I think that one very important aspect should be that CAMD also has an expected and respected role as ‘full’ R&D partner and not only as ‘service provider’.

**John:** To increase “external user function” CAMD needs to upgrade its service to the users we have. The MRI proposal potentially offers a step in the right direction, especially for protein folks and researchers needing tomography. The construction of the new high-energy EXAFS beamline (particularly coupled with a multi-pole wiggler) will also be attractive and very useful to many of our current users as well as to potential users in the South. Also, in our plans is an undulator that could possibly serve two or three beamlines. It would give greatly increased flux to VUV users as well as to X-ray-spectroscopy users with the additional benefit to the latter of a significantly increased spectral range. The CAMD ring was designed and built to accommodate insertion devices, but we have yet to take full advantage of this potential.

### 4. Is there a regional need for CAMD...

- ...in it’s current structure?
- ...in an expanded structure?
- What should that structure/function be?

**David:** Currently CAMD serves 295 users total, 228 from Louisiana, 115 from LSU, and 45 from CAMD.

If the new wiggler is funded by the NSF we would expect to see an additional 50-75 users utilizing the greater flux available at the wiggler.

If the second insertion device is funded, another 20-40 users would find the increased brightness beneficial to their work.

New clean rooms would add (Jost I need you here) The old clean rooms would be used to train students and be essentially class rooms.

I would like to suggest that CAMD become an academic department on its own, called maybe, “Engineering Physics.”

**Les:** My crystal ball shows a \$100M+ X-ray facility will be operational in 5-yrs somewhere in the southern USA. It will not be a simple copy of any existing facility, but will be an "X-ray serves \_\_\_\_\_" center. For the blank, options are health or jobs; I'd vote for jobs.

**Jost:** Regional need in current structure:

If region is the state of LA then yes, there is a need for CR based technology support. The CR can be both, high tech infrastructure accessible for knowledgeable users and vehicle to provide high tech services. The only other place in LA is in Ruston at the IfM.

An expanded structure should split the role of educational facility (CR is trainings facility for university users) and service entity (paid service for interested customer, cost center and eventually also for profit if the market growth). Both can be together initially but eventually become two different units in for example a university based technology park.

A new CR as indicated by Dave would allow to buying new state of the art equipment that is needed in the near future as our existing tools are getting old. What could be added are tools capable of below micrometer patterning to further extend the top-down fabrication approaches into the Nano-regime.

The critical question here is whether the CR must be part of CAMD (SEALS or ROSE both don't mention microfab in their name but focus on the SR aspect) or can become an independent organization?

This is to be further discussed within the 'big picture' campus-wide discussion (flag-ship agenda).

**John:** Many of our users need a lot of help and some continue to need help. There are some excellent researchers and their graduate students who are far removed from being spectroscopists. One of CAMD's strong features is the "user friendly" nature of interaction of users and scientific staff. To accommodate more users, if there are those that truly need and wish to use an SR source, we will need to treat, more seriously, our beam-time distribution. In other words, be rigorous in allotting beam time based on the fact we operate 24 hours per day

##### **5. What should be the role of CAMD's staff scientists (user support, independent researcher, combination)?**

**David:** The primary duty of CAMD staff is to support the user community. One of the functions the staff perform is to train student users. In addition they carry out independent and collaborative research. The User Community seems happy with this approach.

**Les:** Clarity and flexibility. Flexibility: some CAMD staff will transition to tenure-track positions at LSU and elsewhere; this should be encouraged. Clarity: external users cannot identify which staff are assigned 100% or 50% to help users.

**Jost:** While the combination is very effective for users (they not only get technical support but also very often great ideas for their projects) it is problematic for the CAMD staff and it would be easier (if funds are available) to have 'true technical support staff' and the 'research staff members' who are equal partners with the users.

**John:** At CAMD, a Research Faculty member is analogous to an academic faculty member (ideally); in the place of formal classroom and lab teaching CAMD faculty "perform service," which is not always clearly defined and, in the same manner as academic faculty, CAMD faculty have their own research programs. This latter issue should be taken seriously by all of us. CAMD Research Faculty should be expected to generate external funding by having good, solid research programs. We have just begun the policy of supporting our faculty for nine months. salary-wise, giving the added incentive to generate 2/9 or 3/9 for support during the

three available months. I have been both a tenure-track academic faculty (Chemistry Faculty, University of Montana from 1978 to 1990) and a Research Faculty member at LSU CAMD (from 1988 to the present, counting two years during which I was on leave from Montana) and I find the service component at CAMD easily equals the teaching component of an academic faculty member. The title “Research Faculty” at LSU means a number of different things across the campus. What I describe, briefly, here applies uniquely (I think) to CAMD, as a service center.

## 6. How can CAMD better integrate itself with the main campus?

**David:** Move closer to campus. Hold classes for users, become a department as suggested in 2.

**Les:** internet & simple video. The crystal ball shows new facility will be on Ag land.

**Just:** The best way of integration is that we play a role within the LSU community accepted by it. I feel that we should find out who on campus wants to have a CAMD and if this support group is strong enough we will have our role and position. Dave’s points are interesting but becoming an independent department will mean that others get less and therefore people will be unhappy.

**John:** I think moving closer to campus has no basis at this point. Campus could move closer to CAMD with a shuttle service – perhaps connecting South, Northeast and Main campus. If LSU is selected as the site for the South’s third (or fourth) generation light source, then a campus location might be the best. Geography is not the only integrating factor involved; adjunct appointments in appropriate departments for CAMD staff with interaction as well as “Adjunct Title” might help. We have a number of scientific collaborations between campus researchers and CAMD researchers – this is a natural thing in many instances. Faculty from campus often attend our seminars and CAMD staff often attend LSU-departmental seminars. CAMD Research Faculty serve on graduate committees and sometimes support and serve as research advisors to graduate students from departments. CAMD Faculty members also may apply to be members of the Graduate Faculty. All of these areas, of course, could be enhanced and/improved.

## 7. Should CAMD make available lab and office space for department based faculty?

**David:** We provide office space to the best of our ability with our limited space, either shared offices or on the floor.

**Les:** It's past time for more parking, more office and lab space

**John:** Not until we have adequate space for the staff. Campus people and other users should be here to work on or at beamlines. We could provide a room with a computer attached to the internet and a couple of desks, maybe. The office space that we do have consists of three buildings; one permanent and two temporary. These were purchased completely with precious normal CAMD budget money to the tune of about \$1M, total. I would like to have space for campus-based faculty and students as well as for our out-of-town users as this could result in closer collaboration but the cost is high and it is difficult to justify such expense when I know we have many instrumentation needs which, if acquired, upgraded or repaired, would benefit a larger number of users than would the office space. Regarding lab space; we have very little lab space, outside of 2500 square feet of clean room. We are attempting to complete a biology lab for protein crystallography users, but CAMD’s share of the funding is lacking – the majority of

the cost, thus far, have been funded by the Gulf-Coast-Protein-Crystallography Consortium and the Louisiana Bio Initiative (I think). Users do have access to the clean rooms and equipment and we have items such as glove boxes (small portable ones) that can be used for sample handling. What is now the “Nano Lab,” a very productive laboratory, was originally built in 2001 for sample prep, etc and for use by users and staff alike. The decision was made to dedicate it to nano-material synthesis.

#### **8. Should CAMD significantly expand its ties with Industry?**

**David:** Yes! We should work through our Industrial Advisory Committee to find ways to implement closer ties. I would like to contact our Industrial Advisory Committee early in 2007 and work closely with you to initiate some kind of workshop.

**Les:** The first connection between CAMD and local industry is traditional X-ray analysis; this is problematic because of insufficient staff. Next connection is microfab: not sure what obstacles are here, check with Jost, Kevin Kelly, Soper, McCarley, etc. Third connection is new generation X-ray analysis, like tomography; techniques under development, but will soon be limited by staffing.

**Jost:** This is a MUST for microfab but I look to Brooks to find more efficient ways than the ones we tried in the past. We can play a role within LSU to move in this direction and perhaps also create some sort of local market.

**John:** We, by this I mean all appropriate LSU divisions and offices, must understand how a particular industry operates and, on the other hand, the industry must understand how we operate at the state mandated business level. A scientist at CAMD discussing a potential research, analytical or manufacturing process, can occur fairly naturally but when both parties involve the business and legal departments, this can add difficulties and possible loss of the “customer.” When LSU (CAMD) sets a cost for beamline use at around \$1,000 per 8-hour shift plus charges salary (plus fringe benefits and overhead) at an hourly rate for each scientist and technician required, the company may feel that ownership of intellectual property should not even an issue – it’s their project or sample and it belongs to them! [Continue on to number 8].

#### **9. Is there an industrial market for CAMD facilities and services?**

**David:** Several spin off companies have formed and I would expect that several more will come to pass as we expand our contacts. We are working to increase the visibility of CAMD to the community through highlights and we are planning a video as a promotional device. I believe the Advocate covered the workshop. More publicity is essential to bring our facilities to the public’s attention.

**Les:** Big companies have beamlines at APS (DuPont), NSLS (ExxonMobil), etc. For the 230+ chemical plants in south Louisiana area, we should create a "virtual industry" beamline, at least an easy access. SAXS beamline could be a leader.

**Jost:** In microfab there is a market but not for services rather than commercial solutions. And the gap from academic research to products well-positioned in a market is typically too big to cover from either end. We may need to strategically plan to bridge it using the SBIR/STTR opportunities.

**John:** There is need for basic science applications that industry can use. Analysis and crystal-structure determination are two. This is discussed further in number 8.

#### **10. How can CAMD play a more active role in economic development?**

**David:** Through more contact with our industrial neighbors (See the comment to the previous question.)

**Les:** I have high hopes for Russo's APTEC project. It is "right-sized" for area chemical industry. It should also provide role-model for bio-tech, microfab, IT spin-offs.

**John:** Perhaps our Industrial Advisory Board could help educate us in the process of servicing industry. This might require a change of some of its members. Microfabrication has been responsible for the spin-off companies because of its unique "grass roots" work. The basic science end of things will aid in economic development through its "service" functions. Protein crystallography can service the medical and pharmaceutical industries, X-ray micro-tomography offers a non-destructive look inside materials (state archeologists, manufacturers of small precise devices, etc.), EXAFS and XANES are other "non-destructive analytic techniques (you can usually measure a sample without changing it chemically as lab bench techniques often require plus, you can determine the oxidation state of elements which is difficult to do with normal chemical and spectroscopic techniques), IR Spectromicroscopy will require us being educated to its usefulness as we are not IR spectroscopists (literature shows great utility in the medical, environmental and chemical manufacturing industries).

#### **11. Should CAMD move its micro- fabrication facility to South Campus?**

**David:** Eventually the entire facility should be moved. Suggested locations have been the South Campus and the campus itself.

**Les:** Whatever Jost & Soper want. I'm hearing a partial move is likely. However, I'm not a fan of South Campus, it's too far from LSU.

**Jost:** Solely from CAMD's perspective – why should we? We have established a routine operation under the current boundary conditions and the old saying is '...never change a winning team'. However, in view of the big picture (flag-ship agenda) it might be a better thing to do (Campus would even be better than South Campus).

**John:** My answer to this is "no." It is premature to discuss placement of SEALS and, furthermore, doing so now will make issues cloudy. We seem to be in the mode "We made one mistake in moving CAMD 5 miles off campus 17 years go so why not fix it with another hasty mistake." I have visions of the same thing happening again and, 10 years from now, everyone will wonder how such a mistake could have been made. It will cost considerably to move it and all we finally will have is the same facility and similar clean rooms but no storage ring near by. Why not invest the same money in Microfab in its current location and have a much better facility with a storage ring attached?

#### **12. Should CAMD build a 3rd generation light source?**

**David:** If LSU and other CAMD users are to remain competitive LSU eventually will have to consider the construction of a 3<sup>rd</sup> generation light source.

**Les:** Crystal ball says there will be a new X-ray facility in the southern USA. Let's consider the range of scenarios: (a) Best case is facility is on LSU campus. (b) worst case is Lubbock, TX. Lubbock is close enough for protein crystal transportation. If LSU is a strong partner, we get lots of access. Future beamlines will have more capability for remote operation. So, the worst case is still quite good for LSU. Summary, LSU should lead quest for a regional X-ray facility and be flexible with regard to final location.

**Jost:** Not for microfab.

**John:** LSU should take the lead in working up a case for a regional light source. The question is not "Who gets it?" but is "Where will it be built?" If we start the process and because we have an SR source already, we stand a good chance of getting it here. It will not be LSU's light source or even Louisiana's light source – unless the state of Louisiana funds and supports it. Having a strong Materials Science Program at LSU and one that networks other strong Louisiana and regional universities will also be a compelling reason to locate it here.

### **13. Does the SE need an advanced light source?**

**David:** The case can be made for a 3<sup>rd</sup> generation light source for the southeast. There are many researchers in Texas, Mississippi, Alabama, Georgia, and Florida that have not been tapped. The case for NSLS-II is based on arguments that propinquity is an essential ingredient for protein crystallography and nanosciences. CAMD has core expertise in both these research areas.

**Les:** ditto

### **14. How can CAMD fund a 3rd generation light source?**

**David:** Comments from the break-out sessions suggest that CAMD-II will be an integrated facility that will emerge incrementally from add-on insertion devices, increased brightness brought about by decreased ring emittance and upgraded clean rooms. I believe the funding will be a combination of federal, state, industrial and philanthropic.

**Les:** First, CAMD will be upgraded with series of \$1-3M add-ons. (a) NSF MRI for \$1.5M wiggler. (b) CRDF or similar for soft X-ray insertion device (c) BoR for cryocooler-enhanced wiggler (d) State funding for office/lab/parking (f) State increase in overall CAMD funding (what happens to CAMD funding with microfab move?)

### **15. What role can/should CAMD play in building a materials science program at LSU?**

**David:** CAMD already plays an important role in LSU's material science program. There are close collaborations between microfabrication and CBMM, engineering, chemistry, physics, etc. In a typical year about ten different departments use CAMD's facilities. Thus, CAMD will be a vital ingredient in any LSU materials science program.

I would like to suggest some people who may help guide LSU in forming a Materials Science PhD program.

Ward Plummer- University of Tennessee

Miles V. Klein – University of Illinois

Al Sievers –Cornell University



**Les:** What is the driver for materials science? In some places, it was intellectual curiosity (like Univ. of Illinois). In some places, it was an available technique (like ORNL neutrons for Univ of Tennessee). What will be the driver at LSU? What's left? How about job creation?

**Jost:** The cycle of synthesis and analysis presented by Franz Himpsel at the workshop is the best advocate for CAMD's role. Materials science esp. with respect to 'nano-engineering' requires continuous control or analysis of the synthesis effort and SR is well-excepted as versatile and unique tool to perform this analysis. But again, is such a program desired within the flag-ship agenda? Does it get the priority and support?

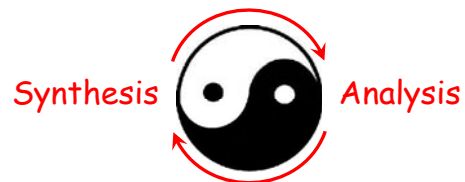
**John:** All of CAMD, not only Microfabrication, has close ties with chemistry, physics, biology, geology, engineering and agronomy to name a few. All interactions can be classed as "materials" in today's definition. CAMD offers unique and very excellent equipment and expertise to enhance a Materials Science Program. Our scientists can also contribute their own research efforts as well as education of students – both graduate and undergraduate. CAMD might even provide a small catalyst to get researchers (we have a fair amount of talent on campus) to figure out what a Materials Science Program is and what one is at LSU. There actually was a formal MS Program started at LSU in the late 70's. Mary Goode was brought in as its chair. Maybe history could teach us what NOT to do.

## The Madison Discovery Institute (Nano + Bio + Info)



The Key to Success in the Rapidly-Moving  
Field of Nanoscience and Nanotechnology:

A Tight Feedback Loop



- Rapid access (like a TEM, "small facility", remote operation?)
- Emulate NNIN (Natl. Nanotech. Infrastructure Network)
- Synthesis and analysis at the same location (DOE nanocenters)

**Report of Medical Radiology Breakout Session  
LSU CAMD Fall 2006 User Meeting Workshop  
November 19-21, 2006**

**Report Contributors**

LSU Dept. of Physics and Astronomy/Medical Physics and Health Physics Program

Joe Dugas, Ken Hogstrom, Kip Matthews, Erno Sajo, Marie Varnes

LSU Dept. of Chemistry

Les Butler, Luigi Marzilli, Patricia Marzilli

CAMD

Kyungmin Ham

MXISystems, Inc.

Frank Carroll

The three topics below, relevant to the use of CAMD for medical radiology research and to questions posed by Vice Chancellor for Research and Economic Development, Brook Keels, were discussed.

**1. Medical Radiological Science**

Current and Proposed Future Areas of Research

- Diagnostic Imaging
  - Dual energy imaging (planar and CT)
  - K-edge imaging (planar and CT)
  - Phase contrast imaging
- Therapy
  - K-edge capture, Auger electron therapy (Z ranging from iodine to platinum)

Targeted Applications of Research

- Mammography
- Thoracic and brain imaging
- Imaging of high-Z labeled pharmaceuticals
- Applications
  - Diagnosis of disease
  - Mapping of pharmaceutical used in chemo-irradiation, e.g. IUdR
  - Therapeutic irradiation of cells and small animals with cancers

Types of Irradiations and Research

- Physical dosimetry measurements
- Image acquisition and analysis
- Biological Irradiations
  - Cells
  - Small animals (mouse or rat)

## 2. Beam-line Requirements

### Utilization of Current Beam-line

- From irradiation of atoms to small animals- currently limited to  $\approx 40$  keV for biological irradiations

### Needed Beam-line Improvements

- Increase photon fluence rate at 80 keV to equal that currently at 35 keV (2 orders of magnitude?)
- Increase beam dimensions from 3 cm to 20 cm for large animal studies (meeting above fluence rates)

### Comments Regarding Mechanisms to Achieve Future Needs

- Proposed new wiggler should increase fluence rate x10 allowing cell and animal irradiations up to  $\approx 60$  keV
- Perhaps it would be possible to increase the fluence rate using a different monochromator (double crystal versus monolayer) allowing studies at  $>60$  KeV for small samples ( $< 3$  cm).
- Irradiation of large animals at highest keV are likely best done using inverse Compton accelerator located at the Vet School. These inverse Compton sources have a lower flux than synchrotrons at lower energies ( $10^{10}$  photons/sec vs.  $10^{12-14}$  photons/sec) and are not phase coherent, but they show good lateral coherence and area geometries at energies of 100 keV or more at excellent fluxes, that are useful for imaging and therapy in animals and humans. They do not require monochromators, as well.
  - Unlikely beam size could be large enough at CAMD without excessively long beam line to widen the beam to useful area geometry
  - Unlikely that new CAMD ring would provide ample fluence rate
  - Location of accelerator near animal facilities is more practical and more enticing for Vet School to participate

## 3. User Interactions with CAMD

### Current Status

- Excellent support; CAMD scientists are very helpful and considered collaborators
- Like easy accessibility of beam time

### Future Requests

- Develop method for scheduling time on beam line well in advance, while maintaining flexibility of having access to some “short-notice” beam time
- Find ways of slightly increasing irradiation area for medical irradiations
- Equip beam line with equipment important for medical uses
  - Dosimetry equipment
  - Imaging equipment
  - Minor equipment to support cell and small animal irradiations

**Report of Soft Materials Breakout Session  
LSU CAMD Fall 2006 User Meeting Workshop  
November 19-21, 2006**

At the workshop, the CAMD director seemed interested in hearing about the experimental capability of the SAXS beamline 1) in its current state within CAMD, 2) in an upgraded/expanded CAMD, and/or 3) in a SPEAR 3 environment. I just wanted to include some comments about possible SAXS use @ CAMD. Please place these comments in an appropriate section of this report. Thanks!

Current SAXS users at LSU have traveled both nationally (SSRL and APS) and internationally (Photon Factory in Japan and LNLS in Brazil) to perform research using synchrotron SAXS.

Local researchers studying the solution structure of proteins could utilize a SAXS beamline at CAMD, but not in its current state. Currently, the flux of the CAMD SAXS beamline is much too low to obtain useful scattering data for a protein (less than 100kDa) in a dilute solution. With the construction of an appropriate sample holder, the CAMD SAXS beamline could be comparable to the SAXS beamline at LNLS in Brazil. However, small angle x-ray scattering curves for dilute protein solutions collected at LNLS by researchers in Dr. Vince LiCata's laboratory at LSU were too noisy to yield publishable results. The LNLS SAXS beamline has no insertion device to increase the flux, and the LiCata lab data was collected on a linear detector.

The CAMD SAXS beamline currently has a 2D CCD detector and with the addition of an insertion device, it may be possible to collect useful SAXS data in the Guinier region to determine overall particle size ( $R_g$ ) and volume.

On the other hand, if the SAXS data is to be used to create bead models of particle shape *ab initio*, then data will have to be collected at both low and high scattering angles. Scattering intensity decays in a somewhat exponential fashion with increasing scattering angle. Therefore, even with an upgraded CAMD SAXS beamline it will be difficult to collect usable high angle scattering data for dilute protein solutions. Thus far, the LiCata lab researchers have only been able to collect modeling-quality high angle scattering data at SPEAR 3 synchrotron sources.

1. The question is confusing.
2. CAMD has a regional user base. In protein crystallography, users have come from Texas, Kansas, Maryland, etc.; in X-ray absorption spectroscopy users have come from Alabama, Virginia, Texas; there are potential users for SAXS out there.

The current configuration of the CAMD ring satisfies a real need and is justified. At expanded level, with insertion devices, the need can also be justified.

3. The qualifications, training and pay scale of the CAMD staff should be improved.
4. A convenient bus route or call drivers should be established. This is particularly true for students without cars.
5. There should be real laboratory facility on CAMD premises close to the experimental hall.
6. How will CAMD benefit from this alliance?
7. The chances of collaboration with the local industry are decreasing as many of them have closed their research facility in and around Baton Rouge. However, there are smaller companies which may want to collaborate with us.
8. Work closely (have monthly meetings) with LETC (Louisiana Emerging Technology Center).
9. If Microfabrication moves to South Campus it may mean closing down of CAMD.
10. Third generation light source:  
  
Instead of asking for \$100 million, we should ask for more, say \$250 million  
How is Rose unique?  
ROSE sounds like more of the same on a show-string budget.
11. Not as much as it needs an innovative national lab that has an advanced light source as part of the purchase.
12. Think bigger than synchrotron, work with governor/director.
13. For the Materials Science program, CAMD can supply much of the needed reality but political issues are for the VC Keel to solve.

**Report of Microfabrication Breakout Session  
LSU CAMD Fall 2006 User Meeting Workshop  
November 19-21, 2006**

**Report Contributors**

Steven Soper (Dept. of Chemistry, LSU )  
Jost Goettert (CAMD)  
Proyag Datta (CAMD)

The topics below, relevant to the microfabrication activities and research at CAMD and to questions posed by Vice Chancellor for Research and Economic Development, Brooks Keal, were discussed.

**CAMD and Main Campus Interaction**

CAMD needs a closer level of interaction with faculty on campus to promote collaborative and multi-disciplinary research in order to pursue unique funding opportunities that depend on such interactions. The type of funding opportunities that depend on active researchers with extensive publication records and state-of-the-art research capabilities, in terms of equipment and personnel expertise, include Engineering Research Centers (NSF), Science and Technology Centers (NSF) and National Centers of Research and Resources (NIH). These types of funding mechanisms can bring a large amount of visibility to CAMD and the LSU campus. Planning meetings between cognizant researchers on campus CAMD staff should proceed immediately so as to be fully aware of these funding opportunities and also, develop and coordinate plans for joint research projects. Another mechanism that would benefit greatly from main campus / CAMD joint efforts would be acquisition of new major equipment through Major Research Instrumentation grants (NSF) and Shared Instrumentation grants (NIH). Joint efforts on this front will allow CAMD to remain state-of-the-art in terms of instrumentation and capabilities.

Secondly, in order to assist in fostering interactions between CAMD and main campus, joint courses of some form are necessary, where students can learn the theoretical aspects of micro-manufacturing and attend laboratory sessions to gain hands-on experience with equipment and processes. Funding for something like this would have to come from the University. There has been in the past efforts on this front such as the nanotechnology graduate level course that was developed by Prof. David Spivak (CHEM), but these courses need to be formalized in terms of continuous and periodic offerings and inclusion of CAMD staff in the instruction aspects of these courses. In addition, mechanisms for receiving class credit for CAMD clean room training needs to be affected. Involvement of faculty on-campus needs to become more engaged in these training sessions.

**Economic Development**

CAMD can play and has played a significant role in education in high technology. It can also provide a strong support structure for start-up companies. Examples include MEZZO, but others need to materialize to effectively utilize this strong resource. With the presence of the Emerging Technology Building and enterprise, the ability to develop start-up companies on the LSU campus is becoming more accommodating and this should help to foster such activities. The CAMD fabrication enterprise needs to become more engaged in these types of activities. CAMD has already developed a user facility structure, which can be further developed to support economic development in the Southeast and make researchers across this region more competitive for scarce research dollars. This can be accomplished by holding regional workshops on fabrication to allow researchers the opportunity to become familiar with the research capabilities of CAMD and discuss possible project collaboration efforts.

**SEALS source**

For microfabrication efforts, the group does not see a strong need for a 3<sup>rd</sup> generation source, since the current source meets the needs for microfabrication. A new synchrotron would also require process development before the X-ray lithography processes are well established.

However, a 3<sup>rd</sup> generation light source would provide unique opportunities for developing some new lithography capabilities (for example x-ray interference lithography) as well as improve basic understanding of surface functionalized microdevices through advanced spectroscopic methods (as illustrated in Franz Himpsel's presentation). It is worthwhile planning a dedicated workshop to further discuss these avenues. However, it is clear that a limited number of applications would evolve from the adoption of a new source and require re-optimization of existing standard operating procedures. It was also noted that with the development of new micro-manufacturing techniques across campus and the development of SU-8 lithographic procedures, the dependency of microfabrication on X-ray lithography has become a minor component of the total processing work load of the fabrication enterprise (~10% of the total work load). While this may be true at the present time, the ability to pattern ultra-high aspect ratio microstructures cannot be ignored and does offer unique process capabilities of the fabrication enterprise on campus.

### **Centralized Facility**

It was strongly noted that the development and organization of a centralized facility for micro- and nanofabrication would definitely move this component of the research mission of CAMD forward both academically and economically as well. However, this would have to be supported by the university as a whole (faculty, and administrators) to formulate a concerted effort towards developing all aspects of microfabrication at this core facility – materials, silicon-MEMS, packaging of microfabricated devices, applications in biology, chemistry etc. This should be done quickly so as not to miss the opportunities in the in micro & nanotechnology areas that are currently here. Choices for location are Main Campus or South Campus. A strong commitment from the University is necessary for this to become a reality. It was felt that the centralization would require the installment of a new clean room, since the existing one is out-dated, and the joint consolidation of the fabrication tools with ancillary and support tools, such as materials characterization. Centralization would provide many benefits to both CAMD and the researchers on campus, such as better collaboration and communication between CAMD staff and faculty on campus, more competitive for Center-type funding opportunities, better utilization of support staff, opportunities in joint projects with the private sector and lower operational costs.

### **Industrial Ties**

The microfab group collaborates well with many industrial partners already and the numbers of collaborations are steadily increasing. Some industrial partners sponsor research, some utilize the 'user facility' aspect of CAMD and use the beamlines and equipment and some are true 'customers' who buy services/products from CAMD. These need to be expanded and increase the customer base of CAMD in order to increase revenues and further justify the expansion of such a resource and add new staff to this resource.



**Report of Chemical Physics/HardCondensed Matter Breakout Session**  
**LSU CAMD Fall 2006 User Meeting Workshop**  
**November 19-21, 2006**

### **Report Contributors**

Erwin Poliakoff, Gary Findley, John Scott, Vic Suller, Rich Kurtz, Ulli Diebold, Kyungmin Ham, Franz Himpsel, Tony Caruso, Orhan Kizilkaya, Kresimir Rupnik, Phillip Sprunger

### **Summary**

Discussion centered on various aspects of condensed matter (hard/dilute materials) and AMO (atomic, molecular, optical)/chemical physics research at CAMD. These research efforts include IR, valence- and core-spectroscopy/absorption. The principle focus of our discussion was on valence-shell and shallow core spectroscopies.

There was a consensus on a few points. (1) CAMD should develop a long term (e.g. 20 year) “road map” that would be based on users’ present and future scientific needs. (2) Incremental change should be the paradigm of this evolution in which facility upgrades and/or development is based on both short-term and long-term considerations.

Focus of discussion centered on three different “epochs” of CAMD: the present, the future (short-term) upgrades, and the long-term development of a new machine.

### Current status

- In general, AMO/Hard-CM researchers were pleased with CAMD’s current beamlines and ring operation. In general, this group, operating in the VUV energy range, has sufficient flux to perform many current levels of experiments.
- The successful commissioning of the VLSG monochromator, beam-shutters, user-friendly endstation allowing for XMCD/XMLD spectroscopy will greatly enhance the “magnetic materials” programs of both LSU and external users.
- Discussion regarding user needs indicated that more scientific/technical staff is needed to better meet the needs of the researchers.

### Short-term development/improvement

- Discussion centered around two key upgrades: upgrading current wiggler and installing new multiple wiggler.
- The upgrade of the current wiggler would not, in general, benefit this group. Although it would access more elements, this would not affect this research community.
- The prospect for installing a new multipole wiggler (100-1200 eV) was highly encouraged and supported by this group. The ability of operating this ID in a concurrent multi-user (20/20/20 or 30/30) mode was encouraged. The higher flux would greatly enhance and extend current research CM efforts. With use of SGM and DCM’s, this includes:
  - Dilute sample characterization (e.g. dilute ferromagnetic semiconductors)

- PEEM / XMCD-PEEM (e.g. better contrast of materials and/or magnetic contrast)
  - High-resolution ARPES (e.g. enable higher resolution at sufficient flux)
  - Spin-resolved PES
  - Increased sensitivity for ionization probe experiments (e.g., combustion dynamics)
- A “scientific case” for acquisition and installation of this multipole wiggler and beamlines should begin at present.
  - The formation of potentially federally-funded “Centers”, or focused research groups, should be encouraged and initiated. It is believed that these units would act as a means by which federal agencies (e.g. DOE, DOD, NSF) would fund operational costs associated with ongoing and enhanced research. Examples might include:
    - Elucidating exchange mechanisms in novel magnetic materials
    - AMO center for ionization dynamics and ionization probes
    - In situ characterization of combustion chemistry
  - Any and all short-term upgrades should incorporate regional input and/or support from CM and chemical-physics university researchers and/or national labs. This includes TX, FL, and perhaps TN (ORNL), AZ (Sandia), NC (Jeff)

#### Long-term future

- The idea and justification of a new 3-generation machine were also discussed. Within the context of a 20-year roadmap of “CAMD’s” future, it was in general agreed that ultimate installation of a 3-generation source should be a vital component. This is based primarily on the need for an expanded vision of potential synchrotron-based research capabilities of the mid-South/ Southeastern Region.
- In the area of CM and chemical physics, the major justification for a new third generation machine would be brightness. Although this property is not, in general, required for all experiments, it would enable a drastic improvement for three activities:
  - spectromicroscopy experiments including PEEM, microprobe, small sample valence/core samples
  - Photon-in-photon-out experiments would benefit greatly
  - High resolution experiments requiring broad spectral coverage

Informal Comments about the 3-rd Generation Synchrotron Planning  
LSU CAMD Fall 2006 User Meeting Workshop  
November 19-21, 2006

Background: Les Butler (CAMD user committee chair) requested additional information from Vic Suller to supplement the excellent talk and powerpoint describing a 3-rd generation X-ray facility.

Nov 29

Hi Les

My reactions to the workshop are:

1. It attracted a reasonable cross section of CAMD staff and Users so that any views and opinions expressed were fairly representative.
2. The presentations clearly demonstrated the vigor and scientific relevance of research using synchrotron radiation. Some research areas obviously benefit from high brightness (imaging, microprobes, protein crystallography), others need high flux (photo emission spectroscopy/dilute samples), while some (micro fabrication) have no requirement for brightness.
3. The convenience of having a light source facility within easy reach of a home laboratory was stressed repeatedly.
4. There is some demand for higher energy photons than CAMD can deliver, to access K-edges of heavier elements and for medical imaging. This implies a higher energy electron beam than CAMD's 1.3 GeV would be useful.
5. There is at the moment no strong support for SEALS/ROSE as a stand alone facility but it could be an essential component for something like a chemistry or materials science center.

My conclusion is that the CAMD User community has to become accustomed to using higher brightness and flux from CAMD itself. This can be achieved by incrementally upgrading CAMD with new insertion devices and by modifying the lattice structure until every ounce of flux and brightness increase has been squeezed from it. Then will be the time to push strongly for SEALS/ROSE.

Vic

Nov 29

Hi Vic,

My apologies for talking \$\$\$, but let's blame that on the upcoming task of coordinating the NSF MRI, \$1.6M proposal. Could you provide more detail about the details of item #6, future upgrades of CAMD. For example, the estimated cost of the second insertion device, anticipated funding agency, types of users writing that proposal. Also, any updates to SEALS/ROSE cost based on news from the workshops, or still in the \$90-\$100M range?

Thanks,

Les

Nov 30

Hi Les

Very approximate costs for CAMD upgrades are:-

New soft X-ray MPW \$2M (including integration into the storage ring)  
Beamline and station to suit \$4M

Improving the brightness with updated quadrupoles and power supplies \$0.5M

Attaining the ultimate CAMD brightness with additional quadrupoles \$3M

The SEALS estimates pretty much stand except inflation needs to be factored in since 2003.

Regards, Vic

## Appendix C.2.

Second Workshop: “Enabling Grand Challenge  
Science: The Light Source of the Future,”

January 28-30, 2008



# Enabling Grand Challenge Science: The Light Source of the Future

a workshop sponsored by the LSU Office of Research & Economic Development\*

In the latter part of the 20th century and the early years of the 21st,  
discoveries in science have advanced at an almost blinding pace...

Join us in an effort to elucidate the dynamic and  
functional behavior of gases and solids at the atomic scale

## January 28-30, 2008

Lod and Carole Cook Conference Center & Hotel  
3848 West Lakeshore Drive, Baton Rouge, Louisiana

# LSU

LOUISIANA STATE UNIVERSITY

\* Cosponsored by the Southeastern Universities  
Research Association (SURA), Florida State  
University, Office of the Vice President for  
Research, and University of Tennessee, Office of  
the Vice Chancellor for Research

### Organizing Committee:

Doris Carver  
David Ederer  
Brooks Keel  
Ward Plummer  
Gwyn Williams

### Local Arrangements Committee:

Caryl Boyet  
Holly Carruth  
Matt Mullenix  
Craig Stevens

# Enabling Grand Challenge Science: The Light Source of the Future

## Conference Agenda

### Monday, January 28, 2008 - Lod Cook Conference Center

8:00 AM – 9:00 AM Registration and Continental Breakfast

#### Session I: Welcome and Introduction to the Grand Challenges – Noland/Laborde

9:00 AM – 11:30 AM Morning Session

9:00 AM – 9:15 AM Welcome – Astrid Merget, Executive Vice Chancellor and Provost, LSU

9:15 AM – 9:30 AM Welcome – Brooks Keel, Vice Chancellor, Office of Research & Economic Development, LSU

9:30 AM – 10:15 AM Directing Matter and Energy: Five Challenges for Science and the Imagination – John Hemminger, Dean, School of Physical Sciences, and Professor University of California, Irvine

10:15 AM – 10:30 AM Coffee Break

10:30 AM – 11:00 AM Addressing the Grand Challenges: What Can Light Sources Contribute – Wolfgang Eberhardt, Director, BESSY Laboratory

11:00 AM – 11:30 AM Motivation and Outcome for the Workshop – Ward Plummer, Professor and Special Assistant to Vice Chancellor of Research & Economic Development, LSU, and Distinguished Professor, University of Tennessee

11:30 AM – 12:30 PM Lunch at Lod Cook

#### Session II: Meeting the Grand Scientific Challenges

12:30 PM – 5:00 PM Afternoon Session

##### Session II – A: Control of Electrons in Atoms, Molecules and Materials: Creating a New Language for the Behavior of Electrons

12:30 PM – 1:00 PM The Challenge of Manipulating and Controlling Material at the Quantum Level: What High Brightness and Source Coherence Means to the Study of Nanomaterials – Lou Terminello, Lawrence Livermore National Laboratory

1:00 PM – 1:30 PM Brighter, Smaller, Faster: X-ray Absorption Spectroscopy and Grand Challenge Science – Josef Hormes, Bonn University and CAMD/LSU

1:30 PM – 2:00 PM Attosecond Science – Ken Schafer, LSU

2:00 PM – 2:30 PM Atomic, Molecular and Cluster Physics with Ultrafast and Ultra-intense Light Sources – Nora Berrah, Distinguished Professor, Western Michigan University

2:30 PM – 2:45 PM Coffee Break

##### Session II – B: Basic Architecture of Matter: Directed Assembly, Structures and Properties: The Challenge of Creating Robust Soft Matter and Tailorable Hard Materials

2:45 PM – 3:15 PM Macromolecular Crystallography in the 21st Century – Robert Sweet, Brookhaven National Laboratory

3:15 PM – 3:45 PM Ab initio Structural Modeling with Small Angle X-ray Scattering Data and the Need for High Intensity Sources – Vincent J LiCata, LSU

3:45 PM – 4:15 PM Structural Biology in the Southeast – Bob Fox, University of Texas Medical Branch

4:15 PM – 4:45 PM Imaging Cells with X-rays: Current Capabilities and Future Challenges – Gerry McDermott, University of California, San Francisco

# Enabling Grand Challenge Science: The Light Source of the Future

## Agenda, continued

- 4:45 PM – 5:15 PM Single Molecule Diffraction – Sebastien Boutet, Stanford Linear Accelerator Center, Stanford University
- 5:15 PM – 6:00 PM Reception – Noland/Laborde Lobby
- 6:00 PM – 7:30 PM Dinner Break – Noland/Laborde Hall
- Session II – C: Emergence, Complex Phenomena and Strongly Correlated Multiparticle Systems: The Challenge of Creating New Correlated Electron Materials**
- 7:30 PM – 8:00 PM Emergent Phenomena in Strongly Correlated Electron Materials: Detection and Characterization - Matthew P. A. Fisher, Microsoft Corporation and University of California, Santa Barbara
- 8:00 PM – 8:30 PM Advances in Photoemission at a Next-Generation Light Source – Tai C. Chiang, University of Illinois at Urbana-Champaign
- 8:30 PM – 9:00 PM Electronic Properties of Nanostructures – Richard Kurtz, LSU

### Tuesday, January 29, 2008 - Lod Cook Conference Center

- 8:00 AM – 8:30 AM Registration – Noland/Laborde Hall
- 8:30 AM – 12:00 PM Morning Session
- Session II – D: Nanoscale Communication–Energy and Information: The Challenge of Creating Nanotechnology with Functionalities that Rival Living Systems**
- 8:30 AM – 9:00 AM Microtechnology Advances in the Light of a Source of the 21st Century – Franco Cerrina, University of Wisconsin
- 9:00 AM – 9:30 AM Bioscience and MEMS – Steve Soper, LSU
- 9:30 AM – 10:00 AM Case for Environmental Science at the ‘Next Generation’ Light Source – Gordon Brown, Stanford University
- 10:00 AM – 10:30 AM Coffee Break
- Session II – E: Matter Far Beyond Equilibrium: The Challenge of Understanding and Controlling Systems that are Far from Equilibrium**
- 10:30 AM – 11:00 AM Science Challenges Far from Equilibrium Using Future Light Sources – Gopal Shenoy, Argonne National Laboratory.
- 11:00 AM – 11:30 PM Probing Molecular Dynamics – Lin Chen, Argonne National Laboratory
- 11:30 AM – 12:00 PM Pump-Probe Processes-time-Resolved X-ray Diffraction and Ultrafast X-ray Optics for the Study of Material Dynamics – David Fritz, Stanford Synchrotron Radiation Laboratory, Stanford University
- 12:00 PM – 1:00 PM Lunch at Lod Cook
- 1:00 PM – 5:00 PM Afternoon Session
- Session II – F: Source Parameters**
- 1:00 PM – 1:30 PM Parameters for Fourth Generation Light Sources – Roger Falcone, UC Berkeley, and Director of the Advanced Light Source, Lawrence Berkeley National Laboratory
- 1:30 PM – 2:00 PM Ultimate Storage Ring Light Sources – Mike Borland, Argonne National Laboratory



# Enabling Grand Challenge Science: The Light Source of the Future

## Agenda, continued

2:00 PM – 2:30 PM Energy Recovery Linacs – Geoffrey Krafft, Jefferson Lab National Accelerator Facility

2:30 PM – 3:00 PM Free Electron Lasers – John Lewellen, Naval Postgraduate School

3:00 PM – 3:30 PM **Coffee Break**

### Session III: Writing the Report

3:30 PM – 5:00 PM Break out Session A – Abell Board Room

3:30 PM – 5:00 PM Break out Session B – Abell Board Room

3:30 PM – 5:00 PM Break out Session C – Shelton 1st Floor

3:30 PM – 5:00 PM Break out Session D – Shelton 2nd Floor

3:30 PM – 5:00 PM Break out Session E – Cook Conference Room

3:30 PM – 5:00 PM Speakers Interact with Break Out Groups

(A) Control of Electrons in Atoms, Molecules and Materials: Creating a New Language for the Behavior of Electrons – The Challenge of Manipulating and Controlling Material at the Quantum Level

(B) Basic Architecture of Matter: Directed Assembly, Structure and Properties – The Challenge of Creating Robust Soft Matter and Tailorable Hard Materials

(C) Emergence, Complex Phenomena and Strongly Correlated Multiparticle System – The Challenge of Creating New Correlated Electron Materials

(D) Nanoscale Communication – Energy and Information: The Challenge of Creating Nanotechnology with Functionalities that Rival Living Systems

(E) Matter Far Beyond Equilibrium – The Challenge of Understanding and Controlling Systems That are Far from Equilibrium

### Wednesday, January 30, 2008 - Lod Cook Conference Center

8:30 AM - 9:00 AM **Session III (Writing the Report) – Abell Board Room**

9:30 AM – 10:00 AM **Coffee Break**

10:00 AM – 11:30 AM Report from breakout sessions

11:30 AM – 12:30 PM **Lunch at Lod Cook**

12:30 PM – 2:00 PM Summary of Workshop

2:00 PM End of workshop

# ***Enabling Grand Challenge Science: The Light Source of the Future***

## ***List of Attendees***

**Ade**, Harald, North Carolina State University  
**Barnett**, Heath, LSU  
**Bellamy**, Henry, CAMD  
**Berrah**, Nora, University of Western Michigan  
**Beuerle**, Johannes, CAMD  
**Boebinger**, Gregory, National High Magnetic Field Laboratory  
**Borland**, Mike, Argonne National Laboratory  
**Boutet**, Sebastian, Stanford Linear Accelerator Center  
**Briski**, Karen, University of Louisiana at Monroe, School of Pharmacy  
**Brown**, Gordon, Stanford University  
**Buckalew**, Katie, LSU  
**Butler**, Les, LSU  
**Carruth**, Holly, LSU  
**Carver**, Doris, LSU  
**Cerrina**, Franco, University of Wisconsin  
**Challa**, Kumar, CAMD  
**Chen**, Lin, Argonne National Laboratory  
**Chiang**, Tai-Chang, University of Illinois - Urbana-Champaign  
**Corbett**, Jeff, Stanford Linear Accelerator Center  
**Crappell**, Alex, CAMD  
**Datta**, Proyag, CAMD  
**DiTusa**, John, LSU  
**Dobbins**, Tabbetha, Louisiana Tech University  
**Dorman**, Derek, LSU  
**Draayer**, Jerry, SURA  
**Dutrow**, Barb, LSU  
**Eberhardt**, Wolfgang, BESSY Laboratory  
**Ederer**, David, CAMD  
**Ellington**, Ross, Florida State University  
**Falcone**, Roger, Lawrence Berkeley National Laboratory  
**Fenwick**, Brad, University of Tennessee  
**Findley**, Gary, University of Louisiana at Monroe  
**Fisher**, Matthew, Microsoft Corporation, Station Q  
**Fox**, Robert, University of Texas Medical Branch  
**Fritz**, David, Stanford Linear Accelerator Center  
**Gearba**, Alina, Southern Mississippi  
**Goettert**, Jost, CAMD  
**Gopalan**, Balaji, CAMD  
**Ham**, Kyungmin, CAMD  
**Hemminger**, John, University of California, Irvine  
**Henry**, Darrell, LSU  
**Hormes**, Josef, CAMD/Bonn University  
**Jenkins**, Brandon, LSU  
**Jiles**, Ronnel, CAMD  
**Jines**, Paul, CAMD  
**Kazan**, Selim, CAMD  
**Keel**, Brooks, LSU  
**Khonsari**, Michael, Louisiana Board of Regents  
**Kizilkaya**, Orhan, CAMD  
**Knott**, Eric, CAMD  
**Krafft**, Geoffrey, Jefferson Lab  
**Kurtz**, Richard, LSU  
**Launey**, Daren, CAMD  
**Lewellen**, John, Naval Postgraduate School  
**Lian**, Kun, CAMD  
**LiCata**, Vince, LSU  
**Logan**, Tim, Florida State University  
**Mankey**, Gary, University of Alabama  
**McDermott**, Gerard, University of California, San Francisco  
**Merchan**, Gregory, CAMD  
**Miller**, Toby, CAMD  
**Morikawa**, Eizi, CAMD  
**Morris**, Kevin, CAMD  
**Neau**, David, CAMD  
**Neil**, George, Jefferson Lab

**Ogunbakin**, Tolulope, LSU  
**Plummer**, Ward, University of  
Tennessee/ORNL/LSU  
**Pourciau**, Todd, LSU  
**Ramachandran**, Bala, Louisiana Tech  
University  
**Rau**, Ravi, LSU  
**Richard**, Allison, LSU  
**Roy**, Amitava, CAMD  
**Roy**, Sumita, CAMD  
**Rupnik**, Kresimir, LSU  
**Russo**, Paul, LSU  
**Schafer**, Ken, LSU  
**Scott**, John, CAMD  
**Shenoy**, Gopal, Argonne National  
Laboratory  
**Singh**, Varshni, CAMD  
**Singleton**, John, National High Magnetic  
Field Laboratory  
**Soper**, Steve, LSU  
**Sprunger**, Phillip, LSU

**Steier**, Christof, Lawrence Berkeley  
National Laboratory  
**Stevens**, Craig, CAMD  
**Suller**, Victor, CAMD  
**Sutherland**, John, East Carolina University  
**Sweet**, Robert, Brookhaven National  
Laboratory  
**Terminello**, Lou, Lawrence Livermore  
National Laboratory  
**van Tol**, Johan, Florida State  
University/NHMFL  
**Wang**, Shaoheng, CAMD  
**Wang**, Yanshan, CAMD  
**Weber**, Andrew, CAMD  
**Williams**, Gwyn, Jefferson Lab  
**Willson**, Clint, LSU  
**Winick**, Herman, Stanford  
University/SLAC/SSRL  
**Yemane**, Dawit, CAMD  
**Zhou**, Pingheng, CAMD

## **Appendix. C.2 Enabling Grand Challenge Science: The Light Source of the Future, January 28-30, 2008**

### **App.C.2.a. Introduction**

As of May 2008 and probably for several years to come, CAMD is and will be the only synchrotron light facility in the southeastern USA. It has operated successfully as a regional facility since 1992 with a growing and diverse research program that has been described in Section II. The overwhelming number of CAMD's over 300 users comes from LSU, and Louisiana. About 50 users are from the rest of the United States with about a dozen coming from Europe. During the course of time new technology emerges and the science horizon changes. Therefore, CAMD and LSU must consider how the user community will be served and developed in the short and long term future. Especially, during the next five to ten years source development must include our current user base. Beyond that time frame, one may consider morphing the current source into a third or fourth generation source, into a laser-based high coherence high, brightness facility or into a combination of the two. In this section we will present several the possibilities but not define the parameters for the future light source at CAMD at this time.

The cost of a future CAMD source will range from about \$100,000,000 to something of order of a billion dollars, and thus the source characteristics will depend almost totally on obtainable funding. The search to define the next source and its funding is necessarily a task that the LSU Vice Chancellor of Research should direct.

What follows is a report of the workshop held in January 2008 that was cosponsored by the Louisiana Board of Regents; the Southeastern Universities Research Association (SURA); Florida State University, Office of the Vice President for Research; University of Tennessee, Office of the Vice Chancellor for Research; the Louisiana Board of Regents and the LSU Office of the Vice Chancellor of Research and Economic Development, to explore some of the possibilities for a fourth generation source. Some of the material was introduced in Section V and will not be extensively repeated here.

The cost of a third-generation source would be of the order of \$100M, including a new building, and is described in Section V.B. The cost of a fourth-generation source will range from several hundred million dollars to something of the order of one billion dollars, depending on the design. Facilities of this magnitude will require a regional effort to obtain funding from state, federal, and private sources. On the other hand, the scientific benefits of such a source will drive cutting-edge science and technology development for all the universities in the Southeast.

### **App.C.2.b. A More Advanced Third Generation Source Concept to Move Beyond the Simplest Kind of Third-Generation Source**

The following paragraphs contain a summary of a report that describes a more elaborate source by Dr. Wolfgang Eberhardt, Director BESSY-II. Professor Eberhardt attended the LSU workshop in January 2008 and has kindly offered these insights.

From my reading of the draft ROSE report, it can be seen that CAMD has more users who are interested in hard X rays than in spectroscopy and VUV/soft x-ray science. The industrial users/connections are almost exclusively in hard X rays (PX, catalysis, materials, LIGA). Nevertheless, there are some very good spectroscopy groups at CAMD. At present, scientists at CAMD are not very interested in time-resolved studies. On the other hand, CAMD's educational capabilities and student training are very important characteristics for CAMD.

Taking these various aspects into account, this clearly points to a multi-user, ring-like source; whether this will be a storage ring or an ERL depends on the time scale of the funding. The ERL offers a substantial increase in brightness of the beam and short pulse characteristics, while the ultimate average beam current achievable in such a source is still an issue. On the other hand, it is definitely a multi-user facility with a very broad spectral range, just as are today's storage rings.

ERLs require some additional developments on the machine side, mainly a high-current gun and development of concepts concerning the stability and timing issues associated with the energy recovery process. In about five years, these issues will probably be solved, and it would be possible to build an ERL source.

There is a strong analogy in looking at the situation at CAMD and comparing it with the user community in Sweden. There, they have some very strong spectroscopy groups (Uppsala, Gothenburg), while the industrial users are mostly interested in PX, catalysis, and materials science. Accordingly, the MAX-IV proposal is for a double-ring source, 1.5 and 3 GeV, on top of each other within the same building and tunnel. Injection would be done with a full energy Linac.

The MAX-IV concept is quite cost effective because it puts two rings into the same building. There is space for about eight IDs in each one of the rings, which is ample, considering the size and scope of the user community in Sweden/Scandinavia.

Putting these thoughts together, we should consider a 3-GeV Linac with the double-ring source as an interesting future perspective for CAMD. The Linac would enable full energy injection—a must for any high-brilliance source—and top-off capabilities for both rings. For users interested in high-brightness applications, this could be set up in such a way that one or maybe even both rings can also be operated as an ERL, if not only an injection line but also a beam return line is constructed for each ring. Then at least three quarters of each of the beamlines would be usable in the ERL mode. At a small extra cost, this would allow for two alternate modes, a high-average brightness mode as a storage ring in top-off operation and a high-peak brightness mode as an ERL.

To my knowledge, such a scheme has not yet been proposed, but no show stoppers are foreseen. Even if the above-mentioned development efforts take longer than expected, it will be possible to run the ERL at lower average beam current with today's available technology.

As the ROSE report clearly states, the user community needs to be continuously developed to take full advantage of a new state of the art source.

- A. Continual interaction with the CAMD User community is essential to help CAMD staff work through the complex multidimensional space to arrive at the parameters of the next source to serve the south.
- B. Realistically, it takes about three years to design, build, and commission a state of the art insertion device and beamline. Given this timeframe and the resources required, whatever is constructed for CAMD now should actually be designed with the concept to transfer the equipment to the new source.
- C. Beamlines and endstations are getting more and more sophisticated --- ***there has to be adequate technical support for the users***. University professors with their graduate students can and should define the specifications required on the basis of the scientific program, the technical solutions, on the other hand, should be provided by the (permanent) staff of the facility.
- D. Microscopy is missing at CAMD. This is a very important aspect of high brightness sources and should be developed. Microfocus applications (tomography) have been developed and will definitely benefit from a brighter hard X-ray source.
- E. Protein crystallography and the life sciences program seems to be quite strong in comparison. A proposed crystal change robot would be a key addition for improving this facility. Successful experiments require literally hundreds of crystals to be characterized quickly in order to find the ones that give the best overall diffraction pattern. Often these are not the obvious choices by visual inspection.
- F. A state of the art ARPES photoemission setup is essential for the solid state physics – advanced materials efforts. This would be a SCIENTA R4000 with a helium cooled manipulator and an appropriate beamline delivering photon energies up to 100 eV with meV resolution and high flux.
- G. Full energy injection would help in many ways. The stability and reliability of the machine would improve greatly; top up injection would be possible, and this addition also would enable the installation of superbends.
- H. As the new source is being planned and later built, ***staffing and other resources will have to be increased substantially***. The exact levels are strongly dependent on the number of experimental stations to be operated by the facility. ***Every facility also needs an adequate capital fund to perform necessary upgrades and improvements at a steady, reliable, and consistent level***. In principle such funds have to be available at the director’s discretion to be used in conjunction with proposals for other external funding.
- I. Once the new source is being built, ***staffing and other resources have to be increased substantially***. The exact levels are strongly dependent on the number of experimental stations to be operated by the facility. ***A facility also needs a capital fund to perform necessary upgrades and improvements at a steady, reliable, and consistent level***. In principle, such funds have to be available at the Director’s discretion to be used in conjunction with proposals for other external funding.

Such a source would have a price tag on the order of \$500M.

The justifications of sources of greater brightness and intensity have been well documented in a series of workshops and websites. Representative ones can be found at the sites listed in the following paragraph and at the sites:

<http://www.science.doe.gov/bes/besac/Hemminger-02-2008.pdf>

<http://www.bnl.gov/nsls2/sciOps/LifeSci/default.asp>

<http://www.4gls.ac.uk/>

<http://cat.inist.fr/?aModele=afficheN&cpsidt=17833628>

<http://meetings.aps.org/Meeting/MAR08/Event/80418>

Worldwide there is a great interest in these advanced sources because of their high coherence and short pulse length. In fact, at least five different facilities in the United States are exploring the possibilities for different fourth generation sources. These sources have been described in various workshops and are based on a seeded-laser superconducting LINAC-undulator combination (proposed by the SRC (<http://www.wifel.wisc.edu/>) and the ALS (<http://www-als.lbl.gov/als/usermtg/talks2008/chu.pdf>)), and energy recovery LINAC's (ERL's) proposed by Cornell University, <http://erl.chess.cornell.edu/>, and by Florida State University, <http://www.magnet.fsu.edu/usershub/scientificdivisions/emr/facilities/fel.html> and as an upgrade at the APS. An operational THz ERL source is located at Jefferson National Laboratory (JLab, <http://www.jlab.org/fel/>) and an x-ray FEL (the LCLS, <http://www-ssrl.slac.stanford.edu/lcls/>) is under construction at Stanford University and will be operational in 2009. Therefore, CAMD is in good company as scientists ponder its future amid the diverse array of current possibilities.

It is clear that the future development of CAMD must be the subject of a parade of workshops that involve the user community, the LSU administration, and regional universities alike to chart the course of action.

The discussion in the following subsections provides some ideas from the most recent workshop that outlines topics for consideration to develop a fourth generation source that can provide the ultimate in radiation to probe the science contained the "Grand Challenges." In Section V.d. the impact of the source and facility on work force development is described. In this section a strong argument is made that a "next" generation light source should be sited at a university based rather than a national laboratory, because universities are key players in the drive to achieve the national mandate (The America COMPETES Act of 2007) to train new scientists to ensure that the United States is competitive in the 21<sup>st</sup> century.

**App.C.2.c. Defining the Road toward the Development of the "Light Source of the Future": A report by the Source Breakout Group attending the workshop, Enabling Grand Challenge Science: The Light Source of the Future.** (M. Borland, J. Corbett, R. Falcone, G. Kraft, J. Lewellen, C. Steier, and V. Suller)

#### **App.C.2.c.1. Overview**

A clear theme emerging from discussions relating to Grand Challenge Science is the desire to develop an understanding of materials at a length scale of 1-100 nm, energy scales of 1-100 meV, and for processes with time scale of 1-1000 femtoseconds. This understanding will ultimately enable the creation of new materials with tailored properties for new technology applications. The report from this breakout group was presented in its entirety in Section V.C.

### **App.C.2.d. Consideration of Advanced Light Sources to Enable Grand Challenge Science**

The following paragraphs contain a portion of a report from break-out sessions dealing with several of the grand challenges (GC) and the advanced sources that would provide a significant impact on these GCs

#### **App.C.2.d.1. Control of Electrons in Atoms, Molecules and Materials: Creating a New Language for the Behavior of Electrons—*The Challenge of Manipulating and Controlling Material at the Quantum Level.***

(GC)—“Nanoparticles, Dynamics, Complexity, Materials in Extreme Environments,” at the LSU 2008 Workshop. This break-out session suggests the defining science and provides a description of a fourth-generation source that could be used to investigate the science. This portion of the report is submitted by Gwyn Williams. Participants were John Scott, Williams, Gary Findley, Ramu Ramachandran, Alina Gearba, and Sumita Roy.

Individuals were asked to write up their own interests as they related to GC No. 1

**Summary:** The meeting focused on atomic, molecular, and optical (AMO) science, with just a couple of other interests, namely self-assembly of nanowires and dynamics of biological systems. It was hard to distinguish the interests of this group from that of GC–No. 5 “Beyond Equilibrium.” Williams suggested that people take the time to read the Grand Challenges and the other reports, such as 4GLS and STARS, and map their own interests onto those.

However, a very rich list of ideas and interests were presented, highly relevant to the grand challenges and to the tools needed to study them. Williams summarized this list, but was not sure at this point how the participants wanted to unify the separate reports into the document.

Interests are in energetics of simple systems such as critical point fluctuations on the free electron energy in rare gases; dynamics of bio-molecules driven specifically out of equilibrium by synchronously produced multiphoton pulses, including THz; bond selective chemistry; quantum trapping; dynamics of molecular Rydberg states; reaction intermediates; coherent control; Born-Oppenheimer breakdown; discovering the magic functional that would relate electron density to ground state molecular properties; electron density in correlated systems using time-of-flight techniques; reactions at interfaces; and the transport of molecular species across interfaces.

Some of the topics discussed included determination of intermolecular attraction potential parameters; exploring efficient coherent excitation techniques to control population transfer between specific atomic or molecular states, including heterogeneous molecules in magneto-optical traps; and studies of an organisms’ ability to remediate toxic metals by changing a hazardous oxidation state to a benign state, including dynamics and microscopy of living cells.

**App.C.2.d.1.i. Energetics of Simple Systems Under Extreme Conditions—*The Energy of the Free Electron in Critical Point Rare Gases.* Gary Findley, Professor of Physical Chemistry, University of Louisiana at Monroe.**



To study the effects of critical point fluctuations on the free electron energy in these systems will require ultrafast pulses to inject electrons at specific energies. We should not try to do everything with one source. In a climate where DOE and NSF are cash-strapped and other fourth generation proposals worldwide are under pressure, we need to be very distinctive.

There are many third-generation light sources either extant or coming on-line, each with research programs pushing current crystallography techniques. There may even be an oversupply of such beamlines soon. We should not try to compete. “Standard” measurements such as protein crystallography, high-resolution imaging (nanostructures), and their near-future developments should therefore be excluded from this discussion. In addition, third-generation sources can probably push down beam sizes for spatially resolved ARPES. Again, we should probably not try to compete.

My view is that the Grand Challenges that we can address with a new light source involve fast processes in materials, chemistry, biology, and artificial materials that mimic biological systems (e.g., new types of solar cells and materials for extreme environments).

This implies femtosecond time resolution and multicolor/pump-probe. The probes should be soft X rays for time-resolved core spectroscopy, ARPES and imaging, and hard X rays for transient structural work (melting, compression waves, spalling, deposition, ultrafast evaporation, optically induced phase transitions).

Biological processes and chemical reactions will need to be initiated by visible or ultraviolet photons (or by “instant heat,” i.e., THz). The femtosecond time resolution *requires* that the initiating photons are produced by the same bunch that drives the x-ray source; electronic timing (i.e., synchronizing an external bench-top laser with the accelerator source) is limited to a jitter of around 1 ps. The latter is two orders of magnitude longer than the phenomena to be probed

**App.C.2.d.1.ii. Ramu Ramachandran, Hazel Stewart Garner Professor of Chemistry, Associate Dean for Research & Graduate Studies, College of Engineering and Science, Louisiana Tech University, Ruston, LA.**

***Bond Selective Chemistry.*** There is a long history of bond selective chemistry. My Ph.D. dissertation (1987) started out with a discussion of this tantalizing possibility, but I came to the conclusion that intramolecular vibrational energy redistribution (IVR) is too fast in almost all “real” molecules. However, Eric Heller (Harvard, then at the University of Washington, Seattle) and Kenneth Kay and I (from Kansas State) came to the same conclusion—if we could prepare molecules in initial states where most of the energy was concentrated in a single mode, the energy could stay trapped in such modes for many vibrational periods. Ken called it “quantum trapping.” Of course, back then, there was almost no chance of preparing such an initial state. Perhaps the next-generation light sources could.

***Probing Molecul.ar Rydberg States and Watching the Collisional Energy Transfer Process.*** I think Gary Findley is on to something here, and he should be encouraged to expand on this.

***Attosecond Pulses.*** This, of course, leads to interesting possibilities including “watching” reactive intermediates as they form and disintegrate, even in cases where transition-state theory fails. An even more intriguing possibility is that “new” superpositions of atomic and molecular initial states (e.g.,

wave packets on Born-Oppenheimer surfaces) can be realized, which would then evolve by coherent “control” to yield interesting possibilities. Paul Brumer’s theoretical work from the 90s is of great relevance here although Rabitz’s optimal control ideas (shaping laser pulses through feedback loops) may be more fashionable in the U.S. (but, in my opinion, less practical).

***Mapping Molecular Electron Density.*** This goes under the “fantasy” category. Most density functional theorists (including Walter Kohn, who was on the BESAC Committee) know that the greatest challenge facing the field right now is “discovering” the magic functional that would relate electron density to ground state molecular properties. Because we have no idea what form that functional would take, various workers have taken various approaches, starting with Fermi’s idea of the uniform electron gas and adding various levels of sophistication. Perhaps John Perdew (Tulane) has the most systematic approach, but at the end of the day, all the functionals currently in use are simply educated guesses. Is it possible to map the electron density of a molecule as a function of the three spatial coordinates using an ultrafast probe? Wow! That would really be something and could lead to the formulation of much better density functional theory (DFT) functionals than we have now

Stepping outside my field of research, experimental data that can help us develop better many-body potentials for liquids will be extremely useful. Some of my colleagues at Louisiana Tech are especially interested in the concentration of ions at the interface, the reactions that occur at interfaces, and the transport of molecular species across interfaces. It is reasonable to expect large molecules, including bio-molecules, to take on different conformations at interfaces compared with the bulk. What can ultrafast, ultraintense probes do to study such processes/species? The highly collimated beam (you want to probe just a few nanometers) would ideally also be intense enough to yield good signal-to-noise ratio.

**App.C.2.d.1.iii. Alina Gearba, Ph.D., Assistant Professor of Physics, Department of Physics and Astronomy, University of Southern Mississippi (USM), 118 College Drive #5046, Hattiesburg, MS.**

My research area lies in the field of controlling atoms and molecules with laser light. At the USM, I have built, from the ground up, a magneto-optical trap for cooling and trapping rubidium atoms. In the near future, I plan to add cesium atoms to the same trap and create ultracold heteronuclear molecules through photoassociation in the dual-species magneto-optical trap. Such heteronuclear ultracold molecules have permanent electric dipole moments and thus could be controlled by electric fields. Another research project than I plan to pursue in the future involves trapping radioactive isotopes of cesium to monitor long-lived nuclear waste. The research project that is probably the most in line with the DOE objectives involves exploring efficient coherent excitation techniques to control population transfer between specific atomic or molecular states. Efficient preparation of an atomic or molecular system on a desired state is important for advances in quantum information, atom optics, laser-assisted chemistry, creation of quantum degenerate molecules, and solid state physics.

**App.C.2.d.1.iv. John Scott, Scientific Director, CAMD/LSU**  
Intermolecular attraction potential parameters have been determined by measuring the effects of pressure of gas solvents on molecular Rydberg transition absorption bands (pressure shift and band-shape changes). Femtosecond pulses of THz radiation could, perhaps, be used to test my

model used for calculations of the potential-well shape and equilibrium of a system when the absorber is in an excited Rydberg state.

A number of CAMD users are doing biological and environmental experiments. Some of the studies deal with an organism's ability to remediate toxic metals by changing a hazardous oxidation state to a benign state. These studies involve XANES. I cannot speak for these users, but some may wish to undertake a study of the mechanism of the oxidation or reduction of metals in the plant's cells. Short pulses of THz radiation might prove to be a useful tool for following such a reaction, *in vivo*. If it is possible to couple the source of this radiation with an IR microscope, equipped with an appropriate detector, single cells could be examined, if necessary. Perhaps the mechanisms can be elucidated at much longer times.

The self-assembly of nanowires on substrates might be better understood, and perhaps, control of the growth could be made possible if fast-time dependence were made possible by short pulses of radiation. I am not certain about the spectral range that would be best—i.e., the study of electronic phenomena in the VUV or study of weak bonding in the THz region.

**Parameters Driving the Source.** We assume that a peak power of 1 GW is required, which is  $100 \mu\text{J}$  in 100 fs. This is  $6.25 \times 10^{12}$  photons per pulse at 100 eV and would require a peak current of 121 A. At 10 eV and 1 keV, the numbers are  $6.25 \times 10^{13}$ ,  $6.25 \times 10^{11}$  photons per pulse and peak currents of 381 and 38 A, respectively. The peak electric fields then, assuming a focus of  $4 \times \lambda^2$ , are  $2.2 \times 10^{16}$  V/m at 1 keV to  $2.2 \times 10^{14}$  V/m at 10 eV. In the machine design which follows, we design for higher peak currents for the contingency.

**The Machine (Fig. 3).** We are proposing a green-field staged approach in which techniques and technologies of ultrafast optics and harmonic generation are first developed using table-top lasers. In parallel, a superconducting Linac of 1 GeV will be designed, together with a multiundulator farm and an injection capability into a storage ring with an energy recovery path. The 1-GeV injector will be designed for later upgrade to a 3-GeV injector. The facility will incorporate synchronized multiphoton capability and will initially cover the range from 0.1 THz in the far infrared to 1 keV in the

soft x-ray region. Later, at higher energies, x-ray photons to 12 keV will be produced. The repetition rate is envisioned to be in the 100-MHz range. The normalized electron beam emittance will be less than a micron, the charge per bunch 200 pC, and the bunch length 100 fs. Multiphoton capability will be available from seeded, sequential undulators and from spontaneous emission.

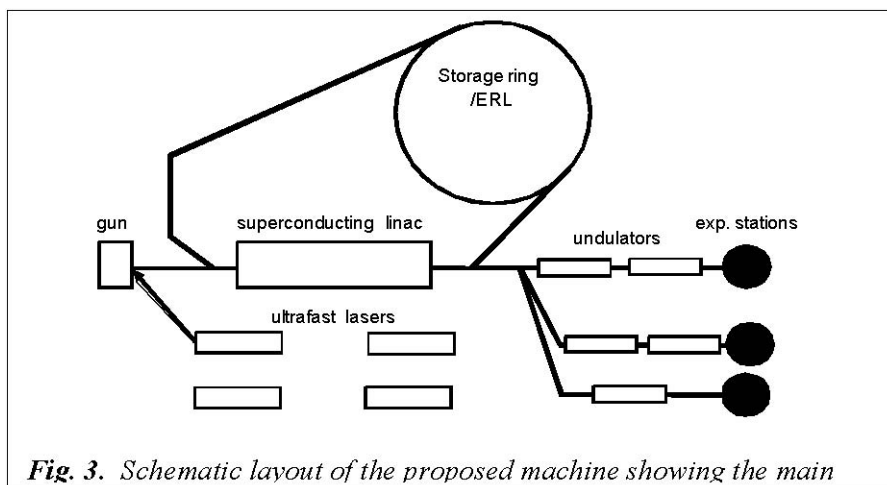


**Fig. 3.** Schematic layout of the proposed machine showing the main

The cost of such a layout would be over \$500M, depending on the energy of the Linac and the number of laser-seeded undulators. High brightness, coherence, and 100-fs pulses over a broad spectral range would be its output as shown in Figure 4.

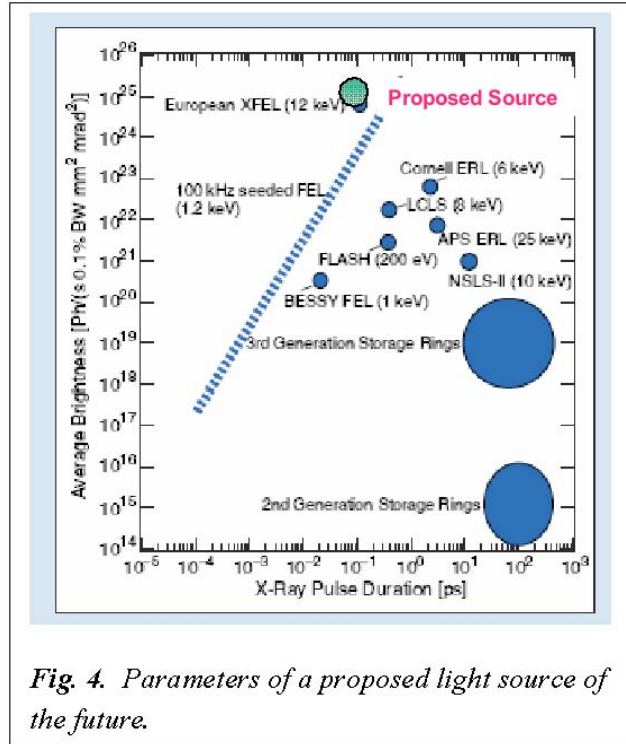


*Fig. 4. Parameters of a proposed light source of the future.*

### **App.C.2.d.2. Matter Far from Equilibrium**

This portion of the report was submitted by Gopal Shenoy. Participants in attendance were Lin Chen (Argonne National Laboratory and Northwestern University), David Fritz (Stanford Linear Accelerator Center), and Gopal Shenoy (Argonne National Laboratory).

#### **App.C.2.d.2.i. Background**

Every living system in nature performs its functions when it is driven to conditions that are far from equilibrium. Extreme length and time scales are characteristic of this behavior and complexity of matter around us, from subatomic sizes up to macroscopic measures, from electronic reaction times in the femtosecond range up to geological periods. Basic physics principles governing systems far from equilibrium stand in close interaction with the neighboring disciplines of chemistry and biology as well as the geosciences and medicine and affect wide fields of the engineering sciences. Research that we will briefly address in this section is strategically interwoven with other sections in this proposal and explores the frontiers of science that are relevant to the critical national and global issues on energy, environment, and life itself.

The scientific interest in understanding the far-from-equilibrium behavior is entering a new era. Powerful experimental tools combined with extraordinary progress in theory, simulations, and computing power have paved new roads that will successfully answer central questions: What are the principles that determine far-from-equilibrium behavior that govern natural processes around us, such as the flow of energy and its efficient conversion from one form to the other? How does the complexity of matter develop in time and space leading to its unique electronic, magnetic, and mechanical properties far from equilibrium? How does matter develop and organize itself in the far-from-equilibrium state during its formation, leading to structures with perfect to chaotic orders? How do we describe multiscale processes in systems with disorder leading to unusual emergent properties? How do we understand materials with hierarchical internal structures like complex fluids and their flow through confined space? What are the universal principles of pattern formation, development, and self-organization in nature and how can they be exploited in future technologies? Answers to these questions will lay the foundation for the far-from-equilibrium processes that determine the novel functions of every material around us. The advancement of appropriate experimental methods—extending from synchrotron radiation, the main focus of this proposal, along with neutron scattering to new sub-Ångstrom transmission electron microscopy and from thin-film techniques to nanostructuring by self-assembly and single-atom manipulation, chemical dynamics to nanofluidics, combined with theoretical concepts—is a generic mission for the participating centers in this proposal. While forging ahead, mastering the behavior of materials in equilibrium with increasing degrees of complexity, our current knowledge has prepared the ground for the field of far-from-equilibrium science central to the focus of this proposal.

#### **App.C.2.d.2.ii. Major Themes**

##### **App.C.2.d.2.ii(a). Understanding the Energy/Electron Flow in Hybrid Materials and Molecular Assemblies**

Energy and electron transfer processes are the most basic reactions in chemistry and control the existence of life on Earth through the photosynthetic conversion of solar energy to chemical or

electrical energy. Efficient light harvesting and charge carrier generation are crucial in developing efficient solar energy conversion using photovoltaic devices and are an important component of the portfolio on renewable energy resources. During the past decade, much attention has been given to dye-sensitized solar cell (DSSC) development which is based on photoinduced electron injection from an excited state molecule to the conduction band of a nanocrystalline metal oxide electrode. In these devices, the interfacial electron transfer processes govern the efficiency of light to electricity conversion. Any progress in this energy conversion technology requires that the most fundamental question be answered: How do the nonequilibrium chemical processes in a cell evolve in time and space following the light excitation? The answer requires (1) measurements of femtosecond electron transfer dynamics between anchored dyes and semiconductor nanostructures, (2) details on concurrent chemical rearrangement of excited state molecule and ensuing structural rearrangement of nanostructure surfaces, and (3) theoretical simulations of the process using next-generation computational tools.

Prototypical candidates for these studies of a photovoltaic cell will include a dye sensitizer containing 3d-or 4d-atoms and nanocrystalline TiO<sub>2</sub> or SnO<sub>2</sub> electrodes. A fourth-generation light source such as an FEL will allow one to perform surface scattering and XANES studies in the time domain with femtosecond resolution required to understand the surface restructuring as well as the electron flow in this ultrafast nonequilibrium processes. It would also be possible to model the measured properties of nanoscale cell systems using a variety of computational strategies. For example, a combination of codes and techniques such as time-dependent DFT (TDDFT), Car–Parrinello molecular dynamics simulations, continuum solvation models, etc., would be considered. Armed with this fundamental knowledge, it would be possible to make progress in optimal design of photovoltaic cells of the future.

While we have only addressed above the most relevant problem in the development of alternative energy technology, the tools are broadly applicable to the vast area of femtochemistry.

#### **App.C.2.d.2.ii(b). Nonequilibrium Processes in Photocatalysis**

Photocatalysis is one of the important ways of generating solar fuels (H<sub>2</sub>, etc.) as well as for removing organic and inorganic pollutants in water. Instead of lowering the activation energy in a reaction as normal catalysts do, photons provide extra energy above the activation energy barrier for the reactant to continue the reaction course to the final product. The photoactivation process driving the catalyst to its nonequilibrium state will have energy higher than required to achieve the activation from the reactant to the intermediate in the reaction path. At the crossing of the activation barrier is the so-called transition state whose structure has been elusive to direct structural measurements, but is only modeled by theoretical calculations, largely because of its ultrashort lifetime in the femtosecond timescale. Having femtosecond time resolution from a fourth-generation source light such as an FEL combined with laser excitation, we would be able to launch a photocatalytic reaction simultaneously among molecules and to capture their barrier crossing act to determine the transition-state structure via x-ray diffuse scattering in solution or from soft x-ray absorption. As we gain the knowledge of the transition-state electronic and geometric structures, we can predict the outcome of the catalytic reactions and design the reaction with a proper combination of the catalysts and reactions to achieve high-efficiency conversion from reactants to products.

### **App.C.2.d.2.ii(c). Micro-and Nano-Fluidics**

Flowing fluids present the most common phenomena in nature as well in technology applications. However, little attention has been paid to the actual transport of fluids in these confined geometries, even though the fluid flow on increasingly smaller scales is critical to so many natural and man-made processes. This includes the design of miniaturized mechanical structures and complex micro-machines through which fluids move to the flow of fluids in the human body to flows through gasoline injectors in combustion engines. Most of the examples represent flow through confined structures represented by the field of micro-and nano-fluidics. These flows that are in a far-from-their-equilibrium state are often turbulent. They develop eddies and form unique patterns such as dendritic structures from tiny fluctuations in their surroundings, and their subsequent development is also controlled sensitively by the fluctuations and the interactions with the atomic variability in the surfaces forming the confined structures.

Measurements of the dynamic processes in confined flows with both nanoscopic-and molecular-resolution and associated hydrodynamic time scales require new approaches and new tools. Hence, the biggest challenges to condensed matter and materials physics in the next decade are to develop novel experimental techniques as well as theories and numerical methods devised to properly describe the confined fluid flow on length scales in the range from 10 to 1000 nm and hydrodynamic time scales from femtoseconds to microseconds. Both the spatial coherence and temporal femtosecond resolution of fourth-generation light sources such as an FEL will be a major key in addressing challenging questions in this field.

### **App.C.2.d.2.ii(d). Extreme Transformational Dynamics of Matter**

There are many mysteries that remain regarding the understanding of the first instances of the transformation of matter. The availability of modern lasers delivering femtosecond pulses allows energy deposition into a material faster than needed for the system to react, leading to confinement of important quantities of energy. This pushes the matter into an extreme state that is far away from equilibrium. Ensuing state and extreme transformational dynamics in the material are determined by the deposited energy, depth of pulse-penetration, the length of the energy pulse, the material's composition, and its electronic, spin, phonon, and diffusion properties. An optical laser pulse, for example, may melt the surface of the material, show phase transformation (such as from an insulating to a conducting state or from a paraelectric to ferroelectric state), initiate material ejection leading to ablation products, or even form a plasma (if the deposited energy exceeds  $\sim 10^{13} \text{ W/cm}^2$ ). For example, photomechanical fragmentation will produce clusters as a result of the mechanical stress imposed by the very rapid thermal expansion of the surface, followed by homogeneous nucleation and vaporization. What microscopic and/or nanoscopic properties govern the nucleation process? Can we control how/when/if nucleation occurs? Understanding the pathways in the extreme transformational dynamics following the formation of the far-from-equilibrium state is the key for the materials control required in the next generation of technologies. A fourth-generation light source that has the capability to map the transformational processes in matter (order/disorder, solid/liquid, liquid/gas, electronic transformations, etc.) with both the relevant spatial and temporal resolution will revolutionize our understanding of these processes.

While we have emphasized the ultrashort laser pulses to drive the system far from equilibrium, there are equally optimal sources that will interact in different ways with matter. For example, one may conceivably use shock waves, FEL pulses from a fourth-generation source (in a two-color or a two-undulator source experiment), or relativistic electron bunches from an accelerator that can generate large electric and magnetic pulse fields with picosecond to femtosecond width. In this last example, a femtosecond magnetic field pulse can interact in a nonlinear fashion with the spins in a confined system (e.g., a nanodot matrix). The relaxation of spins in this chaotic spin system cannot be described by the traditional Landau-Lifshitz-Ginsburg equation. It is our conjecture that a nonuniform distribution of spontaneously self-organized spin regions (so-called dissipative structures in nonequilibrium thermodynamics with nanodimensions) which will vary in time or space (or both) will develop. A relativistic electron beam used in an FEL could be used as a pump to investigate this far-from-equilibrium magnetic phenomenon using holographic imaging of the time development of the spin and spatial structures. Control of the electronic and magnetic behavior of materials has been critical to the technological advancement, and the new class of magnetic excitation experiments should lead the way.

The thermodynamic pathways through the extreme transformational dynamics must also be investigated using modern tools of computational science. This can be accomplished using a combined molecular-dynamics and Monte Carlo approach to describe atom and carrier dynamics, respectively, and investigating the thermodynamic evolution of the system during heating, expansion, and cooling.



### App.C.2.d.3. Emergence, Complex Phenomena, and Strongly Correlated Multiparticle Systems

#### App.C.2.d.3.i. Discipline Defining Science

The discussion of this particular breakout session focused on the application of a fourth-generation light source to probe the exotic many-body behavior of materials where there is a strong coupling and competition between differing ground states (complex charge and orbital order, magnetic local or itinerant order, superconducting, or structurally competing ground states). Based on these discussions, there was a strong agreement that a major key requisite to understanding and predicting the novel properties of highly correlated materials is the ability to spatially resolve key dynamics. To do this, the following experimental parameters are needed:

- A. Relevant length scale: few nanometers to micron scale
- B. Time scale: for electronic relaxations, femtosecond time resolution is needed
- C. Energy scales: the excitations and fluctuations are of the order of meV.

Much of the discussions followed from the material presented in talks during the previous days, including but not limited to: Matthew Fisher's "Emergent Phenomena in Strongly Correlated Electron Materials," which gave an overview of the exotic many-body behavior of materials where there is a strong coupling and competition between differing ground states (complex charge and orbital order, magnetic local or itinerant order, superconducting, or structurally competing ground states); Tai Chiang's "Advances in Photoemission at a Next-Generation Light Source," which presented an overview at the forefront of light source measurement capabilities (3d-nano-ARPES, ultrahigh energy resolution, ultrafast dynamics at the nanoscale and pump-probe techniques) that will be possible with a combination of state-of-the-art electron analyzers and ultrafast/coherent/ultra-intense, low-energy (<900) light from a FEL; and Greg Boebinger's "Unrealized Opportunities for Increased Scientific Impact of High Magnetic Field Research," which outlined a broad scientific case for a THz-IR FEL at the NHMFL.

This group made specific recommendations centered around differing topics:

- A. **Pioneering Experiments Made Possible:** To probe fluctuations, both thermal and quantum (ns to ps), an ultrafast source with extraordinary high energy and spatial resolution is required. For example, exploration of correlation lengths in real space requires the control of pump and probe timing as well as the spatial separation which can only be made possible by a fourth-generation light source.
- B. **On-Site Sample Fabrication:** New capabilities to probe matter require the ability to perform in-situ growth of complex materials within a beam line end station. The desire to judiciously nanoengineer and subsequently probe materials with a particular dopant distribution would open new frontiers both in fundamental science and future technology design. The materials will be fabricated by molecular beam epitaxy (MBE), pulsed-laser deposition (PLD), and/or combinatorial growth capabilities directly within the fourth-generation experimental hall.
- C. **Sample Environments:** To explore the unique properties that strong electron correlations impart on materials, the materials must be studied under extreme environments (e.g., high magnetic fields). For example, a high magnetic field induces

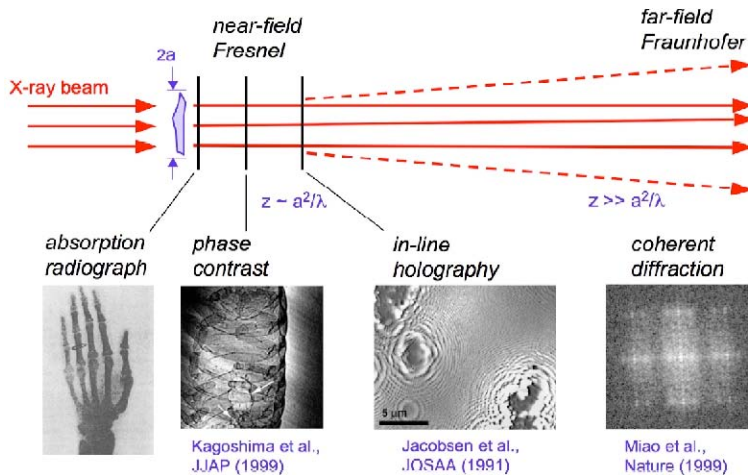
energy level splittings that can be probed with THz spectroscopy. This includes resonant, Raman, and/or pump-probe techniques.

- D. Source Requirements:** A vital interest in studying the next generation of materials is in multicolor pump-probe experiments (UV and soft X rays). To enable this type of multicolor experimental geometry in a given end station, an FEL source geometry similar to the proposed 4GLS may be needed. In this design, IR to soft X rays with precise predetermined timing can be used in a pump-probe arrangement to facilitate time and spatial interrogation of complex phase transitions. In addition to the area of correlated materials, this type of femtosecond-resolved, two-color pump probe would enable investigations of key photochemical and/or catalytic reactions at surfaces and environmentally important systems. We envision that the density of data will be sufficient to produce video-quality images of electron transfer at the atomic scale in such reactions.
- E. Current Capabilities and their Relation to the Proposed Work:** Current advances in both neutron spectroscopy and scanning probe microscopy/spectroscopy have already greatly enhanced our understanding of a variety of strongly correlated materials such as unconventional superconducting transition-metal oxides. However, there are distinct opportunities, as well as a great deal of complementarities, that a fourth-generation light source can offer. For example, although sub-nanometer scanning tunneling spectroscopy/microscopy (STS/STM) images reveal rich information about thermal fluctuations in complex materials, it is as yet unknown whether the domain formations are dictated by inhomogeneities (dopant spatial distribution) or a more interesting competition between ground states and the quantum fluctuations that result. The spatial and spectroscopic resolution that a fourth-generation light source would provide, for example, to perform nano-3dARPES (TOF design triggered from VUV-FEL), would allow investigations of the correlation of sample inhomogeneities (spatial-dependent dopant concentration profiles) and local, nanoscale, ground state fluctuations. Such an ultrafast light source allows exploration of these fluctuations—thermal or quantum in the nanosecond to picosecond time domain. As a final example, understanding the evolution of quantum liquids with disorder or charge carrier addition could be probed with the spatial and temporal resolution of a fourth-generation source.

**App.C.2.d.4. The Scientific Case for Implementing Tomography at a Third/Fourth-Generation Light Source.** Submitted by Les Butler ([lbutler@lsu.edu](mailto:lbutler@lsu.edu)) and Kyungmin Ham ([kham1@lsu.edu](mailto:kham1@lsu.edu))

In the soft x-ray, fast-pulse regime, biological cells can be imaged in 3D using tomographic methods. These rely on the particular characteristics of photons in the “water window” (~500 eV). In this region, water is an order of magnitude more transmissive than the molecules found in biological materials, such as membranes, proteins, DNA, etc. For example, solvent-filled vacuoles absorb minimally, compared with dense lipid droplets or regions of membrane. Because photons in the water window are not particularly damaging to biological cells (at LN<sub>2</sub>), it is possible to acquire tomographic images at ~40 nm, a resolution set by current-generation zone plate optical systems. Using future ERL type sources, together with the next generation of zone plates, it should be possible to image cells in 3D to a resolution of 10 to 15 nm. This level of information fits between high-resolution electron microscopy and lower resolution light-based techniques. Beside biological systems, there are polymer/composite and polymer/additive blends that will also benefit from nanometer-resolution imaging, especially for time-dependent processes in polymer blends. In a more speculative direction, an intense, coherent, soft x-ray pulsed source could provide a route to a novel atom-scale imaging method for insulating samples. Near-femtosecond pulses may allow coherent diffractive imaging of an insulator’s surface as successive layers are ablated with a pulsed optical laser. Coherent diffractive imaging of the ablation cloud could yield atom identification and original location, thus resulting in a 3D image of the original sample. Applications could range from cell membranes, catalysts, semiconductor semiconductor structures, etc.

Tomography is a well established, vibrant, and fastgrowing technique at synchrotrons and neutrons sources worldwide. At the ALS, single-cell imaging is providing new insights into cellular structure and metabolism. The future of tomography depends upon sources with high brilliance and unity coherence. Briefly, tomography operates in several regimes, as shown in Figure 5.



High-brilliance, unity coherence will greatly advance coherent diffraction imaging, yielding 3D tomography at nanometer resolution. The range of applications adapts to fourth-generation source parameters as:

**Fig. 5.** Different contrast regimes for x-ray imaging, depending on the propagation distance between sample and detector. The most current synchrotron tomography beamlines operate in the absorption regime, a few beamlines operate in the near-field Fresnel regime, a couple have the coherence needed for focusing optics (such as ALS single-cell imaging), and coherent diffraction imaging is still in the developmental stage. (Figure prepared by Qun Shen, APS.)

- A. **Soft X Rays (<1 keV):** Applications are to biological and polymer materials. For polymers, active tomography projects include polymer/composite and polymer/additive blends. In addition, the time-evolution of blends, both dissolution and precipitation processes depending upon thermodynamics, are observed.
- B. **Hard X Rays (to 40 keV):** As yet, K-edge-based coherent diffractive imaging has not yet been performed because of source limitations. This experiment would yield important elemental distribution in 3D in composite materials. Applications are then extended to geology, metal alloy structures, bone/metal implant structures, and other high-Z materials.
- C. **Pulsed X-Ray Source:** A multipulse x-ray and laser ablation system may allow a technique analogous to atom probe tomography (APT). APT is a near-ideal 3D imaging method for extremely small, needle-shaped, electrically conducting samples. Near-femtosecond, coherent X rays may allow extension of APT to larger, insulating samples by observing, with time-integrated coherent diffractive imaging, the optical ablation of an insulating surface. This could yield 3D atom identification and location, with applications ranging from cell membranes, catalysts, and semiconductor structures.

### **App.C.2.d.5. Nanoscale Science**

Nanoscale science has both the visual appeal that astronomy provides and holds the promise that the new properties in reduced dimensions can lead to new technologies that will fundamentally change humankind. Ultimately, if we can control synthesis and understand mechanisms such as those that enzymes or proteins use in synthesizing nanocrystals, we may develop new paradigms for creating matter. Furthermore, we can couple the techniques of self-assembly with directed nanoscale fabrication to understand the new physics and chemistry playing out in these materials.

#### **App.C.2.d.5.i. Discipline-Defining Science**

The consensus reached in this breakout session was that the application of VUV-soft X rays to understand the fundamentals of surface chemistry and biology occurring at the nanoscale was discipline defining. Key to the new applications of a next-generation light source was the ability to have small spot sizes to  $\sim 10$  nm to better define the probed structures, femtosecond timing for following chemical and biological dynamics, and coherence for new classes of measurements.

Key issues in understanding nanophase properties are the geometries of nanoclusters, within and *on* the surface, and how this gives rise to new electronic structural properties. These new electronic structures play a central role in determining the chemical reactivity and chemical dynamics occurring at the nanophase interfaces. The ability to focus allows one to study a single nanoparticle and overcome the long-standing problem of ensemble averaging. Many classes of problems could benefit from this, including atmospheric and environmental chemistry, and help us to understand the fundamentals of biological activities such as photosynthesis and charge transfer. This would also allow one to better understand the differing structures of nanoparticles produced in solution in terms of the reactions occurring on their surfaces. The ability to assess the uniformity of nanoscale properties was also seen to be important. The interaction of nanoparticles with biological molecules is an area that will show a significant boost in interest in the future.

In the time domain, the dynamics of cooperative effects including stochastic events or fluctuations in properties such as chemical, optical, magnetic, conductivity, or superconductivity could be addressed with a next-generation light source. Other key studies of chemical dynamics such as melting, dissolution, dynamics of nanocluster formation, and shell encapsulation would be enabled. Even the nature of water at interfaces could be probed to answer questions such as “What is the nature of water near the interface?” and “When does the picture of a liquid break down and become one of an amorphous solid?”

#### **Technical Specifications**

The key features of the next-generation light source include coherence/spatial focusing to  $\sim 10$  nm spot size that allows one to study individual nanoclusters without having to correct for ensemble averaging. This is currently not possible; for example, the STXM limit is  $\sim 15$  nm and TEM with aberration correction roasts samples. One concern is that when focused, one would prefer a high repetition rate to minimize specimen damage. Femtosecond timing will enable a new class of studies of dynamics, and it is likely that this will require additional regional expertise in laser science. Both pump-probe and photon-in photon-out were seen as playing a role, particularly as they enable a high magnetic field or high-pressure studies. Furthermore,

endstation instrumentation should include additional tools for materials characterization including STM, EELS, etc. The conclusion of this breakout group was that a source focused on coherence in the VUV/soft x-ray area, with fs timing structure was the most likely way to have a significant impact.

## App.C.2.e. Work Force Development Implicit with the Development of an Advanced Light Source

### App.C.2.e.1. General Remarks, Nora Berrah (Distinguished University Professor, Western Michigan University)

Sustained investment in scientific research ensures critical national needs such as energy, economic competitiveness, and security. The latter can be achieved by aggressively investing in the production of the future scientific workforce. Recent statistics from the American Institute of Physics Statistical Research Center [1] showed alarming ratios of physics degrees to all bachelor degrees granted in the U.S. The ratio peaked at about 1.45 in the early 1960s but was about 0.4 in 2007. The number of physics majors dipped to about 3800 in 1999 and is now about 5400—still a very low number nationally.

The America COMPETES Act of 2007, signed into law, includes strengthening research but also educational programs. It provides incentives to increase the number of majors and teachers in the STEM fields such as science, technology, engineering, and mathematics. Future light sources should be seen as an opportunity not only to train majors in physics, chemistry, biology, and engineering but also to produce the next generation of scientists that will push forward the frontiers of science.

The fourth-generation light source, with source properties unattainable as of today, will allow some of the recently proposed DOE BESAC scientific grand challenges to be pursued and could also enable much-needed growth in our national scientific workforce. The future light sources will have several specific needs in terms of a workforce that is educated with the skills needed to make it a success. First, there will be a need for both *hardware and instrument development scientists*. Currently, the funding and support mechanisms in the U. S. do not train a sufficient number of these scientists. The demand for trained technical staff is critical enough that new light sources, such as NSLS-2 or LCLS, recruit their needed technical staff from other light sources or accelerator facilities. In addition to the technical staff that directly supports the facility, there is a need to train, fund, and engage young researchers and junior faculty to become the next-generation light source scientists. Furthermore, training *theorists* and hiring them in academia and national laboratories are also important because in order to make significant scientific advances, experimentalists and theorists need to work together.

The DOE has been a steward of major light-source facilities with construction, maintenance, upgrade, and operational leadership provided to various national laboratories. In recent years, DOE has also assumed stewardship for the operation of the experimental stations and other subfacilities at various light sources. This has successfully supported numerous research experiments proposed by the users from academia, industry, and national laboratories producing short-term returns for the investments by the funding agencies. However, in this operational paradigm, because the operational leadership is with the national laboratories, the traditional partners in these facilities—namely the academia, industry, and other agencies—have often disengaged in contributing to the scientific vision, future plans, and innovative design for developing next-generation scientific programs. *The consequence of this new funding strategy has severely precluded the academic institutions from developing a trained workforce.* This, in

turn, limits the number of trained scientists with advanced science and technology skills that could play a significant role at major facilities such as a light source, essential for U.S. scientific and technological competitiveness in the 21<sup>st</sup> century.

The National Academy of Sciences Report in 2003 based on the *Pan-Organizational Summit on the U.S. Science and Engineering Workforce* addressed key issues on the science and engineering (S&E) workforce needs in the U.S. for the 21<sup>st</sup> century and suggested various approaches to this noble goal. The key questions are: How will we capitalize on the growing opportunities for S&E discoveries in the 21<sup>st</sup> century? And, how will we keep pace with the growing competition in these areas with other countries? The simple and only answer to these questions is to develop a highly trained S&E workforce with all the means that we have at our disposal. Unfortunately, it is generally difficult for national laboratories, which currently operate the major light sources, to easily establish a *dedicated effort* to deliver a pipeline of S&E workforce. In our vision of a next-generation light source, this will be the foremost and natural priority for a university consortium that will operate the facility. It will include enhancing the existing programs such as Research Experience for Teachers (RET), teacher workshops, Historically Black Colleges and Universities (HBCU), Partnership for Research and Education in Materials (PREM), and graduate training within the university consortium. The light sources of the future provide an additional important component—the ability for large groups of trained students, undergraduates, graduates, scientists, and engineers from diverse and merging areas (of accelerator physics and technology, materials sciences, life sciences, chemical sciences, medical sciences, earth and planetary sciences, energy and environmental sciences, computational and informational sciences, etc.) to be able to work together as a team—a necessary ingredient for successful workforce development for the future. New inventions and innovations in health, defense, security, and technology, as well as in other areas, will greatly benefit from a qualified workforce capable of working in large teams that can be educated and trained at a next-generation light source.

1. Kerry G. Johnson, American Institute of Physics Statistical Research Center, Capitol Hill Quarterly, February 2008, v3, No 1. [www.aps.org/publications/capitolhillquarterly/index.cfm](http://www.aps.org/publications/capitolhillquarterly/index.cfm).

#### **App.C.2.e.2. Staffing Challenges to Develop the Accelerator, V. Suller, (CAMD)**

The Fourth Generation light source of the future will provide source properties which are unattainable as of today. Development of the necessary technologies is underway at several centers worldwide, including the USA, but no one center can supply all the critical R&D needed to credibly propose construction of such an advanced source. This includes high brightness electron guns, superconducting accelerators, lasers, insertion devices, optics, and related technologies. The team assembled to construct the new light source will initially need to interact and collaborate with these centers, and then instigate well-funded development programs of its own in the most critical areas. Undoubtedly this process would provide technology transfer into, and build up expertise in, the new project. More generic accelerator systems will be less demanding but will nevertheless require highly competent technical staff with the necessary expertise. To move in this direction will require an overall project team which could be constituted from collaborators who could be seconded from US National Labs and perhaps also from overseas centers. Additionally it would include a core group employed by the new facility, which could initially be relatively inexperienced, but visionary. They would gain expertise by



being immersed in the build up phase of the project. Because what is envisioned is a national flagship facility, there should be little difficulty in recruiting top quality staff where needed. Students and postdocs will additionally be drawn to this important frontier work.

### **App.C.2.e.3. Workforce Development through an Existing LSU Program.**

One avenue toward the future development of a 4<sup>th</sup> generation light source would be by expanding Professor Ken Schafer's ultra-fast laser-based program and by hiring accelerator physicists to develop design concepts and costs of new light source schemes. These schemes should include incorporation or upgrades to CAMD with possible relocation. In parallel, under careful guidance by the new CAMD director, science programs at CAMD should be developed, but be well integrated with programs on campus. The programs at CAMD and in ultra-fast laser science, also need to involve as many campuses in the SE as possible.

**App.C.2.e.4. Workforce Development through a University-Federal and State Partnership,** Herman Winick (Stanford), John Sutherland (East Carolina University), Harald Ade (North Carolina State University), John DiTusa (LSU), and Les Butler.

A unique opportunity exists for Government agencies to interact with academic institutions and a whole region outside the traditional national laboratory structure.

The main contact points whose interdigitation has to be considered and defined are:

- A. Education
- B. Research
- C. People: Faculty (Post docs, students)
- D. Facilities (land, etc.)
- E. Operation
- F. Outreach

### **App.C.2.e.4.i. University Partnership:**

It is felt that solid commitments from many universities in the southeast region are needed for the development of advanced research facilities such as light sources to provide the strong intellectual horsepower to make the facility succeed. These commitments are to (a) teaching, (b) on-going research funding, and (c) initial construction.

Workforce development at the 4<sup>th</sup> generation source (4G), and the teaching capacity of the partnering universities should be tightly coupled. If there is a target of 1,000 users/yr, then many, many workshops and graduate courses are needed. The new high-speed internets through the southeast will allow workshops and graduate courses to reach many students; the 4G is seen as the coordinator of workshop and course offerings.

### **App.C.2.e.4.ii. Joint Faculty Appointments:**

Building upon the SSRL joint faculty appointment strategy, one envisions a policy of large scale joint faculty appointments across universities in the south. The driver for joint faculty

appointments is the predicted large teaching load associated with the 4G: workshops and graduate courses.

To implement such a program the following joint faculty appointment strategy is proposed:

- A. Joint faculty appointments, in pairs. That is, a university should split one position into two, with one person having majority appointment at the university (and tenure-track) and the other person sited at the 4G.
- B. The appointments are fixed term: reviewed by the 4G and the university.
- C. 4G courses and workshops are for both graduate, undergraduate.
- D. 4G courses are internet based (see David Attwood's (Berkeley) course on VUV spectroscopy that reaches students and faculty worldwide ([Synchrotron Radiation for Material Science Applications \(http://www.coe.berkeley.edu/AST/srms\)](http://www.coe.berkeley.edu/AST/srms))).

#### **App.C.2.e.4.i ii. Joint Research Funding Support Strategy:**

Beamline scientists, the facility, and faculty at the partnering universities will contribute to a yearly omnibus proposal. The proposal to be submitted for funding consideration by DOE. The DOE funds will be cost shared by the participating universities Offices of Research. In this arrangement the participating universities contribute operational facilities, and faculty positions.

#### **App.C.2.f. Conclusions**

By now the reader has tired eyes, but I hope not a numbed mind! This report has been assembled by the committee of dedicated scientists listed on the cover page of this report.

Of the 40 sources listed at [http://www-als.lbl.gov/als/synchrotron\\_sources.html](http://www-als.lbl.gov/als/synchrotron_sources.html) seven are in the US, seven more are under construction or just beginning operation. The field is intensely competitive and many programs are at the cutting edge of research. It is time for CAMD to continue to push ahead!

## Appendix D.

### Second Insertion Device



# PLANS FOR A 2<sup>ND</sup> INSERTION DEVICE IN CAMD

M Fedurin, P Jines, D Launey, T Miller, V Suller, Y Wang; CAMD, Baton Rouge LA 70806, USA.

## Abstract

To allow the possible installation of a 2<sup>nd</sup> Insertion Device in the CAMD Light Source, the lattice optic needs to be changed. The present configuration has a small vertical beta function in the long straight section containing the 7 Tesla wiggler. The new optic will give a small vertical beta at two long straight sections which are diametrically opposite. Test results with the new optic are presented together with the measured beam parameters. These data are used to predict the photon beam performance for an Insertion Device which could be installed.

## INTRODUCTION

The CAMD Light Source was originally intended as a Lithography facility for microstructures [1] but since coming into operation in 1992 its use for research has steadily broadened. At the present time 15 beamlines are in use for spectroscopy, spectro-microscopy, micro-tomography, molecular and crystal structure determination and for microfabrication. [2]

The source was conceived as a 2<sup>nd</sup> generation facility of moderate brightness using a 4 cell Chasman-Green lattice. The normal beam operating energy is 1.3 GeV. At the injection energy of 200 MeV the lattice is operated in a fully symmetric zero dispersion mode, which is also used during the energy ramp.

In 1998 a 3 pole wavelength shifter [3] was installed whose maximum field is 7 Tesla. This is used to provide hard X-rays for ultra-deep lithography, protein crystallography and other hard X-ray science. To increase the brightness, after the energy ramp is completed the optic is changed to one with finite dispersion in the long straights. This reduces the natural horizontal emittance by about a factor of 2 to 150 nm.rads. In addition the optic is configured to produce a small value of the vertical beta function at the center of the wiggler in order to increase the flux density of the source point. This is known as the minibeta optic.[4]

The wavelength shifter is located in one of the 4 long straights which each have a free length of about 2.5 m. One of these straights contains the injection septum magnet and another contains the single RF cavity. The remaining straight is not presently used. These features may be seen in fig 1 which is a diagram of the CAMD facility.

To enable the lattice to operate in the minibeta configuration, the F and D quadrupoles in the wavelength shifter straight are connected to independent power supplies. In addition these quadrupoles are adjusted to compensate for the focusing effects of the wavelength shifter and so maintain the beta values close to the optimum minibeta.

At the end of the energy ramp the settings for the minibeta are applied smoothly in synchronism as the wavelength shifter is energized without loss of beam current.

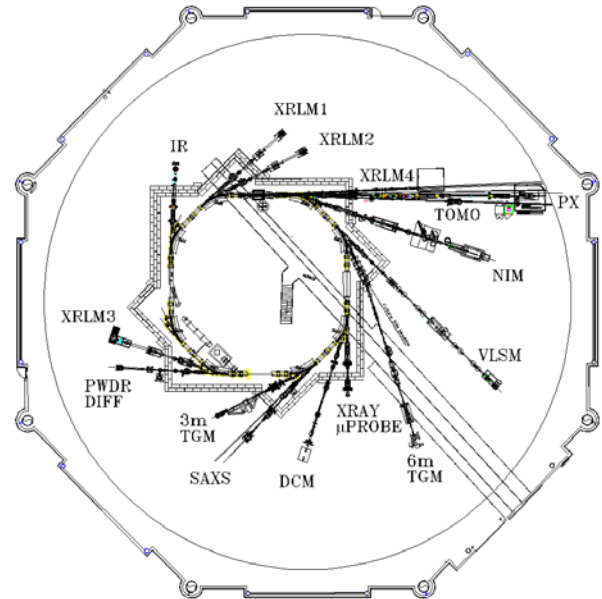


Fig 1. A general view of the CAMD facility.

## A SECOND INSERTION DEVICE

Because one of the long straights is unoccupied consideration has been given to the possibility of installing a 2<sup>nd</sup> Insertion Device (ID) in CAMD. In principle this could be either a wavelength shifter, a multipole wiggler or an undulator. Given that the existing wavelength shifter already provides sufficient coverage of the hard X-ray spectrum and that the CAMD research program has strong emphasis in the soft X-ray region it was decided to base plans on a multipole wiggler. This will be optimized to generate high flux density in the photon energy range 1 – 4 keV and would be designed to serve several beamlines simultaneously.

The requirement for high flux density from the 2<sup>nd</sup> ID implies that the beta values at the source point should be small to give small beam size. Although a minibeta can in principle be arranged at both the existing 7 Tesla ID and the adjoining vacant straight section it is not very practical. Furthermore the asymmetric periodicity which would result in the storage ring is not desirable. For these reasons it has been decided to locate the 2<sup>nd</sup> ID in the straight section diametrically opposite the 7 Tesla ID.

The straight chosen for the 2<sup>nd</sup> ID presently contains the single DORIS type RF cavity and this must be relocated to give sufficient space for the ID. It is intended to move the RF cavity to the unoccupied straight where it would

still be close to the power source and auxiliaries and it will only be necessary to rearrange and lengthen the waveguide.

The additional radiation loss in the 2<sup>nd</sup> ID may limit the beam current which can be maintained at 1.3 GeV, depending on its detailed design. There are several possible ways of overcoming such a limitation such as installing a higher power klystron, or adjusting the RF coupling factor. It would also be possible to install the 2<sup>nd</sup> RF cavity, which is held as a spare, in the same straight. A decision on these alternatives has not yet been made, pending a final design of the 2<sup>nd</sup> ID.

## DOUBLE MINIBETA OPTIC

The design of a lattice optic producing double minibeta has been explored. Several options have been identified, but the most suitable version has a betatron tune quite close to the present working point and has low emittance. The lattice functions of this optic, based on the lattice model which has been developed for CAMD, is shown in fig 2.

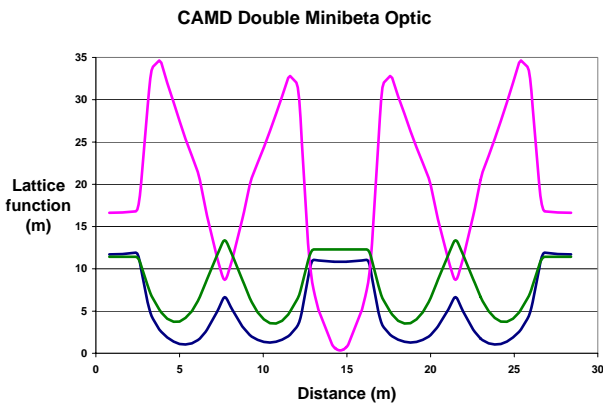


Fig 2. Double mini beta optic for CAMD. Half the circumference is shown. The vertical beta is shown red, the horizontal beta is blue and the dispersion x10 is green.

The double minibeta optic has tune values of  $Q_h=3.23$ ;  $Q_v=1.30$  which are very comparable with the normal tunes of  $Q_h=3.24$ ;  $Q_v=1.15$ . The natural horizontal emittance is calculated as 110 nm.rad but that will increase to 170 nm.rad when the 7 Tesla ID is on. There will be a further emittance growth owing to the 2<sup>nd</sup> ID, estimated as about 10% depending on the field level. The peak value of the vertical beta function is seen to increase from the present value of 25 m to 35 m and that will result in a slight growth in the vertical beam size, which is not expected to be a problem.

This double minibeta optic has been tested experimentally during dedicated beam studies at CAMD. The quadrupole power supplies were reconnected so that the quadrupoles in diametrically opposed straights were in the same families. It proved to be simple to migrate from the symmetric zero dispersion optic at the end of the energy ramp to the new optic.

The values of the lattice functions in the double minibeta optic were measured experimentally by means of the active shunts which are connected across each individual quadrupole. [5] The horizontal and vertical average beta function at each quadrupole were calculated from the resulting tune shifts. The dispersion function also was measured by offsetting the RF and measuring the shift of the beam orbit. The beta function measurements are shown in fig 3 and the dispersion in fig 4.

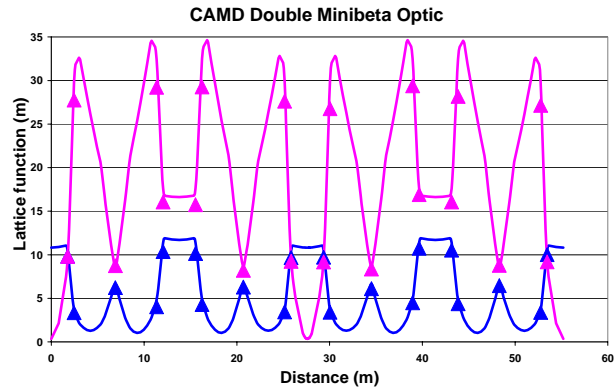


Fig 3. The calculated beta functions compared with the measured values averaged over each quadrupole. The vertical beta is shown red, the horizontal beta is blue

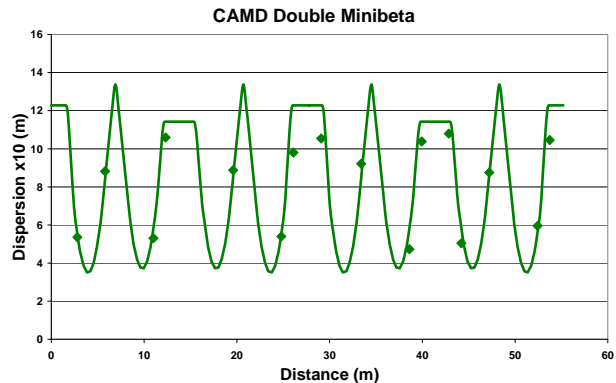


Fig 4. The calculated dispersion function x10 compared with the measured values.

It can be seen from figs 3 & 4 that the lattice functions as measured are in close agreement with the predictions of the lattice model using quadrupole gradients derived from the real magnet currents. These results give confidence that the lattice can be effectively modeled with good accuracy and optimized to give best performance when both IDs are in operation.

## PROPOSED MULTIPOLE WIGGLER

An innovative superconducting multipole wiggler has been proposed for the 2<sup>nd</sup> CAMD ID by N Mesentsev of the Budker Institute, Novosibirsk, Russia. This device would allow the flux from the ID either to be concentrated into one straight ahead beam line or alternatively to be

shared equally between 3 beamlines. This would be achieved by subdividing the multipole wiggler into 3 equal sections with bump correctors between each section and at both ends of the device. Each section would consist of 23 full poles with a half pole at each end. Without the bump correctors energized the entire flux from the ID would be delivered into the forward direction. By powering the bump correctors the 1<sup>st</sup> and 3<sup>rd</sup> sections would be deflected at  $\pm 8$  mrad and could serve independent beamlines set at these angles. The magnetic field configuration is shown in fig 5.

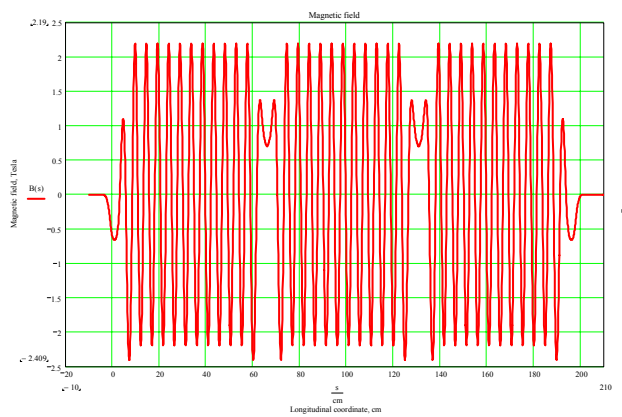


Fig 5. Magnetic field in the Multipole wiggler with the bump correctors energized.

The multipole wiggler has been optimized to generate flux in the 1-4 keV photon energy range. To do this it will have peak fields in the full poles of 2.2 Tesla and the length of a full period will be 42 mm. Each section will contain 11 full periods together with a half pole at each end. The overall length of the ID including its cryostat will enable it to be located in the 2.5 m free space of a CAMD long straight.

The spectral flux density which will be available from the 3 combined sections of this multipole wiggler is shown in fig 6. For comparison the flux density from a CAMD dipole and the 7 Tesla wavelength shifter are also shown. It is apparent that the multipole wiggler will be an excellent source of radiation in the range 1-5 keV with an increased flux density a factor 100 times greater than available from a CAMD dipole.

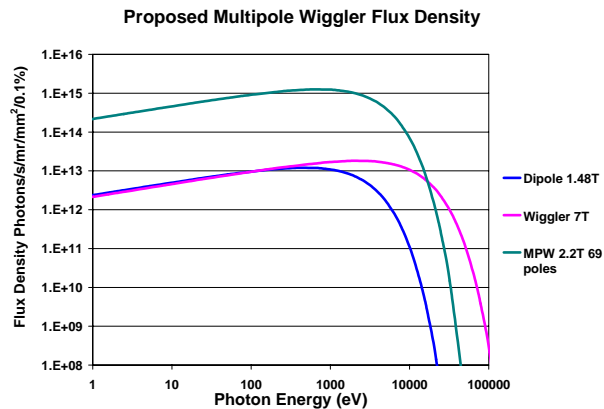


Fig 6. The flux density from the proposed multipole wiggler, the 7 Tesla wavelength shifter and the CAMD dipoles for a beam current of 250 mA.

At the present time the proposed multipole wiggler is not funded but a proposal is being drawn up which would include the ID, the machine modifications and the beamline with experimental station. This will be submitted to the funding authorities available to CAMD as part of a general proposal to increase the level of financial support.

## ACKNOWLEDGMENT

The contribution by N Mesentsev of the BINP, Novosibirsk, Russia in providing the design of the proposed multipole wiggler is gratefully acknowledged.

## REFERENCES

- [1] B C Craft et al., NIM B-40/41, p373, (1989); V P Suller et al., Proc EPAC2004, pp2424-2426.
- [2] F J Hormes et al., SP-005 in Proceedings of SRI 2006, Daegu, Korea.
- [3] VM Borovikov et al, J Synch Rad, vol 5, p440 (1998)
- [4] M Fedurin et al., Proc PAC2003, pp1053-1055.
- [5] V P Suller et al, Proc EPAC2004, pp2427-2429.





## Appendix E:

Possible configuration for the  
source of the 21<sup>st</sup> Century



# THE CONCEPTUAL DESIGN OF 4GLS AT DARESBURY LABORATORY

J. A. Clarke, CCLRC Daresbury Laboratory, Warrington, UK, on behalf of the 4GLS Design Team.

## Abstract

4GLS is a novel next generation proposal for a UK national light source to be sited at Daresbury Laboratory, based on a superconducting energy recovery linac with both high average current photon sources (undulators and bending magnets) and three high peak current free electron lasers. Key features are a high gain, seeded FEL amplifier to generate XUV radiation and the prospect of advanced research arising from unique combinations of sources with femtosecond pulse structure. The conceptual design is now completed and a CDR recently published [1].

## INTRODUCTION

4GLS will enable the study of real time molecular processes and reactions on timescales down to tens of femtoseconds in short-lived, nano-structured or ultra-dilute systems. The emphasis is on molecular and device function, rather than the largely ‘static’ structural focus of work on 3<sup>rd</sup> generation synchrotron radiation sources and X-ray FELs.

The 4GLS facility is planned from the outset to be a multi-source, multi-user facility. This is achieved by superconducting radio-frequency accelerator technology, operating using energy recovery, to provide short pulse spontaneous radiation with pulse length variable from ps to < 100 fs. At long wavelengths this allows the condition for coherent synchrotron radiation production to be met, with the result that 4GLS will provide enormously bright THz radiation. The high quality low emittance electron beam provided by the linacs additionally provides an

ideal source with which to operate free electron lasers (FELs). In the 4GLS conceptual design [1] these are embedded within the facility, delivering ultra-high brightness short-pulse radiation in the IR, VUV and XUV energy ranges, with pulse lengths as short as 50 fs FWHM. In world terms, this gives a unique suite of synchrotron radiation (SR) and FEL sources covering the THz to the soft X-ray range. Many of the light pulses originate from the same electron bunch, thus offering potential levels of internal synchronization at the tens of femtoseconds level. The peak brightness of the 4GLS sources is given in figure 1. There is a typical enhancement of eight orders of magnitude when compared with 3<sup>rd</sup> generation light sources.

Significant aspects of the 4GLS design have been informed by experience gained on the 4GLS Energy Recovery Linac Prototype (ERLP) currently approaching completion at CCLRC Daresbury Laboratory [2, 3].

## OVERVIEW

4GLS consists of three inter-related accelerator systems [12] (see figure 2). The first is the high average current loop (HACL). In this a 600 MeV beam of 77 pC bunches is delivered at repetition rates of up to 1.3 GHz and energy recovery is an essential element. Progressive compression of the electron bunches in this loop allows for photon pulse lengths from a few ps to approximately 100 fs (RMS). The VUV FEL is placed towards the end of the HACL.

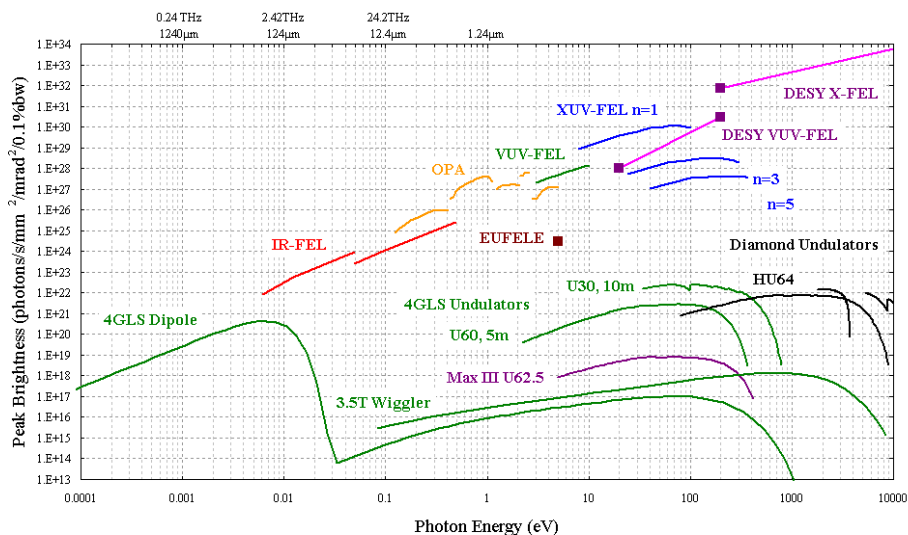


Figure 1. Peak brightness for 4GLS FELs, undulators, wiggler, OPA and dipoles compared with EUFELE, X-FEL, Diamond and Max III undulators.

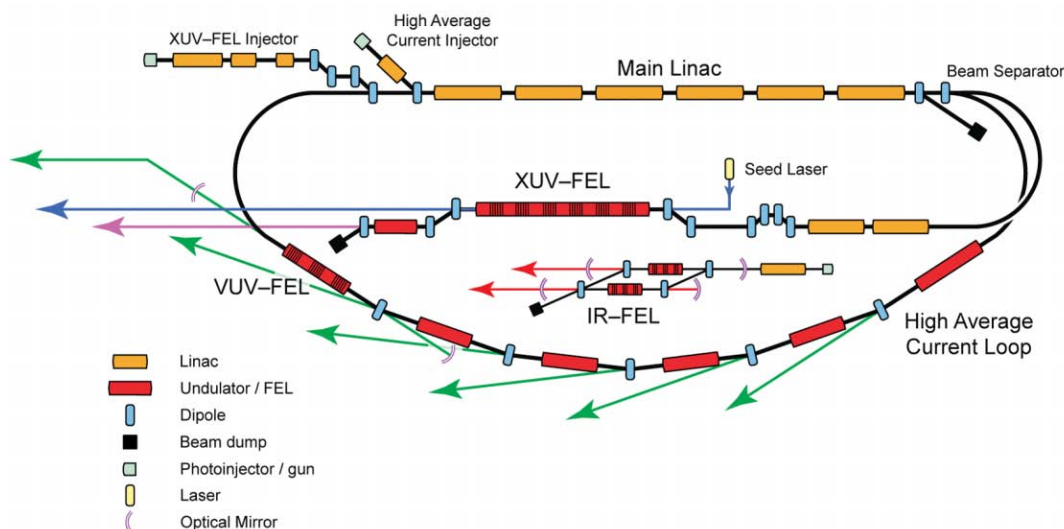


Figure 2. The conceptual layout of 4GLS.

Table 1. Main electron beam parameters of 4GLS

<i>Bunch Parameter</i>	<i>XUV-FEL</i>	<i>100 mA HACL</i>	<i>VUV-FEL HACL</i>	<i>IR-FEL</i>
		<i>Operation</i>	<i>Operation</i>	
Electron Energy	750 to 950 MeV	600 MeV	600 MeV	25 to 60 MeV
Normalised Emittance	2 mm mrad	2 mm mrad	2 mm mrad	10 mm mrad
RMS Projected Energy Spread	0.1 %	0.1 %	0.1 %	0.1 %
RMS Bunch Length	< 270 fs	100 to 900 fs	100 fs	1 to 10 ps
Bunch Charge	1 nC	77 pC	77 pC	200 pC
Bunch Repetition Rate	1 kHz	1.3 GHz	n x 4.33 MHz	13 MHz
Electron Beam Average Power	1 kW	60 MW	n x 200 kW	156 kW

The second major accelerator system is the XUV-FEL branch. The XUV-FEL requires a peak current of  $\sim 1.5$  kA at beam energies from 750 to 950 MeV. This beam is derived from 1 nC bunches produced by a normal conducting RF photo injector operating at 1 kHz. At this repetition rate the 1 kW of beam can be safely dumped after traversing a final spontaneous undulator source.

Although the XUV-FEL beam and the high average-current beam discussed above are derived from separate electron sources after suitable low energy acceleration they are merged and accelerated in a single superconducting linac. The two beams are then separated using magnetic, energy separation for delivery to their respective devices.

The third accelerator system is that required for the IR-FEL. The same linac technology is used to accelerate electrons to between 25 and 60 MeV to provide a fully integrated and synchronised IR-FEL facility. The main electron beam parameters for 4GLS are given in Table 1.

The 4GLS design utilises superconducting linacs to accelerate and manipulate the three beams required to drive the photon sources. The accelerating structures are all based on a fundamental RF frequency of 1.3 GHz and

a modified TESLA type cavity design operating at 2 K or below [4, 5]. A prototype 2 cavity cryomodule is currently being developed at Daresbury Laboratory [6].

The most challenging area of accelerator design for 4GLS is in meeting the requirements of extremely high peak current for the XUV-FEL branch whilst simultaneously transporting and accelerating very high quality high-average current (100 mA) beam to the energy recovery loop.

The bunches within both of these beams have to undergo a significant amount of compression to deliver the required peak currents to drive the XUV- and VUV-FELs and to meet the requirements of the science case for different pulse lengths from undulators in the HACL. An innovative, integrated acceleration and compression scheme is proposed which meets the unique requirements for each of the two beams whilst using the same main superconducting accelerator [7]. By defining appropriate accelerating phases within the linacs, the high compression demands of the XUV-FEL are met using a two-stage compression scheme including a higher harmonic RF system for flexible non-linear correction, whilst progressive compression through the undulator arc

delivers the high peak current in the 77 pC bunches required to drive the VUV-FEL. Wakefield effects in the accelerator are reduced by performing the final compression stage at full energy so that the bunches around the arcs are kept relatively long to control the disruptive effects of coherent synchrotron radiation emission. Acceleration of a 100 mA beam is very challenging; to accelerate and decelerate such a beam requires that the linac transport design is tailored to give a high threshold for the disruptive beam break-up instability. This is achieved through a combination of techniques including substantial damping of HOMs in an advanced design of RF cavity, tight control of beam focussing throughout the linac and optimisation of coupling and overall transport properties in the energy recovery loop [8, 9].

A simple yet robust seeded design for the XUV-FEL is proposed [10] to ensure that ultra-high quality, reproducible, tunable radiation is available in the 8 to 100 eV photon range. The output pulses will have selectable polarisation and a pulse repetition rate of 1 kHz is set by the seed laser and the photoinjector; upgrade paths to 10 kHz for both these items looks likely. Established FEL theory and state-of-the-art simulation codes predict this FEL will generate photon energies at multi giga-watt power levels in pulses of duration  $\sim 50$  fs FWHM. The pulses will have excellent temporal and spatial coherence with time-bandwidth products close to the Fourier transform limit for a Gaussian pulse. Unlike the self amplified spontaneous emission mode of operation, which effectively self-starts from intrinsic noise, the FEL interaction here is acting as a true amplifier. The high quality spectral properties of the radiation input seed pulses are maintained by the amplified output radiation pulses. Recent advances in High Harmonic Generation sources mean that the seed requirements for the XUV-FEL already exist.

The VUV-FEL offers high repetition rates (multiples of 4.33 MHz) with giga-watt peak power and  $> 100$  W average power [11]. Here advantage is taken of mirrors (with hole out-coupling) that are able to operate over the photon energy range of 3 to 10 eV. Photon pulse lengths of  $\sim 170$  fs (FWHM) will be obtained in standard mode and simulations suggest that pulses as short as  $\sim 25$  fs may be possible in a super-radiant mode. The output pulses will have selectable polarisation and be fully tunable.

By using a pair of mirrors to reflect light emitted by the FEL back to the entrance of the device it becomes, in effect, self-seeding and no external conventional laser system is required. Hence high quality, stable light is ensured through a rather simple optical feedback loop. A particular feature of this FEL when compared with similar designs covering the same wavelength range is the tolerance to low mirror reflectivity. Extensive simulations have shown that mirror reflectivities in the range 40 to 60 % are acceptable for this design. Detailed modelling has been used to confirm excellent spatial and temporal coherence and a regime has been identified where the

performance of the device is relatively insensitive to (and can even be enhanced by) degradation of mirror reflectivity.

The IR-FEL has been designed to produce high intensity, spatially and temporally coherent radiation with variable pulse lengths, flexible output pulse patterns and variable polarisation over the wavelength range 2.5 to 200  $\mu\text{m}$ . The high-Q cavity-based design employs two undulators and hence offers the potential to satisfy user experiments at two different wavelengths simultaneously. The provision of short electron bunches offers the potential to operate the FEL in super-radiant mode to produce shorter pulses with higher peak intensities than available in normal operation: simulations predict FWHM pulse lengths of only a few optical cycles can be produced in this way. The implementation of a superconducting RF linac with the IR-FEL will offer highly stable operation and also high average powers ( $> 100$  W) though the option of running in modes that reduce the average power for sensitive samples will also be available.

There are six insertion device straights in the HACL, one of which is allocated to the VUV-FEL. The remaining five will be used to generate spontaneous radiation. To maximise the potential of the spontaneous sources three different undulator straight lengths have been chosen; two 14 m straights; two 10 m straights and two 8 m straights. Thus the total space available for undulators is  $\sim 64$  m, which exceeds all other existing low energy 3rd generation light sources.

## REFERENCES

- [1] 4GLS Conceptual Design Report 2006, available from [www.4gls.ac.uk](http://www.4gls.ac.uk)
- [2] S. L. Smith et al, 'The Status of the Daresbury Energy Recovery Prototype Project', these proc.
- [3] S. L. Smith, 'A Review of ERL Prototype Experience and Light Source Design Challenges', these proc.
- [4] P. A. McIntosh et al, 'RF Requirements for the 4GLS LINAC Systems', these proc.
- [5] S. Pattalwar et al, 'Key Cryogenics Challenges in the Development of the 4GLS', these proc.
- [6] P. A. McIntosh et al, 'Development of a Prototype Superconducting CW Cavity and Cryomodule for Energy Recovery', these proc.
- [7] B. D. Muratori et al, 'Lattice Design for the Fourth Generation Light Source at Daresbury Laboratory', these proc.
- [8] E. Wooldridge and B. D. Muratori, 'Linac Focusing and Beam Break Up for 4GLS', these proc.
- [9] E. Wooldridge, 'Alternate Cavity Designs to Reduce BBU', these proc.
- [10] B. W. J. McNeil et al, 'Design Considerations for the 4GLS XUV-FEL', FEL 2005.
- [11] N. Thompson et al, 'A VUV-FEL for 4GLS: Design Concept and Simulation Results', FEL 2005.
- [12] M. W. Poole and E. A. Seddon, '4GLS and the Energy Recovery Linac Prototype Project at Daresbury Laboratory', PAC 05, Knoxville, p431.